UNIVERSITÀ
DEGLI STUDI
DI PADOVA

Sede Amministrativa: Università degli Studi di Padova

Dipartimento di Geoscienze

CORSO DI DOTTORATO DI RICERCA IN: Scienze della Terra
CURRICOLO: unico
CICLO XXXIV

Are calcareous phytoplankton affected by the onset of the Antarctica ice-sheet at the Eocene-Oligocene transition?

Qual è la risposta del phytoplankton calcareo all'instaurarsi della calotta antartica durante la transizione Eocene-Oligocene?

Coordinatore: Prof.ssa Claudia Agnini
Supervisore: Prof.ssa Claudia Agnini

Dottoranda: Allyson Viganò

Contents

Chapter 5

Calcareous nannofossils across the Eocene-Oligocene transition: preservation signals and biostratigraphic remarks from ODP Site 1209 (NW Pacific, Shatsky Rise) and IODP Hole U1411B (NW Atlantic Ocean, Newfoundland Ridge)

Abstract

Today's icehouse climate, characterized by two glaciated poles, is the result of gradual cooling over tens of millions of years. In the southern hemisphere, no undoubtable evidence for permanent ice on Antarctica existed until 34 Ma, when ice rafted detritus were first deposited on the surrounded sediments. From that time, known as the Eocene-Oligocene transition (E/O), the magnitude of the Antarctic ice sheet has increased unevenly toward the present. This transition also documented main reorganisation of marine and terrestrial ecosystems and paved the way to the establishment of the modern thermohaline circulation. An exceptional record of this climatic change is stored in the deep ocean, where the accumulation of sediments has provided an almost continuous archive of the past. During this time, datasets from around the world document increases in both oxygen and carbon deep-ocean isotopes. However, the role played by calcareous phytoplankton, one of the main carbonate and carbon producers, is still open to questions, primarily due to the lack of high-resolution studies, especially for the mid-low latitudes.

In this context, this Ph.D. project focuses on the ecological, biostratigraphic, morphometric and preservation response of calcareous nannofossils in different sediments retrieved from the Pacific (IODP Site U1509; ODP Site U1209), Indian (ODP Site 756) and Atlantic oceans (IODP Site U1411). The main aim is to add a piece of information on the timing, modes, and magnitude of their response to sea-surface water changes related to the expansion of the Antarctic ice-sheet. Our study indicates shifts and changes within the nannoplankton community at the E-O transition, closely coupled to major isotopic excursions. Throughout the study interval, calcareous nannofossils have responded quite synchronously to glacial expansion, recording a major turnover in the assemblage from a warm-oligotrophic community, that characterized the late Priabonian to a cold eutrophic in the early Rupelian. This major turnover appears to have been triggered by a combination of decreasing temperature and increasing nutrients (**Chapter 2** and **Chapter 4**). The high-resolution dataset also provides new potential biohorizons that can be integrated with available mid-low latitude biozonations allowing for highly refined comparison between mid-low and high latitudes (**Chapter 3**).

Among the investigated taxa, *Clausicoccus subdistichus* gr. has proven to be an extraordinary biostratigraphic and paleoenvironmental proxy for this crucial climatic phase.

The acme of this informal taxonomic group is present and easily recognizable at all the studied sites, even in extremely poorly preserved sediments (e.g., ODP Site 1209). The base common (Bc) of this acme represents the best nannofossil bioevent to approximate the E-O boundary (EOB), while the highest abundance values correlate with the Earliest Oligocene Glacial Maximum - EOGM.

In addition, we clarify the relative ranking between the Top common and continuous of *C. subdistichus* gr. versus the Top of *Ericsonia formosa,* with the latter predating the former (**Chapter 3**).

The morphometric investigation performed on this group provide key information on its sensitivity to paleoenvironmental changes across different latitudes and basins and enabled us to investigate in more detailed the two species ascribed to this group, i.e. *C. subdistichus* and *C. fenestratus* (**Chapter 6**).

The increase in abundance and size of *C. subdistichus* gr. is likely favored by high nutrient concentrations and an oversaturation of $[CO_3^{2-}]$ in the sea surface water across the E-O.

Finally, a preservational variation of the nannofossil assemblages across the EOT is the case study of **Chapter 5**. We described and compared, with the aid of the SEM, the exceptional well preserved sediments at Site U1411 with the poorly preserved of Site 1209, in order to describe the wide spectrum of variation observed across the E/O. A first result is that at Site 1209, diagenesis has severely affected calcareous nannofossil assemblages, preventing any paleoecological interpretation. Despite this, for most of the section, diagenesis did not alter the primary bulk isotopic signal which still retains the main geochemical features of the event, and it has been possible to construct an accurate age model because the biostratigraphic index species are solution-resistant forms.

Sommario

Il sistema climatico dei nostri giorni, caratterizzato dalla presenza di ghiacci su entrambi i poli, è il risultato di un raffreddamento graduale avvenuto nel corso di decine di milioni di anni. La calotta Antartica permanente, si sviluppò 34 Ma, quando i detriti trasportati dal ghiaccio si depositarono per la prima volta sui sedimenti circostanti. Da quel momento, noto come la transizione Eocene-Oligocene (E/O), la calotta glaciale antartica è cresciuta in modo non uniforme fino a raggiungere le dimensioni attuali. Questa transizione portò alla riorganizzazione degli ecosistemi marini e terrestri e aprì la strada all'istituzione della moderna circolazione termoalina. Un record eccezionale di questo cambiamento climatico è conservato nelle profondità oceaniche, dove l'accumulo di sedimenti ha fornito un archivio quasi continuo del passato. Durante questo periodo, i dataset di tutto il mondo documentano un aumento dei valori isotopi dell'ossigeno e del carbonio negli oceani profondi. Tuttavia, il ruolo svolto dal fitoplancton calcareo, uno dei principali produttori di carbonato e carbonio, è ancora aperto a dubbi, principalmente per la mancanza di studi ad alta risoluzione, soprattutto per le latitudini medio-basseIn questo quadro, questa tesi si concentra sulla risposta ecologica, biostratigrafica, morfometrica e preservazionale dei nannofossili calcarei, recuperati in diversi sedimenti provenienti dall'oceano Pacifico (Site IODP U1509; Site ODP U1209), Indiano (Site ODP 756) e Atlantico (Site IODP U1411). L'obiettivo principale è far luce sui tempi, le modalità e l'entità della loro risposta a cambiamenti legati alla chimica oceanica e all'espansione antartica. Questo studio documenta cambiamenti nell'associazione fitoplanctonica strettamente legati alla transizione stessa e alle principali escursioni isotopiche. Durante questo intervallo, i nannofossili calcarei hanno risposto in modo piuttosto sincrono all'espansione glaciale, registrando il passaggio da una comunità caldo-oligotrofica, che caratterizzava il tardo Priaboniano ad una fredda eutrofica nel primo Rupeliano. Questo importante turnover sembra essere stato innescato da una diminuzione di temperatura dell'acqua marina e, al contempo, da un aumento dei nutrienti (**Capitolo 2 e Capitolo 4**).

Il dataset ad alta risoluzione fornisce anche un perfezionamento della biostratigrafia delle medio-basse latitudini e introduce nuovi biorizzonti potenzialmente utili che possono essere a loro volta integrati con altri, consentendo un confronto dettagliato tra alte e medio-basse latitudini (**Capitolo 3**).

Tra i taxa indagati, *Clausicoccus subdistichus* gr. si è rivelato uno straordinario indicatore biostratigrafico e paleoambientale per questo critico intervallo temporale. Il suo acme (i.e. incremento di abbondanza) è infatti presente e facilmente riconoscibile in tutti i siti studiati, perfino in un sedimento estremamente mal preservato (Site ODP 1209). La base comune (Bc) di questo acme, collocata al limite E/O (EOB), rappresenta il migliore bioevento, tra quelli a nannofossili, per approssimare questo limite. Inoltre, i suoi picchi di abbondanza consentono una facile correlazione con il massimo glaciale dell'Oligocene inferiore - EOGM.

In questo lavoro è stato ridefinito il ranking del limite superiore di abbondanza (Tc) di *C. subdistichus* gr. che è stato posto al di sopra dell'estinzione di *E. formosa* (**Chapter 3**).

L'indagine morfometrica eseguita su questo gruppo ha fornito informazioni chiave sulla sensibilità di *Clausicoccus* ai cambiamenti paleoambientali avvenuti alle basse-medie latitudini e ha permesso di condurre un'indagine approfondita riguardo alle due specie appartenenti a questo gruppo, ovvero *C. subdistichus* e C. *fenestratus* (**Capitolo 6**). L'aumento dell'abbondanza e delle dimensioni di *Clausicoccus* è stato probabilmente determinato e favorito da elevate concentrazioni di nutrienti e da un'eccessiva saturazione di [CO_3^{2-}] nell'acqua di mare. Infine, nel **Capitolo 5**, è stata eseguita un'analisi sullo stato di preservazione dell'associazione durante le fasi principali di questa transizione. Con l'aiuto del SEM sono stati confrontati due sedimenti a diversa preservazione (Site U1411 e 1209), con lo scopo di ricostruire l'intero spettro delle variazioni preservazionali. Abbiamo riscontrato come, al Site 1209, la diagenesi influisca in maniera grave sull'associazione, impedendo qualsiasi interpretazione paleoecologica. Nonostante questo, per la maggior parte della sezione, la diagenesi non ha alterato il segnale isotopico originale, il quale conserva le principali caratteristiche geochimiche dell'evento. Allo stesso modo, le specie biostratigrafiche chiave, per lo più forme resistenti alla dissoluzione, non sono state cancellate dai processi diagenetici e hanno quindi permesso di fornire un modello di età accurato.

Chapter 1

Introduction

1.1 Overview

The Eocene-Oligocene transition (EOT) represents a critical phase of Earth's history characterized by an intense climatic change and biotic turnovers in both marine and terrestrial realms (Zachos et al., 2001; Coxall and Pearson, 2007; Hutchinson et al., 2021). During this time, climate shifted from a largely ice-free greenhouse world to a glacial regime, that characterized the Oligocene, with intense cooling and the growth of a major sustained Antarctic ice-sheet (Zachos et al., 2001; Zachos and Kump, 2005; Coxall and Pearson, 2007; Westerhold et al., 2020; Hutchinson et al., 2021), most likely an early East Antarctic Ice Sheet (EAIS) (Shackleton and Kennett, 1975; Miller et al., 1987; Zachos et al., 1992; Coxall et al., 2005; Young et al., 2011; Bohaty et al., 2012; Galeotti et al., 2016).

The transition between the Eocene and Oligocene epochs represents the climax of a long-term cooling, whose onset coincides with the end of a global warm phase, known as Early Eocene Climatic Optimum or EECO (~ 50-52 Ma) and culminated with the beginning, for the first time in the Cenozoic, of a permanent continental-scale glaciation on Antarctica at the Eocene/Oligocene boundary (~34 Ma) (Zachos et al., 2001; 2008). Evidences for this glaciation are provided over the word by marine sedimentary cores, which record large positive excursions (~1.2 to 1.5‰) in benthic foraminifera oxygen isotopes synchronous with a rapid deepening of the calcite compensation depth (CCD) (Coxall et al., 2005; Pälike et al., 2012).

A possible explanation for the CCD deepening is the exposure and consequent dissolution of shallow-marine carbonates caused by the glacio-eustatic sea-level fall (Merico et al., 2008).

The terrestrial record documents significant changes in plants and animals triggered by cold temperature, but, unfortunately the available datasets are sporadic. By contrast, the deep-sea sediments represent the most complete archive of the past, providing a continuous and relatively expanded record, where it is possible to undertake paleoclimatic reconstructions. Microfossils, in this sense, provide the most solid basis for the understanding of the E-O transition (Coxall and Pearson, 2007).

Advances in Cenozoic climate history have been achieved in the last sixty years through the international ocean drilling programs: the Deep Sea Drilling Project (DSDP; 1964-1983), the Ocean Drilling Program (ODP; 1984-2003), the Integrated Ocean Drilling Program (IODP, 2003- 2013) and the International Ocean Discovery Program (IODP; 2013-2023) (Cronin, 2010; https://www.iodp.org/about-iodp/history). However, a major issue is that only few ODP, DSDP and IODP deep-sea sites are suitable to study the EOT and this leads to a number of limits in the knowledge of this transition. In fact, many sections spanning the E-O boundary (EOB) are poorly recovered, extremely condensed, or characterized by gaps, which are, at least in part, attributable to major oceanic reorganization occurred during this time (Kennett, 1976; Miller et al., 1991; Zachos et al., 1996). Among microfossils, calcareous nannofossils, which are the inorganic rests of photosynthetic primary producers (Coccolihophores, Haptophyte algae), provide fundamental constraints on

the past organic and inorganic carbon cycle, since their first appearance in the fossil record (Upper Triassic, ~225 Ma) (Bown et al., 2004), because their role in regulating the Earth system is considerable.

Calcareous nannoplankton use solar energy to drive the conversion of carbon dioxide into organic polysaccharides (***organic carbon pump***), but, at the same time, they precipitate $CaCO_3$ (***carbonate counter pump***) through the secretion of tiny composite exoskeletons (the *coccosphere*, made of multiple *coccoliths*). Precipitation of calcite produces CO_2 that can be released to the atmosphere (Berner et al., 1983). This process is called biomineralisation and plays an important role in controlling the alkalinity and carbonate chemistry of the photic zone of the modern and past ocean.

On one hand coccolithophores play an active role in gas exchange (CO_2) between surface seawater and atmosphere and but, on the other hand, these organisms are also able to export organic matter and carbonate to sea floor (De Vargas et al., 2007). For this reason, they are extremely valuable paleoenvironmental and geochemical proxies.

They are also exceptional dating tools thanks to their wide distribution, high evolutionary rates and their high abundances in the fossil record. These features allow to interpret the modifications in the assemblages as a response/adaptation to climate changes. In addition, the good correlation between Cenozoic nannoplankton diversity and climate trends, with higher diversities associated with warm climates and lower diversity with cooling phases also help to reconstruct their biodiversity patterns and their relation to past environmental conditions (Bown et al., 2004).

The ongoing debate on the response of the major calcifying primary producers as a result of increasing pCO_2 atmospheric concentration is based on in vitro studies but insights are possibly obtainable from the study of fossil records documenting times of significant changes in atmospheric greenhouse gases.

A fundamental limit in the present knowledge of the Earth's dynamics is related to the poor understanding of how and how much changes in climate and ice growth could impact on marine biota, and, in particular, on phytoplankton community. The E–O transition, represents the counterpart of the present global warming but it is equally fundamental in order to model the complex interaction among the different components of the climate system. Several lines of evidence suggest a strong connection between changes observed in calcareous nannoplankton and this climate transition both in low and high resolution studies (Persico and Villa, 2004; Dunkley Jones et al., 2008; Villa et al., 2008; 2021; Blaj et al., 2009; Toffanin et al., 2013; Bordiga et al., 2015; Jones et al., 2019). In this thesis, I will investigate sedimentary records recovered from ODP and IODP sites at low and middle latitudes. The main aim of this research is to address the nannofossil response to the EOT and specifically to provide a detailed record of the nannoplankton community that can be used to address specific questions related to the reconstruction of the paleoenvironmental conditions, as well as to biostratigraphic framework. In order to achieve these goals, we have decided to study calcareous nannofossil assemblages recovered in different oceans and depositional settings from ODP Site 756 (Ninetyeast ridge, Indian Ocean; Peirce et al., 1989), to ODP Site 1209 (Shatsky Rise, NW Pacific; Bralower et al., 2002), to IODP Site U1509 (New Caledonia Trough, Tasman Sea; Sutherland et al., 2019) and, eventually, to IODP Site U1411 (Newfoundland Ridge; Norris et al., 2014b), this will allow to describe nannofossil assemblages shifts across the EOT and to discriminate between local and global dynamics.

1.2 State of the art

Here, we discussed the current state of art of the E-O transition with a detailed analysis of the Paleogene climate evolution, the Eocene-Oligocene transition and the stratigraphic terminology adopted in this work.
The core of this introduction will consider a synthesis of evidence from different environmental parameters (e.g., $\delta^{18}O$, SST and paleoproductivity), the causes of the Antarctic glaciation, calcareous nannofossils (their taxonomy, biostratigraphy and paleoecology), the role of preservation, morphometry and climate change.

1.2.1 Paleogene greenhouse-icehouse climate evolution

In the past Earth's history, climate has changed on different timescales, driven by a multitude of forcing mechanisms (e.g. changes in solar radiation on the scale of Milankovitch cycles or by internal responses and feedbacks, for instance, by changes in concentration of greenhouse gases, albedo and heat transport; for an overview see Ruddiman, 2008).
During the Paleogene (66-23 Ma), climate was characterized by relatively warm global temperatures given by higher concentrations of greenhouse gases and by the absence of permanent ice sheets at the poles (Vandenberghe et al., 2012). During the Eocene, South America and Australia were still not fully separated from the Antarctic continent (e.g. Livermore et al., 2005; Brown et al., 2006), preventing the development of a (proto) Antarctic circumpolar current (Jenkins, 1974; Hutchinson et al., 2018). These climatic conditions have persisted until the late Eocene, when the cooling trend culminated in a major glaciation event in the early Oligocene, paving the way for modern life and climate.
Several lines of evidences for the Antarctic glaciation come from glacio-marine sediments and variations in clay mineralogy – i.e. a shift from smectite to illite-dominated clay materials (Ehrmann and Mackensen, 1992; Diester-Haass and Zahn, 1996; Ehrmann, 1998). Similarly, terrestrial paleontological evidences from fossil plants and palynomorphs have yielded information about cooling climates (Francis, 1999; Francis and Poole 2002), as well as the mass extinction of mammalian faunas recorded in Europe within Chron C13n (Hooker et al., 2004). The mammal extinction was noted almost a century ago by Stehlin (1909), who named it the 'Grande Coupure' (the great break) (Sun et al., 2014; Sheldon et al., 2016).
Major turnovers were observed in marine micro biota, as for instance in radiolaria (Funakawa et al., 2006; Kamikuri et al., 2012) and diatoms (Baldauf, 1992). A variety of long-ranging larger benthic foraminifera, in particular the highly specialized forms, disappeared near the end of the Eocene, events likely triggered by global environmental or ecological mechanisms (Cotton and Pearson, 2011). Important genera that disappeared include *Discocyclina, Asterocyclina* and *Pellatispira*. All these extinctions precede the sea-level regression and are found to occur close to the last appearance of the planktonic foraminiferal family *Hantkeninidae* (Pearson et al., 2008; Wade and Pearson, 2008; Cotton and Pearson, 2011). These quasi-synchronous extinctions suggest that the environmental changes associated with the Eocene-Oligocene boundary affected more than just the plankton communities (see references above). According to Cotton and Pearson (2011), a sudden increase in nutrient availability in the surface waters was responsible for the extinction of oligotrophic foraminifera, particularly among the highly-specialized genera (Figure 1.3).

Undoubtedly, despite all these paleontological and sedimentological data, the main evidence of this event is still based on the marine oxygen ($\delta^{18}O$) and carbon ($\delta^{13}C$) isotope compilations measured in deep-sea sediments (Zachos et al., 2001; 2008; Cramer et al., 2009; Westerhold et al., 2020) (Figure 1.1).

The benthic foraminiferal $\delta^{18}O$ values retain information both on the contribution of deep-water temperatures in which organisms secrete their test (Urey, 1947; Emiliani, 1955; Craig, 1965) and on global ice volumes, the so-called “glacial effect" (Shackleton, 1967). In fact, looking at this dataset, we can see that after the warm early Eocene phase (50-52 Ma), the $\delta^{18}O$-stack indicates a long-term gradual transition to heavier (cooler) values toward the Oligocene. Concomitant to the E-O transition an overall deepening of the carbonate compensation depth (CCD), greater than 1 km, is observed in the Pacific Ocean (Coxall et al., 2005; Pälike et al., 2012). This climatic disruption led to significant ecological changes, which clearly correspond with a decreasing in species diversity in marine calcareous plankton assemblages, as reported by Bown et al. (2004) (Figure 1.1) and by Pearson et al. (2008) (Figure 1.2).

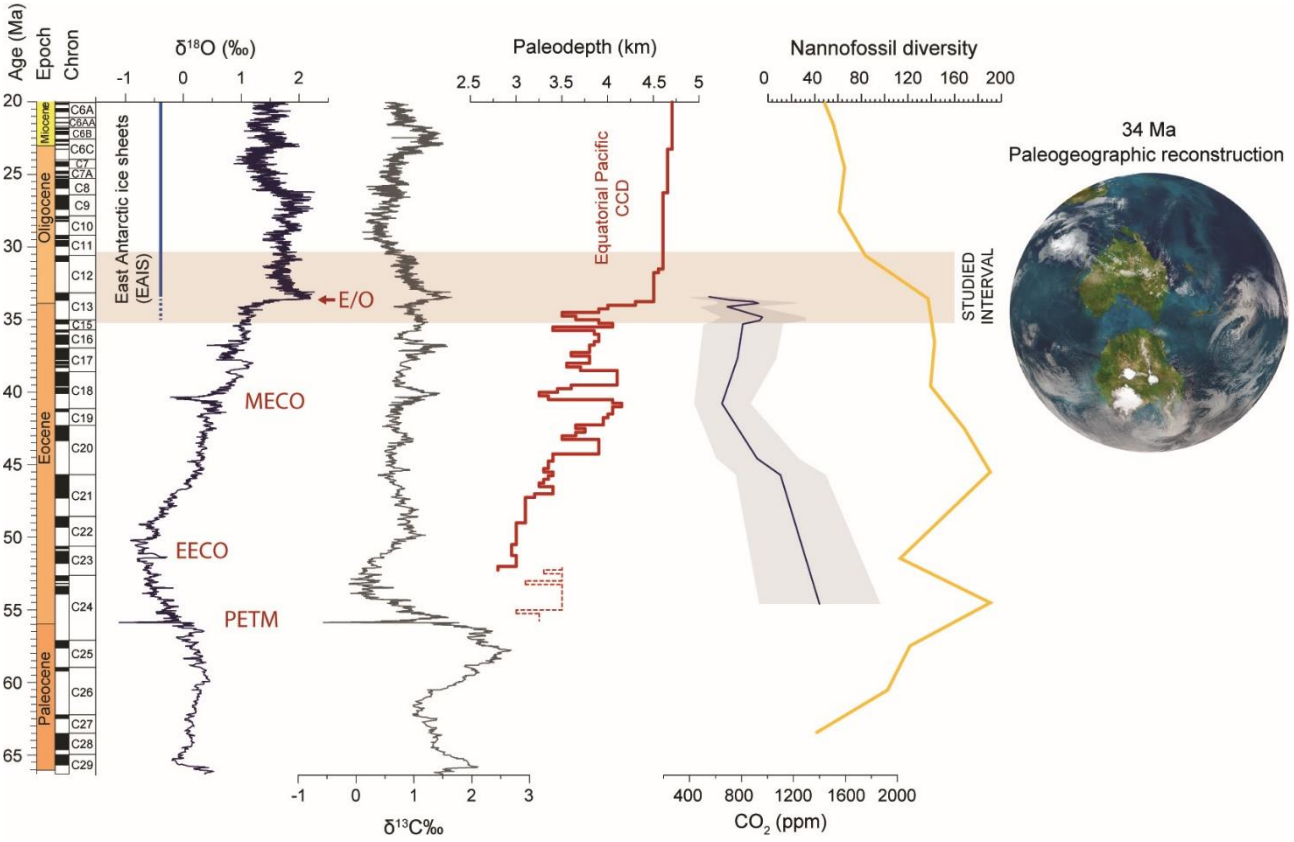

Figure 1.1 Paleogene main climatic events plotted against oxygen and carbon stable isotopes curves from Cramer et al. (2009). Stable isotopes values are recalibrated to GTS12. Isotope curves are obtained by a 9-point moving average. Large-scale features of this transition are here reported, such as: CCD paleodepth, (Pälike et al., 2012), past pCO_2 trend (Anagnostou et al., 2016) and nannofossil diversity (Bown et al., 2004). A 34 Ma paleogeographic Antarctica ice-sheet reconstruction is after Lear et al. (2016). The orange band indicates the study interval. The main Paleogene climate events (i.e., PETM, EECO, MECO and EOT) are also reported in the figure.

Pivotal Cenozoic reconstructions that use foraminiferal isotopes are those of Shackleton and Kennett (1975), and Miller et al. (1987). As underlined before, the isotope ratios of oxygen ($^{18}O/^{16}O$) and carbon ($^{13}C/^{12}C$) constitute the most important paleoclimatic proxies to reconstruct past climate and environmental parameters (e.g., temperature, ice volume, paleoproductivity,.).

Conventionally, the oxygen isotope ratio is expressed as:

$$\delta^{18}O \text{ ‰} = [(^{18}O/^{16}O)_{sample} - (^{18}O/^{16}O)_{standard}]/ (^{18}O/^{16}O)_{standard} \text{ x } 100$$

The ratio of heavy to light oxygen isotope is a function of the fractionation processes within the global hydrological cycle. Since ice sheets store isotopically light oxygen (^{16}O) during glacial periods, the sea-water become enriched in ^{18}O, relative to ^{16}O (e.g. Emiliani, 1966; Kennett, 1976; Shackleton, 2000). However, $\delta^{18}O$ signature preserved in marine microfossils also reflects the water temperature in which the carbonate was secreted, with heavier isotopic values reflecting cooler temperatures. Thus, enriched values of $\delta^{18}O$ can be interpreted in term of either a cooling in water temperatures or increased ice volumes. Hydrological (evaporation, precipitation, sea-water density), biological ("vital effects", non-equilibrium shell secretion) and post-mortem dissolution also contribute to control the values observed in oxygen isotope (see Chapter 5).

Gateways, pCO_2 or orbital forcing? Different climatic drivers have been proposed to explain the possible trigger mechanism for the Antarctic glaciation, but the precise cause is still unknown (Galeotti et al., 2022).

A long-held hypothesis was first attributed to paleogeographic changes, and in particular to the tectonic separation of Antarctica from South America (Drake Passage opening) and Australia (Tasmanian Gateway opening) through the Paleogene, which may have contributed to the thermal isolation of Antarctica (Kennett, 1977) and the development of the Antarctic Circumpolar Current (ACC) in the early Oligocene (Lawver and Gahagan, 2003). But the exact timing of these openings and their role continues to be the matter of the ongoing debate (Barker, 2001; Stickley et al., 2004; Eagles et al., 2006; Livermore et al., 2007; Scher et al., 2015; Sauermilch et al., 2021). Numerical modelling has shown that although the ACC may have played a role in the Antarctic glaciation, the rapid glacial onset was most likely caused by a gradual declining in atmospheric pCO_2, without any change in ocean circulation (DeConto and Pollard, 2003). Pollard and DeConto (2005) modelled the coupled effects of orbital forcing and CO_2 to explain the 34 Ma cooling. In their work, they propose that thresholds in the atmospheric greenhouse gas concentration are the main forcing for the evolution of EAIS (East Antarctic Ice sheet); while a minor role is assigned to ocean heat transport in controlling ice volumes. This idea is also corroborated by a more recent climate model which suggests that only 10% of temperature change can be attributed to ocean gateways reorganization (Inglis et al., 2015). Thus, the authors suggest that bathymetric changes (i.e. the gateway openings) may have been responsible for other specific regional features, e.g. sea surface temperature (SST) shifts. Actually, the hypothesis of gradual atmospheric pCO_2 decline is considered the principal forcing mechanism for the Eocene cooling and the cryosphere unipolar evolution (DeConto and Pollard, 2003; Pagani et al., 2005; 2011; Zachos et al., 2008; Anagnostou et al., 2016; Cramwinckel et al. 2018). Combined to orbital forcings (Coxall et al., 2005) a CO_2 decrease from 1400 ± 470

parts per million (ppm) in the EECO to 550 ± 190 ppm by the early Oligocene (Anagnostou et al., 2016) is most likely responsible for the transition to a glaciated world.

Several methods are used to estimate CO_2 concentrations for geological intervals. A primary method involves the carbon isotopic composition ($\delta^{13}C_{37:2}$) of long-chained alkenones (37 or 39 carbon atoms in a chain) produced by marine (haptophyte) Prymnesiophyceae algae (e.g. Jasper and Hayes, 1990; Pagani et al., 2005; Zhang et al., 2013). Other methods comprise the use different proxies as for instance: 1) the $\delta^{13}C$ of pedogenic (soil) carbonates (paleosols) where CO_2 is produced by the decomposition of organic matter and respiration by roots (Cerling et al., 1991; Ekart et al., 1999); 2) fossil leaf stomata pores, based on the negative correlation between stomatal density (number of stomata per unit leaf area) and the atmospheric pCO_2 at which a plant grows (Franks et al., 2014); 3) the boron isotopic composition in planktonic foraminiferal tests ($\delta^{11}B$), because boron is related to ocean pH and alkalinity, which in turn are influenced by pCO_2 (Pearson et al., 2009; Anagnostou et al., 2016); 4) the sodium carbonate mineral (nahcolite, $NaHCO_3$) precipitation, as a function of pCO_2 and temperature (Lowenstein and Demicco, 2006; Jagniecki et al., 2015) and 5) fossil liverwort (bryophyte) (Fletcher et al., 2008).

DeConto et al. (2008) analysed the sensitivity of polar ice-sheets by using a global climate ice-sheet model forced by orbital insolation and pCO_2. Their results estimated a CO_2 thresohold for Antarctic glaciation of ~750 ppm, which is much higher compared to that estimated for the Northern Hemisphere (~280 ppm). Therefore, the northern glaciation would have required lower levels of CO_2, which are not supported by available geochemical proxies (Pearson and Palmer, 2000; Pagani et al., 2005) and carbon-cycles models (Zachos and Kump, 2005; Merico et al., 2008). For this reason, a bipolar glaciation (e.g. Tripati et al., 2005; Edgar et al., 2007; Spray et al., 2019) is quite unlikely, even if episodic northern-hemispheric ice sheets have been possible starting from ~25 Ma, when CO_2 concentrations reached near pre-industrial levels of 280 ppm (DeConto et al., 2008).

Thus, the most-shared scenario is that of an Oligocene time with different conditions with respect to the modern state, in particular with only Antarctica glaciated (unipolar hypothesis) (Zachos et al., 2001; Liu et al., 2009; Westerhold et al., 2020; Hutchinson et al., 2021). Many hypotheses were considered to explain the Antarctic glaciation, however, as underlined in the past by Zachos et al. (2001) and more recently by Lear and Lunt (2016), given the complex nature of long-term trends, we must consider the ice, ocean and climate as an articulated system where several factors, rather than one, control the Earth's evolution.

1.2.2 The Eocene-Oligocene transition

Terminology, correlation, and calibrations. The Eocene to Oligocene transition culminates in an abrupt ~1.5‰ shift near the boundary between the Eocene and Oligocene epochs (EOB; 33.9 Ma, following the timescale of Gradstein et al., 2012).

High-resolution studies on benthic $\delta^{18}O$ records revealed that the EOT is characterized by a distinct two step-wise pattern (e.g. Coxall et al., 2005). The first of these shifts we referred to as Step 1 and the second to Step 2 (or EOIS - Early Oligocene oxygen Isotope Step, Hutchinson et al., 2021). The two steps are separated by a

more stable plateau interval (Coxall et al., 2005; Coxall and Wilson, 2011) with relatively constant and intermediate values if compared to the values observed at the onset of Step 1 and the end of Step 2 (EOIS).

Recent investigations have attempted to decouple the contribution of ice volume and temperature signals from foraminiferal oxygen isotopes using an independent proxy: the Mg/Ca paleo-thermometer (Lear et al., 2008; Bohaty et al., 2012). A decrease in the foraminiferal Mg/Ca ratio values indicates a tropical near-surface and bottom water cooling of about 2.5 °C, coincident with the initial foraminiferal oxygen isotope increase (Step 1). Instead, the second $\delta^{18}O$ step (Step 2 or EOIS) is primarily dominated by a large ice-volume component (Katz et al., 2008; Lear et al., 2008; Bohaty et al., 2012). In general, Step 1 is less prominent and thus harder to observed compared to the second step, which is more abrupt and easily correlatable (Hutchinson et al., 2021) (Figure 1.2).

In the high resolution record from ODP Site 1218, the shift in the $\delta^{13}C$ profile was also rapid, stepwise, and pretty similar to the $\delta^{18}O$ curve, but with a lag of ~ 10 kyr (Coxall et al., 2005). The $\delta^{13}C$ record is interpreted to reflect an increase in the organic and inorganic carbon production due to enhanced marine export production, wind stress, upwelling and oceanic turnover (e.g. Diester-Haass, 1995; Zachos et al., 1996; Coxall and Pearson, 2007). To summarize, with the term "Eocene-Oligocene transition" (EOT) we define "a phase of accelerated climatic and biotic change that began before and ended after the EOB", as recently revised by Hutchinson et al. (2021), after Coxall and Pearson (2007). The duration of EOT is of ~790 kys and spans from the extinction (top) of *Discoaster saipanensis* and the top of Step 2 (or EOIS). The extinction of *D. saipanensis* represents a reliable bioevent interpreted as the first signal of biotic loss associated with a late Eocene cooling termed as the Late Eocene Event (LEE) (Katz et al., 2008) (Dunkley Jones et al., 2008; Pearson et al., 2008).

This event has been interpreted as a first unsuccesful attempt to enter in an icehouse regime or, in other words, a failed glaciation. Above the EOT, a prolonged interval of maximum ice-extent, corresponding to $\delta^{18}O$ maximum values, was identified and named as the Earliest Oligocene Glacial Maximum (EOGM; Liu et al., 2004). The EOGM is consistently calibrated in the lowermost Oligocene within Chron C13n. The EOT embraces these isotopic steps (Step 1 and 2) with the EOB falling in the plateau between them (Coxall and Pearson, 2007; Dunkley Jones et al., 2008; Pearson et al., 2008; Coxall and Wilson, 2011).

The EOGM event is widely regarded to reflect the onset of a permanent and expanded Antarctic glaciation (e.g., Zachos et al., 2001), a hypothesis that is supported by the remarkable fall of global eustatic sea level (~70 m; Miller et al., 2008; Wilson et al., 2013).

A coherent temporal isotopic response was also provided by a recent high-resolution continental record, from the Hampshire Basin (UK), where an isotopic record derived from *Viviparus lentus,* a freshwater gill-breathing gastropod, reveals the same isotopic pattern, suggesting that strong connections in the hydrological cycle were active between marine and marginal continental environments (Sheldon et al., 2016). Instead, terrestrial records rarely document the positive isotopic excursion (e.g. Sheldon et al., 2012; Zanazzi et al., 2007). This is probably due to the fact that oxygen isotopes from continental records can be compromised by non-temperature related factors or may react to local, rather than global hydrologic cycle drivers (Sheldon et al., 2012; 2016).

The E-O boundary. In the '80s much of the scientific debate on the search for a proper global stratotype section and point (GSSP) to define the base of the Rupelian Stage (Eocene–Oligocene boundary, EOB) was included in the synthesis published by Pomerol and Premoli Silva (1986). The final choise on where to position the GSSP level relies upon many criteria (e.g. biostratigraphic, chemostratigraphic, or magnetostratigraphic) and on the stability and accessibility of the stratotype to correlate other worldwide sections.

There are challenges in correlating GSSPs and other reference sections especially over long distances or between marine and terrestrial sections. Eventually, the GSSP of the EOB has been defined in the pelagic Massignano quarry section, located 10 km southeast of Ancona, on the Adriatic coast of central Italy (Premoli Silva and Jenkins, 1993) in correspondance to the extinction of the tropical planktonic foraminiferal genus *Hantkenina* (Premoli Silva and Jenkins, 1993), which was found within Chron C13r (Berggren et al., 2018) in the GSSP section. In the common biostratigraphic practice, the extinction of species *H. alabamensis* must be considered the "primary marker" for worldwide correlation of the EOB. However, the EOB is preceded or corresponds to other additional events: that the extinction or dramatic diversity reduction in the *Turborotalia cerroazulensis* group and the sudden dwarfing of *Pseudohastigerina micra*, respectively (Pearson et al., 2008). Unluckily, there are important issues related to this reference section that mainly concern with its poor carbonate preservation and its possibly unreliable stable-isotope stratigraphy (Bodiselitsch et al., 2004). Another possible weak point of the formal definition of the EOB is linked to overall scarsity of hantkeninids in several successions worldwide, and the complete absence of these planktonic foraminifera in crucial sites such as Site 744 (Zachos et al., 1996) and Site 1218 (Coxall et al., 2005).

These considerations have opened a discussion among the scientific community on possible criteria to be used to define the base of the Rupelian Stage. As underlined by van Mourik et al. (2005), the current golden spike "based on the local extinction of the tropical planktonic foraminiferal genus *Hantkenina* represents an isolated event that is not suitable for global correlation". However, foraminiferal specialists argue that there is as yet no evidence that the extinction of the Hantkeninidae was locally controlled or diachronous (Coxall and Pearson, 2007; Berggren et al., 2018).

In the past, scientific conflicts have been undertaken between foraminiferal specialists supporting the extinction of *Hantkenina* and nannofossil specialists proposing the extinction of rosetta-shaped discoasters, that unluckily occurred much earlier (Snyder et al., 1984). As previously pointed out, the articulated pattern in the oxygen isotopes observed across the EOB, which includes the top of Step 2 (or EOIS), document a global climate event but, even more importantly in this context, could also serves as an exceptional correlating tool that would allow for worldwide correlations, the ideal criterium to denote a chronostratigraphic unit. In fact, the $\delta^{18}O$ record is extremely useful for global stratigraphic correlations and it is universally accepted as marking the climatic shift toward the modern climate state that culminated, much later, with the Northern Hemisphere glaciation (2.58 Ma; Lisiecki and Raymo, 2005). This line of argumentation has been recently supported also by Miller et al. (2017), which reiterate the idea to avoid the use of biostratigraphic datums for defining of GSSPs that according to the authors should be preferentially defined using magnetostratigraphic or isotopic events. After a couple of decades, the debate is still open but a formal proposal to modify the GSSP

and/or the relative primary marker of the base of the Rupelian Stage has not been received by the International Commission on Stratigraphy (ICS).

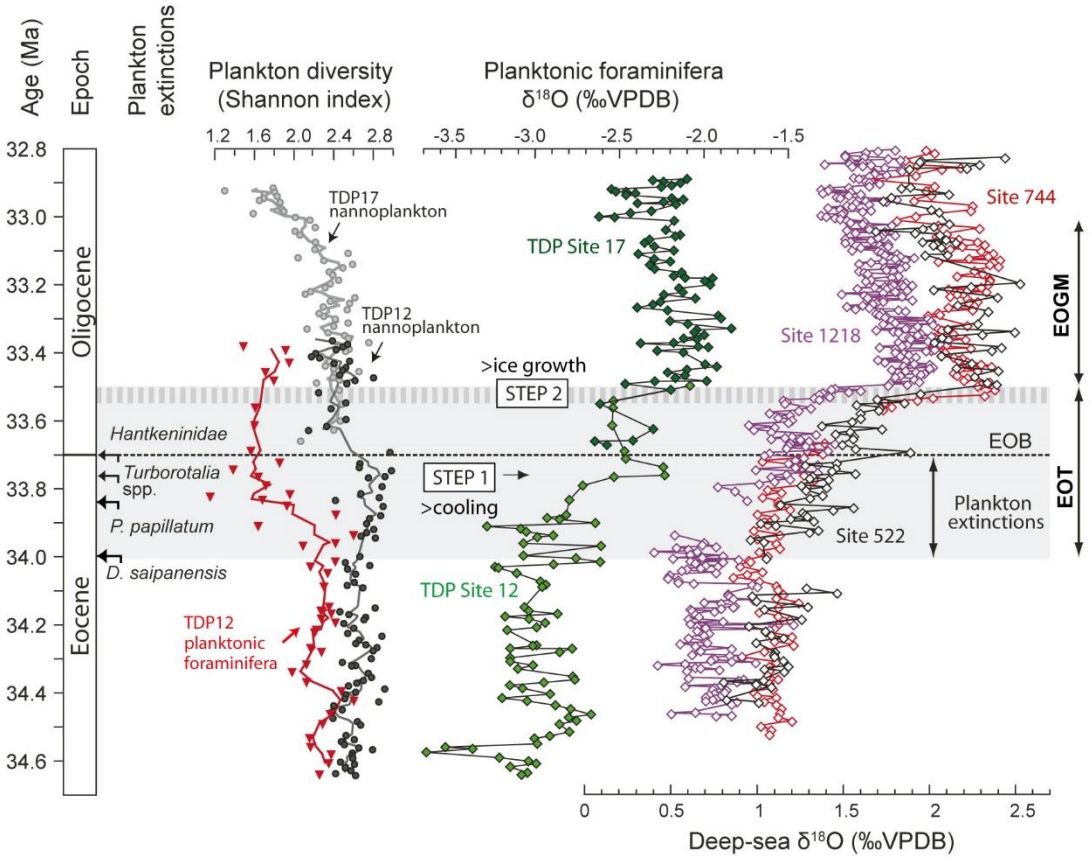

Figure 1.2 High-resolution geochemical and biotic events across Eocene-Oligocene boundary. The $\delta^{18}O$ record from planktonic foraminifera and plankton diversity refers to the Tanzania Drilling Project data (TDP). Deep-sea benthic foraminiferal isotope records are from Site 1218 - Coxall et al. (2005), and Site 522, 744 - Zachos et al. 1996). The age-model is on the time scale of Berggren et al. (1995); EOB here is at 33.7 Ma. The light grey band highlights the EOT, while the dashed grey interval in the upper part of the EOT indicates Step 2 (or EOIS). EOT= Eocene Oligocene transition. EOGM = Earliest Oligocene Glacial Maximum.
Modified from Pearson et al. (2008).

Sea-surface water temperatures. Different proxies have been used to reconstruct global sea water temperatures from multiple ocean localities. A compilation of SST proxies is provided by a recent review by Hutchinson et al. (2021) in two time windows: the first for the late Eocene (38 to 33.9 Ma; red data) and the second for the early Oligocene (33.9 to 30 Ma, blue data) (Figure 1.3).

From the late Eocene (38-33.9 Ma) to the earliest Oligocene (33.9-30 Ma), high latitudes (45-70°) documented a temperature decrease of approximaltely ~5°C (Liu et al., 2009) or 6°C (Inglis et al., 2015) on average, instead evidences from the tropics suggested a decrease in both sea-surface (SST) and bottom temperature of ~2.5°C (Katz et al., 2008; Lear et al., 2008; Inglis et al., 2015) or, as indicated by Evans et al. (2016) and Wade et al. (2012) for the Gulf of Mexico, of ~3-4 °C. During the late Eocene, SST from Tanzania (Pearson et al., 2007; Lear et al., 2008), Ceara Rise (ODP Site 925, ODP Site 929; Liu et al., 2009) and the Atlantic Coast plain recorded temperature consistently warmer than modern, which rarely exceeds 28-29°C (Inglis et al., 2015), even reaching 35°C (Pearson et al., 2007). Despite the SST signal is more heterogeneous than the deep sea, it

is more achievable because there are more proxies available. These proxies are: (1) the marine $\delta^{18}O$ palaeothermometry extracted planktonic foraminifera; (2) Mg/Ca palaeothermometry; (3) clumped isotope ($\Delta47$) paleothermometry; (4) tetrather (TEX_{86}) indices, lipids produced by archaea; (5) alkenone unsaturation index ($U^{K'}_{37}$), lipids produced by haptophyte algae.

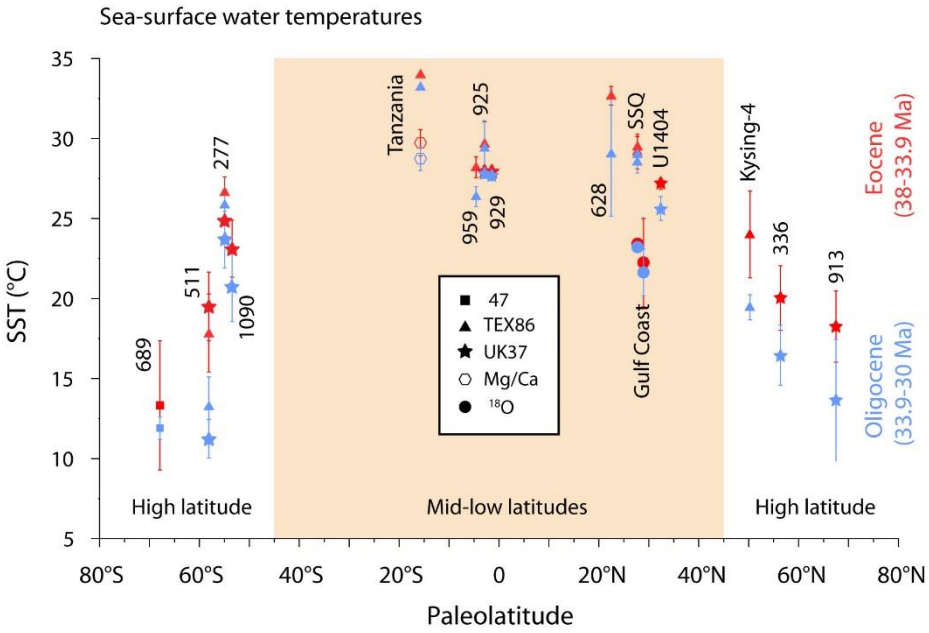

Figure 1.3 Compilation of the sea surface temperature (SST) changes across the EOT from different proxies: TEX_{86}, $U^{K'}_{37}$, $\delta^{18}O$, $\Delta47$, and Mg/ Ca. Late Eocene mean temperature data are plotted in red, early Oligocene in light blue (modified from Hutchinson et al. (2021). High latitudes are comprised between 45-70°.

As reported in Figure 1.3, low-middle latitude temperature proxies suggest an annual mean SST up to 20°C, both in the late Eocene and early Oligocene. A recent comparison between SST estimates from North and South Atlantic during this time support the idea of weak latitudinal temperature gradients and a distinct northern–southern hemispheric thermal asymmetry in the sea surface water cooling (Liu et al., 2018).

According to a coupled ocean-ice-atmosphere model (GFDL's CM2Mc), the opening of the Drake Passage (sill depth: 400-1000 m) interrupted the southward geostrophic flow transport of saline subtropical waters, resulting in the overturning of salty waters to the north that strengthened the North Atlantic Deep Water (NADW) formation, when the Panama Seaway is opened (Yang et al., 2014). The oceanic reorganization also promoted the initiation of the Atlantic Overturning Circulation (AMOC), characterized by the northward flow of warm and saline waters masses, compensated by the southward flow of colder masses at depth (Elsworth et al., 2017). The latter authors argue that "the asymmetry of Northern versus Southern Hemisphere temperature histories would not be expected from CO_2-driven cooling alone but is entirely consistent with a strengthening of the AMOC that warmed the Northern Hemisphere at the expense of the Southern Hemisphere". Thus, the question of what role the opening of the Drake Passage played in the subsequent Antarctic cooling remains much debated.

Certainly, the 37–34 Ma interval is critical to understand the formation of NADW (Coxall et al., 2018), the early history of AMOC and its possible role in increasing silicate weathering (and drawdown of atmospheric pCO_2) (Elsworth et al., 2017).

Changes in paleoproductivity

Changes in ocean circulation/mixing and meridional heat transport, possibly accompanied by latitudinal thermal gradients, are supposed to play a major role for the Eocene-Oligocene climate, increasing the availability of nutrients and determining several modifications among the marine biota (Diester-Haass and Zahn, 2001; Coxall and Pearson, 2007; Dunkley Jones et al., 2008; Wade and Pearson, 2008; Cotton and Pearson, 2011; Barron et al., 2015; Fioroni et al., 2015; Villa et al., 2021).

A common indirect approach to reconstruct paleo-productivity is the analysis of different proxies that reflect changes in nutrients, which include: marine carbonate carbon stable isotopes (Coxall and Pearson, 2007), benthic foraminifera accumulation rates (BFAR) (Coxall and Wilson, 2011), changes in diatoms assemblages (Falkowski et al., 2004), opal accumulation rate (Salamy and Zachos, 1999), changes in micro- and macro-fossil (e.g. echinoderms, ostracods, sponge spicules, diatoms, radiolarians) accumulation rates, carbonate dissolution indices and marine barite ($BaSO_4$) accumulation (Diester-Haass and Zahn, 2001; Diester-Haass and Zachos, 2003; Griffith et al., 2010). Other productivity proxies such as Ba and reactive P may provide independent evidence for changes in export production, since they are not affected by carbonate dissolution (Nilsen et al., 2003). However, in many cases, these proxies are inconsistent, and their interpretation in terms of changes in primary production, export production, and ecosystem structure is not straightforward and/or unique (Anderson and Winckler, 2005; Griffith et al., 2010). For example, an apparent inconsistency exists at Site 1218 between BFAR (Coxall and Wilson, 2011) and BAR (Erhardt et al., 2013). The inconsistency is related to the fact that the two proxies respond to different factors: BFAR reflects food (or organic C) input to the sediment water interface, while BAR represents the amount of C exported out of the surface layer and oxidized between 500 and 1500 m depth, and thus reflecting bacterial activity (which in turn relies upon temperature), responsible for the formation of barite (Erhardt et al., 2013).

Today, the Sub Antarctic Mode Water (SAMW) flows in the Southern Ocean and provides three-quarters of the global nutrient supply to the low latitude surface waters (Sarmiento et al., 2004).

Regarding the E-O, several studies suggest that the removal of land barriers around Antarctica (i.e. gateways deepening) played a crucial role in reorganizing the ocean circulation patterns and temperature distribution around Antarctica (Sauermilch et al., 2021) and likely induced the upwelling of nutrient-rich deep waters, increasing Southern Ocean primary productivity (Diester-Haass, 1991; Diester-Haass and Zahn, 2001; Persico and Villa, 2004; Villa et al. 2008; 2014). At some locations, paleo-productivity was observed to strongly increase in correspondence to the earliest Oligocene in parallel with the positive carbon isotopic anomaly, indicating increased burial of organic matter on a global scale (Coxall and Wilson, 2011; Diester-Haass et al., 1996).

The shift toward higher marine productivity conditions, is possibly related to the transition from calcareous to siliceous dominance in the primary producers, that could had led to the origination of the diatom and krill-based, highly productive, modern glacial ecosystems (Egan et al., 2013).

Across the EOT, a temporary but remarkable pulse in opal deposition has been observed and is likely consistent with the hypothesis of an accelerated silicate weathering (Elsworth et al., 2017), while enhanced weathering of carbonate shelves, exposed by glacio-eustatic sea level fall, resulted in a deepening of the calcium carbonate compensation depth (CCD) (Merico et al., 2008; Coxall and Wilson, 2011). Despite multiple evidences of perturbations in the Southern Ocean ecosystem during this time, global changes in ocean productivity, export production, and organic carbon burial remain poorly constrained (Coxall and Wilson, 2011).

The change in the surface nutrient regime, from oligotrophic to more eutrophic surface waters, is also highlighted in a recent work provided by Villa et al. (2021) from the equatorial Indian Ocean. According to the authors, this transition is strictly related to the initiation of the proto-Antarctic circumpolar current (ACC) and with the formation of nutrient-rich waters at high latitudes.

In Figure 1.4, we reported a synthesis of relevant cores for the EOT with data related paleoproductivity estimations for the following sites: ODP 1218 (Coxall and Wilson, 2011), ODP 709 (Villa et al., 2021), NKKI (Jones et al., 2019), ODP 763 and DSDP 592 (Diester-Haass and Zahn, 2001), ODP 744 and 690 (Diester-Haass, 1996), ODP 689 and 1090 (Egan et al., 2013), DSDP 511 (Plancq et al., 2014), ODP 748, 738, 689 (Villa et al., 2014), ODP 959 (Schumacher and Lazarus, 2004), ODP 756 (this thesis, Chapter 1), IODP U1509 (this thesis, Chapter 3), ODP 1209 and IODP U1411 (this thesis, Chapter 5).

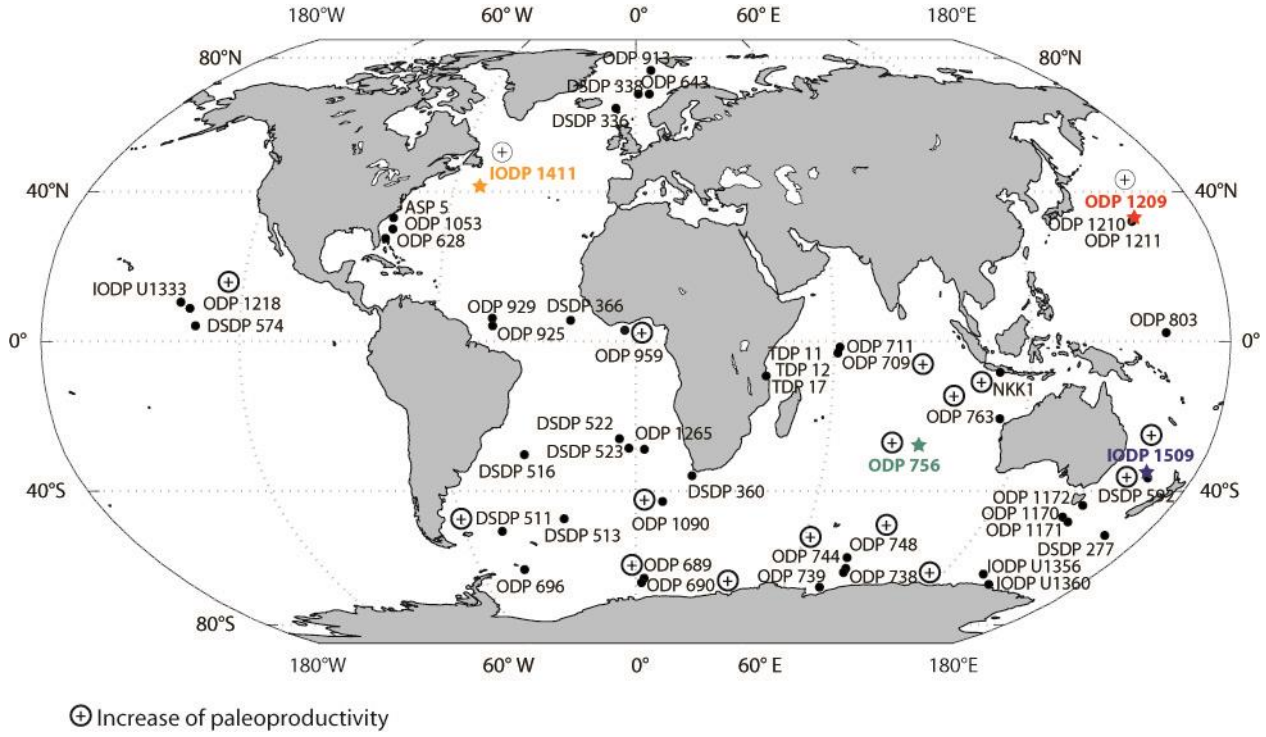

Figure 1.4 Modern-day compilation of relevant cores (see Appendix I for details) for the EOT from low-middle and high latitudes with evidence of paleo-productivity increases for each site indicated as encircled plus. The studied sites investigated in this thesis are also reported with coloured stars.

These records provide a further support for a global increase in productivity, although some equatorial regions were probably less affected due to regional variations in circulation and productivity responses (Nilsen et al., 2003; Schumacher and Lazarus, 2004).

1.2.3 Calcareous nannofossils

Coccolithophores are a group of calcifying haptophyte algae, whose fossil remains are included in calcareous nannofossils. In principle and following the traditional definition calcareous nannofossils are a wider group but most of them belong to the coccolithophores. The latter ones are single cell prostists surrounded by coccoliths, small calcareous plates which cover all the cell surface, forming the *coccosphere*.

These organisms show signs of pervasive ecological disruption through the EOT and a shift toward less diverse assemblages across the boundary (Bown et al., 2004). However, how ice-growth and climatic deterioration affect the phytoplankton community remain largely unknown and is the focus of this PhD thesis.

Thus, the study of their extinct counterpart, i.e. calcareous nannofossils, offer a unique opportunity to disclose the impact of Antarctic ice caps on an important component of the marine sea surface planktonic biota.

Their calcite rests (i.e., coccoliths/nannoliths), typically smaller than 30 µm, provide an abundant and continuous sedimentary archive that allow for high-resolution paleoclimatic reconstructions. They are highly sensitive to changes in the surface-ocean environment and their composition and diversity are strongly related to different ecologic and environmental parameters such as latitudes, ocean circulation and water masses,

turbidity, salinity and light (e.g. Winter et al., 1994) but temperature and nutrients are considered to play a key role (Aubry, 1992) in their distribution in time and space. In the following, we provide an overview of the potential of calcareous nannofossils, especially that related to the application used in this work.

Biostratigraphy

Calcareous nannofossils are primarily used to perform correlations at different geographic scales since they are proved to be an extremely useful tool to determine the age of marine sediments (Bown et al., 2004; Raffi et al., 2016; Agnini et al., 2017). The high potential of calcareous nannofossils in dating marine sediments and rocks mainly derives from their rapid evolutionary changes, small size (that protects them from mechanical damage), high abundances, cosmopolitan marine distribution, and inexpensive and quick preparation methods. In this work, they were essential to refine the current biostratigraphic framework available for the E-O transition that, in turn, allows for an improvement of our capacity in correlating sections worldwide using standard and additional bioevents (e.g., bases, tops, acme) (Agnini et al., 2014; 2017).

In this thesis, we primarily relay on three Paleogene zonations, conceived for low-middle latitudes, which are based on a set of biohorizons with different degrees of reliability (Martini, 1971; Okada and Bukry, 1980; Agnini et al., 2014). A further effort has been also made to integrate new or additional biohorizons to the main framework. As for instance we have tested the reliability of both the base and top of *C. subdistichus* using a semiquantitative and multi-site approach. Absolute age calibrations of bioevents in million years (Ma) are used to calculate linear sedimentation rates, where indipendent age models were not available. In a second step of the study, we have compared, on the basis of a common timescale, the assemblage variations observed at different sites across the EOT at low-middle latitudes.

The high resolutition data acquired in the study successions result in the acquisition of highly reproducible abundance patterns for standard as well as for additional taxa that has eventually allowed for an implementation in locating the relative position of each biohorizon as well as of the time resolution that can be obtained.

This is absolutely fundamental especially for the Oligocene, which is an Epoch characterised by the lowest resolution in the Cenozoic considering the number of biozones (6) and their relative durations (Backman et al., 2012; Agnini et al., 2014; Raffi et al., 2016) (Figure 1.5).

The low resolution available for the Oligocene is surely related to the extremely low nannofossil diversity documented during the Oligocene though the overall climate evololution could have played a role in the decreasing of the evolutionary rates that, at least for the Oligocene, is the result of an enhanced extinction rate and a deacrease in the speciation rate (Bown et al., 2004). However, despite of the low number of potential biohorizons, other important issues concern the presence of taxonomic ambiguities for some taxa that could have caused inconsistent and low quality biostratigraphic data and, consequentually, the apparent decrease in the degree of reliability of some biohorizons. This is, as for instance, the case of *C. subdistichus*.

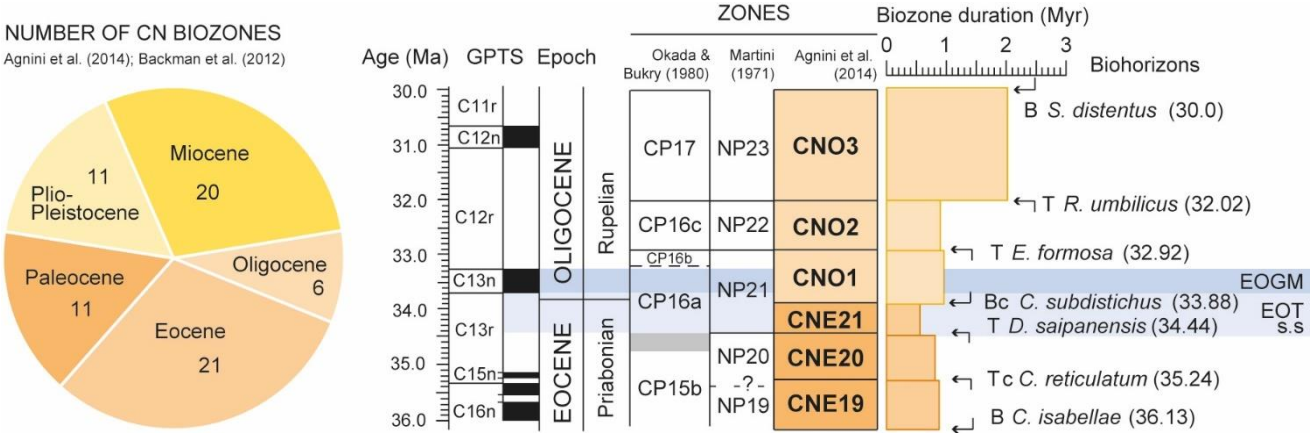

Figure 1.5 To the left: number of calcareous nannofossil biozones (Agnini et al., 2014; Backman et al., 2012; Raffi et al., 2016). To the right: CN zones (Okada and Bukry, 1980; Martini, 1971; Agnini et al., 2014), their duration (Myr) and the standard biohorizons used to define them. The time scale adopted is after Pälike et al. (2006). The blue bars report the EOT range- sensu strictu and the EOGM (which primarily correlates to Chron C13n).

Paleoecology and paleoceanography

Calcareous nannoplankton have a widespread distribution in the marine domain, from the shelf to the open ocean, and represent an important component of the phytoplankton community along with diatoms and photosynthetic dinoflagellates.

As photosynthesizing organisms, they need sunlight to thrive and reproduce; for this reason, they live in the upper photic zone (mainly between 0-100 m) of the water column. Most species have broad ecological tolerances for temperature and salinity conditions. Their distribution is strongly controlled by surface water temperature and macronutrient availability (primarily nitrate and phosphate), which, in turn, are linked to ocean circulation and water mass features (Winter et al., 1994). Modern coccolithophore diversity is strongly influenced by environmental fluctuations. In general, high diversity (and lower biomass) is commonly related to a stable, oligotrophic (low nutrients) and subtropical environment, dominated by K-selected communities (i.e. specialists, e.g., *Discoaster*). By contrast, eutrophic (high nutrient) areas, often associated with continental shelves, polar or upwelling areas, support high-standing populations (higher biomass) and favor low-diversity communities, dominated by one or few species (monospecific blooms) or oppurtunistic r-mode taxa (Bown et al., 2004). This is mainly due to the ecological competition with diatoms, which are more abundant in coastal areas and polar regions and, for their intrinsic physiological features are able to outcompete coccolithophores in those environments (Falkowski et al., 2004;, Katz et al., 2004; Nissen et al., 2018).

Despite the fact that calcareous nannoplankton, as a group, are considered to be eurytopic and thus able to survive in a wide spectrum of environmental conditions, some taxa exhibit specific ecological preferences for warm/oligotrophic or cold/eutrophic water conditions, as well as for neritic or frankly pelagic environments. The paleoecological preferences of modern taxa were initially inferred from their biogeographic distribution that are typically latitude-related (e.g. McIntyre and Bé, 1967; Okada and Honjo, 1973). This approach has successively been translated to the fossil record (e.g. Haq and Lohmann, 1976; Wei and Wise, 1990; Aubry,

1992; Wei et al., 1992; Lees et al., 2005; Mutterlose et al., 2005), and have been used to characterize long-term as short-term environmental fluctuations on the basis of the changes observed in calcareous nannofossil assemblages.

Generally, the ecological preferences of extinct taxa are primarily interpreted as related to temperature and/or fertility gradients but they are potentially deeply linked to the modification of other environmental factors such as carbonate sea water chemistry, salinity, light, etc. A synthesis of ecological assignments for calcareous nannofossil taxa distributed across the EOT was provided by Villa et al. (2014).

However, the ecology of some taxa are likely more complex, being possibly non linearly affected by multiple factors at the same time (Villa et al., 2008; Schneider et al., 2011).

The role of preservation

The continuous stratigraphic record of calcareous nannofossils coupled with their widespread geographical distribution makes them exceptionally useful in paleoceanographic and paleoclimatic reconstructions, as well as in chronostratigraphic issues of crucial time intervals. Despite all these benefits, calcareous nannofossils can also suffer from major disadvantages, related to the low degree of preservation, possibly resulting from their vulnerability to chemical and mechanical stress produced by diagenetic processes.

In addition, further drawbacks are also potentially related to their susceptibility to reworking that could bias the quality of the data obtainable from the study of this group (Bolli et al., 1985; Parker et al., 1985; Ferreira et al., 2008). The preservation of calcareous nannofossils in the geological record depends on how they sink trough the water column and reach the sea floor as well as on the conditions they encounter at the water / seabed interface as well as within the sediments. Phytoplankton, including coccolithophores, is a trophic source for larger organisms, lying at higher trophic levels, such as copepods which, after ingestion, expel them as fecal pellets. This mechanism protects them from being partially or totally disaggregate and dissolved (De Vargas et al., 2007). However, an important component of the pristine assemblages can be pervasively affected during their sink along the water column (Andruleit et al., 2004) and, once on the bottom, coccoliths can be consistently altered by diagenetic processes with a significant loss of fragile and smaller taxa (usually smaller than 3μm), with larger species having a higher preservation potential (Young et al., 2005). Thus, estimations of diversity and paleoclimatic interpretation are strongly influenced by the availability of well-preserved records and of accurate scanning electron microscope studies. Nonetheless, exceptionally preserved sediments, found in the so-called Konservat-Lagerstätte, are very rare and represent unique and exceptional study cases. Two examples of extraordinary well preserved records are those retrieved during the Tanzania drilling project (Kilwa Group; Bown and Jones, 2006) and IODP Exp. 342 (drift sediments; Norris et al., 2014a).

These sediments represent an exceptional and unique archive of the EOT but most of the records come instead from sediments with different degree of preservation. Therefore, a comprehensive understanding of the processes and mechanism active during this climate event pass through the study of good, moderately, and even poorly preserved sediments. Of course, the study of poorly preserved assemblages prevents reliable and comprehensive interpretations of fossil diversity (due to size-preservation effects) and paleoecology, but can

provide insights on site-specific diagenetic processes and, in some cases, can also record primary geochemical signatures (Chapter 5).

Morphometry and climate change

Size is a key feature in algal physiology and impacts phytoplankton metabolic processes in terms of photosynthesis, calcification and growth rates (Aloisi, 2015), respiration, reproduction and sinking velocity (Raven, 1998; Raven and Waite, 2004), as well as abundances and diversity (Finkel, 2007).

In this thesis, we take into account coccolith size, since it is thought to be sensitive to environmental change in a way that is proportional to coccosphere size (Henderiks, 2008; Gibbs et al., 2013). In the past years, coccolith and nannolith size variations have been intensively investigate in the fossil record to evaluate the role of environmental parameters on their morphology, especially in time intervals characterized by high CO_2 concentration, as in the case of the PETM (Tremolada et al., 2008; Gibbs et al., 2013) or the MECO (Salaviale et al., 2018), both events that can be used as analogous for future scenarios (Westerhold et al., 2020).

Our oceans are now acting as a buffer for antropogenic CO_2, that behaves like a weak acid, potentially affecting coccolithophores metabolism and the magnitude of carbon fluxes (Riebesell et al., 2000; Gehlen et al., 2007; Hönisch et al., 2012). In the last two decades, the acidification of the oceans have been the focus of many studies and debates. Recent laboratory and field experiments on the modern and ubiquitous species *Emiliania huxleyi* have shown inconsistent results with different strains displaying contradictory vulnerabilities to CO_2 increases (e.g. D'Amario et al., 2018). In contrast to modern days, during the transition from the Eocene to the Oligocene, oceans experienced opposite trends and very different conditions, as for instance a long-term decrease in $CO_{2(aq)}$ and higher $CaCO_3$ saturation state (Van Andel, 1975; Zachos et al., 1996; Salamy and Zachos, 1999; Coxall et al., 2005; Pagani et al., 2005; Zachos and Kump, 2005; Merico et al., 2008). Nonetheless the comprehensive understanding of the behavior of this group to changes in the carbonate chemistry seawater pass through the recognition of the possible response and the modellization of how this response is related the climate forcing. Several factors are supposed to alter phytplankton community structure and their cell size, they include: carbon dioxide, ozone depletion (i.e. UV-B alterations), coastal eutrophications, pollution, ice cover, temperature and precipitations (Finkel et al., 2010). To date, only few studies document nannofossil morphometric response across the EOT (Bordiga et al., 2015; 2017; Jones et al., 2019) and thus the possible consequences of cooling and glaciation on coccolithophores remain largely unknown for this time interval. An improved understanding of how key EOT taxa respond to change in size is required to better elucidate the role of the biological pump, which in turn have influenced CO_2 uptake and climate.

1.3 Main Aims

Several works have focused on calcareous nannofossil biostratigraphy and paleoecology across the Eocene-Oligocene transition in the southern high latitudes (e.g. Wei and Wise, 1990; Wei 1991a; 2004; Wei et al., 1992; Villa et al., 2003; 2008; Persico and Villa, 2004; Villa and Persico, 2006; Persico et al., 2012) and they all highlighted the great potential and reliability of this group as paleoclimatic tools.

However, many questions are still open and deal with the timing and structure of their response at the low-middle latitudes. This partial gap is essentially due to the relatively few records with high stratigraphic resolution and state of preservation (Dunkley Jones et al., 2008; Blaj et al., 2009; Bordiga et al., 2015; Fioroni et al., 2015; Jones et al., 2019; Villa et al., 2021) available for this crucial interval. Thus, the main aim of this work is to contribute to fill this gap, with a detailed analysis of calcareous nannofossil assemblages.

This Ph.D. thesis focuses on the following question: "Are calcareous phytoplankton affected by the onset of the Antarctica ice-sheet at the Eocene-Oligocene transition?"

To answer to this apparently simple question we have designed a research project that has allowed us to investigate the calcareous nannofossil response in a virtually global perspective, at different latitudes and in different depositional basins. For this reason, we propose to subdivide this thesis in five chapters. Each of these chapters will provide insights and reflections on different aspects, ranging from biostratigraphy, paleoecology/paleoclimate/paleoceanography, preservation and morphometry. More in detail, the main aims of this work are devoted to:

1. analyses the short-term effects of extreme global cooling and ice-growth on calcareous nannofossils, including significant shifts and changes in the assemblages.
2. establish/calibrate a set of palaeoecological indicators and interpret the observed variations in these proxies in terms of paleoclimatic changes.
3. provide a global picture of the reliability (and synchroneity) of calcareous nannofossil bioevents, providing abundance patterns of selected taxa (standard and additional) and their relative age estimates for different settings and locations.
4. carefully analyze the preservation state of nannofossil assemblage during the main phases of this transition and assess the impact of diagenesis on the bulk stable O and C isotopic record.
5. analyze the effect of climate change (and paleoenvironmental factors) on morphometry, also discussing its taxonomic and biostratigraphic implications (i.e. *Clausicoccus subdistichus* group).

1.4 The study material

Four sites were selected to investigate the Eocene-Oligocene transition: ODP Site 756, IODP U1509, U1411 and ODP 1209 (Figure 1.6). These sections have been chosen based on their geographic location and on the availability of an almost complete sedimentary record. The main goal was to correlate data from different oceans, discriminating between local and global changes within the context of low-middle latitudes.

Moreover, the selected sites are located at different distances with respect to Antarctica, where the glaciation really took place. Thus, these sites could have recorded variations in the assemblage composition and/or abundances related to different thermal gradients, generated by a combination of latitudinal and glacial effect. Well-constrained age models which primarily incorporated biostratigraphic and, in some cases, magnestrotratigraphic datums allow correlation between sites.

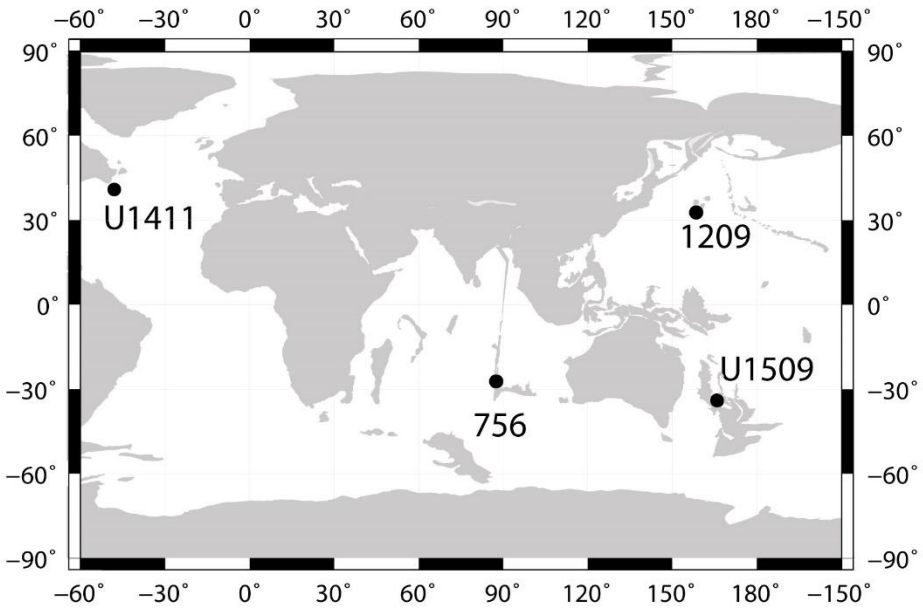

Figure 1.6 Paleo-location (34 Ma) of the studied sites: ODP Site 1209 (Shatsky Rise, Northern Pacific Ocean), ODP Site 756 (Ninetyeast Ridge, Southern Indian Ocean), IODP Site U1509 (Tasman Sea, Southern Pacific Ocean and IODP Site U1411 (Newfoundland Ridge) Northern Atlantic Ocean (https://www.odsn.de/).

ODP Site 756 is located near the crest of the southern end of Ninetyeast Ridge. As part of the Ocean Drilling Program (ODP) Leg 121, Ninetyeast Ridge was one of the drilling targets. One of the objectives of the drilling campaign was to sample an upper Eocene to Holocene sedimentary section for paleo-geographic/climatic studies of the eastern Indian Ocean (Peirce et al., 1989). Four holes (A-D), on a southwest-northeast line, were drilled at this site and we focused on Hole 756C. The study sections provide common to abundant calcareous nannofossils with moderate to good preservation.

IODP Site U1509 is situated on the western margin of New Caledonia Trough (NCT) in the Tasman Sea, at the base of the Lord Howe Rise slope (Sutherland et al., 2019). Nannofossil abundance is generally high, and the preservation is mostly good. At this site, we documented the presence of reworked taxa (especially in the early Oligocene), which is related to the re-deposition of older (middle to upper Eocene) sediments present in

the basin or in the nearby area. Our finding is consistent with preliminary shipboard data and, fortunately, does not impair our biostratigraphic results.

IODP Site U1411 is located on the Southeast Newfoundland Ridge in the Northwest Atlantic and the material retrieved in the interval of interest is a clay-rich drift sediment characterized by high sedimentation rates (Norris et al., 2014a). The high clay content allows for an exceptional preservation of the calcite fossils present in the sediment. This site was chosen, not with the aim of producing a careful analysis on nannoplankton biodiversity, taxonomy and abundances, which was the main purpose of the work by Newsam (2016), but rather to conduct a detailed morphometric analysis on exceptionally preserved specimens of *Clausicoccus subdistichus* gr. In addition, the exceptional preservation found at this site was essential to compare, with detailed SEM investigations, the poor preservation of the calcareous nannofossil assemblages recovered at Site 1209, which represents an example of dissolved material.

ODP 1209 is located close to the most elevated, central part of the Southern High of Shatsky Rise, in the NW Pacific (Bralower et al., 2002). The goal of site coring was primarily linked with the recovery of the sedimentary record of several critical events, included the E-O transition. Our biostratigraphic analysis suggests that the boundary interval is complete. However, dissolution and poor preservation characterized the middle-upper Eocene assemblages, with a slight improvement towards the Oligocene.
This site was primarily chosen to verify the morphometric response of *Clausicoccus* in a less ideal depositional setting, with the aim to shed light on the possible influence of preservation on size. In addition, the poor preservation allows us to reconstruct the diagenetic processes affecting calcareous nannofossils in the main phases of this transition.

1.5 Methods and approaches

Quantitative and semi-quantitavive analysis. We used relative abundances of species/taxa to quantify changes (%) in coccolithophores across the EOT at the low-middle latitudes. High resolution semi-quantitative analysis (n/mm^2) (Backman and Shackleton, 1983) in combination with high resolution sampling, have been performed to refine the precision of nannofossil biostratigraphic datums and the behaviour of individual calcareous nannofossil taxa. The age models derived from the studied sites are primarily based on semi-quantitative data of calcareous nannofossils, magnetostratigraphic polarity reversals and oxygen stable isotopic events. The use of the same tie points, on a common time scale, allow us to develop a precise site-to-site correlation.

Geochemical analysis. For the determination of the paleoclimatic evolution, we relied on the oxygen and carbon stable isotopes, as well as carbonate content (wt%), derived from bulk-carbonate trough mass spectrometer analysis. Since bulk sediments represent a mixture of different biogenic carbonate components (e.g. benthic and planktic foraminifers, and calcareous nannofossils), the C and O stable isotopes reflect the composition of these constituents, which, in turn is a function of the seawater $\delta^{18}O$ value where the organisms

lived. The isotopic composition derived from bulk sediments closely resembles the pattern derived from single planktonic foraminiferal analysis, but unlike this latter approach, bulk analysis has two main advantages: 1) is a non-destructive method (few milligram of sediment are required), 2) is a less intensive procedure (Shackleton et al., 1993). The methodological procedure is explained in detail in Chapter 2 and Chapter 4.

Biometric analysis. In this thesis, we analyzed the relationship between the size variations of *Clausicoccus subdistichus* gr. and the control of environmental factors linked to the onset of Antarctica glaciation (i.e., temperature, paleoproductivity, ocean carbon chemistry and carbon cycling) in affecting the physiology of these organisms and the related biomineralization processes (Chapter 6). However, disentangling the relation between size change and the effect of each single variable is not obvious, because of potentially nonlinear interactions. The maximum and minimum axis, i.e. length and width, of each coccoliths (included the central areas) was measured with a polarized light microscopy combined with a digital camera equipment.
For this study, we used deep-sea sediment samples, selected from a set of low-middle latitude DSDP/ODP drilling sites covering tropical/temperate regions and all major ocean basins (Atlantic, Indian, and Pacific oceans).

Diversity indices. We document shifts in calcareous nannofossil diversity trough time using quantitative count data (%) from the Indian Ocean (ODP Site 756) and Tasman Sea (IODP U1509). The indices considered in this work were performed using the statistical software Past and include: the number of taxa (S), dominance (D), Shannon-Weaver index (H) (Shannon and Weaver, 1949) and Evenness (E) (Buzas and Gibson, 1969).

Scanning electron microscopy (SEM). To evaluate the degree of control exerted by preservation on the different components of the assemblage trough the E-O transition, both at ODP Site 1209 and IODP Site 1411, we conducted an extensive SEM study using the newly installed scanning electron microscope Tescan Solaris (FEG-FIB-EDS-WDS-EBSD) available at the Department of Geosciences (University of Padova).
The methodology adopted for the preparation of samples is extensively described in Chapter 5.

1.6 Summary of the chapters

In this thesis, each chapter is presented as an independent scientific manuscript and will include its own specific abstract, introduction, methods, results, discussion, and conclusion. In the following we present a brief summary of each chapter.

In **Chapter 2,** an in depth understanding of the quantitative distributions of calcareous nannofossils and of the main paleo-environmental factors controlling the assemblage composition in the Indian Ocean (ODP Site 756) was carried out through biostratigraphic, geochemical and statistical analysis. This first case study constituted a starting point for this project and the basis of comparison for the subsequent chapters.

Next, multi-proxy data sets, including calcareous nannofossils, magnetostratigraphy and isotope geochemistry were generated to reconstruct a reliable age model and to provide a paleoclimatic reconstruction for the South Pacific (Tasman Sea, Site U1509). The paleoclimatic evolution was primarily inferred from shifts and trends in the assemblages, using groups of taxa and their known paleoecological affinities, several diversity indices, principal component analysis, and bulk O and C stable isotope geochemistry (**Chapter 4**).

In addition, the high-resolution bio-magnetostratigraphic results obtained at Site U1509 were compared to previously published records from low-middle and high latitudes to produce a comprehensive inter-basinal biochronological global framework of the main calcareous nannofossil bioevents observed during this time (**Chapter 3**).

In **Chapter 5,** we try to reveal the role played by preservation in altering/modifying calcareous nannofossil assemblage and bulk primary isotopic signal, comparing different sediments from the tropical Pacific (ODP Site 1209) and North Atlantic (IODP Site U1411). Ultimately, the main finding of this part of the research project is the construction of reliable age models derived for our case studies (ODP 756 and 1209, IODP U1509 and U1411). This step was essential to present and discuss the new morphometric results obtained for *C. subdistichus* gr. from these multiple localities (**Chapter 6**).

In **Chapter 6**, The unique biostratigraphic, paleoenvironmental and morphometric feature of *C. subdistichus* gr. has been comprehensively discussed. In summary, we consider the biohorizons related to this taxon (i.e., the acme beginning ad end) a reliable biostratigraphic datums that well approximate the EOB at low-middle latitudes. Moreover, the peak interval and the size changes of this taxon observed across the EOT is thought to represent a good indicator for enhanced productivity conditions at low middle latitudes, and a sensitive indicator of sea-water chemistry changes. All together, we hope that these chapters add a piece of information that would lead us towards a better and comprehensive understanding on how nannoplankton react to climate changes occurred at the Eocene Oligocene transition.

References

Agnini, C., Fornaciari, E., Raffi, I., Catanzariti, R., Pälike, H., Backman, J., Rio, D., 2014. Biozonation and biochronology of Paleogene calcareous nannofossils from low and middle latitudes. Newsletters on Stratigraphy 47, 131–181.

Agnini, C., Monechi, S., Raffi, I., 2017. Calcareous nannofossil biostratigraphy: historical background and application in Cenozoic chronostratigraphy. Lethaia 50, 447–463.

Aloisi, G., 2015. Covariation of metabolic rates and cell size in coccolithophores. Biogeosciences 12, 4665–4692.

Anagnostou, E., John, E.H., Edgar, K.M., Foster, G.L., Ridgwell, A., Inglis, G.N., Pancost, R.D., Lunt, D.J., Pearson, P.N., 2016. Changing atmospheric CO_2 concentration was the primary driver of early Cenozoic climate. Nature 533, 380–384.

Anderson, L.D., Delaney, M.L., 2005. Middle Eocene to early Oligocene paleoceanography from Agulhas Ridge, Southern Ocean (Ocean Drilling Program Leg 177, Site 1090). Paleoceanography 20, 1–13.

Anderson, R.F., Winckler, G., 2005. Problems with paleoproductivity proxies. Paleoceanography 20, 1–7.

Andruleit, H., Rogalla, U., Stäger, S., 2004. From living communities to fossil assemblages: Origin and fate of coccolithophores in the northern Arabian Sea. Micropaleontology 50, 5–21.

Aubry, M.-P., 1992. Late Paleogene Calcareous Nannoplankton Evolution: A Tale of Climatic Deterioration. In: Eocene-Oligocene Climatic and Biotic Evolution. p. 272–279.

Backman, J., Raffi, I., Rio, D., Fornaciari, E., Pälike, H., 2012. Biozonation and biochronology of Miocene through Pleistocene calcareous nannofossils from low and middle latitudes. Newsletters on Stratigraphy 45, 221–244.

Backman, J., Shackleton, N.J., 1983. Quantitative biochronology of Pliocene and early Pleistocene calcareous nannofossils from the Atlantic, Indian and Pacific oceans. Marine Micropaleontology 8, 141–170.

Baldauf, J.G., 1992. Middle Eocene through early Miocene diatom floral turnover. In: Prothero, D.R., Berggren, W.A. (Eds.), Eocene–Oligocene Climatic and Biotic Evolution. Princeton University Press, Princeton, NJ.

Barker, P.F., 2001. Scotia sea regional tectonic evolution: Implications for mantle flow and palaeocirculation, Earth-Science Reviews.

Barron, J.A., Stickley, C.E., Bukry, D., 2015. Paleoceanographic, and paleoclimatic constraints on the global Eocene diatom and silicoflagellate record. Palaeogeography, Palaeoclimatology, Palaeoecology 422, 85–100.

Berggren, W.A., Wade, B.S., Pearson, P.N., 2018. Oligocene chronostratigraphy and planktonic foraminiferal biostratigraphy: Historical review and current state-of-the-art. In: Wade, B.S., Olsson, R.K., Pearson, P.N., Huber, B.T., Berggren, W.A. (Eds.), Atlas of Oligocene Planktonic Foraminifera. Cushman Foundation for Foraminiferal Research, Lawrence, USA, p. 19–54.

Berner, R.A., Lasaga, A.C., Garrels, R.M., 1983. The carbonate-silicate geochemical cycle and its effect on atmospheric carbon dioxide over the past 100 million years. American Journal of Science 283, 641–683.

Blaj, T., Backman, J., Raffi, I., 2009. Late Eocene to Oligocene preservation history and biochronology of

calcareous nannofossils from paleo-equatorial Pacific Ocean sediments. Rivista Italiana di Paleontologia e Stratigrafia 115, 67–85.

Bodiselitsch, B., Montanari, A., Koeberl, C., Coccioni, R., 2004. Delayed climate cooling in the Late Eocene caused by multiple impacts: High-resolution geochemical studies at Massignano, Italy. Earth and Planetary Science Letters 223, 283–302.

Bohaty, S.M., Zachos, J.C., Delaney, M.L., 2012. Foraminiferal Mg/Ca evidence for Southern Ocean cooling across the Eocene-Oligocene transition. Earth and Planetary Science Letters 317–318, 251–261.

Bolli, H.M., Saunders, J.B., Perch-Nielsen, K., 1985. Plankton Stratigraphy. Cambridge University Press.

Bordiga, M., Henderiks, J., Tori, F., Monechi, S., Fenero, R., Legarda-Lisarri, A., Thomas, E., 2015. Microfossil evidence for trophic changes during the Eocene-Oligocene transition in the South Atlantic (ODP Site 1263, Walvis Ridge). Climate of the Past 11, 1249–1270.

Bordiga, M., Sulas, C., Henderiks, J., 2017. Reticulofenestra daviesii: biostratigraphy and paleogeographic distribution across the Eocene–Oligocene boundary. Geobios 50, 349–358.

Bown, P.R., Jones, T.D., 2006. New Paleogene calcareous nannofossil taxa from coastal Tanzania: Tanzania Drilling Project Sites 11 to 14.

Bown, P.R., Lees, J.A., Young, J.R., 2004. Calcareous nannoplankton evolution and diversity through time, Coccolithophores - From Molecular Process to Global Impact. Springer, London.

Bralower, T.J., Premoli Silva, I., Malone, M.J., Shipboard Scientific Party, 2002. Site 1209. In: Proceedings of the Ocean Drilling Program, Initial Reports Volume 198, College Station, TX (Ocean Drilling Program). p. 1–102.

Brown, B., Gaina, C., Müller, R.D., 2006. Circum-Antarctic palaeobathymetry: Illustrated examples from Cenozoic to recent times. Palaeogeography, Palaeoclimatology, Palaeoecology 231, 158–168.

Buzas, M.A., Gibson, T.G., 1969. Species diversity: benthonic foraminifera in Western North Atlantic. Science 163, 72–75.

Cerling, T.E., Solomon, D.K., Quade, J., Bowman, J.R., 1991. On the isotopic composition of carbon in soil carbon dioxide. Geochimica et Cosmochimica Acta 55, 3403–3405.

Cotton, L.J., Pearson, P.N., 2011. Extinction of larger benthic foraminifera at the Eocene/Oligocene boundary. Palaeogeography, Palaeoclimatology, Palaeoecology 311, 281–296.

Coxall, H.K., Huck, C.E., Huber, M., Lear, C.H., Legarda-Lisarri, A., O'Regan, M., Sliwinska, K.K., Van De Flierdt, T., De Boer, A.M., Zachos, J.C., Backman, J., 2018. Export of nutrient rich Northern Component Water preceded early Oligocene Antarctic glaciation /704/106/413 /704/829 /704/106/2738 article. Nature Geoscience 11, 190–196.

Coxall, H.K., Pearson, P.N., 2007. The Eocene-Oligocene Transition. In: Williams, M., Haywood, A.M., Gregory, J., Schmidt, D.N. (Eds.), Deep-Time Perspectives on Climate Change: Marrying the Signal from Computer Models and Biological Proxies, Micropaleontology Society Special Publication. Geological Society, London, p. 351–387.

Coxall, H.K., Wilson, P.A., 2011. Early Oligocene glaciation and productivity in the eastern equatorial Pacific: Insights into global carbon cycling. Paleoceanography 26, 1–18.

Coxall, H.K., Wilson, P.A., Pälike, H., Lear, C.H., Backman, J., 2005. Rapid stepwise onset of Antarctic glaciation and deeper calcite compensation in the Pacific Ocean. Nature 433, 53–7.

Craig, H., 1965. The measurements of oxygen isotope paleotemperature. In: Tongiori E. (Ed.), Second Conference on Oceanographic Studies and Paleotemperatures. Spoleto (Italy): Consiglio Nazionale delle Ricerche, p. 161–182.

Cramer, B.S., Toggweiler, J.R., Wright, J.D., Katz, M.E., Miller, K.G., 2009. Ocean overturning since the Late Cretaceous: Inferences from a new benthic foraminiferal isotope compilation. Paleoceanography 24, PA4216.

Cramwinckel, M.J., Huber, M., Kocken, I.J., Agnini, C., Bijl, P.K., Bohaty, S.M., Frieling, J., Goldner, A., Hilgen, F.J., Kip, E.L., Peterse, F., Van Der Ploeg, R., Röhl, U., Schouten, S., Sluijs, A., 2018. Synchronous tropical and polar temperature evolution in the Eocene letter. Nature 559, 382–386.

Cronin, T.M., 2010. Paleoclimates: Understanding climate change past and present. Columbia University Press, New York, NY.

D'Amario, B., Ziveri, P., Grelaud, M., Oviedo, A., 2018. Emiliania huxleyi coccolith calcite mass modulation by morphological changes and ecology in the Mediterranean Sea. PLoS ONE 13, 1–17.

De Vargas, C., Aubry, M., Probert, I., Young, J.R., 2007. Origin and evolution of coccolithophores: from coastal hunters to oceanic farmers, Evolution of primary …. Elsevier Inc.

DeConto, R.M., Pollard, D., 2003. Rapid Cenozoic glaciation of Antarctica induced by declining atmospheric CO_2. Nature 1317, 1313–1317.

DeConto, R.M., Pollard, D., Wilson, P.A., Pälike, H., Lear, C.H., Pagani, M., 2008. Thresholds for Cenozoic bipolar glaciation. Nature 455, 652–656.

Diester-Haass, L., 1995. Middle Eocene to early Oligocene paleoceanography of the Antarctic Ocean (Maud Rise, ODP Leg 113, Site 689): change from a low to a high productivity ocean. Palaeogeography, Palaeoclimatology, Palaeoecology 113, 311–334.

Diester-Haass, L., 1991. Eocene/Oligocene paleoceanography in the Antarctic Ocean, Atlantic sector (Maud Rise, ODP leg 113, Site 689B and 690B). Marine Geology 100, 249–276.

Diester-Haass, L., 1996. Late Eocene-Oligocene paleoceanography in the southern Indian Ocean (ODP Site 744). Marine Geology 130, 99–119.

Diester-Haass, L., Robert, C., Chamley, H., 1996. The Eocene-Oligocene preglacial-glacial transition in the Atlantic sector of the Southern Ocean (ODP Site 690). Marine Geology 131, 123–149.

Diester-Haass, L., Zachos, J.C., 2003. The Eocene-Oligocene transition in the Equatorial Atlantic (ODP Site 925); Paleoproductivity increase and positive $\delta^{13}C$ excursion. In: Prothero, D.R., Ivany, C.L., Nesbitt, E.A. (Eds.), From Greenhouse to Icehouse; The Marine Eocene-Oligocene Transition. Columbia Univ. Press, New York, NY, USA, p. 397–416.

Diester-Haass, L., Zahn, R., 1996. Eocene-Oligocene transition in the Southern Ocean: History of water mass circulation and biological productivity. Geology 24, 163–166.

Diester-Haass, L., Zahn, R., 2001. Paleoproductivity increase at the Eocene - Oligocene climatic transition: ODP/DSDP sites 763 and 592. Palaeogeography, Palaeoclimatology, Palaeoecology 172, 153–170.

Dunkley Jones, T., Bown, P.R., Pearson, P.N., Wade, B.S., Coxall, H.K., Lear, C.H., 2008. Major shifts in calcareous phytoplankton assemblages through the Eocene-Oligocene transition of Tanzania and their implications for low-latitude primary production. Paleoceanography 23, 1–14.

Eagles, G., Livermore, R., Morris, P., 2006. Small basins in the Scotia Sea: The Eocene Drake Passage gateway. Earth and Planetary Science Letters 242, 343–353.

Edgar, K.M., Wilson, P.A., Sexton, P.F., Suganuma, Y., 2007. No extreme bipolar glaciation during the main Eocene calcite compensation shift. Nature 448, 908–911.

Egan, K.E., Rickaby, R.E.M., Hendry, K.R., Halliday, A.N., 2013. Opening the gateways for diatoms primes Earth for Antarctic glaciation. Earth and Planetary Science Letters 375, 34–43.

Ehrmann, W.U., 1998. Implications of late Eocene to early Miocene clay mineral assemblages in McMurdo sound (Ross sea, Antarctica) on paleoclimate and ice dynamics. Palaeogeography, Palaeoclimatology, Palaeoecology 139, 213–231.

Ehrmann, W.U., Mackensen, A., 1992. Sedimentological evidence for the formation of an East Antarctic ice sheet in Eocene/Oligocene time. Palaeogeography, Palaeoclimatology, Palaeoecology 93, 85–112.

Ekart, D.D., Cerling, T.E., Montañez, I.P., Tabor, N.J., 1999. A 400 million year carbon isotope record of pedogenic carbonate: Implications for paleoatmospheric carbon dioxide. American Journal of Science.

Elsworth, G., Galbraith, E., Halverson, G., Yang, S., 2017. Enhanced weathering and CO 2 drawdown caused by latest Eocene strengthening of the Atlantic meridional overturning circulation. Nature Geoscience 10, 213–216.

Emiliani, C., 1955. Pleistocene temperatures. Journal of Geology 63, 538–578.

Emiliani, C., 1966. Paleotemperature analysis of Caribbean cores P6304–8 and P6304–9 and a generalized temperature curve for the past 425,000 years. The Journal of Geology 74, 109–124.

Erhardt, A.M., Pälike, H., Paytan, A., 2013. High-resolution record of export production in the eastern equatorial Pacific across the Eocene-Oligocene transition and relationships to global climatic records. Paleoceanography 28, 130–142.

Evans, D., Wade, B.S., Henehan, M., Erez, J., Müller, W., 2016. Revisiting carbonate chemistry controls on planktic foraminifera Mg/Ca: Implications for sea surface temperature and hydrology shifts over the Paleocene-Eocene Thermal Maximum and Eocene-Oligocene transition. Climate of the Past 12, 819–835.

Falkowski, P.G., Katz, M.E., Knoll, A.H., Quigg, A., Raven, J.A., Schofield, O., Taylor, F.J.R., 2004. The evolution of modern eukaryotic phytoplankton. Science 305, 354–360.

Ferreira, J., Cachão, M., González, R., 2008. Reworked calcareous nannofossils as ocean dynamic tracers: The Guadiana shelf case study (SW Iberia). Estuarine, Coastal and Shelf Science 79, 59–70.

Finkel, Z. V., 2007. Does Phytoplankton Cell Size Matter? The Evolution of Modern Marine Food Webs. In: Falkowski, P.G., Knoll, A.H. (Eds.), Evolution of Primary Producers in the Sea. Elsevier Academic Press, p. 333–350.

Finkel, Z. V., Beardall, J., Flynn, K.J., Quigg, A., Rees, T.A. V., Raven, J.A., 2010. Phytoplankton in a changing world: Cell size and elemental stoichiometry. Journal of Plankton Research 32, 119–137.

Fioroni, C., Villa, G., Persico, D., Jovane, L., 2015. Middle Eocene-Lower Oligocene calcareous nannofossil biostratigraphy and paleoceanographic implications from Site 711 (equatorial Indian Ocean). Marine Micropaleontology 118, 50–62.

Fletcher, B.J., Brentnall, S.J., Anderson, C.W., Berner, R.A., Beerling, D.J., 2008. Atmospheric carbon dioxide linked with Mesozoic and early Cenozoic climate change. Nature Geoscience 1, 43–48.

Francis, J.E., 1999. Evidence from fossil plants for Antarctica palaeoclimates over the past 100 million years. Terra Antarctica 3, 43–52.

Francis, J.E., Poole, I., 2002. Cretaceous and early Tertiary climates of Antarctica: Evidence from fossil wood. Palaeogeography, Palaeoclimatology, Palaeoecology 182, 47–64.

Franks, P.J., Royer, D.L., Beerling, D.J., Van De Water, P.K., Cantrill, D.J., Barbour, M.M., Berry, J.A., 2014. New constraints on atmospheric CO_2 concentration for the Phanerozoic. Geophysical Research Letters 41, 4685–4694.

Funakawa, S., Nishi, H., Moore, T.C., Nigrini, C.A., 2006. Radiolarian faunal turnover and paleoceanographic change around Eocene/Oligocene boundary in the central equatorial Pacific, ODP Leg 199, Holes 1218A, 1219A, and 1220A. Palaeogeography, Palaeoclimatology, Palaeoecology 230, 183–203.

Galeotti, S., Bijl, P., Brinkuis, H., M. DeConto, R., Escutia, C., Florindo, F., G.W. Gasson, E., Francis, J., Hutchinson, D., Kennedy-Asser, A., Lanci, L., Sauermilch, I., Sluijs, A., Stocchi, P., 2022. The Eocene-Oligocene boundary climate transition: an Antarctic perspective. In: Antarctic Climate Evolution. BV, p. 297–361.

Galeotti, S., DeConto, R.M., Naish, T., Stocchi, P., Florindo, F., Pagani, M., Barrett, P., Bohaty, S.M., Lanci, L., Pollard, D., Sandroni, S., Talarico, F.M., Zachos, J.C., 2016. Antarctic Ice Sheet variability across the Eocene-Oligocene boundary climate transition. Science 352, 76–80.

Gehlen, M., Gangstø, R., Schneider, B., Bopp, L., Aumont, O., Ethe, C., 2007. The fate of pelagic CaCO3 production in a high CO2 ocean: A model study. Biogeosciences 4, 505–519.

Gibbs, S.J., Poulton, A.J., Bown, P.R., Daniels, C.J., Hopkins, J., Young, J.R., Jones, H.L., Thiemann, G.J., Dea, S.A.O., Newsam, C., 2013. Species-specific growth response of coccolithophores to Palaeocene – Eocene environmental change. Nature Geoscience 6, 1–5.

Gradstein, F.M., Ogg, J.G., Schmitz, M.D., Ogg, G.M., 2012. The Geologic Time Scale 2012. Elsevier, Amsterdam, Netherlands.

Griffith, E., Calhoun, M., Thomas, E., Averyt, K.B., Erhardt, A.M., Bralower, T.J., Lyle, M.W., Olivarez-Lyle, A., Paytan, A., 2010. Export productivity and carbonate accumulation in the Pacific Basin at the transition from a greenhouse to icehouse climate (late Eocene to early Oligocene). Paleoceanography 25, 1–15.

Haq, B.U., Lohmann, G.P., 1976. Early Cenozoic calcareous nannoplankton biogeography of the Atlantic Ocean. Marine Micropaleontology 1, 119–194.

Henderiks, J., 2008. Coccolithophore size rules - Reconstructing ancient cell geometry and cellular calcite quota from fossil coccoliths. Marine Micropaleontology 67, 143–154.

Hönisch, B., Ridgwell, A., Schmidt, D.N., Thomas, E., Gibbs, S.J., Sluijs, A., Zeebe, R., Kump, L., Martindale,

R.C., Greene, S.E., Kiessling, W., Ries, J., Zachos, J.C., Royer, D.L., Barker, S., Marchitto, T.M., Moyer, R., Pelejero, C., Ziveri, P., Foster, G.L., Williams, B., 2012. The geological record of ocean acidification. Science 335, 1058–1063.

Hooker, J.J.J., Collinson, M.E.E., Sille, N.P.P., 2004. Eocene-Oligocene mammalian faunal turnover in the Hampshire Basin, UK: Calibration to the global time scale and the major cooling event. Journal of the Geological Society 161, 161–172.

Hutchinson, D.K., Coxall, H.K., Lunt, D.J., Steinthorsdottir, M., de Boer, A.M., Baatsen, M., von der Heydt, A., Huber, M., Kennedy-Asser, A.T., Kunzmann, L., Ladant, J.B., Lear, C.H., Moraweck, K., Pearson, P.N., Piga, E., Pound, M.J., Salzmann, U., Scher, H.D., Sijp, W.P., Śliwińska, K.K., Wilson, P.A., Zhang, Z., 2021. The Eocene–Oligocene transition: a review of marine and terrestrial proxy data, models and model–data comparisons. Climate of the Past 17, 269–315.

Hutchinson, D.K., De Boer, A.M., Coxall, H.K., Caballero, R., Nilsson, J., Baatsen, M., 2018. Climate sensitivity and meridional overturning circulation in the late Eocene using GFDL CM2.1. Climate of the Past 14, 789–810.

Inglis, G.N., Farnsworth, A., Lunt, D.J., Foster, G.L., Hollis, C.J., Pagani, M., Jardine, P.E., Pearson, P.N., Markwick, P., Galsworthy, A.M.J., 2015. Descent toward the Icehouse: Eocene sea surface cooling inferred from GDGT distributions. Paleoceanography 30, 1000–1020.

Jagniecki, E.A., Lowenstein, T.K., Jenkins, D.M., Demicco, R. V., 2015. Eocene atmospheric CO_2 from the nahcolite proxy. Geology 43, 1075–1078.

Jasper, J.P., Hayes, J.M., 1990. A carbon isotope record of CO_2 levels during the late Quaternary. Nature 347, 462–464.

Jenkins, D.G., 1974. Initiation of the proto circum-Antarctic current. Nature 252, 371–373.

Jones, A.P., Dunkley Jones, T., Coxall, H.K., Pearson, P.N., Nala, D., Hoggett, M., 2019. Low-Latitude Calcareous Nannofossil Response in the Indo-Pacific Warm Pool Across the Eocene-Oligocene Transition of Java, Indonesia. Paleoceanography and Paleoclimatology 34, 1833–1847.

Kamikuri, S.I., Moore, T.C., Ogane, K., Suzuki, N., Pälike, H., Nishi, H., 2012. Early Eocene to early Miocene radiolarian biostratigraphy for the low-latitude Pacific Ocean. Stratigraphy 9, 77–108.

Katz, M.E., Finkel, Z. V., Grzebyk, D., Knoll, A.H., Falkowski, P.G., 2004. Evolutionary Trajectories and Biogeochemical Impacts of Marine Eukaryotic Phytoplankton. Annual Review of Ecology, Evolution, and Systematics 35, 523–556.

Katz, M.E., Miller, K.G., Wright, J.D., Wade, B.S., Browning, J. V., Cramer, B.S., Rosenthal, Y., 2008. Stepwise transition from the Eocene greenhouse to the Oligocene icehouse. Nature Geoscience 1, 329–333.

Kennett, J.P., 1976. Oxygen isotopic evidence for the development of the psychrosphere 38 Myr ago. Nature 260, 513–515.

Lawver, L.A., Gahagan, L.M., 2003. Evolution of cenozoic seaways in the circum-antarctic region. Palaeogeography, Palaeoclimatology, Palaeoecology 198, 11–37.

Lear, C.H., Bailey, T.R., Pearson, P.N., Coxall, H.K., Rosenthal, Y., 2008. Cooling and ice growth across the

Eocene-Oligocene transition. Geology 36, 251–254.

Lear, C.H., Lunt, D.J., 2016. How Antarctica got its ice. Science 352, 34–35.

Lees, J.A., Bown, P.R., Mattioli, E., 2005. Problems with proxies? Cautionary tales of calcareous nannofossil paleoenvironmental indicators. Micropaleontology 51, 333–343.

Lisiecki, L.E., Raymo, M.E., 2005. A Pliocene-Pleistocene stack of 57 globally distributed benthic δ 18O records. Paleoceanography 20, 1–17.

Liu, Z., He, Y., Jiang, Y., Wang, H., Liu, W., Bohaty, S.M., Wilson, P.A., 2018. Transient temperature asymmetry between hemispheres in the Palaeogene Atlantic Ocean. Nature Geoscience 11, 656–660.

Liu, Z., Pagani, M., Zinniker, D., Deconto, R.M.R.., Huber, M., Brinkhuis, H., Shah, S.. S.R., Leckie, R.M.M., Pearson, A., 2009. Global cooling during the Eocene-Oligocene climate transition. Science 323, 1187–1190.

Liu, Z., Tuo, S., Zhao, Q., Cheng, X., Huang, W., 2004. Deep-water earliest Oligocene glacial maximum (EOGM) in South Atlantic. Chinese Science Bulletin 49, 2190–2197.

Livermore, R., Hillenbrand, C.D., Meredith, M., Eagles, G., 2007. Drake Passage and Cenozoic climate: An open and shut case? Geochemistry, Geophysics, Geosystems 8.

Livermore, R., Nankivell, A., Eagles, G., Morris, P., 2005. Paleogene opening of Drake Passage. Earth and Planetary Science Letters 236, 459–470.

Lowenstein, T.K., Demicco, R. V., 2006. Elevated eocene atmospheric CO2 and its subsequent decline. Science 313, 1928.

Martini, E., 1971. Standard Tertiary and Quaternary calcareous nannoplankton zonation. In: Farinacci, A. (Ed.), Proceedings of the 2nd International Conference on Planktonic Microfossils. Edizioni Tecnoscienza, Rome, p. 739–785.

McIntyre, A., Bé, A.W.H., 1967. Modern coccolithophoridae of the atlantic ocean-I. Placoliths and cyrtoliths. Deep-Sea Research and Oceanographic Abstracts 14.

Merico, A., Tyrrell, T., Wilson, P.A., 2008. Eocene/Oligocene ocean de-acidification linked to Antarctic glaciation by sea-level fall. Nature 452, 979–982.

Miller, K.G., Browning, J. V., Aubry, M.-P., Wade, B.S., Katz, M.E., Kulpecz, A.A., Wright, J.D., 2008. Eocene-Oligocene global climate and sea-level changes: St. Stephens Quarry, Alabama. Bulletin of the Geological Society of America 120, 34–53.

Miller, K.G., Fairbanks, R.G., Mountain, G.S., 1987. Tertiary oxygen isotope synthesis, sea level history, and continental margin erosion. Paleoceanography 2, 1–19.

Miller, K.G., Wright, J.D., Fairbanks, R.G., 1991. Unlocking the Ice House: Oligocene-Miocene oxygen isotopes, eustasy, and margin erosion. Journal of Geophysical Research: Solid Earth 96, 6829–6848.

Mutterlose, R.G., Herrle, J.O., Mutterlose, J., 2005. Mesozoic calcareous nannofossils-state of the art. Paläontologische Zeitschrift 79/1, 113–133.

Newsam, C., 2016. Calcareous nannoplankton evolution and the Paleogene greenhouse to icehouse climate-mode transition.

Nilsen, E.B., Anderson, L.D., Delaney, M.L., 2003. Paleoproductivity, nutrient burial, climate change and the

carbon cycle in the western equatorial Atlantic across the Eocene/Oligocene boundary. Paleoceanography 18.

Nissen, C., Vogt, M., Münnich, M., Gruber, N., Alexander Haumann, F., 2018. Factors controlling coccolithophore biogeography in the Southern Ocean. Biogeosciences 15, 6997–7024.

Norris, R.D., Wilson, P.A., Blum, P., Fehr, A., Agnini, C., Bornemann, A., Boulila, S., Bown, P.R., Cournede, C., Friedrich, O., Ghosh, A.K., Hollis, C.J., Hull, P.M., Jo, K., Junium, C.K., Kaneko, M., Liebrand, D., Lippert, P.C., Liu, Z., Matsui, H., Moriya, K., Nishi, H., Opdyke, B.N., Penman, D., Romans, B., Scher, H.D., Sexton, P., Takagi, H., Turner, S.K., Whiteside, J.H., Yamaguchi, T., Yamamoto, Y., 2014a. Expedition 342 summary. Proceedings. IODP, 342: College Station, TX (Integrated Ocean Drilling Program) 342.

Norris, R.D., Wilson, P.A., Blum, P., Fehr, A., Agnini, C., Bornemann, A., Boulila, S., Bown, P.R., Cournede, C., Friedrich, O., Ghosh, A.K., Hollis, C.J., Hull, P.M., Jo, K., Junium, C.K., Kaneko, M., Liebrand, D., Lippert, P.C., Liu, Z., Matsui, H., Moriya, K., Nishi, H., Opdyke, B.N., Penman, D.E., Romans, B.W., Scher, H.D., Sexton, P., Takagi, H., Turner, S.K., Whiteside, J.H., Yamaguchi, T., Yamamoto, Y., 2014b. Site U1411. Proceedings of the Integrated Ocean Drilling Program 342.

Okada, H., Bukry, D., 1980. Supplementary modification and introduction of code numbers to the low-latitude coccolith biostratigraphic zonation. Marine Micropaleontology 5, 321–325.

Okada, H., Honjo, S., 1973. Distribution of Oceanic Coccolithophorids in the Pacific. Deep Sea Res 20, 355–374.

Pagani, M., Huber, M., Liu, Z., Bohaty, S.M., Henderiks, J., Sijp, W., Krishnan, S., DeConto, R.M., 2011. The role of carbon dioxide during the onset of antarctic glaciation. Science 334, 1261–1264.

Pagani, M., Zachos, J.C., Freeman, K.H., Tipple, B., Bohaty, S.M., 2005. Marked Decline in Atmospheric Carbon Dioxide Concentrations During the Paleogene. Science 309, 600–603.

Pälike, H., Lyle, M.W., Nishi, H., Raffi, I., Ridgwell, A., Gamage, K., Klaus, A., Acton, G., Anderson, L., Backman, J., Baldauf, J., Beltran, C., Bohaty, S.M., Bown, P.R., Busch, W., Channell, J.E.T., Chun, C.O.J., Delaney, M.L., Dewangan, P., Dunkley Jones, T., Edgar, K.M., Evans, H., Fitch, P., Foster, G.L., Gussone, N., Hasegawa, H., Hathorne, E.C., Hayashi, H., Herrle, J.O., Holbourn, A.E., Hovan, S., Hyeong, K., Iijima, K., Ito, T., Kamikuri, S.I., Kimoto, K., Kuroda, J., Leon-Rodriguez, L., Malinverno, A., Moore, T.C., Murphy, B.H., Murphy, D.P., Nakamura, H., Ogane, K., Ohneiser, C., Richter, C., Robinson, R., Rohling, E.J., Romero, O., Sawada, K., Scher, H.D., Schneider, L., Sluijs, A., Takata, H., Tian, J., Tsujimoto, A., Wade, B.S., Westerhold, T., Wilkens, R., Williams, T., Wilson, P.A., Yamamoto, Y., Yamamoto, S., Yamazaki, T., Zeebe, R.E., 2012. A Cenozoic record of the equatorial Pacific carbonate compensation depth. Nature 488, 609–614.

Parker, M.E., Clark, M., Wise, S.W., 1985. Calcareous nannofossils of Deep Sea Drilling Project Sites 558 and 563, North Atlantic Ocean: biostratigraphy and the distribution of Oligocene braarudosphaerids. Initial reports DSDP, Leg 82, Ponta Delgada to Balboa 559–589.

Pearson, P.N., Foster, G.L., Wade, B.S., 2009. Atmospheric carbon dioxide through the Eocene-Oligocene climate transition. Nature 461, 1110–1113.

Pearson, P.N., McMillan, I.K., Wade, B.S., Dunkley Jones, T., Coxall, H.K., Bown, P.R., Lear, C.H., 2008. Extinction and environmental change across the Eocene-Oligocene boundary in Tanzania. Geology 36, 179–182.

Pearson, P.N., Palmer, M.R., 2000. Atmospheric carbon dioxide concentrations over the past 60 million years. Nature 406, 695–699.

Pearson, P.N., van Dongen, B.E., Nicholas, C.J., Pancost, R.D., Schouten, S., Singano, J.M., Schouten, S., Singano, J.M., Wade, B.S., 2007. Stable warm tropical climate through the Eocene Epoch. Geology 35, 211–214.

Peirce, J., Weissel, J., et al., 1989. Site 756. Proceeding ODP, Initial Reports, 121: College Station, TX (Ocean Drilling Program).

Persico, D., Fioroni, C., Villa, G., 2012. A refined calcareous nannofossil biostratigraphy for the middle Eocene-early Oligocene Southern Ocean ODP sites. Palaeogeography, Palaeoclimatology, Palaeoecology 335–336, 12–23.

Persico, D., Villa, G., 2004. Eocene-Oligocene calcareous nannofossils from Maud Rise and Kerguelen Plateau (Antarctica): Paleoecological and paleoceanographic implications. Marine Micropaleontology 52, 153–179.

Plancq, J., Mattioli, E., Pittet, B., Simon, L., Grossi, V., 2014. Productivity and sea-surface temperature changes recorded during the late Eocene-early Oligocene at DSDP Site 511 (South Atlantic). Palaeogeography, Palaeoclimatology, Palaeoecology 407, 34–44.

Pollard, D., DeConto, R.M., 2005. Hysteresis in Cenozoic Antarctic ice-sheet variations. Global and Planetary Change 45, 9–21.

Pomerol, C., Premoli Silva, I., 1986. The Eocene-Oligocene Transition: Events and Boundary. In: Terminal Eocene Events. Elsevier, Amsterdam, p. 1–24.

Premoli Silva, I., Jenkins, D.G., 1993. Decision on the Eocene-Oligocene boundary stratotype. Episodes 16, 379–382.

Raffi, I., Agnini, C., Backman, J., Catanzariti, R., Pälike, H., 2016. A Cenozoic calcareous nannofossil biozonation from low and middle latitudes: A synthesis. Journal of Nannoplankton Research 36, 121–132.

Raven, J.A., 1998. The twelfth Tansley Lecture. Small is beautiful: The picophytoplankton. Functional Ecology 12, 503–513.

Raven, J.A., Waite, A.M., 2004. The evolution of silicification in diatoms: Inescapable sinking and sinking as escape? New Phytologist 162, 45–61.

Riebesell, U., Zondervan, I., Rost, B., Tortell, P.D., Zeebe, R.E., Morel, F.M.M., 2000. Reduced calcification of marine plankton in response to increased atmospheric CO2. Nature 407, 364–366.

Ruddiman, W.F., 2008. Earth's climate: past and future. Earth's climate : past and future.

Salamy, K.A., Zachos, J.C., 1999. Latest Eocene-Early Oligocene climate change and Southern Ocean fertility: Inferences from sediment accumulation and stable isotope data. Palaeogeography, Palaeoclimatology, Palaeoecology 145, 61–77.

Salaviale, C., Gollain, B., Mattioli, E., 2018. Calcareous nannofossil fluxes and size fluctuations in the middle Eocene (48–39 Ma) from Ocean Drilling Program (ODP) Site 1209 in the tropical Pacific Ocean. Palaeogeography, Palaeoclimatology, Palaeoecology 490, 240–251.

Sarmiento, J.L., Gruber, N., Brzezinski, M.A., Dunne, J.P., 2004. High-latitude controls of thermocline nutrients and low latitude biological productivity. Nature 427, 56–60.

Sauermilch, I., Whittaker, J.M., Klocker, A., Munday, D.R., Hochmuth, K., Bijl, P.K., LaCasce, J.H., 2021. Gateway-driven weakening of ocean gyres leads to Southern Ocean cooling. Nature Communications 12, 1–8.

Scher, H.D., Whittaker, J.M., Williams, S.E., Latimer, J.C., Kordesch, W.E.C., Delaney, M.L., 2015. Onset of Antarctic Circumpolar Current 30 million years ago as Tasmanian Gateway aligned with westerlies. Nature 523, 580–583.

Schneider, L.J., Bralower, T.J., Kump, L.R., 2011. Response of nannoplankton to early Eocene ocean destratification. Palaeogeography, Palaeoclimatology, Palaeoecology 310, 152–162.

Schumacher, S., Lazarus, D., 2004. Regional differences in pelagic productivity in the late Eocene to early Oligocene—a comparison of southern high latitudes and lower latitudes. Palaeogeography, Palaeoclimatology, Palaeoecology 214, 243–263.

Shackleton, N., 1967. Oxygen isotope analyses and pleistocene temperatures re-assessed. Nature 215, 15–17.

Shackleton, N.J., 2000. The 100,000-year ice-age cycle identified and found to lag temperature, carbon dioxide, and orbital eccentricity. Science 289, 1897–1902.

Shackleton, N.J., Hall, M.A., Pate, D., Meynadier, L., Valet, J.P., 1993. High resolution stable isotope stratigraphy from bulk samples. Paleoceanography 8, 141–148.

Shackleton, N.J., Kennett, J.P., 1975. Paleotemperature history of the Cenozoic and the initiation of Antarctic glaciation: oxygen and carbon isotope analysis in DSDP sites 277, 279, and 281. Initial Report of the Deep Sea Drilling Project 29, 743–755.

Shannon, C.E., Weaver, W., 1949. The Mathematical Theory of Communication. University of Illinois Press, Champaign, IL.

Sheldon, N.D., Costa, E., Cabrera, L., Garcés, M., 2012. Continental climatic and Weathering Response to the Eocene-Oligocene transition. Journal of Geology 120, 227–236.

Sheldon, N.D., Grimes, S.T., Hooker, J.J., Collinson, M.E., Bugler, M.J., Hren, M.T., Price, G.D., Sutton, P.A., 2016. Coupling of marine and continental oxygen isotope records during the Eocene-Oligocene transition. Bulletin of the Geological Society of America 128, 502–510.

Snyder, S.W., Muller, C., Miller, K.G., 1984. Eocene-Oligocene boundary: Biostratigraphic recognition and gradual paleoceanoghraphic change at DSDP Site 549. Geology 12, 112–115.

Spray, J.F., Bohaty, S.M., Davies, A., Bailey, I., Romans, B.W., Cooper, M.J., Milton, J.A., Wilson, P.A., 2019. North Atlantic evidence for a unipolar icehouse climate state at the Eocene-Oligocene Transition. Paleoceanography and Paleoclimatology 2019PA003563.

Stehlin, H.G., 1909. Remarques sur les faunules de Mammiferes des couches Eocenes et Oligocenes du Bassin de Paris. Bulletin de la Societe Geologique de France 29, 488–520.

Stickley, C.E., Brinkhuis, H., Schellenberg, S.A., Sluijs, A., Röhl, U., Fuller, M., Grauert, M., Huber, M., Warnaar, J., Williams, G.L., 2004. Timing and nature of the deepening of the Tasmanian Gateway. Paleoceanography 19, 1–18.

Sun, J., Ni, X., Bi, S., Wu, W., Ye, J., Meng, J., Windley, B.F., 2014. Synchronous turnover of flora, fauna, and climate at the Eocene-Oligocene Boundary in Asia. Scientific Reports 4, 1–6.

Sutherland, R., Dickens, G.R., Blum, P., Agnini, C., Alegret, L., Bhattacharya, J., Bordenave, A., Chang, Li., Collot, J., Cramwinckel, M.J., Dallanave, E., Drake, M.K., Etienne, S.J.G., Giorgioni, M., Gurnis, M., Harper, D.T., Huang, H., Keller, A.L., Lam, A.R., Li, H., Matsui, H., Morgans, H.E.G., Newsam, C., Park, Y.H., Pascher, K.M., Pekar, S.F., Penman, D.E., Saito, S., Stratford, W.R., Westerhold, T., Zhou, X., 2019. Site U1509. Tasman Frontier Subduction Initiation and Paleogene Climate. Proceedings of the International Ocean Discovery Program, 371: College Station, TX (International Oce 371.

Toffanin, F., Agnini, C., Rio, D., Acton, G., Westerhold, T., 2013. Middle eocene to early oligocene calcareous nannofossil biostratigraphy at IODP site U1333 (equatorial pacific). Micropaleontology 59, 69–82.

Tremolada, F., De Bernardi, B., Erba, E., 2008. Size variations of the calcareous nannofossil taxon Discoaster multiradiatus (Incertae sedis) across the Paleocene-Eocene thermal maximum in ocean drilling program holes 690B and 1209B. Marine Micropaleontology.

Tripati, A., Backman, J., Elderfield, H., Ferretti, P., 2005. Eocene bipolar glaciation associated with global carbon cycle changes. Nature 436, 341–346.

Urey, H.C., 1947. The thermodiynamic properties of isotopic substances. Journal of the Chemical Society (London) 562–581.

Van Andel, T.H., 1975. Mesozoic/cenozoic calcite compensation depth and the global distribution of calcareous sediments. Earth and Planetary Science Letters 26, 187–194.

Van Mourik, C.A., Brinkhuis, H., Mourik, C.A. Van, Brinkhuis, H., 2005. The Massignano Eocene-Oligocene golden spike section. Stratigraphy 2, 13–30.

Vandenberghe, N., Hilgen, F.J., Speijer, R.P., 2012. The Paleogene period. In: Gradstein, F.M., Ogg, J.C., Schmitz, M.D., Ogg, G.M. (Eds.), The Geological Timescale 2012. Amsterdam: Elsevier, p. 855–922.

Villa, G., Fioroni, C., Pea, L., Bohaty, S.M., Persico, D., 2008. Middle Eocene-late Oligocene climate variability: Calcareous nannofossil response at Kerguelen Plateau, Site 748. Marine Micropaleontology 69, 173–192.

Villa, G., Fioroni, C., Persico, D., Roberts, A.P., Florindo, F., 2014. Middle Eocene to Late Oligocene Antarctic glaciation/deglaciation and Southern Ocean productivity. Paleoceanography 29, 223–237.

Villa, G., Florindo, F., Persico, D., Lurcock, P., de Martini, A.P., Jovane, L., Fioroni, C., 2021. Integrated calcareous nannofossil and magnetostratigraphic record of ODP Site 709: Middle Eocene to late Oligocene paleoclimate and paleoceanography of the Equatorial Indian Ocean. Marine Micropaleontology 169, 102051.

Villa, G., Persico, D., 2006. Late Oligocene climatic changes: Evidence from calcareous nannofossils at Kerguelen Plateau Site 748 (Southern Ocean). In: Palaeogeography, Palaeoclimatology, Palaeoecology. Elsevier, p. 110–119.

Villa, G., Persico, D., Bonci, M.C., Lucchi, R.G., Morigi, C., Rebesco, M., 2003. Biostratigraphic characterization and Quaternary microfossil palaeoecology in sediment drifts west of the Antarctic Peninsula - Implications for cyclic glacial-interglacial deposition. Palaeogeography, Palaeoclimatology, Palaeoecology 198, 237–263.

Wade, B.S., Houben, A.J.P., Quaijtaal, W., Schouten, S., Rosenthal, Y., Miller, K.G., Katz, M.E., Wright, J.D., Brinkhuis, H., 2012. Multiproxy record of abrupt sea-surface cooling across the Eocene-Oligocene transition in the Gulf of Mexico. Geology 40, 159–162.

Wade, B.S., Pearson, P.N., 2008. Planktonic foraminiferal turnover, diversity fluctuations and geochemical signals across the Eocene/Oligocene boundary in Tanzania. Marine Micropaleontology 68, 244–255.

Wei, W., 1991. Middle Eocene-lower Miocene calcareous nannofossil magnetobiochronology of ODP Holes 699A and 703A in the subantarctic South Atlantic. Marine Micropaleontology 18, 143–165.

Wei, W., 2004. Opening of the Australia-Antarctica Gateway as dated by nannofossils. Marine Micropaleontology 52, 133–152.

Wei, W., Wise, S.W., 1990. Biogeographic gradients of middle Eocene-Oligocene calcareous nannoplankton in the South Atlantic Ocean. Palaeogeography, Palaeoclimatology, Palaeoecology 79, 29–61.

Wei, W.C., Villa, G., Wise, S.W., Wuchang Wei, Villa, G., Wise, S.W., 1992. Paleoceanographic implications of Eocene-Oligocene calcareous nannofossils from Sites 711 and 748 in the Indian Ocean. Proceedings of the Ocean Drilling Program, 120 Scientific Results 120, 979–999.

Westerhold, T., Marwan, N., Drury, A.J., Liebrand, D., Agnini, C., Anagnostou, E., Barnet, J.S.K., Bohaty, S.M., De Vleeschouwer, D., Florindo, F., Frederichs, T., Hodell, D.A., Holbourn, A.E., Kroon, D., Lauretano, V., Littler, K., Lourens, L.J., Lyle, M.W., Pälike, H., Röhl, U., Tian, J., Wilkens, R.H., Wilson, P.A., Zachos, J.C., 2020. An astronomically dated record of Earth's climate and its predictability over the last 66 million years. Science 369, 1383–1388.

Wilson, D.S., Pollard, D., Deconto, R.M., Jamieson, S.S.R., Luyendyk, B.P., 2013. Initiation of the West Antarctic Ice Sheet and estimates of total Antarctic ice volume in the earliest Oligocene. Geophysical Research Letters 40, 4305–4309.

Winter, A., Jordan, R.W., Roth, P.H., 1994. Biogeography of living coccolithophores in ocean waters. In: Winter, A., Siesser, W.G. (Eds.), Coccolithophores. Cambridge University Press, Cambridge, p. 161–177.

Yang, S., Galbraith, E., Palter, J., 2014. Coupled climate impacts of the Drake Passage and the Panama Seaway. Climate Dynamics 43, 37–52.

Young, D.A., Wright, A.P., Roberts, J.L., Warner, R.C., Young, N.W., Greenbaum, J.S., Schroeder, D.M., Holt, J.W., Sugden, D.E., Blankenship, D.D., Van Ommen, T.D., Siegert, M.J., 2011. A dynamic early East Antarctic Ice Sheet suggested by ice-covered fjord landscapes. Nature 474, 72–75.

Young, J.R., Geisen, M., Probert, I., 2005. A review of selected aspects of coccolithophore biology with implications for paleobiodiversity estimation. Micropaleontology 51, 267–288.

Zachos, J.C., Dickens, G.R., Zeebe, R.E., 2008. An early Cenozoic perspective on greenhouse warming and carbon-cycle dynamics. Nature 451, 279–283.

Zachos, J.C., Kump, L.R., 2005. Carbon cycle feedbacks and the initiation of Antarctic glaciation in the earliest Oligocene. Global and Planetary Change.

Zachos, J.C., Pagani, M., Sloan, L., Thomas, E., Billups, K., 2001. Trends, Global Rhythms, and Aberrations in Global Climate 65 Ma to Present. Science 292, 686–693.

Zachos, J.C., Quinn, T.M., Salamy, K.A., 1996. High-resolution (10^4 years) deep-sea foraminiferal stable isotope records of the Eocene-Oligocene climate transition. Paleoceanography 11, 251–266.

Zachos, J.C., Rea, D.K., Seto, K., Nomura, R., Niitsuma, N., 1992. Paleogene and Early Neogene Deep Water Paleoceanography of the Indian Ocean as Determined from Benthic Foraminifer Stable Carbon and Oxygen Isotope Records. In: Duncan, R.A., Rea, D.K., Kidd, R.B., Rad, U. von, Weissel, J.K. (Eds.), Synthesis of Results from Scientific Drilling in the Indian Ocean, Volume 70. American Geophysical Union, p. 351–385.

Zanazzi, A., Kohn, M.J., MacFadden, B.J., Terry, D.O., 2007. Large temperature drop across the Eocene-Oligocene transition in central North America. Nature 445, 639–642.

Zhang, Y.G., Pagani, M., Liu, Z., Bohaty, S.M., DeConto, R.M., 2013. A 40-million-year history of atmospheric CO_2. Philosophical Transactions of the Royal Society 1–20.

Chapter 2

Calcareous nannofossils across the Eocene-Oligocene transition at Site 756 (Ninetyeast Ridge, Indian Ocean): implications for biostratigraphy and paleoceanographic clues[1]

Abstract. The timing and modalities of calcareous phytoplankton community and evolutionary responses to the Eocene-Oligocene transition (EOT, ~ 34 Ma) are still under investigated. In order to better constrain the dynamics of these pelagic primary producers during the climate transition, we conducted high resolution assemblage analysis on calcareous nannofossils across a ~19 m-thick interval of nannofossil ooze at Ocean Drilling Program (ODP) Site 756 (Ninetyeast Ridge, Indian Ocean; Peirce et al., 1989) (paleolatitude ~43°S; Zachos et al., 1992). We explored the diversity patterns against a new integrated planktonic foraminifera and calcareous nannofossil biostratigraphy produced for the site, as well as new benthic foraminifera stable isotope (C, O) record, which documents ocean-climate changes, and provides independent chemostratigraphy.
The study section spans nannofossil Zones NP20-NP23 (equivalent to CNE20-CNO4) and lasts 5.6 Myr.
The results show that the hankeninid extinction falls within the ~4.5 m-thick EOT isotopic interval (0.67 m below the base of the second positive $\delta^{18}O$ shift - EOIS), which is consistent with previous works, making Hole 756C one of a few sites globally boasting both the familiar stepped $\delta^{18}O$ and $\delta^{13}C$ structure of the EOT and the primary biostratigraphic marker defining the base of the Oligocene. A series of potentially useful new calcareous nannofossil bioevents were identified that could help improve dating and correlation of this crucial interval. In this context, changes in calcareous nannofossil assemblages observed across EOT are interpreted in terms of modifications of paleoecological parameters that typically control the abundance and distribution of different taxa. Variations in sea surface temperature and nutrient availability are considered to be the most likely triggers for the calcareous phytoplankton changes observed across EOT. Specifically, our data suggest that increased nutrients in the mixed layer played a key role in shaping the late Eocene - early Oligocene calcareous nannofossil assemblages.

Keywords: calcareous nannofossils, biostratigraphy, paleoecology, Eocene-Oligocene transition, ODP Hole 756C.

[1] Allyson Viganò[1*], Helen K. Coxall[2], Max Holmström[2], Martina Vinco[1], Caroline Lear[3], Claudia Agnini[1]
[1]Dipartimento di Geoscienze, Università di Padova, Via Gradenigo 6 – 35131, Padova, Italy;
[2]Department of Geological Sciences, Stockholm University, SE-106 91 Stockholm, Sweden;
[3]School of Earth and Environmental Sciences, Cardiff University, Main building, Park Place, Cardiff CF10 3AT, UK

Authors contributions: A.V. and C.A. designed the study and developed the methodology. A.V. was responsible for data creation and presentation. A.V. and C.A. were the project administrator. M.H. and M.V. have collected data. H.K.C. and C.L. provided the samples used in this study. H.K.C. and C.A. have provided laboratories techniques and instrumentation for analysis. A.V. wrote the original draft. C.A. and H.K.C. have provided editings and revisions on the original draft and C.L. provided comments and suggestions.
All the co-authors discussed the data and agreed on their interpretation and contributed to the final polishing of the manuscript.
Submitted to *Newsletters on Stratigraphy* journal.

2.1 Introduction

The Eocene-Oligocene transition denotes a period of profound change during the Cenozoic and coincides with the onset of permanent ice caps on Antarctica (e.g. Coxall and Pearson, 2007; Hutchinson et al., 2021).

The transition from a largely ice-free greenhouse world (Eocene) to an icehouse climate (Oligocene) characterized by a major glaciation on the South Pole and global cooling (e.g. Zachos et al., 2001) is documented by diverse geological evidence from around the world including glacio-marine deposits, sea water cooling, ice growth, sea-level fall, calcite compensation depth (CCD) deepening and important extinction and turnover in the marine biota (Pälike et al., 2006; 2012; Coxall and Pearson, 2007; Pearson et al., 2008;, Coxall and Wilson, 2011; Hutchinson et al., 2021). During this time, the marine ecosystem suffered a variety of abrupt modifications - e.g. major turnovers were observed in radiolarians and diatoms (Baldauf, 1992; Funakawa et al., 2006; Moore et al., 2014), planktonic foraminifera (Diester-Haass and Zahn, 2001; Pearson et al., 2008; Wade and Pearson, 2008; Wade and Olsson, 2009) and calcareous nannofossils (Dunkley Jones et al., 2008; Bordiga et al., 2015; Jones et al., 2019), dramatic extinctions have been documented in large benthic foraminifera (Cotton and Pearson, 2011), diverse proxies recorded variations in the global carbon cycling, productivity (Coxall and Pearson, 2007) and silica supply (Egan et al., 2013; Fontorbe et al., 2017).

The possible triggers for the EOT are still lively debated and include different mechanisms: (1) the opening of the southern oceanic gateways, the Drake Passage and the Tasman Gateway, which led to the initiation of the Antarctic Circumpolar current (ACC) and the thermal isolation of Antarctica (Kennett, 1977), (2) a long-term decrease in atmospheric pCO_2 (DeConto and Pollard, 2003) that associated an eccentricity minimum and a low-amplitude obliquity, eventually promoted cooler summers – inhibiting ice, accumulated during the winter season, from melting (Coxall et al., 2005), or (3) a combination of the two (e.g. Drake Passage opening resulting in reduced pCO_2), as recently suggested by Lear and Lunt (2016).

Strong evidence for ice expansion comes from a two-stepped positive shift documented in benthic (1.5‰) and planktonic (~1‰) foraminiferal oxygen stable isotopes ($\delta^{18}O$) (Coxall et al., 2005; Coxall and Wilson, 2011). Following the terminology recently proposed by Hutchinson et al. (2021), these two steps are here referred to as “Step 1” and “EOIS”, and all together constitute the EOT, which is bounded at the base by the extinction of calcareous nannofossil *Discoaster saipanensis*. The Eocene-Oligocene boundary (EOB) appears to fall in the plateau between the two isotopic steps, although only a limited number of studies have sufficiently well preserved planktonic foraminifera records and benthic foraminifera $\delta^{18}O$ and $\delta^{13}C$ to document this pattern and none, thus far from the pelagic Indian Ocean (Coxall and Pearson, 2007; Dunkley Jones et al., 2008; Pearson et al., 2008; Coxall and Wilson, 2011; Hutchinson et al., 2021). The phase following the EOT and characterized by maximum $\delta^{18}O$ values, is here denoted as the ‘Early Oligocene Glacial Maximum’ (EOGM; Liu et al., 2004; Hutchinson et al., 2021).

It is commonly accepted that the changes in $\delta^{18}O$, observed during the Eocene-Oligocene transition, reflect variations both in ice-volume and sea water temperature (Zachos et al., 2001). In order to quantify the contribution of ice-volume signal from $\delta^{18}O$ record, Lear et al. (2008) have provided a $\delta^{18}O$-independent SST record from the Tanzanian planktonic Mg/Ca paleothermometry. According to this study, the initial planktonic $\delta^{18}O$ step (Step 1) coincides with a decrease in Mg/Ca value (equivalent to ~2.5 °C cooling), recently

corroborated by Bohaty et al. (2012), instead the second $\delta^{18}O$ step (EOIS) primarily reflects the expansion of the Antarctic cryosphere.

The stepwise pattern documented in $\delta^{18}O$ seems to be associated, with a 10 kyr lag, to a perturbation in the benthic and planktonic foraminiferal $\delta^{13}C$ records. The positive excursion in $\delta^{13}C$, as well as the deepening of the CCD, have been proposed to be related to an increased sea surface productivity and consequent enhanced global burial of organic carbon in the deep sea, which would have caused an abnormally high storage of ^{12}C in the sediments (Zachos et al., 1996; Salamy and Zachos, 1999; Zachos and Kump, 2005; Coxall et al., 2005; 2018; 2021; Merico et al., 2008; Ravizza and Paquay, 2008; Coxall and Wilson, 2011; Bordiga et al., 2015; Armstrong Mckay et al., 2016; Jones et al., 2019; López-Quirós et al., 2021).

More recently, a shelf-to-basin shift in marine carbonate deposition in response to the sea level fall has been hypothesized as an additional mechanism behind the shift in $\delta^{13}C$ toward more positive values (Merico et al,. 2008; Pälike et al., 2012) coupled to the sequestration of ^{12}C-enriched carbon into carbon capacitors (e.g. permafrost and marine methane hydrates) and possibly increased ocean ventilation (Armstrong Mckay et al., 2016).

A commonly held opinion is that the greenhouse-to-icehouse transition might have coincided with the onset of Arctic-imprinted North Component Water (NCW) mass, the ancient precursor of the North Atlantic Deep Water (NADW), which in turn probably impacted the poleward heat transport in both hemispheres (Davies et al., 2001; Via and Thomas, 2006; Abelson and Erez, 2017; Coxall et al., 2018).

Changes in deep water circulation, as a consequence of differences in temperature and salinity, the so-called thermohaline circulation, are fundamental to understand the evolution of climate because they are at the base of the very complicated balances and fluxes between deep waters and upper and mixed ocean layers.

Among the marine plankton, planktonic foraminifera were deeply affected during this time and suffered several losses. Wade and Pearson (2008) reported the abrupt extinction of all five remaining planktonic foraminifera species of the family Hantkeninidae, which formally defines the Eocene-Oligocene boundary (EOB; Premoli Silva and Jenkins, 1993). The extinction of *Hantkenina* has been associated with a period of profound climate instability and increased nutrients in the photic zone (Pearson and Coxall, 2014).

Unlike planktonic foraminifera, calcareous nannoplankton experienced a major turnover and a distinct shift toward less diverse assemblages rather than dramatic extinctions at the boundary.

To date, calcareous nannofossil response still lacks a global perspective and only few high-resolution studies are available for the EOT at high (Southern Ocean; Persico and Villa, 2004; Villa et al., 2008; 2014) and low-middle latitudes (Tanzania, Dunkley Jones et al., 2008; South Atlantic, Bordiga et al., 2015; Equatorial Indian Ocean, Fioroni et al., 2015, Villa et al., 2021; Indonesia, Jones et al., 2019). From a biostratigraphic point of view, the E-O transition is characterized by a low rate of evolution which is reflected in a scarcity of useful calcareous nannofossil biohorizons (Raffi et al., 2016). In some cases, the ranking and spacing of some bioevents, but also their quality and reliability, are still ambiguous and need to be further evaluated (Agnini et al., 2014). From a paleoecological perspective, the environmental pressure seems to have triggered important changes in the relative abundance of calcareous nannofossil species/taxa, diversity index, community structure and ecology. The present work focuses on three main goals: (1) to document ocean, climate and biotic

responses in the eastern Indian Ocean at high-resolution across the Eocene-Oligocene transition at Site 756 (ODP Leg 121), (2) to potentially refine the number and position of calcareous nannofossil bioevents during this crucial time for future correlations over wide areas, (2) to provide a paleoecological interpretation based on abundance variations and distributions of calcareous nannofossil genera in order to reconstruct the characteristics of the sea surface waters in terms of temperature and productivity

2.2 Material and methods

2.2.1 ODP Site 756

Sediments documenting the Eocene-Oligocene transition (EOT) were retrieved in the eastern Indian Ocean during ODP Leg 121 (Peirce et al., 1989). ODP Site 756 is the southern end member of a north-south paleoceanographic transect of seven sites drilled on Broken Ridge and Ninetyeast Ridge. At this site, a 227 m-thick section was drilled at four holes (A-D) and spans from the upper Eocene through Pleistocene. The drilling was terminated after penetrating 82 m of volcanic basalt in Hole 756D (Peirce et al., 1989b). The lithostratigraphic units (reported as meter below seafloor, mbsf) comprises: Subunit IA (0-144.5 m; nannofossils and foraminifera ooze), Subunit IB (144.5-150.3 m; foraminifera limestone) and Unit II (150.3-221.0 m; composed of vesicular basalts) (Peirce et al., 1989). Importantly, the drilled Paleogene carbonate ooze sequence contains a continuous sequence across the Eocene-Oligocene boundary, and is thus suitable to carry out a high-resolution study. Many other open-ocean E/O sequences are either incomplete or poorly preserved (Hutchinson et al., 2021 and references therein). In this study we analyzed samples from Hole 756C, which is located at 27°21.25'S, 87°35.89'E, in a water depth of 1516 m, near the crest of Ninetyeast Ridge (Figure 2.1).

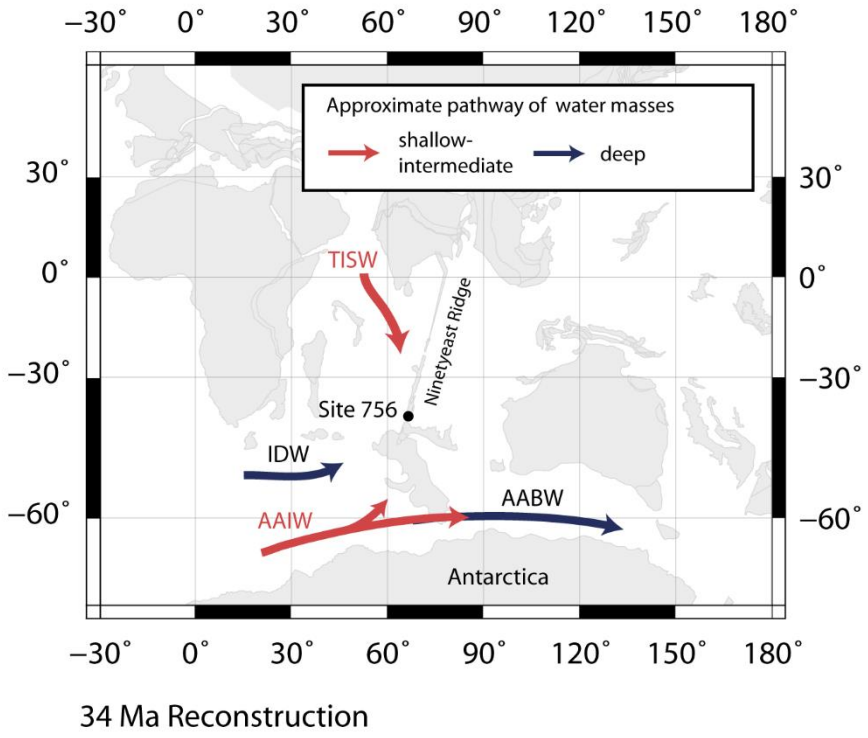

Figure 2.1 Location of ODP Site 756 shown on a paleomap (Mercator projection) at 34 Ma, reconstruction from http://www.odsn.de/ The approximate pathway of shallow-intermediate and deep waters masses during the EOT, as inferred from Zachos et al. (1992), is also shown. IDW = Indian Deep Water; AAIW=Antarctic Intermediate Water; AABW = Antarctic Bottom Water; TISW = Tethyan-Indian saline water.

The investigated material belongs to the Subunit IA (0-144.5 m) and consists of a white nannofossil ooze with foraminiferal content varying between 5% and 20%. Trace amounts of radiolarians, sponge spicules, and silicoflagellates occur throughout the ooze (Peirce et al., 1989). The samples analyzed span from 113.46 to 132.70 mbsf, with an average spacing of ~20 cm and a temporal resolution of ca. 55kyr.

2.2.2 Geological setting and Indian Ocean paleoceanography

During the Eocene, the Ninetyeast Ridge, today situated at a lower bathyal depth and bathed by Indian Central Water (Sverdrup et al., 1942), was influenced by several water masses operating simultaneously: the Indian Deep Water (IDW), the warm low-latitude Tethyan-Indian saline water (TISW, likely originating from the Tethyan or northern Indian Ocean) probably very similar in character to present day intermediate waters from the Arabian and Red seas, and possibly by other cold high latitude water masses, i.e. the Antarctic Intermediate Water (AAIW) and Antarctic Bottom Water (AABW) (Zachos et al., 1992).

ODP Site 756 has an estimated paleodepth of ~400 m (Zachos et al., 1992) and was likely bathed by the TISW. The reconstructed paleolatitude indicate a significantly further South position (~43°S) during the Eocene relative to the present day (~7°S) (Zachos et al., 1992). During the study interval, this site thus represents an intermediate biogeographic domain located between low-middle and high latitudes (Figure 2.1).

At the onset of the Oligocene, the two shallow-intermediate water-masses (TISW and AAIW) were still flowing in the Indian Ocean, but are thought to experience a significant cooling related to the early Oligocene onset of the Antarctica ice-cap. During the E-O transition, the cool AABW was likely reinforced by a more vigorous circulation promoted by the onset of Antarctica, and eventually lead to the upwelling of nutrient rich waters (Zachos et al., 1996) and to a further cooling (~2-3°) of deep-surface (thermocline) waters (Bohaty et al., 2012). Moreover, the location of this site on a southeastern slope with irregular topography might have favored the direct upwelling of these deeper water masses (Nomura, 1991).

2.2.3 Calcareous nannofossil data

Counts on the calcareous nannofossil assemblages have been carried out on a total of 102 samples, prepared using standard smear slide technique (Bown and Young, 1998). Smear slides were analyzed using a Zeiss optical microscope, at 1250× magnification, in cross-polarized (XPL) and phase-contrast (PC) light. Calcareous nannofossils were identified to species/genus level, depending on coccolith preservation.

For an instance, the overgrowth of *Discoaster* and the etching of *Chiasmolithus* in some cases prevent the identification at species level. With few exceptions, the taxonomy adopted is that of Aubry (1984, 1988, 1989), Perch-Nielsen (1985), Bown (2005), Bown and Dunkley Jones (2012) and Bown and Newsam (2017).

In particular, in accordance with Romein (1969), we ascribe *formosa* to genus *Ericsonia* (Agnini et al., 2014). We also separate genus *Dictyococcites* from genus *Reticulofenestra* to maintain these genera as distinct taxonomic units (Agnini et al., 2014; Fornaciari et al., 2010; Perch-Nielsen, 1985).

We define *Reticulofenestra umbilicus* using the morphometric definition of Backman and Hermelin (1986), which includes specimens > 14μm. Relative abundance (%) data (Dataset S1) have been collected for species and genera based on counts of at least 300 specimens per sample (Pospichal, 1991). Semi-quantitative

abundance of selected taxa (Dataset S2) was determined by counting the number of specimens in a prefixed area (n/mm^2; Backman and Shackleton, 1983). This method allows to catch in detail the occurrence of selected taxa, even those showing a sporadic occurrence (Agnini et al., 2014). The position of biostratigraphic and isotopic tie-points were compiled to construct an age-depth model for Hole 756C and calculate LSRs, based on the Geological Time Scale 2012 (GTS2012; Gradstein et al., 2012).

Principal component analysis (PCA), based on the correlation matrix (Q-mode; variables normalized with respect to variance), was performed on a set of relative abundance data, for a total of 13 taxa (Dataset S3), using the statistical software Past (Paleontological Statistic; Hammer et al., 2001).

PCA is a descriptive and explorative method that allows us to reduce the redundancy of the dataset producing a two-dimensional representation of the samples (Hammer and Harper, 2006). This approach facilitates the visualization of our data, helping us to detect the major loading genera and to investigate the main environmental factors affecting changes on calcareous nannofossil assemblage. Shannon's index (H) was used to quantify the diversity of nannoplankton for each sample, with low values indicating lower species richness and high values corresponding to dominance assemblages (Shannon and Weaver, 1949). Microphotos of markers species, as well as several calcareous nannofossil taxa, are provided (Plate 2.1, 2.2, 2.3).

2.2.4 Foraminifera sample preparation and planktonic foraminifera biostratigraphic analysis

A total of 122 x 20 cc sand-fraction samples were prepared for foraminifera analysis. Bulk sediment samples were first disaggregated in deionized water on a shaker table at 175 rpm for at least one hour. The suspended sample was then poured onto a 63µm mesh sieve and washed with deionized water to separate the sand size particles. The >63µm residues were dried in an oven at 50 °C overnight before being transferred to labelled glass vials for storage. Planktonic foraminiferal biostratigraphy was based on assemblage-counts performed on a subset of fifty-three of the samples. Here we focus on documentation of the position of relevant EOT biostratigraphic markers only, especially species of *Hantkenina*, *Globigerinatheka, Pseudohastigerina* and *Turborotalia*. Full planktonic foraminiferal assemblage counts are not reported here. Assemblages were examined using a Zeiss binocular stereo light microscope. Taxonomic determinations follow Pearson et al. (2006) and Wade et al. (2018). Counts were based on the standard 300-specimen approach. Samples were first reduced to a split containing several hundred whole planktonic foraminifera specimens using a microsplitter (Shaw, 1964). For the counting, each split sample was randomly strewn on a picking tray with a numbered grid (squares from 1 to 45). In order to reach the 300-specimen target, a random number generator was used to select grid squares. The order generated was followed until approximately 300 planktonic foraminifera specimens had been counted. This was repeated for both the >180 µm and 63 µm fractions. For the extinction of *Hantkenina*, which denotes the E/O boundary (Premoli Silva and Jenkins, 1993), additional (non-quantitative) scouring of the whole samples was performed to pin-down the event (>180µm and 63 µm fractions). Selected planktonic and benthic foraminifera were imaged using the scanning electron microscopes (SEM) installed at the Department of Geological Sciences (IGV), Stockholm University to document important taxa and test preservation states (Plate 2.4).

2.2.5 Geochemical analyses

Bulk stable isotope data and $CaCO_3$ content. Bulk carbon and oxygen stable isotopes ($\delta^{13}C$ and $\delta^{18}O$) and calcium carbonate content (% $CaCO_3$) (Dataset S4) were analyzed using a Thermo Scientific Delta V Advantage spectrometer equipped with a Gas Bench II device at the Department of Geosciences (University of Padova). A known mass of sample (~0.30 mg) was weighed using the precision balance Mettler Toledo AT21 and placed into vials, subsequently flushed with helium. Each sample was then treated with 10 ml of orthophosphoric acid (EMSURE ® ≥ 99 %) for ca. 3 hours before the mass spectrometer analysis. Isotopic values are reported in standard delta notation relative to the Vienna Pee Dee Belemnite (VPDB). Raw $\delta^{13}C$ and $\delta^{18}O$ values were normalized through an internal standard (white Carrara marble Maq1: $\delta^{13}C$ = 2.58‰; $\delta^{18}O$= −1.15‰VPDB) periodically calibrated to NBS-19 IAEA reference material (Coplen et al., 2006).
For quality assurance, we used another internal standard, named as marble Gr1 ($\delta^{13}C$ = 0.68‰; $\delta^{18}O$= −10.44‰ VPDB). The CO_2 beam height (mV), which is a function of the carbonate content of the sample (Spofforth et al. 2010), was obtained during the mass spectrometer analysis. To calculate the carbonate content of each sample, a ramp of at least 10 samples of Maq1 (with weights ranging from 0.050 to 0.500 mg) was distributed along the run, and used to construct a linear fit (with R^2= 0.99).

Benthic foraminifera stable C and O isotopes. Benthic foraminifera were picked from the 250-500 µm fraction of the sand-sized sample set (see above for sample preparation). 122 monospecific samples were prepared, comprising the epifaunal species *Cibicidoides mundulus* and *Cibicidoides havanensis.*
The *C. mundulus* and *C. havanensis* sample sets were generated at different times (2014 and 2015 respectively); *C. havanensis* is more consistently present in the upper part of the studied section. Comparison of the data for the different species shows minimal differences, thus we present an integrated species record (Dataset S5) for our EOT chemostratigraphy. Benthic foraminifera taxonomy followed Morkhoven et al. (1986) and Nomura et al. (1991). Test preservation was determined as moderate to well-preserved.
For each sample, 2-3 specimens were analysed to provide a target weight of 0.1-0.3 mg $CaCO_3$, as determined by the detection limits of the mass spectrometer. Sample weights were determined using a Sartorius MC5 microbalance (0.001 mg resolution). Benthic $\delta^{13}C$ and $\delta^{18}O$ was measured at Stockholm University using a Thermo Scientific MAT252 mass spectrometer attached to a GasBench II flow preparation and inlet system. An offline preparation step involved first drying the samples in an oven at 50° to remove any excess water before flushing the vials with helium. Each sample was reacted with 100 µl of 99% phosphoric acid before introduction to the mass spectrometer. Isotopic values were calibrated against the international standard VPDB. The reproducibility was determined to be 0.07‰ for $\delta^{13}C$ and 0.15‰ for $\delta^{18}O$.

2.3 Results

2.3.1 Biostratigraphy

Abundance patterns of index calcareous nannofossil species obtained from semi-quantitative counts (Figure 2.3) were used to biostratigraphically frame the succession with reference to the biohorizons proposed in standard (Martini, 1971; Okada and Bukry, 1980) and additional biozonations (Agnini et al., 2014) (Figure 2.2).

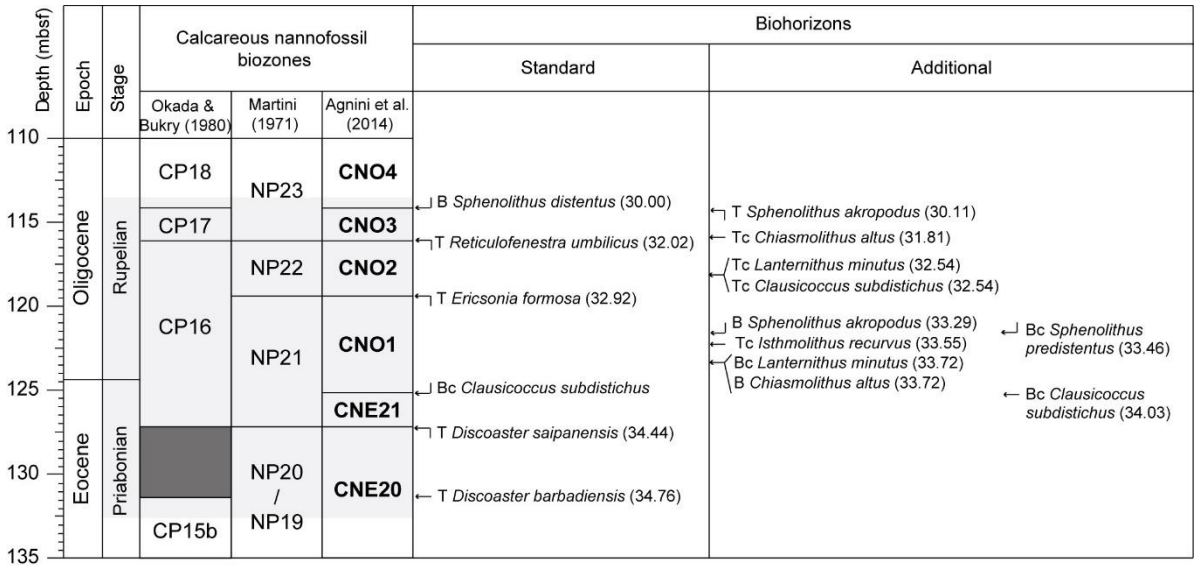

Figure 2.2 Biostratigraphic classification of the study succession at Hole 756C based on calcareous nannofossils. The adopted schemes are those of Okada and Bukry 1980 (CP), Martini, 1971 (NP) and Agnini et al., 2014 (CNE). Biohorizons are also indicated and defined as B (Base), Bc (Base common), T (Top), Tc (Top common). Biochronological estimations calibrated to the GTS12 are provided. Chronostratigraphy is also plotted along depth (mbsf).

Biohorizons have been labelled according to published Cenozoic calcareous nannofossil biozonations (Backman et al., 2012; Agnini et al., 2014; Raffi, et al., 2016) as follows: Base (B; stratigraphic lowest occurrence of a taxon), Top (T; stratigraphic highest occurrence of a taxon), Base common and continuous (Bc) and Top common and continuous (Tc), respectively the lowest and highest common and continuous occurrence of a taxon.

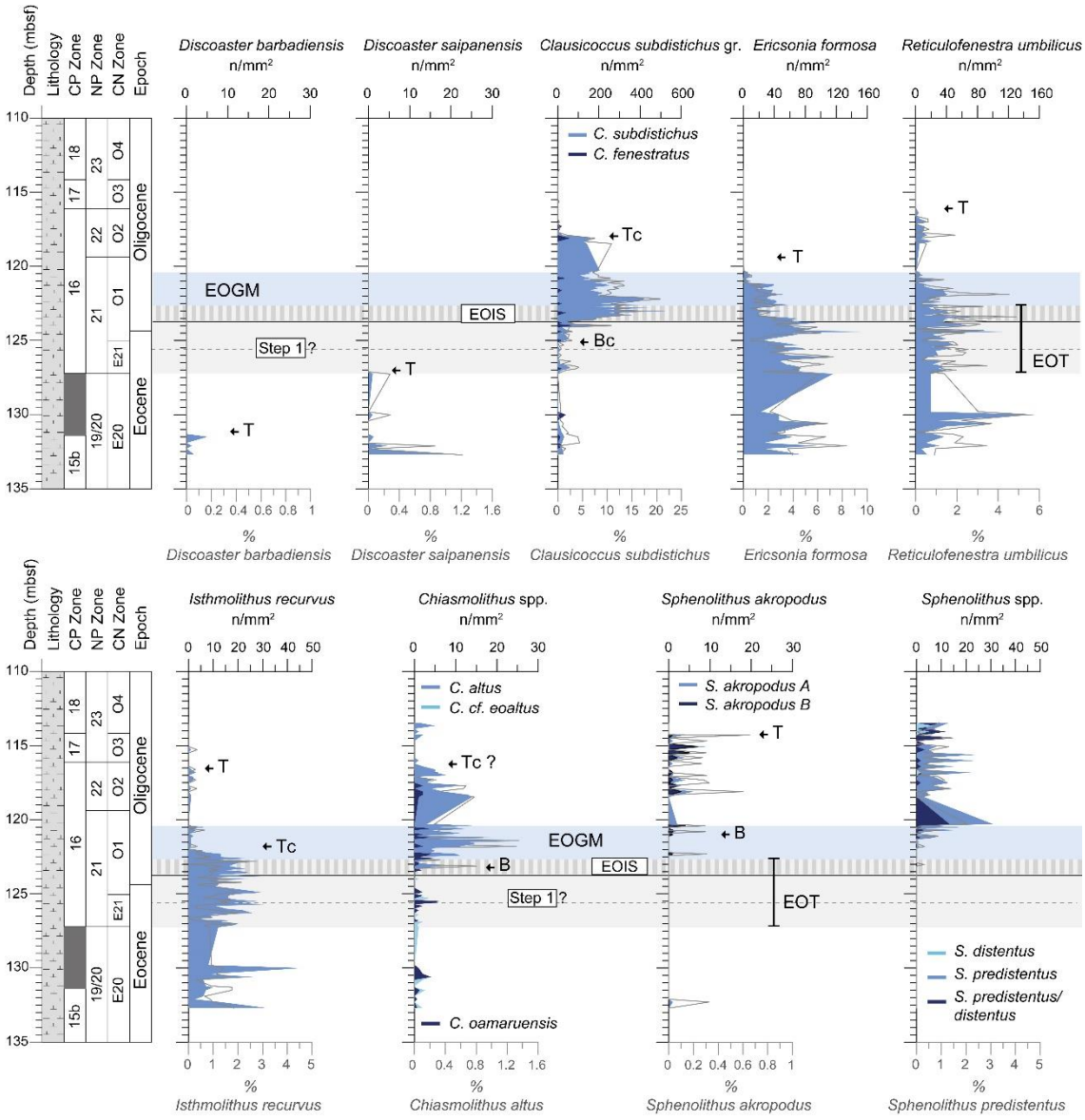

Figure 2.3 Semi-quantitative (n/mm²) and relative (%, grey line) abundance patterns of biostratigraphically significant taxa from Hole 756C are plotted versus depth (mbsf), lithology, calcareous nannofossil biostratigraphy (NP, Martini, 1971; CP, Okada and Bukry, 1980; CN, Agnini et al., 2014) and chronostratigraphy. Events are termed as: B = Base, Bc= Base common and continuous, T = Top, Tc= Top common and continuous. The EOGM (light blue bar) and EOT (grey bar) are also reported and refer to the oxygen stable isotopes results from paragraph 2.3.2.

At Hole 756C, three planktonic foraminifera bioevents were recognized: the Top (T) of *Globigerinatheka index*, the Top of *Hantkenina* (comprising *H. alabamensis* and *H. primitva*), and the Top of large (>180µm) *Pseudohastigerina* (Table 2.1). In particular, we find the Top of *G. index* at 126.8 mbsf. It is recorded again in a sample 2 meters above this level (124.80 mbsf) (Dataset S6). However, the preservation is poor here and its possible that this is reworked or a misidentified dentoglobigerinid, which can look rather similar. We therefore take the lower level for the Top *G. index* event. It is also noted that there is a shift to a *'Dentoglobigerina taci'*-type assemblage above this horizon. Hantkeninids, belonging to the species *H. alabamensis* and *H. primitiva* only, are not common at Site 756 (<1%). However, they are extremely distinctive, biostratigraphically critical

thus worth hunting down. The highest occurrence of *Hantkenina* in our count data is at 125.0 mbsf. More detailed scouring of the whole samples around this horizon, including in the >63 µm fraction where sometimes broken tubulospines are the only remaining trace, pinned the Top *Hantkenina* spp. event down to 124.50 mbsf. *Pseudohastigerina micra* and *P. naguewichiensis* are also rare (Plate 2.4. Figs. 15-20) but persistent throughout the section. Significantly, at 127.0 mbsf, *Pseudohastigerina* no longer occurs in the >180 µm fraction but continues in the <63 µm fraction (Dataset S6). This we interpret as the '*Pseudohastigerina* dwarfing' event recognized previously (Nocchi et al., 1986; Wade and Pearson, 2008). We are unable to place the *Turborotalita cerroazulensis-cunialensis* group extinction due to the absence of this group at Site 756.

Table 2.1 Datum Type		**Interval (hole-core-section, cm)**		**Top sample (mbsf)**	**Base sample (mbsf)**	**Mid-point (mbsf)**	**Error (mbsf)**	**Age (Ma) GTS12**	**Sed. rate (cm kyr^{-1})**	**Age (Ma) This study**
	Event	**Top sample**	**Base sample**							
CN	**B *S. distentus***	756C-5X-5W, 60.0-63.0	756C-5X-5W, 79.0-81.0	114.06	114.25	**114.16**	0.09	**30.00**		
CN	T *S. akropodus*	756C-5X-5W, 79.0-81.0	756C-5X-6W, 0.0-2.0	114.25	114.28	114.27	0.02		0.10	30.11
CN	Tc *C. altus*	756C-5X-7W, 20.0-22.0	756C-5X-7W, 40.0-42.0	115.81	116.01	115.91	0.10		0.10	31.81
CN	**T *R. umbilicus***	756C-5X-7W, 40.0-42.0	756C-5X-7W, 60.0-62.0	116.01	116.21	**116.11**	0.10	**32.02**		
CN	T *I. recurvus*	756C-5X-7W, 79.0-81.0	756C-5X-7W, 100.0-102.0	116.40	116.61	116.51	0.10		0.36	32.13
CN	Tc *L. minutus*	756C-5X-8W, 79.0-81.0	756C-5X-8W, 100.0-102.0	117.90	118.10	118.00	0.10		0.36	32.54
CN	Tc *C. subdistichus*	756C-5X-8W, 79.0-81.0	756C-5X-8W, 100.0-102.0	117.90	118.10	118.00	0.10		0.36	32.54
CN	**T *E. formosa***	756C-5X-CCW, 10.5-12.5	756C-6X-1W, 10.0-12.0	118.47	120.30	**119.38**	0.92	**32.92**		
CN	B *S. akropodus*	756C-6X-1W, 80.0-82.0	756C-6X-1W, 90.0-92.0	121.00	121.10	121.05	0.05		0.46	33.29
CN	Bc *S. predistentus*	756C-6X-2W, 10.0-12.0	756C-6X-2W,19.5-21.5	121.80	121.90	121.85	0.05		0.46	33.46
CN	Tc *I. recurvus*	756C-6X-2W, 50.0-52.0	756C-6X-2W, 60.0-62.0	122.20	122.30	122.25	0.05		0.46	33.55
IS	**T EOIS**					**122.71**		**33.65**		
CN	Bc *L. minutus*	756C-6X-2W, 142.0-144.0	756C-6X-3W, 10.0-12.0	123.12	123.30	123.21	0.09		0.69	33.72
CN	B *C. altus*	756C-6X-2W, 142.0144.0	756C-6X-3W, 10.0-12.0	123.12	123.30	123.21	0.09		0.69	33.72
PF	**T *Hantkenina***	756C-6X-3W, 102.5-104.5	756C-6X-3W, 129.5-131.5	124.23	124.50	**124.37**	0.13	**33.89**		
CN	Bc *C. subdistichus*	756C-6X-4W, 30.0-32.0	756C-6X-4W, 41.5-43.5	125.00	125.12	125.06	0.06		0.51	34.03
PF	T *G. index*	756C-6X-5W, 40.0-42.0	756C-6X-5W, 60.0-22.0	126.60	126.80	126.70	0.10		0.51	34.35
PF	*T Pseudohastigerina* (>180 µm)	756C-6X-5W, 80.0-82.0	756C-6X-CC W, 10.0-12.0	127.00	127.25	127.13	0.13		0.51	34.43
CN	**T *D. saipanensis***	756C-6X-5W, 90.0-92.0	756C-6X-CCW, 10.0-12.0	127.10	127.25	**127.18**	0.08	**34.44**		
CN	**T *D. barbadiensis***	756C-7X-2W, 19.0-21.0	756C-7X-2W, 0.0-2.0	131.30	131.49	**131.40**	0.09	**34.76**		

Table 2.1 Position (in mbsf) of calcareous plankton (calcareous nannofossils, planktonic foraminifera *Hantkenina, P. micra* and *G. index*) and geochemical events at ODP Hole 756C. The grey bars represent the tie-points (in bold) used in the construction of the age model. The ages of tie-points were assigned using the Geological Time Scale calibration ages (GTS12, Gradstein et al. 2012). Other investigated bioevents are calculated by applying linear interpolation between tie-points, assuming constant sedimentation rates. Datum type is also reported: CN (calcareous nannofossil), PF (planktonic foraminifera) and IS (oxygen stable isotopes).

In the following, the calcareous nannofossil bioevents identified in this study are discussed and listed in stratigraphic order.

We do not further explore planktonic foraminifera events, except with respect to the stable isotope records (below).

The Top of *Discoaster barbadiensis* and *Discoaster saipanensis*

The extinction of *D. saipanensis* marks the base of Zone NP21 (Martini, 1971), whereas the extinction of both *D. saipanensis* and *D. barbadiensis* are proposed to be used to mark the base of Subzone CP16a (Okada and Bukry, 1980). In Agnini et al. (2014) the Top of *D. saipanensis* defines the base of Zone CNE21.

The Top of *D. saipanensis* (Plate 2.3, Figs. 3-5) and *D. barbadiensis* (Plate 2.3, Fig. 2) are calibrated at 34.44 Ma and 34.77 Ma, respectively (Blaj et al., 2009). As expected, at Hole 756C, the Top of *D. barbadiensis* and *D. saipanensis* occurred before the Eocene-Oligocene boundary (EOB), which was reported at 124.365 ± 0.13 mbsf. The Top of *D. saipanensis* is observed at a depth of 127.18 mbsf, whereas the Top of *D. barbadiensis* falls at a depth of 131.40 mbsf. This datum indicates that their extinctions are closely spaced.

The disappearance of these taxa dramatically modifies the discoaster assemblage that in the early Oligocene is characterized by a lower diversity and the dominance of few species ascribable to the flower-shape discoasters (e.g., *D. deflandrei, D. tanii* and *D. tanii nodifer).* These taxa will remain the dominant species within this genus for all the Oligocene and part of the Miocene (Young, 1998).

The acme of *Clausiccocus subdistichus* group

At Hole 756C, we have merged *C. subdistichus* and *C. fenestratus* into a single informal group, named as *C. subdistichus* group (Figure 2.3). The Bc of *C. subdistichus* (Plate 2.1, Figs. 13, 14) is considered a potential reliable bioevent that allows to approximate quite well the Eocene-Oligocene boundary (EOB), being constantly found in the upper part of Chron C13r (e.g. Tethyan region, Coccioni et al., 1988; Southern Ocean, Marino and Flores, 2002; Hyland et al., 2009; Equatorial Pacific, Toffanin et al., 2013; NW Atlantic, Norris et al., 2014).

In Agnini et al. (2014), the Bc of *C. subdistichus* (33.88 Ma) marks the base of Zone CN01 which corresponds to upper Zone NP21. At Hole 756C, *C. subdistichus* becomes common and continuous (Bc) at 125.06 mbsf shortly below the EOB (124.37 mbsf). The estimated age for the Bc *of C. subdistichus* at Hole 756C is slightly older (34.03 Ma). It should be noted that the gradual and scattered increase in abundance of *C. subdistichus* makes it difficult to properly recognize and place this event, making any site-to-site correlation challenging.

The end of the acme interval (Tc) of *Clausicoccus subdistichus* defines the base of the Subzone CP16b in Okada and Bukry (1980). At ODP Hole 756C, the Tc of *C. subdistichus* is a neat event, characterized by a sharp decrease in abundance of the species (from 166 to 23 n/mm^2), occurring at 118 mbsf and shortly afterward the extinction (T) of *Ericsonia formosa* (119.38 mbsf). Our datum perfectly agrees with the ranking reported for the Top of *E. obruta* (= *C. subdistichus*) by Backman (1987) in the South Atlantic.

However, this result is in disagreement with previous data indicating that the Tc of *C. subdistichus* (33.43 Ma) should precede the disappearance of *E. formosa* (Berggren et al., 1995). Comparing all the data available, this event displays a certain degree of discrepancy and further high-resolution investigations in different depositional settings are needed in order to evaluate the reliability of the event, especially considering that some of previous results are qualitative and/or use old poor-quality age models (Perch-Nielsen, 1986; Moran and Watkins, 1988; Nocchi et al., 1988; Catanzariti et al., 1997).

The Top of *Ericsonia formosa*

The Top of *Ericsonia formosa* defines the base of Zone NP22 and Subzone CP16c (Martini, 1971; Okada and Bukry, 1980). The extinction of *E. formosa* (Plate 2.1, Fig. 12) marks the base of Zone CNO2 and has an estimated age of 32.92 Ma (Agnini et al., 2014). This biohorizon is generally easily recognizable in terms of abundance decline (Backman, 1987) and represents a highly reliable event at low-middle latitudes where occurs from the uppermost C13n and lower C12r (Berggren et al., 1995; Marino and Flores, 2002). *Ericsonia formosa* disappeared very early from the southern high latitudes, in association with the polarity Chronozone C18, and thus is considered strongly diachronous between low-middle and high latitudes (Berggren et al., 1995). At ODP Hole 756C, *E. formosa* has a continuous and abundant pattern and its final extinction occurs at 119.38 mbsf.

The observed abundance pattern is well comparable with previous data available from equatorial Pacific Ocean (Blaj et al., 2009; Toffanin et al., 2013) and South Atlantic (Bordiga et al., 2015) confirming the high reliability of this event. At Hole 756C, the disappearance of *E. formosa* precedes the Top common of *C. subdistichus*.

The Top of *Reticulofenestra umbilicus*

The disappearance of *R. umbilicus* (Plate 2.1, Figs. 1, 2) defines the base of Zone CP17 and Zone NP23 (Martini, 1971; Okada and Bukry, 1980). In Agnini et al. (2014), the Top of *R. umbilicus* is used to define the base of Zone CNO3 and has an estimated age of 32.02 Ma. Zone CNO3 corresponds to the lower part of Zone NP23 (Martini, 1971) and to Zone CP17 (Okada and Bukry, 1980). This event is diachronous between low-middle and southern high latitudes (Berggren et al., 1995; Marino and Flores, 2002).

At ODP Hole 756C, the abundance pattern of *R. umbilicus* shows a high variability, and the final part of its range is characterized by a gradual decrease with the last occurrence of the species observed at 116.11 mbsf.

The Top of *R. umbilicus* seems to be a quite good bioevent, though the low abundances observed toward the end of its range could make the precise positioning of this biohorizon difficult.

The Base of *Sphenolithus distentus*

In Okada and Bukry (1980) the appearance (B) of *Sphenolithus distentus* (Plate 2.3, Figs. 15-16) defines the base of Zone CP18, which corresponds in Martini (1971) to the upper part of Zone NP23. In Agnini et al. (2014), the Base of *S. distentus* marks the base of Zone CNO4 with an estimated age of 30.0 Ma. At ODP Hole 756C, the Base of *S. distentus* is recognized at 114.16 mbsf. It is worth to note that the close spacing between the Top of *R. umbilicus* (115.81 mbsf) and the Base of *S. distentus* (114.16 mbsf) indicate a decrease in LSR and indicates a condensed Zone CP17.

2.3.2 Geochemical data

Bulk stable isotopes ($\delta^{13}C$ and $\delta^{18}O$) and calcium carbonate (% $CaCO_3$) have been compared along with deep sea benthic foraminifera (i.e., *Cibicidoides havanensis* and *Cibicidoides mundulus*) isotopes data, calcareous nannofossil genera and diversity index (Figure 2.4). Both bulk and benthic stable isotopes display the two-stepped oxygen isotope pattern described for complete successions (e.g. Hutchinson et al., 2021), suggesting that the EOT is well recorded at Ninetyeast Ridge.

Benthic stable isotope record. Benthic $\delta^{18}O$ varies between a 0.23‰ and 1.47‰, with a mean value of 0.91‰ and a standard deviation (σ) of 0.31‰ (Figure 2.4). Overall, the $\delta^{18}O$ trend shows a progressive increase from the base of the section upward, with a first positive step (step 1) starting at 127.1 mbsf and lasting up to 125.92 mbsf (initial increase of ~0.6 ‰). A second positive shift (EOIS) is located at 123.70 mbsf and ends at 122.71 mbsf (increase of 0.97‰). Above, $\delta^{18}O$ values remain relatively high and constant (122.71 mbsf - 120.4 mbsf), forming a plateau that is consistent with the EOGM (Earliest Oligocene Glacial Maximum; Hutchinson et al., 2021). Benthic $\delta^{13}C$ values range between 0.72‰ and 1.93‰ with a mean value of 1.24‰ ± 0.27‰ (σ).
Key features of the curve are a minimum in $\delta^{13}C$ at 126.40 mbsf (0.72 ‰), corresponding with a minimum in $\delta^{18}O$ (0.55‰), with $\delta^{13}C$ increasing thereafter in parallel with the stepped $\delta^{18}O$ pattern, to produce a temporary maximum in $\delta^{13}C$, as is typical in deep marine EOT records. Unlike the $\delta^{18}O$, from 122.30 mbsf the benthic $\delta^{13}C$ gradually returns to a new baseline of ca. 1-1.2‰. Shorter term variability in $\delta^{18}O$ and $\delta^{13}C$ on the order of 0.1-0.2‰, hints at cyclicity, although the resolution of the record is at the limits of being able to resolve this.

Bulk stable isotope record and carbonate content. The Hole 756C bulk carbonate $\delta^{18}O$ and $\delta^{13}C$ records are very similar to the benthic records in structure, although the absolute values are a little offset (0.18 and 0.31, respectively). Bulk $\delta^{18}O$ varies between 0.10‰ and 1.19‰, with a mean value of 0.73‰ ± 0.28‰ (σ).
$\delta^{13}C$ values range between 1.13‰ and 1.95‰ with a mean value of 1.55‰ and a standard deviation of ± 0.22‰. The mean $\delta^{18}O$ value (0.37‰) on the lower part of the study section (127.25-132.70 mbsf), is lower if compared with the average values calculated for rest of the section (0.80‰). The EOIS bulk $\delta^{18}O$ increase is much more pronounced compared to Step 1. Moreover, while $\delta^{18}O$ 'Step 1' is not apparent where we might expect it to be, there is a clear bulk $\delta^{13}C$ increase at the 'Step-1' level, as predicted using the nannofossil definition of the base of the EOT (127.18 mbsf). In fact, like the benthic $\delta^{18}O$ record, if there is a 'Step-1' $\delta^{18}O$ increase it seems to occur at the base of Zone E21. Bulk $\delta^{13}C$ in contrast shows the same positive excursion centered around the EOGM as the benthic record.
The succession is characterized by generally high $CaCO_3$ content, ranging between 59% and 100%, with an average value of 81%. The high values documented during the early Oligocene are in agreement with previous data from the Pacific Ocean that have been interpreted as the result of a dramatic deepening of CCD and the consequent increased availability of carbonate sea water ions $(CO_3)^{2-}$ (Coxall et al., 2005), although due to much shallower paleodepths (ca. 400 m) it is unclear whether this relative increase in $CaCO_3$ is the result of ocean carbonate chemistry changes or changes in the contribution of other sediment types.

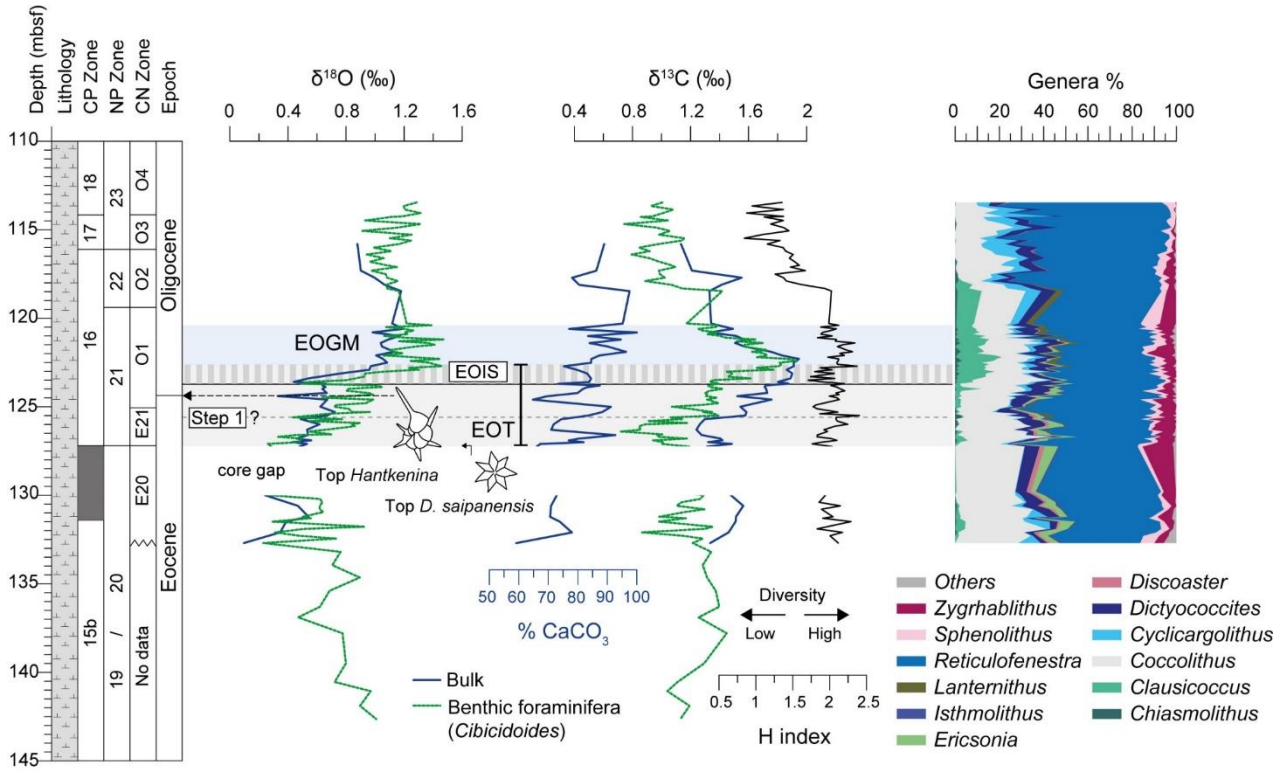

Figure 2.4 $\delta^{18}O$ (‰), $CaCO_3$ (%), $\delta^{13}C$ (‰), H index, cumulative percentage of calcareous nannofossils genera from ODP Hole 756C plotted against depth (mbsf), lithology, calcareous nannofossil biozones (NP, Martini, 1971; CP, Okada and Bukry, 1980; CN, Agnini et al., 2014) and chronostratigraphy. Benthic foraminiferal stable isotopes were analyzed on *Cibicidoides havanensis* and *C. mundulus.* We highlight the EOT-shift as well as the two $\delta^{18}O$ steps (horizontal grey bar) using the terminology of Hutchinson et al. (2021). The early Oligocene $\delta^{18}O$ maximum, referred to as the Early Oligocene Glacial Maximum (EOGM) is denoted by a light blue bar.

2.3.3 Planktonic assemblages

Planktonic foraminifera. The Hole 756C samples contain relatively diverse (20-30 species) assemblages of planktonic foraminifera. The most common species belong to the genera *Dentoglobigerina* and *Subbotina,* with *D. galavisi* and *S. utilusindex* being most common throughout the section. *Catapsydrax unicavus* and *Globorotaloides suteri* are additional common components. *Globigerinahteka index* (Plate 2.4, Fig. 6) is abundant between 137.8-130.21 mbsf, accompanied by lower numbers of *G. tropicalis* and *G. luterbacheri*. Hantkeninids, represented by the species *H. alabamensis* (Plate 2.4., Figs. 1-3) and *H. primitiva* only, are scarce and the *Turborotalita cerroazulensis-cunialensis* group, common elsewhere in the tropics and sub-tropics (Nocchi et al., 1986; Katz et al., 2008; Pearson et al., 2008; Edgar et al., 2020 Coxall et al., 2021; Wade et al., 2021) is virtually absent. The less angular/more globular relatives *Turborotalita ampliapertura* and *T. increbescens* are, however, common (Plate 2.4, Figs. 8 and 9). The fine sand fraction 63-150 µm contains abundant *Chiloguembelina ototara* and common *Tenuitella gemma* throughout (Plate 4, Figs. 10-14). In these respects, the Hole 756C assemblages appear transitional between the late Eocene-Oligocene Southern Ocean assemblages found on the Kerguelen Plateau (Huber, 1991) and the more diverse tropical Indian Ocean assemblages (e.g. Pearson et al., 2008).

Calcareous nannofossils. Calcareous nannofossils are common to abundant throughout the studied interval, showing a general decrease in diversity (H index) in the Oligocene samples (Figure 2.4). The Shannon's index values calculated for the study succession are relatively low ($0.84 \leq H \leq 2.40$). This is partially the result of the fact that not all the specimens have been determined at species level, but rather grouped into larger taxonomic units (see Appendix II for details). However, the H index shows a certain degree of variability during the EOT and a remarkable decline after the EOGM. The lower heterogeneity and evenness of the assemblages during the Oligocene reflect a community structure with a few dominant taxa (*Reticulofenestra, Coccolithus* and *Clausicoccus*). The preservation varies from moderate to good and dissolution and/or overgrowth seems to have minimally affected the assemblages, as these processes are not pervasive in the study material. There is no obvious change in preservation state through the section.

At ODP Hole 756C, *Reticulofenestra* is the dominant genus throughout all the studied interval (33.2-78.2%), with a relative abundance showing a gradual and relatively small increasing trend toward the top of the succession (Figure 2.5). Conversely, *Coccolithus* (8.3-40.4%) displays an opposite trend with highly variable abundances recorded across the EOT. *Cyclicargolithus* (0-2.76%) shows a gradual increase in abundance across the EOT which persists throughout the lower Oligocene. *Clausicoccus*, *Dictyococcites* and *Zyghrablithus* display similar abundances varying from 0 to ca. 20%. Specifically, *Clausicoccus* (0-20.8%; primarily represented by *C. subdistichus* and *C. fenestratus*) displays a sudden peak of abundance (acme) above the EOB followed by remarkable high values persisting during the EOGM.

Dictyococcites (0.6-14.0%) (*D. bisectus, D.* aff. *D. bisectus, D. hesslandii, D. filewiczii*) shows an increase in abundance in the first step while the pattern becomes highly variable during the second step (EOIS) but overall, it does not display any dramatic change in the study interval. *Zyghrablithus* (0-13.9%) is continuously present and well preserved, the abundance pattern shows a general decrease across the EOT.

The most common taxon among *Sphenolithus* (0.9-8.7%) is *S. moriformis* group but the sphenolith assemblages display relatively high diversity including *S. akropodus*, *S. predistentus, S. predistentus-distentus* transitional forms*, S. distentus* and very sporadic occurrences of *S. radians, S. tribulosus* and *S. intercalaris*.

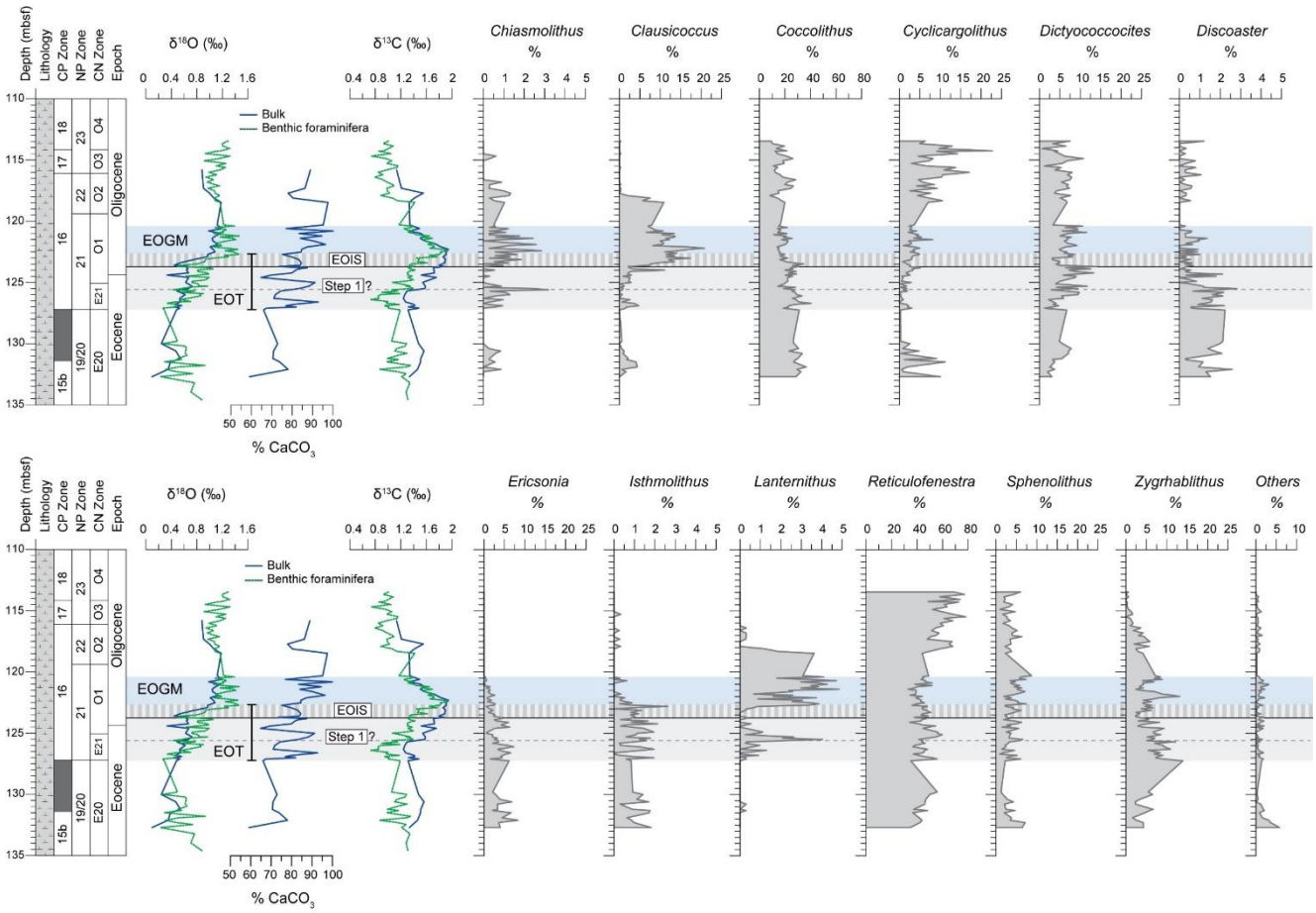

Figure 2.5. Nannofossil genera (%) are compared along with geochemical data ($\delta^{18}O$‰, $CaCO_3$%, $\delta^{13}C$ ‰) from Hole 756C. Data are plotted against depth (mbsf), lithology, calcareous nannofossils biostratigraphy (NP, Martini, 1971; CP, Okada and Bukry, 1980; CN, Agnini et al., 2014) and chronostratigraphy. The horizontal grey bar indicates the two positive steps in $\delta^{18}O$ recognized at the EOT and the light blue bar indicates the maximum values of $\delta^{18}O$ (EOGM).

Genus *Ericsonia* (0-8.3 %) shows a general decrease in abundance across the two steps that eventually led to its extinction. A minor but interesting component of the assemblages is *Lanternithus* (0-5%), which is rare and scattered during the late Eocene and becomes more common and abundant in the early Oligocene.

Other genera that occurred less frequently are *Chiasmolithus* (0-3.2%), *Discoaster* (0-2.8%, mainly represented by *D. tani gr.*) and *Isthmolithus* (0-2.62%). Discoasters are usually affected by diagenetic overgrowth, and, thus, several specimens could not be confidently identified at species level.

Genera with sporadic occurrences have been reported as 'others' (0-5.8%) and include: *Coronocyclus, Helicosphaera, Pontosphaera, Thoracosphaera, Umbilicosphaera*, reworked and undetermined nannofossils.

2.3.4 Age-depth model

The age-depth model (Figure 2.6) for the Eocene-Oligocene section of Hole 756C was developed using the position of calcareous nannofossil events with additional control provided by the top of the planktonic foraminifera *Hantkenina* and the Top of EOIS. Tie-points were placed at midpoints (mbsf) between bounding samples and their ages were assigned using the Geological Time Scale 2012 calibration ages (GTS12; Gradstein et al., 2012) (Table 2.1). The maximum LSR of 1.3 cm kyr^{-1} was recorded in the late Eocene (132.7-127.18 mbsf). During the EOT and EOGM, we have recorded an average LSR of 0.6 cm kyr^{-1} (127.18-119.38 mbsf). Our data indicate a gradual decrease of LSRs during the Oligocene with LSR of 0.4 cm/kyr from 119.39 to 116.11 mbsf and a very low LSR of 0.1 cm kyr^{-1} in the upper interval (from 116.11 to 113.4 mbsf). If we assume that linear sedimentation rate has remained constant during this latter interval, this extremely low value of LSR (0.1 cm kyr^{-1}) denotes an extremely condensed Oligocene sequence. Otherwise, LSR might have been higher than the estimated value (>0.1 cm kyr^{-1}) during part of the range and zero for the remaining interval, inferring the presence of a *hiatus*. Even if this second hypothesis is likely from a stratigraphic point of view, from a biostratigraphic perspective the succession is complete since the bioevents (i.e. the Base of *S. distentus* and the Top of *R. umbilicus*) are slightly spaced. Based on the identified bioevents described above, the sedimentary section corresponds to the time interval from 34.86 to 29.27 Ma (5.6 Myr).

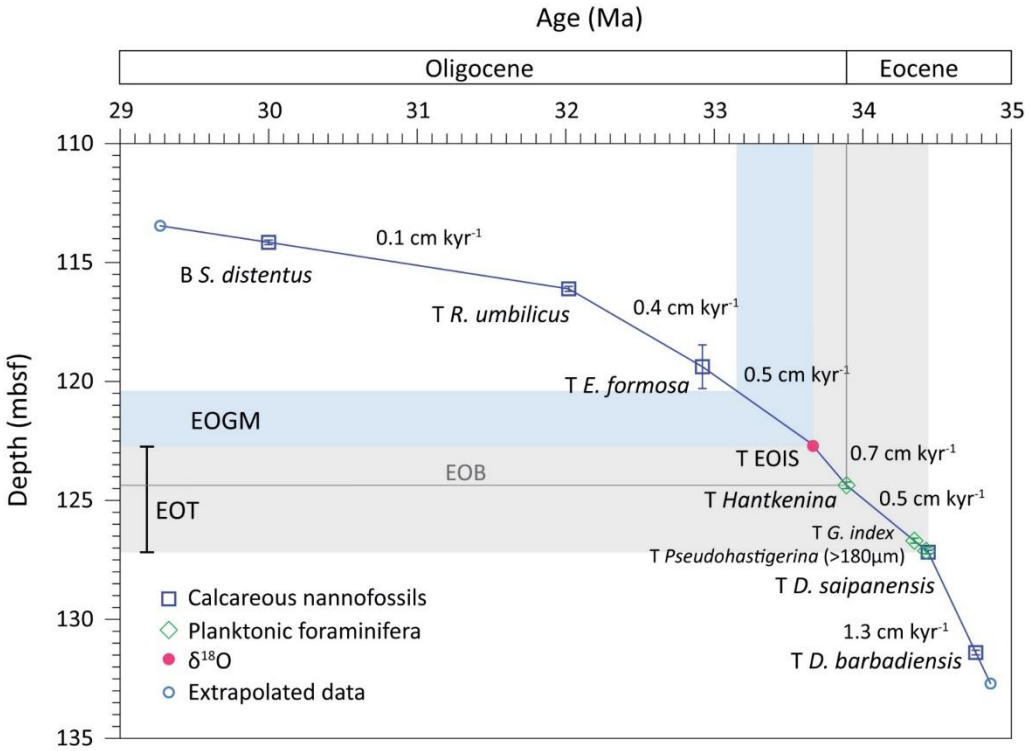

Figure 2.6 Age-depth plot and sedimentation rates across the E-O transition, Hole 756C. Tie-points ages are based on calcareous nannofossil datums (blue squares), planktonic foraminifera *Hantkenina* spp. extinction (green diamond) and EOIS (magenta circle). The position of the T of *G. index* and pseudohastigerinid dwarfing event (green diamonds) are also reported in the plot but they were not included in the age-model. Symbols are shown with error bars in the depth domain, representing the lowermost and uppermost depths of biohorizons. See Table 1 for data points. EOGM, EOB and EOT are also shown.

2.3.5 Principal component analysis

Our multivariate dataset consists of points (= samples) in a high multidimensional space projected down to a two-dimensional plot. The PCA analysis allows us to identify and interpret the axes of maximal variance (principal components) of our dataset, which are linear combinations of the original variables.

Results from PCA at ODP Hole 756C provide two significant principal component which explain 49.8% (PC1 27.88%; PC2 21.96%) of the total variance in our dataset. The screen plot reported in Figure 2.7 shows where the variance explained (%) by each component starts to flatten out. Beyond that point, we have excluded the other components, that are possibly related to a "noise" component. The loadings of each component (PC1 and PC2 loadings) represent the contribution of each variable (% genus) to the component.

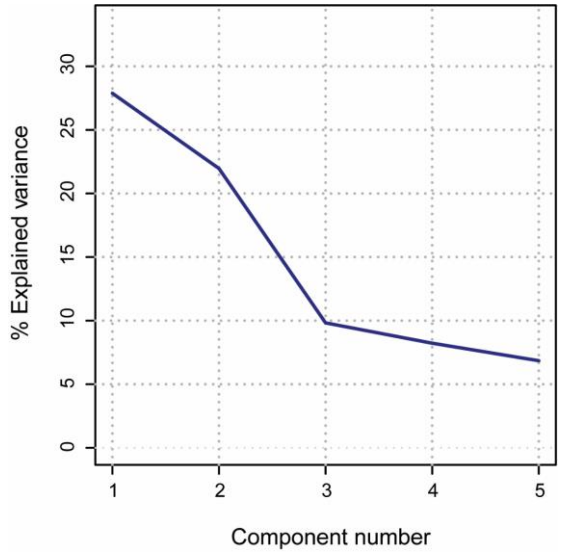

Figure 2.7 Screen plot from PCA, showing the relative importance of the principal components (PCs) in terms of explained variance.

PC1 is positively loaded by *Ericsonia* (0.44), *Coccolithus* (0.38), *Discoaster* (0.34), *Zygrhablithus* (0.33), *Isthmolithus* (0.31) and negatively only by *Reticulofenestra* (-0.40) and *Cyclicargolithus* (-0.36).

The most meaningful genus loading on PC2 is *Lanternithus* (positively loading 0.51), but it is also loaded positively by *Clausicoccus* (0.47), *Chiasmolithus* (0.36) and *Sphenolithus* (0.35). PC2 is negatively loaded by *Coccolithus* (-0.24), *Reticulofenestra* (-0.24), *Ericsonia* (-0.19), *Discoaster* (-0.18). The loadings of the other genera are extremely low and are not further considered (Figure 2.8).

A four-way separation of samples was used in order to recognize changes in the composition of the assemblage in the PCA biplot through time**:** late Eocene, EOT (defined by samples belonging to the E-O transition, Step 1 and EOIS), EOGM (samples characterized by maximum $\delta^{18}O$ values) and Oligocene (marked by samples above the EOGM) (Figure 2.8).

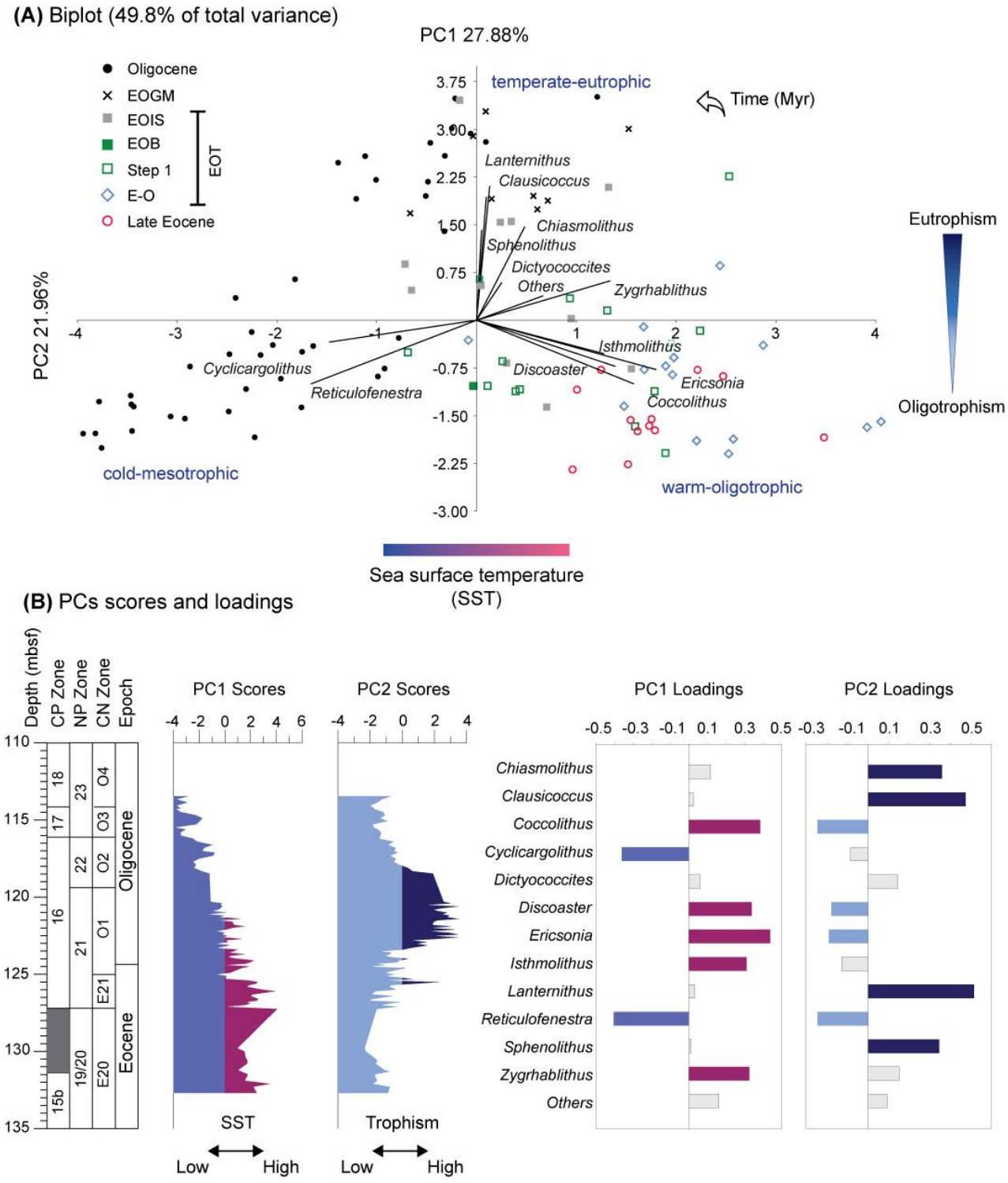

Figure 2.8 Results of principal component analysis (PCA; correlation matrix) based on calcareous nannofossil assemblage from ODP Site 756. (A) PCA biplot showing PC1 (interpreted as sea surface temperature SST) and PC2 (interpreted as trophic conditions). Samples are divided in: "Late Eocene", "EOT", "EOGM" and "Oligocene" based on the position of the isotopic shifts. (B) Principal component scores and loadings of calcareous nannofossil taxa on the two principal components. Data are plotted against depth (mbsf), calcareous nannofossil biozones (NP, Martini ,1971; CP, Okada and Bukry, 1980; CN, Agnini et al., 2014) and chronostratigraphy.

2.4 Discussion

2.4.1 Site 756 stable isotope and biostratigraphy

In the few sites world-wide containing both the *Hantkenina* spp. extinction and having a reliable stable isotope record, the extinction of *Hantkenina* spp. has been found occurring between the two successive isotopic shifts (Coxall and Pearson, 2007; Pearson et al., 2008; Hutchinson et al., 2021). The position of the Top of *Hantkenina* spp. at Hole 756C is generally in excellent agreement with previous data (Figure 2.4), implying that while hantkeninids survived the ocean climate changes associated with the high-latitude cooling at Step 1 (Bohaty et al., 2012), they were unable to adapt to subsequent environmental disruptions. There is no temporary $\delta^{18}O$ increase in the late Eocene, suggesting that the 'late Eocene (glaciation) Event' found elsewhere (Hutchinson et al., 2021), is not recorded or falls in the interval of the coring/recovery gap (Figure 2.4). The benthic foraminifera $\delta^{18}O$ and $\delta^{13}C$ shows a rather clear signal of stepped isotopic change, with a magnitude comparable to other sites and consistent with the global ice volume increase (Hutchinson et al., 2021). Although bulk carbonate and benthic foraminifera $\delta^{18}O$ records show strong similarities (Figure 2.4), minor offsets exist between these two signals. This is consistent with the idea that bulk carbonate stable isotopes primarily reflect mixed layer ocean conditions (Reghellin et al., 2015). At Hole 756C, the first bulk $\delta^{18}O$ increase (Step 1) is not as clear as that derived from benthic foraminiferal, suggesting limited sea-surface cooling at this step compared to the cooler deep waters bathing the seafloor. In contrast, the second positive $\delta^{18}O$ shift (EOIS) is sharp and synchronous in both bulk and benthic foraminifera records, consistent with a major ice expansion on Antarctica and significant glacial activity in the early Oligocene.

2.4.2 Calcareous nannofossil biostratigraphy remarks

The biozonations of Martini (1971) and Okada and Bukry (1980) are characterized by widely spaced biohorizons. For this reason, quantitative distribution patterns of alternative taxa have been considered in this work in order to provide supplementary bioevents across the EOT both for regional and worldwide correlations. According to Fornaciari and Rio (1996), a biohorizon is reliable when it is easily reproducible and identifiable by different workers and it can be systematically correlated over wide areas, maintaining the same ranking and spacing. The taxa discussed in the following have been previously observed by different authors but due to low abundances, poor preservation of the study material or lack of exhaustive studies, their extrapolated ages are not confidently determined. These bioevents are reported in Table 1.

In some cases, distinct biohorizons are found to lie at the same stratigraphic position, as for example the Tc of *C. subdistichus* and Tc of *L. minutus*. A reasonable explanation for this coincidence is possibly related to the relatively low sedimentation rates at this specific interval of the study site.

The reliability and reproducibility of the examined bioevents are discussed below:

The range of *Sphenolithus akropodus*

Sphenolithus akropodus was first described in north-eastern Atlantic Ocean sediments (Iberia Abyssal Plain) as a relatively large species (7-9 μm) with a long elongated apical spine, sometimes bifurcated, and with short proximal elements extending laterally to form a small base. At 0° to the crossed nicols, the apical spine is

weakly birefringent. In cross-polarized light at 45°, the apical spine is completely bright (de Kaenel and Villa, 1996). In this work, we have observed two different morphotypes: *S. akropodus* morphotype A and *S. akropodus* morphotype B that can be differentiated if observed at XPL at 0°. *S. akropodus* morphotype A (Plate 2.3, figs. 7-8) is characterized by a single apical spine (not divided by a central extinction line), while *S. akropodus* morphotype B (Plate 2.3, figs. 9-10) shows an apical spine subdivided in two elements by a central extinction line. Our data indicate overlapping abundance patterns for these morphotypes (Figure 2.3), suggesting a morphological variability within the same species, rather than intergradational forms.

At Hole 756C, the first appearance of this taxon is difficult to define due to its sporadic occurrence, but we tentatively placed its base at 121.05 mbsf (33.29 Ma), within Zone NP21, equivalent to Zone CNO1 (Figure 2.3). Our datum is consistent with those provided by de Kaenel and Villa (1996), Bordiga et al. (2015) and more recently by Villa et al. (2021), which indicate that this event occurs in the early Oligocene.

The base of *S. akropodus* could be used for a good approximation of this time interval, but further data are required to confirm its reliability. The top of *S. akropodus* is found at 114.265 mbsf within Zone CNO3 (Agnini et al., 2014), corresponding to the lower part of Zone NP23 of Martini (1971) and has an extrapolated age of 30.11 Ma.

The Base common of *Sphenolithus predistentus*

At ODP Hole 756C, the species becomes common and continuous (Bc) up to 121.85 mbsf (estimated age of 33.46 Ma, early Oligocene), while data from the equatorial Indian Ocean (Fioroni et al., 2015) indicates that *S. predistentus* is very abundant and commonly present already within Chron C13r (late Eocene).

The diachrony observed for this event suggests a low potential as possible additional bioevent. Specimens of *S. predistentus* (Plate 2.3, figs. 11-14) at ODP Hole 756C are relatively rare (0-31 n/mm^2, Figure 2.3) and, in some cases, this species is not easy to recognize essentially because of either (1) the absence of the two low quadrants or 'feet' due to preservation issues, 2) taxonomic ambiguities between *S. predistentus* and *S. akropodus* (Bown and Dunkley Jones, 2012) or the presence of transitional forms (Blaj et al., 2010). For these reasons, and with the available data, we do not recommend the use of the Bc of *S. predistentus.*

The range of *Chiasmolithus altus*

At high latitudes, the biohorizons (Base and Top) related to *Chiasmolithus altus* are considered highly reliable (Fioroni et al., 2012; Persico et al., 2008). At Hole 756C, the Base (B) of *C.altus* (Plate 2.1, figs. 15-16) was found at 123.21 mbsf (33.72 Ma) within Zone CNO1 (Figure 2.3), in the lower Oligocene. This datum is consistent with data reported from the Southern Ocean (Fioroni et al., 2012). At 115.91 mbsf (31.81 Ma), *C. altus* becomes discontinuous and rare (Tc) shortly above the Top of *R. umbilicus* (within Zone CNO3).

Data from the Southern Ocean document that *C. altus* first appears (Base) in the lower Oligocene after an interval following the Top of *C. eoaltus* (or *C. altus-like*), a species restricted to the middle-late Eocene (Persico and Villa, 2008). *Chiasmolithus. eoaltus* slightly morphologically differs from *C. altus* (Persico and Villa, 2008) by having a larger central opening, a thinner rim, and one cross-bar not perfectly aligned (i.e. slightly sigmoidal). Overall, at Hole 756C, late Eocene specimens of *Chiasmolithus* are commonly affected by

dissolution of the cross-bar structure present in the central area, precluding, in some cases, the unambiguous identification at the species level. The rarity of the taxon and the lack of the cross-bar structure suggests caution in ascribing the forms observed in the middle-late Eocene to *C. eoaltus* and, consequently, we have preferred to refer these specimens to as *C. cf. eoaltus* (Figure 2.3). The Top common (Tc) and Base (B) of *Chiasmolithus altus* here presented seem to represent potential useful biohorizons, although these events require further investigations, especially at low-middle latitudes where they have been poorly tested.

The Top and Top common of *Isthmolithus recurvus*

At ODP Hole 756C*, I. recurvus* (Plate 2.2, figs. 6-7) displays a high variance in abundance (0-46 n/mm^2, Figure 2.3), but toward the end of its range it showed a neat decrease followed by a final discontinuous occurrence. In our samples, *I. recurvus* is often overgrown, but thanks to its distinct shape it is still easily recognizable. The final occurrence of this species at ODP Hole 756C is positioned at 116.51 mbsf (32.13 Ma) just below the Top of *R. umbilicus* (116.11 mbsf). This finding is in agreement with previous estimations from mid latitudes (Premoli Silva et al., 1988), as well as from the central equatorial Pacific (Lyle et al., 2002).

At low-middle latitudes (South Atlantic), Backman (1987) reported the extinction of this taxon below the Top of *E. formosa*. In the Equatorial Indian Ocean (ODP 711), Fioroni et al. (2015) did not use this event, since *I. recurvus* is extremely rare and poorly preserved in the studied material. The supposed diachroneity between low and middle latitudes has been interpreted by Wei and Wise (1990) as related to a paleoecological preference of this species for cool waters. In the studied section, *I. recurvus* shows a sharp drop at 122.25 mbsf (33.55 Ma), which is used to define the Top common of this species. The reliability of the Top common of *I. recurvus* remains debatable but future data will confirm or not the real potential of this biohorizon.

The acme of *Lanternithus minutus*

The abundance pattern of *Lanternithus minutus* (Plate 2.2, Figs. 8-9) at Hole 756C (Figure 2.5) is noteworthy for at least three reasons: (1) there are only two high resolution datasets reporting the relative abundance pattern of this taxon across the EOT (Dunkley Jones et al., 2008; Bordiga et al., 2015); (2) at ODP Hole 756C, the abundance pattern of *L. minutus* is very similar to that of *C. subdistichus*; (3) in the study section, *L. minutus* is well preserved though holococcoliths are generally considerate to be particularly fragile and not easily preserved in carbonate-rich pelagic sediments (Young et al., 2005; Bown et al., 2008; Dunkley Jones et al., 2008). At Hole 756C, *L. minutus* suddenly increases in abundance (acme) at 123.21 mbsf (33.72 Ma). This change is used to mark the Bc of this taxon. The Top common of *L. minutus* is located at 118 mbsf (32.54 Ma) and coincides with the Top common of *C. subdistichus*. Unluckily, the acme interval of *L. minutus* seems not be a global feature, showing different patterns at different sites. In SE Atlantic Ocean (Bordiga et al., 2015), this taxon shows an increase in abundance above EOIS (0-12% in abundance; dataset A), while data from Tanzania (Dunkley Jones et al., 2008) reports an unrecoverable decline through the EOT.

L. minutus is not considered as a valuable biohorizon because of its high susceptibility to dissolution (especially in deep waters) and the high vulnerability during diagenetic processes (Moran and Watkins, 1988). Despite these conflicting views, the species could be used as a paleoenvironmental indicator in regional contexts.

2.4.3 Paleoenvironmental changes across the late Eocene – early Oligocene

Calcareous nannofossils are excellent proxies for inferring paleoenvironmental reconstructions because of their sensitivity to environmental conditions. Variations in calcareous nannofossil assemblages can be related to changes in sea surface water temperature (SST), nutrient availability, intensity of solar radiance, salinity and many other factors (e.g. Aubry, 1992; Winter et al., 1994; Flores and Sierro, 2013). However, the complicated interaction between these abiotic parameters with the physical properties of the water masses (i.e. upwelling, turbulence, stratification, and turbidity), atmospheric processes and biotic components (i.e. competition, predation, disease, etc.) makes the disentangling of each contribution difficult.

In modern coccolithophore communities, sea water temperature is considered one of the most significant parameters, playing a key role in defining the latitudinal distribution of species (Baumann et al., 2005). Nevertheless, on more local scales, in modern tropical and subtropical regions, temperature variations seem to be less informative and important (Andruleit et al., 2003). In these cases, what comes into play is another fundamental parameter for coccolithophore growth and diversification: the availability of bio-limiting nutrients. Despite the overall eurytopic nature of coccolithophores, taxa are subdivided in two different ecological groups: k-specialist (oligotrophs, efficiency maximized, high H index) and r-opportunist (eutrophs, grow rate maximized, low H index), although many species are considered to be mesotrophs (Bralower, 2002). Temperature and trophic conditions are often intimately correlated since eutrophic taxa are generally more common in cold waters (high nutrients availability) and oligotrophic taxa are more abundant in warm waters (low nutrients availability). To date, the ecological preferences of many species have received a wide consensus among the scientific community, but others appear to have more complex and controversial ecologies (Villa et al., 2008; Newsam et al., 2017).

At ODP Hole 756C, the PCA analysis was used to group coccolith taxa and to relate their temporal distribution to the paleoecological structure of the upper photic zone (UPZ) during the E-O interval. From the analysis of the major loading taxa, we tentatively correlate the changes observed in the assemblages with the main paleoenvironmental parameters (principal components: PC1 and PC2). Major and minor loading taxa were interpreted and compared in terms of temperature and trophic preferences with previously published paleoecological assignments (Table 2.2). However, many taxa display broad ecological affinities and require further study, as in the case of *Isthmolithus, Zygrhablithus, Sphenolithus and Dictyoccocites.*

Their abundance is likely the result of the complex interaction of abiotic and/or biotic parameters.

For instance, the debate on the apparently inconsistent ecological behavior of *Sphenolithus* and *Dictyoccocites* is probably related to the fact that species belonging to these genera show species-specific responses, hampering any ecological categorization at genus level (Langer et al., 2006; Toffanin et al., 2011; Cappelli et al., 2021).

According to our PCA results (Figure 2.8), PC1 is positively loaded by *Coccolithus, Ericsonia, Discoaster, Zygrablithus* and *Isthmolithus. Coccolithus* is thought to have changed its temperature preferences through time, from warmer waters in the Paleogene to colder waters in the Neogene (Agnini et al., 2007). Pleistocene and modern *C. pelagicus* prefer cold and/or eutrophic waters (Cachão and Moita, 2000).

At high latitudes, the most abundant species of this genus, *C. pelagicus*, is considered to be indicative of temperate water conditions during the Eocene-Oligocene transition (Wei and Wise, 1990; Persico and Villa, 2004; Villa et al., 2008). *Ericsonia* is thought to have thrived in warm-waters in the Paleogene (Haq and Lohmann, 1976; Wei and Wise, 1990; Aubry, 1992; Kelly et al., 1996; Bralower, 2002) and is considered a warm water indicator (Villa et al., 2008; 2014; 2021). *Discoaster* has been consistently considered as a warm-water taxon, common in oligotrophic environments (Aubry, 1998; Bralower, 2002).

Finally, several studies have suggested that *Zygrablithus* is a near shore indicator (e.g. Heirtzler et al., 1977; Coccioni et al., 1988; Nocchi et al., 1988; Wei and Wise, 1990; Monechi et al., 2000). However, the paleoecology of this taxon remains elusive based on the review reported in Villa et al. (2008), who highlighted highly inconsistent paleoecological affinities for *Z. bijugatus* among different authors. Our result possibly indicates a preference for warm and mesotrophic waters, but we are skeptical that the record of this taxon is only related to environmental conditions and rather support the hypothesis that diagenetic processes could have played an important role in favoring or disfavoring the preservation of this fragile taxon (Agnini et al., 2016).

Isthmolithus has been interpreted as temperature-dependent taxon, with preferences for cool (Wei and Wise, 1990; Wei et al., 1992; Monechi et al., 2000) or temperate waters (Persico and Villa, 2004). In our opinion *Isthmolithus* ecological interpretation remains enigmatic. In the PCA biplot, *Isthmolithus recurvus* lies in the warm-oligotrophic field (Figure 2.8) but this datum is essentially the result of the stratigraphic occurrence of this taxon that is not present in the early Oligocene, except in the lower part. The negative loadings on PC1 are *Reticulofenestra* and *Cyclicargolithus*. *Reticulofenestra* is an eurytopic cosmopolitan taxon, thriving in a wide range of environmental conditions with a preference for temperate waters (Wei and Wise, 1990; Shcherbinina, 2010; Cappelli et al., 2019), while *Cyclicargolithus floridanus* is considered a species with preferences for eutrophic-high productivity environments (Aubry, 1992; Dunkley Jones et al., 2008; Villa et al., 2021).

PC2 is positively loaded by *Lanternithus, Clausicoccus, Chiasmolithus*, *Sphenolithus* and *Dictyococcites.* The paleoecological preferences of *Lanternithus* (represented by *L. minutus*) are poorly known, nevertheless a number of studies have suggested that holococcoliths usually prefer more oligotrophic waters (Kleijne, 1991; Winter et al., 1994; Cros et al., 2000; Baumann et al., 2005; Gibbs et al., 2006; Dunkley Jones et al., 2008; Bordiga et al. 2015). Nocchi et al. (1988) observed high abundances of *Lanternithus* and *Zygrablithus* in near shore settings and used these taxa as shallow-water indicators and cold-water tolerant species.

Our results seem to indicate an eutrophic affinity for *Lanternithus* that is supported by the general increase in abundance observed starting with the middle Eocene, and the correlative eutrophication of the oceans (Agnini et al., 2006; Schneider et al., 2011; Cappelli et al., 2019). In general, the carbonate ocean chemistry together with local environmental conditions can possibly affect the preservation potential of holococcoliths and, in turn, their abundances (Young et al., 2005). However, the relatively shallow paleowater depth (~400 m) makes Site 756 less prone to dissolution and thus the abundance pattern of *Lanternithus* potentially reflects a true signal, not compromised by poor preservation. As regard to the paleoecology of *Clausicoccus*, Wei and Wise (1990) reported a common presence of this taxon in the middle latitudes, though the distribution of this genus may be controlled also by factors (e.g. nutrients, insolation, salinity) other than temperature.

Our data suggest a temperate-water affinity for this taxon, but also point out a strong control exerted by the high nutrient availability in favoring the distribution of this species.

Chiasmolithus is thought to be indicative of cool-cold water conditions (Wei and Wise, 1990; Wei et al., 1992; Bralower, 2002; Persico and Villa, 2004; Tremolada and Bralower, 2004; Villa and Persico, 2006;, Villa et al., 2008), an ecological affinity that is confirmed in our study. Genus *Sphenolithus* is known to be considered a warm water taxon (Villa et al., 2021) adapted to oligotrophic environments (Aubry, 1998; Bralower, 2002; Gibbs et al., 2004; Kalb and Bralower, 2012), even so the study carried out by Wade and Bown (2006) shows a strong increase of sphenoliths during eutrophic conditions.

It is becoming increasingly evident that species belonging to the same genus can in fact better thrive in a wide trophic continuum (Dunkley Jones et al., 2008; Toffanin et al., 2011; Cappelli et al., 2021) showing species-specific responses to climate/environmental changes. In this view the constant abundance displayed at genus level (Figure 2.5) blurs the more nuanced ecological preferences at species level, where *S. akropodus* and *S. predistentus* partially substitute the warm-oligotrophic *S. moriformis* during the EOT, suggesting a more eutrophic/temperate affinity for the former taxa. The paleoecological affinities of *Dictyococcites* are still under debate and this is essentially due to the controversial taxonomy of this group and insufficient data available. For instance, different preferences have been proposed for *D. bisectus* which is designated as a temperate-water (Persico and Villa, 2004), warm to temperate (Wei and Wise, 1990) or warm taxon (Monechi et al., 2000). The PCA results suggest a temperate/mesotrophic affinities with different species possibly lying in a different position of the trophic resource continuum (TRC; Hallock, 1987).

Based on these considerations, PC1 (27.88% of the total variance) and PC2 (21.96% of the total variance) were distinguished as representative, respectively, of paleotemperature and trophic conditions.

According to our paleoecological interpretation, calcareous nannofossil taxa are, when possible and supported by straightforward data, subdivided in three eco-groups:

1) **Warm-oligotrophic group**, that includes *Coccolithus, Ericsonia, Discoaster,* characterized by warm temperatures (high PC1 scores) and low nutrients affinity (low PC2 scores).
2) **Temperate-eutrophic group**, to which belong *Clausicoccus, Lanternithus* and *Chiasmolithus*.
   This eco-group is characterized by high trophic (high PC2 scores) and intermediate temperatures preferences. Within these groups, *Clausicoccus* and *Lanternithus* seems to be highly sensitive to trophic conditions and their peaks in abundance across the EOGM were probably induced by a high availability of nutrients.
3) **Cold-mesotrophic group** that comprises *Reticulofenestra* and *Cyclicargolithus* genera characterized by low temperature and a return to slightly oligotrophic paleoenvironmental conditions.

The following taxa have been excluded from the three main eco-groups because of more difficult interpretation and include: *Zygrhablithus* (warm-mesotrophic), *Dictyococcites* (temperate-mesotrophic; species-specific affinities), *Sphenolithus* (species-specific affinities) and *Isthmolithus,* for which we require further investigations.

Table 2									
	Authors								
Genus	Bukry (1973)	Wei and Wise (1990)	Aubry (1992, 1998)	Monechi et al. (2000)	Bralower (2002)	Tremolada and Bralower (2004)	Villa et al. (2008)	Villa et al. (2014)	This study
Chiasmolithus	Inshore or cool-water (*C. oamaruensis*)	Cool	Mesotrophic or eutrophic-cold (*C. oamaruensis*)	Eutrophic (*C. oamaruensis*)	Cool-eutrophic		Cool	Cool-eutrophic	Temperate-eutrophic
Clausicoccus									Temperate-eutrophic
Coccolithus		Temperate (*C. pelagicus*)		Warm or oligotrophic (*C. pelagicus*)			Temperate (*C. pelagicus*)	Temperate-eutrophic (*C. pelagicus*)	Warm-oligotrophic
Cyclicargolithus	Temperate-cool (*C. floridanus*)	Temperate (*C. floridanus*)	Eutrophic temperate-cold (*C. floridanus*)	Eutrophic (*C. floridanus*)					Cold-mesotrophic (*C. floridanus*)
Dictyococcites		Warm-temperate (*D. cf. D. bisectus*)		Warm (*D. bisectus*)			Temperate (*D. bisectus*)	Temperate-oligotrophic (*D. bisectus*)	Temperate-mesotrophic
Discoaster		Warm	Oligotrophic-warm	Oligotrophic	Warm-oligotrophic	Warm-oligotrophic	Warm-oligotrophic	Warm-oligotrophic	Warm-oligotrophic
Ericsonia	Warm-temperate	Warm	Warm	Warm	Warm-oligotrophic	Warm-oligotrophic	Warm-oligotrophic	Warm	Warm-oligotrophic (*E. formosa*)
Isthmolithus	Inshore or cool-water (*I. recurvus*)	Cool (*I. recurvus*)		Cool (*I. recurvus*)				Temperate, eutrophic (*I. recurvus*)	
Lanternithus				Near shore or shallow water (*L. minutus*)					Temperate-eutrophic (*L. minutus*)
Reticulofenestra		Temperate (*R. samodurovii/R. umbilica*); cool or cold (*R. daviesii*)	Oligotrophic-mesotrophic warm (*R. umbilicus)*	Cool (*R. hillae* and *R. daviesii*)			Mesotrophic; temperate (*R. umbilicus*); cool (*R. daviesii*)	Temperate-eutrophic; cool-eutrophic (*R. daviesii*)	Cold-mesotrophic; warm-oligotrophic (*R. umbilicus* and *Reticulofenestra* spp. 10-14 µm); cold-mesotrophic (*Reticulofenestra* spp. 4-10 µm)
Sphenolithus		Warm	Warm	Warm (*S. moriformis*)	Warm-oligotrophic		Warm-oligotrophic	Warm-oligotrophic	Temperate-eutrophic (*S. akropodus* and *S. predistentus*); warm-oligotrophic (*S. moriformis*)
Zygrhablithus		Depth and/or paleoproductivity controlled (*Z. bijugatus*)	Oligotrophic (*Z. bijugatus*)	Near shore or shallow water (*Z. bijugatus)*	Warm-oligotrophic (*Z. bijugatus*)	Cool-mesotrophic (*Z. bijugatus*)	Temperate (*Z. bijugatus*)		Warm-mesotrophic (*Z. bijugatus*)

Table 2.2 Synthesis of calcareous nannofossil paleoecological affinities based on previous literature and on this study.

2.4.4 Comparison with other nannofossil studies

At Hole 756C, the loss of the warm-oligotrophic community is one the main changes observed in the nannoplankton assemblage, together with the massive increase of the temperate-eutrophic taxa (*Clausicoccus*, *Chiasmolithus* and *Lanternithus*) closely coupled to the EOIS and the EOGM (Figure 2.8A). No specifically assemblage response was observed at Step 1. Instead, the only significant change that occurred close to the EOB, is a remarkable increase of abundance (acme) of *Clausicoccus*.

Our data suggest that the causes of calcareous nannofossil changes at ODP Hole 756C are related to both temperature and trophic conditions, in agreement with previous studies from low-middle latitudes (Dunkley Jones et al., 2008; Jones et al., 2019; Villa et al., 2021). Specifically, if compared with the record available from Tanzania (Dunkley Jones et al., 2008) our data similarly record an increase in the relative abundance of

C. floridanus and *S. predistentus,* but important differences have been observed with regard to holococcolith abundances. While our dataset displays an unusual increase in abundance of *L. minutus,* the record from Tanzania indicates a marked reduction of holococcoliths (i.e. *Varolia macleodi, Lanternithus minutus* and *Zygrhablithus bijugatus*) during the E-O transition. The overall comparison with other low-middle latitude datasets (Tanzania; Dunkley Jones et al., 2008; Equatorial Indian Ocean; Fioroni et al., 2015; Villa et al., 2021 and Indo-Pacific; Jones et al., 2019; Equatorial Pacific; Blaj et al., 2009) highlights important similarities and a substantial synchronicity in the changes documented in the calcareous nannofossil record.

Noteworthy, the abundance pattern of *I. recurvus* recorded in the Southern Kerguelen Plateau (Site 748; Wei et al., 1992; Villa et al., 2008) is similar to our record (0-3%) and differs from that recorded in the Equatorial Indian Ocean (Sites 711, 709; Fioroni et al., 2015; Villa et al., 2021), where this species is strongly reduced or virtually absent. Similarly, limited *Chiasmolithus* and *Reticulofenestra daviesii* were recorded, in contrast to much higher abundances documented in the Kerguelen Plateau (Wei et al., 1992; Villa et al., 2008) and to the rarity or absence of these taxa in the Equatorial Indian Ocean (Wei et al., 1992; Fioroni et al., 2015; Villa et al., 2021). Thus, as observed for the planktonic foraminifera assemblages, at Hole 756C, the E-O calcareous nannofossil assemblages appear transitional between the assemblages found on the Kerguelen Plateau (Wei et al., 1992) and from the equatorial Indian Ocean (Fioroni et al., 2015; Villa et al., 2021).

The water masses formed in the Southern Ocean and flowing northward were characterized by low temperature and high nutrients levels (Sarmiento et al., 2004). The deep circulation of these water masses was likely invigorated close to the EOT providing an enhanced nutrient supply at low-middle latitudes which eventually leads to more eutrophic conditions in the Indian Ocean (Villa et al., 2021). As a result, the transition from the Eocene to the Oligocene was marked by a progressive increase in abundance of opportunistic taxa better adapted to thrive in cooler and more eutrophic environments (Dunkley Jones et al., 2008; Fioroni et al., 2015; Jones et al., 2019;, Villa et al., 2021). Other than changes in ocean circulation, an alternative possible explanation for the eutrophic conditions recorded at ODP Hole 756C likely involved the weathering of shelf sediments in response to sea level fall (e.g. Merico et al., 2008), but the paleoceanographic changes that occurred in the Antarctic area remain the most plausible mechanisms to explain all the modification observed in calcareous nannofossils. Moreover, our paleoproductivity proxy (PC2 scores; Figure 2.8B) also highlights the presence of a transient and large increase in nutrients coeval with the global maximum $\delta^{18}O$ values (EOGM) and major ice build-up on Antarctica. Our interpretation is that this temporary nutrient overshoot, might have been caused by an additional short-term event, such as a sudden and massive input of micro-nutrients to the ocean due to maximum glacial expansion in the earliest Oligocene (Diester-Haass and Zahn, 1996).

2.4.5 The paleoecological significance of *Reticulofenestra*

Reticulofenestra is thought to be a cosmopolitan taxon, but different species or informal groups ascribed to this genus can lie in different positions of TRC. For this reason and, in order to better constrain their paleoecological significance, we decide to consider them separately. Our results indicate a long-term decrease in relative abundance (%) of medium to large reticulofenestrids (*Reticulofenestra* spp. 10-14 μm and *Reticulofenestra umbilicus* >14 μm) starting in the late Eocene and culminating after the EOT.

This group was replaced by small-sized reticulofenestrids (*Reticulofenestra* spp. 4-10 µm), which show a remarkable increase after the EOGM (Figure 2.9). The decrease in size of *Reticulofenestra* perfectly matches with the SST paleoenvironmental proxy (derived from PC1), confirming a temperature-dependence of this group. A possible explanation is that larger reticulofenestrids were probably better adapted to warmer Eocene sea-surface temperatures, while smaller forms were more competitive in Oligocene cold waters.

Moreover, this macroevolutionary size-decrease reflects the long-term decline of pCO_2: the bio-limiting levels of $[CO_2]_{aq}$ characterizing the surface waters during the Oligocene have likely reduced the diffusive CO_2 uptake of larger reticulofenestrids (low SA:V ratio) with a competitive advantage for smaller forms (high SA:V ratio) (Henderiks and Pagani, 2008). Finally, among reticulofenestrids, *Rerticulofenestra daviesii* displays a complex behavior. The abundance pattern of this species suggests a wide temperature tolerance as proposed by Bordiga et al. (2017). Nevertheless, the high abundance observed across the EOT is possibly a response to the eutrophic conditions inferred for this interval and is consistent with the eutrophic ecological affinity recently proposed for this taxon (Villa et al., 2014; 2021). Finally, we should also consider the importance of the competitive dynamics within a biological community in regulating the ecological success or failure of a group/taxon.

In this regard, at ODP Hole 756C, *R. daviesii* seems not as competitive as small reticulofenestrids, especially after the EOGM and could have been ecologically marginalized by these forms, as well as the larger reticulofenestrids in the late Eocene.

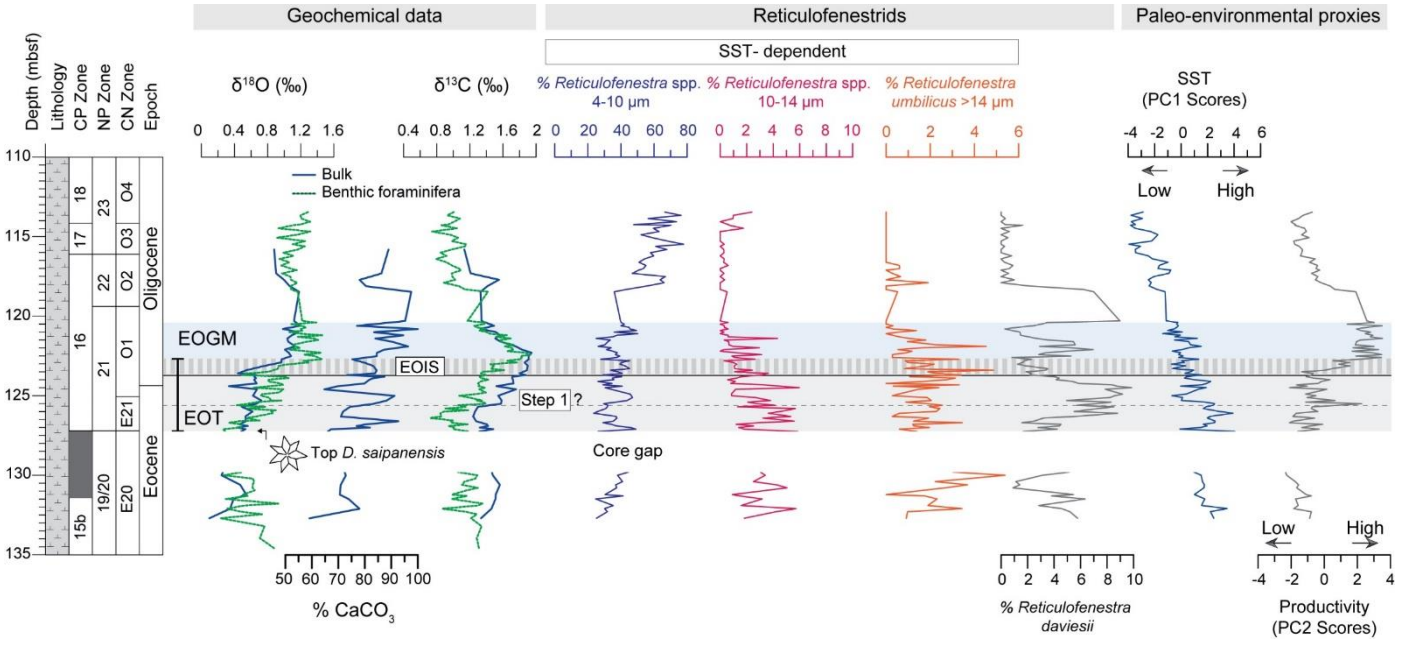

Figure 2.9 Relative (%) abundance of reticulofenestrids at ODP Hole 756C are plotted against stable oxygen and carbon isotopes ($\delta^{18}O$; $\delta^{13}C$) from bulk and benthic foraminifera (*C. mundulus* and *C. havanensis*) and bulk carbonate content ($CaCO_3$%). Principal component scores (PC1 and PC2) are also reported as indices, respectively, of temperature and paleoproductivity. Data are plotted against depth (m), lithology, calcareous nannofossils biozones (NP, Martini, 1971; CP, Okada and Bukry, 1980; CN, Agnini et al., 2014) and chronostratigraphy. The horizontal grey bar indicates the two positive steps in $\delta^{18}O$ recognized at the EOT (Step 1 and EOIS) and the light blue bar indicates the maximum values of $\delta^{18}O$ (EOGM). The base of the EOT is marked by the extinction of *D. saipanensis* (Hutchinson et al. 2021).

2.5 Conclusions

Our integrated benthic foraminifera and bulk stable isotope stratigraphies, and nannofossil and planktonic foraminifera biostratigraphies across the late Eocene and early Oligocene of Indian Ocean ODP Hole 756C, demonstrate well-defined and familiar geochemical structure within a consistent relative chronological framework. These constraints make Site 756 an excellent site for exploring pelagic changes in the subtropical Indian Ocean during the greenhouse to icehouse transition. An important aspect of Site 756 is that the shallow water depths facilitate good planktonic foraminifera as well as nannofossil preservation, and this includes preservation of the E/O boundary marker genus *Hantkenina*. The extinction of *Hantkenina* spp. in Hole 756C at 124.4 mbsf, occurs during an intermediate plateau between positive $\delta^{18}O$ and $\delta^{13}C$ isotopic shifts, as has been shown elsewhere. This is the first open-ocean Indian Ocean record to demonstrate this pattern, confirming the global synchroneity of this extinction event with respect to the familiar sequence of ocean-climate changes occurring during the EOT.

The new integrated isotopic and biostratigraphic framework allows a detailed examination of nannofossil assemblage variability at Hole 756C, leading to further refinements to local and potentially global EOT nannofossil biostratigraphy and nannofossil palaeoceanographic interpretations. The biostratigraphy of Indian Ocean ODP Hole 756C has been refined based on a semi-quantitative high-resolution calcareous nannofossil record across the E-O transition. This study confirms the reliability of classical or already known bioevents, but we also present new alternative biohorizons, which possibly implement the overall biostratigraphic framework of this interval: the acme of *Clausicoccus subdistichus* gr. and *Lanternithus minutus*, the total range of *Sphenolithus akropodus* and *Chiasmolithus altus* and the Tc of *Isthmolithus recurvus*, at least at regional scale. During the late Eocene/early Oligocene transition, calcareous nannofossil assemblages underwent an abrupt turnover with a permanent decline of warm-oligotrophic taxa, a decrease in species diversity and a remarkable increase in eutrophic taxa. We interpret this profound reorganization in nannoplankton assemblage as the result of two major paleoenvironmental changes: a decrease in SST coupled with an increase in nutrient availability. We hypothesize that the new paleoenvironmental conditions likely favored the expansion of temperate/cold water taxa better adapted to a nutrient-rich environment at the expense of warm-water oligotrophic taxa. Our multivariate analysis suggests a main disruption in the taxonomic composition of the assemblage between the EOT and EOGM triggered by enhanced nutrient levels.

This interpretation is further corroborated by strong evidence of invigorated ocean circulation that might be able to transport colder and nutrient-enriched waters at low-middle latitudes (Diester-Haass and Zachos, 2003; Dunkley Jones et al., 2008; Coxall and Wilson, 2011; Fioroni et al., 2015; Jones et al., 2019; Villa et al., 2021). Beyond the overall eutrophication recorded across the EOT, a transient and large nutrient overshoot was recorded at the EOGM, as supported by the high relative abundance of the temperate-eutrophic eco-group.

In a long-term perspective, smaller reticulofenestrids gradually increase across the E-O transition to the detriment of the larger forms, which display an opposite decreasing trend.

Acknowledgements

The authors are grateful to the Integrated Ocean Drilling Program (IODP) for providing samples and data used in this study. The IODP is sponsored by the U.S. National Science Foundation (NSF) and participating countries under the management of Joint Oceanographic Institutions, Inc. Thanks to Elias Chadli for planktonic foraminifera sample washing and benthic foraminifera stable isotope picking and to Heike Sigmund for stable isotope analysis at Stockholm University. We sincerely thank Paul Pearson for his insightful comments on the manuscript. Isabella Raffi and Davide Persico are deeply thanked for their constructive comments in the capacity of reviewers of A.V.' s PhD thesis during the evaluation process required by Italian law.

A. V. and C. A. were supported by University of Padova.

Dataset S1 to S6 are provided in the **Appendix III**.

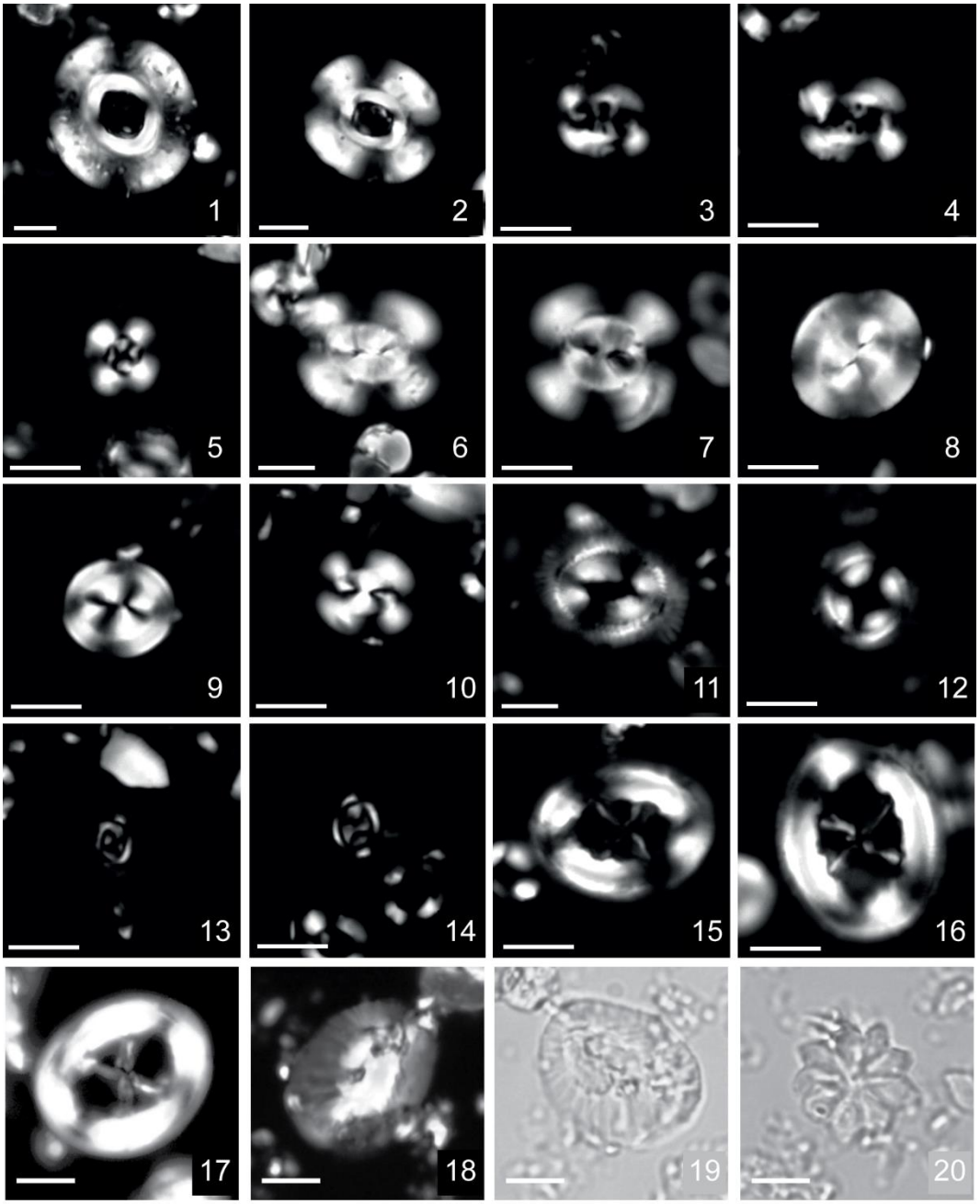

Plate 2.1 LM (magnification 1250x) microphotographs of selected calcareous nannofossil taxa from ODP Hole 756C. Scale bar = 5 µm. Photos **1-18** are in crossed nicols; **19, 20** in parallel light.
1, 2. *Reticulofenestra umbilicus*. Samples 756C-6X-1W, 140 cm (121.60 mbsf); 756C-7X-2W, 140 cm (132.70 mbsf). **3, 4.** *Reticulofenestra daviesii*, Sample 756C-6X-5W, 80 cm (127.00 mbsf). **5.** *Cyclicargolithus floridanus*. Sample 756C-5X-7W, 140 cm (117.01 mbsf). **6,7.** *Dictyococcites bisectus.* Sample 756C-6X-1W, 20 cm (120.40 mbsf). **8, 9.** *Dictyococcites* spp. Samples 756C-6X-1W, 140 cm (121.60 mbsf); 756C-6X-4W, 80 cm (125.50 mbsf). **10.** *Dictyococcites hesslandii.* Sample 756C-6X-4W, 60 cm (125.30 mbsf). **11.** *Coccolithus eopelagicus.* Sample 756C-7X-2W, 140 cm (132.70 mbsf). **12.** *Ericsonia formosa*.Sample 756C-7X-1W, 80 cm (130.60 mbsf). **13, 14.** *Clausicoccus subdistichus*. Sample 756C-6X-5W, 80 cm (127.00 mbsf). **15, 16.** *Chiasmolithus altus*. Samples 756C-5X-7W, 140 cm (117.01 mbsf); 756C-6X-1W, 20 cm (120.40 mbsf). **17.** *Chiasmolithus oamaruensis*. Sample 756C-6X-4W, 90 cm (125.60 mbsf). **18, 19.** *Helicosphaera compacta*. Sample 756C-5X-8W, 20 cm (117.31 mbsf). **20.** *Discoaster barbadiensis*. Sample 756C-7X-2W, 60 cm (131.90 mbsf).

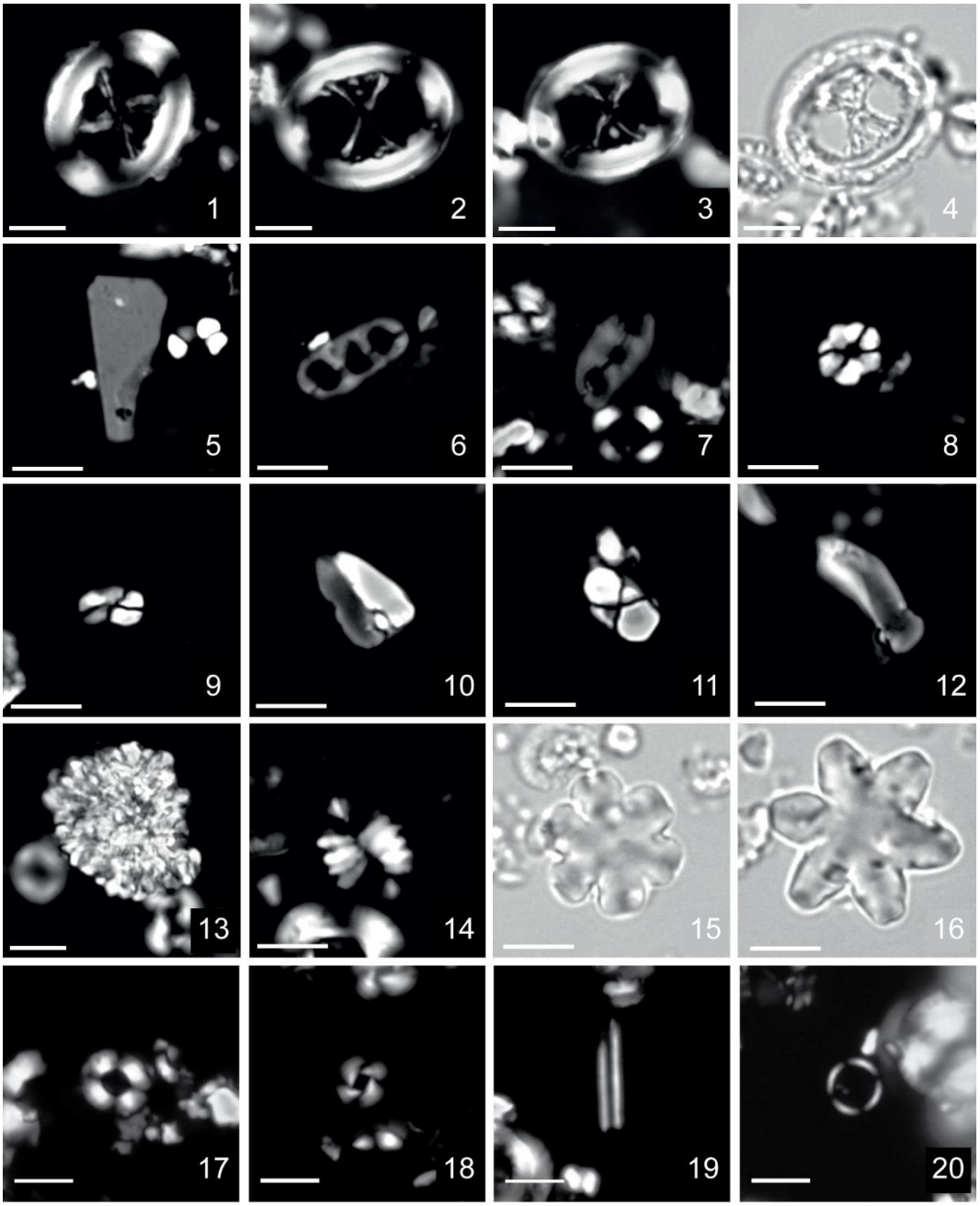

Plate 2.2 LM (magnification 1250x) microphotographs of selected calcareous nannofossil taxa from ODP Hole 756C. Scale bar = 5 µm. All photos are in crossed nicols except for **4, 15, 16** which are in parallel light.
1, 2. *Chiasmolithus altus*. Samples 756C-6X-1W, 140 cm (121.60 mbsf), 756C-6X-4W, 80 cm (125.50 mbsf). 3, 4. *Chiasmolithus cf. C. oamaruensis.* Sample 756C-6X- 4W, 80 cm (125.50 mbsf). **5.** *Bramletteius serraculoides*. Sample 756C-6X-4W, 80 cm (125.50 mbsf). **6, 7.** *Isthmolithus recurvus*. Samples 756C-6X-5W, 80 cm (127.00 mbsf); 756C-7X-2W, 140 cm (132.70 mbsf). **8, 9.** *Lanternithus minutus*. Samples 756C-6X-4W, 129 cm (125.99 mbsf); 756C-6X-5W, 70 cm (126.90 mbsf). **10, 12.** *Zygrhablithus bijugatus*. Sample 756C-6X-3W, 50 cm (123.70 mbsf). **11.** *Zygrhablithus bijugatus* base. Sample 756C-6X-3W, 50 cm (123.70 mbsf). **13.** *Thoracosphaera* spp. Sample 756C-6X-1W, 20 cm (120.40 mbsf). **14.** *Pontosphaera* spp. Sample 756C-7X-2W, 140 cm (132.70 mbsf). **15.** *Discoaster* cf. *D. deflandrei*. Sample 756C-6X-4W, 129 cm (125.99 mbsf). **16.** *Discoaster tanii*, 756C-6X-5W, 80 cm (127.00 mbsf). **17.** *Reticulofenestra* spp. Sample 756C-5X-5W, 60 cm (114.06 mbsf). **18.** *Reticulofenestra dictyoda.* Sample 756C-7X-2W, 19 cm (131.49 mbsf). **19.** *Blackites* cf. *B. singulus.* Sample 756C-6X-1W, 140 cm (121.60 mbsf). **20.** *Umbilicosphaera* spp. Sample 756C-6X-3W, 69 cm (123.89 mbsf).

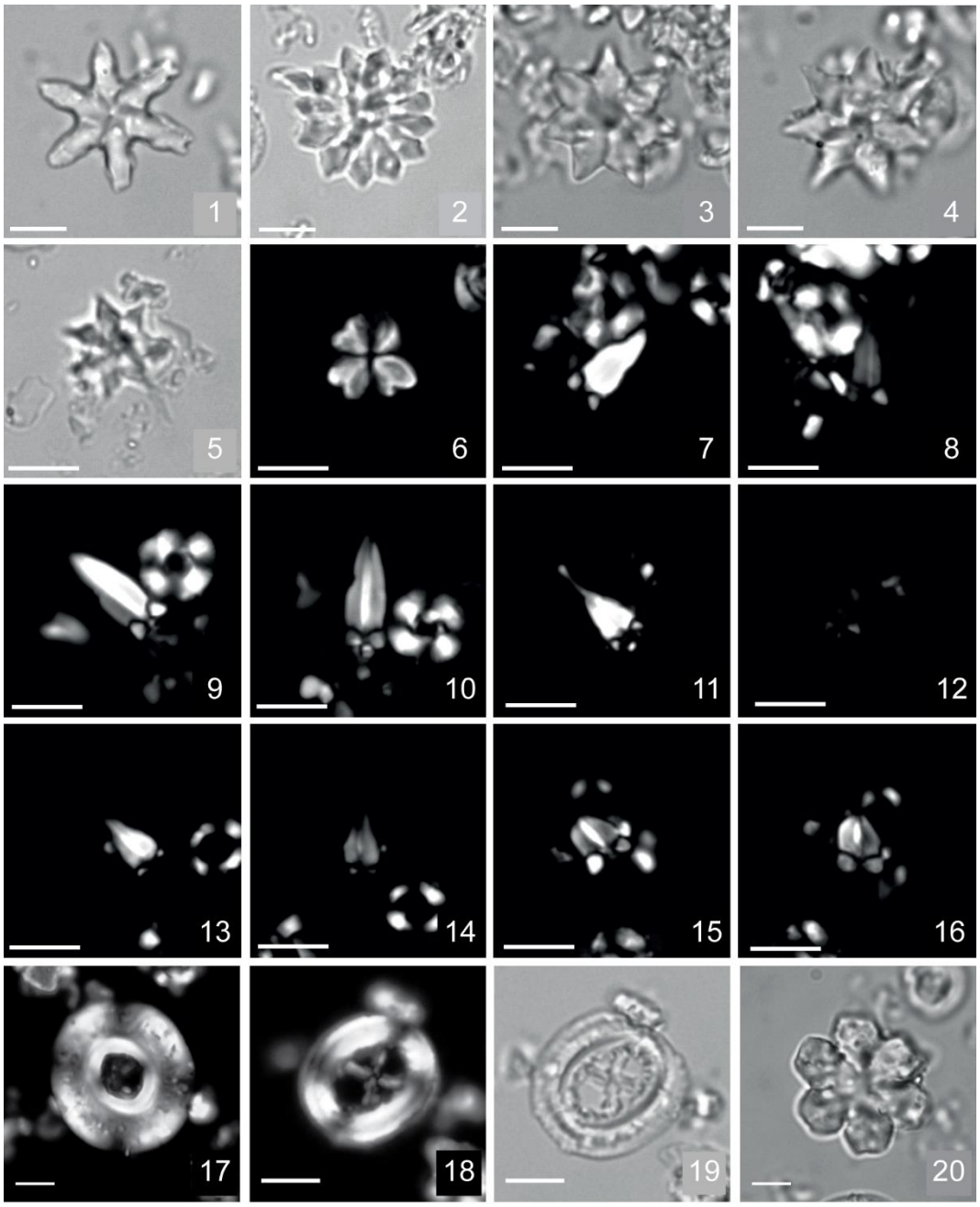

Plate 2.3 LM (magnification 1250x) microphotographs of selected calcareous nannofossil taxa from ODP Hole 756. Scale bar = 5 µm. Photos **1-5** and **19, 20** are in parallel light; photos **6-18** are in crossed nicols.
1. *Discoaster tanii nodifer*. Sample 756C-6X-5W, 80 cm (127.00 mbsf). **2.** *Discoaster barbadiensis*. Sample 756C-7X-2W, 19 cm (131.49 mbsf). **3-5.** *Discoaster saipanensis*. Sample 756C-7X-2W, 19 cm (131.49 mbsf). **6.** *Sphenolithus moriformis* gr. Sample 756C-7X-2W, 80 cm (132.10 mbsf). **7, 8.** *Sphenolithus akropodus* morphotype A (45°, 0°). Sample 756C-6X-1W, 20 cm (120.40 mbsf). **9, 10**. *Sphenolithus akropodus* morphotype B (45°, 0°). Sample 756C-6X-1W, 20 cm (120.40 mbsf). **11-14.** *Sphenolithus predistentus* (45°, 0°). Samples 756C-5X-6W, 0 cm 114.28 mbsf); 756C-5X-7W, 140 cm (117.01 mbsf). **15, 16.** *Sphenolithus distentus* (45°, 0°). Sample 756C-5X-6W, 0 cm (114.28 mbsf). **17.** *Reticulofenestra umbilicus.* Sample 756C-6X-1W, 140 cm (121.60 mbsf). **18, 19.** *Chiasmolithus altus*. Sample 756C-6X-1W, 140 cm (121.60 mbsf). **20.** *Discoaster* cf. *D. deflandrei.* Sample 756C-5X-7W, 140 cm (117.01 mbsf).

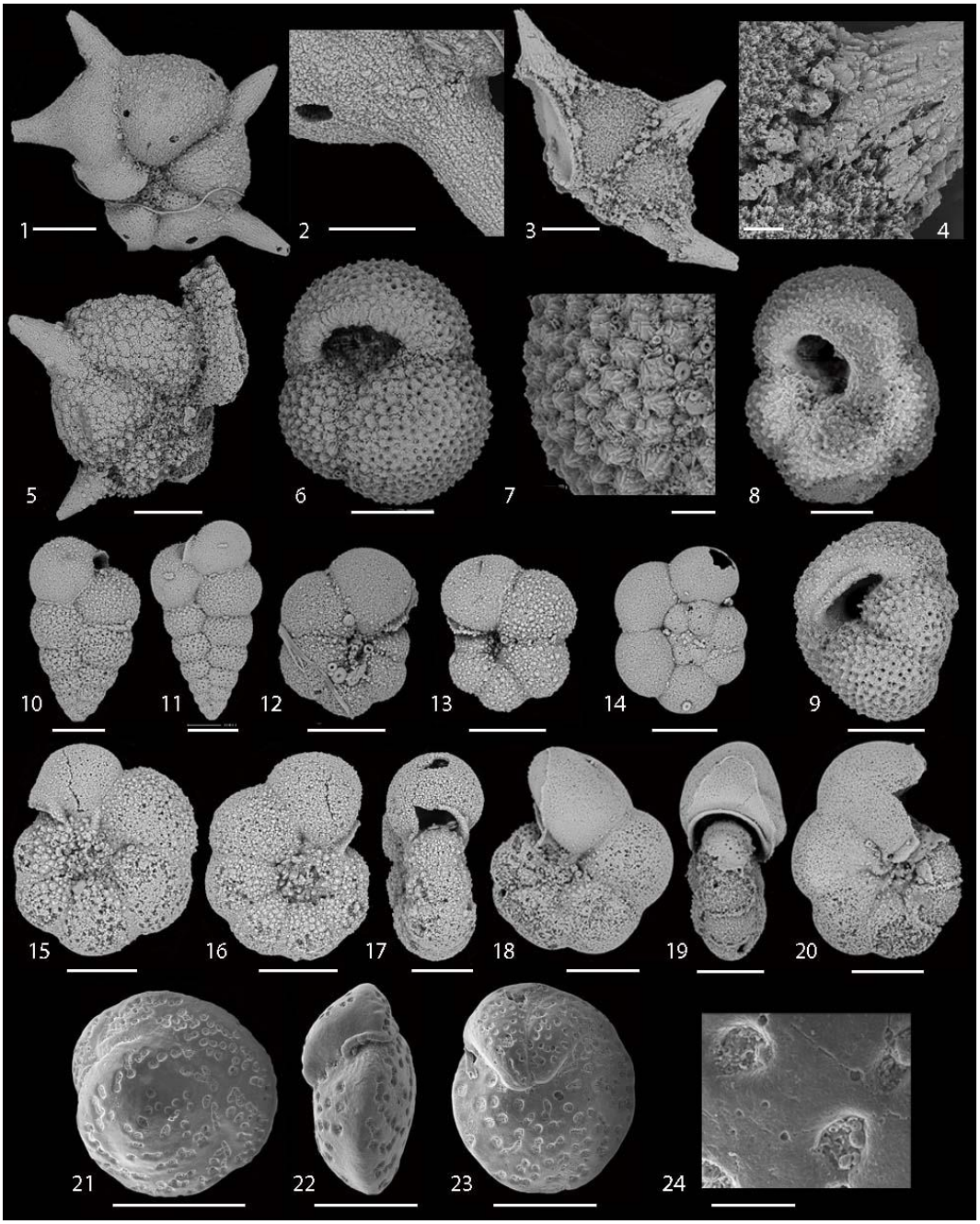

Plate 2.4 SEM images of selected Eocene-Oligocene foraminifera from Hole 756C. Scale bars: **21**, 400 µm; **22** and **23**, 300 µm; **1**, **3**, **5**, **6**, **8**, **9**, **19**, **20**, 100 µm; **2** and **10-18**, 50 µm; **24**, 40 µm; **4** and **7**, 20 µm.
1. *Hantkenina alabamensis* with post depositional borings. Sample 756C-6X-5, 20-22 cm. **2.** *H. alabamensis* close-up**,** showing surface striations and dissolution. Sample 756C-6X-5, 20-22 cm. **3.** *H. alabamensis* test fragment*,* strongly dissolved, peeled and partially recrystallized. Sample 756C-6X-3,129.5-131.5 cm. **4.** *H. alabamensis* close-up. Sample 756C-6X-3,129.5-131.5 cm. **5.** *H. alabamensis*. Sample 756C-6X-4, 10 cm. **6.** *Globigerinahteka index*. Sample 756C-7X-1, 115 cm. **7.** *G. index* zoom in showing recrystallized test. Sample 756C-7X-1, 115 cm. **8.** *Turborotalia ampliapertura.* Sample 756C-5X-8, 100-102 cm. **9.** *T. increbescens.* Sample 756C-6X-4,10 cm. **10.** *Chiloguembelina ototara.* Sample 756C-5X-8, 40-42 cm. **11**. *C. ototara.* Sample 756C-6X-2, 131.5-133.5 cm. **12.** *Tenuitella gemma.* Sample 756C-5X-8, 40-42 cm. **13, 14.** *Tenuitella gemma.* Sample 756C-6X-2, 131.5-133.5 cm. **15-17.** *Pseudohastigerina naguewichiensis.* Sample 756C-6X-2, 131.5-133.5 cm. **18.** *P. micra* or *P. naguewichiensis*. Sample 756C-6X-2, 131.5-133.5 cm. **19, 20.** *P. micra*? Sample 756C-6X-2, 131.5-133.5 cm. **21.** *Cibicidoides* cf. *havanensis*. Sample 756C-7X-4, 110 cm. **22, 23.** *Cibicidoides mundulus?* Sample 756C-7X-4, 110 cm. **24.** Zoom in of *Cibicidoides mundulus?* wall showing the relatively good preservation. Sample 756C-7X-4, 110 cm.

References

Abelson, M., Erez, J., 2017. The onset of modern-like Atlantic meridional overturning circulation at the Eocene-Oligocene transition: Evidence, causes, and possible implications for global cooling. Geochemistry, Geophysics, Geosystems 18, 2177–2199.

Agnini, C., Fornaciari, E., Raffi, I., Catanzariti, R., Pälike, H., Backman, J., Rio, D., 2014. Biozonation and biochronology of Paleogene calcareous nannofossils from low and middle latitudes. Newsletters on Stratigraphy 47, 131–181.

Agnini, C., Fornaciari, E., Rio, D., Tateo, F., Backman, J., Giusberti, L., 2007. Responses of calcareous nannofossil assemblages, mineralogy and geochemistry to the environmental perturbations across the Paleocene/Eocene boundary in the Venetian Pre-Alps. Marine Micropaleontology 63, 19–38.

Agnini, C., Muttoni, G., Kent, D. V., Rio, D., 2006. Eocene biostratigraphy and magnetic stratigraphy from Possagno, Italy: The calcareous nannofossil response to climate variability. Earth and Planetary Science Letters 241, 815–830.

Agnini, C., Spofforth, D.J.A., Dickens, G.R., Rio, D., Pälike, H., Backman, J., Muttoni, G., Dallanave, E., 2016. Stable isotope and calcareous nannofossil assemblage record of the late Paleocene and early Eocene (Cicogna section). Climate of the Past 12, 883–909.

Andruleit, H., Stäger, S., Rogalla, U., Čepek, P., 2003. Living coccolithophores in the northern Arabian Sea: ecological tolerances and environmental control. Marine Micropaleontology 49, 157–181.

Armstrong Mckay, D.I., Tyrrell, T., Wilson, P.A., 2016. Global carbon cycle perturbation across the Eocene-Oligocene climate transition. Paleoceanography 31, 311–329.

Aubry, M.-P., 1984. Handbook of Cenozoic calcareous nannoplankton, book 1, Ortholithae (Discoaster). American Museum of Natural History Micropaleontology Press, New York.

Aubry, M.-P., 1988. Handbook of Cenozoic calcareous nannoplankton, book 2, Ortholithae (Holococcoliths, Ceratoliths and others). American Museum of Natural History Micropaleontology Press, New York.

Aubry, M.-P., 1989. Handbook of Cenozoic Calcareous Nannoplankton, book 3, Ortholithae (Pentaliths, and Others) Heliolithae (Fasciculiths, Sphenoliths and Others). American Museum of Natural History Micropaleontology Press., New York.

Aubry, M.-P., 1992. Late Paleogene Calcareous Nannoplankton Evolution: A Tale of Climatic Deterioration. In: Eocene-Oligocene Climatic and Biotic Evolution. p. 272–279.

Aubry, M.-P., 1998. Early Paleogene Calcareous nannoplankton evolution: a tale of climatic amelioration. In: Aubry, M.-P., et al. (Eds.), Late Paleocene–Early Eocene Biotic and Climatic Events in the Marine and Terrestrial Records. Columbia University Press, New York, p. 158–201.

Backman, J., 1987. Quantitative Calcareous Nannofossil Biochronology of Middle Eocene through Early Oligocene Sediment from DSDP Sites 522 and 523. Abhandlungen der Geologischen Bundesanstalt 39, 21–31.

Backman, J., Hermelin, J.O.R., 1986. Morphometry of the Eocene nannofossil Reticulofenestra umbilicus lineage and its biochronological consequences. Palaeogeography, Palaeoclimatology, Palaeoecology 57, 103–116.

Backman, J., Raffi, I., Rio, D., Fornaciari, E., Pälike, H., 2012. Biozonation and biochronology of Miocene through Pleistocene calcareous nannofossils from low and middle latitudes. Newsletters on Stratigraphy 45, 221–244.

Backman, J., Shackleton, N.J., 1983. Quantitative biochronology of Pliocene and early Pleistocene calcareous nannofossils from the Atlantic, Indian and Pacific oceans. Marine Micropaleontology 8, 141–170.

Baldauf, J.G., 1992. Middle Eocene through early Miocene diatom floral turnover. In: Prothero, D.R., Berggren, W.A. (Eds.), Eocene–Oligocene Climatic and Biotic Evolution. Princeton University Press, Princeton, NJ.

Baumann, K.-H., Andruleit, H., Bockel, B., Geisen, M., Kinkel, H., 2005. The significance of extant coccolithophores as indicators of ocean water masses, surface water temperature, and paleoproductivity: a review. Paläontologische Zeitschrift 79, 93–112.

Berggren, W.A., Kent, D. V., Swisher, C.C., Aubry, M.-P., 1995. A Revised Cenozoic geochronology and chronostratigraphy. In: Berggren, W. A., Kent, D.V., Aubry, M.-P., Hardenbol, J. (Eds.), Geochronology, Time Scales, and Global Stratigraphic Correlation: A Unified Temporal Framework for an Historical Geology. Special publication - Society of Economic Paleontologists and Mineralogists, p. 129–212.

Blaj, T., Backman, J., Raffi, I., 2009. Late Eocene to Oligocene preservation history and biochronology of calcareous nannofossils from paleo-equatorial Pacific Ocean sediments. Rivista Italiana di Paleontologia e Stratigrafia 115, 67–85.

Blaj, T., Henderiks, J., Young, J.R., Rehnberg, E., 2010. The Oligocene nannolith Sphenolithus evolutionary lineage: morphometrical insights from the palaeo-equatorial Pacific Ocean. Journal of Micropalaeontology 29, 17–35.

Bohaty, S.M., Zachos, J.C., Delaney, M.L., 2012. Foraminiferal Mg/Ca evidence for Southern Ocean cooling across the Eocene-Oligocene transition. Earth and Planetary Science Letters 317–318, 251–261.

Bordiga, M., Henderiks, J., Tori, F., Monechi, S., Fenero, R., Legarda-Lisarri, A., Thomas, E., 2015. Microfossil evidence for trophic changes during the Eocene-Oligocene transition in the South Atlantic (ODP Site 1263, Walvis Ridge). Climate of the Past 11, 1249–1270.

Bordiga, M., Sulas, C., Henderiks, J., 2017. Reticulofenestra daviesii: biostratigraphy and paleogeographic distribution across the Eocene–Oligocene boundary. Geobios 50, 349–358.

Bown, P.R., 2005. Paleogene calcareous nannofossils from the Kilwa and Lindi areas of coastal Tanzania (Tanzania Drilling Project 2003-4). Journal of Nannoplankton Research 27, 21–95.

Bown, P.R., Dunkley Jones, T., 2012. Calcareous nannofossils from the Paleogene equatorial Pacific (IODP Expedition 320 Sites U1331-1334). Journal of Nannoplankton Research 32, 3–51.

Bown, P.R., Dunkley Jones, T., Lees, J.A., Randell, R.D., Mizzi, J.A., Pearson, P.N., Coxall, H.K., Young, J.R., Nicholas, C.J., Karega, A., Singano, J.M., Wade, B.S., 2008. A Paleogene calcareous microfossil Konservat-Lagerstätte from the Kilwa Group of coastal Tanzania. Geological Society of America Bulletin 120, 3–12.

Bown, P.R., Newsam, C., 2017. Calcareous nannofossils from the Eocene North Atlantic Ocean (IODP Expedition 342 Sites U1403–1411). Journal of Nannoplankton Research 37, 25–60.

Bown, P.R., Young, J.R., 1998. Techniques. In: Bown, P.R. (Ed.), Calcareous Nannofossil Biostratigraphy. Kluwer Academic Publishers, London, p. 16–28.

Bralower, T.J., 2002. Evidence of surface water oligotrophy during the Paleocene-Eocene Thermal Maximum: nannofossil assemblage data from Ocean Drilling Program Site 690, Maud Rise, Weddell Sea. Paleoceanography 17, 1023.

Cachão, M., Moita, M.T., 2000. Coccolithus pelagicus, a productivity proxy related to moderate fronts off Western Iberia. Marine Micropaleontology 39, 131–155.

Cappelli, C., Bown, P.R., de Riu, M., Agnini, C., 2021. The evolution of Eocene (Ypresian/Lutetian) sphenoliths: biostratigraphic implications and paleoceanographic significance from North Atlantic Site IODP U1410. Newsletters on Stratigraphy 54, 405–431.

Cappelli, C., Bown, P.R., Westerhold, T., Bohaty, S.M., De Riu, M., Lobba, V., Yamamoto, Y., Agnini, C., 2019. The early to middle Eocene transition: an integrated calcareous nannofossil and stable isotope record from the Northwest Atlantic Ocean (IODP Site U1410). Paleoceanography and Paleoclimatology 34, 1–18.

Catanzariti, R., Rio, D., Martelli, L., 1997. Late Eocene to Oligocene calcareous nannofossil Biostratigraphy in Northern Apennines: the Ranzano sandstone. Memorie di Scienze Geologiche 49, 207–253.

Coccioni, R., Monaco, P., Monechi, S., Nocchi, M., Parisi, G., 1988. Biostratigraphy of the Eocene-Oligocene bonudary at Massignano (Ancona, Italy). In: Premoli Silva, I., Coccioni, R., Montanari, A. (Eds.), The Eocene–Oligocene Boundary in the March-Umbria Basin (Italy). Fratelli Anniballi, Ancona, p. 81–96.

Coplen, T.B., Brand, W.A., Gehre, M., Gröning, M., Meijer, H.A.J., Toman, B., Verkouteren, R.M., 2006. New guidelines for $\delta^{13}C$ measurements. Analytical Chemistry 78, 2439–2441.

Cotton, L.J., Pearson, P.N., 2011. Extinction of larger benthic foraminifera at the Eocene/Oligocene boundary. Palaeogeography, Palaeoclimatology, Palaeoecology 311, 281–296.

Coxall, H.K., Dunkley Jones, T., Jones, A.P., Lunt, P., MacMillan, I., Marliyani, G.I., Nicholas, C.J., O'Halloran, A., Piga, E., Sanyoto, P., Rahardjo, W., Pearson, P.N., 2021. The Eocene−Oligocene transition in Nanggulan, Java: lithostratigraphy, biostratigraphy and foraminiferal stable isotopes. Journal of the Geological Society 178.

Coxall, H.K., Huck, C.E., Huber, M., Lear, C.H., Legarda-lisarri, A., Regan, M.O., Sliwinska, K.K., Flierdt, T. Van De, Boer, A.M. De, Zachos, J.C., O'Regan, M., Sliwinska, K.K., Van De Flierdt, T., De Boer, A.M., Zachos, J.C., Backman, J., 2018. Export of nutrient rich Northern Component Water preceded early Oligocene Antarctic glaciation. Nature Geoscience 11, 190–196.

Coxall, H.K., Pearson, P.N., 2007. The Eocene-Oligocene Transition. In: Williams, M., Haywood, A.M., Gregory, J., Schmidt, D.N. (Eds.), Deep-Time Perspectives on Climate Change: Marrying the Signal from Computer Models and Biological Proxies, Micropaleontology Society Special Publication. Geological Society, London, p. 351–387.

Coxall, H.K., Wilson, P.A., 2011. Early Oligocene glaciation and productivity in the eastern equatorial Pacific: Insights into global carbon cycling. Paleoceanography 26, 1–18.

Coxall, H.K., Wilson, P.A., Pälike, H., Lear, C.H., Backman, J., 2005. Rapid stepwise onset of Antarctic

glaciation and deeper calcite compensation in the Pacific Ocean. Nature 433, 53–7.

Cros, L., Kleijne, A., Zeltner, A., Billard, C., Young, J.R., 2000. New examples of holococcolith-heterococcolith combination coccospheres and their implications for coccolithophorid biology. Marine Micropaleontology 39, 1–34.

Davies, R., Cartwright, J., Pike, J., Line, C., 2001. Early Oligocene initiation of North Atlantic Deep Water formation. Nature 410, 917–920.

de Kaenel, E., Villa, G., 1996. Oligocene Miocene calcareous nannofossil biostratigraphy and paleoecology from the Iberia Abyssal plain. Proceedings of the Ocean Drilling Program, Scientific results 149, 79–145.

DeConto, R.M., Pollard, D., 2003. Rapid Cenozoic glaciation of Antarctica induced by declining atmospheric CO_2. Nature 1317, 1313–1317.

Diester-Haass, L., Zachos, J.C., 2003. The Eocene-Oligocene transition in the Equatorial Atlantic (ODP Site 925); Paleoproductivity increase and positive $\delta^{13}C$ excursion. In: Prothero, D.R., Ivany, C.L., Nesbitt, E.A. (Eds.), From Greenhouse to Icehouse; The Marine Eocene-Oligocene Transition. Columbia Univ. Press, New York, NY, USA, p. 397–416.

Diester-Haass, L., Zahn, R., 2001. Paleoproductivity increase at the Eocene - Oligocene climatic transition: ODP/DSDP sites 763 and 592. Palaeogeography, Palaeoclimatology, Palaeoecology 172, 153–170.

Diester-Haass, L., Zahn, R., 1996. Eocene-Oligocene transition in the Southern Ocean: History of water mass circulation and biological productivity. Geology 24, 163–166.

Dunkley Jones, T., Bown, P.R., Pearson, P.N., Wade, B.S., Coxall, H.K., Lear, C.H., 2008. Major shifts in calcareous phytoplankton assemblages through the Eocene-Oligocene transition of Tanzania and their implications for low-latitude primary production. Paleoceanography 23, 1–14.

Edgar, K.M., Bohaty, S.M., Coxall, H.K., Bown, P.R., Batenburg, S.J., Lear, C.H., Pearson, P.N., 2020. New composite bio- And isotope stratigraphies spanning the Middle Eocene Climatic Optimum at tropical ODP Site 865 in the Pacific Ocean. Journal of Micropalaeontology 39, 117–138.

Egan, K.E., Rickaby, R.E.M., Hendry, K.R., Halliday, A.N., 2013. Opening the gateways for diatoms primes Earth for Antarctic glaciation. Earth and Planetary Science Letters 375, 34–43.

Fioroni, C., Villa, G., Persico, D., Wise, S.W., Pea, L., 2012. Revised middle Eocene-upper Oligocene calcareous nannofossil biozonation for the Southern Ocean. Revue de Micropaleontologie 55, 53-70.

Fioroni, C., Villa, G., Persico, D., Jovane, L., 2015. Middle Eocene-Lower Oligocene calcareous nannofossil biostratigraphy and paleoceanographic implications from Site 711 (equatorial Indian Ocean). Marine Micropaleontology 118, 50–62.

Flores, J.A., Sierro, F.J., 2013. Coccolithophores. In: Encyclopedia of Quaternary Science. p. 783–794.

Fontorbe, G., Frings, P.J., De La Rocha, C.L., Hendry, K.R., Carstensen, J., Conley, D.J., 2017. Enrichment of dissolved silica in the deep equatorial Pacific during the Eocene-Oligocene. Paleoceanography 32, 848–863.

Fornaciari, E., Agnini, C., Catanzariti, R., Rio, D., Bolla, E.M.E.M., Valvasoni, E., 2010. Mid-latitude calcareous nannofossil biostratigraphy and biochronology across the middle to late eocene transition.

Stratigraphy 7, 229–264.

Fornaciari, E., Rio, D., 1996. Latest Oligocene to Early Middle Miocene Quantitative Calcareous Nannofossil Biostratigraphy in the Mediterranean Region. Micropaleontology 42, 1–36.

Funakawa, S., Nishi, H., Moore, T.C., Nigrini, C.A., 2006. Radiolarian faunal turnover and paleoceanographic change around Eocene/Oligocene boundary in the central equatorial Pacific, ODP Leg 199, Holes 1218A, 1219A, and 1220A. Palaeogeography, Palaeoclimatology, Palaeoecology 230, 183–203.

Gibbs, S.J., Bralower, T.J., Bown, P.R., Zachos, J.C., Bybell, L.M., 2006. Shelf and open-ocean calcareous phytoplankton assemblages across the Paleocene-Eocene thermal maximum: Implications for global productivity gradients. Geology 34, 233–236.

Gibbs, S.J., Shackleton, N.J., Young, J.R., 2004. Orbitally forced climate signals in mid-Pliocene nannofossil assemblages. Marine Micropaleontology 51, 39–56.

Gradstein, F.M., Ogg, J.G., Schmitz, M.D., Ogg, G.M., 2012. The Geologic Time Scale 2012. Elsevier, Amsterdam, Netherlands.

Hallock, P., 1987. Fluctuations in the trophic resource continuum: A factor in global diversity cycles? Paleoceanography 2, 457–471.

Hammer, Ø., Harper, D.T., 2006. Paleontological data analysis. Blackwell publishing, Malden, USA.

Hammer, Ø., Harper, D.T., Ryan, D.D., 2001. Past: Paleontological Statistics Software Package for Education and Data Analysis. Palaeontologia Electronica 4, 5–7.

Haq, B.U., Lohmann, G.P., 1976. Early Cenozoic calcareous nannoplankton biogeography of the Atlantic Ocean. Marine Micropaleontology 1, 119–194.

Heirtzler, J.R., Bolli, H.M., Davies, T.A., Saunders, J.B., Sclater, J.G., 1977. Indian Ocean Geology and biostratigraphy. Washington, D.C.

Henderiks, J., Pagani, M., 2008. Coccolithophore cell size and the Paleogene decline in atmospheric CO_2. Earth and Planetary Science Letters 269, 576–584.

Huber, B.T., 1991. Paleogene and early Neogene planktonic foraminifer biostratigraphy of Sites 738 and 744, Kerguelen Plateau (southern Indian Ocean). In: Barron, J., Larsen, B., et al. (Eds.), Proceedings of the Ocean Drilling Program, Scientific Results, Volume 119: College Station, TX, Ocean Drilling Program. p. 427–449.

Hutchinson, D.K., Coxall, H.K., Lunt, D.J., Steinthorsdottir, M., de Boer, A.M., Baatsen, M., von der Heydt, A., Huber, M., Kennedy-Asser, A.T., Kunzmann, L., Ladant, J.B., Lear, C.H., Moraweck, K., Pearson, P.N., Piga, E., Pound, M.J., Salzmann, U., Scher, H.D., Sijp, W.P., Śliwińska, K.K., Wilson, P.A., Zhang, Z., 2021. The Eocene–Oligocene transition: a review of marine and terrestrial proxy data, models and model–data comparisons. Climate of the Past 17, 269–315.

Hyland, E., Murphy, B.H., Varela, P., Marks, K., Colwell, L., Tori, F., Monechi, S., Cleaveland, L., Brinkhuis, H., Van Mourik, C.A., Coccioni, R., Bice, D.M., Montanari, A., 2009. Integrated stratigraphic and astrochronologic calibration of the Eocene-Oligocene transition in the Monte Cagnero section (northeastern Apennines, Italy): A potential parastratotype for the Massignano global stratotype section and point (GSSP). In: Koeberl, C., Montanari, A. (Eds.), The Late Eocene Eart Hothouse, Icehouse, and

Impacts. The Geological Society of America Special Paper 452, p. 303–322.

Jones, A.P., Dunkley Jones, T., Coxall, H.K., Pearson, P.N., Nala, D., Hoggett, M., 2019. Low-Latitude Calcareous Nannofossil Response in the Indo-Pacific Warm Pool Across the Eocene-Oligocene Transition of Java, Indonesia. Paleoceanography and Paleoclimatology 34, 1833–1847.

Kalb, A.L., Bralower, T.J., 2012. Nannoplankton origination events and environmental changes in the late Paleocene and early Eocene. Marine Micropaleontology 92–93, 1–15.

Katz, M.E., Miller, K.G., Wright, J.D., Wade, B.S., Browning, J. V., Cramer, B.S., Rosenthal, Y., 2008. Stepwise transition from the Eocene greenhouse to the Oligocene icehouse. Nature Geoscience 1, 329–333.

Kelly, D.C., Bralower, T.J., Zachos, J.C., Silva, I.P., Thomas, E., 1996. Rapid diversification of planktonic foraminifera in the tropical Pacific (ODP Site 865) during the late Paleocene thermal maximum. Geology 24, 423–426.

Kennett, J.P., 1977. Cenozoic evolution of Antarctic glaciation, the circum-Antarctic Ocean, and their impact on global paleoceanography. Journal of Geophysical Research 82, 3843–3859.

Kleijne, A., 1991. Holococcolithophorids from the Indian Ocean, Red Sea, Mediterranean Sea and North Atlantic Ocean. Marine Micropaleontology 17, 1–76.

Langer, G., Geisen, M., Baumann, K.H., Kläs, J., Riebesell, U., Thoms, S., Young, J.R., 2006. Species-specific responses of calcifying algae to changing seawater carbonate chemistry. Geochemistry, Geophysics, Geosystems 7, 1–12.

Lear, C.H., Bailey, T.R., Pearson, P.N., Coxall, H.K., Rosenthal, Y., 2008. Cooling and ice growth across the Eocene-Oligocene transition. Geology 36, 251–254.

Lear, C.H., Lunt, D.J., 2016. How Antarctica got its ice. Science 352, 34–35.

Liu, Z., Tuo, S., Zhao, Q., Cheng, X., Huang, W., 2004. Deep-water earliest Oligocene glacial maximum (EOGM) in South Atlantic. Chinese Science Bulletin 49, 2190–2197.

López-Quirós, A., Escutia, C., Etourneau, J., Rodríguez-Tovar, F.J., Roignant, S., Lobo, F.J., Thompson, N., Bijl, P.K., Bohoyo, F., Salzmann, U., Evangelinos, D., Salabarnada, A., Hoem, F.S., Sicre, M.A., 2021. Eocene-Oligocene paleoenvironmental changes in the South Orkney Microcontinent (Antarctica) linked to the opening of Powell Basin. Global and Planetary Change 204, 103581.

Lyle, M.W., Wilson, P.A., Janecek, T.R., 2002. Leg 199 Summary. Proceedings of the Ocean Drilling Program, Initial Reports, College Station, TX (Ocean Drilling Program) 199, 1–87.

Marino, M., Flores, J.A., 2002. Middle Eocene to early Oligocene calcareous nannofossil stratigraphy at Leg 177 Site 1090. Marine Micropaleontology 45, 383–398.

Martini, E., 1971. Standard Tertiary and Quaternary calcareous nannoplankton zonation. In: Farinacci, A. (Ed.), Proceedings of the 2nd International Conference on Planktonic Microfossils. Edizioni Tecnoscienza, Rome, p. 739–785.

Merico, A., Tyrrell, T., Wilson, P.A., 2008. Eocene/Oligocene ocean de-acidification linked to Antarctic glaciation by sea-level fall. Nature 452, 979–982.

Monechi, S., Buccianti, A., Gardin, S., 2000. Biotic signals from nannoflora across the iridium anomaly in the

upper Eocene of the Massignano section: evidence from statistical analysis. Marine Micropaleontology 39, 219–237.

Moore, J.C., Wade, B.S., Westerhold, T., Erhardt, A.M., Coxall, H.K., Baldauf, J., Wagner, M., 2014. Equatorial Pacific productivity changes near the Eocene-Oligocene boundary. Paleoceanography 29, 825–844.

Moran, M.J.J., Watkins, D.K.K., 1988. Oligocene Calcareous-Nannofossil Biostratigraphy from Leg 101, Site 628, Little Bahama Bank Slope. Proceedings of the Ocean Drilling Program, 101 Scientific Results 101, 87–103.

Morkhoven, F., Berggren, W.A., Edwards, A.S., Oertli, H.J., 1986. Cenozoic cosmopolitan deep-water benthic foraminifera., Bulletin des centres de recherches Exploration-production Elf-Aquitaine: Mémoire 11.

Newsam, C., Bown, P.R., Wade, B.S., Jones, H.L., 2017. Muted calcareous nannoplankton response at the Middle/Late Eocene Turnover event in the western North Atlantic Ocean. Newsletters on Stratigraphy 50, 297–309.

Nocchi, M., Parisi, G., Monaco, P., Monechi, S., Madile, M., 1988. Eocene and early Oligocene micropaleontology and paleoenvironments in SE Umbria, Italy. Palaeogeography, Palaeoclimatology, Palaeoecology 67, 181–244.

Nocchi, M., Parisi, G., Monaco, P., Monechi, S., Madile, M., Napoleone, G., Ripepe, M., Orlando, M., Premoli Silva, I., Bice, D.M., 1986. The Eocene-Oligocene Boundary in the Umbrian Pelagic Sequences, Italy. In: Developments in Palaeontology and Stratigraphy. Elsevier, Amsterdam, p. 25–40.

Nomura, R., 1991. Oligocene to Pleistocene benthic foraminifer assemblages at Sites 754 and 756, eastern Indian Ocean. Proc., scientific results, ODP, Leg 121, Broken Ridge and Ninetyeast Ridge 121, 31–75.

Norris, R.D., Wilson, P.A., Blum, P., the Expedition 342, 2014. Proceedings. IODP, 342: College Station, TX (Integrated Ocean Drilling Program).

Okada, H., Bukry, D., 1980. Supplementary modification and introduction of code numbers to the low-latitude coccolith biostratigraphic zonation. Marine Micropaleontology 5, 321–325.

Pälike, H., Lyle, M.W., Nishi, H., Raffi, I., Ridgwell, A., Gamage, K., Klaus, A., Acton, G., Anderson, L., Backman, J., Baldauf, J., Beltran, C., Bohaty, S.M., Bown, P.R., Busch, W., Channell, J.E.T., Chun, C.O.J., Delaney, M.L., Dewangan, P., Dunkley Jones, T., Edgar, K.M., Evans, H., Fitch, P., Foster, G.L., Gussone, N., Hasegawa, H., Hathorne, E.C., Hayashi, H., Herrle, J.O., Holbourn, A.E., Hovan, S., Hyeong, K., Iijima, K., Ito, T., Kamikuri, S.I., Kimoto, K., Kuroda, J., Leon-Rodriguez, L., Malinverno, A., Moore, T.C., Murphy, B.H., Murphy, D.P., Nakamura, H., Ogane, K., Ohneiser, C., Richter, C., Robinson, R., Rohling, E.J., Romero, O., Sawada, K., Scher, H.D., Schneider, L., Sluijs, A., Takata, H., Tian, J., Tsujimoto, A., Wade, B.S., Westerhold, T., Wilkens, R., Williams, T., Wilson, P.A., Yamamoto, Y., Yamamoto, S., Yamazaki, T., Zeebe, R.E., 2012. A Cenozoic record of the equatorial Pacific carbonate compensation depth. Nature 488, 609–614.

Pälike, H., Norris, R.D., Herrle, J.O., Wilson, P.A., Coxall, H.K., Lear, C.H., Shackleton, N.J., Tripati, A.K., Wade, B.S., 2006. The heartbeat of the Oligocene climate system. Science 314, 1894–1898.

Pearson, P.N., Coxall, H.K., 2014. Origin of the Eocene planktonic foraminifer Hantkenina by gradual

evolution. Palaeontology 57, 243–267.

Pearson, P.N., McMillan, I.K., Wade, B.S., Dunkley Jones, T., Coxall, H.K., Bown, P.R., Lear, C.H., 2008. Extinction and environmental change across the Eocene-Oligocene boundary in Tanzania. Geology 36, 179–182.

Pearson, P.N., Olsson, R.K., Huber, B.T., Hemleben, C., Berggren, W.A., 2006. Atlas of Eocene planktonic foraminifera (No. 41). Cushman Foundation for Foraminiferal Research.

Peirce, J., Weissel, J., et al., 1989a. Leg 121 Background and objectives. Proceeding ODP, Initial Reports, 121: College Station, TX (Ocean Drilling Program).

Peirce, J., Weissel, J., et al., 1989b. Site 756. Proceeding ODP, Initial Reports, 121: College Station, TX (Ocean Drilling Program).

Perch-Nielsen, K., 1985. Cenozoic calcareous nannofossils. In: Bolli, H.M., Saunders, J.B., Perch-Nielsen, K. (Eds.), Plankton Stratigraphy. Cambridge University Press, Cambridge, p. 427–555.

Perch-Nielsen, K., 1986. Calcareous nannofossil events at Eocene/Oligocene boundary. In: Pomerol, C., Premoli Silva, I. (Eds.), Terminal Eocene Events. Elsevier, Amsterdam, p. 275–282.

Persico, D., Villa, G., 2004. Eocene-Oligocene calcareous nannofossils from Maud Rise and Kerguelen Plateau (Antarctica): Paleoecological and paleoceanographic implications. Marine Micropaleontology 52, 153–179.

Persico, D., Villa G., 2008. A new Eocene Chiasmolithus species: hypothetical reconstruction of its phyletic lineage. Journal of Nannoplankton Research 30, 23-33

Pospichal, J.J., 1991. Calcareous nannofossils across Cretaceous/Tertiary boundary at Site 752, eastern Indian Ocean. Proceedings of the Ocean Drilling Program, College Station, TX, 121 395–413.

Premoli Silva, I., Jenkins, D.G., 1993. Decision on the Eocene-Oligocene boundary stratotype. Episodes 16, 379–382.

Premoli Silva, I., Orlando, M., Monechi, S., Madile, M., Napoleone, G., Ripepe, M., 1988. Calcareous plankton biostratigraphy and magnetostratigraphy at the Eocene-Oligocene transition in the Gubbio area. International Subcommission on Paleogene Stratigraphy, Eocene/Oligocene Meeting, Spec. Publ., II 6, 137–161.

Raffi, I., Agnini, C., Backman, J., Catanzariti, R., Pälike, H., 2016. A Cenozoic calcareous nannofossil biozonation from low and middle latitudes: A synthesis. Journal of Nannoplankton Research 36, 121–132.

Ravizza, G., Paquay, F., 2008. Os isotope chemostratigraphy applied to organic-rich marine sediments from the Eocene-Oligocene transition on the West African margin (ODP Site 959). Paleoceanography 23, 1–11.

Reghellin, D., Coxall, H.K., Dickens, G.R., Backman, J., 2015. Carbon and oxygen isotopes of bulk carbonate in sediment deposited beneath the eastern equatorial Pacific over the last 8 million years. Paleoceanography 30, 1261–1286.

Salamy, K.A., Zachos, J.C., 1999. Latest Eocene-Early Oligocene climate change and Southern Ocean fertility: Inferences from sediment accumulation and stable isotope data. Palaeogeography, Palaeoclimatology,

Palaeoecology 145, 61–77.

Sarmiento, J.L., Gruber, N., Brzezinski, M.A., Dunne, J.P., 2004. High-latitude controls of thermocline nutrients and low latitude biological productivity. Nature 427, 56–60.

Schneider, L.J., Bralower, T.J., Kump, L.R., 2011. Response of nannoplankton to early Eocene ocean destratification. Palaeogeography, Palaeoclimatology, Palaeoecology 310, 152–162.

Shannon, C.E., Weaver, W., 1949. The Mathematical Theory of Communication. University of Illinois Press, Champaign, IL.

Shaw, A.B., 1964. Adequacy of the Fossil Record. In: Time in Stratigraphy. Mc Graw-Hill, p. 105–117.

Shcherbinina, E., 2010. Response of early Paleogene nannofossils to periodically increased nutrient availability in the NE Peri-Tethys. Geophysical Research Abstracts 12, 13597.

Spofforth, D.J.A., Agnini, C., Pälike, H., Rio, D., Fornaciari, E., Giusberti, L., Luciani, V., Lanci, L., Muttoni, G., 2010. Organic carbon burial following the middle Eocene climatic optimum in the central western Tethys. Paleoceanography 25, PA3210.

Sverdrup, H.U., Johnson, M.W., Fleming, R.H.., 1942. The Oceans: their physics, chemistry, and general biology. Prentice-Hall, Inc., New York.

Toffanin, F., Agnini, C., Fornaciari, E., Rio, D., Giusberti, L., Luciani, V., Spofforth, D.J.A., Pälike, H., 2011. Changes in calcareous nannofossil assemblages during the Middle Eocene Climatic Optimum: Clues from the central-western Tethys (Alano section, NE Italy). Marine Micropaleontology 81, 22–31.

Toffanin, F., Agnini, C., Rio, D., Acton, G., Westerhold, T., 2013. Middle eocene to early oligocene calcareous nannofossil biostratigraphy at IODP site U1333 (equatorial pacific). Micropaleontology 59, 69–82.

Tremolada, F., Bralower, T.J., 2004. Nannofossil assemblage fluctuations during the Paleocene-Eocene Thermal Maximum at Sites 213 (Indian Ocean) and 401 (North Atlantic Ocean): palaeoceanographic implications. Marine Micropaleontology 52, 107–116.

Via, R.K., Thomas, D.J., 2006. Evolution of Atlantic thermohaline circulation: Early Oligocene onset of deep-water production in the North Atlantic. Geology 34, 441–444.

Villa, G., Fioroni, C., Pea, L., Bohaty, S.M., Persico, D., 2008. Middle Eocene-late Oligocene climate variability: Calcareous nannofossil response at Kerguelen Plateau, Site 748. Marine Micropaleontology 69, 173–192.

Villa, G., Fioroni, C., Persico, D., Roberts, A.P., Florindo, F., 2014. Middle Eocene to Late Oligocene Antarctic glaciation/deglaciation and Southern Ocean productivity. Paleoceanography 29, 223–237.

Villa, G., Florindo, F., Persico, D., Lurcock, P., de Martini, A.P., Jovane, L., Fioroni, C., 2021. Integrated calcareous nannofossil and magnetostratigraphic record of ODP Site 709: Middle Eocene to late Oligocene paleoclimate and paleoceanography of the Equatorial Indian Ocean. Marine Micropaleontology 169, 102051.

Villa, G., Persico, D., 2006. Late Oligocene climatic changes: Evidence from calcareous nannofossils at Kerguelen Plateau Site 748 (Southern Ocean). In: Palaeogeography, Palaeoclimatology, Palaeoecology. Elsevier, p. 110–119.

Wade, B.S., Aljahdali, M.H., Mufrreh, Y.A., Memesh, A.M., Alsoubhi, S.A., Zalmout, I.S., 2021. Upper

Eocene planktonic foraminifera from northern Saudi Arabia: Implications for stratigraphic ranges. Journal of Micropalaeontology 40, 145–161.

Wade, B.S., Bown, P.R., 2006. Calcareous nannofossils in extreme environments: the Messinian Salinity Crisis, Polemi Basin, Cyprus. Palaeogeography, Palaeoclimatology, Palaeoecology 233, 271–286.

Wade, B.S., Olsson, R.K., 2009. Investigation of pre-extinction dwarfing in Cenozoic planktonic foraminifera. Palaeogeography, Palaeoclimatology, Palaeoecology 284, 39–46.

Wade, B.S., Olsson, R.K., Pearson, P.N., Huber, B.T., Berggren, W.A., 2018. Atlas of Oligocene Planktonic Foraminifera. Cushman Foundation Special Publication 46, Washington D.C.

Wade, B.S., Pearson, P.N., 2008. Planktonic foraminiferal turnover, diversity fluctuations and geochemical signals across the Eocene/Oligocene boundary in Tanzania. Marine Micropaleontology 68, 244–255.

Wei, W., Wise, S.W., 1990. Biogeographic gradients of middle Eocene-Oligocene calcareous nannoplankton in the South Atlantic Ocean. Palaeogeography, Palaeoclimatology, Palaeoecology 79, 29–61.

Wei, W.C., Villa, G., Wise, S.W., Wuchang Wei, Villa, G., Wise, S.W., 1992. Paleoceanographic implications of Eocene-Oligocene calcareous nannofossils from Sites 711 and 748 in the Indian Ocean. Proceedings of the Ocean Drilling Program, 120 Scientific Results 120, 979–999.

Winter, A., Jordan, R.W., Roth, P.H., 1994. Biogeography of living coccolithophores in ocean waters. In: Winter, A., Siesser, W.G. (Eds.), Coccolithophores. Cambridge University Press, Cambridge, p. 161–177.

Young, J.R., 1998. Neogene. In: Bown, P. (Ed.), Calcareous Nannofossil Biostratigraphy. Kluwer Academic Publishers, p. 225–265.

Young, J.R., Geisen, M., Probert, I., 2005. A review of selected aspects of coccolithophore biology with implications for paleobiodiversity estimation. Micropaleontology 51, 267–288.

Zachos, J.C., Kump, L.R., 2005. Carbon cycle feedbacks and the initiation of Antarctic glaciation in the earliest Oligocene. Global and Planetary Change 47, 51–66.

Zachos, J.C., Pagani, M., Sloan, L., Thomas, E., Billups, K., 2001. Trends, Global Rhythms, and Aberrations in Global Climate 65 Ma to Present. Science 292, 686–693.

Zachos, J.C., Quinn, T.M., Salamy, K.A., 1996. High-resolution (10^4 years) deep-sea foraminiferal stable isotope records of the Eocene-Oligocene climate transition. Paleoceanography 11, 251–266.

Zachos, J.C., Rea, D.K., Seto, K., Nomura, R., Niitsuma, N., 1992. Paleogene and Early Neogene Deep Water Paleoceanography of the Indian Ocean as Determined from Benthic Foraminifer Stable Carbon and Oxygen Isotope Records. In: Duncan, R.A., Rea, D.K., Kidd, R.B., Rad, U. von, Weissel, J.K. (Eds.), Synthesis of Results from Scientific Drilling in the Indian Ocean, Volume 70. American Geophysical Union, p. 351–385.

Chapter 3

Calcareous nannofossils biostratigraphy and biochronology from IODP Site U1509 across the Eocene-Oligocene transition: a global overview[1]

Abstract

Over the last 50 years, calcareous nannofossils have been widely used in Cenozoic marine biostratigraphy and biochronology. The special bonus of this group is that first and last appearance are typically high and thus provide reliable data that could be used for dating aims and worldwide correlations. In the last decades, new calcareous nannofossil biostratigraphic biohorizons have been proposed, for the Paleogene (Agnini et al., 2007, 2014) and the Neogene (Raffi et al., 2016). In the Paleogene, the Oligocene represents an exception with low resolved calcareous nannofossil biozonations, mainly due to low evolutionary rates and species diversity (Raffi et al., 2016). In this work we present a continuous and well-resolved sequence across the Eocene-Oligocene transition from IODP Site U1509 located in the New Caledonia Trough (Tasman Sea) which offers a unique opportunity to implement the available bistratigraphic/biochronologic framework and allows for an improved age model of the study section. High resolution biostratigraphic data are consistent with the preliminary on-board data (Sutherland et al., 2019) but point to additional biohorizons that could potentially be integrated with classic (Martini, 1971; Okada and Bukry, 1980) and recently published (Agnini et al., 2014) biozonations, that are here described. Comparison of the age estimates from Site U1509 with those of previous works from low-middle and high latitudes allows us to critically evaluate the accuracy, reliability, synchroneity or diachroneity of all the biohorizons considered and to test them over different oceanographic domains.

Keywords: calcareous nannofossils, biostratigraphy, biochronology, Eocene-Oligocene transition, IODP Site U1509.

[1] Allyson Viganò[1], Edoardo Dallanave[2], Laia Alegret[3], Thomas Westerhold[4], Rupert Sutherland[5], Gerald R. Dickens[6], Cherry Newsam[7], Claudia Agnini[1]

[1]Dipartimento di Geoscienze, Università di Padova, Padova, Italy
[2]Faculty of Geosciences - Research Group Marine Geophysics, University of Bremen, Bremen, Germany
[3]Facultad de Sciencias, Universidad de Zaragoza, Zaragoza, Spain
[4]Center for Marine Environmental Sciences (Marum), University of Bremen, Bremen, Germany
[5]School of Geography, Environment and Earth Sciences, Victoria University of Wellington, Kelburn Parade, Wellington 6012, New Zealand
[6]Earth, Environmental and Planetary Sciences, Rice University, 6100 Main Street, Houston, TX 77005, USA
[7]Department of Earth Sciences, University College London, Gower Street, London, UK, WC1E 6BT

Authors contributions: A.V. and C.A. designed the study and developed the methodology. A.V. was responsible for data creation and presentation. A.V. and C.A. were the project administrator. A.V. wrote the original draft. L.A, T.W., R.S., G.D. and C.A. have provided the samples used in this study. E.D. have provided data, comments and suggestions. C.N. have provided further data used in this work.
All the co-authors contributed to the final polishing of the manuscript.

3.1 Introduction

Calcareous nannofossils have a high potential as stratigraphic tool in Mesozoic (Bown, 1998) and Cenozoic (Agnini et al., 2017) deep-sea sediments and provide well refine datasets to date sediments and rocks. Despite the Paleogene calcareous nannofossil biostratigraphy has improved significantly over the last years, through intensive studies on many deep-sea cores, the Eocene-Oligocene interval, though it represents a crucial climate transition, still remains understudied.

It is worth to say that classical Cenozoic biozonations suffer from a series of pitfalls primarily related to ambiguous taxonomic concepts and the low reliability of some biohorizons. Moreover the low degree in the standardizations of counting methods and inconsistent nomenclature definitions sometimes results in low quality data that make them hardly correlatable (Agnini et al., 2017). During the late Eocene and early Oligocene, quantitative biostratigraphy can answer to same specific questions: are there additional E-O calcareous nannofossil horizons that could be used globally? Besides biozonal biohorizons, which bioevents could provide useful regional correlation tools? How could we explain non-spatial homogeneity and conflicting correlations in different areas? Is there any substantial difference between shallow-water and deep-water paleo-environments? To fill this gap and try to answer these questions, we have carried out a quantitative analysis of selected calcareous nannofossil taxa from Site U1509 recovered during International Ocean Discovery Program (IODP) Expedition 371 (Sutherland et al., 2018).

IODP Site U1509 records an expanded late Eocene- early Oligocene sequence with moderate to well preserved calcareous nannofossils, offering the opportunity to tie calcareous nannofossil data to magnetostratigraphy. This section is thus suitable to potentially improve the biostratigraphic and biochronological framework provided by calcareous nannofossils during the late Eocene early Oligocene time, specifically from Chron C15n to the upper part of Chron C12r (35.24 to 30.33 Ma; CNE19-CNO3) (Agnini et al., 2014).

Main aims of this work are to (1) semi-quantitatively investigate standard and additional biohorizons at Site U1509 in order to obtain a high-resolution bio-magnetochronostratigraphic framework and, in turn, an implemented age model; (2) to compare, using a common time scale (GTS2012; Gradstein et al., 2012), the ages obtained for calcareous nannofossil bioevents at Site U1509 with the biochronologic data published for a number of sites located at low-middle and high latitudes; (3) to evaluate their accuracy and significance, in term of global/regional validity, synchronicity and preservation potential. To achieve these goals, our high-quality data are compared along with other existing records available from the Indian, Equatorial Pacific, South Atlantic and Southern oceans in order to obtain a global biochronological model and to assess the presence -if any- of latitudinal inconsistencies (e.g., diachrony, paleobiogeographic provincialism and/or regional constraints) that would also provide insights on the Eocene-Oligocene climate evolution.

3.2 Geological settings

For this study, the age estimates of calcareous nannofossil events, has been compiled from nine low-middle latitude sites (Figure 3.1A): IODP Site U1509, ODP Site 1218 (Equatorial Pacific; Blaj et al., 2009), IODP Site U1333 (Equatorial Pacific; Toffanin et al., 2013); IODP Site U1411 (NW Atlantic; Newsam, 2016), DSDP Sites 522 and523 (SE Atlantic; Backman, 1987), DSDP Site 516 (SW Atlantic, Wei and Wise, 1989); ODP Site 711 (Equatorial Indian; Fioroni et al., 2015) and ODP Site 756 (Indian Ocean; Chapter 2).

To obtain a global overview, we also compared our results with four high-latitude sites (Figure 3.1B): ODP Site 1090 (Agulhas Ridge; Marino and Flores, 2002), ODP Site 689 (Maud Rise; Persico and Villa, 2004), ODP Site 744 (Kerguelen Plateau; Persico and Villa, 2004), ODP Site 748 (Kerguelen Plateau; Villa et al., 2008). The present geographic location as well as the today and paleo depths are provided in Table 3.1.

The study site, IODP Site U1509, is situated ~640 km west of the northern tip of New Zealand, currently positioned at a water depth of 2911 m, and it is supposed to have been at least lower bathyal during the E-O transition (Sutherland et al., 2019; 2022). The location is on the western margin of the New Caledonia Trough at the base of the Lord Howe Rise slope, near the mouth of a canyon (Sutherland et al., 2018; 2019).

DSDP/ODP/IODP	Location	Latitude	Longitude	Water depth (m)	Paleodepth (m)	Reference
Site U1509	New Caledonia Trough, Pacific Ocean	34°39.13'S	165°49.66'E	2911	lower bathyal	Sutherland et al. (2019)
Site 1218	Eastern Equatorial Pacific	8°53.378'N	135°22.00'W	4826	~3700–4300	Blaj et al. (2009)
Site U1333	Eastern Equatorial Pacific	10°30.996'N	138°25.159'W	4853	lower bathyal to abyssal	Toffanin et al. (2013)
Site 711	Equatorial Indian Ocean	2°44.56'S	61°09.78'E	4428	~3450-3750	Fioroni et al. (2015)
Site 756	Ninetyeast Ridge (Indian Ocean)	27°21.25'S	87°35.89'E	1516	~400	This thesis (Chapter 2)
Site U1411	Newfoundland Ridge (NW Atlantic)	41°37'N	48°6'W	3300	~2800	Newsam (2016)
Site 522	Walvis Ridge (SE Atlantic)	26°6.843'S	5°7.748'W	4441	~3000-3500	Backman (1987)
Site 523	Walvis Ridge (SE Atlantic Ocean)	28°33.131'S	2°15.078'W	4562	~3450-3550	Backman (1987)
Site 516	Rio Grande Rise (SW Atlantic Ocean)	30°16.59'S	35°17.10'W	1313	middle bathyal	Wei and Wise (1989)
Site 1090	Agulhas Ridge (SE Atlantic Ocean)	42°54'S	8°53'E	3702	~3200	Marino and Flores (2002)
Site 689	Maud Rise (Southern Ocean)	64°31.009'S	03°06.026'E	2080	~1500-2000	Persico and Villa (2004)
Site 744	Kerguelen Plateau (Southern Ocean)	61°34.66'S	80°35.46'E	2307	~2250	Persico and Villa (2004)
Site 748	Kerguelen Plateau (Southern Ocean)	58°26.45'S	78°58.89'E	1291	~1200	Villa et al. (2008)

Table 3.1 Current location of the study site (IODP Site U1509) and other sites used for comparison. Location, geographic coordinates, current water depth (m), paleodepth (m) and references are reported for each IODP, DSDP and ODP site.

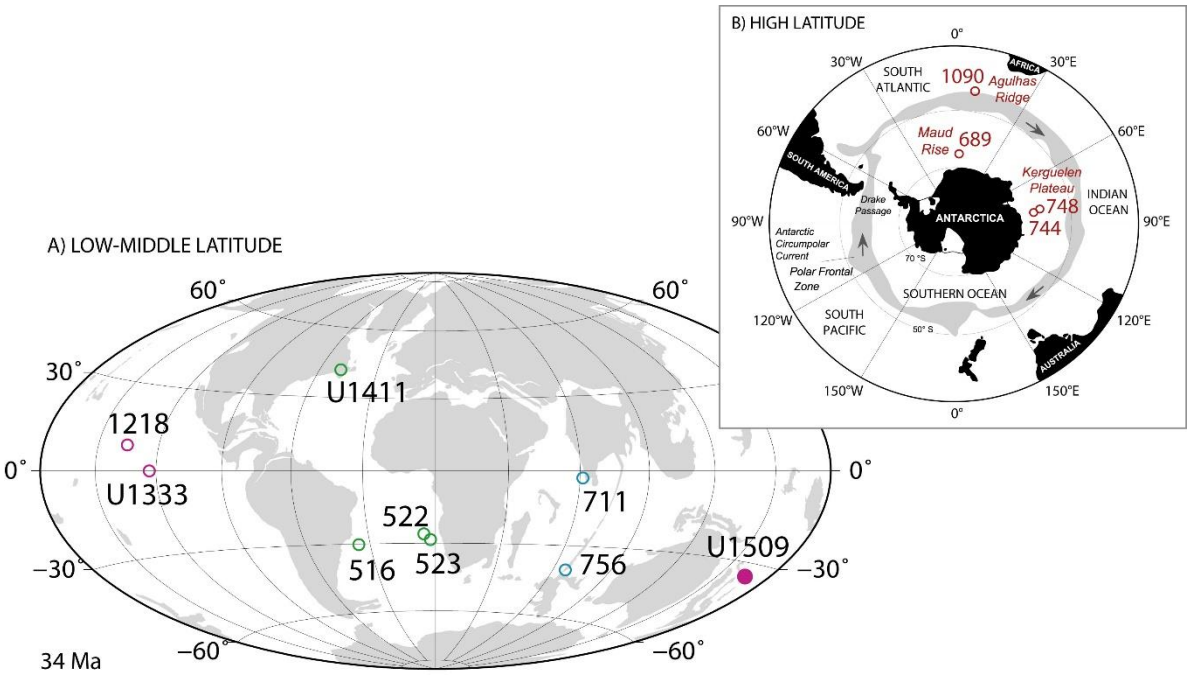

Figure 3.1 A) Paleo map reconstruction (www.odsn.de) for the E-O transition (~34 Ma) showing the location of IODP Site U1509 (solid purple circle, IODP Exp. 371) and other low-middle latitude sites (IODP Site U1411, IODP Exp. 342; Sites 522/523, DSDP Leg. 73; 516, DSDP Leg. 72; Site 711, ODP Leg. 115; Site 756, ODP Leg. 121; Site 1218, ODP Leg 199; Site 1333, IODP Exp. 320; references are reported in the main text). **B)** Present day location of Southern Ocean sites used herein for comparison (Site 1090, ODP Leg. 177; Site 744, ODP Leg. 119; Site 748, ODP Leg. Site 120; 689, ODP Leg. 113; references in the text) (modified from Diekmann et al. 2004).
Purple circle = Pacific Ocean; green circle = Atlantic Ocean; light blue circles: Indian Ocean.

Sediments recovered at Site U1509 (Hole 1509A) belongs to two lithostratigraphic units: Unit I, which consists of ~415 m of Pleistocene to upper Paleocene calcareous ooze, chalk, and limestone, and the underlying Unit II, which comprises ~275 m of Paleocene to Upper Cretaceous claystone. In turn, lithostratigraphic Unit I is further divided into three subunits: Subunit Ia (~ 100 m -thick- sediment of Pliocene to upper Oligocene sediments dominated by calcareous ooze and chalk with varying foraminifera abundances), Subunit Ib (~ 40 m of upper to lower Oligocene greenish grey calcareous chalk, with dominant nannofossils and common to abundant foraminifers) and Subunit Ic (~275 m of lower Oligocene to upper Paleocene calcareous chalk and limestone with varying amounts of siliceous microfossils or chert nodules). Subunit Ic is dominated by a calcareous component which consists of calcareous nannofossils with rare to common foraminifera. Biosilica was also observed and consists of sponge spicules, radiolaria, and silicoflagellates (Sutherland et al., 2019). The succession investigated in this work belongs to Subunit Ic and ranges from 267.305 to 183.305 m CSF-a, spanning ~5 Myr.

3.3 Methods

3.3.1 Calcareous nannofossils

A total of 129 samples from Hole U1509A were prepared using standard methodologies (Bown and Young, 1998). The study interval is ~ 84m -thick interval and the sampling resolution is ~66 cm.

Selected calcareous nannofossil index species were investigated using a transmitted light microscope (Zeiss Axioscope 40), at 1250× magnification, to determine semi-quantitative abundance patterns. The temporal resolution across studied interval is of approximately 40 kyrs, which duplicates around the EOT (20 kyrs). Nannofossil biostratigraphic data are based on semi-quantitative analysis obtained counting the number of specimens of the considered taxon present in a 1 mm^2 (n/mm^2; Backman and Shackleton, 1983).

Bioevents are labelled following the terminology proposed by Agnini et al. (2014): the Base (B) as the lowest occurrence of a taxon; the Top (T) as the highest occurrence of a taxon; the Base common and continuous (Bc) as the first and continuous presence of a taxon and the Top common and continuous (Tc) as the last continuous and common presence of a taxon. We decided to adopt this nomenclature, because we share the opinion that semiquantitative abundance fluctuations, can more consistently be correlated than qualitative on first and last occurrence data (Agnini et al., 2014). In this regard, the followed strategy was to compare the pattern of abundance of individual taxa, rather than just their final extinction or appearance, and thus using both the top commons and base commons. In this work we adopted the classical low-middle latitude calcareous nannofossil zonations of Martini (1971) and Okada and Bukry (1980), and Agnini et al. (2014).

The main criteria used for site selection were the availability of magnetostratigraphic data coupled with high-quality and well-resolved nannofossil records from different latitudes (low, middle, and high), ocean basins, depth and depositional settings, providing a representative overview of the global biostratigraphic dynamics through the EOT interval.

3.3.2 Paleomagnetism

At Site U1509 shipboard biostratigraphic data constrain the Eocene-Oligocene boundary between samples U1509A-28R-CC and U1509A-29R-CC (254.31 ± 5.63 m CSF-A) based on the Top of the planktonic foraminifer *Globigerinatheka index*. This correlation was further supported by the identification of the Chron C13n/C13r boundary, but the very low intensity of the paleomagnetic signal resulted in very high background noise (Sutherland et al. 2019).

To refine the correlation with the geomagnetic polarity time scale of the interval of interest, we collected a total of 47 oriented paleomagnetic samples (8 cm^3) in the interval between Cores 34 and 26 of Hole U1509A (299.5–221.35 m CSF-A) (Figure 3.2). Reliable paleomagnetic directions have been provided from 40 samples. The obtained improved magnetic sequence allows a robust correlation with Chrons from C17n to C12r, considerably improving the correlation with the adopted time scale (Gradstein et al., 2012).

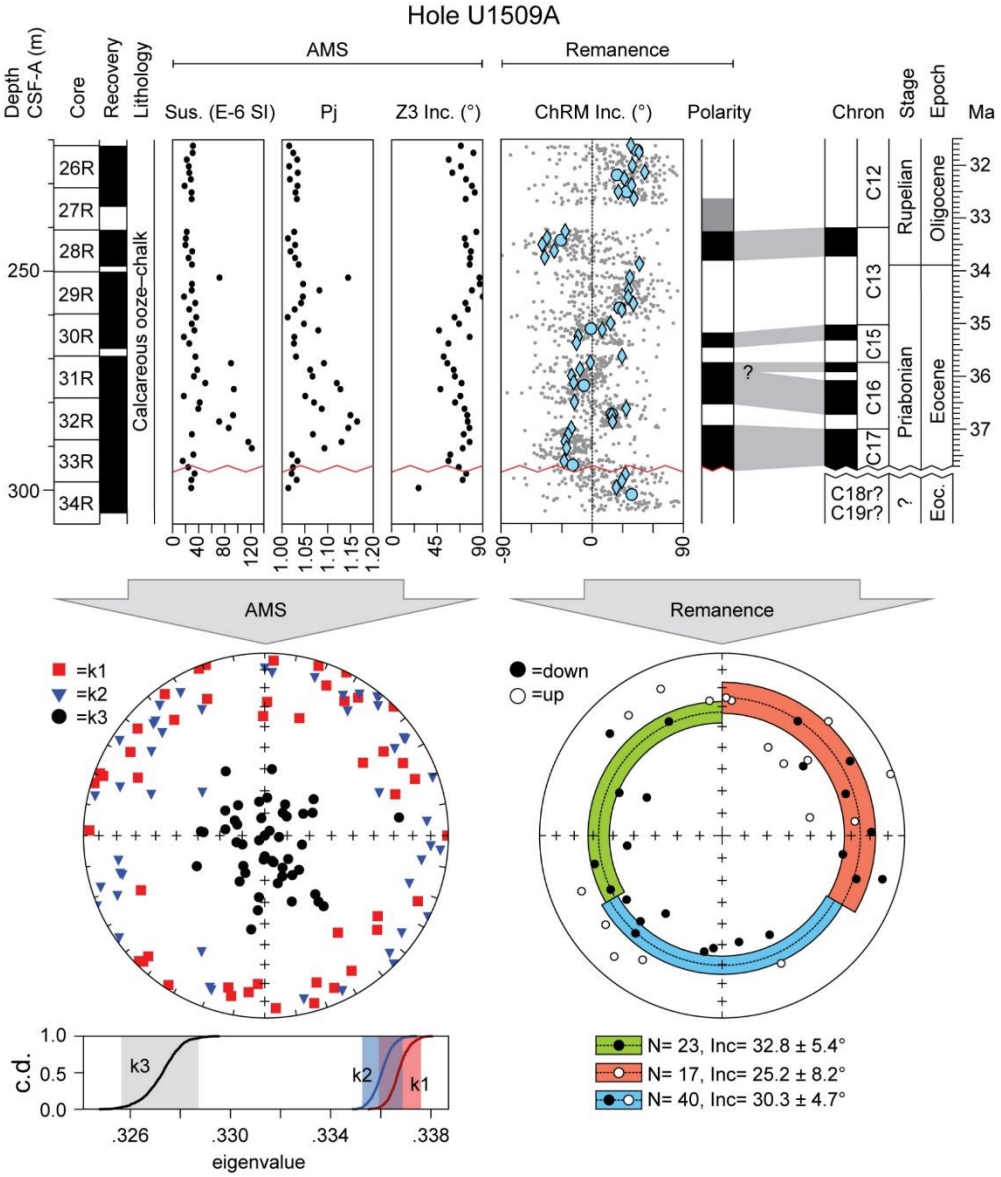

Figure 3.2 Anisotropy of magnetic susceptibility (AMS; left panel) and paleomagnetic remanence (right panel) analysis. AMS has the typical sedimentary fabric (k3 vertical) indicating the absence of deformation. Paleomagnetic directions (light blue diamonds) constrain the E-O boundary within Chron C13r.
Note: Sus.= magnetic susceptibility; Pj= anisotropy degree; Z3 Inc.= inclination of the minor AMS axis; ChRM Inc.= inclination of the characteristic remanent magnetization; c.d.= eigenvalues cumulative distribution of 1000 sets of bootstrapped AMS pseudosamples. Paleomagnetic directions are shown with the average inclination.

3.3.3 Age models

The age model proposed for Site U1509 (Figure 3.3) used the position of the paleomagnetic chron boundaries as tie-points. The ages of the magnetic polarity reversal are after Ogg et al. (2012) (GTS2012).

Absolute ages of calcareous nannofossil biostratigraphic events were calculated by applying a linear interpolation between nearest reversal boundaries. Linear sedimentation rates (LSRs) were assumed to remain constant between tie points, with an average LSR of 1.5 cm/kyr for the EOT interval. The inferred position of the E-O boundary (EOB, 33.89 Ma – GTS12) was extrapolated by applying a linear interpolation between magnetic Chron boundaries. This estimate placed the EOB at 250.085 m CSF-A, ~ 5 m above the Top of *G. index* (254.31 ± 5.63 m CSF-A), within calcareous nannofossil Zone NP21 (Martini, 1971), and near the top of Chron C13r (Gradstein et al., 2012).

Age calibrations of important nannofossil bioevents recognized at IODP Site U1509 were compared with age estimates from published records (assigned using available Chron boundaries and calibrated with respect to the GTS12) to provide a set of 'reliable' events (Appendix IV).

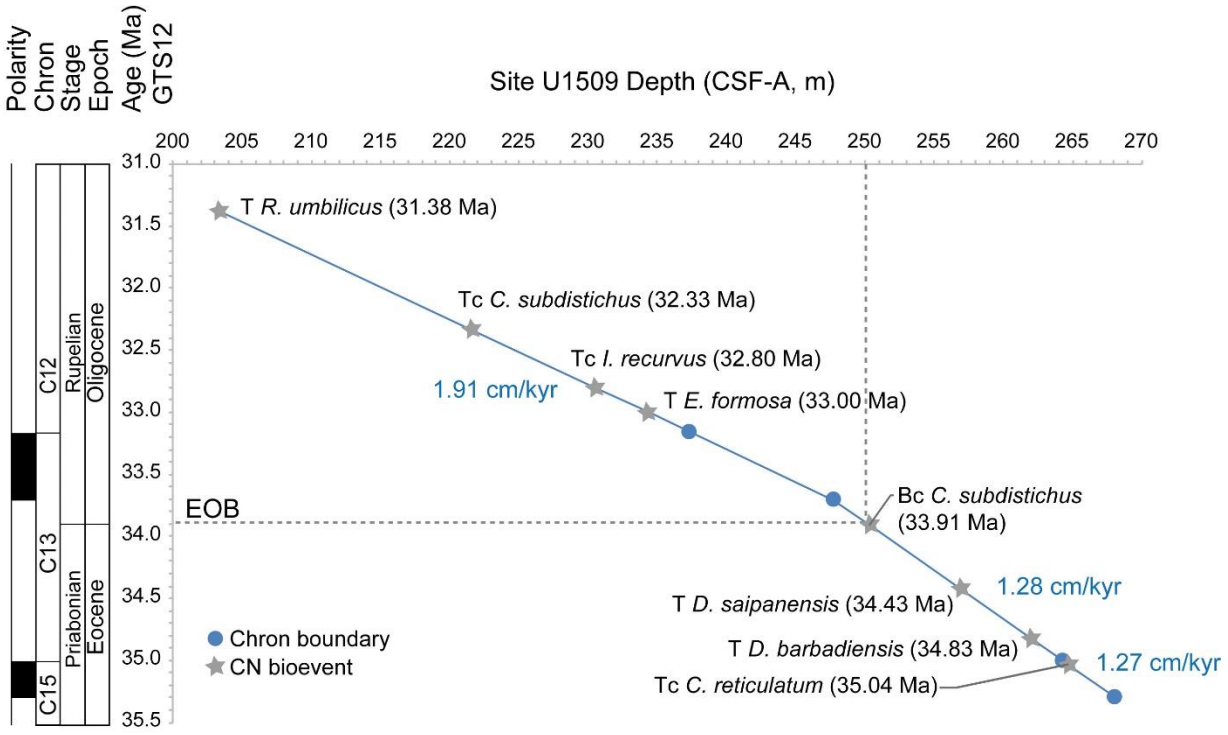

Figure 3.3 Age model for the late Eocene-early Oligocene interval based on magnetostratigraphy, IODP Site U1509. Ages of calcareous nannofossil bioevents (grey stars) were calculated by linear interpolation between successive Chron boundaries (blue dots). Data are reported in the Appendix IV. LSRs are also shown. The position of the EOB (Eocene-Oligocene boundary; 250.085 m CSF-A) was extrapolated by applying linear interpolation between magnetic Chron boundaries (blue dots) and falls within the range limits provided by the Top of *G. index* (254.31 ± 5.63 m CSF-A).

In addition, in order to better compare the reliability of additional bioevents (e.g,. the acme beginning and end of *Clausicoccus subdistichus* gr. and *Lanternithus minutus* or the Tc of *Isthmolithus recurvus*) with those acquired from ODP Site 756, for which magnetostratigraphic data were not available, we decided to use an alternative age model based on the same tie-points applied at Site 756 (Table 3.2), except for the Top of *Hantkenina*, which was not reported at Site U1509.

IODP SITE U1509	Interval (hole-core-section, cm)							
Event	Top sample	Base sample	Top depth (CSF-a, m)	Base depth (CSF-a, m)	**Mid point (CSF-a, m)**	Error (m)	**Age (Ma) GTS12**	Age (Ma) (This study)
T *Reticulofenestra umbilicus*	U1509A-23R-1W, 100-101	U1509A-23R-2W, 8-9	203.105	203.685	**203.395**	0.29	**32.02**	
T *Sphenolithus akropodus*	U1509A-24R-2W, 132-133	U1509A-24R-3W, 42-43	209.405	210.005	209.705	0.30		32.20
Tc *Chiasmolithus altus*	U1509A-24R-3W, 42-43	U1509A-24R-3W, 102-103	210.005	210.605	210.305	0.30		32.22
Tc *Clausicoccus subdistichus*	U1509A-26R-1W, 11-12	U1509A-26R-2W, 2-3	221.415	221.705	221.560	0.14		32.55
Tc *Lanternithus minutus*	U1509A-26R-3W, 122-123	U1509A-26R-4W, 32-33	224.405	225.005	224.705	0.30		32.64
Tc **(2)** *Isthmolithus recurvus*	U1509A-26R-8W, 15-16	U1509A-26R-8W, 45-46	230.405	230.705	230.555	0.15		32.81
T *Ericsonia formosa*	U1509A-27R-3W, 9-10	U1509A-27R-3W, 70-71	233.995	234.605	**234.300**	0.31	**32.92**	
B *Sphenolithus akropodus*	U1509A-27R-3W, 70-71	U1509A-28R-1W, 40-41	234.605	240.905	237.755	3.15		33.13
Tc *Sphenolithus intercalaris*	U1509A-28R-1W, 40-41	U1509A-28R-1W, 100-101	240.905	241.505	241.205	0.30		33.34
Tc **(1)** *Isthmolithus recurvus*	U1509A-28R-2W, 130-131	U1509A-28R-3W, 40-41	243.305	243.905	243.605	0.30		33.49
Bc *Lanternithus minutus*	U1509A-28R-3W, 40-41	U1509A-28R-3W, 100-101	243.905	244.505	244.205	0.30		33.52
T EOIS					**246.300**		**33.65**	
Bc *Clausicoccus subdistichus*	U1509A-29R-1W, 40-40	U1509A-29R-1W, 9-10	250.195	250.505	250.350	0.16		33.95
T *Discoaster saipanensis*	U1509A-29R-5W, 67-68	U1509A-29R-5W, 96-97	256.815	257.105	**256.960**	0.15	**34.44**	
Bc *Sphenolithus intercalaris*	U1509A-30R-1W, 130-131	U1509A-30R-2W, 9-10	261.005	261.295	261.150	0.15		34.70
T *Discoaster barbadiensis*	U1509A-30R-2W, 70-71	U1509A-30R-2W, 100-101	261.910	262.205	**262.058**	0.15	**34.76**	
B S. predistentus	U1509A-30R-5W, 65-66	U1509A-30R-5W, 95-96	266.105	266.405	266.255	0.15		35.02

Table 3.2 Positions and age estimates of selected biohorizons at IODP Site U1509 based on calcareous nannoplankton and Step 2 ($\delta^{18}O$ bulk isotopes) tie points (in bold). Note: B = Base, Bc= Base continuous and common, T = Top, Tc= Top continuous and common.

3.4 Results

The sediment section from IODP Site U1509 is comprised from sample U1509A-30R-CCW, 19-20 (267.305 m, CSF-A) to sample U1509A-21R-1W, 30-31 (183.305 m, CSF-A) and spans from Zone CNE19 to CNO3 (Agnini et al., 2014) equivalent to Zone NP20-NP23 (Martini, 1971) and to Zone CP15b-CP17 (Okada and Bukry, 1980). Calcareous nannofossils are common to abundant and the preservation varies from moderate to good throughout the study section. Semi-quantitative abundance data allow us to investigate biostratigraphically significant CN taxa (Figure 3.4) and to extrapolate their ages assuming constant LSRs between Chron boundaries.

In the Appendix IV, we provide additional information about the age (Ma), errors (Myr) and relative distance of the examined biohorizons from the nearest higher geomagnetic Chron boundary (position from Top Chron). Our strategy for the E-O transition was to investigate taxa displaying robust and marked abundance patterns and/or taxa which are easily recognizable. Unfortunately, this critical interval resulted in a lack of good biostratigraphic markers, forcing us also to consider poorly studied bioevents characterized by low abundances and/or significant fluctuactions, as the case of *L. minutus* or *I. recurvus*.

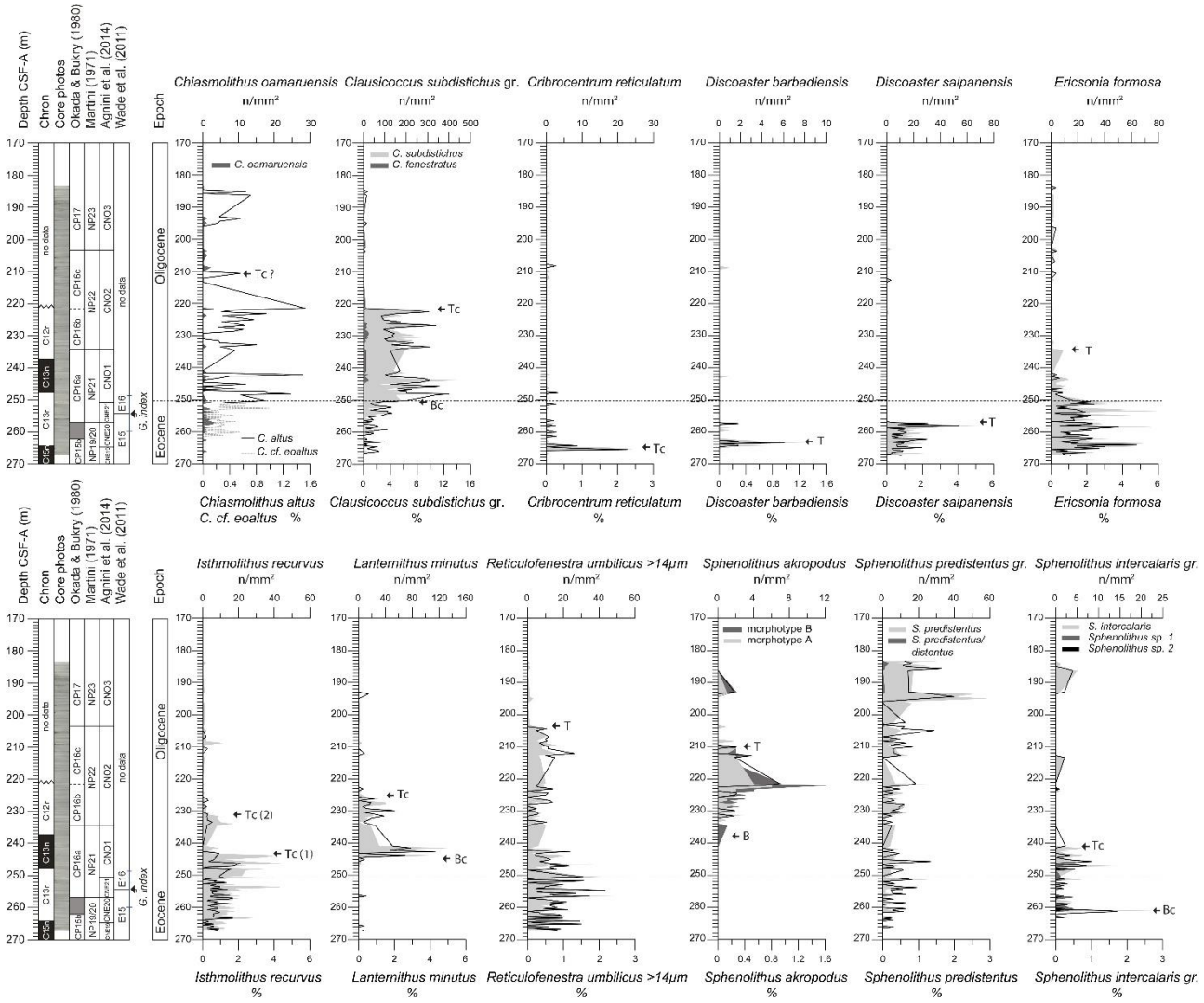

Figure 3.4 Semi-quantitative (n/mm^2, in solid grey area) and relative (%, black line and dotted grey line) abundance patterns of biostratigraphically useful calcareous nannofossil taxa from Site U1509, compared along with depth (CSF-A, m), magnetostratigraphy, calcareous nannofossil (CN) (Martini, 1971; Okada & Bukry, 1980; Agnini et al., 2014) planktonic foraminiferal (PF) (Wade et al., 2011) biozonations and chronostratigraphy. The dashed horizontal line specifies the extrapolated position of the EOB based on LSR. We also indicate the position of the bioevents as B = Base, Bc= Base continuous and common, T = Top, Tc= Top continuous and common.

Some of the bioevents reported in this study (e.g., the base of *S. akropodus*, the Top common and Base common of *L. minutus*, the Top common of *Clausicoccus subdistichus* gr. and *Istmolithus recurvus,..*) have not been systematically tested in different geographical areas and/ or depositional settings and certainly require further investigations, however, they show a high potential and we thus decide to discuss them, in addition to the classical biohorizons, in the following:

The Top common of Cribrocentrum reticulatum

Recently, Agnini et al. (2014) have proposed the Top common (Tc) of *C. reticulatum* to mark the base of Zone CNE20, enabling the subdivision of the long stratigraphic interval between the Base of *Cribrocentrum isabellae* and the Top of *Discoaster saipanensis*. At Site U1509 *C. reticulatum* reaches a peak of 25

specimens/mm^2 at 265.485 m, CSF-A and then sharply dropped. The extinction of *C. reticulatum* in our dataset occurs within Chron C15n consistently with data reported from different low-middle latitude areas (Shafik, 1981; Backman, 1987; Premoli Silva et al., 1988; Wei and Wise, 1989). In this work the Tc of this species falls 13% down from the top of Chron C15n. At high latitude this event occurs within C16n as reported by different authors (Wei, 1991; Aubry, 1992; Marino and Flores, 2002; Persico et al., 2012), confirming a strong diachroneity between low-middle and high latitudes.

The Top of rosetta-shaped discoasterids

The shortly-spaced successive extinctions of rosetta-shaped *D. saipanensis* and *D. barbadiensis* mark the base of Subzone CP16a (Okada and Bukry, 1980), whereas the extinction of *Discoaster saipanensis* defines the base of Zone NP21 (Martini, 1971), which coincides with the base of Zone CNE21 (Agnini et al., 2014).

At Site U1509, the Top of *D. barbadiensis* falls 5.10 meters below the Top of *D. saipanensis* (256.960 ± 0.15 m. CSF-A), both within Chron C13r. These datums are consistent with published data from low-middle latitude sites (Backman and Hermelin, 1986; Wei and Wise, 1989; Blaj et al., 2009). The extinction of rosette-shaped discoasters is a diachronous event, which occurs at ~40 Ma in high latitudinal settings (Wei and Wise, 1990; Persico and Villa, 2004; Villa et al., 2008; Fioroni et al., 2015) and ~5.5 Myr later in low-middle latitudes (see discussion in Berggren et al., 1995 and reference herein).

The acme interval of Clausicoccus subdistichus group

The acme event of *C. subdistichus* was identified at different sites worldwide (Backman, 1987; Coccioni et al., 1988; Marino and Flores, 2002; Hyland et al., 2009; Toffanin et al., 2013; Norris et al., 2014; Fioroni et al., 2015; Jovane et al., 2015; Newsam, 2016) and recently at ODP Site 756 (Indian Ocean; Chapter 1).

At Site U1509, this species is characterized by high and variable abundances with a marked increase in the number of specimens (reaching ~450 specimens/mm2) during Chron C13n (Figure 3.4).

The Base common (Bc) of this species was used by Agnini et al. (2014) to identify the onset of Zone CNO1, which corresponds to the lower part of Zone NP21 (Martini, 1971). In our dataset, a remarkable increase in abundance (Bc) of *C. subdistichus* gr. is observed at 250.35 m ± 0.16 m CSF-A in the upper part of Chron C13r. In particular, the biohorizon lies at 16% down from the top of this polarity chron (considering its duration equals to 100%), a datum that is in very good agreement with that reported in Agnini et al. (2014; 13%). Unfortunately, the Bc of *C. subdistichus* gr., also known as acme beginning, is not easily located because the increase in the abundance pattern at the onset of the acme interval is not always neat.

At Site U1509, we place the Bc of *C. subdistichus* gr. at 250.35 m CSF-A, which corresponds to the highest increment of specimens recorded in 1 mm^2 (Δ= 121 n/mm^2, i.e. from 56 to 177 specimens) within Chron C13r. However, as underlined before, the positioning of this bioevent could be not straightforward at different sites though the acme interval of this taxon represents a valuable and unique datum to approximate the Earliest Oligocene Glacial Maximum (EOGM) (Chapter 2).

At Hole U1334A, stratigraphic range charts report a significant increase in abundance of *C. subdistichus* (Bc) (Bown and Dunkley Jones, 2012). Consistently with the previous datum, at Hole U1333C (Eq. Pacific; Exp.

320), a notable increase in abundance of this species (up to 100 n/mm^2) occurs in the upper part of Chron C13r (Toffanin et al., 2013). Instead, in the nearby Holes U1331A, U1332A and U1333A, only few and sporadic specimens were found (Bown and Dunkley Jones, 2012). However, these qualitative data need to be further checked. The extinction of *Clausicoccus subdistichus* was proposed as zonal marker by Bukry (1973) and Okada & Bukry (1980) to mark the base of Subzone CP16b. Bukry (1973) pointed out the objective difficulty to distinguish among three different species belonging to genus *Clausicoccus* (i.e., *C. subdistichus, C.obrutus* and *C. fenestratus*) in overgrown assemblages and underlined the potential bias in the abundance peaks documented in very well preserved sediments that would account for a high abundances.

In this work, *C. obrutus* and *C. fenestratus* and *C. subdistichus* were included in the *C. subdistichus* group concept following Agnini et al. (2014). As far as *C. fenestratus* versus *C. subdistichus* is concerned, our data indicate that these two taxa have the same biostratigraphic significance but *C. subdistichus* is usually found to be most common (reaching a maximum of 12.8% within Chron C13n), if compared with *C. fenestratus* that typically shows sporadic abundances (0-25 n/mm^2).

At Site U1509, the abundance pattern of *C. subdistichus* shows a sharped decline (Tc) from 326 to 3 specimens/mm^2 at 221.560 ± 0.14 m CSF-A in the lower part of Chron C12r. This biohorizon is thus recorded above the Top of *Ericsonia formosa*, consistently with findings of Backman (1987) and Catanzariti et al. (1997). The Tc of this species, early in Chron C12r, is recorded also at high latitudes and always above the Top of *E. formosa* (Madile and Monechi, 1991). Similarly, in the equatorial Pacific (Site U1333; Toffanin et al., 2013) and in the South Atlantic (Site 1263; Bordiga et al., 2015), this species seems to be present and common even after the Top of *E. formosa*. In conclusion, the reversed relative ranking of these two biohorizons as previously proposed by Okada and Bukry (1980) seems to be inconsistent with virtually all the available data. Possible explanations for these inconsistencies are likely related to misleading correlations between T and Tc, these are in fact spaced biohorizons with the latter preceding the former. In addition, low resolution qualitative data and taxonomic ambiguity could have biased the quality of the datums and caused the reverse ranking found in some studies (e.g. Wise, 1983; Madile and Monechi, 1991). As documented in the Tasman Sea as well as in many other cases, the Tc of *C. subdistichus* gr. is neat event postponed to the Top of *E. formosa* but other data could serve to confirm the high realiability of this biohorizon.

The Top of Ericsonia formosa

The Top of *E. formosa* formally defines the base of Zone NP22 (Martini, 1971) and Zone CNO2 (Agnini et al., 2014). At Site U1509, the species is quite common in the lower part of the section, with a long tail of distribution towards the end of its range. Despite the presence of a long and scattered final distribution, we recognized the Top of *E. formosa* in the lowermost part of Chron C12r (234.300 ± 0.31 m, CSF-A), a datum that is consistent with most of the low-middle latitude data (Backman, 1987; Wei and Wise, 1989; Blaj et al., 2009; Toffanin et al., 2013). This event is diachronous between low-middle and high latitudes, with the last occurrence of this species lying within Chron C18 at high latitudes (Berggren et al., 1995).

The Top and the Top common of Istmolithus recurvus

In the classical biozonations, the Base of *I. recurvus* defines both the base of undifferentiated Zone NP19/ NP20 (Martini, 1971) and Subzone CP15b (Okada and Bukry, 1980), however, many authors have pointed out the low reliability of this late Eocene biohorizon. In particular, Agnini et al. (2014) underlined that the position of the first occurrence of this species with respect to magnetostratigraphy is highly inconsistent ranging from Chron C17n to Chron C15n. In a similar way, the final sporadic occurrence of this taxon is often difficult to be recognized. Moreover, Bukry (1978) suggested that *I. recurvus* is likely affected by latitudinal thermal gradients which consequently results in a diachronic extinction if low-middle and high latitudes are compared. At Site U1509, the final distribution of *I. recurvus* is characterized by a sporadic occurrence that has not permitted an unambiguous positioning of the Top of this taxon. However, we have instead identified the Top common and continuous, of this species at 230.555 ± 0.15 m, CSF-A, within Chron C12r. This datum seems to be quite consistent with data from northern middle latitudes (Martini, 1971), South Atlantic (Backman, 1987) and southern high latitudes (Persico and Villa, 2004; Villa et al., 2008).

The acme interval of Lanternithus minutus

Biohorizons based on the abundance pattern of *Lanternithus minutus* are not used to biostratigraphically subdivide the Oligocene, but the potential of this holococcolith as a regional index species is supported in the discussion of this study. This species was first found in upper Eocene Austrian glauconite sediments (Stradner, 1962). More recently Bown and Newsam (2017) reported the common presence of this species in middle to upper Eocene sediments from Tanzania and sporadic occurrences in the North Atlantic Exp. 342 sites. The stratigraphic range of *L. minutus* spans from Subzone NP14b (middle Eocene) to Zone NP23 (lower Oligocene) (Bown, 2005). At Site U1509, we document a remarkable increase in abundance across late Eocene - early Oligocene with maximum values (>100 specimens/mm^2) observed between 246.905 to 223.205 m CSF-A, within Chron C13n to C12r. At Site U1509, the Bc of *L. minutus* was found at 244.205 ± 0.30 m CSF-A, lying 66% down from the top of Chron C13n. The Tc of this species occurs at 224.705 ± 0.30 m CSF-A within Chron C12r. A similar trend has been observed in the Indian Ocean at Site 756 (see Chapter 2) and seems to perfectly correlates with the acme interval observed in the Tasman Sea Site U1509.

The Top of Reticulofenestra umbilicus

This event is known to be diachronous between low-middle and high latitudes (e.g., Backman, 1987). Following Backman and Hermelin (1986) we decide to include in *R. umbilicus* only specimens >14μm.

In a most recent biozonation (Agnini et al., 2014), the extinction of *R. umbilicus* marks the base of Zone CNO3. In our dataset, the abundance pattern of this species displays a progressive decline and the presence of reworked specimens as already highlighted in the shipboard reports (Sutherland et al., 2019). However, the Top of *R. umbilicus* was placed at 203.395 ± 0.29 m CSF-A in coincidence with its sharpest decline in abundance and is consistent with a constant LSR.

3.5 Discussion

3.5.1 Biochronological global comparison

The degree of reliability of a bioevent it is based on the evaluation of the synchronicity over wide areas (Raffi 1999), the high repeatability among different workers and the respect of the ranking if compared with other biohorizons (Catanzariti et al., 1997).

Calcareous nannofossil biostratigraphic data investigated at Site U1509 have been compiled along with low-middle and high latitude data from South Atlantic (DSDP Sites 522/523, Backman, 1987; DSDP Site 516, Wei and Wise, 1989), North Atlantic (IODP Site U1411, Newsam, 2016), Indian Ocean (ODP Site 711, Fioroni et al., 2015; ODP Site 756), Equatorial Pacific (IODP 1218, Blaj et al., 2009; ODP Hole U1333C, Toffanin et al., 2013) and Southern Ocean (ODP 1090, Marino and Flores, 2002; ODP 689 and 744, Persico and Villa, 2004; ODP 748, Villa et al., 2008). We collected calcareous nannofossil biochronological data available in literature for the E-O transition with the aim to correlate age estimates obtained for selected biohorizons from different biogeographic domains and depositional settings (Figure 3.5; Appendix IV).

To facilitate the comparison, we have recalibrated all the biochronological estimates to the Geological Time Scale 2012 (GTS12; Gradstein et al., 2012). The precision of age estimates used for this exercise generally depends on the mass accumulation rates, the sampling resolution, the counting methods (quantitative counts are preferred), the intrinsic quality of datum (e.g., % of recovery), and, even more importantly, the assumption of constant LSRs between chron boundaries. All these boundary conditions could bias, even heavily, the final age assignment provided. We are aware that the age estimates derived from only magnetostratigraphic tie-points are less accurate compared to those obtainable using astronomically tuned records (Blaj et al., 2009) because the latter are capable to provide age models based on the Earth's orbital parameters (i.e., precession, obliquity and eccentricity) (Berggren, 2001). Clearly, the best solution is to have sections with available cyclostratigraphy in order to capture any variation in the accumulation rates (Raffi et al., 2016). but the reality is that for most of the sections these data are not available.

However, magnetostratigraphic constrains remain a primary tool to assess the global reliability of a specific biohorizon (e.g. Gradstein et al., 2012). In this work, new age calibrations are provided and discussed in order to test the reliability of the identified calcareous nannofossil events for global correlations and to provide possible additional biohorizons for the late Eocene early Oligocene. In the following discussion, we will emphasize the limits and bonuses of some of the main biohorizons:

The **Top of *Reticulofenestra umbilicus*** is a possible tricky marker due to the scattered occurrences towards the end of its range. Its extinction shows some inconsistencies among workers and ocean basins as shown in Figure 3.5. The Top of *R. umbilicus* has been commonly applied as an early Oligocene marker (Martini, 1971; Okada and Bukry, 1980) based on its morphometrical differentiation. As suggested by Backman and Hermelin (1986), the criterion to distinguish *R. umbilicus* from other morphologically similar taxa is based on the size limit of 14µm, which is what we used in this study. Age estimates for this bioevent from low-middle latitude sites are highly variable (31.15- 32.98 Ma) if compared with the age derived at Site U1509 (31.38 Ma, GTS12). The age of the extinction of *R. umbilicus* shows small inconsistencies in the same oceanographic domain that

could be related to ambiguous taxonomic concepts. In addition, the significant difference with the reference age estimate (32.02 Ma) could, at least in part, be explained by the further uncertainty due to the lack of Chron C12r/C12n boundary. Because of this, the age assignment for the Top of *R. umbilicus* was calculated using the same LSR of the previous Chron interval (Chron C12r). Notably, the shipboard data from IODP Site U1509 placed this event 1.38 Myr younger (midpoint 177.07 ± 1.38 m CSF-A) than our result.

Clearly, we recommend caution using the Top of *R. umbilicus* since the reliability of this datum is considered relatively low.

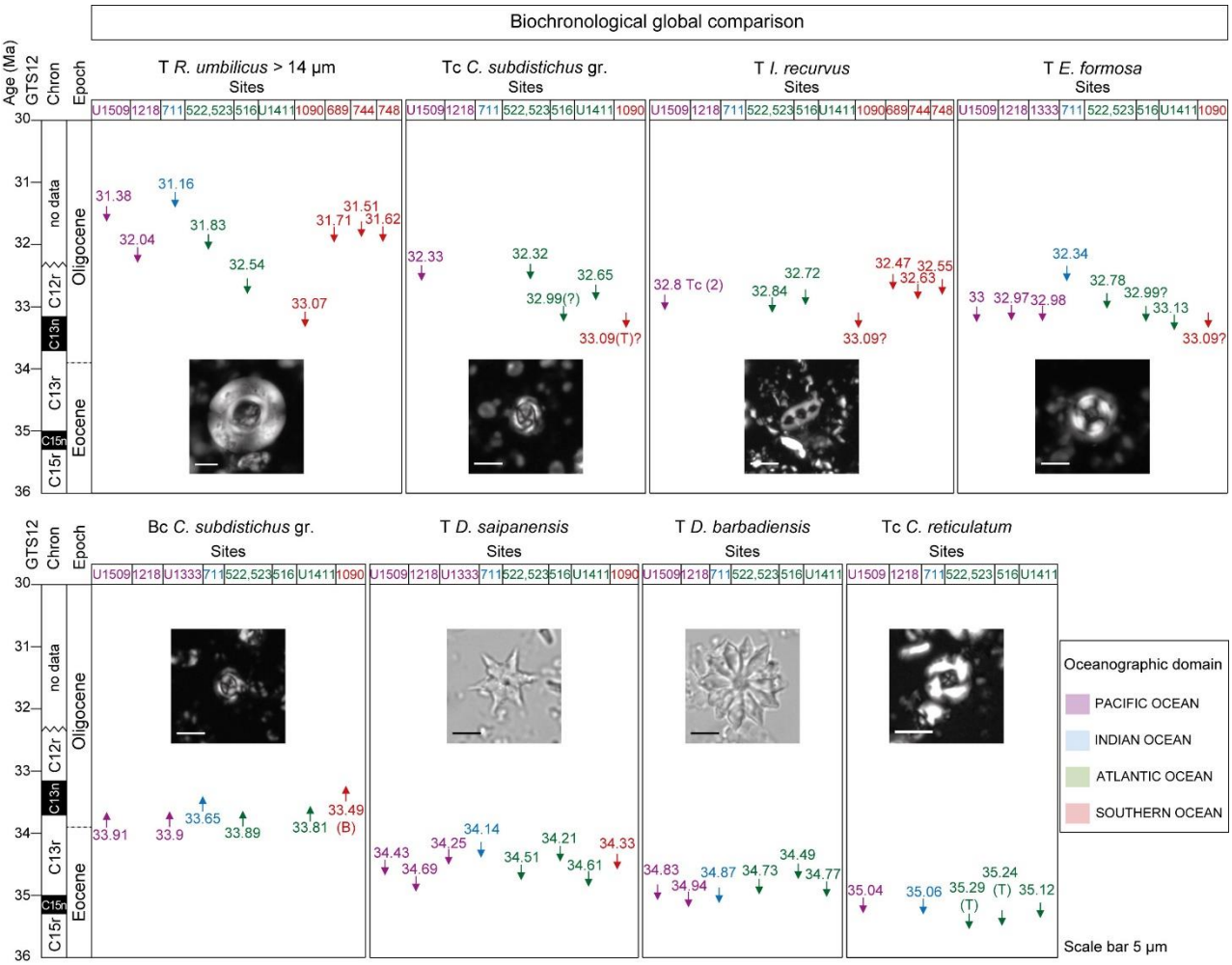

Figure 3.5 Correlation of the main biostratigraphic events based on magnetostratigraphy as recognized in different low-middle and high latitude sites. Age estimates were recalibrated to GTS of Gradstein et al. (2012).
Data come from: Tasman Sea (Site U1509), Eq. Pacific Ocean (Site 1218, Blaj et al., 2009); Site U1333, Toffanin et al., 2013), Equatorial Indian Ocean (Site 511; Fioroni et al., 2015), South Atlantic (Sites 522, 523; Backman, 1987; Site 516 from Wei and Wise, 1989), North Atlantic (Site U1411; Newsam, 2016) and Southern Ocean (Site 1090; Marino and Flores, 2002; Site 689 and Site 744: Persico and Villa, 2004; Site 748; Villa et al., 2008).
Microphotos: scale bar = 5 µm. Note: age estimates from the investigated sites are based on taxa semiquantitative abundances, expressed as n/mm^2, except for Site U1411 where are based on percentage (%) of the total assemblage.

The **Top common of *Clausicoccus subdistichus*** gr. is considered either diachronous in different regions (Backman, 1987) or not well defined because of the lack of sufficient data (Toffanin et al., 2013). In our opinion, it represents a promising biohorizon and seems to be a synchronous event at least in the Pacific (Tasman Sea, Site U1509) and South Atlantic (Site 523) oceans.

As reported by previous studies (e.g., Chapter 2; Monechi, 1986a) the top of the acme interval of this species postdates the Top of *E. formosa*. Despite minor inconsistencies, our result is in good agreement with the position of this event ~58% from the top of Zone CNO2 at ODP Site 756, corroborating the idea that the Tc of *C. subdistichus* gr. could represent an excellent bioevent, at least in some depositional settings. The Tc of *Clausicoccus subdistichus* gr. recorded at ODP Site 756 has an age estimate of 32.54 Ma, that perfectly matches with that calibrated at Site U1509. On this basis, we think that the Tc of *C. subdistichus* could be useful to subdivide the long Zone CNO2 (duration: 900 kyr). Furthermore, the neat pattern of this event is easy to detect even if more studies are required to assess the reproducibility at high latitudes and in different depositional settings.

The biostratigraphic significance of the **Top of *Istmolithus recurvus*** is controversial (Backman, 1987). A common opinion is that the Top of *I. recurvus* better works at middle to high latitudes, this species is found to be rare or absent at low latitudes, as confirmed by data from the Tanzanian Drilling Project (TDP) cores (TDP Site 12 and 17) (Bown and Jones, 2006; Dunkley Jones et al., 2009). The age calculated for the Tc of *I. recurvus* at IODP Site U1509 (32.8 Ma) is extremely consistent with the age estimates from middle latitude South Atlantic Sites 522, 523 and 516 (Figure 3.5). This result is also in agreement with the placement of this event within Chron C12r, as reported by Wei (1991) for the nearby Site 699. Our results indicate that *I. recurvus* is characterized by a slightly early exit at middle latitudes (32.72 – 32.84 Ma) compared to high latitudes (32.47-32.63 Ma; Site 689, 744 and 748). The only exception is the 290 kyr older estimate from Site 1090 that, however, suffers from a likely condensation supported by the shortly spaced occurrence of several bioevents (i.e., the top of *I. recurvus, E. formosa* and *C. subdistichus*). Based on to these data, a small diachrony is confirmed between low-middle and high southern latitudes, as also suggested by Berggren et al. (1995). Further investigations are desirable in order to further test the reliability of this bioevent, especially at low-middle latitudes. Our data also further corroborate the hypothesis that the abundance of *I. recurvus* strongly relies on latitudinal thermal gradients and ecological affinity of this taxon for high latitudes. This rationale is consistent with the distribution model found for this species: with low abundances per square mm at low-middle latitudes and higher abundances at higher latitudes (Monechi, 1986b). In the Southern Ocean this taxon is extremely abundant (up to 200 n/mm^2) (Persico and Villa, 2004; Villa et al., 2008) while data from IODP Site U1509 and ODP Site 756 indicate similar patterns but with lower absolute abundances (up to 50 n/mm^2).

The **Top of *Ericsonia formosa*** is a widely used biohorizon that benefits from the easy recognition of the species even in poorly preserved sediments (Wise, 1973). The disappearance of *E. formosa* (33.00 ± 0.016 Ma) at Site U1509 was recorded in the lower middle part of Chron C12r (Figure 3.5) and perfectly correlates with the age estimates from the Equatorial Pacific Ocean (32.97 ± 0.004 Ma – Site 1218; 32.98 ± 0.251 – Hole U1333C). A quite good correlation is also reported for the Atlantic Ocean, with age estimates ranging between 32.78 and 33.09 Ma. A significative discrepancy has been observed with the age estimate from the Equatorial Indian Ocean (32.34 Ma), which provides 657 kyr younger age estimate. This inconsistency is likely related

to the relatively low sedimentation rate calculated at Site 711. In conclusion, the extinction of this taxon is globally synchronous and represents an excellent and consistent biohorizon.

The **Base common and continuous of *Clausicoccus subdistichus*** gr. is the only calcareous nannofossil event suitable to approximate the EOB, and, as discussed in this work, it seems to be globally synchronous, although sometimes difficult to place. One possible limit of this event is the need of quantitative counts in order to obtain an abundance profile and, eventually, place the increase in abundance. At IODP Site U1509, the Bc of *C. subdistichus* gr. is calibrated at 33.91 ± 0.012 Ma, slightly predating the EOB (~33.89 Ma; GTS12). The age estimate of the Bc of *C. subdistichus* gr. from the Equatorial Indian Ocean (Site 711; Fioroni et al., 2015) is 51 kyr younger than the age estimate at Site U1509, while the one reported from the Monte Cagnero section (Jovane et al., 2015) is 120 kyrs older (34.03 Ma). All these data confirm the high reliability of this biohorizon in different geographic domains and depositional settings.

At Site U1509 the **Top of *Discoaster saipanensis*** occurs at 34.428 ± 0.011 Ma, an age that is extremely consistent with the age derived from astronomical tuning (Appendix IV). Possible minor discrepancies in age estimates are observed from Equatorial Pacific, Indian and Atlantic oceans. At sites 1218 and 711, sedimentation rates are relatively low within Chron C13r (0.5 cm/kyr). Possible small inconsistencies are thus, likely the result of the summed effect of low sedimentation rates and/or poor magnetostratigraphic records, as the case of Site 516 (Wei and Wise, 1989).

The **Top of *Discoaster barbadiensis*** occurs 400 kyr before the Top of *D. saipanensis* at Site U1509. Age estimates from low-middle South and North Atlantic sites (Figure 3.5) are consistently younger. Age derived from the Equatorial Indian Ocean are instead perfectly synchronous (34.874 ± 0.106 Ma). However, the extinction of *D. barbadiensis* in the Equatorial Pacific Ocean (Site 1218) occurs 116 kyr before our age estimate. This event is fairly reliable.

The **Top common and continuous of *Cribrocentrum reticulatum*** represents a virtually synchronous bioevent at low-middle latitudes. Our age estimate from the Tasman Sea (35.038 ± 0.012 Ma) correlates extremely well with that reported for the Equatorial Indian Ocean (35.057 ± 0.070 Ma) (Fioroni et al., 2015). The only significant discrepancy comes from South Atlantic Sites 522 and 516, where the Top of this species is 256 kyr and 202 kyr older, respectively. Data from the GSSP section, (Monte Cagnero; Hyland et al., 2009) provide an age of 35.12 Ma for the extinction (T) of this species. Hence, the Tc of this species appears to be extremely consistent among different basins at low to middle latitudes.

3.5.2 Other investigated taxa

Lanternithus minutus has never been considered to be potentially reliable because of the high abundance variability of this species that seems to be site-specific. However, the Bc and Tc of *L. minutus* seem promising, at least in some depositional settings. The acme interval of *L. minutus* has a short duration both at IODP Site U1509 and ODP Site 756 (Chapter 2), where it shows relatively low abundances (<5%). An acme interval of *L. minutus* was also reported from the shelf areas of Central Paratethys (Ozsvárt et al., 2016; Nyerges et al., 2020), but with considerably higher quantitative abundances. However, it is undeniable that this species strongly relies on local dynamics and specific conditions, since it is extremely rare or even absent in some environments, as the case of North Atlantic (IODP Site U1411) and North Pacific (ODP Site 1209) (Chapter 4). In the latter case, the absence of *L. minutus* may be also due to poor preservation. The Bc and Tc of *L. minutus* are not equally promising, with the Tc of this species that looks more consistent with an estimated age of 32.54 Ma at ODP Site 756 and 32.64 Ma at IODP Site U1509. In the South Atlantic Ocean (ODP Site 1263; Bordiga et al., 2015) and in Tanzania (TDP Site 12,17; Dunkley Jones et al., 2008), *L. minutus* displays similar and quite high abundances, respectively between 0-16% and 0-20%, but different profiles and, in the latter case, a gradual decreasing in abundances. More data are therefore required to assess the usefulness of this species in regional settings.

Among the other investigated taxa (***S. akropodus, S. predistentus*** and ***C. altus***), the Base of *S. predistentus* seems to be meaningless from a biostratigraphic point of view, as suggested also by the results acquired from Site 756 (Chapter 2). Instead, the Base of *S. akropodus* might be helpful, at least as a regional indicator, since this species is extremely rare or even absent at some sites (e.g. IODP Site U1411; Newsam, 2016).

As far as the Tc of *C. altus* is concerned, we currently do not have sufficient data to evaluate its reliability, although the comparison of the abundance patterns of this taxon seems to suggest some spatial homogeneity and consistency between Site U1509 and Site 756 (Chapter 2). In this work, late Eocene forms of *Chiasmolithus* were ascribed to *C.* cf. *eoaltus* (Figure 3.4). Unfortunately, the lack of an unambiguous recognition of *C. eoaltus* hampers from any biostratigraphic interpretations, especially considering that we do not find the supposed gap between the Top of *C. eoaltus* and the base of *C. altus* (see Chapter 2).

A further degree of complexity comes from the sporadic finding of specimens of *C. eoaltus* (Chapter 4, Plate 4.1, fig. 26) between 184.50-231.31 CSF-A m (early Oligocene), that has been interpreted as reworked (see Figure 4.3 in Chapter 4). More data are needed to sort this issue out but the rarity and/or low preservation degree of this species at low-middle latitudes could have bias our data and make a confident correlation with high latitudes (Persico and Villa 2008; Fioroni et al., 2012) elusive at this state.

In our study no strong correlation was found between the considered events and the paleodepth estimated for each site. Most of the discussed bioevents can be considered global and synchronous in Pacific, Indian and Atlantic oceans. However, some slightly inconsistencies have been found for the Top of *R. umbilicus*.

Instead, more studies are required to assess the reliability of the Tc of *C. subdistichus* gr. and *I. recurvus*, and, in particular,for the latter a slight latitudinal dependency is suggested.

3.6 Conclusions

Magnetostratigraphic age estimates were established for Site U1509 and globally compared with those derived from Indian, Pacific, Atlantic and Southern Ocean sites. Data provided by this work lay the basis for the evaluation of the synchroneity of the calcareous nannofossil events during and the late Eocene early Oligocene and, at the same time, provide several clues on the reliability of the Tc of *C. subdistichus* and the Tc of *I. recurvus*, as new valuable stratigraphic tools to correlate Chron C12r.

At Site U1509, the global age estimates obtained for the Top of *E. formosa, D. saipanensis, D. barbadiensis,* the Bc of *C. subdistichus* and the Tc of *C. reticulatum* appears to be extremely consistent with those from Equatorial Pacific, Indian and Atlantic oceans. As a result, most bioevents can considered by and large synchronous at low-middle latitudes. The major discrepancy is the one observed for the extinction of *Reticulofenestra umbilicus* within Chron C12r. Possible explanations for this incongruity includes: (i) a possible bias based on the assumption of constant linear sedimentation during Chrons C13n and C12r (ii) the possible effect of reworked specimens in placing the event (iii) intrinsic errors due to the morphometric definition of this taxon. For all these reasons, the Top of *R. umbilicus* should be used with caution, as also emphasized by Backman (1987) and Blaj et al. (2009).

At all locations, the only calcareous nannofossil biohorizon able to approximate the Eocene/Oligocene boundary (EOB) is the Bc of *C. subdistichus* gr. (33.91 Ma, GTS12). This event is preceded by the top of *D. saipanensis* and the Top of *D. barbadiensis* that have an age estimation of 34.43 Ma and 34.83 Ma, respectively. The Bc of *C. subdistichus* gr. represents an alternative marker to approximate the position of the EOB, especially in the absence of planktonic foraminiferal biostratigraphy and/or oxygen isotopic data. Moreover, this work provides an additional set of potentially useful bioevents (i.e., the Tc of *L. minutus,* the Tc of *C. altus* and the Base *S. akropodus*), with a possible regional extension that could pave the way for future regional schemes.

Acknowledgements

The authors are grateful to the Integrated Ocean Drilling Program (IODP) for providing samples and data used in this study. The IODP is sponsored by the U.S. National Science Foundation (NSF) and participating countries under the management of Joint Oceanographic Institutions, Inc.

Isabella Raffi and Davide Persico are deeply thanked for their constructive comments in the capacity of reviewers of A.V.' s PhD thesis during the evaluation process required by Italian law.

Datasets can be found in the **Appendix IV**.

References

Agnini, C., Fornaciari, E., Raffi, I., Catanzariti, R., Pälike, H., Backman, J., Rio, D., 2014. Biozonation and biochronology of Paleogene calcareous nannofossils from low and middle latitudes. Newsletters on Stratigraphy 47, 131–181.

Agnini, C., Fornaciari, E., Raffi, I., Rio, D., Röhl, U., Westerhold, T., 2007. High-resolution nannofossil biochronology of middle Paleocene to early Eocene at ODP Site 1262: Implications for calcareous nannoplankton evolution. Marine Micropaleontology 64, 215–248.

Agnini, C., Monechi, S., Raffi, I., 2017. Calcareous nannofossil biostratigraphy: historical background and application in Cenozoic chronostratigraphy. Lethaia 50, 447–463.

Aubry, M.-P., 1992. Late Paleogene Calcareous Nannoplankton Evolution: A Tale of Climatic Deterioration. In: Eocene-Oligocene Climatic and Biotic Evolution. p. 272–279.

Backman, J., 1987. Quantitative Calcareous Nannofossil Biochronology of Middle Eocene through Early Oligocene Sediment from DSDP Sites 522 and 523. Abhandlungen der Geologischen Bundesanstalt 39, 21–31.

Backman, J., Hermelin, J.O.R., 1986. Morphometry of the Eocene nannofossil Reticulofenestra umbilicus lineage and its biochronological consequences. Palaeogeography, Palaeoclimatology, Palaeoecology 57, 103–116.

Backman, J., Shackleton, N.J., 1983. Quantitative biochronology of Pliocene and early Pleistocene calcareous nannofossils from the Atlantic, Indian and Pacific oceans. Marine Micropaleontology 8, 141–170.

Berggren, W.A., 2001. International Time Scale. Encyclopedia of Life Sciences 1–5.

Berggren, William A., Kent, D. V., Swisher, C.C., Aubry, Marie-Pierre, 1995. A Revised Cenozoic geochronology and chronostratigraphy. In: Berggren, W. A., Kent, D.V., Aubry, M.-P., Hardenbol, J. (Eds.), Geochronology, Time Scales, and Global Stratigraphic Correlation: A Unified Temporal Framework for an Historical Geology. Special publication - Society of Economic Paleontologists and Mineralogists, p. 129–212.

Blaj, T., Backman, J., Raffi, I., 2009. Late Eocene to Oligocene preservation history and biochronology of calcareous nannofossils from paleo-equatorial Pacific Ocean sediments. Rivista Italiana di Paleontologia e Stratigrafia 115, 67–85.

Bordiga, M., Henderiks, J., Tori, F., Monechi, S., Fenero, R., Legarda-Lisarri, A., Thomas, E., 2015. Microfossil evidence for trophic changes during the Eocene-Oligocene transition in the South Atlantic (ODP Site 1263, Walvis Ridge). Climate of the Past 11, 1249–1270.

Bown, P.R., 1998. Calcareous nannofossil biostratigraphy. Chapman and Hall (Kluwer Academic Publishers), London, UK.

Bown, P.R., 2005. Paleogene calcareous nannofossils from the Kilwa and Lindi areas of coastal Tanzania (Tanzania Drilling Project 2003-4). Journal of Nannoplankton Research 27, 21–95.

Bown, P.R., Dunkley Jones, T., 2012. Calcareous nannofossils from the Paleogene equatorial Pacific (IODP Expedition 320 Sites U1331-1334). Journal of Nannoplankton Research 32, 3–51.

Bown, P.R., Jones, T.D., 2006. New Paleogene calcareous nannofossil taxa from coastal Tanzania: Tanzania

Drilling Project Sites 11 to 14.

Bown, P.R., Newsam, C., 2017. Calcareous nannofossils from the Eocene North Atlantic Ocean (IODP Expedition 342 Sites U1403–1411). Journal of Nannoplankton Research 37, 25–60.

Bown, Paul R., Young, J.R., 1998. Techniques. In: Bown, P.R. (Ed.), Calcareous Nannofossil Biostratigraphy. Kluwer Academic Publishers, London, p. 16–28.

Bukry, D., 1973. Low-latitude coccolith biostratigraphic zonation. Initial Reports of the Deep Sea Drilling Project, 15 685–703.

Bukry, D., 1978. Biostratigraphy of Cenozoic marine sediment by calcareous nannofossils. Micropaleontology 24, 44–60.

Catanzariti, R., Rio, D., Martelli, L., 1997. Late Eocene to Oligocene calcareous nannofossil Biostratigraphy in Northern Apennines: the Ranzano sandstone. Memorie di Scienze Geologiche 49, 207–253.

Coccioni, Rodolfo, Monaco, P., Monechi, S., Nocchi, M., Parisi, G., 1988. Biostratigraphy of the Eocene-Oligocene bonudary at Massignano (Ancona, Italy). In: Premoli Silva, I., Coccioni, R., Montanari, A. (Eds.), The Eocene–Oligocene Boundary in the March-Umbria Basin (Italy). Fratelli Anniballi, Ancona, p. 81–96.

Dunkley Jones, T., Bown, P.R., Pearson, P.N., 2009. Exceptionally well preserved upper Eocene to lower Oligocene calcareous nannofossils (Prymnesiophyceae) from the Pande Formation (Kilwa Group), Tanzania. Journal of Systematic Palaeontology 7, 359–411.

Dunkley Jones, T., Bown, P.R., Pearson, P.N., Wade, B.S., Coxall, H.K., Lear, C.H., 2008. Major shifts in calcareous phytoplankton assemblages through the Eocene-Oligocene transition of Tanzania and their implications for low-latitude primary production. Paleoceanography 23, 1–14.

Fioroni, C., Villa, G., Persico, D., Wise, S.W., Pea, L., 2012. Revised middle Eocene-upper Oligocene calcareous nannofossil biozonation for the Southern Ocean. Revue de Micropaleontologie 55, 53-70.

Fioroni, C., Villa, G., Persico, D., Jovane, L., 2015. Middle Eocene-Lower Oligocene calcareous nannofossil biostratigraphy and paleoceanographic implications from Site 711 (equatorial Indian Ocean). Marine Micropaleontology 118, 50–62.

Gradstein, F.M., Ogg, J.G., Schmitz, M.D., Ogg, G.M., 2012. The Geologic Time Scale 2012. Elsevier, Amsterdam, Netherlands.

Hyland, E., Murphy, B.H., Varela, P., Marks, K., Colwell, L., Tori, F., Monechi, S., Cleaveland, L., Brinkhuis, H., Van Mourik, C.A., Coccioni, R., Bice, D.M., Montanari, Alessandro, 2009. Integrated stratigraphic and astrochronologic calibration of the Eocene-Oligocene transition in the Monte Cagnero section (northeastern Apennines, Italy): A potential parastratotype for the Massignano global stratotype section and point (GSSP). In: Koeberl, C., Montanari, A. (Eds.), The Late Eocene Eart Hothouse, Icehouse, and Impacts. The Geological Society of America Special Paper 452, p. 303–322.

Jovane, Luigi, Savian, J.F., Coccioni, R., Frontalini, F., Bancala, G., Catanzariti, R., Luciani, V., Bohaty, S.M., Wilson, P.A., Florindo, F., 2015. Integrated magnetobiostratigraphy of the middle Eocene – lower Oligocene interval from the Monte Cagnero section , central Italy Ocean and Earth Science , University of Southampton , National Oceanography Centre. In: Jovane, L., Herrero-Bervera, E., Hinnov, L.A.,

Housen, B.A. (Eds.), Magnetic Methods and the Timing of Geological Processes. Geological Society, London, Special Publications, p. 79–95.

Madile, M., Monechi, S., 1991. Late Eocene to early Oligocene calcareous nannofossil assemblages from Sites 699 and 703, subantarctic South Atlantic Ocean. Proc., scientific results, ODP, Leg 114, subantarctic South Atlantic 114, 179–192.

Marino, M., Flores, J.A., 2002. Middle Eocene to early Oligocene calcareous nannofossil stratigraphy at Leg 177 Site 1090. Marine Micropaleontology 45, 383–398.

Martini, E., 1971. Standard Tertiary and Quaternary calcareous nannoplankton zonation. In: Farinacci, A. (Ed.), Proceedings of the 2nd International Conference on Planktonic Microfossils. Edizioni Tecnoscienza, Rome, p. 739–785.

Monechi, S., 1986a. Biostratigraphy of Fuente Caldera Section by Means of Calcareous Nannofossils. Developments in Palaeontology and Stratigraphy 9, 65/69.

Monechi, S., 1986b. Calcareous nannofossil events around the Eocene-Oligocene boundary in the Umbrian Appenines (Italy). Palaeogeography, Palaeoclimatology, Palaeoecology 57, 61–69.

Newsam, C., 2016. Calcareous nannoplankton evolution and the Paleogene greenhouse to icehouse climate-mode transition.

Norris, R.D., Wilson, P.A., Blum, P., Fehr, A., Agnini, C., Bornemann, A., Boulila, S., Bown, P.R., Cournede, C., Friedrich, O., Ghosh, A.K., Hollis, C.J., Hull, P.M., Jo, K., Junium, C.K., Kaneko, M., Liebrand, D., Lippert, P.C., Liu, Z., Matsui, H., Moriya, K., Nishi, H., Opdyke, B.N., Penman, D.E., Romans, B.W., Scher, H.D., Sexton, P., Takagi, H., Turner, S.K., Whiteside, J.H., Yamaguchi, T., Yamamoto, Y., 2014. Site U1411. Proceedings of the Integrated Ocean Drilling Program 342.

Nyerges, A., Kocsis, Á.T., Pálfy, J., 2020. Changes in calcareous nannoplankton assemblages around the Eocene-Oligocene climate transition in the Hungarian Palaeogene Basin (Central Paratethys). Historical Biology 00, 1–14.

Okada, H., Bukry, D., 1980. Supplementary modification and introduction of code numbers to the low-latitude coccolith biostratigraphic zonation. Marine Micropaleontology 5, 321–325.

Ozsvárt, P., Kocsis, L., Nyerges, A., Győri, O., Pálfy, J., 2016. The Eocene-Oligocene climate transition in the Central Paratethys. Palaeogeography, Palaeoclimatology, Palaeoecology 459, 471–487.

Persico, D., Fioroni, C., Villa, G., 2012. A refined calcareous nannofossil biostratigraphy for the middle Eocene-early Oligocene Southern Ocean ODP sites. Palaeogeography, Palaeoclimatology, Palaeoecology 335–336, 12–23.

Persico, D., Villa, G., 2004. Eocene-Oligocene calcareous nannofossils from Maud Rise and Kerguelen Plateau (Antarctica): Paleoecological and paleoceanographic implications. Marine Micropaleontology 52, 153–179.

Persico, D., Villa G., 2008. A new Eocene Chiasmolithus species: hypothetical reconstruction of its phyletic lineage. Journal of Nannoplankton Research 30, 23-33

Premoli Silva, I., Orlando, M., Monechi, S., Madile, M., Napoleone, G., Ripepe, M., 1988. Calcareous plankton biostratigraphy and magnetostratigraphy at the Eocene-Oligocene transition in the Gubbio area.

International Subcommission on Paleogene Stratigraphy, Eocene/Oligocene Meeting, Spec. Publ., II 6, 137–161.

Raffi, I., 1999. Precision and accuracy of nannofossil biostratigraphic correlation. Philosophical Transactions of the Royal Society A: Mathematical, Physical and Engineering Sciences 357, 1975–1993.

Raffi, I., Agnini, C., Backman, J., Catanzariti, R., Pälike, H., 2016. A Cenozoic calcareous nannofossil biozonation from low and middle latitudes: A synthesis. Journal of Nannoplankton Research 36, 121–132.

Shafik, S., 1981. Nannofossil biostratigraphy of the Hankenina (foraminiferal) interval in the upper Eocene of southern Australia. BMR Journal of Australian Geology & Geophysics 6, 108–116.

Stradner, H., 1962. Über neue und wenig bekannte Nannofossilien aus Kreide und Alttertiär. Sonderabdruck aus den Verhandlungen der Geologischen Bundesanstalt 2, 363–377.

Sutherland, R., Dickens, G.R., Blum, P., Agnini, C., Alegret, L., Bhattacharya, J., Bordenave, A., Chang, Li., Collot, J., Cramwinckel, M.J., Dallanave, E., Drake, M.K., Etienne, S.J.G., Giorgioni, M., Gurnis, M., Harper, D.T., Huang, H., Keller, A.L., Lam, A.R., Li, H., Matsui, H., Morgans, H.E.G., Newsam, C., Park, Y.H., Pascher, K.M., Pekar, S.F., Penman, D.E., Saito, S., Stratford, W.R., Westerhold, T., Zhou, X., 2019. Site U1509. Tasman Frontier Subduction Initiation and Paleogene Climate. Proceedings of the International Ocean Discovery Program, 371: College Station, TX (International Oce 371.

Sutherland, R., Dickens, G.R., Blum, P., and the Expedition 371 Scientists, 2018. Expedition 371 Preliminary Report: Tasman Frontier Subduction Initiation and Paleogene Climate. International Ocean Discovery Program.

Sutherland, R., Dos Santos, Z., Agnini, C., Alegret, L., Lam, A.R., Westerhold, T., Drake, M.K., Harper, D.T., Dallanave, E., Newsam, C., Cramwinckel, M.J., Dickens, G.R., Collot, J., Etienne, S.J.G., Bordenave, A., Stratford, W.R., Zhou, X., Li, H., Asatryan, G., 2022. Neogene Mass Accumulation Rate of Carbonate Sediment Across Northern Zealandia, Tasman Sea, Southwest Pacific. Paleoceanography and Paleoclimatology 37, 1–22.

Toffanin, F., Agnini, C., Rio, D., Acton, G., Westerhold, T., 2013. Middle eocene to early oligocene calcareous nannofossil biostratigraphy at IODP site U1333 (equatorial pacific). Micropaleontology 59, 69–82.

Villa, G., Fioroni, C., Pea, L., Bohaty, S.M., Persico, D., 2008. Middle Eocene-late Oligocene climate variability: Calcareous nannofossil response at Kerguelen Plateau, Site 748. Marine Micropaleontology 69, 173–192.

Wei, W., 1991. Middle Eocene-lower Miocene calcareous nannofossil magnetobiochronology of ODP Holes 699A and 703A in the subantarctic South Atlantic. Marine Micropaleontology 18, 143–165.

Wei, W., Wise, S.W., 1989. Paleogene calcareous nannofossil magnetobiochronology: Results from South Atlantic DSDP Site 516. Marine Micropaleontology 14, 119–152.

Wei, W., Wise, S.W., 1990. Biogeographic gradients of middle Eocene-Oligocene calcareous nannoplankton in the South Atlantic Ocean. Palaeogeography, Palaeoclimatology, Palaeoecology 79, 29–61.

Wise, S.W., 1983. Mesozoic and Cenozoic calcareous nannofossils recovered by Deep Sea Drilling Project Leg 71 in the Falkland Plateau region, southwest Atlantic Ocean. Init. Repts. DSDP, 71 481–550.

Wise, S.W., 1973. Calcareous nannofossils from cores recovered during Leg 18, Deep Sea Drilling Project: biostratigraphy and observations on diagenesis. In: Kulm, L.D., Huene, R. von, Et, A. (Eds.), Initial Reports of the Deep Sea Drilling Project, 18. U.S. Government Printing Office, Washington, D.C., p. 569–515.

Chapter 4

Calcareous nannofossil record at the Eocene-Oligocene transition from Site U1509 (IODP Exp. 371): paleoclimatic evolution and bulk stable isotopes[1]

Abstract The Eocene-Oligocene transition (EOT; ~34 Ma) represents one of the most prominent climate transition of the entire Cenozoic. Calcareous nannoplankton experienced significant assemblage changes in coincidence with the long-term modifications in sea-surface temperature and trophic conditions, suggesting a cause-effect relationship between the onset of the first sustained Antarctic glaciation and the response of phytoplanktonic communities.

To better evaluate the timing and nature of this relationship, we generated a high-resolution calcareous nannofossil and geochemical datasets ($\delta^{18}O$, $\delta^{13}C$ and % $CaCO_3$) from IODP Site U1509 (New Caledonia Trough) with the final aim to provide an overview of the paleoclimatic and paleoceanographic evolution of the study area. Based on the trends and shifts observed in the assemblages, the ~5 Myr study interval is subdivided in 4 distinct phases: *warm-oligotrophic*, *precursor*, *cold-eutrophic* and *steady-state*. These changes are interpreted as an overall decline of warm-oligotrophic communities which favors the incoming of taxa better adapted to cooler and more eutrophic conditions. The most prominent shift in the assemblages occurred during a ~520 kyr interval, referred to as the *precursor phase*, with relatively high bulk $\delta^{18}O$ and % $CaCO_3$ values, that predated the phase of maximum glacial expansion (Earliest Oligocene Glacial Maximum – EOGM).

Keypoints

- Dramatic changes in nannofossil assemblage occurred during the '*precursor phase'*, in coincidence with the onset of the Eocene-Oligocene transition (EOT);
- diversity dramatically decreases during the EOT, with the loss of warm oligotrophic community and the replacement by the cold-eutrophic taxa;
- An increased of paleoproductivity and a decreased in temperature, respectively inferred from PC2 and PC1 scores, is documented in coincidence with the EOGM;

[1] Allyson Viganò[1], Edoardo Dallanave[2], Laia Alegret[3], Thomas Westerhold[4], Rupert Sutherland[5], Gerald R. Dickens[6], Claudia Agnini[1]
[1]Dipartimento di Geoscienze, Università di Padova, Padova, Italy
[2]Faculty of Geosciences - Research Group Marine Geophysics, University of Bremen, Bremen, Germany
[3]Facultad de Sciencias, Universidad de Zaragoza, Zaragoza, Spain
[4]Center for Marine Environmental Sciences (Marum), University of Bremen, Bremen, Germany
[5]School of Geography, Environment and Earth Sciences, Victoria University of Wellington, Kelburn Parade, Wellington 6012, New Zealand
[6]Earth, Environmental and Planetary Sciences, Rice University, 6100 Main Street, Houston, TX 77005, USA

Authors contributions: A.V. and C.A. designed the study and developed the methodology. A.V. was responsible for data creation and presentation. A.V. and C.A. were the project administrator. L.A, T.W., R.S., G.D. and C.A. have provided the samples and data used in this study. E.D. have provided data, comments and suggestions. All the co-authors contributed to the final polishing of the manuscript.

4.1 Introduction

The Eocene–Oligocene transition (EOT, ~34 Ma) is characterized by a decrease in global temperatures and the permanent onset of Antarctic glaciation (Zachos et al., 1996; 2001; Lear et al., 2000; Pearson et al., 2009). The transition from the Eocene greenhouse to Oligocene icehouse conditions occurred in two orbitally-paced steps, which are denoted by positive shifts in benthic foraminiferal oxygen isotopes ($\delta^{18}O$).

The $\delta^{18}O$ signal (Figure 4.1) reflects both an increase in continental ice volume and a decrease in ocean temperature, due to the preferential enrichment of ^{16}O in ice sheets by the hydrological cycle and isotopic fractionation during the calcification process. Most of the cooling occurred during Step 1 (Lear et al., 2008), where Mg/Ca ratio and oxygen isotope data indicate a deep-sea water cooling of ~2°C (Haiblen et al., 2019). The second step (Step 2 or EOIS, Hutchinson et al., 2021) is dominated by an increase in ice volume with a minor component related to temperature (Lear et al., 2008). This positive shift denotes the end of the EOT and the onset of the Early Oligocene Glacial Maximum (EOGM) (Miller et al., 1991; Zachos et al., 1996;, Liu et al., 2004; Coxall et al., 2005; Coxall and Pearson, 2007). The EOGM coincides with a phase of relatively constant positive $\delta^{18}O$ values that roughly corresponds to Chron C13n and represents the first appearance and expansion of permanent ice sheets on east Antarctica (Zachos et al., 1996; Liu et al., 2004). Associated with the global EOGM event, fundamental components of the Earth system including sea level, atmospheric CO_2, orbital configuration, land/sea surface coverage, continental weathering rates, ocean chemistry, circulation, productivity as well as the role of many positive climate feedbacks dramatically changed triggering transient and permanent modifications in marine and terrestrial faunas and floras (Coxall and Pearson, 2007).

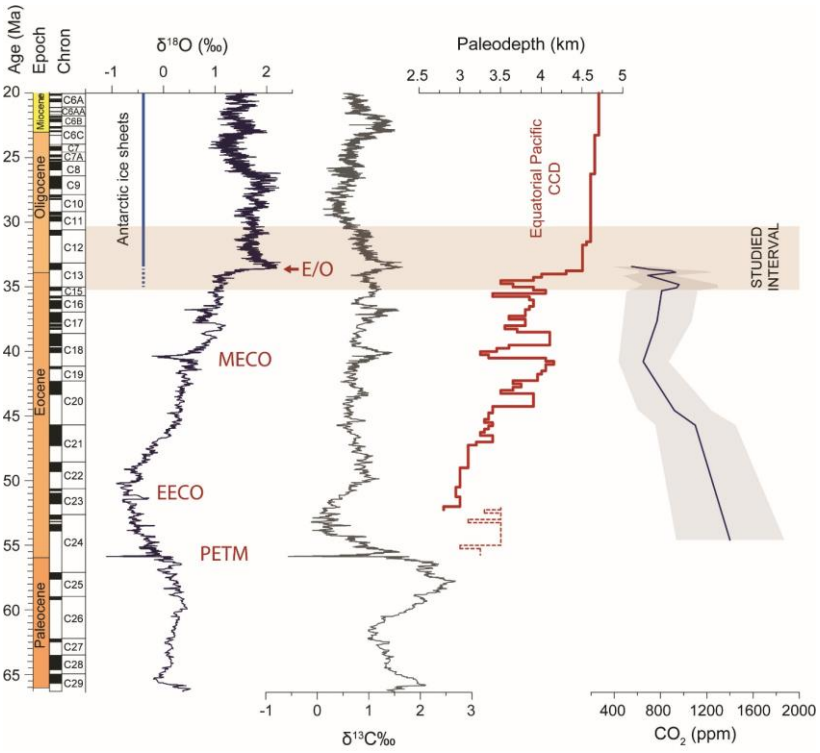

Figure 4.1 Position of the main Paleogene climatic events (PETM, EECO, MECO and EOT) plotted against oxygen and carbon stable isotope compilations (9-point moving average) (Cramer et al., 2009 recalibrated to GTS12), equatorial Pacific CCD (Pälike et al., 2012), mean CO_2 (Anagnostou et al., 2016 converted to GTS12) enveloped by a shaded standard deviation band.

Two main hypotheses exist to explain the Antarctic glaciation: "the CO_2 hypothesis" and "the ocean-gateway hypothesis". The first proposes that the global decline in CO_2 caused the drop in global temperature leading to emplacement of the Antarctic ice sheet (DeConto and Pollard, 2003; Zachos and Kump, 2005; Pearson et al., 2009; Pagani et al., 2011; Anagnostou et al., 2016). The second hypothesis suggests that the opening of the Southern Ocean gateways (i.e., the Drake Passage and the Tasman Seaway) allowed for the initiation of the Antarctic circumpolar current (ACC) which, in turn, reduced poleward heat transfer and thermally isolated Antarctica (Kennett, 1977; Sijp et al., 2004). Paleoestimates of CO_2 concentrations unravel a gradual decreasing with values ranging from 1400 ± 470 ppm during the Early Eocene climatic Optimum (EECO; 51-53 Ma) to 550 ± 190 ppm in the early Oligocene (Anagnostou et al., 2016). This dramatic change in atmospheric CO_2 indicates that carbon dioxide could have been the principal forcing of long-term middle-late Eocene cooling (Figure 4.1). Although there is evidence for both theories, the common view is that the gradual decline in atmospheric CO_2 has acted as the main driver of the EOT, with ice-sheet feedbacks and paleogeography forcing playing a secondary role (Hutchinson et al., 2021). The variation in orbital parameters has likely controlled the Earth system dynamics (DeConto and Pollard, 2003; Huber et al., 2004; Coxall et al., 2005; Pearson et al., 2009; Pagani et al., 2011; Lefebvre et al., 2012; Goldner et al., 2014; Ladant et al., 2014; Sijp et al., 2011). A piece of information on the paleoclimatic evolution during the late Eocene – early Oligocene is possibly inferred from the distribution and abundances of calcareous nannofossils, which mainly consist of the fossil rest of coccolithophores. In the modern oceans, coccolithophorids are one of the most important primary organic and inorganic carbon producers. The cell of these organisms is surrounded by small calcite plates (*coccoliths*), which form a calcareous test named *coccosphere* (Perch-Nielsen, 1985). In virtue of their biological/physiological traits, calcareous nannofossils are extremely sensitive indicators of oceanographic and climatic conditions in the marine photic zone and is thus considered as a fundamental tool to shed light into the evolution of the bio-geosphere during the Paleogene. At present, the response of calcareous nannofossils to the onset of Antarctic glaciation is still puzzled lacking a global perspective. Although the late Eocene - early Oligocene witnessed one of the most crucial climate transition on the Earth during the Cenozoic, relatively few highly resolved studies have documented the calcareous nannofossil response to this event (Persico and Villa, 2004; Dunkley Jones et al., 2008; Villa et al., 2008; 2014; 2021; Bordiga et al., 2015; Fioroni et al., 2015; Jones et al., 2019). This lack is mainly due the fact that the Eocene-Oligocene transition is very often characterized by condensed sequences, or even worst hiatuses, that typically display moderate to poor preservation.

The shift from a greenhouse to an icehouse world was accompanied by a decrease in nannofossil diversity, which reached minimum values during the EOGM (Bown et al., 2004) in coincidence with the lowest rates of evolution of the entire Paleogene (Haq, 1973). In the last decades, a cause-effect relationship has been proposed for decline in diversity, on one side, and the global cooling, on the other side (Aubry, 1992). An alternative explanation for the decrease in the number of species is a nutrient-controlled contraction of oceanic trophic resource continuum (TRF), that would have resulted from enhanced eutrophic conditions (Hallock, 1987). The sustained eutrophication together with the decrease in temperature are considered the possible forcings for the evolutionary turnovers and extinctions observed in calcareous nannoplankton (Aubry, 1992). The earliest

Oligocene was dominated by few opportunistic taxa displaying high abundances, which typically better thrive in stressed and unstable environments. Almost in correspondence to the onset of the EOT, calcareous nannofossil assemblages experienced the dramatic extinction of warm and k-selected rosetta-shaped discoasterids (i.e., *Discoaster saipanensis* and *D. barbadiensis*). This event is preceded by the disappearance of *Cribrocentrum reticulatum* and followed by the rapid and remarkable increase of *Clausicoccus subdistichus* gr.

The long-term decrease in diversity is mainly related to an increase in the extinction rate during the late Eocene and becomes more and more intense as the EOB approaches indicating an increase in the environmental pressure, such as a change in ocean thermal structure and/or nutrient availability. This phase is followed by the incoming of cold-tolerant and cosmopolitan species. A major paleoceanographic change is the global deepening of the CCD (approximately > 1 km; Coxall et al., 2005; Pälike et al., 2012) that has resulted in a huge exchange of carbonate from the shallow water domain to the deep-sea: This transfer is due to a shelf to basin fractionation change across the E-O transition that is remarkable considering that shallow-shelves areas, were extensive carbonate precipitation sites in the Eocene but ,as a result of the marine global regression this was not the case anymore in the Oligocene, (e.g. Coxall and Wilson, 2011). In this work we have developed highly resolved calcareous nannofossil and geochemical (bulk $\delta^{13}C$, bulk $\delta^{18}O$, $\%CaCO_3$) records from IODP Site U1509 (New Caledonia Trough – Tasman Sea, Sutherland et al., 2019) spanning from the late Eocene to the early Oligocene.

Main aims of this work are: (1) to analyze diversity and abundances of calcareous nannofossil assemblage data; (2) to reconstruct the paleoclimatic evolution of the study area and its possible connection with the Antarctic glaciation. Records generated at Site U1509 provide new insights on how calcareous phytoplankton have reacted to the onset of global "icehouse" conditions and contribute to a better understanding of the dynamics active during this key transition.

4.2 Material and methods

4.2.1 IODP Site U1509

Site U1509 (34°39.13'S, 165°49.66'E) (Figure 4.2) was drilled during International Ocean Discovery Program (IODP) Expedition 371 on the western margin of New Caledonia Trough (NCT) at the base of the Lord Howe Rise slope in the Tasman Sea (Sutherland et al., 2019).

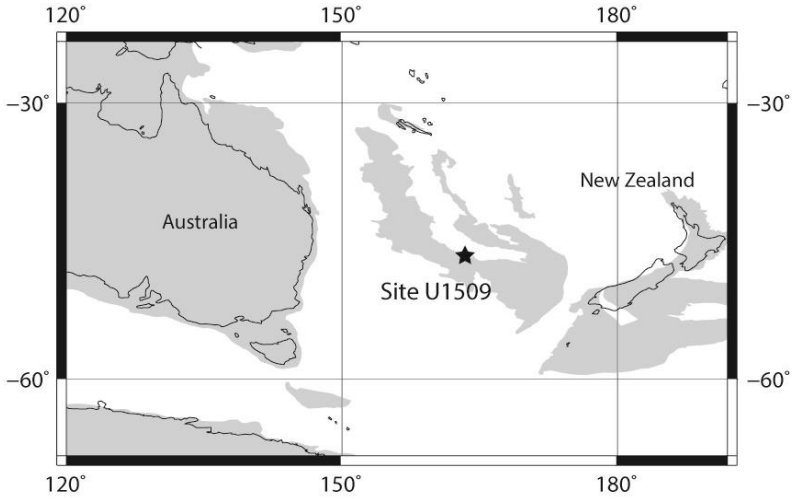

Figure 4.2 Paleogeographic reconstruction at 34 Ma, showing the approximate location of IODP Site U1509 (black star). In grey: plate fragments; black lines: present day shorelines. Base map projection (equidistant cylindrical) is available online http://www.odsn.de/odsn/services/paleomap/paleomap.html.

Today, the oceanography of study area is influenced by the Antarctic Circumpolar Current (ACC) and the shallow wind-driven East Australian Current (EAC) (Sutherland et al., 2018) whose strength is observed to vary seasonally in response to changes in basin-scale winds (Chiswell et al., 1997). This area is also influenced by the Subtropical Water (STW), the warmest (T>15°) and most saline surface water (higher than 34.5‰), which arrives as complex vortexes in the New Zealand region by EAC. At about 32°S part of these vortexes propagates into the central Tasman Sea, forming the Tasman Front (TF) (Chiswell et al., 2015; Sutherland et al., 2022).

The intermediate (~1000 m) circulation consists of the Antarctic Intermediate Water (AAIW) subtype 3 as revised by Bostock et al. (2013). Site U1509 currently sits at 2911 m water depth and the estimated paleodepth for the interval of interest is lower bathyal (Sutherland et al., 2019) based on the upper depth limit (ca. 1000 m) of benthic foraminifera *C. mundulus* and *N. umbonifera* (van Morkhoven et al., 1986).

Notably, the middle Eocene to Oligocene interval at Site U1509 where found to contain biosilica (Sutherland et al., 2019). This is particularly relevant since the presence of siliceous microfossils (i.e., diatoms, radiolarians, sponge spicules, silicoflagellates) is usually associated either with enhanced surface water productivity or preservation.

4.2.2 Calcareous nannofossils data

At Hole U1509A, the study succession spans from 267.305 to 183.305 (CSF-a, m), roughly corresponding to a time interval of 4.91 Myr (i.e., 35.24 to 30.33 Ma). In the interval of interest, we have analyzed a total number of 124 samples with an average sampling resolution of 66 cm, which duplicates (ca. 33 cm) around the EOT. All samples were prepared following the standard procedure for smear slides preparation (Bown & Young, 1998) and then analyzed using a Zeiss transmitted light microscope with a magnification of 1250×. In this work, we provide the distribution patterns of taxa across the late Eocene- early Oligocene time. Relative abundance patterns (%) of the total assemblage were obtained counting at least 300 specimens per sample. The taxonomy follows Aubry (1984, 1988, 1989), Perch-Nielsen (1985), Bown (2005), Bown & Dunkley Jones (2012), Newsam et al. (2017), except for *Dictyococcites* and *Reticulofenestra* for which we follow Agnini et al. (2014). Here, we have adopted the Cenozoic calcareous nannofossil NP of (Martini,1971), CP (Okada and Bukry, 1980) zonations, and CN biostratigraphic scheme of Agnini et al. (2014). A comprehensive discussion regarding the selected biohorizons, their global comparison and the age model here adopted is provided in the Chapter 3). Microphotographs of calcareous nannofossils investigated are presented in Plates 4.1, 4.2, 4.3 and 4.4. Principal component analysis (PCA) was performed on the most abundant calcareous nannofossil taxa (%) of the assemblage using the statistical software PAST (PAleontological STatistic; Hammer et al., 2001). The PCA allow us to detect the main factors affecting variations in assemblage composition. For this analysis, we considered the following 17 taxa: *Chiasmolithus, Clausicoccus, Coccolithus, Cyclicargolithus, Dictyococcites, Discoaster, Ericsonia, Isthmolithus, Lanternithus, Reticulofenestra, Sphenolithus, Zygrablithus, Helicosphaera, Cribrocentrum, Blackites*, "Reworking" (reworked specimens) and "Others" (genera with extremely low abundances). We also performed an alternative PCA based exclusively on placoliths, to evaluate their specific role during the E-O climate transition. This analysis involved the following 18 taxa: *Cribrocentrum, Chiasmolithus, Clausicoccus, Coccolithus pelagicus* (6-13µm)*, Cyclicargolithus floridanus, Dictyococcites* (<4µm)*, Dictyococcites* (4-10µm), *D. bisectus* (>10µm), *D.* cf. *D. bisectus* (<10µm), *D.* cf. *D. filewiczii*, *D. filewiczii*, *Dictyococcites hesslandii*, *Ericsonia formosa*, *Reticulofenestra* (<4µm), *Reticulofenestra* (4-10µm), *Reticulofenestra* (10-14µm), *Reticulofenestra daviesii*, *Reticulofenestra umbilicus* (>14µm). In this second PCA analysis we also included: reworking, not placoliths and others minor components.

4.2.3 Geochemical proxies

A total of 183 samples were powdered using an agate mortar and inserted into generic polyethylene capsules. For each sample, a mass equal to ~0.300 mg, was weighed using the precision balance Mettler Toledo AT21 and placed into borosilicate vials to be analyzed for bulk sediment carbon and oxygen stable isotope composition and calcium carbonate content (% $CaCO_3$). The analysis was carried out using a Delta V Advance Isotopic Ratio Mass Spectrometer equipped with a Gas Bench II device. Each sample was flushed with He5.5 and then treated with 10 drops of orthophosphoric acid (EMSURE ® ≥ 99 %) for ca. 3 hours at 70°C. Isotopic values are reported in standard delta notation relative to the Vienna Pee Dee Belemnite (VPDB). For the

calibration and the quality check, we used, respectively, two internal standards: Maq1 (white Carrara marble; $\delta^{13}C$= 2.58‰; $\delta^{18}O$= −1.15‰ VPDB) and Gr1 (marble; $\delta^{13}C$= 0.68 ‰; $\delta^{18}O$= −10.44 ‰ VPDB).

For each run sequence we used 12 Maq1 samples and 3 Gr1 samples, each one with a weight range between 0.200-0.250 mg. The precision was better than 0.06‰ for $\delta^{13}C$ and better than 0.09‰ for $\delta^{18}O$, during sample runs. Every rack also contained a ramp of 8 samples of Maq1 with weights ranges from 0.050 to 0.500 mg equally distributed along the run. The Maq1 ramp samples allow the construction of a linear regression equation (based on the of CO_2 beam intensity - mV- and the standard weight - mg) to extrapolate $CaCO_3$ content of the investigated samples (Spofforth et al., 2010).

4.2.4 Paleoecological indices

Calcareous nannofossil species are considered excellent paleoenvironmental proxies and paleoceanographic indicators, thanks to their broad geographic distribution and their sensitivity to common paleoenvironmental parameters (e.g., Wei and Wise, 1990; Aubry, 1992; Bown, 1998; Persico and Villa, 2004; Dunkley Jones et al., 2008; Villa et al., 2008; 2021; Bordiga et al., 2015). In this work we decided to group key EOT calcareous nannofossil taxa which share similar paleoecological traits, such as warm-water oligotrophic and cold-water eutrophic taxa. We considered only taxa for which ecological affinities are well established from previous studies. In particular, *Discoasters* (e.g., *D. saipanensis* and *D. barbadiensis*) are considered warm-water oligotrophs due to their predilection for low-middle latitudes (Wei and Wise, 1990; Villa et al., 2008). *Ericsonia formosa* displays a clear preference for low-middle latitudes and it usually thrives in warm waters (Wei and Wise, 1990; Monechi et al., 2000) and oligotrophic environments (Bralower, 2002; Tremolada and Bralower, 2004; Villa et al., 2008). On this basis, we have grouped and graphically plotted these taxa as warm-oligotrophic water indicators (%). Instead, among the cold-eutrophic group (%) we have included the following taxa: *Reticulofenestra daviesii, Chiasmolithus* spp. and *Clausicoccus subdistichus* group. *R. daviesii* is especially abundant at high latitudes and is considered by many authors a cold-eutrophic water taxon (Monechi et al., 2000; Persico and Villa, 2004; Villa et al., 2008; 2014; Fioroni et al., 2015), however, Bordiga et al. (2017) recently reported a more plastic and tolerant behavior for this species. Genus *Chiasmolithus* is well-established as a cold-water taxon (Bukry, 1973; Wei and Wise, 1990; Persico and Villa, 2008; Villa et al., 2014), possibly adapted to moderate to high nutrients environments (Aubry, 1992; 1998; Bralower, 2002). *Clausicoccus subdistichus* gr. (i.e., *C. subdistichus* and *C. fenestratus*) shows a distinctive increase in abundance at Site U1509, with higher peaks roughly coincident with the EOGM. Recent observations from ODP Site 756 indicates a cold-eutrophic affinity of this group and a high sensitivity during the shift into glacial conditions (Chapter 2).

Warm-oligotrophic taxa	**Cold-eutrophic taxa**
Discoaster barbadiensis	*Chiasmolithus* spp.
Discoaster saipanensis	*Reticulofenestra daviesii*
Ericsonia formosa	*Clausicoccus subdistichus* gr.

Table 4.1 Paleoecological affinities assigned to calcareous nannofossil taxa.

4.2.5 Diversity indices

In this work we estimate the diversity in calcareous nannofossil communities through time by the computation of different diversity indices. The calculations of these indices were made by applying the statistics to quantitative count (%) assemblage data. We decide to use multiple diversity indices for diversity evaluation since the application of one single likely oversimplifies the real biodiversity signal. The indices adopted are as follows: number of taxa (S), dominance (D), Shannon-Weaver index (H) (Shannon and Weaver, 1949) and Evenness (E). Our biodiversity analysis was undertaken within the community-taxa (α-diversity) level (Whittaker, 1972). At this level, the Shannon diversity index (H) is commonly used to evaluate the information entropy of a system. This index incorporates both the number of taxa and evenness, and it is calculated from the equation: $H(S) = -\Sigma p_i \ln p_i$, where p_i represents the probability of occurrence of taxon individuals in a community or quadrat and S is the number of taxa observed. High H values indicate a community with many taxa, each with equal abundances. We also consider Buzas-Gibson Evenness (E) (Buzas and Gibson, 1969) calculated by $E = e^H/S$. Evenness (or equitability) represents a standard measure of diversity on a normalized scale (from 0 to 1, where 0 represents one dominant taxon in the assemblage and 1 embodies an equal proportion of taxa) and expresses how evenly the individuals in a community are distributed among different taxa. Dominance was calculated as $D= \Sigma (n_i/n)^2$, where n_i is the number of individuals of taxon i, and ranges from 0 (all taxa are equally present) to 1 (one taxon dominates the community completely). However, it is important to note that diversity indices are not always comparable between different datasets since they depend on the limits within which they may varies and on the taxonomic groups adopted.

4.3 Results

4.3.1 Relative changes in calcareous nannofossil assemblages

Calcareous nannofossil assemblages at Site U1509 show several variations in abundance (%) and changes in their composition (Figure 4.3). The late Eocene-early Oligocene assemblages are dominated by *Reticulofenestra* which shows a mean abundance of ~67% over the entire ~5 Myr interval. The taxonomy of reticulofenestrids is not well constrained due to the heterogeneity of this group (Young, 1990). For this reason, we decide to include different species ascribed to *Reticulofenestra* into size groups (*Reticulofenestra* <4μm, between 4-10μm and 10-14μm) to capture any possible difference in the abundance behavior of the three size subgroups. The larger forms of *Reticulofenestra* (10-14μm) slightly decreases towards the top of the interval, whereas the smaller forms (<4μm) increase in abundance (Figure 4.4). The smaller forms have a mean value of 25.96% within the total assemblage. At Site 1509, we discriminate between broadly elliptical/subcircular coccoliths characterized by faintly visible or imperceptible net in the central area assigned to *Reticulofenestra* and elliptical forms with a relatively solid central plug closing the central area (*Dictyococcites*) (e.g., Haq, 1971; Backman, 1980; Perch-Nielsen, 1985; Young 1990). *Coccolithus* represents the second most abundant taxon with a mean value of 11.4%. Its abundance pattern varies notably throughout the interval with a peak of 20.7% in the upper part, even if the average values (~13%) are recorded between 267.305 and 240.905 m (CSF-A). *Dictyococcites* is a common component of the assemblages (on average ~8%). For this genus we have differentiated three dimensional groups (*Dictyococcites* spp. <4μm, between 4-10μm and 10-14μm) and

some specific taxa (*D. bisectus* >10µm, *D.* cf. *bisectus* <10µm, *D. filewiczii* and *D. hesslandii*). These taxa are characterized by different and highly variable abundance through the study section (Figure 4.4), although the higher abundances are those of *D.* cf. *D. bisectus* (<10µm) and *D. bisectus* (>10µm), with a mean value of 4.2% and 1.8%, respectively. *Cyclicargolithus* shows a distinct increasing trend from ~2% in the lower part of the to 8.4% in the upper part of the succession, above 217.360 m (CSF-A). *Clausicoccus* rapidly increases in abundance (from 7.1% to 11.5%) at 250.350 m (CSF-A) with high values (~6.3% on average) that persisted up to 221.415 m (CSF-A) and then rapidly dropped to a mean value of 0.1%. *Ericsonia* is rare at the base of the section, from 267.305 to 247.495 m (CSF-A), with a mean value of 1.4%. Above 247.495 m (CSF-A), *Ericsonia* displays a scattered decrease in abundance. Similarly, to *Ericsonia*, *Isthmolithus* is continuously present at the base of the interval with percentages <1.7%. *Discoaster* is rare to frequent in the lower part of the study interval with a peak in abundance (5.5%) between 267.305 and 256.960 m (CSF-A). Upward, *Discoaster* progressively decreases to values <1.2%. *Cribrocentrum* displays a similar pattern with a positive peak of 2.3% at 265.485 m (CSF-A) and then gradually disappears. *Lanternithus* is a minor component in the lower Oligocene assemblage but displays a significant positive peak in abundance (up to 5.3%) at 242.705 m (CSF-A) near the base of Chron C13n. Other components of the assemblage are: *Blackites* (mean value 1.6%), *Sphenolithus* (mean value 1.5%), *Zyghrablithus* (average of 1.1%), *Chiasmolithus* (mean value 0.4%), *Helicosphaera* (mean value 0.1%). The category 'Others' includes very rare and discontinuous taxa, e.g., *Bramletteius, Coronocyclus, Markalius, Pontosphaera, Thoracosphaera, Umbilicosphaera* and indetermined placoliths.

At Site U1509, a low percentage (<1%) of the assemblages consists of reworked calcareous nannofossils, mainly derived from re-elaborated middle-late Eocene sediments. Reworked specimens are recorded in the upper part of the section, starting from 223.205 m (CSF-A) and lasting up to 183.305 m (CSF-A). Images of a representative selection of reworked nannofossils are provided in the Appendix V (Plates S4.1 and S4.2).

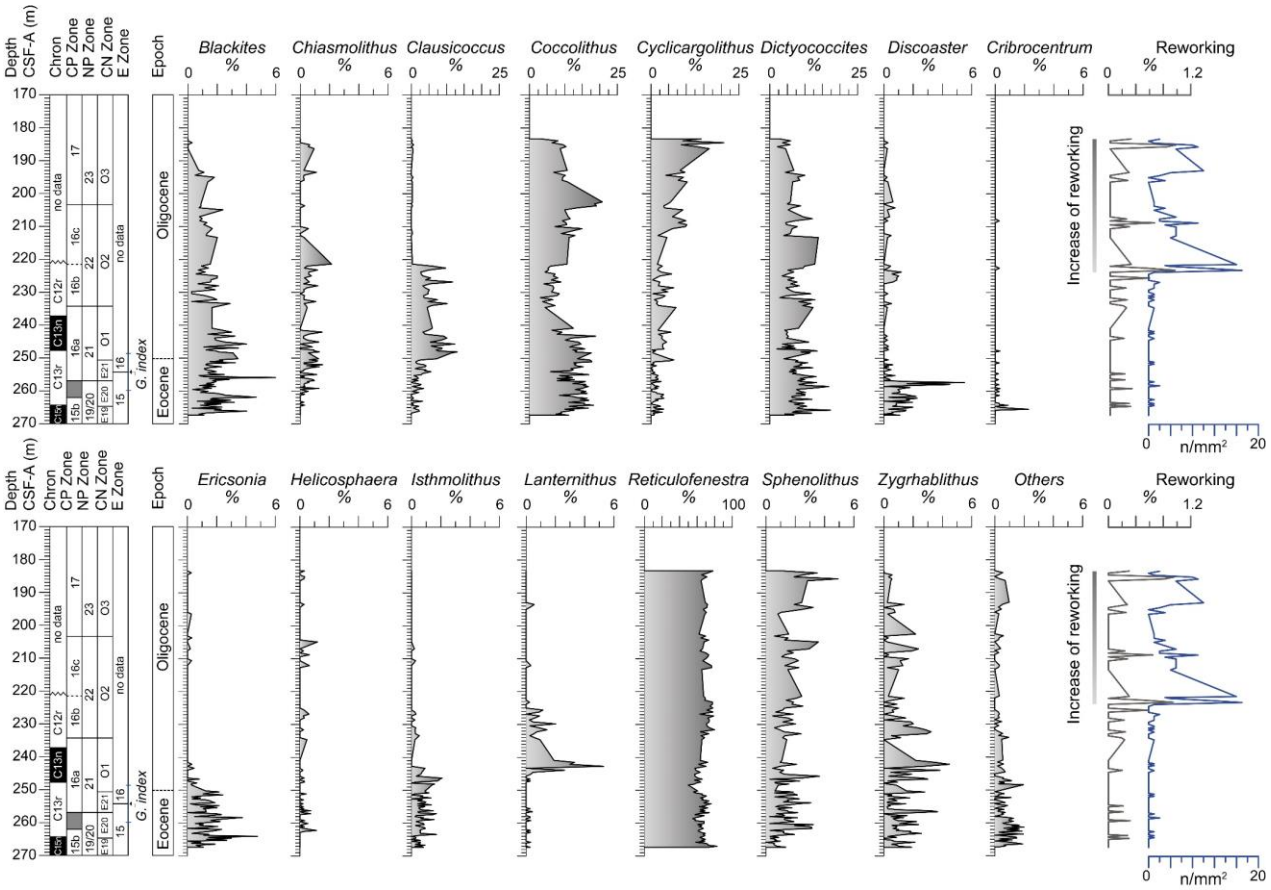

Figure 4.3 Relative abundances (%) of calcareous nannofossil genera at Site U1509.To the right, percentage of reworking and number of reworked specimens (n) in 1 mm^2. To the left, depth (CSF-A, m), magnetostratigraphy, calcareous nannofossil biozonations (CP Zone: Okada & Bukry, 1980; NP Zone: Martini, 1971; CN Zone: Agnini et al., 2014) and planktonic foraminifera biostratigraphy (E Zone: Wade et al., 2011).

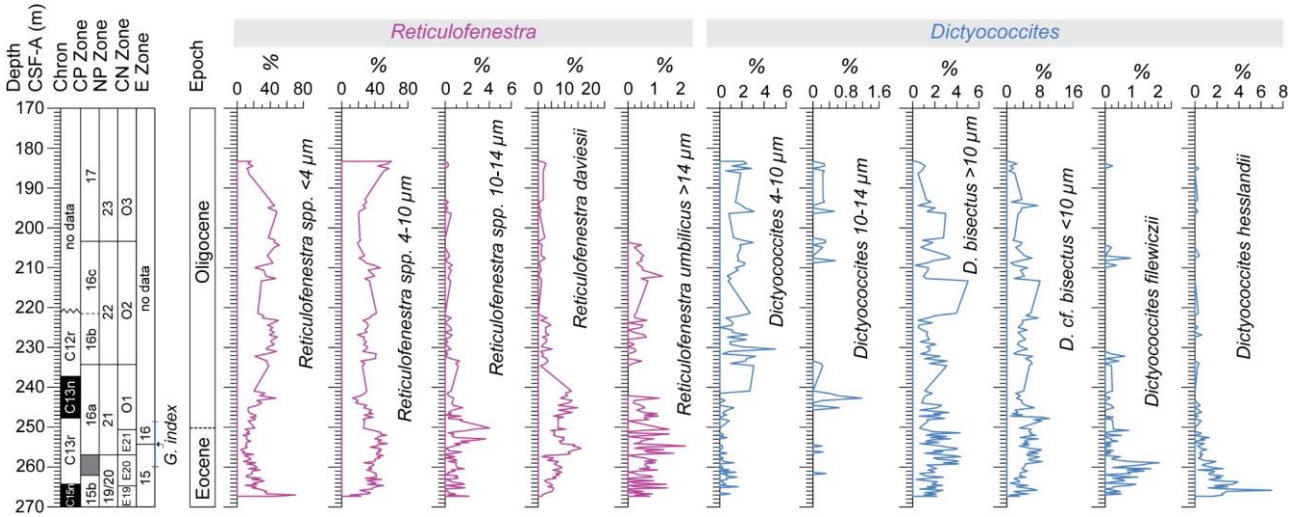

Figure 4.4 Additional relative abundances (%) of formal and informal (size groups) belonging to calcareous nannofossil genera *Reticulofenestra* and *Dictyococcites* at Site U1509.

4.3.2 Paleoclimatic evolution

Significant changes and trends in the calcareous nannofossil data occur across the ~5 Myr study interval. These variations allow the definition of four intervals and 2 subintervals (1-4, Figure 4.5) that are:

1) **Interval 1** (267.305 – 256.960 m, CSF-A)
2) **Interval 2** (256.960 – 250.350 m, CSF-A)
3) **Interval 3** (250.350 – 217.360 m, CSF-A). Interval 3 was further subdivided into two sub-intervals:
    - **Interval 3A** (250.213 – 237.755 m, CSF-A)
    - **Interval 3B** (237.755 – 217.360 m, CSF-A)
4) **Interval 4** (217.360 – 183.305 m, CSF-A). The main traits of the four intervals are discussed below.

Interval 1: late Eocene greenhouse conditions

Interval 1 is defined by the presence of relatively high abundance of mainly rosetta-shaped *Discoaster* and the relatively low abundances of *Clausicoccus* (0-3.5%). From the base to close to the top of interval 1, *Discoaster* varies in abundance from 1.4 to 5.5%. At 256.960 m, CSF-A, discoasters abruptly decrease with values never exceeding 1.2% for the rest of the succession. The relatively high abundances detected for these warm and k-selected taxa suggest that this possibly indicates generally warmer conditions and/or a pre-glaciated world. Common components of Interval 1 also include *D.s filewiczii* and *D.s hesslandii.* Secondary components of this interval are represented by *Cribrocentrum* (0-2.3%) and *Ericsonia* (0-4.8%).

Interval 2: pre-EOGM

Interval 2 displays a sharp decline of discoasters and a first slight increase of *Clausicoccus subdisthicus* gr. During this interval, the assemblage of Interval 1 is gradually replaced by cold water meso/eutrophs taxa, as documented by the remarkable increase of *R. daviesii* from ~3 to 12%.

Interval 3: EOGM and post-EOGM

- ***Interval 3A (EOGM)*** lies within Chron C13n which globally roughly correlates with the phase of maximum positive $\delta^{18}O$ values (EOGM) (Dunkley Jones et al. 2008). The peculiar feature of Interval 3a is the sudden increase of *Clausicoccus subdisthicus* gr. starting from 33.91 Ma. The average abundance of this taxon is of 2.8% but positive peaks in abundance (up to 13%) characterized this subinterval. *Lanternithus minutus* shows positive peaks during this subinterval, then gradually declines during subinterval 3B.
- ***Interval 3B (post-EOGM)*** is characterized by a gradual decline of *Clausicoccus subdisthicus* gr.*, Lanternithus* and *R. daviesii*. *Coccolithus* also displays a remarkable decrease, returning to previous values right at the onset of Interval 4.

Interval 4: Oligocene world. This interval is denoted by the virtual absence of *Clausicoccus* subdisthicus gr. and a significant increase of *Cyclicargolithus.* The Oligocene assemblages consists of few dominant taxa with high numbers of individuals (e.g., *Reticulofenestra*, and *Cyclicargolithus*).

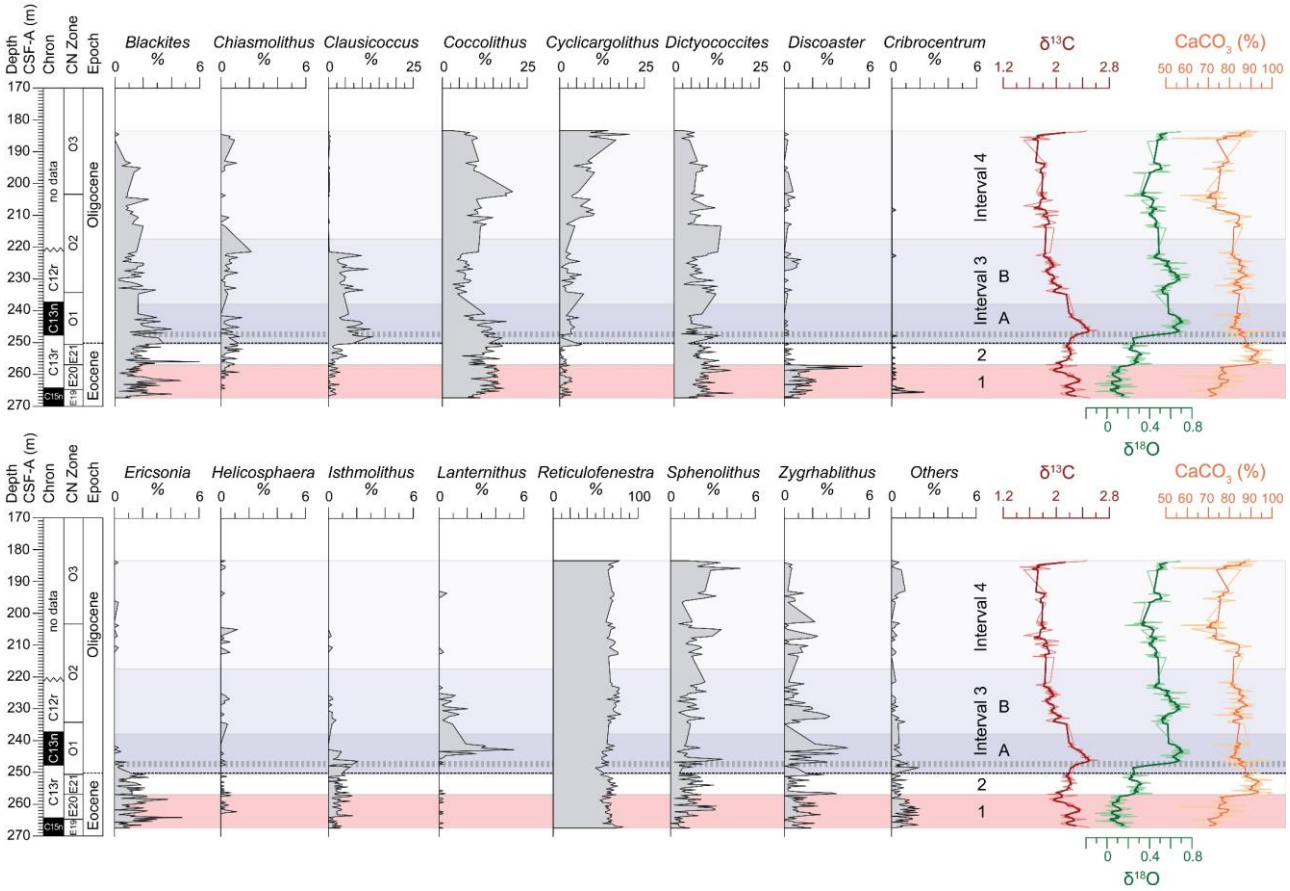

Figure 4.5 Calcareous nannofossil genera (%) along with bulk carbon and oxygen stable isotope and carbonate (%) records at Site U1509. Different colored bands highlight the four intervals in which calcareous nannofossils show significant abundance variations. To the left: depth (m, CSF-A), magnetrostratigraphy, and CN zones (Agnini et al., 2014). Bulk stable isotopes and carbonate content (%) are shown with a 5-point running average.

4.3.3 Bulk carbon and oxygen stable isotope data and carbonate content

A subdivision in four intervals was also found in the bulk carbonate carbon ($\delta^{13}C$) and oxygen ($\delta^{18}O$) isotopes record, and carbonate content (%$CaCO_3$) data (Figure 4.5, 4.6).

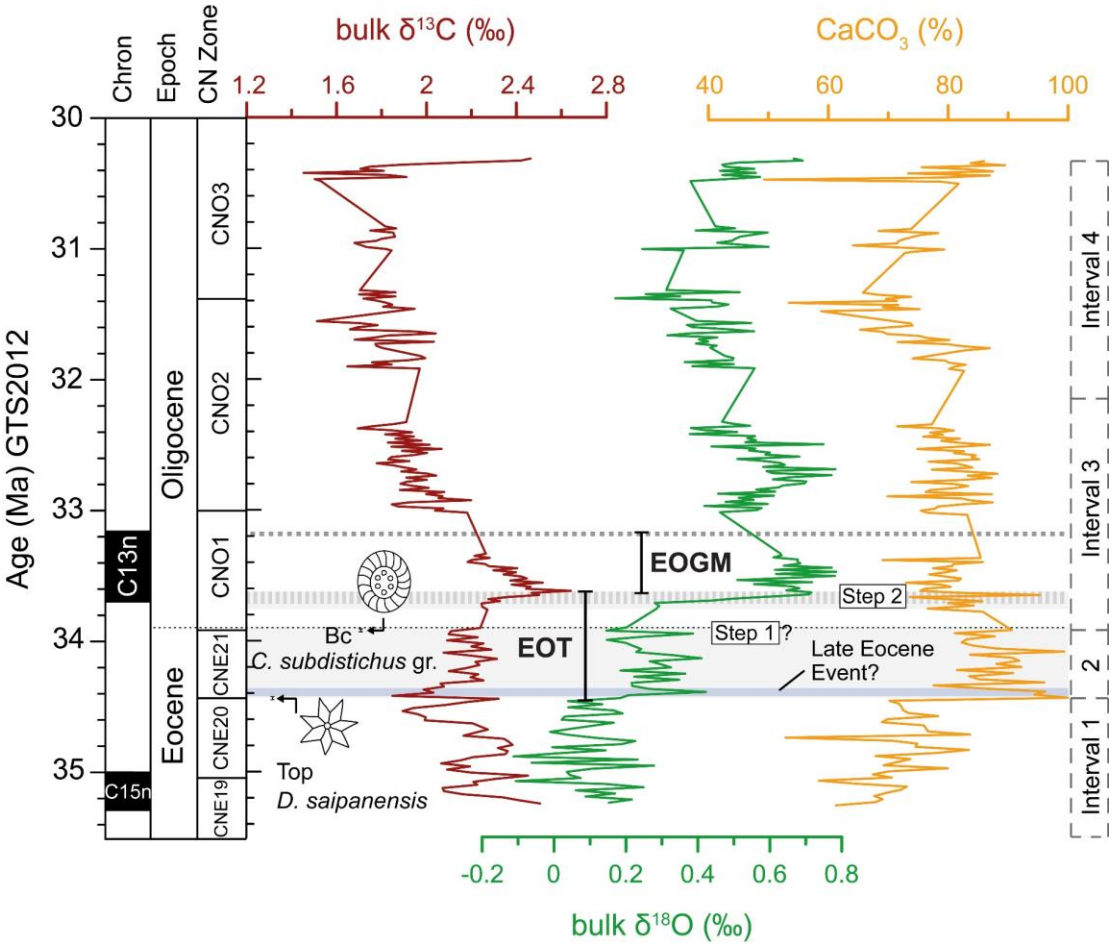

Figure 4.6 Bulk stable isotopes (oxygen, carbon) and carbonate content (%) from IODP U1509 versus chrono-stratigraphy, calcareous nannofossil (CN) biozones (Agnini et al., 2014) and related EOT terminology. Tie-points are available Chron boundaries (see Chapter 3 for details) calibrated to the GTS 2012. timescale (Gradstein et al., 2012).

4.3.3.1 Oxygen isotopes

In the study section, bulk oxygen isotope values vary between -0.11‰ and 0.78‰, with a mean value of 0.41‰. Interval 1 (~7.35 m, 810 kyrs) is characterized by the lowest $\delta^{18}O$ mean value of the entire succession (0.10‰) (± ‰ 0.10). Oxygen isotopic values sharply increase by ~0.4‰ between ~256.5 and ~257.4 CSF-A m (34.46-34.39 Ma), marking the base of Interval 2. This shift is interpreted to correlate with the so-called 'Late Eocene Event' recorded at Sites 522 and 1218 (Katz et al., 2008) which may represent a failed glaciation or a transient cooling event (Hutchinson et al. 2021). The onset of this event is coincident, within a 12 kyrs analytical error with the extinction of *D. saipanensis* (34.428 Ma) as recorded at Site 1509 and perfectly agrees with that reported from Site 1218 (Coxall et al., 2005). At the base of Interval 3, a positive $\delta^{18}O$ shift occurs that is associated with a remarkable increase in abundance of *C. subdistichus* gr. (Bc; 33.91 Ma). However, Step 1, the first increase in $\delta^{18}O$ vales, is hard to identify at Site U1509 because it likely lies in a gap of recovery

(from 33.9 to 33.76 Ma). At Site U1509, the base of Step 2 is calibrated at 33.71 Ma ($\delta^{18}O$ value of 0.28‰) while the Top of this shift has an estimated age of ~33.63 Ma ($\delta^{18}O$ value of 0.72‰)

Step 2 thus represents a rapid $\delta^{18}O$ increase (0.44‰) within the lowermost part of Chron C13n reaching a maximum value of 0.71‰ at 246.6 m The $\delta^{18}O$ highest values are recorded within Chron C13n, which approximately corresponds to the EOGM. Throughout Interval 4, $\delta^{18}O$ values display an average value of 0.45‰ (± ‰ 0.10).

4.3.3.2 Carbon isotopes

Bulk carbon isotope values in the study section range between 1.45‰ and 2.64‰ with an average of 2.04‰ (± 0.24‰). In our record, the $\delta^{13}C$ increase occurred in parallel with the $\delta^{18}O$, and shows the same two-stepped profile. In the lower part of the section (Interval 1), $\delta^{13}C$ values have an average value of 2.21‰ (±0.15‰). The following interval (Interval 2) is characterized by slightly lower mean values (2.15‰ ±0.11‰). From 250.350 to 217.360 m CSF-A (Interval 3), the $\delta^{13}C$ curve displays a trend to lower values with an average of 2.10‰ (±0.23‰). In the lower part of Interval 3 (subinterval 3a) several positive peaks reaching values up to 2.64‰ occur just above the base of Chron C13n. From 217.360 to 183.305 m CSF-A (Interval 4), the $\delta^{13}C$ plot shows relatively low and stable values that has an average value of 1.82‰ (±0.18‰).

4.3.3.3 Carbonate content

Interval 1 is characterized by the lowest $CaCO_3$ content of the entire succession, varying between 53% and 84% and averaging at 71%. Interval 2 is characterized by highest values, ranging roughly between 70% and 100%. Above this interval and in the uppermost ~3.6 Myr (Interval 3 and 4), the carbonate content remains stable with a mean value of 78.3% (± 6.8%). Thus, the carbonate content did not increase during the EOGM but, instead during Interval 2, in contrast to the findings of other sites, specifically in the Indian (Site 756; Chapter 1) and in the Pacific Ocean (Coxall et al., 2005; Coxall and Wilson, 2011).

4.4 Discussion

4.4.1 Paleoclimatic evolution and implications

At Site U1509, the calcareous nannofossil record reveals several shifts in the relative abundance and diversity indices across the Eocene-Oligocene study section, which suggests a causal link between the climatic changes observed and the response of the phytoplanktonic community. A distinctive shift in the assemblage coincides with the base Chron C13n that, in turn, means with the Early Oligocene Glacial Maximum (EOGM). Specifically, the decrease of warm-water oligotrophic taxa (*D. barbadiensis, D. saipanensis* and *E. formosa*) is consistent with both enhanced eutrophic conditions and decreased temperatures, with assemblage modifications primarily controlled by temperature and nutrients (Figure 4.7).

The shift towards cooler and eutrophic assemblages appears to be a consistent feature of the EOT (e.g., Site 756, Chapter 1) with low-middle and high latitude sites suggesting increased nutrient availability (e.g. Dunkley Jones et al., 2008; Villa et al., 2008; Jones et al., 2019). The Shannon H index and the number of taxa show an overall decrease throughout the investigated section, from 2.32 to 1.20 and 30 to 12, respectively. Based on

trends and shifts in the diversity indices, PCs scores and paleoecological groups, our section was subdivided in four phases: (1) a warm-oligotroph phase, (2) a precursor phase, (3) a cold-eutrophic phase and (4) a steady-state phase.

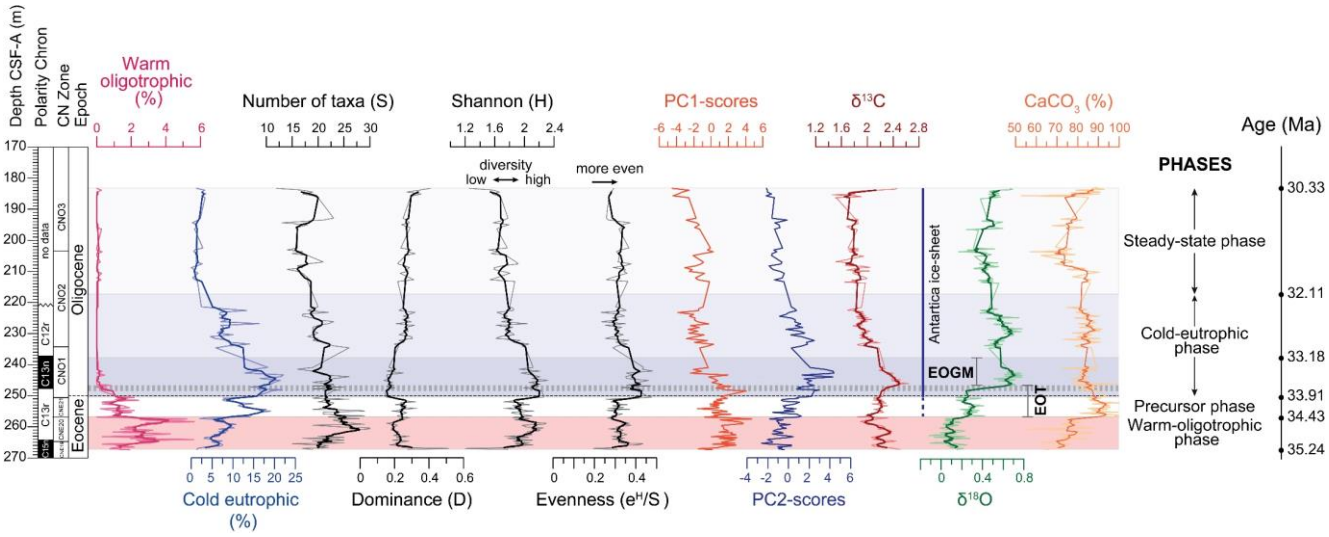

Figure 4.7 Warm oligotrophic taxa (%) and cold eutrophic taxa (%) plotted against magnetostratigraphy and calcareous nannofossil biozonation – CN zones (Agnini et al. 2014). PC1 and PC2 scores here refers to CN genera data (%). Quantitative diversity indices (number of taxa, dominance, Shannon index and evenness). All plots are shown with a 5-point running average, except for PC1 and PC2 scores. The main paleoenvironmental phases are also reported.

The Warm-Oligotrophic phase (35.24 to 34.43 Ma)

This phase is constrained to the lower part of the section and is dominated by warm and oligotrophic taxa and by a highly even and diverse assemblages. Positive peaks in warm water taxa suggest sustained late Eocene warm oligotrophic conditions. Species richness recorded at Site U1509 is relatively high during this phase reaching 30 taxa but dramatically collapses upward. The high values observed in the Shannon index values during this phase indicate a high diverse community structure. At the same time PC2 displays relatively low values, ranging from a minimum of -2.61 to a maximum of 0.46, likely reflecting a stable-warm and oligotrophic environment (Bown et al., 2004). The presence of a highly diversified community, mainly characterized by warm-oligotrophic taxa, is consistent with relatively low $\delta^{18}O$ values documented in the interval. The end of this phase is marked by the onset of the Late Eocene Event (LEE), which is coincident with the extinction of the warm-water *D. saipanensis* (34.43 Ma) and denotes the base of the EOT. The extinction of the last representative of the rosette-shaped discoasters can be read as the first clear symptom of biotic sufferance due to cooling inferred to have occurred during t the LEE (Dunkley Jones et al., 2008; Pearson et al., 2008; Hutchinson et al., 2021) (Figure 4.6).

The Precursor Phase (34.43 to 33.91 Ma)

In this interval, warm oligotrophic taxa dramatically decrease, suggesting either an extreme sensitivity of calcareous nannoplankton even to minor perturbations in the thermo/nutricline or the passage of a climate threshold that is able to trigger dramatic upheavals in the nannoplankton community. The marked decline of

warm-oligotrophic taxa observed during this phase is likely related to a global transition toward cooler and higher nutrient conditions. During the pre-EOGM phase, nannoplankton rapidly react to the modified climate conditions displaying a contraction of the k-selected community and the expansion of few r-mode opportunist taxa, better adapted to cooler and eutrophic conditions. Throughout this phase, major changes in calcareous nannofossil assemblages are also recorded by diversity indices, especially emphasized by the dramatic decrease in species richness (number of taxa) and Shannon indices. The shift from the Eocene warm-oligotrophic community to the Oligocene cold-eutrophic community occurred in a time window of ~520 kyr, suggesting a strong and prompt response of the nannoplankton assemblage to oceanographic changes.

The Cold-Eutrophic Phase (33.91 to 32.11 Ma)

In the lower part of this interval, PC1 significantly decreases as the warm-oligotrophs taxa do and PC2 progressively increases. This phase indicates a period of intense perturbation within the marine ecosystem. At Site U1509, the acme intervals of *Clausicoccus subdisthicus* gr. and *Lanternithus* spp. represent a distinctive feature of the Eocene-Oligocene transition (EOT) that is inferred to be related to a better adaptation of these taxa to the enhanced eutrophication hypothesized for the EOGM. These acme intervals are temporary events lasting for~1.58 and 1.03 Myr, respectively and the specific ecological affinities of *Clausicoccus subdisthicus* gr. and *Lanternithus* spp. allow these taxa to immediately adapt to the new environmental conditions and, successively, to become a fundamental component of the earliest Oligocene assemblages. During this phase, Shannon index values gradually return to pre-transitional values, reaching new relatively stable values. The cold-eutrophic phase initiated in the uppermost part of Chron C13r (~33.91 Ma) and is interpreted to reflect deep changes in ocean circulation which gave rise to in an intensified nutrient availability in surface waters, providing a certain competitive advantage for cold eutrophic taxa. Positive peaks in cold eutrophic taxa, such as *Chiasmolithus* spp. and *R. daviesii*, are recorded within Chron C13n, which corresponds to extreme glacial conditions (EOGM), suggesting a strong connection between climate and nannoplankton changes.

The Steady-State Phase (32.11 to 30.33 Ma)

The Steady-State phase is characterized by the persistent dominance of few taxa which are thought to belong to the survivors-opportunists group, such as *Reticulofenestra* and *Cyclicargolithus*. Decreasing Shannon index values confirm discrete changes in the assemblage structure, as reported also by the gradual decrease in the number of taxa. The virtually constant diversity values (H) documented during this phase possibly reflect a more stable ocean configuration, suggesting a gradual return to mesotrophic or more oligotrophic conditions.

4.4.2 Major changes in calcareous nannofossil placoliths

The E-O transition represents a tipping point in the Cenozoic climate evolution, documenting the transition from warm oligotrophic to cold eutrophic communities, dominated by few taxa. Data collected at IODP Site 1509 allow us to analyze the tempo and mode of this transition, as well as the biodiversity community structure, as we have discussed above. However, the role of an important component of calcareous nannofossils remains to be clarified. The potential paleoenvironmental information contained in this informal group was investigated by using an additional PCA, performed on placolith census data (%), that allow identification of a different distributions in the study samples that is related to the different relative abundance of placoliths. In particular, *C. pelagicus, Cribrocentrum* spp.*, D. hesslandii, D. filewiczii* and medium size (4-10 µm) reticulofenestrids, as well as the above-mentioned *E. formosa* are distributed in the right lower quadrant in the PCA plot suggesting an affinity for warm and oligotrophic conditions. Samples documenting the transitional (i.e. the *precursor phase*) and EOGM conditions are instead distributed in the right upper quadrants and are characterized by the higher abundances of the following placoliths: *D. bisectus* gr., large-sized reticulofenestrids (10-14 µm and >14 µm), *Clausicoccus, Chiasmolithus* and *R. daviesii*. Finally, the earliest Oligocene assemblages, distributed in the left upper quadrant is dominated by small reticulofenestrids (<4 µm) and small to medium size *Dictyococcites* spp., *C. floridanus* and reworked taxa. The latter assemblage supports the hypothesis that, once the steady-state is reached, the new environmental conditions, characterized by cold and nutrient enriched waters, have persisted stable and unvaried for at least 1.8 Myrs. A further support to an early Oligocene eutrophication at Site U1509 is provided by the presence of small opportunists reticulofenestrids (<4 µm), as similarly observed at ODP Site 756 (Chapter 2).

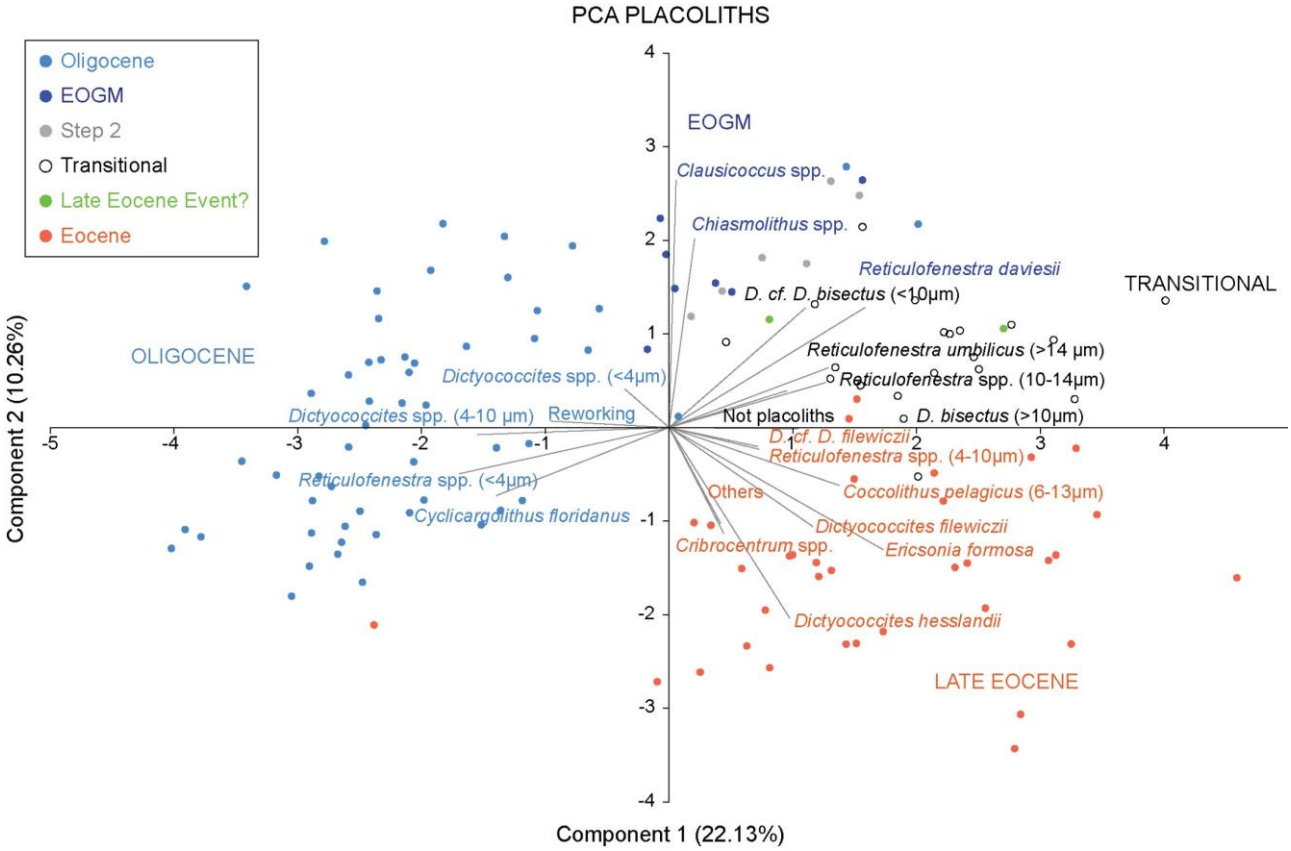

Figure 4.8 Principal component analysis (PCA) plot of placoliths (%) from IODP Site 1509 in terms of the first and second component. Placoliths are subdivided into 18 taxa: *Cribrocentrum, Chiasmolithus, Clausicoccus, Coccolithus pelagicus* (6-13µm)*, Cyclicargolithus floridanus, Dictyococcites* (<4µm)*, Dictyococcites* (4-10µm), *D. bisectus* (>10µm), *D. cf. D. bisectus* (<10µm), *D. cf. D. filewiczii*, *D. filewiczii*, *Dictyococcites hesslandii*, *Ericsonia formosa*, *Reticulofenestra* (<4µm), *Reticulofenestra* (4-10µm), *Reticulofenestra* (10-14µm), *Reticulofenestra daviesii*, *Reticulofenestra umbilicus* (>14µm). Reworking, not placoliths and others are also included in the plot.

An interesting note that arises from this plot, is that the Late Eocene event is characterized by a transitional assemblage rather than a Late Eocene calcareous nannofossil community, further supporting the idea of a transient cooler or glacial event during the late Eocene.

4.5 Conclusions

Nannofossil assemblage data from Site U1509 reveal a major shift from a late Eocene k-selected community, characterized by warm and oligotrophic taxa to an early Oligocene opportunistic assemblage, better adapted to colder and more eutrophic conditions. We think that this profound change in the assemblage composition was the result of sea surface cooling caused by the Antarctica glaciation but also related to an enhanced nutrient availability. The paleoceanigraphic reorganization, likely including the initiation of the Antarctic Circumpolar current (ACC), that took place during this time, caused an intensified nutrient upwelling systems or nutrient delivery to the cooler and more active Oligocene oceans.

These factors together with changed ocean surface conditions were probably able to enhance productivity, as documented in several low, middle and high latitude sites (Salamy and Zachos, 1999; Dunkley Jones et al., 2008; Cramer et al., 2009; Coxall and Wilson, 2011; Houben et al., 2013; Tibbett et al. 2021).

The four paleoclimatic phases highlighted at Site U1509 confirm that the signature of the stable carbon and oxygen isotopes, corresponds to synchronous changes in the marine phytoplankton communities, that indicated a strong and direct interaction between the changes observed in the geosphere and the modifications recorded in the biosphere. A major turnover in the calcareous nannofossil assemblage took place during the *precursor phase*, a transitional time interval of ~ 500 kyrs, which almost corresponds to the EOT s.s.

In the Tasman Sea, the increase in marine productivity have reached maximum values in coincidence with the EOGM, as suggested by high abundance of cold eutrophic taxa and PC2 scores, implying the presence of a larger-scale effects on nannoplankton community associated with sea ice formation and ocean overturning. However, our assemblage data indicate that the amplified ocean fertilization, likely have persisted far beyond the EOGM, at least until 32 Ma, though with minor intensity.

The Oligocene steady-state phase is characterized by few dominant placoliths (*Cyclicargolithus, Reticulofenestra and Dictyoccocites*) and small to medium reticulofenestrids this assemblage, depict a scenario of cold temperature and eutrophic conditions.

Acknowledgments

The authors are grateful to the Integrated Ocean Drilling Program (IODP) for providing samples and data used in this study. The IODP is sponsored by the U.S. National Science Foundation (NSF) and participating countries under the management of Joint Oceanographic Institutions, Inc.

Isabella Raffi and Davide Persico are deeply thanked for their constructive comments in the capacity of reviewers of A.V.' s PhD thesis during the evaluation process required by Italian law.

A. V. and C. A. were supported by University of Padova.

Dataset and supplementary information used in this work are provided in the **Appendix V**.

PLATES

PLATE 4.1 LM (magnification 1250x) microphotographs of selected calcareous nannofossil taxa from Site U1509. **S**cale bar = 5 µm. Photos **15, 17, 19, 21, 23, 25, 27, 29** are in parallel light; photos **1-14** and **16, 18, 20, 22, 24, 26, 28, 30** are in crossed nicols.
1-4. *Zygrhablithus bijugathus*. Sample 242.71 CSF-A (m). **5.** *Z. bijugathus* (base). Sample 242.10 CSF-A (m). **6.** *Z. bijugathus* (base). Sample 241.51 CSF-A (m). **7.** *Z. bijugathus* (base). Sample 232.21 CSF-A (m). **8.** *Umbilicosphaera bramlettei.* Sample 263.71 CSF-A (m). **9**. *U. bramlettei***.** Sample 261.91 CSF-A (m). **10.** *Bramletteius serraculoides.* Sample 264.91 CSF-A (m). **11.** *Bramletteius serraculoides* (base). Sample 256.21 CSF-A (m). **12.** *Blackites* cf. *singulus*. Sample 212.71 CSF-A (m). **13.** *B.* cf. *singulus*. Sample 261.91 CSF-A (m). **14, 15.** *Chiasmolithus altus*. Sample 184.51 CSF-A (m). **16, 17.** *Chiasmolithus altus.* Sample 230.41 CSF-A (m). **18, 19.** *Chiasmolithus altus.* Sample 231.60 CSF-A (m). **20, 21.** *Chiasmolithus altus.* Sample 232.21 CSF-A (m). **22, 23.** *Chiasmolithus altus.* Sample 251.11 CSF-A (m). **24, 25.** *Chiasmolithus* cf. *eoaltus*. Sample 223.21 CSF-A (m). **26, 27.** *C. eoaltus.* Sample 223.21 CSF-A (m). **28, 29.** *C. oamaruensis*. Sample 203.69 CSF-A (m). **30.** *C. floridanus.* Sample 231.61 CSF-A (m).

PLATE 4.2 LM (magnification 1250x) microphotographs of selected calcareous nannofossil taxa from Site U1509. **S**cale bar = 5 µm. Photos **2, 4, 6, 8, 10, 15, 17, 24** and **26-30** are in parallel light; photos **1, 3, 5, 7, 9, 10, 25** and **18-23** are in crossed nicols.
1, 2. *Chiasmolithus oamaruensis*. Sample 203.69 CSF-A (m). **3, 4.** *C. oamaruensis*. Sample 193.51 CSF-A (m). **5, 6.** *C. oamaruensis*. Sample 257.41 CSF-A (m). **7, 8.** *C. oamaruensis*. Sample 260.11 CSF-A (m). **9, 10.** *C. oamaruensis*. Sample 262.51 CSF-A (m). **11.** *Cribrocentrum reticulatum*. Sample 263.71 CSF-A (m). **12.** *C. reticulatum*. Sample 261.30 CSF-A (m). **13.** *Clausicoccus subdistichus.*Sample 222.01 CSF-A (m). **14, 15.** *C. subdistichus.* Sample 231.61 CSF-A (m). **16, 17.** *C. subdistichus.* Sample 246.61 CSF-A (m). **18.** *C. subdistichus.* Sample 248.41 CSF-A (m). **19.** *C. subdistichus.* Sample 251.11 CSF-A (m). **20**. *Coronocyclus nitescens***.** Sample 193.51 CSF-A (m). **21.** *Dictyococcites* cf. *bisectus* (<10µm). Sample 232.21 CSF-A (m). **22.** *Dictyococcites* cf. *bisectus* (<10µm). Sample 261.91 CSF-A (m). **23, 24.** *Dictyococcites bisectus.* Sample 251.41 CSF-A (m). **25.** *Dictyococcites hesslandii*. Sample 261.61 CSF-A (m). **26, 27.** *Discoaster barbadiensis.* Sample 242.71 CSF-A (m). **28, 29.** *D. barbadiensis.* Sample 263.71 CSF-A (m). **30.** *D. barbadiensis.* Sample 266.11 CSF-A (m).

PLATE 4.3 LM (magnification 1250x) microphotographs of selected calcareous nannofossil taxa from Site U1509. **S**cale bar = 5 µm. Photos **1, 12, 14, 16, 18, 20, 22, 29** and **3-8** are in parallel light; photos **2, 13, 15, 17, 19, 21, 30, 9-11** and **23-28** are in crossed nicols.
1. *Discoaster deflandrei* Sample 223.21 CSF-A (m). **2.** *Dictyococcites hesslandii*. Sample 263.71 CSF-A (m). **3.** *Discoaster saipanensis.* Sample 261.61 CSF-A (m). **4.** *D. saipanensis.* Sample 261.91 CSF-A (m). **5.** *D. saipanensis.* Sample 263.71 CSF-A (m). **6.** *D. saipanensis.* Sample 257.41 CSF-A (m)**. 7.** *D. saipanensis.* Sample 264.91 CSF-A (m). **8** *Discoaster* spp. Sample 242.10 CSF-A (m). **9.** *Ericsonia formosa*. Sample 261.91 CSF-A (m). **10.** *Dictyococcites* spp. Sample 261.91 CSF-A (m). **11, 12.** *Helicosphaera* cf. *truempyi* Sample 230.41 CSF-A (m). **13, 14.** *H.* cf. *wilcoxonii.* Sample 230.41 CSF-A (m). **15, 16.** *H. compacta.* Sample 232.21 CSF-A (m). **17, 18.** *H. compacta.* Sample 263.71 CSF-A (m). **19, 20.** *H. recta.* Sample 183.31 CSF-A (m). **21, 22.** *Isthmolithus recurvus.* Sample 258.61 CSF-A (m). **23.** *I. recurvus.* Sample 242.10 CSF-A (m). **24.** *I. recurvus.* Sample 263.71 CSF-A (m). **25.** *Lanternithus minutus.* Sample 242.10 CSF-A (m). **26.** *L. minutus.* Sample 242.71 CSF-A (m). **27.** *L. minutus.* Sample 251.11 CSF-A (m). **28, 29.** *Markalius inversus.* Sample 246.61 CSF-A (m). **30.** *M. inversus.* Sample 263.71 CSF-A (m).

PLATE 4.4 LM (magnification 1250x) microphotographs of selected calcareous nannofossils, biosilica and planktonic foraminifera from Site U1509. **S**cale bar = 5 µm. Photos **29, 30** are in parallel light; photos **1-28** are in crossed nicols.
1. *Reticulofenestra daviesii.* Sample 261.91 CSF-A (m). **2.** *Reticulofenestra umbilicus*. Sample 246.61 CSF-A (m). **3.** *R. umbilicus*. Sample 261.91 CSF-A (m). **4.** *Reticulofenestra dictyoda.* Sample 261.91 CSF-A (m). **5.** *Sphenolithus moriformis.* Sample 261.91 CSF-A (m). **6, 7.** *Sphenolithus akropodus* A. Sample 231.61 CSF-A (m). **8, 9.** *Sphenolithus akropodus* A. Sample 193.51 CSF-A (m). **10, 11.** *Sphenolithus akropodus* B. Sample 224.41 CSF-A (m). **12, 13.** *Sphenolithus akropodus* B. Sample 231.61 CSF-A (m). **14, 15.** *Sphenolithus akropodus* B. Sample 193.51 CSF-A (m). **16, 17.** *Sphenolithus* cf. *spiniger*. Sample 263.71 CSF-A (m). **18, 19.** *Sphenolithus intercalaris.* Sample 263.71 CSF-A (m). **20, 21.** *Sphenolithus intercalaris.* Sample 262.51 CSF-A (m). **22-25.** *Sphenolithus predistentus.* Sample 193.51 CSF-A (m). **26-27.** *Sphenolithus predistentus.* Sample 248.41 CSF-A (m). **28.** *Thoracosphaera* spp. Sample 261.91 CSF-A (m). **29.** Biosilica. Sample 222.01 CSF-A (m). **30.** Planktonic foraminifer. Sample 222.01 CSF-A (m).

PLATE 4.1

Scale bar = 5µm

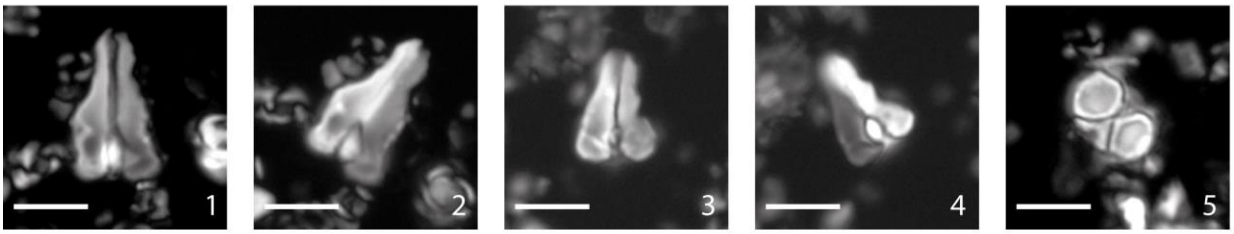

Z. bijugatus U1509A-28R-2W, 70-71 | *Z. bijugatus* U1509A-28R-2W, 70-71 | *Z. bijugatus* U1509A-28R-2W, 70-71 | *Z. bijugatus* U1509A-28R-2W, 70-71 | *Z. bijugatus* U1509A-28R-2W, 9-10

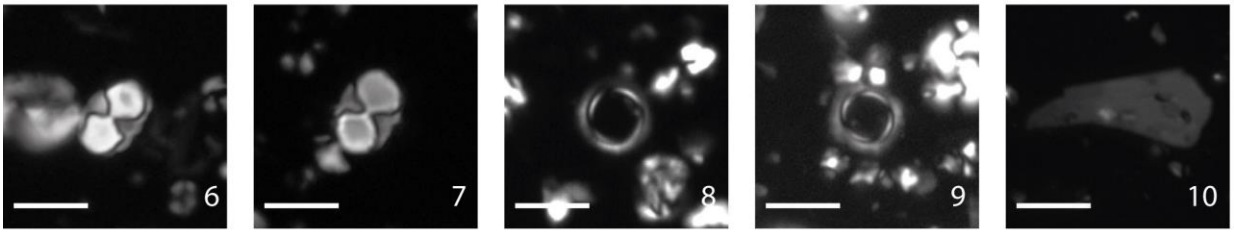

Z. bijugatus U1509A-28R-1W, 100-101 | *Z. bijugatus* U1509A-27R-1W, 130-131 | *U. bramlettei* U1509A-30R-3W, 125-126 | *U. bramlettei* U1509A-30R-2W, 70-71 | *B. serraculoides* U1509A-30R-4W, 95-96

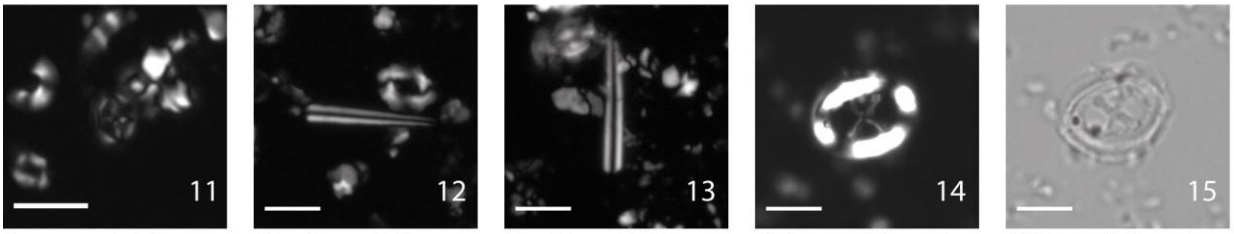

B. serraculoides U1509A-29R-5W, 6-7 | *Blackites* cf. *singulus* U1509A-25R-1W, 100-101 | *Blackites* cf. *singulus* U1509A-30R-2W, 70-71 | *Chiasmolithus altus* U1509A-21R-2W, 0-1 | *Chiasmolithus altus* U1509A-21R-2W, 0-1

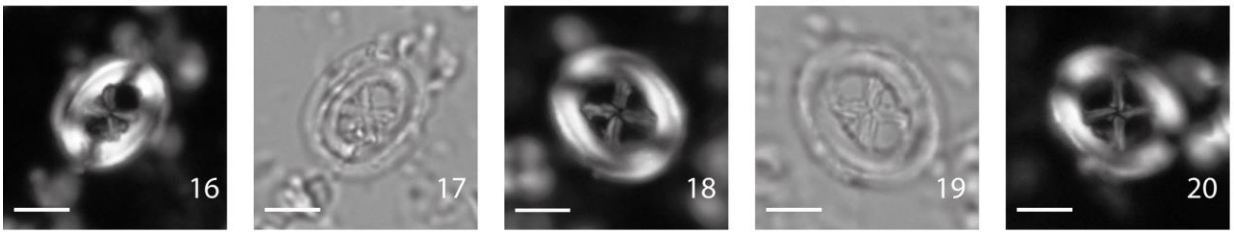

Chiasmolithus altus U1509A-26R-8W, 15-16 | *Chiasmolithus altus* U1509A-26R-8W, 15-16 | *Chiasmolithus altus* U1509A-27R-1W, 70-71 | *Chiasmolithus altus* U1509A-27R-1W, 70-71 | *Chiasmolithus altus* U1509A-27R-1W, 130-131

Chiasmolithus altus U1509A-27R-1W, 130-131 | *Chiasmolithus altus* U1509A-29R-1W, 100-101 | *Chiasmolithus altus* U1509A-29R-1W, 100-101 | *C.* cf. *eoaltus* U1509A-26R-3W, 2-3 | *C.* cf. *eoaltus* U1509A-26R-3W, 2-3

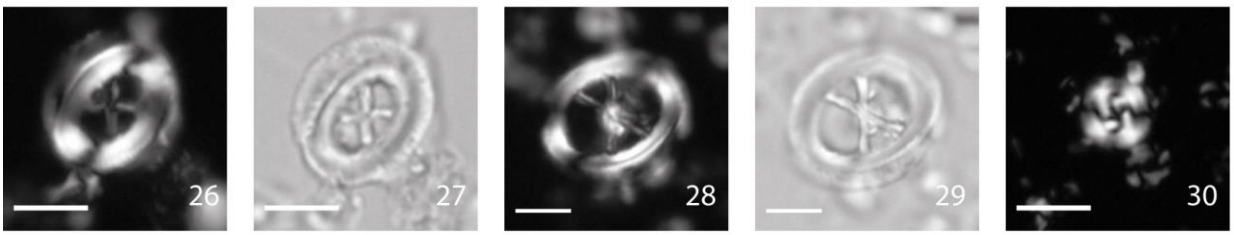

C. eoaltus U1509A-26R-3W, 2-3 | *C. eoaltus* U1509A-26R-3W, 2-3 | *C. oamaruensis* U1509A-23R-2W, 8-9 | *C. oamaruensis* U1509A-23R-2W, 8-9 | *C. floridanus* U1509A-27R-1W, 70-71

PLATE 4.2

Scale bar = 5µm

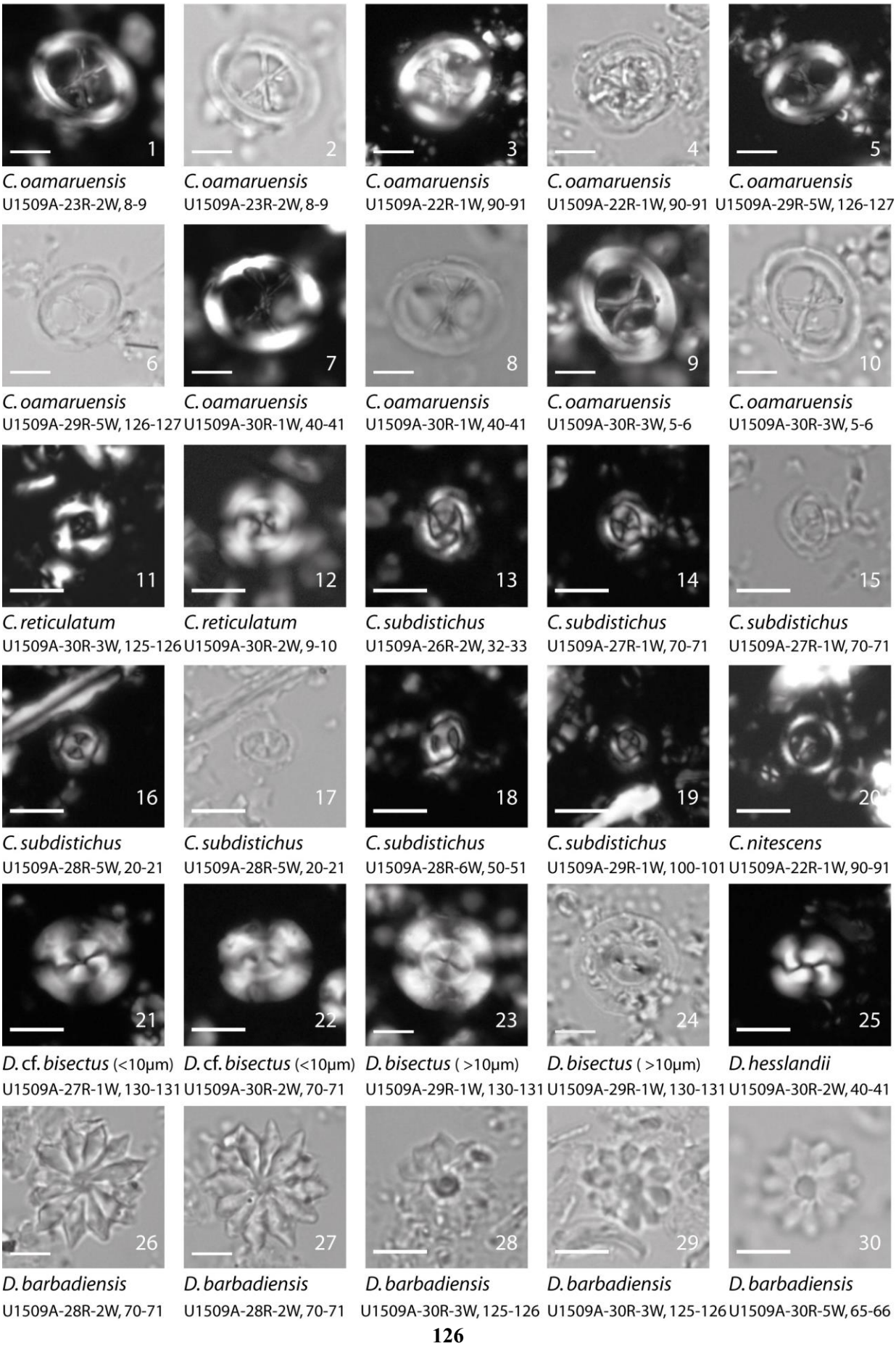

PLATE 4.3

Scale bar = 5µm

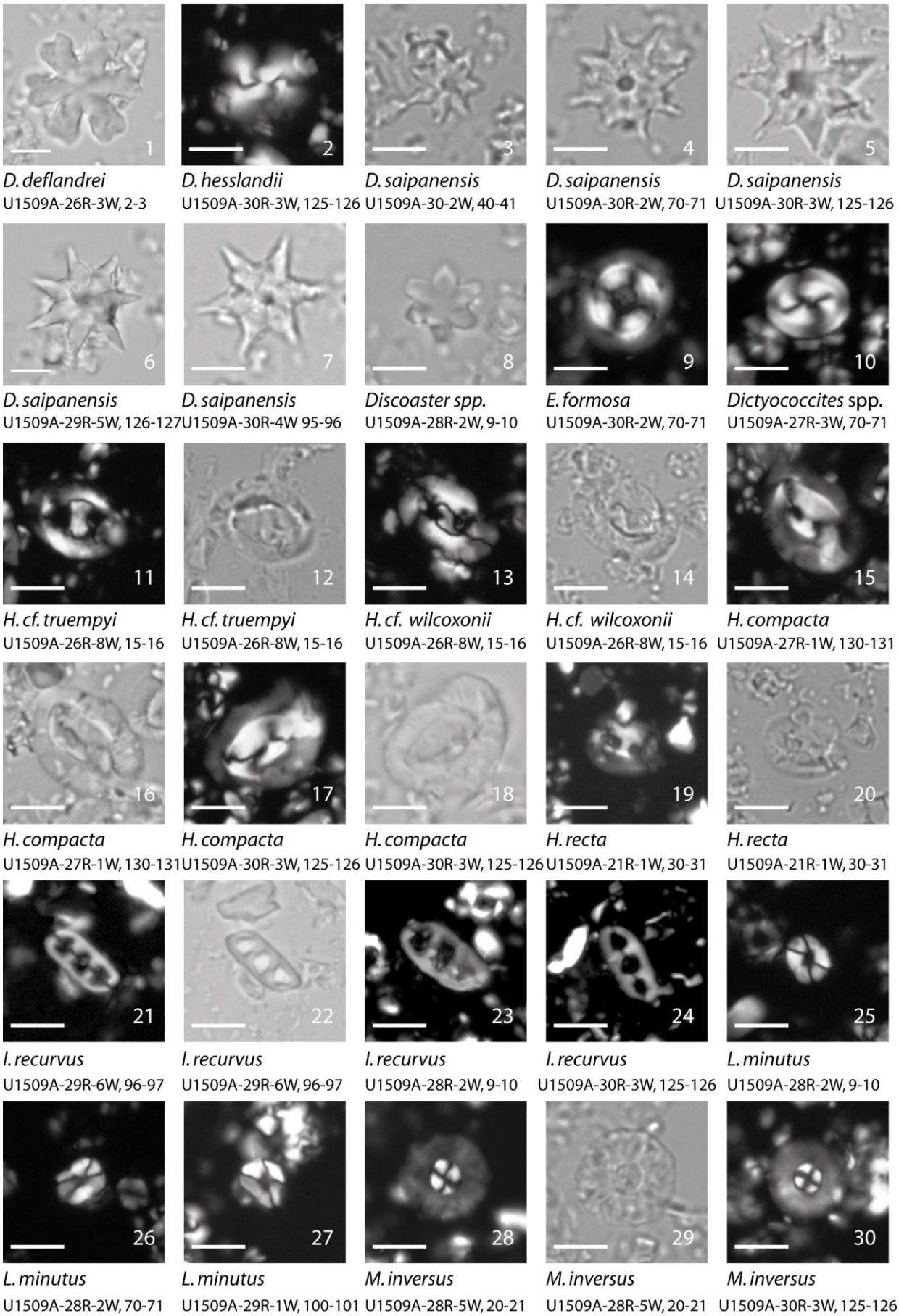

D. deflandrei U1509A-26R-3W, 2-3
D. hesslandii U1509A-30R-3W, 125-126
D. saipanensis U1509A-30-2W, 40-41
D. saipanensis U1509A-30R-2W, 70-71
D. saipanensis U1509A-30R-3W, 125-126
D. saipanensis U1509A-29R-5W, 126-127
D. saipanensis U1509A-30R-4W 95-96
Discoaster spp. U1509A-28R-2W, 9-10
E. formosa U1509A-30R-2W, 70-71
Dictyococcites spp. U1509A-27R-3W, 70-71
H. cf. truempyi U1509A-26R-8W, 15-16
H. cf. truempyi U1509A-26R-8W, 15-16
H. cf. wilcoxonii U1509A-26R-8W, 15-16
H. cf. wilcoxonii U1509A-26R-8W, 15-16
H. compacta U1509A-27R-1W, 130-131
H. compacta U1509A-27R-1W, 130-131
H. compacta U1509A-30R-3W, 125-126
H. compacta U1509A-30R-3W, 125-126
H. recta U1509A-21R-1W, 30-31
H. recta U1509A-21R-1W, 30-31
I. recurvus U1509A-29R-6W, 96-97
I. recurvus U1509A-29R-6W, 96-97
I. recurvus U1509A-28R-2W, 9-10
I. recurvus U1509A-30R-3W, 125-126
L. minutus U1509A-28R-2W, 9-10
L. minutus U1509A-28R-2W, 70-71
L. minutus U1509A-29R-1W, 100-101
M. inversus U1509A-28R-5W, 20-21
M. inversus U1509A-28R-5W, 20-21
M. inversus U1509A-30R-3W, 125-126

PLATE 4.4

Scale bar = 5µm

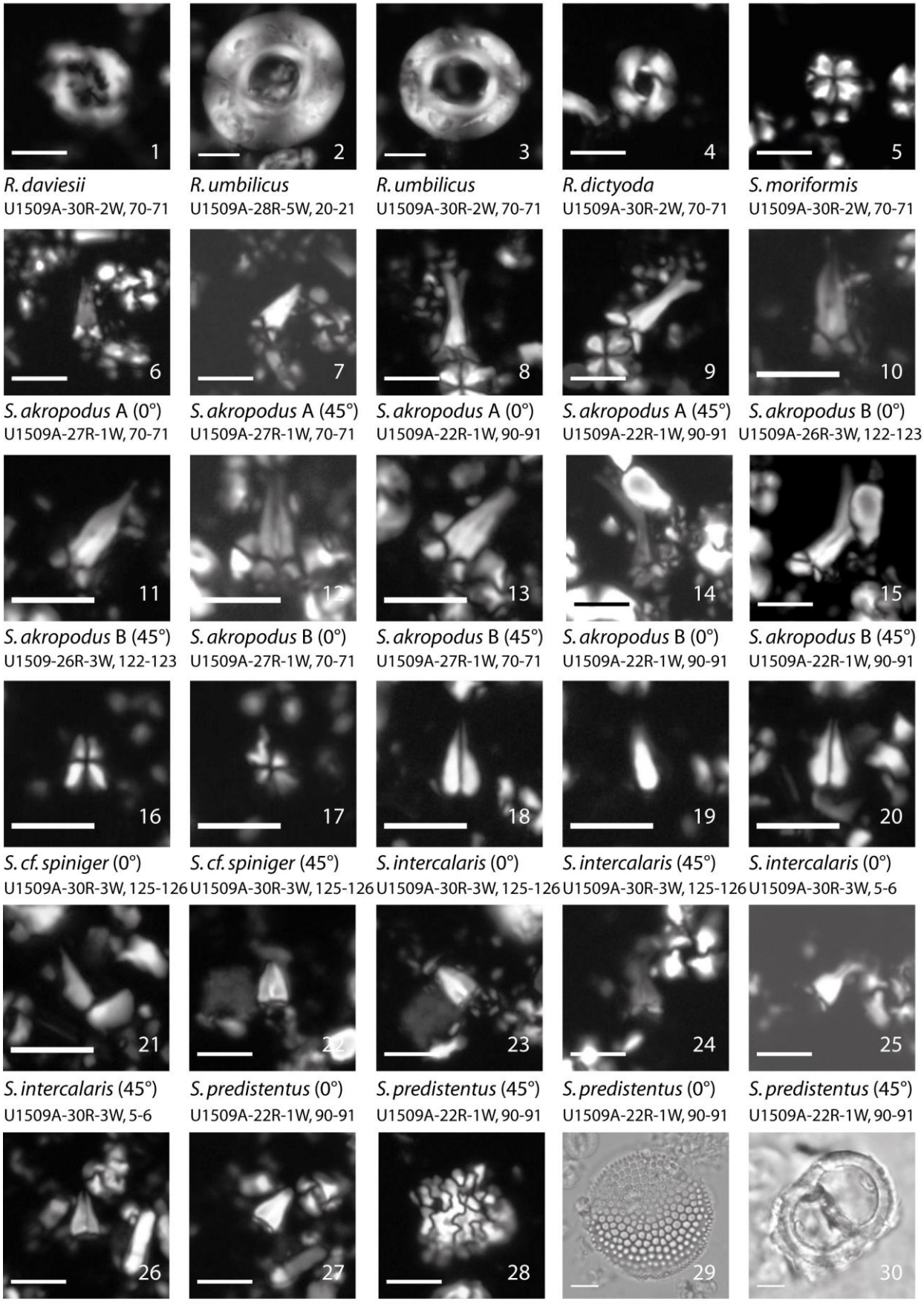

References

Agnini, C., Fornaciari, E., Raffi, I., Catanzariti, R., Pälike, H., Backman, J., Rio, D., 2014. Biozonation and biochronology of Paleogene calcareous nannofossils from low and middle latitudes. Newsletters on Stratigraphy 47, 131–181.

Anagnostou, E., John, E.H., Edgar, K.M., Foster, G.L., Ridgwell, A., Inglis, G.N., Pancost, R.D., Lunt, D.J., Pearson, P.N., 2016. Changing atmospheric CO_2 concentration was the primary driver of early Cenozoic climate. Nature 533, 380–384.

Aubry, M.-P., 1992. Late Paleogene Calcareous Nannoplankton Evolution: A Tale of Climatic Deterioration. In: Eocene-Oligocene Climatic and Biotic Evolution. p. 272–279.

Aubry, M.-P., 1984. Handbook of Cenozoic calcareous nannoplankton, book 1, Ortholithae (Discoaster). American Museum of Natural History Micropaleontology Press, New York.

Aubry, M.-P., 1988. Handbook of Cenozoic calcareous nannoplankton, book 2, Ortholithae (Holococcoliths, Ceratoliths and others). American Museum of Natural History Micropaleontology Press, New York.

Aubry, M.-P., 1989. Handbook of Cenozoic Calcareous Nannoplankton, book 3, Ortholithae (Pentaliths, and Others) Heliolithae (Fasciculiths, Sphenoliths and Others). American Museum of Natural History Micropaleontology Press., New York.

Aubry, M.-P., 1998. Early Paleogene Calcareous nannoplankton evolution: a tale of climatic amelioration. In: Aubry, M.-P., et al. (Eds.), Late Paleocene–Early Eocene Biotic and Climatic Events in the Marine and Terrestrial Records. Columbia University Press, New York, p. 158–201.

Bordiga, M., Henderiks, J., Tori, F., Monechi, S., Fenero, R., Legarda-Lisarri, A., Thomas, E., 2015. Microfossil evidence for trophic changes during the Eocene-Oligocene transition in the South Atlantic (ODP Site 1263, Walvis Ridge). Climate of the Past 11, 1249–1270.

Bordiga, M., Sulas, C., Henderiks, J., 2017. Reticulofenestra daviesii: biostratigraphy and paleogeographic distribution across the Eocene–Oligocene boundary. Geobios 50, 349–358.

Bostock, H.C., Sutton, P.J., Williams, M.J.M., Opdyke, B.N., 2013. Reviewing the circulation and mixing of Antarctic Intermediate Water in the South Pacific using evidence from geochemical tracers and Argo float trajectories. Deep-Sea Research Part I: Oceanographic Research Papers 73, 84–98.

Bown, P.R., 2005. Paleogene calcareous nannofossils from the Kilwa and Lindi areas of coastal Tanzania (Tanzania Drilling Project 2003-4). Journal of Nannoplankton Research 27, 21–95.

Bown, P.R., 1998. Calcareous nannofossil biostratigraphy. Chapman and Hall (Kluwer Academic Publishers), London, UK.

Bown, P.R., Dunkley Jones, T., 2012. Calcareous nannofossils from the Paleogene equatorial Pacific (IODP Expedition 320 Sites U1331-1334). Journal of Nannoplankton Research 32, 3–51.

Bown, P.R., Lees, J.A., Young, J.R., 2004. Calcareous nannoplankton evolution and diversity through time, Coccolithophores - From Molecular Process to Global Impact. Springer, London.

Bown, Paul R., Young, J.R., 1998. Techniques. In: Bown, P.R. (Ed.), Calcareous Nannofossil Biostratigraphy. Kluwer Academic Publishers, London, p. 16–28.

Bralower, T.J., 2002. Evidence of surface water oligotrophy during the Paleocene-Eocene Thermal Maximum:

nannofossil assemblage data from Ocean Drilling Program Site 690, Maud Rise, Weddell Sea. Paleoceanography 17, 1023.

Bukry, D., 1973. Low-latitude coccolith biostratigraphic zonation. Initial Reports of the Deep Sea Drilling Project, 15 685–703.

Buzas, M.A., Gibson, T.G., 1969. Species diversity: benthonic foraminifera in Western North Atlantic. Science 163, 72–75.

Chiswell, S.M., Bostock, H.C., Sutton, P.J.H., Williams, M.J., 2015. Physical oceanography of the deep seas around New Zealand: A review. New Zealand Journal of Marine and Freshwater Research 49, 286–317.

Chiswell, S.M., Toole, J., Church, J., 1997. Transports across the Tasman Sea from WOCE repeat sections: The East Australian Current 1990–94. New Zealand Journal of Marine and Freshwater Research 31, 469–475.

Coxall, H.K., Pearson, P.N., 2007. The Eocene-Oligocene Transition. In: Williams, M., Haywood, A.M., Gregory, J., Schmidt, D.N. (Eds.), Deep-Time Perspectives on Climate Change: Marrying the Signal from Computer Models and Biological Proxies, Micropaleontology Society Special Publication. Geological Society, London, p. 351–387.

Coxall, H.K., Wilson, P.A., 2011. Early Oligocene glaciation and productivity in the eastern equatorial Pacific: Insights into global carbon cycling. Paleoceanography 26, 1–18.

Coxall, H.K., Wilson, P.A., Pälike, H., Lear, C.H., Backman, J., 2005. Rapid stepwise onset of Antarctic glaciation and deeper calcite compensation in the Pacific Ocean. Nature 433, 53–7.

Cramer, B.S., Toggweiler, J.R., Wright, J.D., Katz, M.E., Miller, K.G., 2009. Ocean overturning since the Late Cretaceous: Inferences from a new benthic foraminiferal isotope compilation. Paleoceanography 24, PA4216.

DeConto, R.M., Pollard, D., 2003. Rapid Cenozoic glaciation of Antarctica induced by declining atmospheric CO_2. Nature 1317, 1313–1317.

Dunkley Jones, T., Bown, P.R., Pearson, P.N., Wade, B.S., Coxall, H.K., Lear, C.H., 2008. Major shifts in calcareous phytoplankton assemblages through the Eocene-Oligocene transition of Tanzania and their implications for low-latitude primary production. Paleoceanography 23, 1–14.

Fioroni, C., Villa, G., Persico, D., Jovane, L., 2015. Middle Eocene-Lower Oligocene calcareous nannofossil biostratigraphy and paleoceanographic implications from Site 711 (equatorial Indian Ocean). Marine Micropaleontology 118, 50–62.

Goldner, A., Herold, N., Huber, M., 2014. Antarctic glaciation caused ocean circulation changes at the Eocene-Oligocene transition. Nature 511, 574–577.

Haiblen, A.M., Opdyke, B.N., Roberts, A.P., Heslop, D., Wilson, P.A., 2019. Midlatitude Southern Hemisphere Temperature Change at the End of the Eocene Greenhouse Shortly Before Dawn of the Oligocene Icehouse. Paleoceanography and Paleoclimatology 34, 1995–2004.

Hallock, P., 1987. Fluctuations in the trophic resource continuum: A factor in global diversity cycles? Paleoceanography 2, 457–471.

Hammer, Ø., Harper, D.T., Ryan, D.D., 2001. Past: Paleontological Statistics Software Package for Education

and Data Analysis. Palaeontologia Electronica 4, 5–7.

Haq, B.U., 1973. Transgressions, climatic change and the diversity of calcareous nannoplankton. Marine Geology.

Houben, A.J.P., Bijl, P.K., Pross, J., Bohaty, S.M., Passchier, S., Stickley, C.E., Röhl, U., Sugisaki, S., Tauxe, L., Flierdt, T. van de, Olney, M., Sangiorgi, F., Sluijs, A., Escutia, C., Brinkhuis, H., Scientists, and the E. 318, 2013. Reorganization of Southern Ocean Plankton Ecosystem at the onset of Antarctic Glaciation. Science 340, 341–344.

Huber, M., Brinkhuis, H., Stickley, C.E., Döös, K., Sluijs, A., Warnaar, J., Schellenberg, S.A., Williams, G.L., 2004. Eocene circulation of the Southern Ocean: Was Antarctica kept warm by subtropical waters? Paleoceanography 19, 1–12.

Hutchinson, D.K., Coxall, H.K., Lunt, D.J., Steinthorsdottir, M., de Boer, A.M., Baatsen, M., von der Heydt, A., Huber, M., Kennedy-Asser, A.T., Kunzmann, L., Ladant, J.B., Lear, C.H., Moraweck, K., Pearson, P.N., Piga, E., Pound, M.J., Salzmann, U., Scher, H.D., Sijp, W.P., Śliwińska, K.K., Wilson, P.A., Zhang, Z., 2021. The Eocene–Oligocene transition: a review of marine and terrestrial proxy data, models and model–data comparisons. Climate of the Past 17, 269–315.

Jones, A.P., Dunkley Jones, T., Coxall, H.K., Pearson, P.N., Nala, D., Hoggett, M., 2019. Low-Latitude Calcareous Nannofossil Response in the Indo-Pacific Warm Pool Across the Eocene-Oligocene Transition of Java, Indonesia. Paleoceanography and Paleoclimatology 34, 1833–1847.

Katz, M.E., Miller, K.G., Wright, J.D., Wade, B.S., Browning, J. V., Cramer, B.S., Rosenthal, Y., 2008. Stepwise transition from the Eocene greenhouse to the Oligocene icehouse. Nature Geoscience 1, 329–333.

Kennett, J.P., 1977. Cenozoic evolution of Antarctic glaciation, the circum-Antarctic Ocean, and their impact on global paleoceanography. Journal of Geophysical Research 82, 3843–3859.

Ladant, J.B., Donnadieu, Y., Lefebvre, V., Dumas, C., 2014. The respective role of atmospheric carbon dioxide and orbital parameters on ice sheet evolution at the Eocene-Oligocene transition. Paleoceanography 29, 810–823.

Lear, C.H., Bailey, T.R., Pearson, P.N., Coxall, H.K., Rosenthal, Y., 2008. Cooling and ice growth across the Eocene-Oligocene transition. Geology 36, 251–254.

Lear, C.H., Elderfield, H., Wilson, P.A., 2000. Cenozoic deep-sea temperatures and global ice volumes from Mg/Ca in benthic foraminiferal calcite. Science 287, 269–272.

Lefebvre, V., Donnadieu, Y., Sepulchre, P., Swingedouw, D., Zhang, Z.S., 2012. Deciphering the role of southern gateways and carbon dioxide on the onset of the Antarctic Circumpolar Current. Paleoceanography 27, 1–9.

Liu, Z., Tuo, S., Zhao, Q., Cheng, X., Huang, W., 2004. Deep-water earliest Oligocene glacial maximum (EOGM) in South Atlantic. Chinese Science Bulletin 49, 2190–2197.

Miller, K.G., Wright, J.D., Fairbanks, R.G., 1991. Unlocking the Ice House: Oligocene-Miocene oxygen isotopes, eustasy, and margin erosion. Journal of Geophysical Research: Solid Earth 96, 6829–6848.

Monechi, S., Buccianti, A., Gardin, S., 2000. Biotic signals from nannoflora across the iridium anomaly in the

upper Eocene of the Massignano section: evidence from statistical analysis. Marine Micropaleontology 39, 219–237.

Morkhoven, F., Berggren, W.A., Edwards, A.S., Oertli, H.J., 1986. Cenozoic cosmopolitan deep-water benthic foraminifera., Bulletin des centres de recherches Exploration-production Elf-Aquitaine: Mémoire 11.

Newsam, C., Bown, P.R., Wade, B.S., Jones, H.L., 2017. Muted calcareous nannoplankton response at the Middle/Late Eocene Turnover event in the western North Atlantic Ocean. Newsletters on Stratigraphy 50, 297–309.

Pagani, M., Huber, M., Liu, Z., Bohaty, S.M., Henderiks, J., Sijp, W., Krishnan, S., DeConto, R.M., 2011. The role of carbon dioxide during the onset of antarctic glaciation. Science 334, 1261–1264.

Pälike, H., Lyle, M.W., Nishi, H., Raffi, I., Ridgwell, A., Gamage, K., Klaus, A., Acton, G., Anderson, L., Backman, J., Baldauf, J., Beltran, C., Bohaty, S.M., Bown, P.R., Busch, W., Channell, J.E.T., Chun, C.O.J., Delaney, M.L., Dewangan, P., Dunkley Jones, T., Edgar, K.M., Evans, H., Fitch, P., Foster, G.L., Gussone, N., Hasegawa, H., Hathorne, E.C., Hayashi, H., Herrle, J.O., Holbourn, A.E., Hovan, S., Hyeong, K., Iijima, K., Ito, T., Kamikuri, S.I., Kimoto, K., Kuroda, J., Leon-Rodriguez, L., Malinverno, A., Moore, T.C., Murphy, B.H., Murphy, D.P., Nakamura, H., Ogane, K., Ohneiser, C., Richter, C., Robinson, R., Rohling, E.J., Romero, O., Sawada, K., Scher, H.D., Schneider, L., Sluijs, A., Takata, H., Tian, J., Tsujimoto, A., Wade, B.S., Westerhold, T., Wilkens, R., Williams, T., Wilson, P.A., Yamamoto, Y., Yamamoto, S., Yamazaki, T., Zeebe, R.E., 2012. A Cenozoic record of the equatorial Pacific carbonate compensation depth. Nature 488, 609–614.

Pearson, P.N., Foster, G.L., Wade, B.S., 2009. Atmospheric carbon dioxide through the Eocene-Oligocene climate transition. Nature 461, 1110–1113.

Pearson, P.N., McMillan, I.K., Wade, B.S., Dunkley Jones, T., Coxall, H.K., Bown, P.R., Lear, C.H., 2008. Extinction and environmental change across the Eocene-Oligocene boundary in Tanzania. Geology 36, 179–182.

Perch-Nielsen, Katharina, 1985. Cenozoic calcareous nannofossils. In: Bolli, H.M., Saunders, J.B., Perch-Nielsen, K. (Eds.), Plankton Stratigraphy. Cambridge University Press, Cambridge, p. 427–555.

Persico, D., Villa, G., 2004. Eocene-Oligocene calcareous nannofossils from Maud Rise and Kerguelen Plateau (Antarctica): Paleoecological and paleoceanographic implications. Marine Micropaleontology 52, 153–179.

Persico, D., Villa, G., 2008. A new Eocene Chiasmolithus species: hypothetical reconstruction of its phyletic lineage. Journal of Nannoplankton Research 30, 23–33.

Salamy, K.A., Zachos, J.C., 1999. Latest Eocene-Early Oligocene climate change and Southern Ocean fertility: Inferences from sediment accumulation and stable isotope data. Palaeogeography, Palaeoclimatology, Palaeoecology 145, 61–77.

Shannon, C.E., Weaver, W., 1949. The Mathematical Theory of Communication. University of Illinois Press, Champaign, IL.

Sijp, W.P., England, M.H., Huber, M., 2011. Effect of the deepening of the Tasman Gateway on the global ocean. Paleoceanography 26, 1–18.

Sijp, W.P., England, M.H., Sijp, W.P., England, M.H., 2004. Effect of the Drake Passage Throughflow on Global Climate. Journal of physical oceanography 34, 1254–1266.

Spofforth, D.J.A., Agnini, C., Pälike, H., Rio, D., Fornaciari, E., Giusberti, L., Luciani, V., Lanci, L., Muttoni, G., 2010. Organic carbon burial following the middle Eocene climatic optimum in the central western Tethys. Paleoceanography 25, PA3210.

Sutherland, R., Dickens, G.R., Blum, P., Agnini, C., Alegret, L., Bhattacharya, J., Bordenave, A., Chang, Li., Collot, J., Cramwinckel, M.J., Dallanave, E., Drake, M.K., Etienne, S.J.G., Giorgioni, M., Gurnis, M., Harper, D.T., Huang, H., Keller, A.L., Lam, A.R., Li, H., Matsui, H., Morgans, H.E.G., Newsam, C., Park, Y.H., Pascher, K.M., Pekar, S.F., Penman, D.E., Saito, S., Stratford, W.R., Westerhold, T., Zhou, X., 2019. Site U1509. Tasman Frontier Subduction Initiation and Paleogene Climate. Proceedings of the International Ocean Discovery Program, 371: College Station, TX (International Oce 371.

Sutherland, R., Dickens, G.R., Blum, P., and the Expedition 371 Scientists, 2018. Expedition 371 Preliminary Report: Tasman Frontier Subduction Initiation and Paleogene Climate. International Ocean Discovery Program.

Tibbett, E.J., Scher, H.D., Warny, S., Tierney, J.E., Passchier, S., Feakins, S.J., 2021. Late Eocene record of hydrology and temperature from Prydz Bay, East Antarctica. Paleoceanography and Paleoclimatology 1–21.

Tremolada, F., Bralower, T.J., 2004. Nannofossil assemblage fluctuations during the Paleocene-Eocene Thermal Maximum at Sites 213 (Indian Ocean) and 401 (North Atlantic Ocean): palaeoceanographic implications. Marine Micropaleontology 52, 107–116.

Villa, G., Fioroni, C., Pea, L., Bohaty, S.M., Persico, D., 2008. Middle Eocene-late Oligocene climate variability: Calcareous nannofossil response at Kerguelen Plateau, Site 748. Marine Micropaleontology 69, 173–192.

Villa, G., Fioroni, C., Persico, D., Roberts, A.P., Florindo, F., 2014. Middle Eocene to Late Oligocene Antarctic glaciation/deglaciation and Southern Ocean productivity. Paleoceanography 29, 223–237.

Villa, G., Florindo, F., Persico, D., Lurcock, P., de Martini, A.P., Jovane, L., Fioroni, C., 2021. Integrated calcareous nannofossil and magnetostratigraphic record of ODP Site 709: Middle Eocene to late Oligocene paleoclimate and paleoceanography of the Equatorial Indian Ocean. Marine Micropaleontology 169, 102051.

Wei, W., Wise, S.W., 1990. Biogeographic gradients of middle Eocene-Oligocene calcareous nannoplankton in the South Atlantic Ocean. Palaeogeography, Palaeoclimatology, Palaeoecology 79, 29–61.

Whittaker, R.H., 1972. Evolution and Measurement of Species Diversity. Taxon 21, 213–251.

Zachos, J.C., Kump, L.R., 2005. Carbon cycle feedbacks and the initiation of Antarctic glaciation in the earliest Oligocene. Global and Planetary Change 47, 51–66.

Zachos, J.C., Pagani, M., Sloan, L., Thomas, E., Billups, K., 2001. Trends, Global Rhythms, and Aberrations in Global Climate 65 Ma to Present. Science 292, 686–693.

Zachos, J.C., Quinn, T.M., Salamy, K.A., 1996. High-resolution (10^4 years) deep-sea foraminiferal stable isotope records of the Eocene-Oligocene climate transition. Paleoceanography 11, 251–266.

Chapter 5

Calcareous nannofossils across the Eocene-Oligocene transition: preservation signals and biostratigraphic remarks from ODP Site 1209 (NW Pacific, Shatsky Rise) and IODP Hole U1411B (NW Atlantic Ocean, Newfoundland Ridge)[1]

Abstract. Changes in the preservation state of calcareous nannofossils observed across the Eocene-Oligocene transition has been described at ODP Site 1209 (Shatsky Rise; North Pacific, Bralower et al., 2002a) and IODP Site U1411 (Newfoundland ridge, NW Atlantic; Norris et al., 2014a). Biostratigraphic refinements were performed at Hole U1411B and Site 1209 and provide the basis for the implementation of the age models available for the study sections, allowing a precise site-to-site correlation. The excellent preservation, recorded at Hole U1411B by an almost pristine calcareous nannofossil assemblage, is used here as a reference for comparison. In this work, we discuss the main post-depositional processes that impact the calcareous nannofossil ooze at Site 1209. Our detailed SEM study highlights some differences before, during and after the EOT, suggesting local diagenetic dynamics. The main aim was to understand the extent to which the bulk $\delta^{18}O$ and $\delta^{13}C$ records and their sources (mainly calcareous nannofossils) are altered by diagenesis. At Site 1209, a distinctive change, both in the assemblage composition and preservation state, is observed from the PRE-EOT phase to the Late Eocene Event (LEE), with a shift in the dominant process from dissolution to recrystallisation. Surprisingly, despite the overall poor preservation, only the interval between 141 to 142.4 (adj. rmcd) was severely compromised. This interval, recorded in the late Eocene, was characterized by severe dissolution, concomitant to deposition of secondary calcite on solution-resistant forms. Diagenetic processes have strongly biased the $\delta^{18}O$ isotopic signal, resulting in a positive oxygen isotope anomaly during the late Eocene that is difficult to reconcile with other curves available and still retaining the pristine signal. Instead, for the remaining time interval, diagenesis does not alter the bulk $\delta^{18}O$ profile, which closely resembles to that of other sites across the world, and is particularly consistent with other data from the Pacific (Site U1509). In summary, diagenesis even if clearly visible both at SEM and optical microscope is not always able to cause a pervasive alteration of the pristine isotopic signal and can instead provide important clues on local depositional dynamics.

Keywords: calcareous nannofossils; EOT; preservation; biostratigraphy; IODP Hole U1411B; ODP 1209

[1] Allyson Viganò[1], Thomas Westerhold[2], Paul R. Bown[3], Tom Dunkley Jones[4], Claudia Agnini[1]

[1]Dipartimento di Geoscienze, Università di Padova, Padova, Italy

[2]Center for Marine Environmental Sciences (Marum), University of Bremen, Bremen, Germany

[3] School of Geography, Earth and Environmental Sciences Birmingham, Birmingham, United Kingdom

[4] Department of Earth Sciences, University College London, London, United Kingdom

Authors contribution: A.V. and C.A. designed the study and developed the methodology. A.V. was responsible for the formal analysis and data collection. C.A. was the project administrator. T.W., P.R.B and T.D.J. provided data and samples used in this work. All the co-authors have contributed to the final polishing of the draft.

5.1 Introduction

The global cooling trend, starting at the end of the Early Eocene Climatic Optimum (EECO; ~50 Ma), reached a maximum during the Eocene-Oligocene transition (EOT) at ~34 Ma, with the onset of the Antarctica ice sheet (Zachos et al., 2001; 2008; Coxall and Pearson, 2007; Westerhold et al., 2020). The effects of the EOT on calcareous nannoplankton have been documented at different sites worldwide, providing important paleoenvironmental insight and biostratigraphic implications during this fundamental event (Persico and Villa, 2004; Dunkley Jones et al., 2008; Villa et al., 2008; 2014; 2021; Bordiga et al., 2015; Jones et al., 2019).

The hallmark of this event is globally recognizable by a two-stepped positive excursion in the oxygen ($\delta^{18}O$) and carbon ($\delta^{13}C$) values that are hereafter referred as to Step 1 and Step 2 (or EOIS) (Coxall and Pearson, 2007; Hutchinson et al., 2021). An even stronger geochemical signal is denoted by the EOGM (Early Oligocene Glacial Maximum) which encompassed the $\delta^{18}O$ maxima (Zachos et al., 1996; Liu et al., 2004) and corresponds to an extended glaciation during the earliest Oligocene (Hutchinson et al., 2021) concomitant to a >1 km drop in the calcite compensation depth (CCD) recorded in the Pacific Ocean (Coxall et al., 2005; Pälike et al., 2012). The EOGM coincides with a cold-eutrophic phase in marine environments that persisted for ca. 730 kyrs (Chapter 4). This interpretation is supported by changes observed in calcareous nannofossil assemblages, which consists of an increase in abundance of taxa better adapted to an intensified nutrient availability and cooler regime (e.g. Dunkley Jones et al., 2008; Fioroni et al., 2015; Jones et al., 2019; Villa et al., 2021; see Chapter 2).

The EOT strongly influences the calcifying sea surface plankton communities that dramatically change their thermal and trophic structure. Although calcareous nannofossil sensitivity to the Antarctic glaciation was recently well documented (above references), questions remain still open on the relationship between preservation of microfossils in the sediments and major climate state shifts.

In some cases, understanding of the interconnection between diagenetic and ecological signals is somewhat difficult. Particular in pelagic carbonate-rich sediments. The quality of biological and ecological information is strongly affected by preservation due to dissolution and/or overgrowth of calcareous nannofossil specimens. Dissolution preferentially obliterates the more delicate structures and is determined by the Carbonate Compensation Depth (CCD) as well as the lysocline (Honjo, 1976). Overgrowth generally affects the larger crystallites of coccoliths and nannoliths. This secondary calcite deposition is mainly controlled by the variation of pore fluids in the sediments. Therefore, the assemblage can be strongly biased by these two major chemical processes (Roth and Thierstein, 1972; Roth, 1978). Our study is designed as a survey of different preservation states among nannofossil communities in four well defined and documented phases across the E-O.

One important question to be address in this work is whether the bulk $\delta^{18}O$ and $\delta^{13}C$ records is biased by carbonate diagenesis with preferential recrystallization or dissolution of nannofossils at or beneath the seafloor.

To disclose the effective role of preservation and taxonomic composition, we decide to compare two sites (ODP Site 1209, Bralower et al., 2002b; IODP Site U1411, Norris et al., 2014b) with different preservation state and lithologies. Finally we comprehensively discuss the biostratigraphic data and their possible relation with the

assemblage components, changes in sea-water carbon geochemistry, carbonate content and porosity. To achieve these goals, we first provide an estimate of the abundances and preservation of nannofossils at Hole U1411B and ODP Site U1209 by means of LM and scanning electron micrograph analyses on the assemblage.

5.2 Materials and methods

5.2.1 Hole U1411B and Site 1209

The present study is based on the E-O cores recovered during Exp. 342 (Norris et al., 2012; 2014b) at Hole U1411B (SE Newfoundland Ridge; NW Atlantic Ocean) and during Leg. 198 (Bralower et al., 2002a) at Site 1209 (Shatsky Rise; NW Pacific) (Figure 5.1).

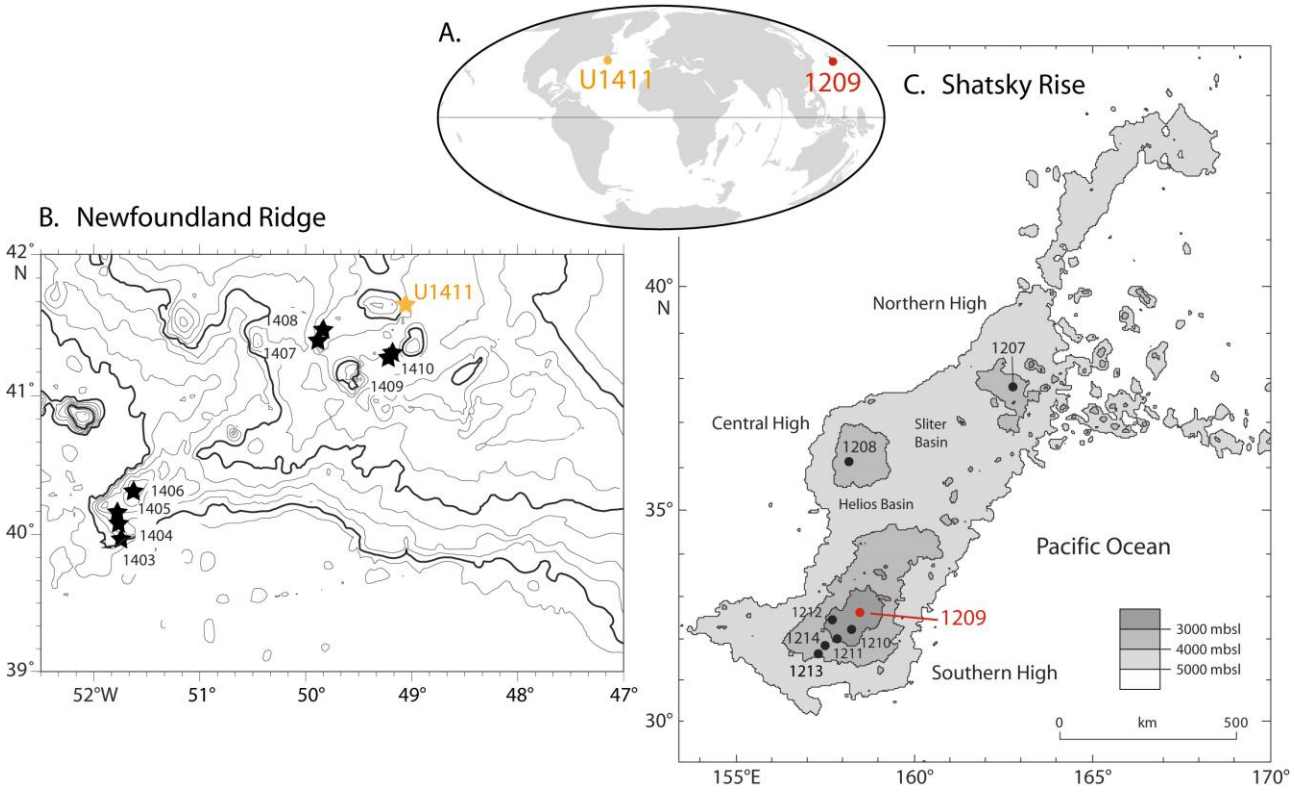

Figure 5.1 A) present-day locations of the study sites, Site U1411 (yellow circle) and Site 1209 (red circle), respectively on Newfoundland Ridge (NW Atlantic) and Shatsky Rise (NW Pacific). B, C) Maps showing the location of IODP/ODP sites drilled on Newfoundland Ridge (modified after Norris et al. 2014) and Shatsky Rise (bathymetric map modified after Bown et al. 2005).

During the drilling of the northwest Atlantic Site U1411 (~3300 m water depth) a 254.5 m-thick sedimentary succession of deep-sea sediment of Pleistocene to late Eocene age was retrieved. The sedimentary sequence at Site U1411 consists of three lithostratigraphic units: Unit I (14.45 m of Pleistocene sediments; composed of clayey foraminiferal ooze), Unit II (a 198.23 m-thick succession of early Miocene to late Eocene age; composed of silty clay, clay with nannofossils, silty nannofossil clay, and clayey nannofossil ooze with silt) and Unit III (41.92 m-

thick of upper Eocene sediments composed by clayey nannofossil chalk and clayey nannofossil chalk with foraminifers) (Norris et al., 2014b). Three holes (A, B, C) were drilled at this site, allowing to recover an expanded clay-rich (~25-50 %) supra-CCD drift sequence with exceptionally well preserved calcareous nannofossils and high accumulation rates (Norris et al., 2014b). In this work, we focus our sampling on sediments recovered from Hole U1411B. Upper Eocene sediments are included in the lithological Unit II and predominantly consists of clayey nannofossil ooze with increased carbonate content across the EOT. Here, we analyzed an expanded record of the Eocene-Oligocene transition from core 342-U1411B-22X to core 342-U1411B-11H, spanning from 187.35 to 96.25 mbsf.

ODP Site 1209, situated on the Southern High of Shatsky Rise in middle bathyal water depth, has been chosen for its geographical location. Three holes (Holes A, B, C) were drilled at this site, whose cores have been aligned and placed into a composite adj. rmcd depth scale (Westerhold and Röhl, 2006). Sediments from Site 1209 mainly consists of nannofossil ooze and nannofossil ooze with clay. The EOT record is characterized by a gradual color change from a light brown nannofossil ooze with clay to a light grey nannofossil ooze (Bralower et al., 2002b). This lithological change corresponds to an increase in carbonate content that occurs in the early Oligocene and well fits with the deepening of the CCD (Pälike et al., 2012).At present, Site 1209 is situated at 2387 m, well above both the lysocline and the CCD, which are at 3500 and 4100 m, respectively (Bralower et al., 2002b). During the E-O transition, the inferred paleodepth was relatively shallower, approximately ~2000 m (Bralower et al., 2002a). The studied section spans the late Eocene to early Oligocene and ranges from 144.95 to 125.80 adj. rmcd (samples U1209B-15H-3W, 95 cm to U1209A-13H-2W, 87 cm), across Zone CNE20 to CNO2 (Agnini et al., 2014).

5.2.2 Calcareous nannofossil assemblage counts

Micropaleontological analyses were performed on a total of 88 samples, recovered from Site 1209 (58 samples) and Hole U1411B (30 samples). Calcareous nannofossils were semi-quantitatively investigated in standard smear-slides (Bown & Young, 1998), using a transmitted light microscope (LM), under cross-polarized (XPL) and phase contrast light (PC) at 1250× magnification. The abundance of each taxon was determined by counting the number of the observed specimens in a predetermined area of 1 mm^2 (Backman & Shackleton, 1983) and then plotted versus depth. Biohorizon nomenclature follows that given by Agnini et al. (2014): base (B), base common (Bc), top (T) and top common (Tc).

Preservation of carbonates on the sea floor varied significantly because of two different processes, etching and calcite overgrowth. Preliminary observations to estimate the preservation state of the samples were performed using a transmitted light microscope. The abundance and etching level were used to estimate the general preservation state. Preservation was defined as follows (Norris et al., 2014b):

G = good (slight or no sign of dissolution and/or overgrowth; principal morphological characteristics unaltered; specimens identifiable to the species level).

M = moderate (some evidence of etching and/or overgrowth; primary morphostructures slightly altered; most specimens identifiable to the species level).

P = poor (severe etching and/or overgrowth; morphological characteristics largely destroyed; fragmentation; specimens could not be identified at the species and/or generic level).

VP = very poor (extreme etching and/or overgrowth; distinctive morphological features unrecognizable; fragmentation; presence of only few highly resistant species; difficulties in identifying specimens also at the genus level).

Calcareous nannofossil abundances were recorded based on qualitative observations on the relative abundance of identifiable specimens per field of view: **A** = abundant, **C** = common, **F** = Few and **R** = rare.

Accordingly to Roth (1983), we made an attempt to evaluate the degree of etching using the three following categories:

E1 slight etching; subtle central area structures are affected by dissolution but are generally still visible.

E2 moderate etching; dissolution of delicate central structures in many specimens; some isolate shields with irregular outlines are present.

E3 strong dissolution; only dissolution-resistant species are present; abundant coccoliths fragments.

5.2.3 Stable isotopes and carbonate content analysis

Geochemical analyses ($CaCO_3$ wt%, C and O stable isotopes) were carried out on a total of 206 bulk samples from ODP Site 1209. Samples were analyzed every 5 cm, ranging from 142.40 adj. rmcd (sample U1209C-4H-3W, 93 cm) to 130.85 adj. rmcd (1209C-3H-2W, 70 cm). All results are given in standard delta notation (‰) with Vienna Pee Dee Belemnite (VPDB) as the reference standard. Analyses were carried out at the Department of Geosciences (University of Padova) using a Delta V Advance Isotopic Ratio Mass Spectrometer equipped with a Gas Bench II device. A known mass (~250 µg) was placed into a headspace vial and flushed with helium. To each sample, 10 mL of 100% phosphoric acid was added and allowed to react. Two standards, Carrara marble Maq 1 ($\delta^{13}C$ = 2.58‰; $\delta^{18}O$=−1.15‰VPDB) and marble Gr1 ($\delta^{13}C$ = 0.68‰; $\delta^{18}O$= −10.44‰ VPDB) were used for instrument calibration and quality assurance and repeated with precisions better than 0.06‰ for $\delta^{13}C$ and better than 0.09‰ for $\delta^{18}O$ during sample runs. The amount of $CaCO_3$ was calculated from the beam height (Spofforth et al., 2010) of the CO_2 liberated during isotope mass spectrometer measurements.

5.2.4 Scanning electron microscopy (SEM)

SEM investigations allow an evaluation of the preservation quality of coccoliths, which includes the description of any evidence of diagenetic alteration (i.e., etching, overgrowth). Analyses on the preservation and composition of the assemblages were performed at the Department of Geosciences (University of Padova) using a Tescan Solaris Scanning Electron Microscope (SEM) on both processed and unprocessed samples. Processed samples were treated as follows: a small amount (~5 mg) of sediment was suspended in distilled water (1.5 ml) and

centrifuged using a Rotofix 32A for 2 min at 2000 rpm. The suspension was then place in a rotating plate (Heidolph Unimax 1010) for 10 hours (6 speed intensity) to disaggregate clay particles from calcareous nannofossils. The supernatant was poured off, and the residual was treated ultrasonically for 1 minute. This methodology was necessary to reduce the high amount of clay found in the samples recovered from Hole U1411B. Finally, a drop of the intermediate suspension was placed on a sticky carbon tab placed on a 12.5 mm stub and dried in the oven at 30/40°C for ~20 minutes. The stubs were then coated with carbon, deposited through a double-tilted vacuum evaporation procedure using the EMITECH K950X sputter coater. The graphite rod evaporation has the advantage to produce an all-round coating layer, with very fine grain size, ideal for high magnification applications. All images were taken under a high-vacuum mode (<0.04 Pa; HighVac) using the In-beam SE detector, considering two different scanning modes: the UH-resolution scan mode for ultrahigh-resolution imaging and the analysis scan mode for compositional assemblage analyses. This latter modality has the benefit to increase the field of view and thus the dynamic survey of the sample. The disadvantage is a lower resolution compared to the UH-resolution scan mode.

5.3 Results

5.3.1 Calcareous nannofossils

Biostragraphic studies carried out at Site 1209 and Hole U1411B are based on the recent biozonation scheme proposed by Agnini et al. (2014). Analyses performed at these sites reveal some distinct trends in the semi-quantitative abundance patterns of selected taxa, which include: *C. subdistichus* gr. (*C. subdistichus* and *C. fenestratus*), *D. barbadiensis, D. saipanensis, E. formosa, I. recurvus, R. umbilicus, C. reticulatum, S. predistentus, S. akropodus* and *S. intercalaris.*

IODP Hole U1411B. Calcareous nannofossil biostratigraphy from Hole U1411B is based on the analysis of core catcher and additional working section half samples. Depth positions and age estimates of biostratigraphic events are shown in Table 5.1. In the study samples calcareous nannofossil are common to abundant and the preservation varies from moderate to good. Only few samples, recorded in the upper part of the section, were classified as poorly preserved. A succession of bioevents (Figure 5.2) is observed from the late Eocene Zone CNE19 to the uppermost part Oligocene Zone CNO2 (Agnini et al., 2014). The total duration of the study interval is of 4.3 Myr (top section 31.9 Ma; base section 36.2 Ma). Site U1411 represents one of the best successions for studying this time interval and this is due to the high sedimentation rates and the good magnetostratigraphic signal (Norris et al., 2014b). At this site, the Eocene/Oligocene boundary was positioned within Chron C13r with the top of *Hantkenina alabamensis* planktonic foraminiferal shipboard datum (157.46 ± 0.75 mbsf; Norris et al., 2014) following the formal definition of the GSSP of base of the Rupelian Stage (Premoli Silva and Jenkins, 2001). The lack of isotopic data at Hole U1411B has been compensated by the integration with magnetostratigraphy, calcium

carbonate data (from Norris et al., 2014b) and calcareous nannofossil events, which allow to identify the most significant changes occurred during this time.

ODP Site 1209. Calcareous nannofossils are generally common to abundant trough the studied section. Strong dissolution (E2/E3) and very poor preservation (VP) characterized almost all the samples investigated in the lower part of the section (ca. from 145 to 141 adj. rmcd). The pervasive dissolution in the upper Eocene is also supported by the high relative abundance (with respect to other taxa) of dissolution-resistant forms belonging to calcareous nannofossil and planktonic foraminifera, including *Globigerinatheka senni, Catapsydrax unicavus, and Globoturborotalita euapertura* (Bralower et al., 2002b). The preservation state slightly improves in the upper part, concomitant to an increase of overgrowth (Figure 5.3). Calcareous nannofossil assemblages present at Site 1209 are characterized by an extremely low diversity, caused by the presence of few dominant dissolution-resistant taxa (e.g., *Discoaster, S. predistentus, Dictyococcites*,..), and by the sporadic occurrence of reworked species (e.g., *Chiasmolithus grandis, C. consuetus, C. solitus, Discoaster multiradiatus*), which become more common (up to 8/mm^2) in the late Eocene and in the uppermost part of the succession (up to 3/mm^2) where the assemblages show a very poor preservation and strong etching. Despite all these issues, we obtained a reliable age model, based on the presence of age-diagnostic taxa. In fact, for what concern biostratigraphic consistency, the reliability of an age assignment in poorly preserved material is not necessarily less than in well preserved one, since, at least in this time interval, it strongly depends on the presence of solution-resistant forms (Perch-Nielsen, 1979). Fortunately, many of the key EOT nannofossil taxa are relatively robust, and thus the biostratigraphic events here reported are reliable. It is worth noting that the Top of *Hantkenina* spp. is reported at 140.36 adj. rmcd (1209A- 14H-5, 36–37 cm; (Bralower et al., 2002a) well below the expected level especially if this datum is compared with both calcareous nannofossil biostratigraphy (Top of D. *saipanensis*) and isotope stratigraphy (LEE) (Figure 5.3). For this reason, the Eocene/Oligocene boundary is positioned in correspondence with Top of *Hantkenina* spp. but we are aware that this biohorizon is anticipated with respect to the onset of the EOT, suggesting a very low reliability for this planktonic foraminiferal biohorizon. LSRs are extremely low for all the studied interval (mean value of 0.4 cm/kyr), especially during the late Eocene and early Oligocene. The succession spans nannofossil Zones CNE20 to CNO2 (Agnini et al., 2014) and lasts 3.8 Myr.

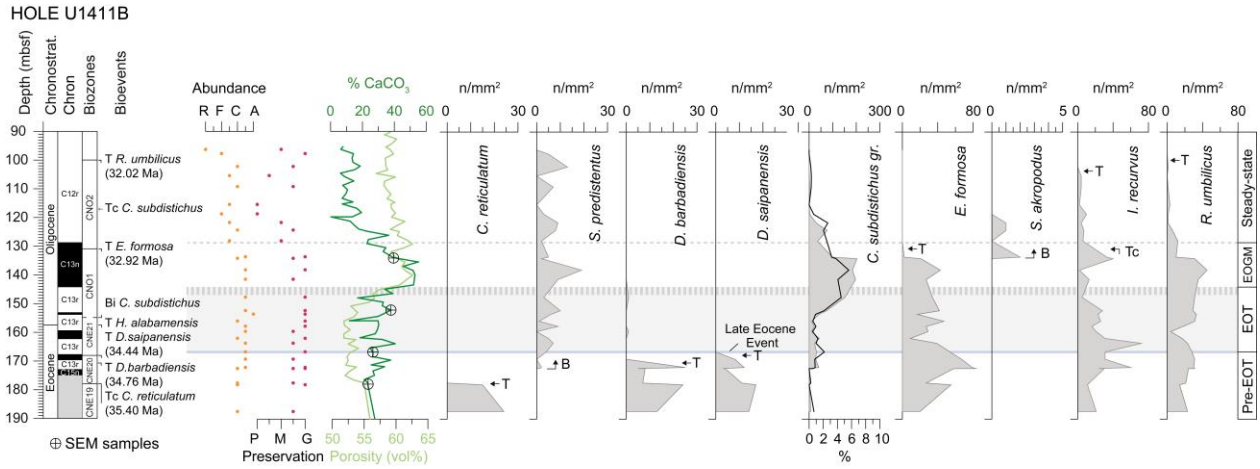

Figure 5.2 Semi-quantitative abundance patterns (n/mm^2) of selected taxa from IODP Hole U1411B are plotted against depth (mbsf), chronostratigraphy, magnetostratigraphy (Norris et al., 2014), CN biozone (Agnini et al., 2014), abundance, and preservation. Nannofossil data are also compared to carbonate content (wt%) and porosity (vol%) (from Norris et al., 2014). The grey band highlights the EOT (base coinciding with the Top of *D. saipanensis*), while the dashed grey line in the upper part is inferred to denote Step 2 (or EOIS). The light blue line indicates the Late Eocene Event (LEE). See text for discussion. Four phases are identified: Pre-EOT, EOT, EOGM and steady-state.

In the following, we report the main bioevents observed at Hole U1411B and Site 1209, listed in stratigraphic order (Figures 5.2, 5.3; Table 5.1):

a) The Top of ***Cribrocentrum reticulatum*** occurs at 177.74 ± 0.31 mbsf at Hole U1411B, whereas at Site 1209 *C. reticulatum* was not found likely because of the pervasive dissolution observed in the late Eocene samples.

b) At Hole U1411B, the Base of ***Sphenolithus predistentus*** was found at 172.39 mbsf, within Chron C13r. At Site 1209, this species becomes abundant and continuous starting from 140.68 adj. rmcd. In this latter site, in the upper part of the section, we detected some transitional morphologies that we grouped as *S. predistentus/S. distentus* morphotype. *S. predistentus* is extremely abundant at Site 1209 (up to 300 n/mm^2), while at Hole U1411B the abundance is lower (up to 30 n/mm^2).

c) At Hole U1411B, the Top of ***Discoaster barbadiensis*** (170.58 ± 1.44 mbsf) and the Top of *Discoaster. saipanensis* (167.87 ± 1.27 mbsf), within Chron C13r. At Site 1209, the synchronous extinction of *D. barbadiensis* and *D. saipanensis* at 139.73 adj. rmcd indicate the presence of a short gap in the sedimentation. Sporadic reworked specimens (1-4 n/mm^2) belonging to these two species were also documented along the succession.

d) At Hole U1411B, we identify the base of major increase, here termed as Bi (= Bi = base of major increase) of ***Clausicoccus subdistichus* gr**. within Chron C13r at 154.71 ± 1.27 mbsf, 2.75 m above the extinction of *H. alabamensis* (Norris et al., 2014b). A similar pattern for *C. subdistichus* gr., with comparable abundances, was documented at Site 1209, where this event was placed at a depth of 137.78 ± 0.22 adj.

rmcd. The Bc of ***Clausicoccus subdistichus* gr**. was instead found below in both the sections, at 172.39 ± 0.02 mbsf and 140.23 ± 0.13 adj. rmcd, respectively.

e) The Top of ***Ericsonia formosa*** was placed at 130.80 mbsf at Hole U1411B, falling within C13n. However, the position of last occurrence of this taxon is not precisely located due to the low sampling resolution that leads to an error of ± 2.8 m. At Site 1209, the top of *E. formosa* occurs at 132.83 ± 0.08 adj. rmcd.

f) The Base (B) of ***Sphenolithus akropodus*** occurs at 133.85 ± 0.27 mbsf at Hole U1411B within Chron C13n, and at 134.20 ± 0.25 adj. rmcd at Site 1209.

g) The Top common (Tc) of ***C. subdistichus* gr.** was reported 117.02 mbsf (Hole U1411B) and at 130.98 adj. rmcd (Site 1209). These data are extremely consistent, falling 55% and 70% from the Top of *Reticulofenestra umbilicus*, respectively, considering the entire duration of Zone CNO2 equals to 100%.

h) At Hole U1411B, ***Isthmolithus recurvus*** is continuously present with relatively high abundances (up to 80 n/mm^2) and its Top common (Tc) is detected at 130.80 ± 2.79 mbsf, coinciding with the Top of *E. formosa*. At Site 1209, the Tc of *I. recurvus* occurs at 133.33 ± 0.13 adj. rmcd, 0.50 m below the Top of *E. formosa,* within Zone CNO1. In this work, we have also monitored the extinction (T) of *I. recurvus*, which occurs at 103.78 ± 1.58 mbsf (Hole U1411B) and at 128.05 ± 0.25 adj. rmcd (Site 1209).

i) At Site 1209 the extinction (T) of *R. umbilicus* was recorded at 126.68 adj. rmcd, instead at Hole U1411B it occurs at 99.95 mbsf.

At Site 1209, we also reported the abundance pattern of *S. intercalaris*, which is particularly abundant (up to 40 n/mm^2) during the late Eocene.

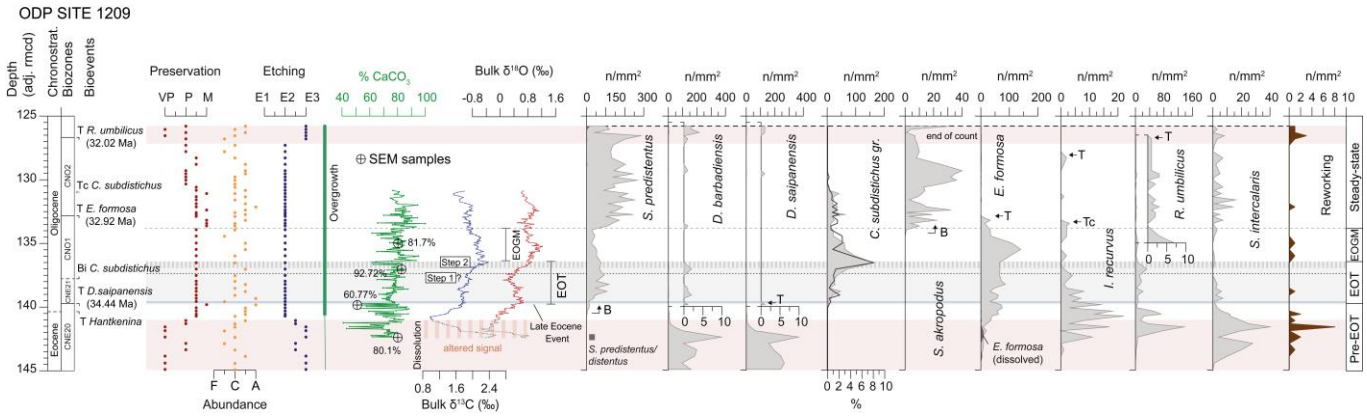

Figure 5.3 Semi-quantitative abundance patterns (n/mm^2) of selected taxa from ODP Site 1209 are plotted against depth (adj. rmcd), chronostratigraphy, CN biozone (Agnini et al., 2014), preservation, abundance, etching, geochemistry (stable O, C isotopes and %$CaCO_3$). Reworking is also present all over the section and especially during the dissolution phases (shaded pink bar). The grey band highlights the EOT (base coinciding with the Top of *D. saipanensis*), while the dashed grey line in the upper part is inferred to denote Step 2 (or EOIS). The light blue line indicates the Late Eocene Event (LEE). See text for discussion. Four phases are identified: Pre-EOT, EOT, EOGM and steady-state. The dashed pink bar highlights the altered geochemical signature linked to the dissolution interval. Reworking corresponds to interval of higher dissolution, as highlighted by the pink bar.

5.3.2 Geochemistry

At Site 1209, calcareous nannofossil biostratigraphy was correlated with a high-resolved (ca. 20 kyrs) bulk geochemical record (Figure 5.4), which allows to subdivide the studied section in different intervals based on distinctive trends and variations, outlined in paragraph 5.3.4. The oxygen isotope values ($\delta^{18}O$) average 0.56 ± 0.38‰ (1σ), while the $\delta^{13}C$ data average 1.87 ± 0.30‰ (1σ). From the base of the section (142.40 adj. rmcd) to 140.90 adj. rmcd, we recognize anomalous high positive $\delta^{18}O$ and $\delta^{13}C$ values, respectively around 0.82‰ and 2.55‰. These anomalous values, recorded during the late Eocene, coincide with an interval of extremely poor preservation and with high abundance peaks of discoasters (up to 400 n/mm^2; Figure 5.2). These data likely indicate a residual assemblage resulting from pervasive dissolution. Moreover, the oligotypic assemblage and the absence of fragile taxa suggest that sediments were strongly affect by diagenetic processes in the lower part of the section. Based on these considerations, the interval with anomalous $\delta^{18}O$ and $\delta^{13}C$ values in the lower part of the section will be discarded and any paleo-environmental interpretations avoided (Figure 5.4, dashed pink bar).

Instead, stable isotopic values recorded above are extremely consistent with global deep-marine records with apparently no or minimal alterations of original $\delta^{18}O$ and $\delta^{13}C$ bulk values, despite the presence of minor dissolution and major overgrowth observed throughout the succession. Between 140.90 adj. rmcd and 139.73 adj. rmcd, both $\delta^{18}O$ and $\delta^{13}C$ bulk values gradually start to increase. The interval between the bottom of the section and 139.73 adj. rmcd, corresponds to the "PRE-EOT" phase. A transient positive $\delta^{18}O$ excursion from 0.46 to 0.57‰ (from 139.80 to 139.65 adj. rmcd) was recognized and interpreted as the Late Eocene Event (LEE; Hutchinson et al., 2021).

This transient event virtually occurs in correspondence with the extinction of *D. saipanensis* (139.73 ± 0.13 adj. rmcd). Between 137.40 (33.88 Ma; B Step 2) and 136.45 adj. rmcd (33.65 Ma; T Step 2), $\delta^{18}O$ rapidly increases by 0.71‰, shifting from 0.20 to 0.91‰. This positive shift is interpreted as Step 2 (or EOIS) and thus the end of the EOT. Above 136.45 adj. rmcd and up to 133.85 adj. rmcd, the oxygen isotopes record an interval of positive $\delta^{18}O$ values, with a maximum peak of 1.22‰ (135.20 adj. rmcd). This interval corresponds to the EOGM (the "EOGM" phase). From 133.85 adj. rmcd upsection, $\delta^{18}O$ values remain relatively stable with absolute high values (0.82‰). This phase is defined as "steady-state" in this work.

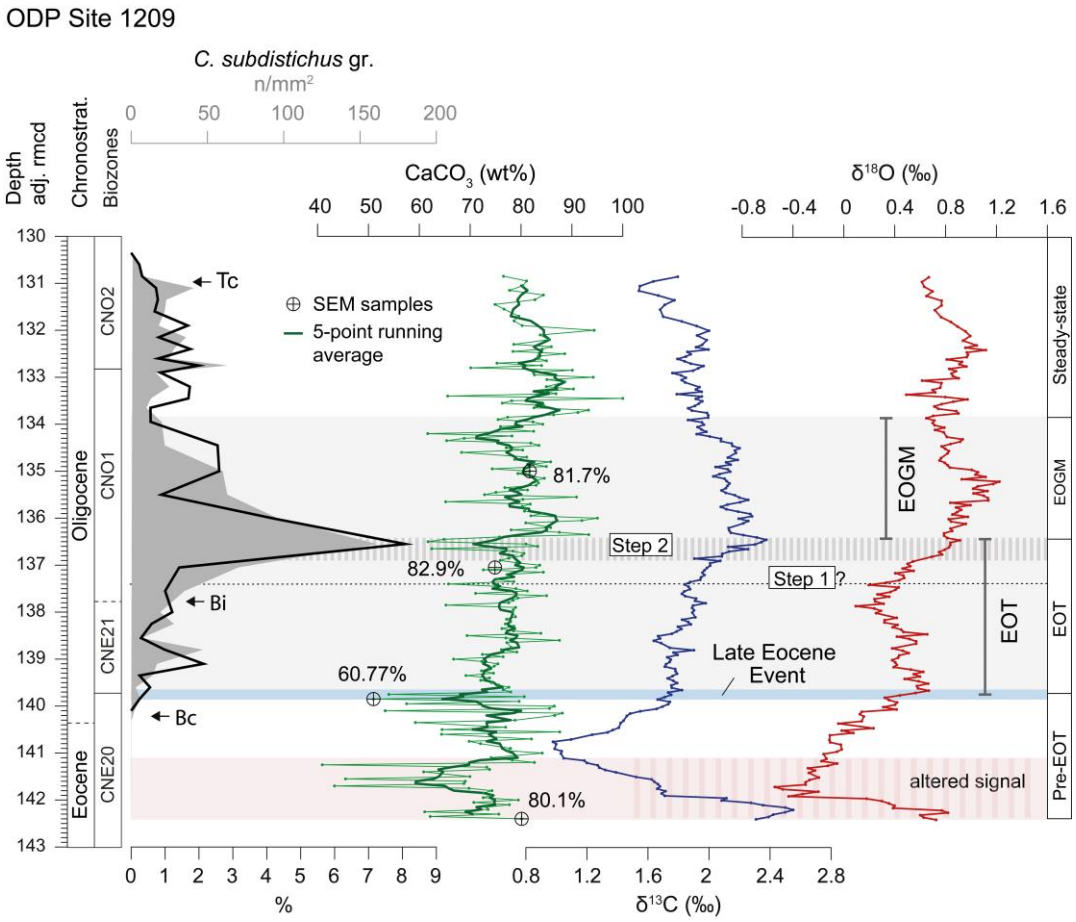

Figure 5.4 Profile of carbonate content (wt %), stable oxygen and carbon isotopes (‰ VPDB), *C. subdistichus* abundance (n/mm² and %) plotted against chronostratigraphy, CN biozone (Agnini et al., 2014) and the four main phases: pre-EOT, EOT, EOGM and steady state. The altered geochemical signature is highlighted by the pink bar. The main oxygen stable isotopic events are reported: Late Eocene Event (LLE), EOT (step 1 and step 2) and EOGM. Bi = base of major increase; Bc= base common and continuous; Tc= top common and continuous refers to *C. subdistichus* (n/mm²) plot.

The general trend documented in the carbon oxygen isotopes show a quite high variability and generally correlates with the main events recognized in the $\delta^{18}O$ curve, with no significant lags. The bulk carbonate content (wt, %)

also shows high variability, with a mean value of 77.5%. Instead, at Hole U1411B the carbonate content (wt, %) is considerably lower (14% - 55.21%; Norris et al., 2014b).

5.3.3 Age models

The age models and the correlation between the two sites rely on tie-points based on calcareous nannofossils, oxygen stable isotope stratigraphy and magnetic reversal stratigraphy listed in Table 5.1.

Using the same chronology, records at Hole U1411B and Site 1209 were aligned in the time domain.

Events	Hole U1411B		Site 1209		Hole U1411B			Age (Ma)
	Mid-depth (mbsf)	Error (± m)	Mid-depth (adj. rmcd)	Error (± m)	Age U1411[#]	Age U1411[@]	Age 1209[$]	GTS12
***T R. umbilicus** **	99.95	2.25	126.68	0.13	32.13	32.02	32.02	**32.02**
T *I. recurvus*	103.78	1.58	128.05	0.25	32.26	32.17	32.22	
Tc *C. subdistichus* gr.	117.02	1.64	130.98	0.13	32.74	32.69	32.65	
***T E. formosa** **	130.80	2.79	132.83	0.08	33.23	33.23	32.92	**32.92**
Base Chron C12r*	128.79	0.73	NA	NA	33.157	33.157	33.157	**33.157**
Tc *I. recurvus*	130.80	2.79	133.33	0.13	33.23	33.23	33.02	
B *S. akropodus*	133.85	0.27	134.20	0.25	33.34	33.34	33.20	
T Step 2 *	NA	NA	136.45	NI	NA	NA	33.65	**33.65**
Base Chron C13n*	144.15	0.05	NA	NA	33.705	33.705	33.157	**33.705**
Bi *C. subdistichus* gr.	154.71	1.20	137.78	0.22	34.18	34.03	33.97	
Bc *C. subdistichus* gr.	172.39	0.02	140.23	0.13	34.97	34.94	34.56	
Top *Hantkenina* spp.	157.46	0.75	140.36	NI	34.30	34.30	34.59	**33.89**
***T D. saipanensis** **	167.87	1.27	139.73	0.13	34.77	34.44	34.44	**34.44**
T *D. barbadiensis*	170.58	1.44	139.73	0.13	34.89	34.76	34.44	**34.76**
B *S. predistentus*	172.39	0.02	140.68	0.08	34.97	34.94	34.67	
Base Chron C13r *	172.98	0.08	NA	NA	34.999	34.999	33.157	**34.999**
T *C. reticulatum*	177.74	0.31	NI	NI	35.21	35.21	NI	**35.40**

Table 5.1 Age and mid-depth of selected calcareous nannofossil biohorizons from Hole U1411B and from Site 1209. Ages are from Agnini et al (2014) recalibrated to GTS2012 (Gradstein et al., 2012). *Points chosen as tie points. [#]Ages for Hole U1411B calibrated with respect to magnetostratigraphy (Norris et al., 2014). [@]Ages for Hole U1411B given with respect to magnetostratigraphic Chron boundaries (Norris et al., 2014) and calcareous nannofossil tie-points (except for Top of *E. formosa*). [$]Ages for Site 1209 are calibrated with respect to nannofossil and oxygen stable datums. NA= not available; NI = not identified. Bi = base of major increase (informal); T = top; Tc= top common; Bc =base common; B= base. Bi= base of acme increase.

The age model for Hole U1411B was constructed using calcareous nannofossil bioevents and magnetostratigraphic data (Norris et al., 2014b) as tie-points (Table 5.1, grey column), since oxygen stable isotope records were not available. Given the uncertainty of the Top of *E. formosa* (error ± 2.79), we decided to exclude this datum from the age model. Instead, for ODP Site 1209, the age-depth model is tied to nannofossil and oxygen stable isotope datums. At this site bio-chemostratigraphic constraints indicate a condensed sequence, characterized by very low

sedimentation rate (average LSR of 0.3 cm/kyr). The synchronous extinction of the two rosetta-shaped discoasters (i.e., *D. barbadiensis* and *D. saipanensis;* 139.73 adj. rmcd) that are usually spaced in time (34.76 and 34.44 Ma) supports the presence of a short hiatus especially considering the high sampling resolution (ca. 20kyr).

5.3.4 Preservation of calcareous nannofossils

In this work, samples from Hole U1411B and Site 1209 have been visually compared with the help of SEM analyses to evaluate the state of preservation of calcareous nannofossil assemblages. We selected four samples from Hole U1411B collected from four different time slices across the late Eocene – early Oligocene: the first sample was collected in the "Pre-EOT" phase, which is the interval lying below the extinction of *D. saipanensis* (167.87 adj. rmcd; 34.44 Ma). The second sample comes from the level corresponding to the Late Eocene Event - LEE (corresponding to the T of *D. saipanensis*). The third sample was taken within the EOT, that is embraced by the two positive $\delta^{18}O$ excursions (Step 1 and Step 2) and that corresponds to most of Chron C13r. the fourth sample was collected in the EOGM, the interval that starts from the top of Step 2 (33.65 Ma include the highest $\delta^{18}O$ values). Four comparative samples were selected from ODP Site 1209 from the same phases. The position of samples analyzed with scanning electron microscope (SEM) is reported in Figure 5.2 and Figure 5.3 along the carbonate record. In the following, a brief description of calcareous nannofossil assemblage composition and preservation from Hole U1411B and Site 1209 is reported in stratigraphic order, from the oldest sample to the younger, and summarizes the main observation made with the SEM analyses:

5.3.4.1 Pre-EOT phase

IODP Site U1411 (Sample U1411B-21X-CC, 25-33 cm). In the upper Eocene, calcareous nannofossils show few to common abundances with moderate to good preservation and no sign of dissolution or recrystallization. The carbonate content is relatively low as reported in Figure 5.2 and shipboard data (20-30%; Norris et al., 2014).
The sample is dominated by clay minerals that produce an important decrease in the porosity of the bulk sediment (Figure 5.3). Clay minerals may derive from detrital sources or from authigenic or late-stage mineral growth. In our investigation clay seems to occur as small plates (Plate 5.1, Fig. 4). The clay-rich ooze contains well preserved coccoliths, as shown by the intact specimens of *Coccolithus, Clausicoccus, Ericsonia, Cribrocentrum,* and *Reticulofenestra* (Plate 5.1, Fig. 16, 17, 23, 18, and 24). The latter two still preserving the original fine nets of the central areas. The late Eocene nannoliths (i.e., rosetta-shaped discoasterids) dominate the assemblage, showing no signs of secondary overgrowth. The most common species are *D. barbadiensis* and *D. saipanensis*. We also documented the presence of several specimens of *Discoaster robustus,* whose stem is barely distinguishable from the body, and form in a pyramid-like structure (Plate 5.1, Fig. 13-15). Many well-preserved specimens of *C. reticulatum,* with their delicate grid in the central area, were observed in the sample (Plate 5.1, Fig. 18).

ODP Site 1209 (Sample 1209C-4H-3, 93 cm). The PRE-EOT interval at Site 1209 coincides with a phase of strong dissolution and reworking. Reworked taxa are mainly from the middle-late Eocene and include *C. grandis, C. consuetus, C. solitus, D. multiradiatus*, *Sphenolithus spiniger,* and others. The carbonate content of the sample is ca. 80%. Overall, placoliths of *E. formosa* are extremely affected by dissolution (Plate 5.2, Fig. 15) and the most common component of the assemblage is represented by fragments of coccoliths where the proximal and distal shields are usually disconnected. These broken coccoliths belong to relatively large *Dictyococcites* and *Reticulofenestra,* which are known to be extremely resistant to dissolution.

The presence of isolated shields, widened central areas and micrite particles generally describe strongly etched samples (Hill, 1975). Poorly preserved distal shield of *C. pelagicus* occur together with well-preserved ones. Dissolution processes seems to primarily affects distal shields, especially corroding the central area of *E. formosa*, as reported by preliminary LM observations and counts, where several specimens of *E. formosa* were strongly affected by dissolution (Figure 5.3). Fragmentation and dissolution are accompanied by the severe overgrowth of discoasters and other solution-resistant forms. In some cases, discoasters are indeterminable due to secondary calcite deposition, especially along their rays. The calcite accretion is particularly evident in some specimens (Plate 5.2, Fig. 12, 13) which show differential growth of their elements (rays or stem).

The original structure of *I. recurvus* and *Bramletteius serraculoides* is also masked by a secondary thick calcite overgrowth (Plate 5.2, Fig. 7, 17). The preferential deposition of overgrowth cement strongly depends on the taxon considered: in the case of *D. bisectus* considerable amounts of calcite are deposited in the central plug (Plate 5.2, Fig. 8, 9). Many specimens of *R. umbilicus* have lost their grid in the central area (Plate 5.2, Fig. 14, 19). Small as well fragile specimens are extremely rare to absent. All these observations confirm the hypothesis that the pristine assemblage has been substantially altered by diagenetic processes.

5.3.4.2 Late Eocene Event

The Late Eocene Event (LEE) represents a crucial point of the Eocene-Oligocene transition, so far understudied. This event documents an extremely important change in the phytoplanktonic assemblage: the extinction of the last member of rosetta-shaped discoasters (i.e. *D. saipanensis*). From that moment on discoaster assemblages include flower-shaped, free-rayed morphotype which can be ascribed to a number of different species as for instance of *D. tanii* gr., *D. distinctus* and *D. deflandrei*.

IODP Site U1411 (Sample U1411B-19H-4W, 30 cm). Preservation is quite similar to the previous sample (U1411B-21X-CC), as well as calcium carbonate content that remains low (Figure 5.4). With the advent of the LEE, the rosetta-shaped discoasterids are replaced by flower-shaped discoasters. Specimens of *Discoaster* show varying degrees of preservation within the same sample: some forms are well preserved with prominent lateral nodes on their rays and ray-end bifurcations (Plate 5.3, Fig. 6), while other individuals show a certain degree of overgrowth (Plate 5.3, Fig. 11). The good preservation of this sample is also confirmed by the presence of

extremely well-preserved specimens of *I. recurvus*, *R. umbilicus*, *R. daviesii* and by the dissolution-resistant species *D. bisectus*, which shows no signs of overgrowth (Plate 5.3, Fig. 7-9, 12, 14).

ODP Site 1209 (Sample 1209A-14H-4W, 115 cm). By contrast to the previous sample (U1209C-4H-3W, 93), where the main processes involved fragmentation, dissolution, and overgrowth, in this sample the assemblage is almost exclusively dominated by recrystallization. Calcareous nannofossils show strong signs of secondary calcite reprecipitation during early diagenesis phases, that resulted in the formation of massive and resistant forms, including *Dictyococcites*, *Discoasters and Sphenolithus pseudoradians.* Fragmented coccoliths are very common and constitute the groundmass of the sediment. Accretion of secondary calcite is evident along *Discoaster* arms, in which distinct (euhedral) crystal faces are developed (Plate 5.4, Fig. 7).
This sample is characterized by the presence of common *Thoracosphaera* and specimens of *Hayella situliformis* (Plate 5.4, Fig. 3). The dominant component of the assemblage is represented by *Dictyococcites,* which is almost completely welded by accretion of cement on the central plug (Plate 5.4, Fig. 4, 15).
An interesting note is that *E. formosa* exhibits preferential deposition of overgrowth cement on the elements surrounding the central area (Plate 5.4, Fig. 11). This diagenetic observation can be explained taking into consideration the topographic structure of coccolith shield of *Ericsonia*. A possible explanation for this post-depositional feature is that the funnel-like central area has likely facilitated the accumulation of interstitial fluids, favoring dissolution and/or overgrowth processes.

5.3.4.3 EOT

IODP Site U1411 (Sample U1411B-17H-7A, 25 cm). The high clay content of this sample leads to an extremely well-preserved assemblage, dominated by abundant and exceptionally preserved specimens of *C. subdistichus* gr. (Plate 5.5, Fig. 7, 8, 13). Certain coccolith taxa, as previously reported, are more readily dissolved or recrystallized than others. This is the case of *I. recurvus*, a taxon that seems to be extremely susceptible to secondary overgrowth. This murolith is characterized by relatively high wall with three openings aligned along the longitudinal axis and separated by two transverse segments of single-calcite crystals. In case of exceptional preservation, as in this sample, muroliths present several parallel ribs on the external lateral side (wall) and two for each transvers (Plate 5.5, Fig. 11, 12). These ultrastructural details observed on the surface of the individual at Hole U1411B, as well as the central openings, are instead totally obliterated at Site 1209. The exceptional preservation of Hole U1411B is also confirmed by the presence of complete coccospheres, which are typically encountered in clay-rich hemipelagic sediments (Bown et al., 2014). In Plate 5.5, we report the occurrence of a coccosphere ascribed to *E. formosa* (Fig. 17, 19), that was detected during the scan mode analysis and then imaged at better resolution with the UH-resolution scan mode. Reticulofenestrids (e.g., *R. umbilicus* and *R. daviesii*) retain their pristine and fragile central nets (Plate 5.5, Fig. 16, 19). The same original structure is maintained by the small base of *B. serraculoides* (Plate 5.5, Fig. 14).

ODP Site 1209 (Sample 1209C-3H-6, 90 cm). The sample is characterized by common to abundant nannofossils, which are partially dissolved - especially along the edges of the distal shields and in the central area – and then heavily recrystallized. In carbonate-rich (~83%) ooze, *S. predistentus* displays a common abundance and its bifurcated spines are found broken off and spread all over the sample (Plate 5.6, Fig. 1), and are usually overgrown (Plate 5.6, Fig. 7, 8). Rest of foraminiferal tests and *Thoracosphaera* skeletons are also commonly found (Plate 5.6, Fig. 3, 6). *Hayella situliformis* is present and abundant in this sample. *Discoaster* and *Dictyococcites* accreted a large amount of secondary calcite forming a thick overgrowth along the rays and in the central plug (Plate 5.6, Fig. 9, 10, 12). Sporadic specimens of *Chiasmolithus* without the central cross were found during the LM investigation. Also in this sample, the central holes of *I. recurvus* are fill-in by calcite overgrowth.

5.3.4.4 EOGM

IODP Site U1411 (Sample U1411-16H-1W, 50 cm). Calcareous nannofossils from the EOGM at IODP Site U1411 are extremely well-preserved. However, some morphological features are slightly obscured by a thin film of clay that persists despite the intensive treatment carried out to remove it (Plate 5.7; Fig. 1-6). The sample is characterized by common specimens of *I. recurvus* (Plate 5.7; Fig. 8), *Blackites* spp. (Plate 5.7; Fig. 10), rabdolith fragments (Plate 5.7; Fig. 16), small reticulofenestrids (e.g., *R. minuta*), *Pontosphaera* spp. (Plate 5.7; Fig. 7, 18) and *Helicosphaera* spp. (Plate 5.7; Fig. 21). The optimal preservation permits the observation of a finely perforate grill on the proximal side of *C. subdistichus*. These micro-pores are visible underneath the larger ones in the distal shield (Plate 5.7; Fig. 11, 13).

ODP Site 1209 (U1209-3H-5, 35 cm). The sample is characterized by a very high carbonate content (82%). Recrystallization, during the EOGM at Site 1209, is still the dominant diagenetic factor. Many fragments of planktonic foraminifera (Plate 5.8; Fig. 1) are present. Several (and difficult to determine) placoliths have proximal shields elements extremely welded together, because of secondary calcite accretion (Plate 5.8; Fig. 16). The sample is characterized by extremely abundant heavily-resistant calcareous nannofossils, including many placoliths of *Dictyococcites* (Plate 5.8; Fig. 9, 19)*, Reticulofenestra* (Plate 5.8; Fig. 9) and *Coccolithus* (Plate 5.8; Fig. 12)*, B. serraculoides* (Plate 5.8; Fig. 17, 18) and *Sphenolithus* spp. (Plate 5.8; Fig. 10).

5.4 Discussion

5.4.1 Biostratigraphic frameworks

In the following, we compared the biostratigraphic events and species quantitative distribution patterns (Figure 5.2 and Figure 5.3) recognized at Hole U1411B and Site 1209, from section base to top:

(i) The top of ***C. reticulatum*** was recovered at Hole U1411B, but the extinction of this taxon was not found at Site 1209. The absence of *C. reticulatum* could be explained as due to ecological factors but it is more likely that it is a preservation artifact resulted from the extremely poor preservation of the samples encountered at the base of the section. This hypothesis is consistent with the fact that this species is thought to be relatively prone to dissolution (Toffanin et al., 2013).

(ii) The reliability of the base of ***S. predistentus*** is much debated, because of the scattered presence of this sphenolith close to its appearance. We found that the base of this event slightly predates the extinction of rosetta-shaped discoasters at both studied sites, lying in the upper part of Zone CNE20, as also reported by Fioroni et al. (2015). Similarly, results from Site U1509 documents an extremely punctuated presence of this species starting from the late Eocene (Chron C15n) (Chapter 3). However, the positions at Site 1209 and Hole U1411B are not consistent with that recorded at Site 756, where the Base of this species was found later within CNO2 (see Chapter 2). Differences in abundances between Site 1209 (0-300 n/mm^2) and Hole U1411B (0-30 n/mm^2) are likely related to both preservation and ecological preferences, since the Site 1209 has been interpreted as characterized by oligotrophic condition while Site U1411B was located in a more eutrophic environment (Schneider et al., 2011; Cappelli et al., 2019).

(iii) The Base common of ***C. subdistichus* gr.** is not easy to detect (see Chapter 2 and Chapter 3), due to an objective difficulty to fix the exact beginning of the acme interval. At different sites, this taxon shows different relative and absolute abundances, and it is thus impossible to define the Base of common and continuous abundance of this species with a single value. This issue possibly results in a certain degree of uncertainty though the acme interval itself surely represent an invaluable tool to correlate earliest Oligocene successions. Inconsistent data available for the Top common of ***I. recurvus*** suggest caution. In particular, the ranking between the Tc of *I. recurvus* and the Top of *E. formosa* seems to be problematic. For example, at Site U1509 this event falls in the lower part of Zone CNO2, corresponding to an age of 32.8 Ma. thus above the Top of *E. formosa* (Chapter 3), while at Site 1209 was recorded at 33.02 Ma. Conversely, the extinction (T) of *I. recurvus* is well recognized at Site 1209 and Hole U1411B, with an age of 32.22 and 32.17, respectively. However, its extinction is commonly considered "one of the most inconsistent datums" (Berggren et al., 1995).

(iv) The base (B) of ***S. akropodus*** documented at Site 1209 and Hole U1411B (age estimate of 33.20 Ma and 33.34 Ma, respectively) is extremely consistent with the datums from South Atlantic (Site 1263; Bordiga et al., 2015), being found in the upper part of Zone CNO1. The age estimate reported from

the Tasman Sea for this event is 33.18 Ma (Chapter 3), and 33.29 Ma in the Indian Ocean Site (756) (Chapter 2), incredibly consistent. Our datum is also consistent with data from the northeastern Atlantic Ocean, as reported in de Kaenel and Villa (1996), where it was used to approximate Zone NP21/NP22. Nonetheless, our result is in disagreement with that reported by Fioroni et al. (2015) who extended this species down to the late Eocene, within Chron C13r. Apart from this minor discrepancy, our data seems to confirm that the base of *S. akropodus* represents a valid and reliable marker, helping to further subdivide the long CNO1.

(v) The Top common of ***C. subdistichus* gr.**, reported at Hole U1411B (. age estimate of 32.74 Ma) and at Site 1209 (age estimate of 32.65 Ma), seems to be fairly consistent and reliable, as previously suggested (Chapter 2 and 3), being constantly found above the Top of *E. formosa*, within Chron C12r.

(vi) The Top of ***R. umbilicus*** is not easy to detect because of the scattered occurrence of the taxon in the final tail of distribution.

At Site 1209, the occurrence of *S. intercalaris* in the upper Eocene (up to 40 n/mm^2) is consistent with previous studies from Shatsky Rise (Site 1208; Bown, 2005), Equatorial Pacific (Toffanin et al., 2013) and Tasman Sea (Chapter 3; up to 22 n/mm^2). Therefore, the presence of this taxon is found to be well documented in the Pacific Ocean. However, no evidence of the presence of *S. intercalaris* was reported from the North Atlantic (Hole U1411B; this study) or from the Indian Ocean (Hole 756C; Chapter 2).

5.4.2 Reconstructing past preservation

Since the 70's, the availability of the scanning electron microscope (SEM) and the beginning of the study of the deep-sea cores have literally promoted an explosion in the study of possible consequences in calcareous nannofossil assemblages related to diagenetic processes (van der Lingen and Packham, 1975). The landmarks works by Fisher et al. (1967) and Adelseck et al. (1973) have provided some general trends as the diagenetic processes become more pervasive described: small coccoliths tends to disarticulate along sutures due to dissolution, producing large amounts of micron-sized particles; placoliths with overlapping elements in the distal shields offers greater resistance to dissolution; discoasters tend to overgrow with the precipitation of highly euhedral calcite, becoming several times more massive than the original; larger coccoliths tend to persist in highly recrystallized sediments. Accordingly, recrystallization and dissolution severely affect nannofossils, and may result in the loss of the pristine ecological and geochemical signal. Understanding how preservation affects the phytoplankton community can help in disentangling the paleoenvironmental information from diagenetic overprint. Our qualitative SEM study provides a detailed picture of the variations occurred on the nannofossil assemblages throughout the studied interval. Furthermore, the comparative LM and SEM observations has been useful for understanding how diagenetic processes can alter the make-up of the assemblage.

Previous results from EOT sediments (e.g. Bordiga et al., 2015; Dunkley Jones et al., 2008; Jones et al., 2019) suggest a quite homogeneous response of calcareous nannofossils to the environmental changes occurred during

the E-O transition. A possible interpretation is that productivity and temperatures have changes globally in the same direction and were thus able to produce quite similar ecological changes in sediments characterized by comparable states of preservation. However, in poorly preserved sediments, as is the case of Site 1209, any paleoecological interpretation should be avoided because the fossil nannoplankton assemblages are deeply biased by taxon-dependent preferential dissolution. At ODP Site1209, our morphological analysis indicates that diagenetic processes have played a crucial role in controlling the presence and/or relative variation of some taxa. Herein, we combine the results described above for Site 1209, in order to provide a brief discussion of the four key intervals that have coherent biostratigraphic and geochemical features.

In the critical PRE-EOT phase at ODP Site 1209, the assemblage is the result of strong dissolution (E3). Despite this, the most resistant and biostratigraphically/ecologically relevant forms (i.e., rosetta-shaped discoasters and *E. formosa*) are still present, even though slightly altered by diagenesis. In fact, the unusual high abundances of *D. saipanensis* and *D. barbadiensis* are clearly a diagenetic artifact, since discoasters are one of the most solution-resistant forms (e.g. Raffi and De Bernardi, 2008). Strong dissolution is also witnessed by the low abundance and poor preservation of the less resistant species such as *E. formosa* and by the high abundance of dissolved/fragmented placoliths (almost exclusively of *Dictyoccocites*), consistently detected both at the LM and, SEM observations.

Upward, during the Late Eocene event (LEE), overgrowth assumes a stronger relevance, going along with minor dissolution (E2). At Site 1209, there is no systematic increase in overgrowth with depth of burial. This evidence agrees with preliminary shipboard observations (Bralower et al. 2005) but disagrees with other studies that document direct proportionality between increasing depth and overgrowth (Hill, 1975; Matter et al., 1975). Thus, preservation, in this case, is exclusively related to altered conditions at or near the sea-floor, as initially suggested by Bralower et al. (2002b) and can further be correlated to a frankly pelagic environment, not buffered by the clay minerals input from inland hydrolysis. The increase in calcite overgrowth suggests a local basification of marine pore fluids and secondary precipitation during post-depositional processes in the thanatocoenosis, rather than a direct response to environmental changes on the biocenosis.During the EOT, preservation tends to gradually improve, although overgrowth is still pervasive: as dissolution decreases, also micro-sized calcite particles (“micarbs”) and fragmentation decrease. In the EOGM, the preservation shows no major differences compared to the previous phases. The diagenetic process seems to reach a sort of stability that persisted during the early Oligocene.

In summary, the low-diverse and poorly preserved nannofossil assemblage from Shatsky Rise is the result of an early diagenetic overprinting. Some taxa are more prone than others in recording diagenetic overgrowth, as for instance *Discoaster*, *B. serraculoides, I. recurvus, Dictyococcites, S. radians* gr. and *S. predistentus*. Other coccoliths proved to be extremely solution-resistant, as the case of *S. intercalaris* probably due to its knob-like massive structure and *H. situliformis*, with strongly imbricated elements. Other taxa with delicate structures are

instead more susceptible to differential dissolution, as the case of the central area of *E. formosa* and the central nets of reticulofenestrids.

At ODP Site 1209, carbonate content is high and ranges between ~41 to 100%. This site represents a typical deep-sea sequence, commonly encountered studying the E-O transition, and characterized by a pervasive overgrowth and/or dissolution due to diagenetic processes typically active in a carbonate-rich nannofossil ooze. In contrast with this case, the clay-rich nature of the drift sediments recovered at Hole U1411B has resulted in extraordinarily high species diversity and predominance of delicate central structures and small forms (Newsam, 2016).

5.4.3 Diagenetic effects on bulk isotopic data

Bulk sediment is composed by the contribution of multiple, mostly biogenic, carbonate components (calcareous nannofossils, planktonic/benthic foraminifera, and fragments). However, as recently underlined by Reghellin et al. (2015), calcareous nannofossils often dominate bulk marine carbonate in open ocean sediments, as in this case, carrying signals of mixed-layer conditions. Consequently, bulk stable isotopic composition ($\delta^{18}O$ and $\delta^{13}C$), coupled with carbonate content (%) have the potential to provide a valuable archive for paleoceanographic studies, as well as stratigraphic correlations. However, the successful application of bulk stable isotopes for accurate paleoceanographic reconstructions relies on the maintaining of the primary isotopic signal of deep-sea carbonates. For this reason, reliable paleoclimatic interpretations are strongly dependent to good or exceptionally preserved sediments. Despite this, paleoclimatologists very often, want to use and interpret data obtained by poorly to moderate preserved material. Overall, carbonate preservation strongly relies on depth, because the undersaturation of seawater increases with pressure and decreasing temperature: as the depth of deposition increases, so does the rate of carbonate dissolution (Berger 1974). So, shallow depositional or more elevated sites tend to promote preservation in contrast to deeper open-ocean sites (Berger, 1971; McIntyre and McIntyre, 1971; Johnson et al., 1977). ODP Site 1209 is well above the lysocline, and consequently the general poor preservation observed is primarily related to diagenesis.

Our results indicate that, within the PRE-EOT phase, precisely from 35.09 to 34.72 Ma, $\delta^{18}O$ values shift from a minimum of -0.54‰ to a maximum of 0.82‰, recording improbable late Eocene values, that are not consistent with the long-term and short-term climate evolution depict in a global oxygen isotope reference curves (Figure 5.5; Westerhold et al., 2020). This interval coincides with a high dissolution phase concomitant to moderate recrystallisation. The dissolution-precipitation reaction often took place simultaneously (van der Lingen and Packham, 1975) and must has started before or soon after the burial. During this interval, both these processes contribute to high and low anomalous $\delta^{18}O$ values. Instead, no evidence of signal distortion was observed above this level, as observed comparing the $\delta^{18}O$ profiles from different Pacific Ocean sites (Figure 5.5), despite overgrowth of coccoliths is well recorded (Plates 5.4, 5.6, 5.8). The $\delta^{18}O$ bulk profile at Site 1209 closely parallels that from Site U1509 (Chapter 4). Bulk $\delta^{18}O$ values at Site 1209 are slightly higher (mean $\delta^{18}O$ 0.56‰ ± 0.38‰) than those of associated bulk from a well-preserved sediment (Site U1509, mean $\delta^{18}O$ 0.41‰ ± 0.21‰), but fall

within quite close standard deviation ranges, indicating a negligible contribution of recrystallization in raising $\delta^{18}O$.

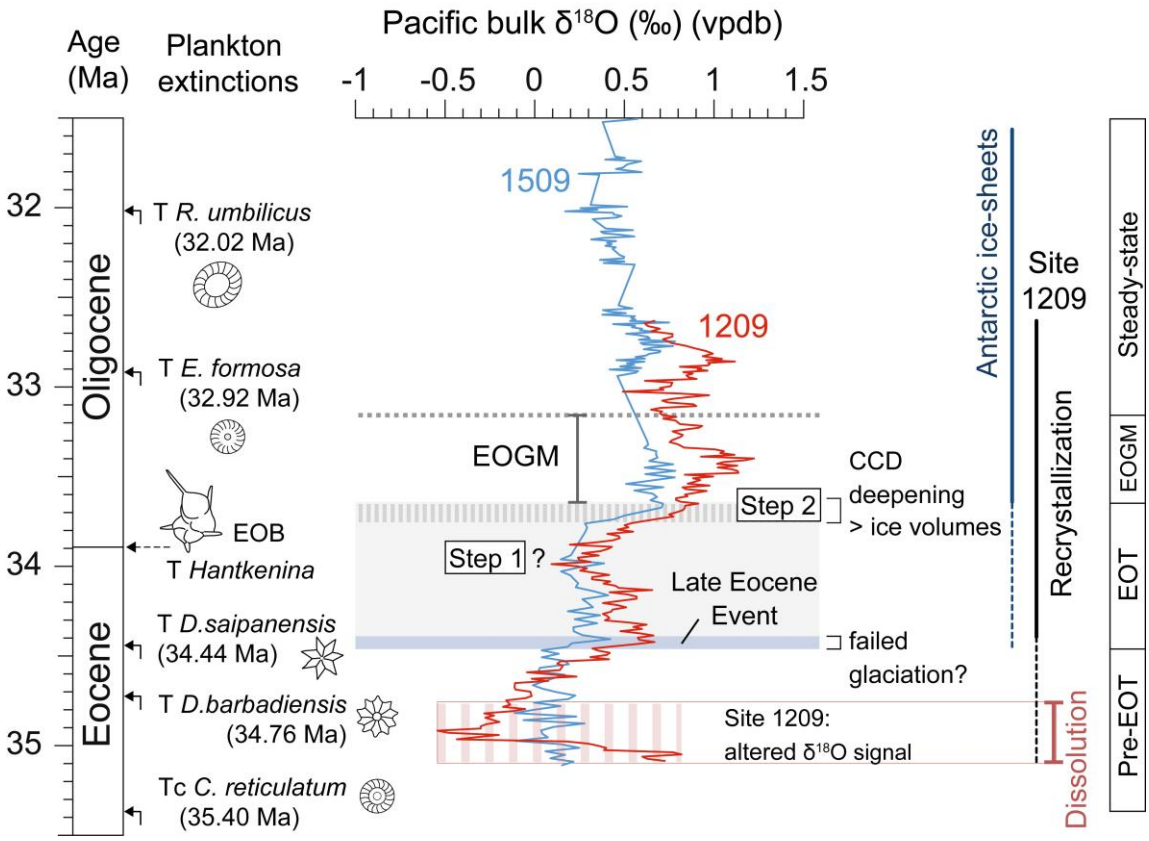

Figure 5.5 Pacific Ocean bulk stable oxygen isotopes records (‰ VPDB) from Site 1209 (this work) and Site U1509 (Chapter 4). A summary of the main environmental and geochemical events occurring across the E-O transition is also reported, as well as the main plankton extinctions. The dissolution phase is highlighted by a shaded pink bar, corresponding to strongly altered geochemical signature at Site 1209, concomitant to modest recrystallization.

5.5 Conclusions

In this study we observed large inter-site differences in the preservation state of calcareous nannofossil coccoliths implying very different diagenetic histories. At Hole U1411B, calcareous nannofossil assemblages are almost pristine and no significant alterations were found during the investigated phases. The presence of clay, very abundant during the PRE-EOT and EOT, and the relatively low $CaCO_3$ (wt, %), allowed for an excellent preservation of specimens, including the most fragile and delicate forms. This contrasts with the results obtained from the frankly pelagic sediments of Shatsky Rise (ODP Site 1209), where dissolution and recrystallization were dominant in controlling the nannofossil assemblage make-up. Dissolution and reprecipitation were extremely efficient in altering the original morphology of several taxa (e.g. Discoaster, *E. formosa*, *Dictyoccocites,..*) as well

as in completely dissolving other, normally common, but fragile EOT taxa (e.g. small reticulofenestrids), thus precluding any paleo-environmental interpretation.

The effects of diagenetic alteration occurred during the PRE-EOT phase in the basal portion of the succession, severely altered the bulk stable isotopic data, resulting in extremely anomalous $\delta^{18}O$ and $\delta^{13}C$ values. On the other hand, the geochemical signature recorded in the remaining part of the study interval, approximately started from 34.7 Ma, seems to be not compromised, although the effects of recrystallization on the nannofossil assemblage were severe during this phase. Thus, despite some diagenetic issues, we were able to recognize the primary global signature of the Eocene-Oligocene transition. To conclude, while our result seems to suggest the maintenance of the primary EOT $\delta^{18}O$ signal even in a poorly preserved carbonate-rich sediment, this outcome should be further tested over wide areas, in similar depositional settings.

Acknowledgements

The authors are grateful to the Integrated Ocean Drilling Program (IODP) for providing samples and data used in this study. The IODP is sponsored by the U.S. National Science Foundation (NSF) and participating countries under the management of Joint Oceanographic Institutions, Inc. Isabella Raffi and Davide Persico are deeply thanked for their constructive comments in the capacity of reviewers of A.V.' s PhD thesis during the evaluation process required by Italian law. TW was funded by the Deutsche Forschungsgemeinschaft (DFG, German Research Foundation) under Germany´s Excellence Strategy – EXC-2077 – 390741603.

A. V. and C. A. were supported by University of Padova.

Datasets used in this work can be found in the **Appendix VI**.

PLATE 5.1

Scanning electron photomicrographs showing the preservation of PRE-EOT calcareous nannofossils from Site U1411 (sample U1411-21X-CC, 25-33cm). **Figures**:

1-6 Analysis scan mode micrographs showing the assemblage constituents.

7-8 Same specimen of ***Discoaster barbadiensis*** shown in UH resolution (7) and analysis scan mode (8). The UH resolution micrographs (8, 9) highlight the extremely good preservation of the specimen.

9 Another specimen of ***Discoaster barbadiensis*** with no evidence for diagenetic overgrowth on the rays.

10-12 UH resolution (11) and analysis scan mode (10) of ***Discoaster saipanensis***.

13-15 Specimens of ***Discoaster robustus*** with 10 (13-14) and 11 rays (15), respectively**.**

16 Distal view of ***Coccolithus pelagicus*** with intact elements.

17 Distal view of ***Clausicoccus fenestratus*** with its high perforated plate in the central area.

18 ***Cribrocentrum reticulatum*** (<12 μm), proximal view. The narrow central area is spanned by a robust and visible grid.

19-20 UH resolution (19) and analysis scan mode (20) of ***Chiasmolithus*** **cf.** ***C. altus*** in distal view. The micrograph shows the cross bars with their complex construction.

21 ***Discoaster saipanensis*** showing a high-defined central stem and distinct radial sutural ridges and depressions.

22 Distal view of ***Chiasmolithus oamaruensis*****.**

23 ***Ericsonia formosa,*** distal view**.**

24. Proximal view of reticulofenestrids. The right specimen (***Reticulofenetra daviesii***) exhibits a delicate and well-preserved net in the central area.

PLATE 5.1

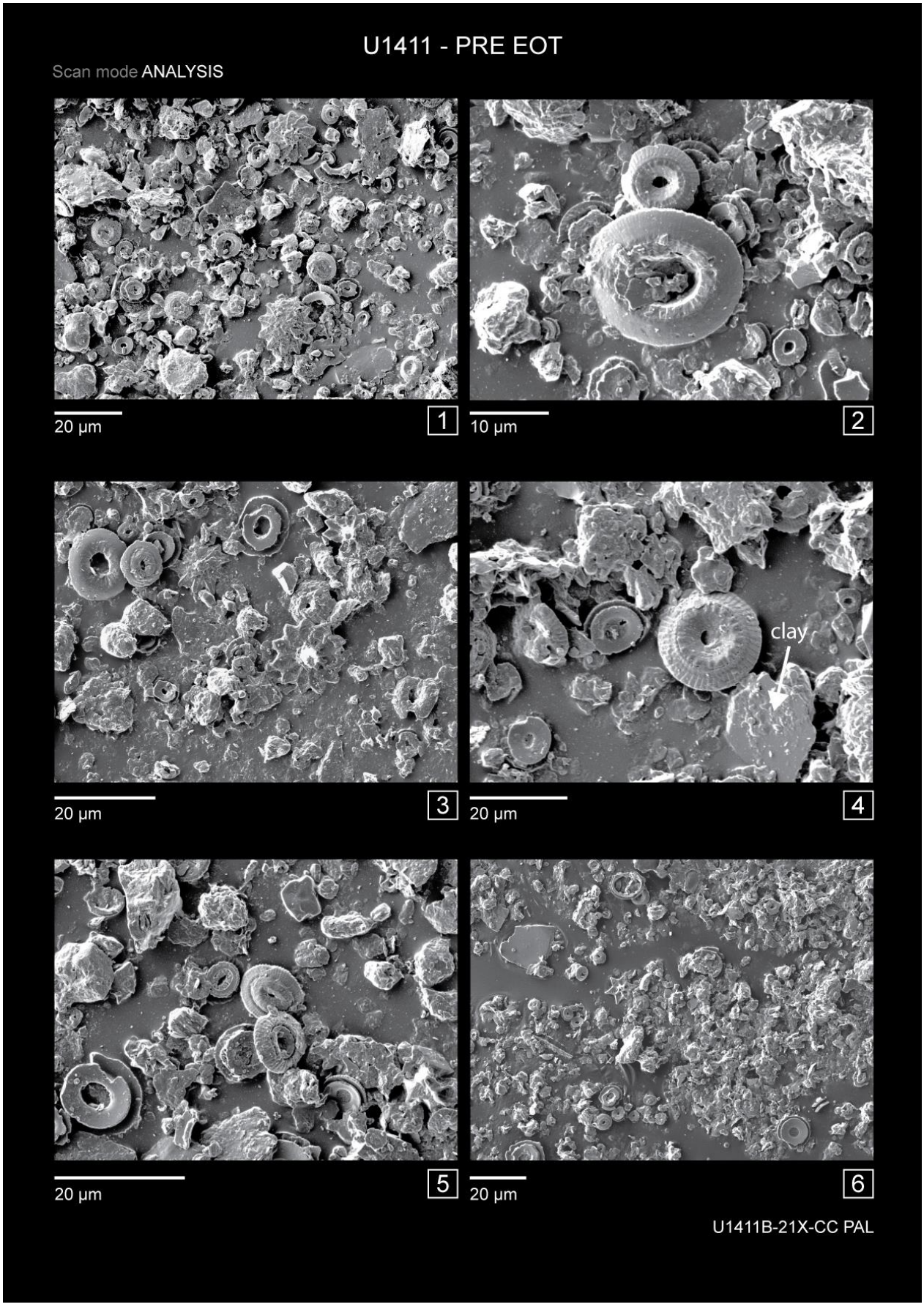
U1411 - PRE EOT
Scan mode ANALYSIS
20 µm
1
10 µm
2
20 µm
3
clay
20 µm
4
20 µm
5
20 µm
6
U1411B-21X-CC PAL

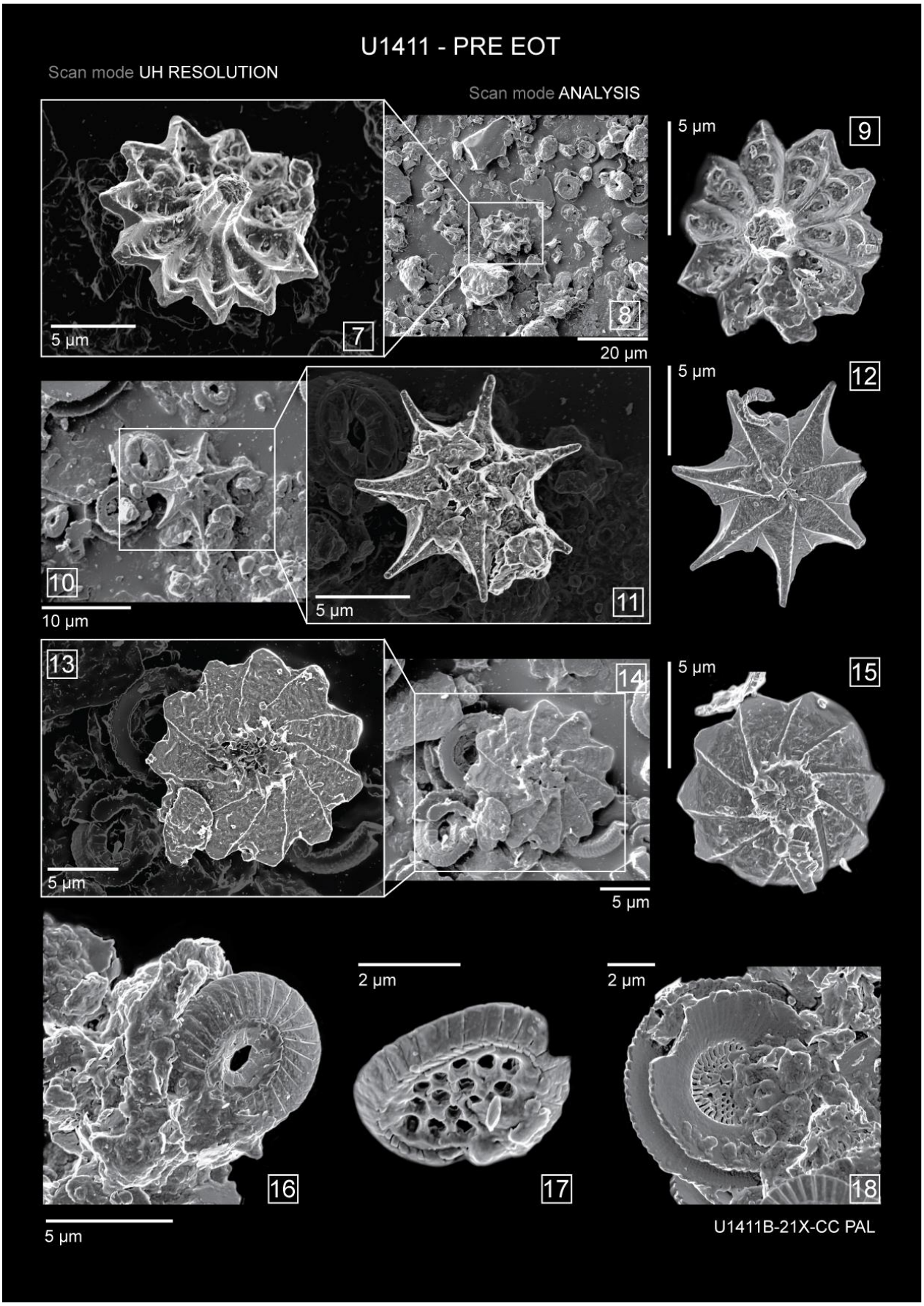
U1411 - PRE EOT
Scan mode UH RESOLUTION
Scan mode ANALYSIS
5 µm
7
8
20 µm
5 µm
9
10
10 µm
5 µm
11
5 µm
12
13
5 µm
14
5 µm
5 µm
15
2 µm
2 µm
16
17
18
5 µm
U1411B-21X-CC PAL

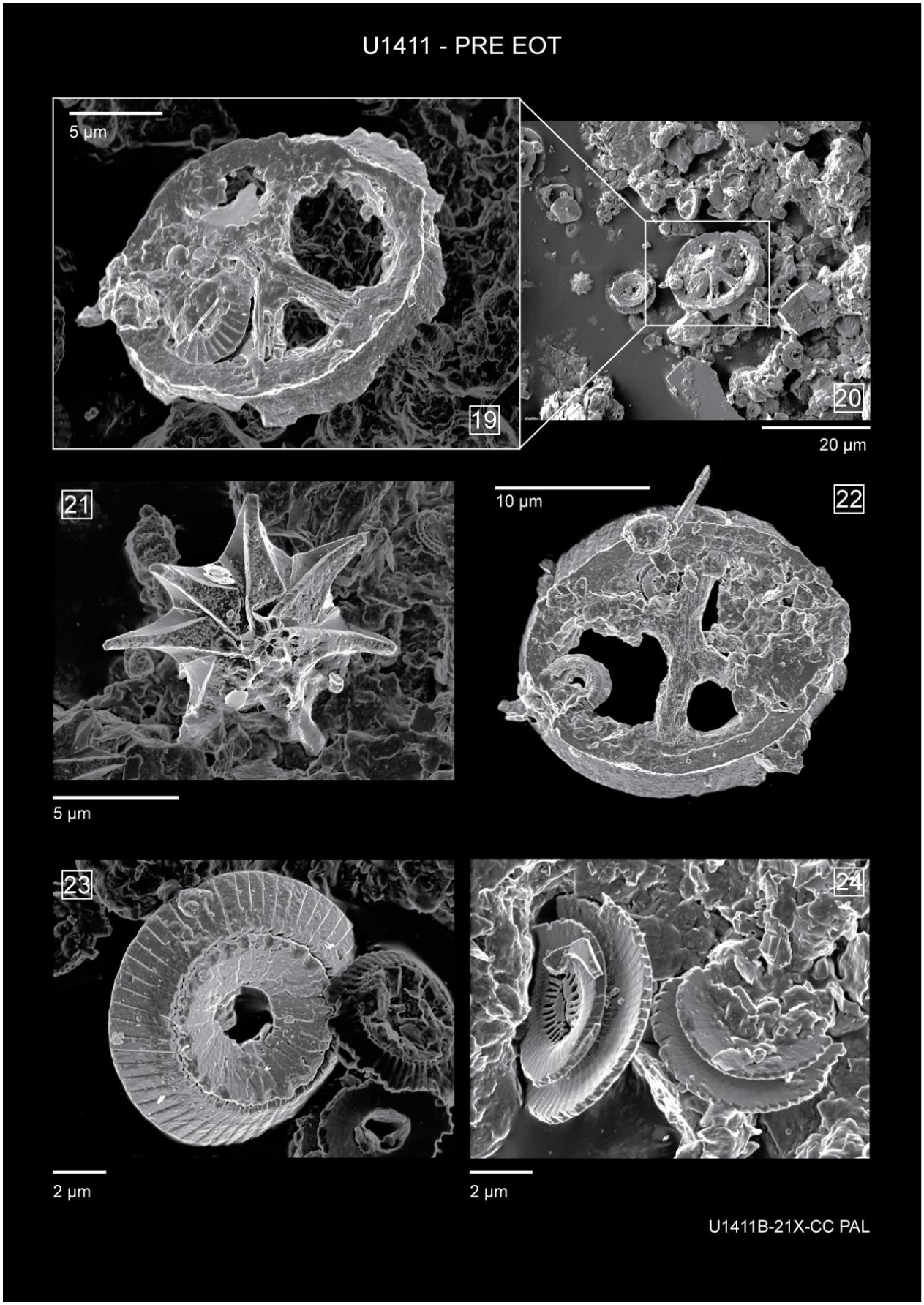
U1411 - PRE EOT
5 µm
19
20
20 µm
21
10 µm
22
5 µm
23
24
2 µm
2 µm
U1411B-21X-CC PAL

PLATE 5.2

Scanning electron photomicrographs showing the preservation of PRE-EOT calcareous nannofossils from Site 1209 (sample 1209C-4H-3, 93cm). **Figures**:

1-6 Analysis scan mode micrographs showing the assemblage constituents.

7 ***Bramletteius serraculoides*** with severe overgrowth along the c-axis.

8-9 ***Dictyococcites bisectus,*** one of the most dissolution-resistant species at the E-O transition, here displays blocky accretions in its central plug due to secondary calcite deposition **(9).**

10 ***Discoaster saipanensis*** showing slight overgrowth.

11 ***Discoaster barbadiensis*** which has accreted a large amount of calcite cement.

12-13 ***Discoaster*** **spp.** displaying heavily overgrowth.

14 ***Reticulofenestra umbilicus*** lacking the central area delicate grid.

15 Distal shield of ***Ericsonia formosa*** partially fractured and dissolved. Dissolution also affects the elements of the distal central area.

16 Distal view of poorly preserved ***Coccolithus pelagicus*.**

17 ***Isthmolithus recurvus*** fully coated by secondary calcite deposition.

18 Moderately preserved ***Discoaster saipanensis***.

19 ***Discoaster saipanensis*** to the left and ***Reticulofenestra umbilicus*** (>14 μm) to the right.

PLATE 5.2

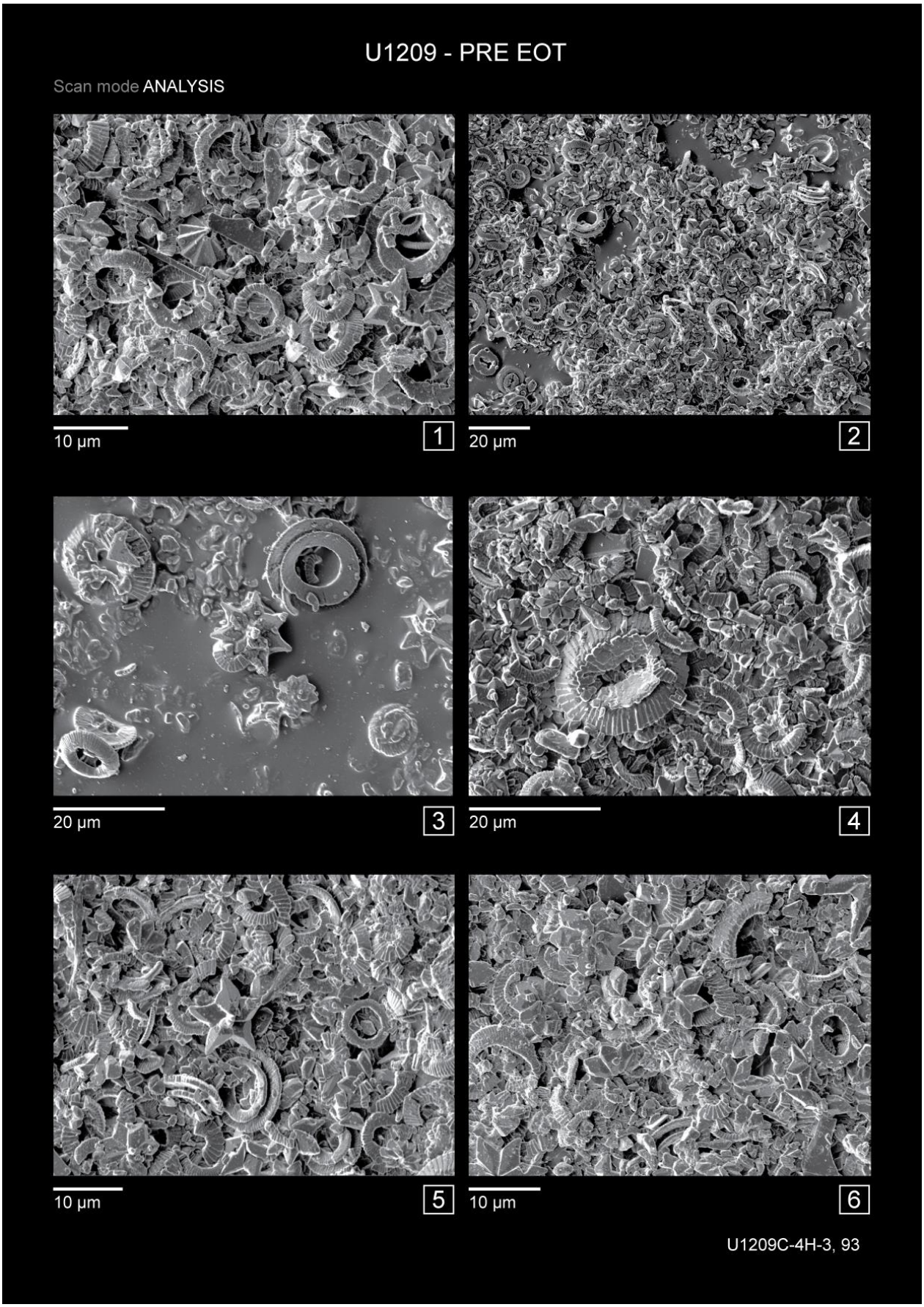
U1209 - PRE EOT
Scan mode ANALYSIS
10 µm
1
20 µm
2
20 µm
3
20 µm
4
10 µm
5
10 µm
6
U1209C-4H-3, 93

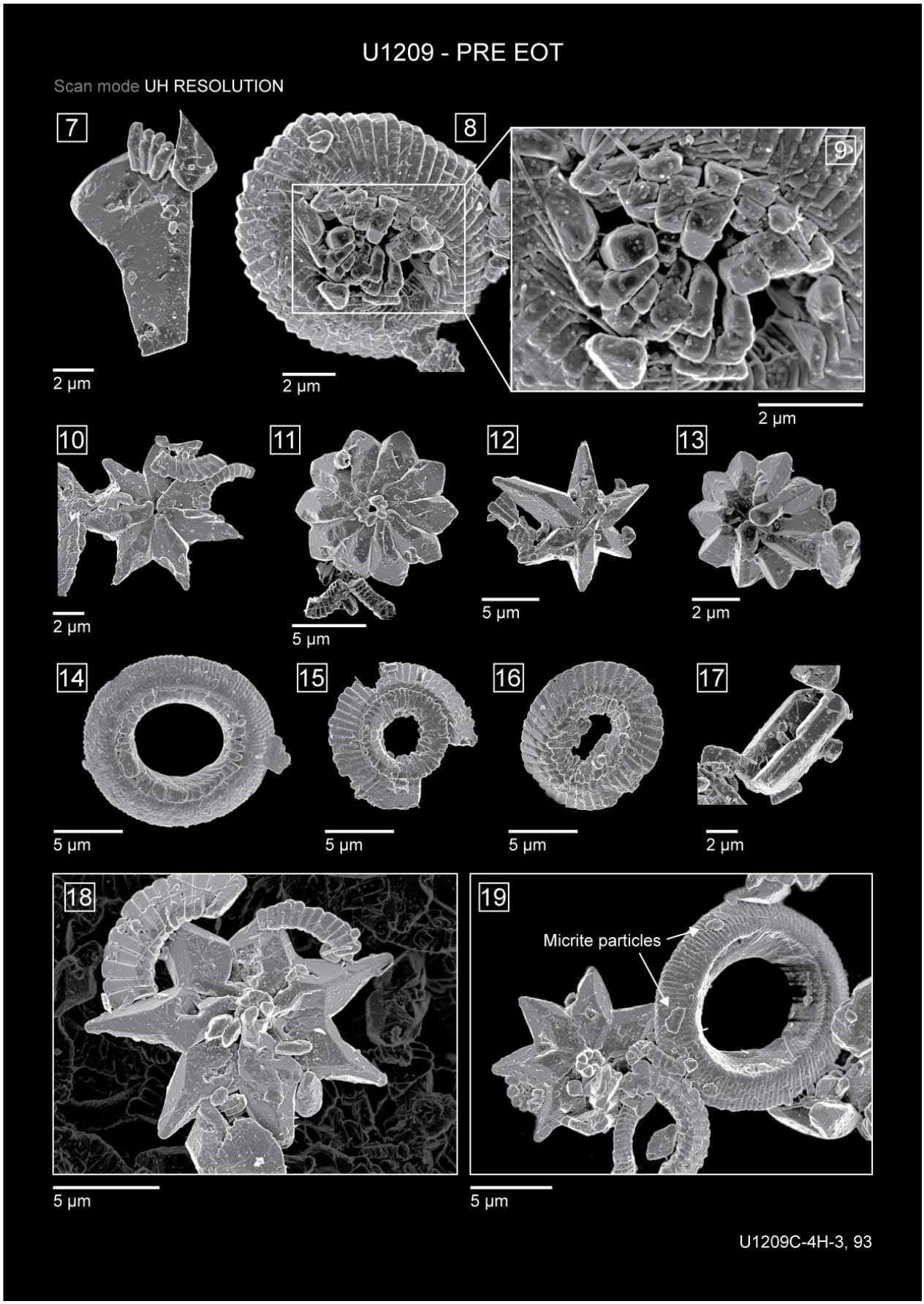
U1209 - PRE EOT
Scan mode UH RESOLUTION
7
8
9
2 µm
2 µm
2 µm
10
11
12
13
2 µm
5 µm
5 µm
2 µm
14
15
16
17
5 µm
5 µm
5 µm
2 µm
18
19
Micrite particles
5 µm
5 µm
U1209C-4H-3, 93

PLATE 5.3

Scanning electron photomicrographs showing the preservation of Late Eocene Event calcareous nannofossils from Site U1411 (sample U1411B-19H-4W, 30cm). **Figures**:

1-6 Analysis scan mode micrographs showing the assemblage constituents.

7-8 Well preserved ***R. umbilicus*** (> 14 μm) with open central area spanned by delicate net remains.

9 Proximal view of ***R. daviesii*** with a robust grill with elongated perforations.

10 Distal view of ***C. pelagicus***.

11 ***Discoaster*** **cf.** ***D. tanii*** with a prominent stem on one side showing minor overgrowth.

12 ***I. recurvus*** exceptionally well preserved.

13 ***S. moriformis*** **gr.,** lateral view.

14 ***D. bisectus*** shows no sign of dissolution and/or overgrowth.

15 Extremely well preserved specimen of ***E. formosa***.

PLATE 5.4

Scanning electron photomicrographs showing the preservation of Late Eocene Event calcareous nannofossils from Site 1209 (sample 1209A-14H-4W, 115cm). **Figures**:

1-6 Analysis scan mode micrographs showing the assemblage components. The arrow in Fig. 1 shows the welded elements of the proximal shield that characterize most of placoliths.

7 ***Discoaster tanii*** showing euhedral crystal faces along the rays.

8 Distal view of ***D. bisectus*** showing extreme overgrowth of its central plug. Some fragments and other species are cemented to its distal shield.

9 Broken wall of ***Thoracosphaera*** **spp.** showing the mosaic grains.

10 Unknown fragment.

11 ***E. formosa*** showing extremely well-preserved external rim giving the placolith a smooth circular outline. The elements of the central area are characterized by severe recrystallization.

12 ***R. umbilicus*** in distal view lacking the central area net.

13 ***B. ovatus*** displaying moderate overgrowth with the two column-like shields partly welded.

14 ***Sphenolithus pseudoradians*****.**

15 Several specimens of ***D. bisectus*** showing differential growth of central plug elements by accretion of secondary calcite.

16 Micrographs showing some of the major assemblage constituents, including ***Sphenolithus moriformis,*** ***Dictyococcites*** **spp.,** ***Reticulofenestra*** **spp.**. An "euhedral" ***Discoaster*** is also shown, the center of which is pitted (arrow).

PLATE 5.3

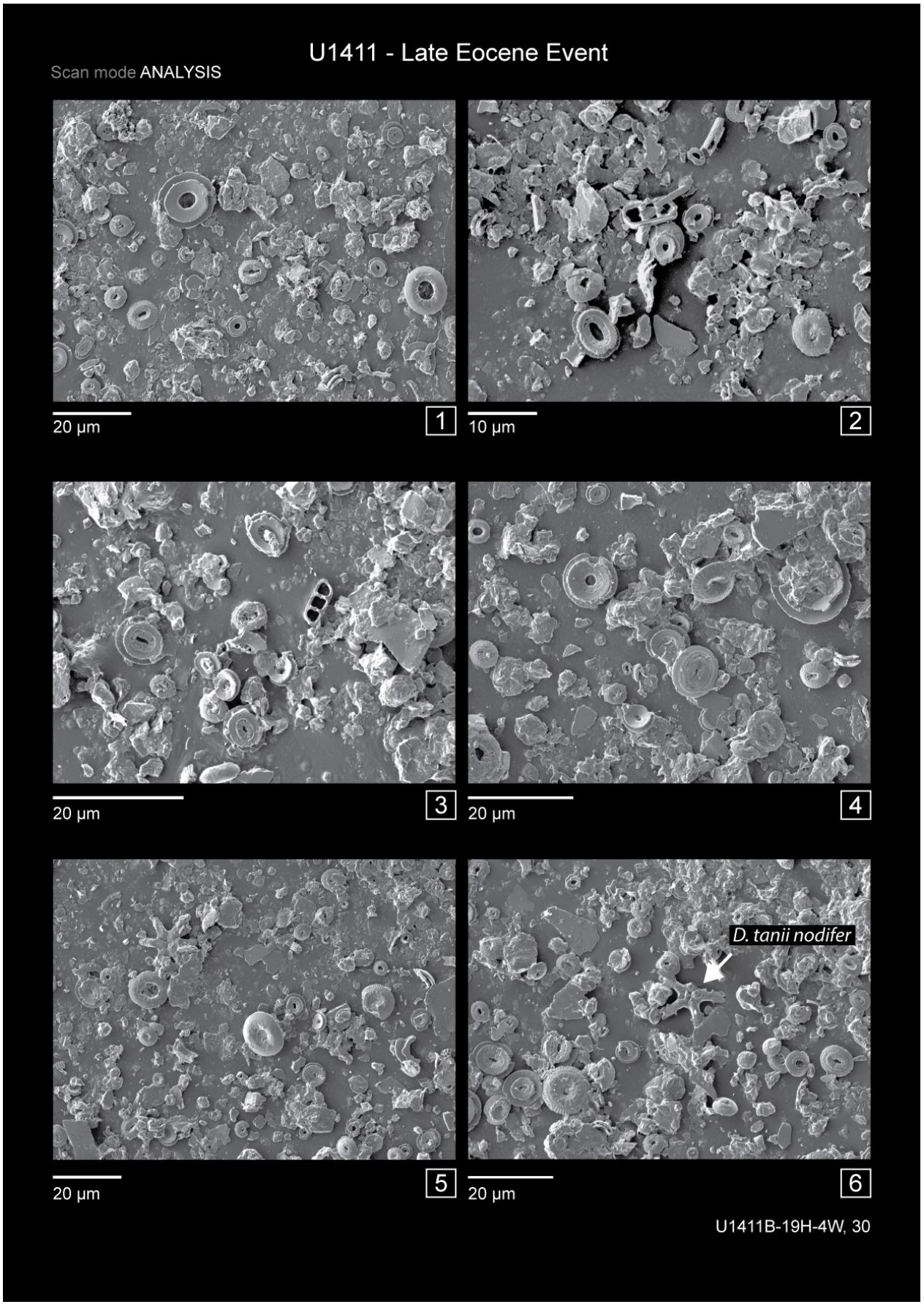
U1411 - Late Eocene Event
Scan mode ANALYSIS
20 µm
1
10 µm
2
20 µm
3
20 µm
4
20 µm
5
D. tanii nodifer
20 µm
6
U1411B-19H-4W, 30

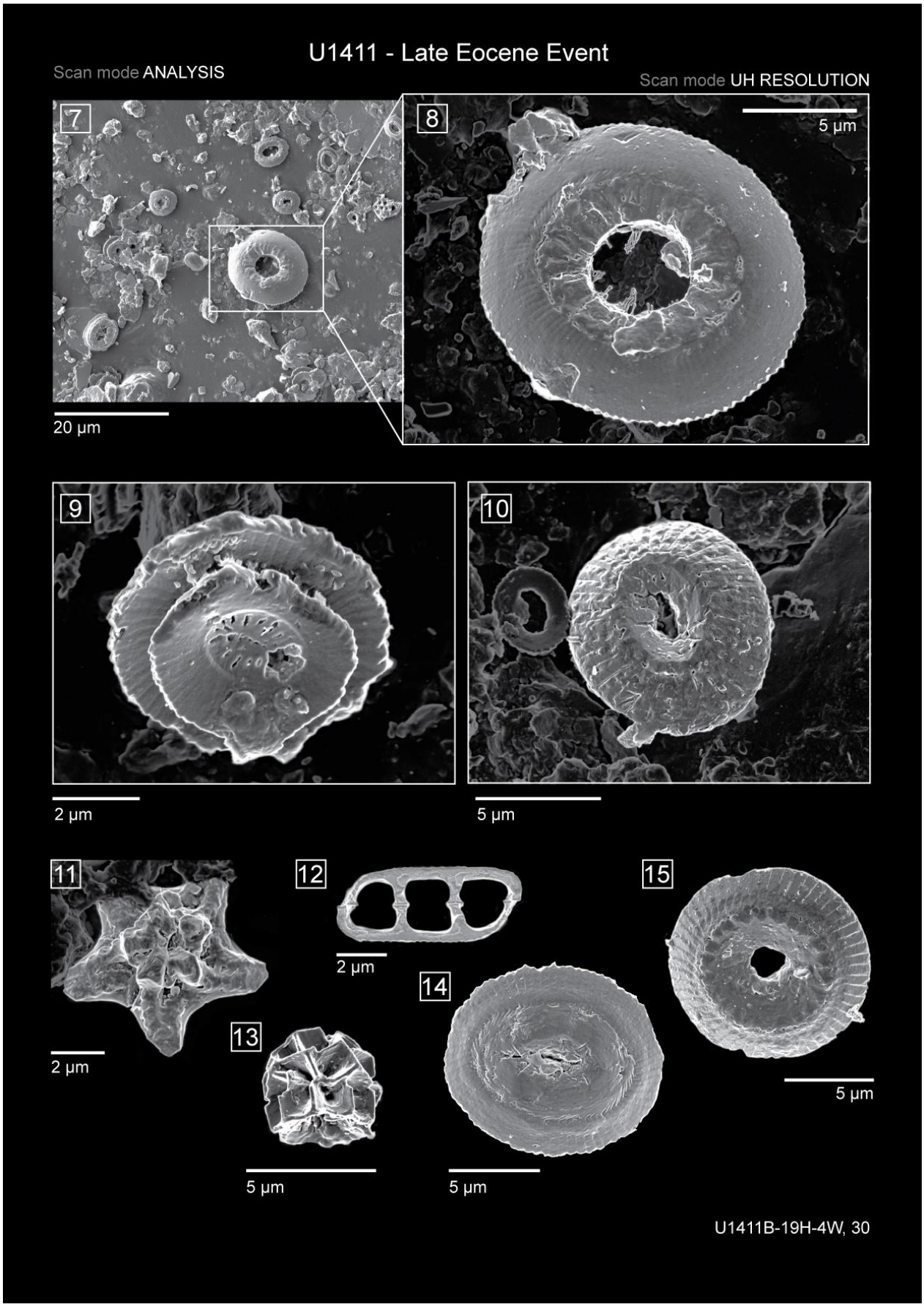
U1411 - Late Eocene Event
Scan mode ANALYSIS
Scan mode UH RESOLUTION
7
8
5 µm
20 µm
9
10
2 µm
5 µm
11
12
15
2 µm
14
13
2 µm
5 µm
5 µm
U1411B-19H-4W, 30

PLATE 5.4

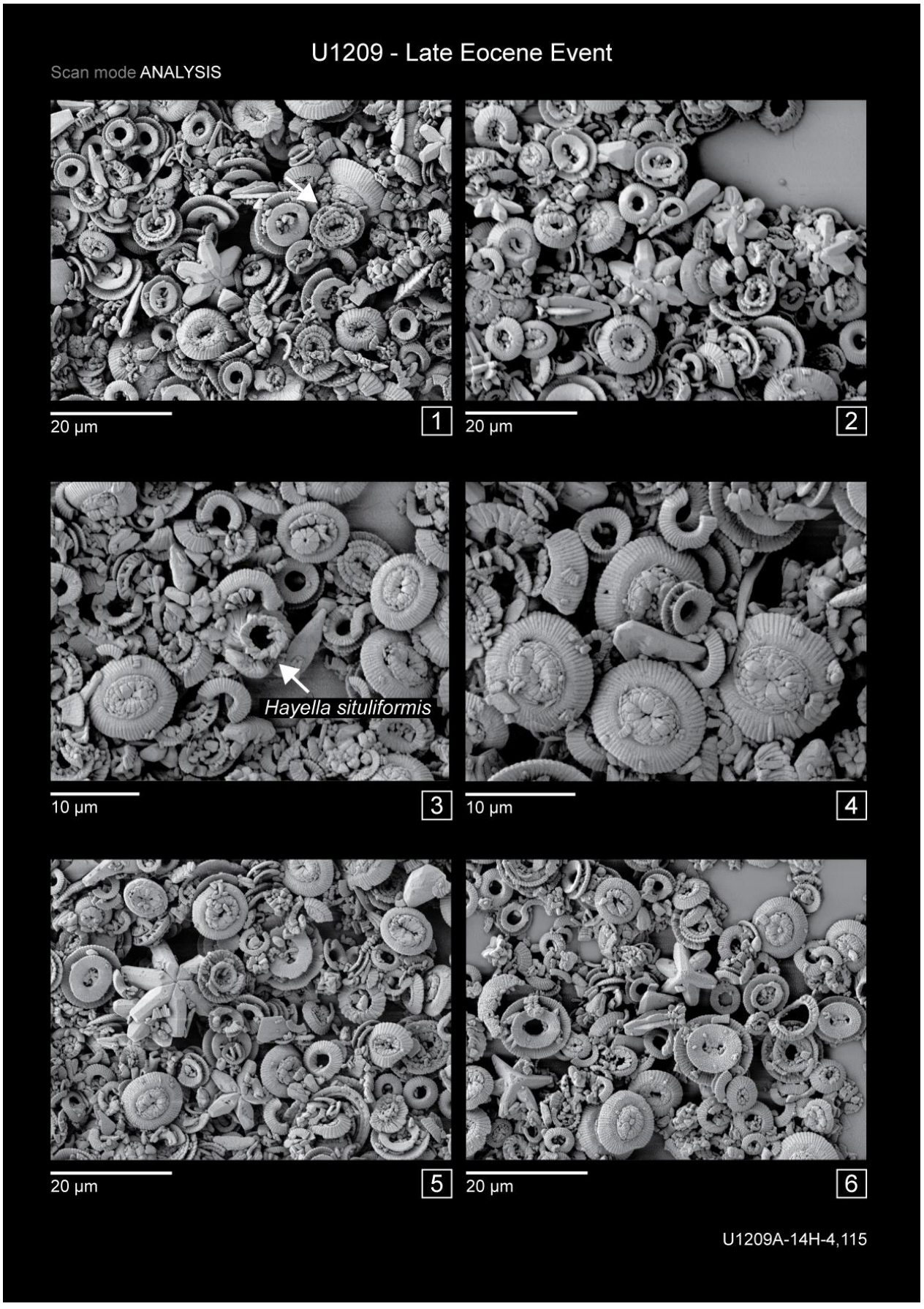
U1209 - Late Eocene Event
Scan mode ANALYSIS
20 µm
1
20 µm
2
Hayella situliformis
10 µm
3
10 µm
4
20 µm
5
20 µm
6
U1209A-14H-4,115

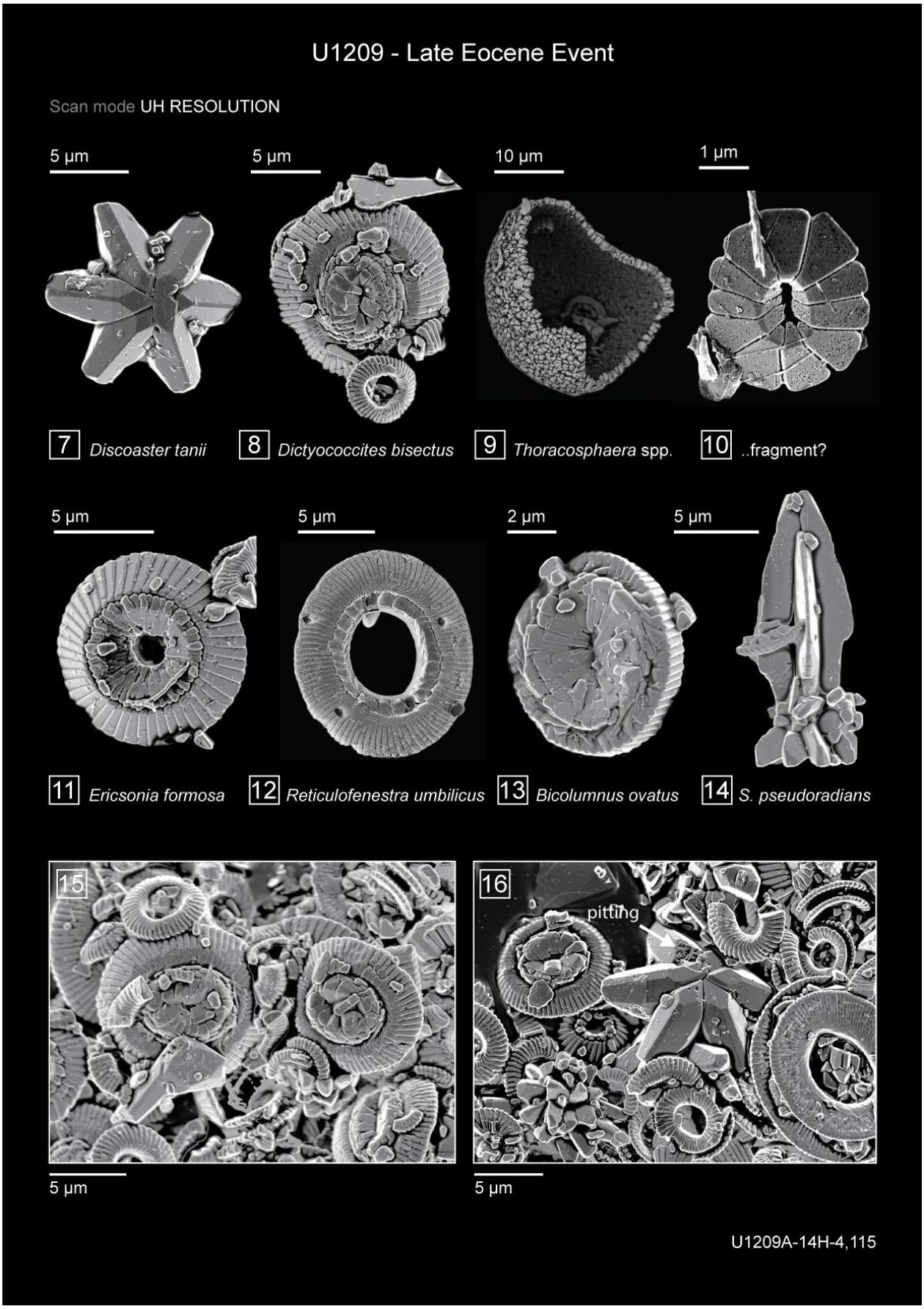
U1209 - Late Eocene Event
Scan mode UH RESOLUTION
5 µm
5 µm
10 µm
1 µm
7 Discoaster tanii
8 Dictyococcites bisectus
9 Thoracosphaera spp.
10 ..fragment?
5 µm
5 µm
2 µm
5 µm
11 Ericsonia formosa
12 Reticulofenestra umbilicus
13 Bicolumnus ovatus
14 S. pseudoradians
15
16
pitting
5 µm
5 µm
U1209A-14H-4,115

PLATE 5.5

Scanning electron photomicrographs showing the preservation of EOT calcareous nannofossils from Site U1411 (sample U1411B-17H-7A, 25 cm). **Figures**:

1-6 Analysis scan mode micrographs showing the assemblage constituents.

7-8 ***C. subdistichus,*** distal view.

9 ***E. formosa,*** distal view.

10 ***Pontosphaera*** **spp.**

12 ***I. recurvus*** specimens showing exceptional preservation.

13 ***C. subdistichus,*** proximal view.

14 Proximal view of the basal disc of ***B. serraculoides***, which is slightly dissolved along the edges.

15 ***I. recurvus*** overlaying a proximal placolith.

16 Proximal view of ***R. umbilicus*** displaying the central grid.

17-18 Coccosphere of ***E. formosa*** acquired with the analysis and (**17**) with UH resolution scan mode (**18**).

19 Proximal view of ***R. daviesii***.

20. ***S. moriformis***.

21 ***D. tanii nodifer***.

22 ***C. pelagicus***.

PLATE 5.6

Scanning electron photomicrographs showing the preservation of EOT calcareous nannofossils from Site 1209 (sample 1209C-3H-6, 90 cm). **Figures**:

1-6 Analysis scan mode micrographs showing the assemblage constituents.

7-8 ***S. predistentus*** acquired with the analysis and (**7**) with UH resolution scan mode (**8**).

9-10 ***Discoaster*** **spp**. in UH resolution (**9**) and analysis scan mode (**10**). The specimens show heavy overgrowth.

11 ***Coccolithus pelagicus*** with the R elements of the upper tube slightly overgrown.

12 ***D. bisectus*** with secondary calcite overgrowths in the central plug.

PLATE 5.5

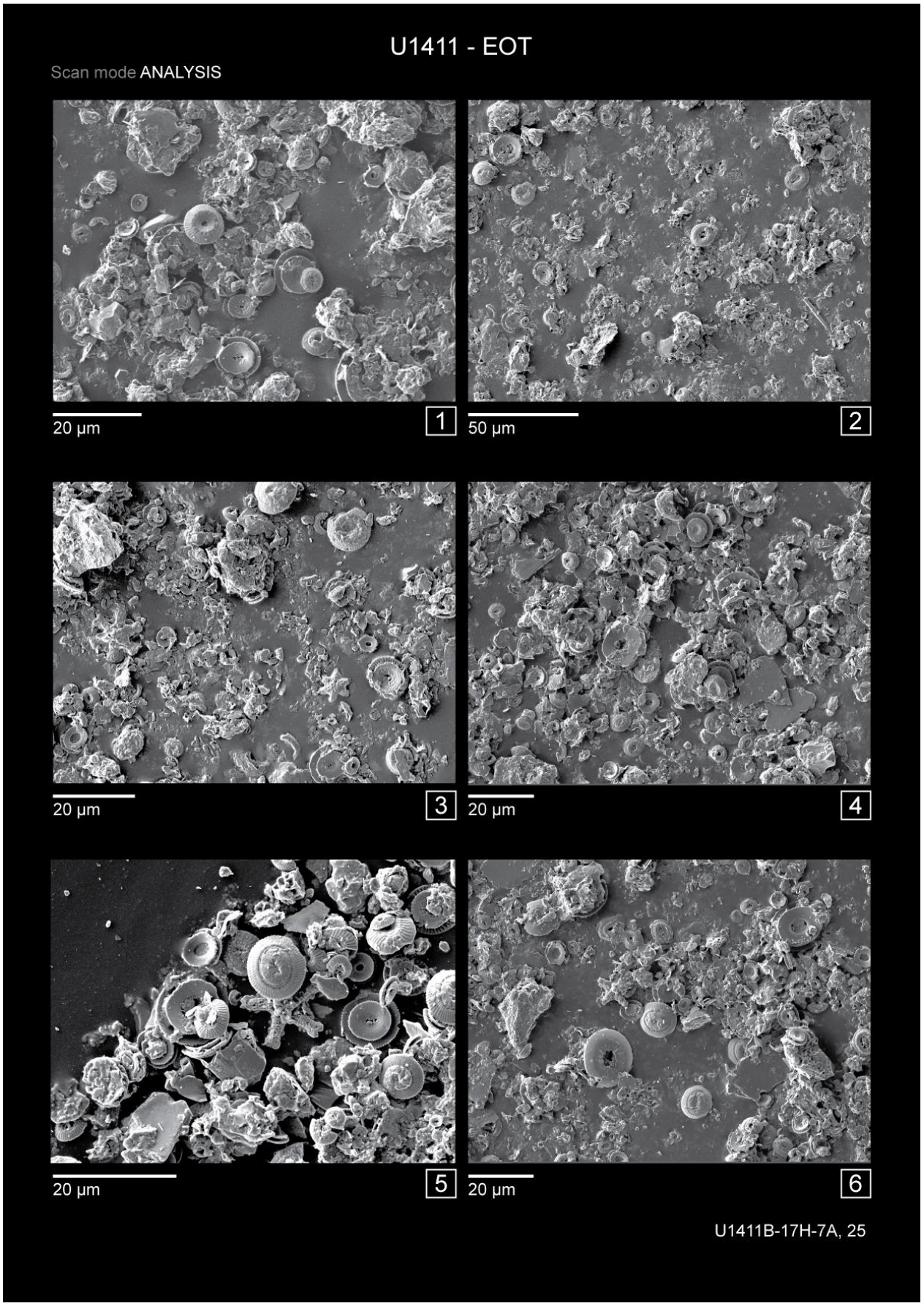
U1411 - EOT
Scan mode ANALYSIS
20 µm
1
50 µm
2
20 µm
3
20 µm
4
20 µm
5
20 µm
6
U1411B-17H-7A, 25

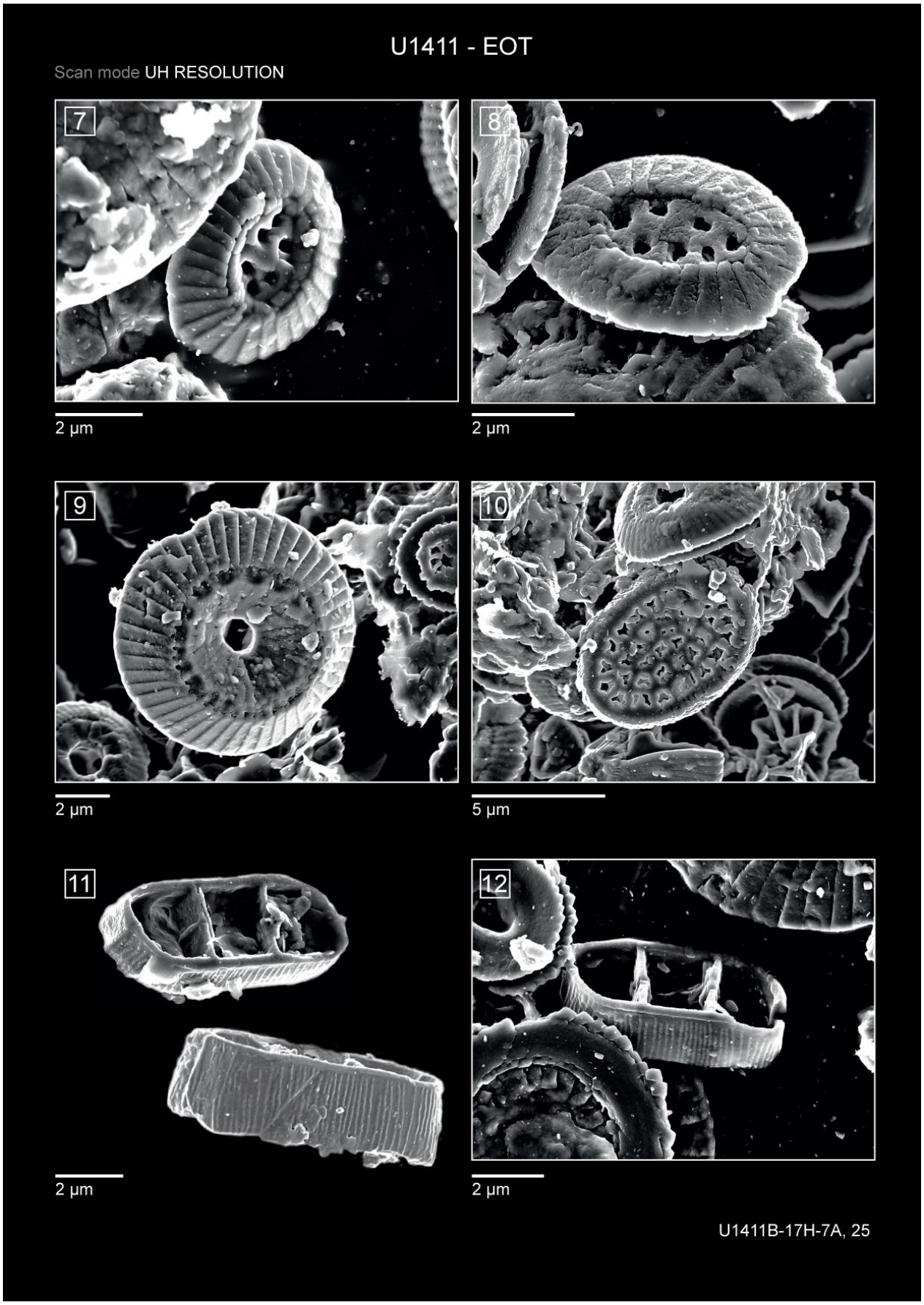
U1411 - EOT
Scan mode UH RESOLUTION
7
2 µm
8
2 µm
9
2 µm
10
5 µm
11
2 µm
12
2 µm
U1411B-17H-7A, 25

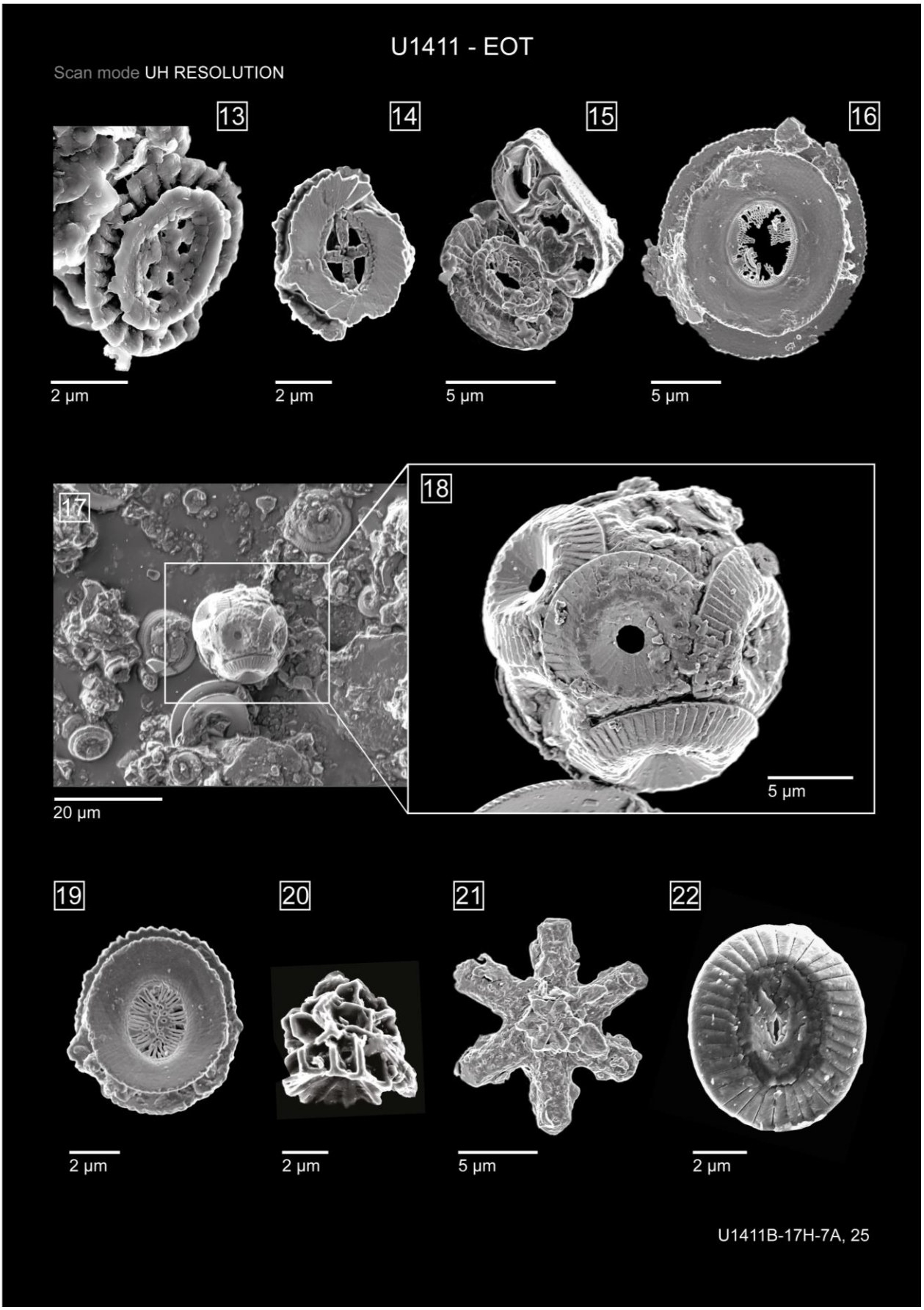
U1411 - EOT
Scan mode UH RESOLUTION
13
14
15
16
2 µm
2 µm
5 µm
5 µm
17
18
20 µm
5 µm
19
20
21
22
2 µm
2 µm
5 µm
2 µm
U1411B-17H-7A, 25

PLATE 5.6

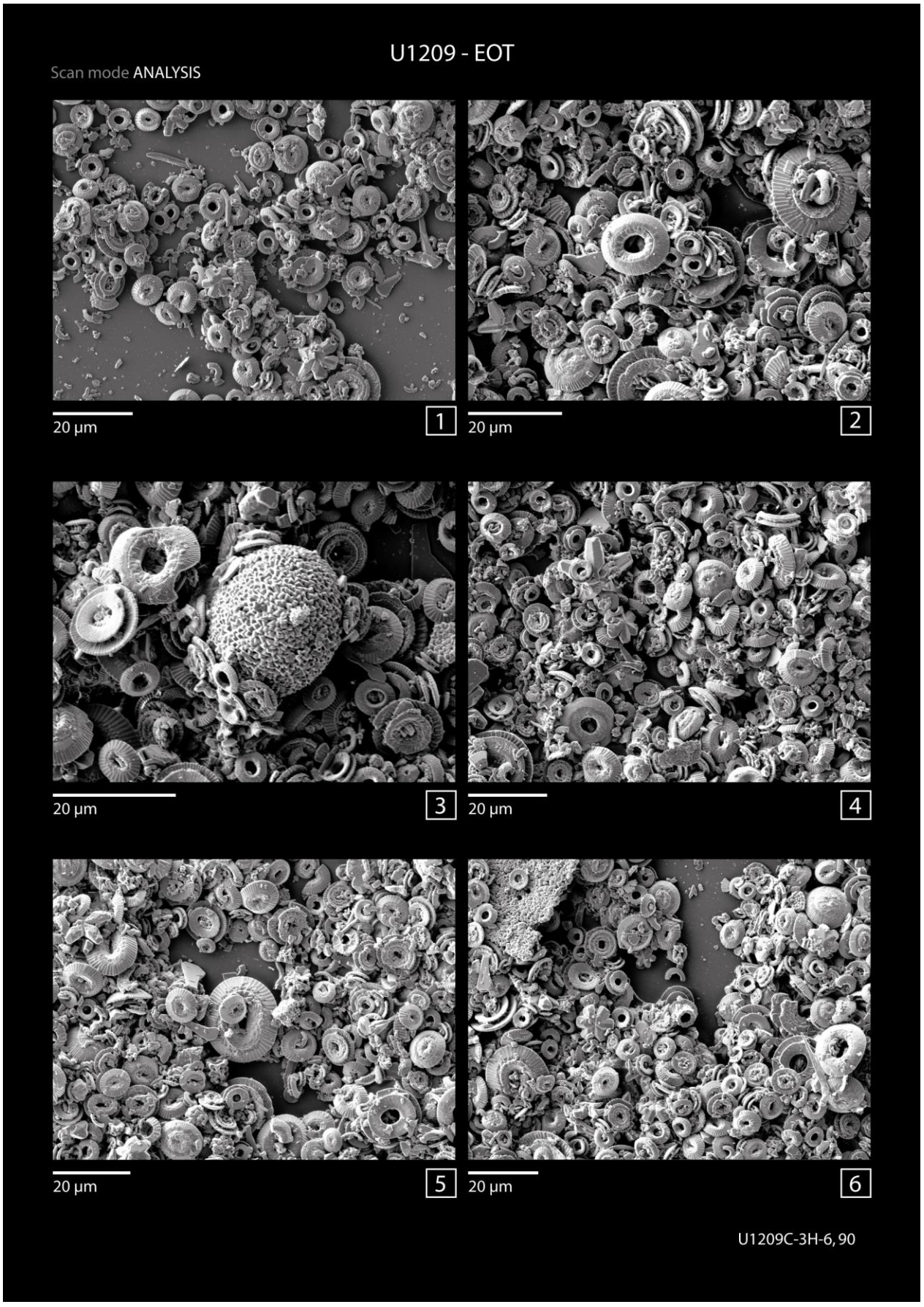
U1209 - EOT
Scan mode ANALYSIS
20 µm
1
20 µm
2
20 µm
3
20 µm
4
20 µm
5
20 µm
6
U1209C-3H-6, 90

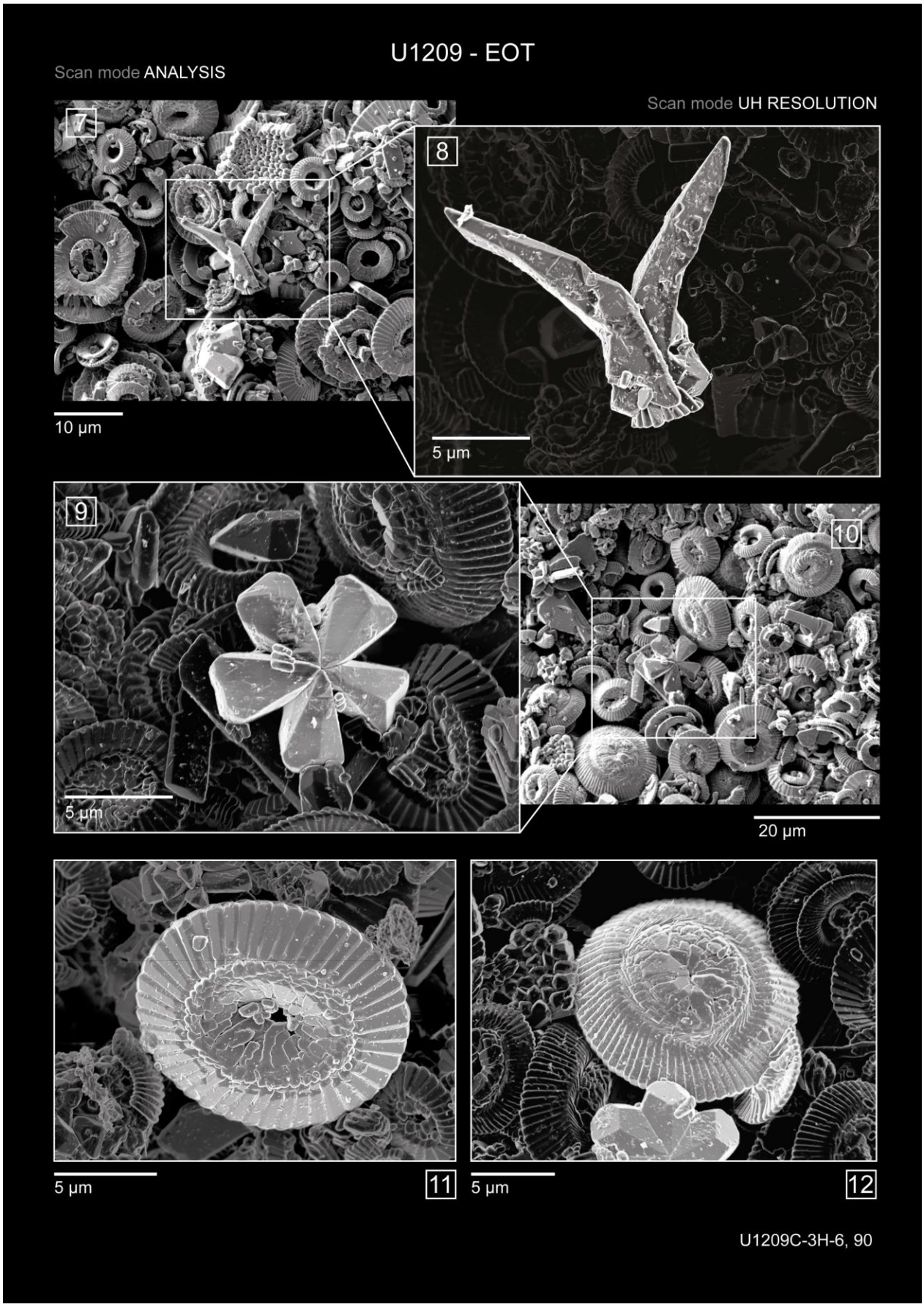
U1209 - EOT
Scan mode ANALYSIS
Scan mode UH RESOLUTION
7
8
10 µm
5 µm
9
10
5 µm
20 µm
5 µm
11
5 µm
12
U1209C-3H-6, 90

PLATE 5.7

Scanning electron photomicrographs showing the preservation of EOGM calcareous nannofossils from Site U1411 (Sample U1411-16H-1W, 50 cm). **Figures**:

1-6 Analysis scan mode micrographs showing the assemblage constituents, which are partly covered by a thin coating of clay minerals.

7 ***Pontosphaera*** **spp**.

8 ***Isthmolithus recurvus***.

9 ***Dictyococcites bisectus*** showing exceptional preservation.

10 ***Blackites*** **spp.**

11 ***Clausicoccus subdistichus*** (distal side) and small reticulofenestrid (proximal side).

12 ***E. formosa,*** distal shield.

13 ***R. umbilicus*** with ***C. subdistichus*** leaning over.

14 ***Discoaster distinctus***.

15 Proximal side of ***R. umbilicus***.

16 ***Sphenolithus moriformis*** and a spine fragment of ***Blackites***.

17 Proximal view of ***R. dictyoda***.

18 ***Pontosphaera pulcheroides***.

19 Undetermined coccosphere.

20 ***Bramletteius serraculoides,*** base.

21 ***Helicosphaera reticulata***.

PLATE 5.8

Scanning electron photomicrographs showing the preservation of EOGM calcareous nannofossils from Site 1209 (Sample 1209-3H-5, 35 cm). **Figures**:

1-6 Analysis scan mode micrographs showing the assemblage constituents.

7 ***Sphenolithus moriformis***.

8 ***Hayella situliformis***.

9 ***Dictyococcites bisectus***.

10 ***Sphenolithus*** **spp**.

11 ***Reticulofenestra umbilicus*** lacking the perforate net in the central area.

12 ***Coccolithus pelagicus***.

13, 14 ***E. formosa***.

15 ***Discoaster tanii***.

16 Indetermined placolith (proximal).

17, 18 ***Bramletteius serraculoides*** lateral view (**17**) and along the c-axis orientation (**18**).

19 ***Dictyococcites cf. D. hesslandii***.

PLATE 5.7

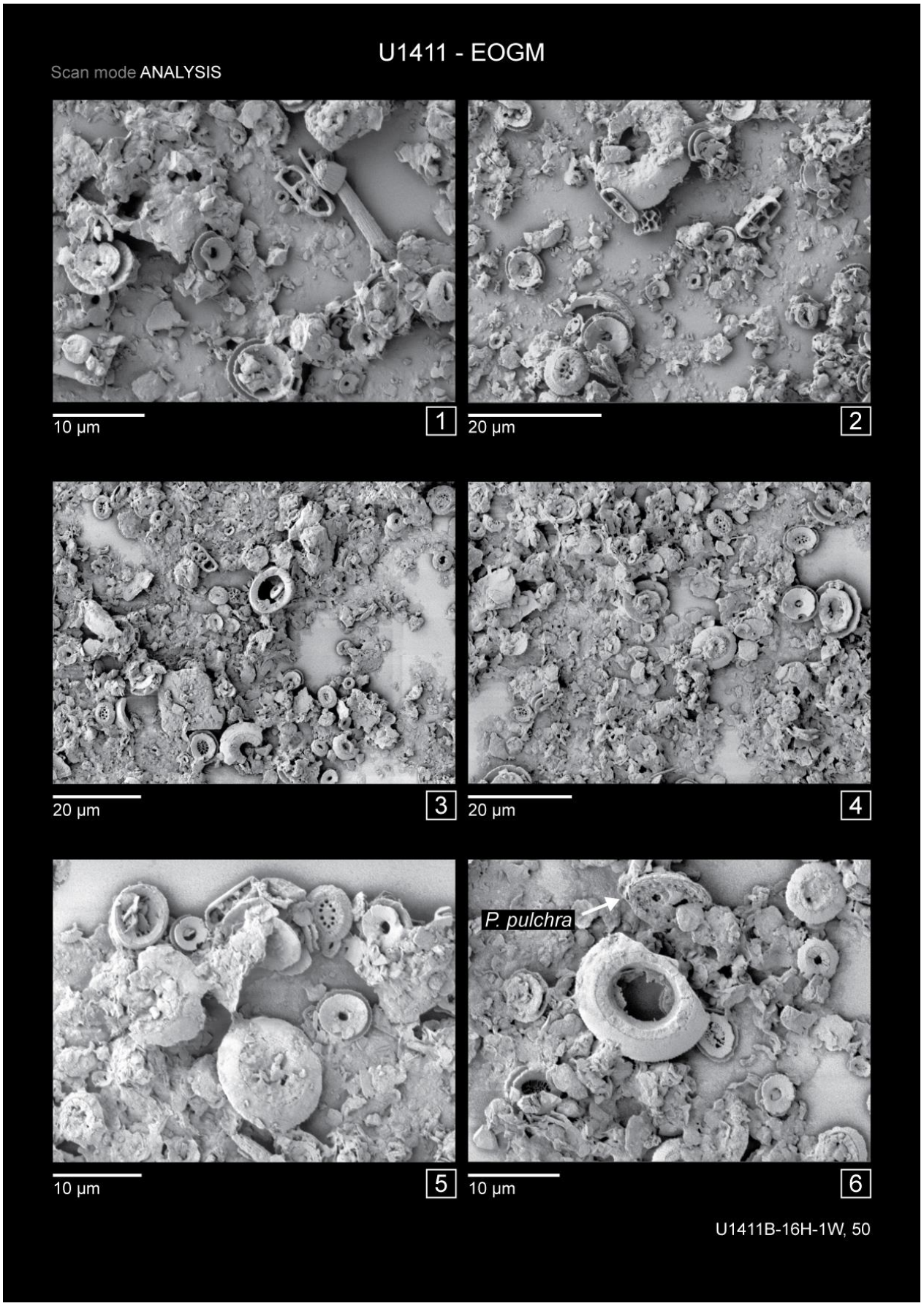
U1411 - EOGM
Scan mode ANALYSIS
10 µm
1
20 µm
2
20 µm
3
20 µm
4
10 µm
5
P. pulchra
10 µm
6
U1411B-16H-1W, 50

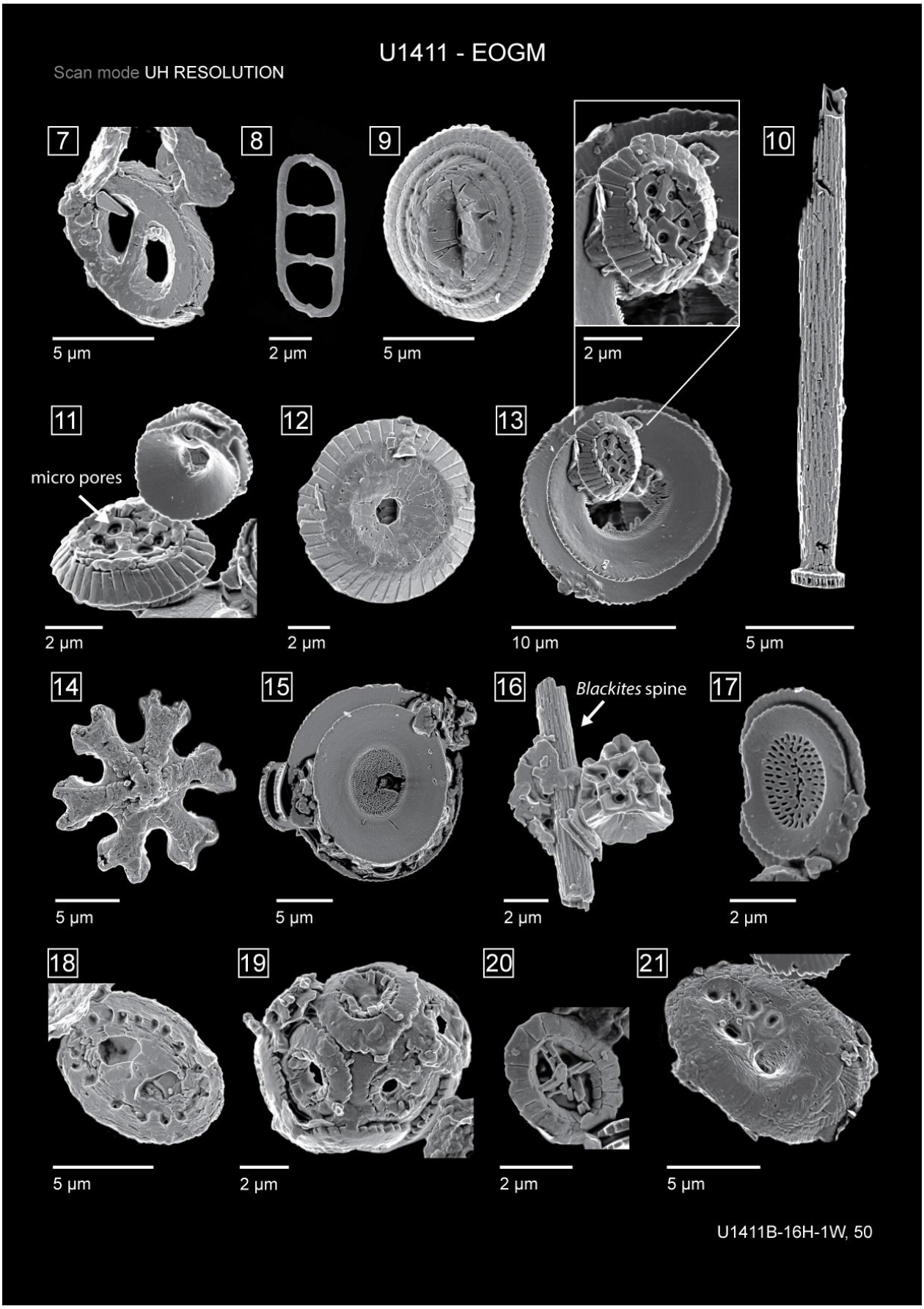
U1411 - EOGM
Scan mode UH RESOLUTION
7
8
9
10
5 µm
2 µm
5 µm
2 µm
11
12
13
micro pores
2 µm
2 µm
10 µm
5 µm
14
15
16
17
Blackites spine
5 µm
5 µm
2 µm
2 µm
18
19
20
21
5 µm
2 µm
2 µm
5 µm
U1411B-16H-1W, 50

PLATE 5.8

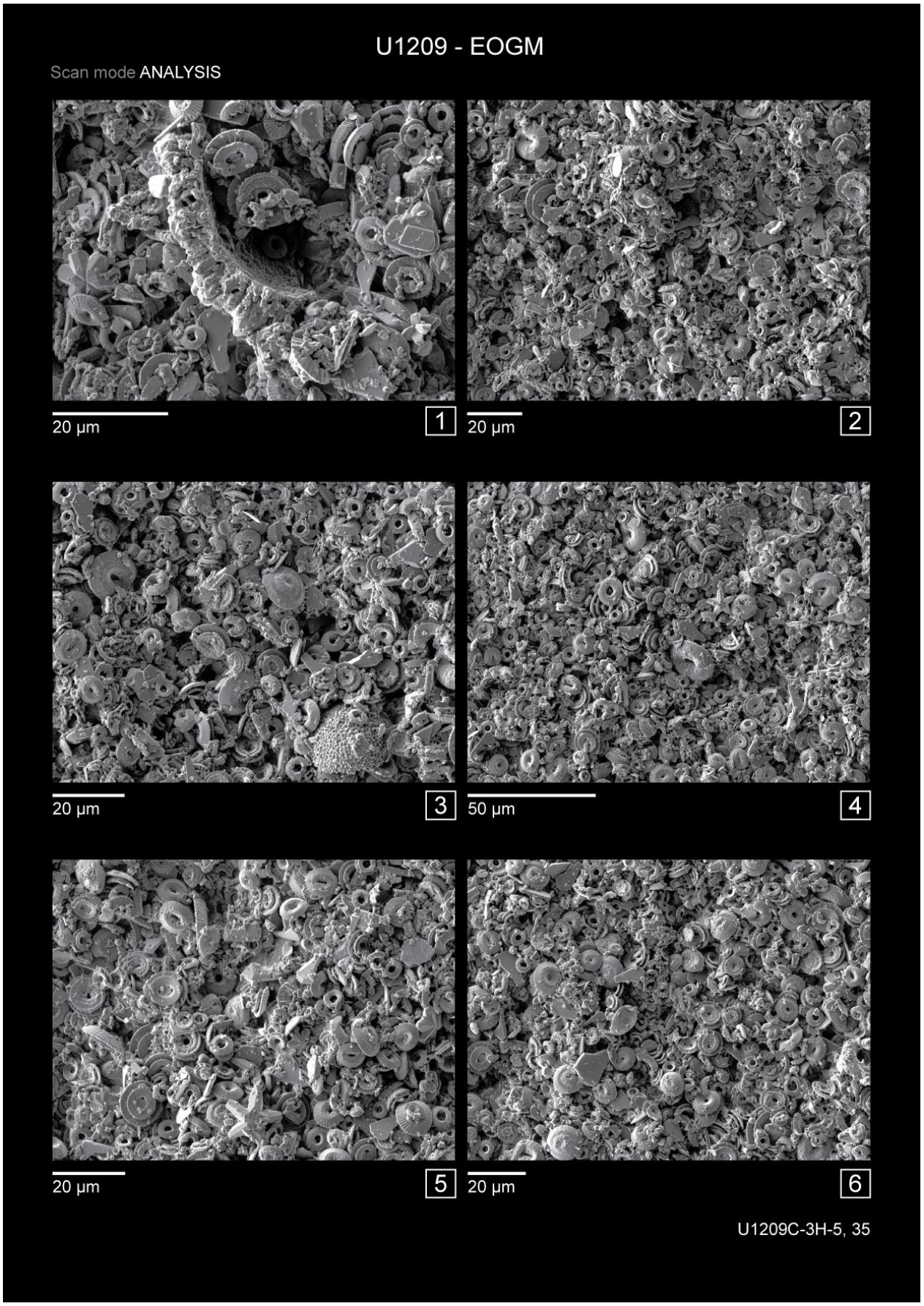
U1209 - EOGM
Scan mode ANALYSIS
20 µm
1
20 µm
2
20 µm
3
50 µm
4
20 µm
5
20 µm
6
U1209C-3H-5, 35

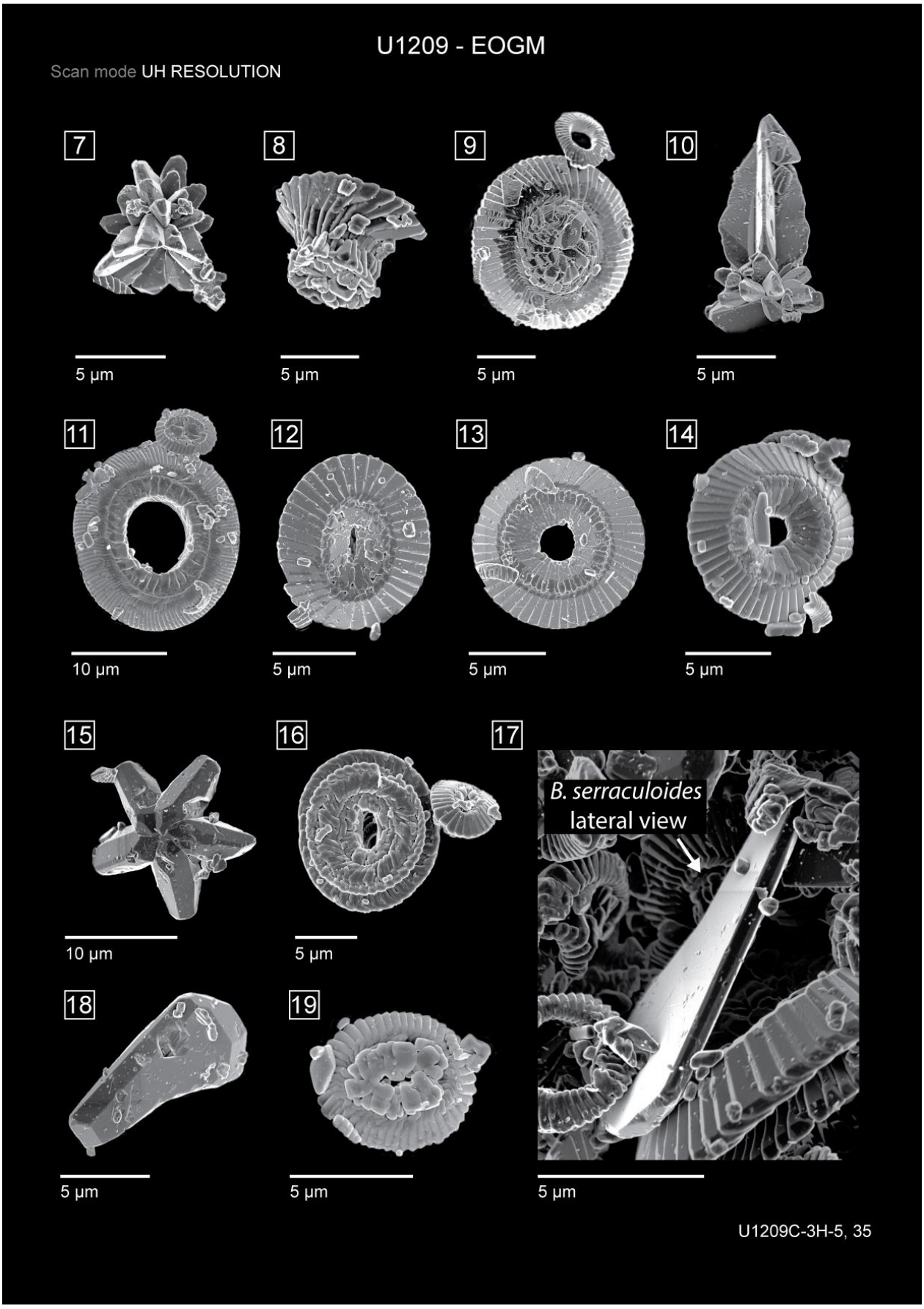
U1209 - EOGM
Scan mode UH RESOLUTION
7
8
9
10
5 µm
5 µm
5 µm
5 µm
11
12
13
14
10 µm
5 µm
5 µm
5 µm
15
16
17
10 µm
5 µm
B. serraculoides
lateral view
18
19
5 µm
5 µm
5 µm
U1209C-3H-5, 35

References

Adelseck, C.G., Geehan, G.W., Roth, P.H., 1973. Experimental evidence for the selective dissolution and overgrowth of calcareous nannofossils during diagenesis. Bulletin of the Geological Society of America 84, 2755–2762.

Agnini, C., Fornaciari, E., Raffi, I., Catanzariti, R., Pälike, H., Backman, J., Rio, D., 2014. Biozonation and biochronology of Paleogene calcareous nannofossils from low and middle latitudes. Newsletters on Stratigraphy 47, 131–181.

Berger, W.H., 1974. Deep-sea sedimentation. In: Burk, C.A., et al. (Eds.), The Geology of Continental Margins. Springer Science+Business Media New York, p. 213–241.

Berger, W.H., 1971. Sedimentation of planktonic foraminifera. Marine Geology 11, 325–358.

Berggren, W.A., Kent, D. V., Swisher, C.C., Aubry, M.-P., 1995. A Revised Cenozoic geochronology and chronostratigraphy. In: Berggren, W. A., Kent, D.V., Aubry, M.-P., Hardenbol, J. (Eds.), Geochronology, Time Scales, and Global Stratigraphic Correlation: A Unified Temporal Framework for an Historical Geology. Special publication - Society of Economic Paleontologists and Mineralogists, p. 129–212.

Bordiga, M., Henderiks, J., Tori, F., Monechi, S., Fenero, R., Legarda-Lisarri, A., Thomas, E., 2015. Microfossil evidence for trophic changes during the Eocene-Oligocene transition in the South Atlantic (ODP Site 1263, Walvis Ridge). Climate of the Past 11, 1249–1270.

Bown, P.R., 2005. Cenozoic calcareous nannofossil biostratigraphy, ODP Leg 198 Site 1208 (Shatsky Rise, northwest Pacific Ocean). Proceedings of the Ocean Drilling Program, Scientific Results, 198: College Station, Tx: Ocean Drilling Program 198, 1–44.

Bown, P.R., Gibbs, S.J., Sheward, R., Sarah, O., 2014. Searching for cells: the potential of fossil coccospheres in coccolithophore Searching for cells: the potential of fossil coccospheres in coccolithophore research. Journal of Nannoplankton Research.

Bralower, T.J., Premoli Silva, I., Malone, M.J., 2005. Data report: Paleocene-early Oligocene calcareous nannofossil biostratigraphy, ODP Leg 198 Sites 1209, 1210, and 1211 (Shatsky Rise, Pacific Ocean). In: Proceedings of the Ocean Drilling Program, Scientific Results, 198, College Station, TX (Ocean Drilling Program). p. 1–15.

Bralower, T.J., Premoli Silva, I., Malone, M.J., et al., 2002a. Leg 198 Summary. In: Proceedings of the Ocean Drilling Program, Initial Reports Volume 198, College Station, TX (Ocean Drilling Program). p. 1–148.

Bralower, T.J., Premoli Silva, I., Malone, M.J., Shipboard Scientific Party, 2002b. Site 1209. In: Proceedings of the Ocean Drilling Program, Initial Reports Volume 198, College Station, TX (Ocean Drilling Program). p. 1–102.

Cappelli, C., Bown, P.R., Westerhold, T., Bohaty, S.M., De Riu, M., Lobba, V., Yamamoto, Y., Agnini, C., 2019. The early to middle Eocene transition: an integrated calcareous nannofossil and stable isotope record from the Northwest Atlantic Ocean (IODP Site U1410). Paleoceanography and Paleoclimatology 34, 1–18.

Coxall, H.K., Pearson, P.N., 2007. The Eocene-Oligocene Transition. In: Williams, M., Haywood, A.M., Gregory, J., Schmidt, D.N. (Eds.), Deep-Time Perspectives on Climate Change: Marrying the Signal from Computer Models and Biological Proxies, Micropaleontology Society Special Publication. Geological Society, London, p. 351–387.

Coxall, H.K., Wilson, P.A., Pälike, H., Lear, C.H., Backman, J., 2005. Rapid stepwise onset of Antarctic glaciation and deeper calcite compensation in the Pacific Ocean. Nature 433, 53–7.

Dunkley Jones, T., Bown, P.R., Pearson, P.N., Wade, B.S., Coxall, H.K., Lear, C.H., 2008. Major shifts in calcareous phytoplankton assemblages through the Eocene-Oligocene transition of Tanzania and their implications for low-latitude primary production. Paleoceanography 23, 1–14.

Fioroni, C., Villa, G., Persico, D., Jovane, L., 2015. Middle Eocene-Lower Oligocene calcareous nannofossil biostratigraphy and paleoceanographic implications from Site 711 (equatorial Indian Ocean). Marine Micropaleontology 118, 50–62.

Fisher, A.G., Honjo, S., Garrison, R.E., 1967. Electron micrographs of limestones and their nannofossils. Princeton University Press, Princeton, New Jersey.

Hill, M.E., 1975. Selective dissolution of mid-Cretaceous (Cenomanian) calcareous nannofossils. Micropaleontology 21, 227–235.

Honjo, S., 1976. Coccoliths: Production, transportation and sedimentation. Marine Micropaleontology 1, 65–79.

Hutchinson, D.K., Coxall, H.K., Lunt, D.J., Steinthorsdottir, M., de Boer, A.M., Baatsen, M., von der Heydt, A., Huber, M., Kennedy-Asser, A.T., Kunzmann, L., Ladant, J.B., Lear, C.H., Moraweck, K., Pearson, P.N., Piga, E., Pound, M.J., Salzmann, U., Scher, H.D., Sijp, W.P., Śliwińska, K.K., Wilson, P.A., Zhang, Z., 2021. The Eocene–Oligocene transition: a review of marine and terrestrial proxy data, models and model–data comparisons. Climate of the Past 17, 269–315.

Johnson, T.C., Hamilton, E.L., Berger, W.H., 1977. Physical properties of calcareous ooze: Control by dissolution at depth. Marine Geology 24, 259–277.

Jones, A.P., Dunkley Jones, T., Coxall, H.K., Pearson, P.N., Nala, D., Hoggett, M., 2019. Low-Latitude Calcareous Nannofossil Response in the Indo-Pacific Warm Pool Across the Eocene-Oligocene Transition of Java, Indonesia. Paleoceanography and Paleoclimatology 34, 1833–1847.

Liu, Z., Tuo, S., Zhao, Q., Cheng, X., Huang, W., 2004. Deep-water earliest Oligocene glacial maximum (EOGM) in South Atlantic. Chinese Science Bulletin 49, 2190–2197.

Matter, A., Douglas, R.G., Perch-Nielsen, Katharina, Larson, R.L., Moberly, R., Matter, A., Douglas, R.G., Perch-Nielsen, K., 1975. Fossil Preservation, Geochemistry, and Diagenesis, of Pelagic Carbonates from Shatsky Rise, Northwest Pacific. Initial Reports of the Deep Sea Drilling Project, 32.

McIntyre, A., McIntyre, R., 1971. Coccolith concentrations and differential solution in oceanic sediments. In: Funnel, B.M., Riedel, W.R. (Eds.), The Micropalaeontology of the Oceans. Cambridge University Press, p. 253–261.

Newsam, C., 2016. Calcareous nannoplankton evolution and the Paleogene greenhouse to icehouse climate-mode transition.

Norris, R.D., Wilson, P.A., Blum, P., Fehr, A., Agnini, C., Bornemann, A., Boulila, S., Bown, P.R., Cournede, C., Friedrich, O., Ghosh, A.K., Hollis, C.J., Hull, P.M., Jo, K., Junium, C.K., Kaneko, M., Liebrand, D., Lippert, P.C., Liu, Z., Matsui, H., Moriya, K., Nishi, H., Opdyke, B.N., Penman, D., Romans, B., Scher, H.D., Sexton, P., Takagi, H., Turner, S.K., Whiteside, J.H., Yamaguchi, T., Yamamoto, Y., 2014a. Expedition 342 summary. Proceedings. IODP, 342: College Station, TX (Integrated Ocean Drilling Program) 342.

Norris, R.D., Wilson, P.A., Blum, P., Fehr, A., Agnini, C., Bornemann, A., Boulila, S., Bown, P.R., Cournede, C., Friedrich, O., Ghosh, A.K., Hollis, C.J., Hull, P.M., Jo, K., Junium, C.K., Kaneko, M., Liebrand, D., Lippert, P.C., Liu, Z., Matsui, H., Moriya, K., Nishi, H., Opdyke, B.N., Penman, D.E., Romans, B.W., Scher, H.D., Sexton, P., Takagi, H., Turner, S.K., Whiteside, J.H., Yamaguchi, T., Yamamoto, Y., 2014b. Site U1411. Proceedings of the Integrated Ocean Drilling Program 342.

Norris, R.D., Wilson, P.A., Blum, P., Fehr, A., Agnini, C., Bornemann, A., Boulila, S., Bown, P.R., Cournede, C., Friedrich, O., Kumar Ghosh, A., Hollis, C.J., Hull, P.M., Jo, K., Junium, C.K., Kaneko, M., Liebrand, D., Lippert, P.C., Liu, Z., Matsui, H., Moriya, K., Nishi, H., Opdyke, B.N., Penman, D., Romans, B., Scher, H.D., Sexton, P., Takagi, H., Kirtland Turner, S., Whiteside, J.H., Yamaguchi, T., Yamamoto, Y., Scully, C., Brinkhuis, D.F., Flemings, P.B., Iturrino, G.J., Meissner, E., Pettigrew, T.L., Polito, P.J., Aduddell, R., Barnes, H., Beck, J., Bertoli, M., Bloxom, T., Cannon, M., Claassen, E., Cobine, T., Davis, R., Fulton, T., Gustafson, T., Herrmann, S., Meiring, M., Midgley, S., Moortgat, E., Morgan, A., Peng, C., Prinz, S., Swain, K., Vasilyeva, Y., Weymer, B., James Zhao, H., 2012. Paleogene newfoundland sediment drifts. Integrated Ocean Drilling Program, Expedition 342, Preliminary Report 1–263.

Pälike, H., Lyle, M.W., Nishi, H., Raffi, I., Ridgwell, A., Gamage, K., Klaus, A., Acton, G., Anderson, L., Backman, J., Baldauf, J., Beltran, C., Bohaty, S.M., Bown, P.R., Busch, W., Channell, J.E.T., Chun, C.O.J., Delaney, M.L., Dewangan, P., Dunkley Jones, T., Edgar, K.M., Evans, H., Fitch, P., Foster, G.L., Gussone, N., Hasegawa, H., Hathorne, E.C., Hayashi, H., Herrle, J.O., Holbourn, A.E., Hovan, S., Hyeong, K., Iijima, K., Ito, T., Kamikuri, S.I., Kimoto, K., Kuroda, J., Leon-Rodriguez, L., Malinverno, A., Moore, T.C., Murphy, B.H., Murphy, D.P., Nakamura, H., Ogane, K., Ohneiser, C., Richter, C., Robinson, R., Rohling, E.J., Romero, O., Sawada, K., Scher, H.D., Schneider, L., Sluijs, A., Takata, H., Tian, J., Tsujimoto, A., Wade, B.S., Westerhold, T., Wilkens, R., Williams, T., Wilson, P.A., Yamamoto, Y., Yamamoto, S., Yamazaki, T., Zeebe, R.E., 2012. A Cenozoic record of the equatorial Pacific carbonate compensation depth. Nature 488, 609–614.

Perch-Nielsen, K., 1979. Clacareous nannofossils from the Cretaceous between the North Sea and the Mediterranean. Aspekte der Kreide Europas. IUGS Series A 6, 223–272.

Persico, D., Villa, G., 2004. Eocene-Oligocene calcareous nannofossils from Maud Rise and Kerguelen Plateau (Antarctica): Paleoecological and paleoceanographic implications. Marine Micropaleontology 52, 153–179.

Raffi, I., De Bernardi, B., 2008. Response of calcareous nannofossils to the Paleocene-Eocene Thermal Maximum: Observations on composition, preservation and calcification in sediments from ODP Site 1263 (Walvis Ridge - SW Atlantic). Marine Micropaleontology 69, 119–138.

Reghellin, D., Coxall, H.K., Dickens, G.R., Backman, J., 2015. Carbon and oxygen isotopes of bulk carbonate in sediment deposited beneath the eastern equatorial Pacific over the last 8 million years. Paleoceanography 30, 1261–1286.

Roth, P.H., 1983. Jurassic and Lower Cretaceous calcareous nannofossils in the western North Atlantic (Site 534): biostratigraphy, preservation, and some observations on biogeography and paleoceanography. Initial reports DSDP, Leg 76, Norfolk to Fort Lauderdale 587–621.

Roth, P.H., Thierstein, H., 1972. Calcareous Nannoplankton: Leg 14 of the Deep Sea Drilling Project. Initial Reports of the Deep Sea Drilling Project, 14.

Roth, P.R., 1978. Cretaceous Nannoplankton Biostratigraphy and Oceanography of the Northwestern Atlantic Ocean. Initial Reports of the Deep Sea Drilling Project, 44.

Schneider, L.J., Bralower, T.J., Kump, L.R., 2011. Response of nannoplankton to early Eocene ocean destratification. Palaeogeography, Palaeoclimatology, Palaeoecology 310, 152–162.

Toffanin, F., Agnini, C., Rio, D., Acton, G., Westerhold, T., 2013. Middle eocene to early oligocene calcareous nannofossil biostratigraphy at IODP site U1333 (equatorial pacific). Micropaleontology 59, 69–82.

van der Lingen, G.J., Packham, G.H., 1975. Relationships between Diagenesis and Physical Properties of Biogenic Sediments of the Ontong- Java Plateau (Sites 288 and 289, Deep Sea Drilling Project). Initial Reports of the Deep Sea Drilling Project, 30 443–481.

Villa, G., Fioroni, C., Pea, L., Bohaty, S.M., Persico, D., 2008. Middle Eocene-late Oligocene climate variability: Calcareous nannofossil response at Kerguelen Plateau, Site 748. Marine Micropaleontology 69, 173–192.

Villa, G., Fioroni, C., Persico, D., Roberts, A.P., Florindo, F., 2014. Middle Eocene to Late Oligocene Antarctic glaciation/deglaciation and Southern Ocean productivity. Paleoceanography 29, 223–237.

Villa, G., Florindo, F., Persico, D., Lurcock, P., de Martini, A.P., Jovane, L., Fioroni, C., 2021. Integrated calcareous nannofossil and magnetostratigraphic record of ODP Site 709: Middle Eocene to late Oligocene paleoclimate and paleoceanography of the Equatorial Indian Ocean. Marine Micropaleontology 169, 102051.

Westerhold, T., Marwan, N., Drury, A.J., Liebrand, D., Agnini, C., Anagnostou, E., Barnet, J.S.K., Bohaty, S.M., De Vleeschouwer, D., Florindo, F., Frederichs, T., Hodell, D.A., Holbourn, A.E., Kroon, D., Lauretano, V., Littler, K., Lourens, L.J., Lyle, M.W., Pälike, H., Röhl, U., Tian, J., Wilkens, R.H., Wilson, P.A., Zachos, J.C., 2020. An astronomically dated record of Earth's climate and its predictability over the last 66 million years. Science 369, 1383–1388.

Westerhold, T., Röhl, U., 2006. Data report: revised composite depth records for Shatsky Rise Sites 1209, 1210, and 1211. In: Bralower, T.J., Premoli Silva, I., Malone, M.J. (Eds.), Proceedings of the Ocean Drilling Program, Scientific Results Volume 198: College Station, TX (Ocean Drilling Program). p. 1–26.

Zachos, J.C., Dickens, G.R., Zeebe, R.E., 2008. An early Cenozoic perspective on greenhouse warming and carbon-cycle dynamics. Nature 451, 279–283.

Zachos, J.C., Pagani, M., Sloan, L., Thomas, E., Billups, K., 2001. Trends, Global Rhythms, and Aberrations in Global Climate 65 Ma to Present. Science 292, 686–693.

Zachos, J.C., Quinn, T.M., Salamy, K.A., 1996. High-resolution (10^4 years) deep-sea foraminiferal stable isotope records of the Eocene-Oligocene climate transition. Paleoceanography 11, 251–266.

Chapter 6

Enhanced primary productivity and carbonate oversaturation across the Eocene Oligocene Transition: a global perspective[1]

Abstract. In the late Eocene - early Oligocene (EOT; 34 Ma), Earth's climate transitioned from a warm (unglaciated) state to a cold (glaciated) state, characterized by the development of large dynamic ice-sheet on Antarctica. For decades, the response of calcareous nannoplantkon was thought to be negligible or, when documented, it seems to precede the EOT of ~500 Kyr, suggesting a subdued response of one the main primary producers in modern and past oceans to this fundamental climate phase. Here we present morphometric and abundance data performed on *Clausicoccus subdistichus* gr. from the Indian (Site 756, Peirce et al., 1989), Pacific (Site U1509, Sutherland et al., 2019; Site 1209, Bralower et al., 2002) and Atlantic oceans (Site U1411, Norris et al., 2014). At these sites, we document a synchronous increase in the placolith size and abundance (acme interval) of this taxon. The continuous records investigated worldwide and in different depositional settings confirm the global nature of this event, at least at low-middle latitudes, and the high potential to be recognized, with its fine articulation, even in poorly preserved sediments. This event is likely induced by an oversaturation of [CO_3^{2-}] in the sea-water and by a progressive eutrophication of the oceans, culminated in the "Early Oligocene Glacial Maximum" (EOGM).

Keywords *Clausicoccus*, Eocene Oligocene, morphometry, paleoproductivity, carbonate oversaturation.

[1] Allyson Viganò[1], Paul R. Bown[2] Paul N. Pearson[3], Claudia Agnini[1],

[1]Dipartimento di Geoscienze, Università di Padova, Via Gradenigo 6 – 35131, Padova, Italy;
[2]Department of Earth Sciences, University College London, London WC1E 6BT, UK.
[3]School of Earth and Environmental Sciences, Cardiff University, Main building, Park Place, Cardiff CF10 3AT, UK
[2] School of Geography, Earth and Environmental Sciences Birmingham, Birmingham, United Kingdom

Authors contributions: A.V. and C.A. designed the study and developed the methodology. A.V. was responsible for data creation and presentation. A.V. and C.A. were the project administrator. P.R.B and P.N.P. have contributed to the drafting of this manuscript. All the co-authors contributed to the final polishing of the manuscript.

6.1 Introduction

The E-O transition (EOT, ~34 Ma) denotes a period of intense change in climate and a crucial point towards the development of the modern ice-house climate, marked by the onset of the first sustained Antarctic ice-sheet (e.g. Miller et al., 1991; Zachos et al., 1996, 2008). The main signature of this transition involved two positive shifts in deep-sea oxygen stable isotopes (i.e., Step 1 and EOIS, which constrains the EOT; Hutchinson et al., 2021) and reflects a combination of global cooling and ice volume (Coxall et al., 2005; Lear et al., 2008; Bohaty et al., 2012). The EOT is marked at the base by the extinction of calcareous nannofossil *D. saipanensis* and is followed by maximum $\delta^{18}O$ values (EOGM; Hutchinson et al., 2021). Virtually the onset of the EOT, a transient interval of positive $\delta^{18}O$ values, was recognised worldwide and named as the "Late Eocene Event" (LEE; Hutchinson et al., 2021; Katz et al., 2008)

Several studies document a rapid and permanent deepening (≥1 km) of the calcite compensation depth (CCD), supporting a strong coupling between Antarctic glaciation and global carbon cycle (Coxall et al., 2005; Coxall and Wilson, 2011; Wade et al., 2020). The shared understanding for explaining the CCD deepening and the related increase in seawater $\delta^{13}C$ values, is that a shelf-to-basin shift in marine carbonate sedimentation in response to sea level fall with the consequent erosion of widespread neritic carbonates and the input of isotopically heavy carbon in the ocean occurred (e.g. Merico et al., 2008; Pälike et al., 2012; Armstrong Mckay et al., 2016).

Several lines of evidences for increased productivity and cooling were provided by recent studies on calcareous nannofossil assemblages at various worldwide locations (Dunkley Jones, 2008; Bordiga et al., 2015; Fioroni et al., 2015; Jones et al., 2019; Villa et al., 2021), but the actual extent and intensity of productivity changes are still strongly debated (Nilsen et al., 2003; Ladant et al., 2018; Wade et al., 2020). The striking acme interval of *Clausicoccus subdistichus* gr. observed at the EOT, has been recently interpreted as a further support for ocean eutrophication (see also Chapter 2 and 4, Sites 756, U1509).

Moreover, the base of this event represents a synchronous biohorizon with a high correlation potential (Monechi, 1986a; Nocchi et al., 1988; Wei and Wise, 1990; Fornaciari et al., 2010; Agnini et al., 2014) and, could serve to denote the EOB at least at low-middle latitudes (Monechi, 1986b; Backman, 1987).

The end of this acme is proved to be extremely consistent and reliable among different successions (see previous chapters; Nocchi et al., 1986; Monechi, 1986a; Perch-Nielsen, 1986; Backman, 1987) and constrain the perturbation observed in calcareous nannofossil assemblage. Here, we provide a high-resolution (~10 kyrs) biometric analysis on *C. subdistichus* gr. in different depositional settings from the low-middle latitudes to better constraint the effect of the late Eocene – early Oligocene climate perturbation on the size and abundance of this group and interpret those changes in terms of paleoceanographic/climate evolution.

6.2 Material and methods

All samples were prepared using the standard smear slide tecnique (Bown and Young, 1998) and then analyzed at trasmitted light microscopy at 1250X. Biometric analyses on *C. subdistichus* gr. (see the taxonomy notes in the supplementary) were performed on a total of 108 samples collected in a ~3 Myr time interval from ODP Hole 756C (Indian Ocean; Peirce et al., 1989), IODP Site U1509 (Tasman Sea; Sutherland et al., 2019), ODP Site 1209 (NW Pacific Ocean; Bralower et al., 2002) and IODP Hole U1411B (NW Atlantic Ocean; Norris et al., 2014) (Figure 6.1). These sediments are characterized by high $CaCO_3$ content (40-100 wt%) with good (Sites 756 and U1509) to poor preservation (Site 1209), except Site U1411, which is characterized by a clay-rich sediment with excellent preservation and lower $CaCO_3$ content (0-60 wt%) (Chapter 5, Figure S6.1).
This approach is intended to investigate heterogeneous sediments in order to evaluate the role of carbon geochemistry and preservation on shaping this event. For each sample, the images of at least 30 specimens of *Clausicoccus subdistichus* gr. were captured using an Invenio 5D camera and the placolith length and width were measured with the DeltaPix InSight software. An additional biometric parameter considered is the central opening area (a) to total area (A) ratio, was determined on a total of 621 specimens of *C. subdistichus* (584) and *C. fenestratus* (37) from Site U1411, where the excellent preservation allow us to distinguish the two species. Morphometric data were then processed using Mathlab and PAST softwares (Hammer et al., 2001). Quantitative (n/mm^2) and relative abundance analysis (%) on *Clausicoccus subdistichus* gr., as well as bulk and benthic foraminifera geochemical records (C, O stable isotopes and carbonate content), have been provided by previous studies (Chapters 2, 3, 4, 5). Consistent age models, based on the time scale of Gradstein et al. (2012), were generated at each site, in order to guarantee a robust site-to-site correlation.

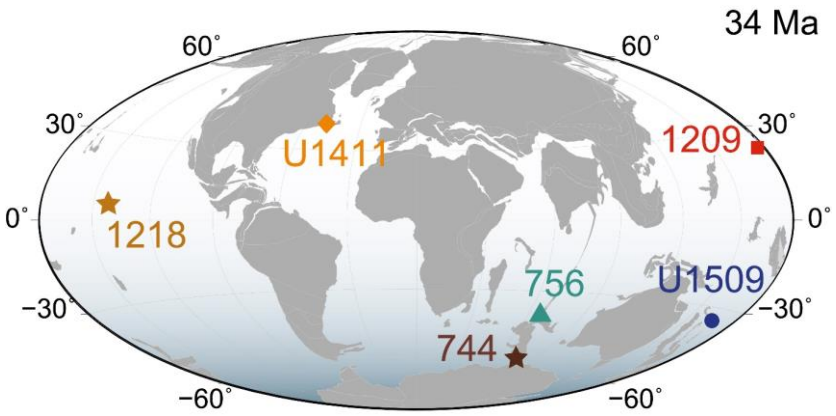

Figure 6.1 Location map of the investigated sites (IODP U1411, IODP U1509, ODP 1209, ODP 756) at 34 Ma (paleomap from http:// www.odsn.de/odsn/index.html) and other key sites discussed in this paper (stars; 1218 and 744).

6.3 Results

Our morphometric investigations reveal that the mean length of placoliths belonging to *Clausicoccus subdistichus* gr. significantly increases across all the studied sections and through time (Figure 6.2D). The patterns of variations are remarkably similar among sites and documents a progressive increase starting from the late Eocene (PRE-EOT, mean length 5.34 µm), through the EOT (mean length 5.88 µm) and up to the early Oligocene (mean length 6.49 µm) (Figure 6.2E).

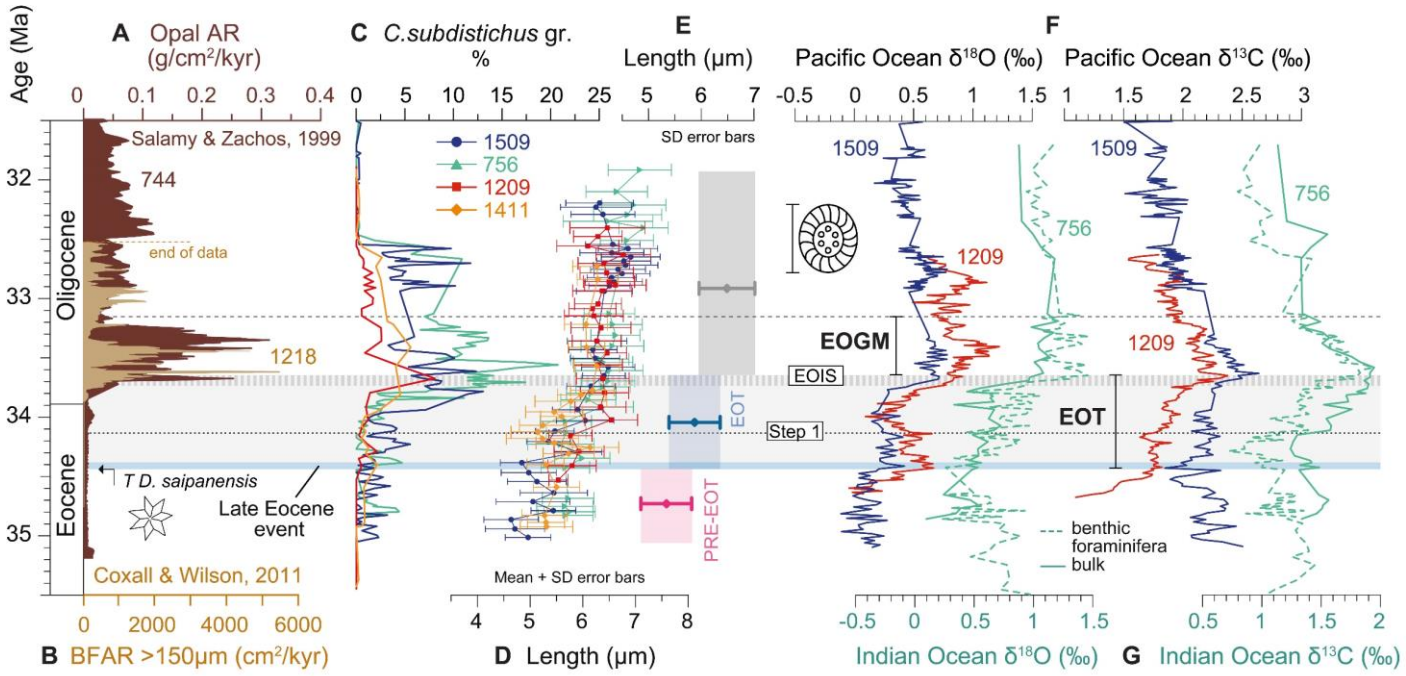

Figure 6.2 Biotic and geochemical changes across the Eocene-Oligocene transition. **A.** Site 744 opal accumulation rate (Salamy & Zachos, 1999). **B.** Site 1218 benthic foraminifera accumulation rate (>150 µm). **C**. *C. subdistichus* gr. relative abundances (%). **D.** *C. subdistichus* gr. mean length with SD error bars at the studied sites. **E.** Total mean length with SD error bars for the PRE-EOT, EOT and early Oligocene interval. **F**. Bulk $\delta^{13}C$ and $\delta^{18}O$ from the Pacific Ocean (Chapter 4 and 5, Site U1509 and Site 1209). **G.** Bulk $\delta^{13}C$ and $\delta^{18}O$ (solid line) curves and benthic foraminifera $\delta^{13}C$ and $\delta^{18}O$ profiles (dashed line) from the Indian Ocean (Chapter 1, Site 756).
Conversion of Site 744 to our time scale is approximate. The two steps of increase in $\delta^{18}O$ (step 1 and EOIS) that constitute the EOT (grey bar) are reported, as well as the EOGM and the Late Eocene Event (blue bar). The base of the EOT is defined by the top of *D. saipanensis* (Hutchinson et al., 2021). The two positive shifts in $\delta^{18}O$ (Step 1 and EOIS), the EOT (grey bar), the EOGM and the Late Eocene Event (blue bar) are reported. The base of the EOT is defined by the Top of *D. saipanensis* (Hutchinson et al., 2021).

More specifically, our results show that the first remarkable size increase started slightly above the onset of Step 1 (i.e., the Late Eocene Event - LEE) while the second increase in size coincides with the EOIS and $\delta^{13}C$ excursion. Finally, largest and stable size where reached during the early Oligocene (Figure 6.2D and Figure 6.4).

At all study site, associated to the increase in size, there is a synchournous increase in the relative (%) abundances (acme) of *C. subdistichus* gr. (Figure 6.2C). The positive peaks in abundances of *C. subdistichus* gr. well correlates with remarkable pulses of opal accumulation rate (opal AR) (Site 744, Southern Ocean) and benthic foraminifera accumulation rate (BFAR >150 µm) (Site 1218, Equatorial Pacific) (Figure 6.2), which

are interpreted to represent increased surface productivity associated with the early Oligocene glacial expansion (Salamy and Zachos, 1999; Coxall and Wilson, 2011).

At Hole 756C, the size of placoliths ascribable to *Clausicoccus subdistichus* gr. ranges from 4 to 8.5 µm. Specimens are relatively larger (average length of 6.3 µm) and abundant (up to 21% and 522 n/mm^2; mean value 4.8%) (Figure 6.4). Major fluctuations in size were recorded during the late Eocene at Site U1509, with the occurrence of relatively smaller forms (<4 µm). Here, the relative and semiquantitative abundances of this taxon reach 13% and 472 n/mm^2 (mean value 2.8%), respectively.

A similar relative abundance pattern (up to ~12%) was recorded in the South Atlantic (Site 1263; Bordiga et al., 2015). At ODP Site 1209, the frequency histrogram reveals an average length of 6.33 µm and a relatively small stardard deviation (σ) of 0.54 (Figure S6.3), which is probably due to preservation issues. At this site, the abundances of *Clausicoccus subdistichus* gr. are relatively low (max value of ~8% and of 161 n/mm^2; mean value 0.7%), if compared with other sites. At Hole 1411B, *Clausicoccus subdistichus* gr. has an average length of 5.7 µm and maximum abundance of 5.6% and 203 n/mm^2 (mean value 1.4%) (Figure 6.2 and Figure 6.4).

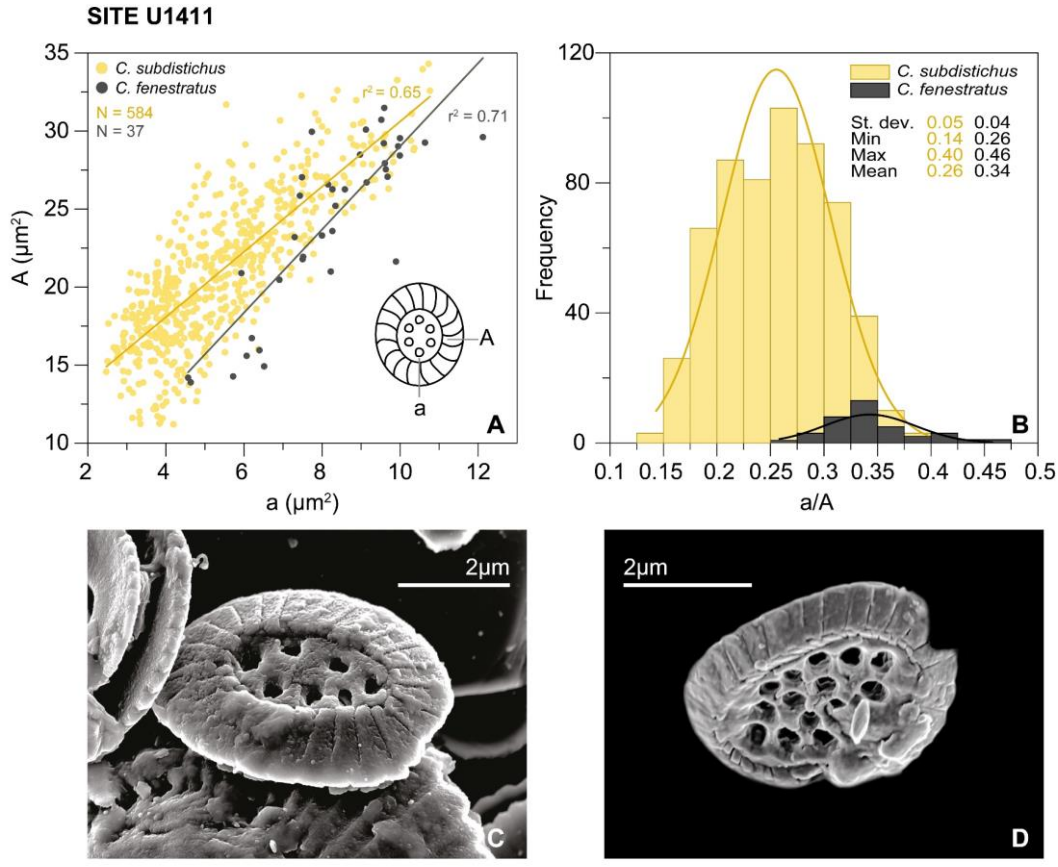

Figure 6.3 Morphometric parameters investigated for *C. fenestratus* and *C. subdistichus* at Site U1411. **A.** Scatter plot of central area (a) vs total placolith area (A). **B.** Frequency histogram of a/A ratio. **C** SEM image of *C. subdistichus* from IODP Site U1411. Sample U1411B-17H-7A, 25. **D.** SEM image of *C. fenestratus* from IODP Site U1411. Sample U1411B-21X-CC PAL.

The results of the morphometric analyses performed on *C. subdistichus* and *C. fenestratus* at Site U1411 do not show any significant correlation between the central area (a) and the total placolith area (A) or any bimodal distribution in the central to total area (a/A) ratio (Figure 6.3). The frequency histogram show that the mean a/A ratio of *C. fenestratus* is slightly higher (0.34) compared to that of *C. subdistichus* (0.26), but reflects the same normal distribution of *C. subdistichus* (Figure 6.3B).

6.4 Discussion

The similar timing and intensity in both size and abundance increase of *Clausicoccus subdistichus* gr. at the study sites suggest a widespread low-middle latitude response of this group in the two hemispheres. This is best illustrated in Figure 6.4, where the size-distribution plots of *Clausicoccus subdistichus* gr. are compared with the relative (%) and semiquantitative (n/mm^2) abundances.

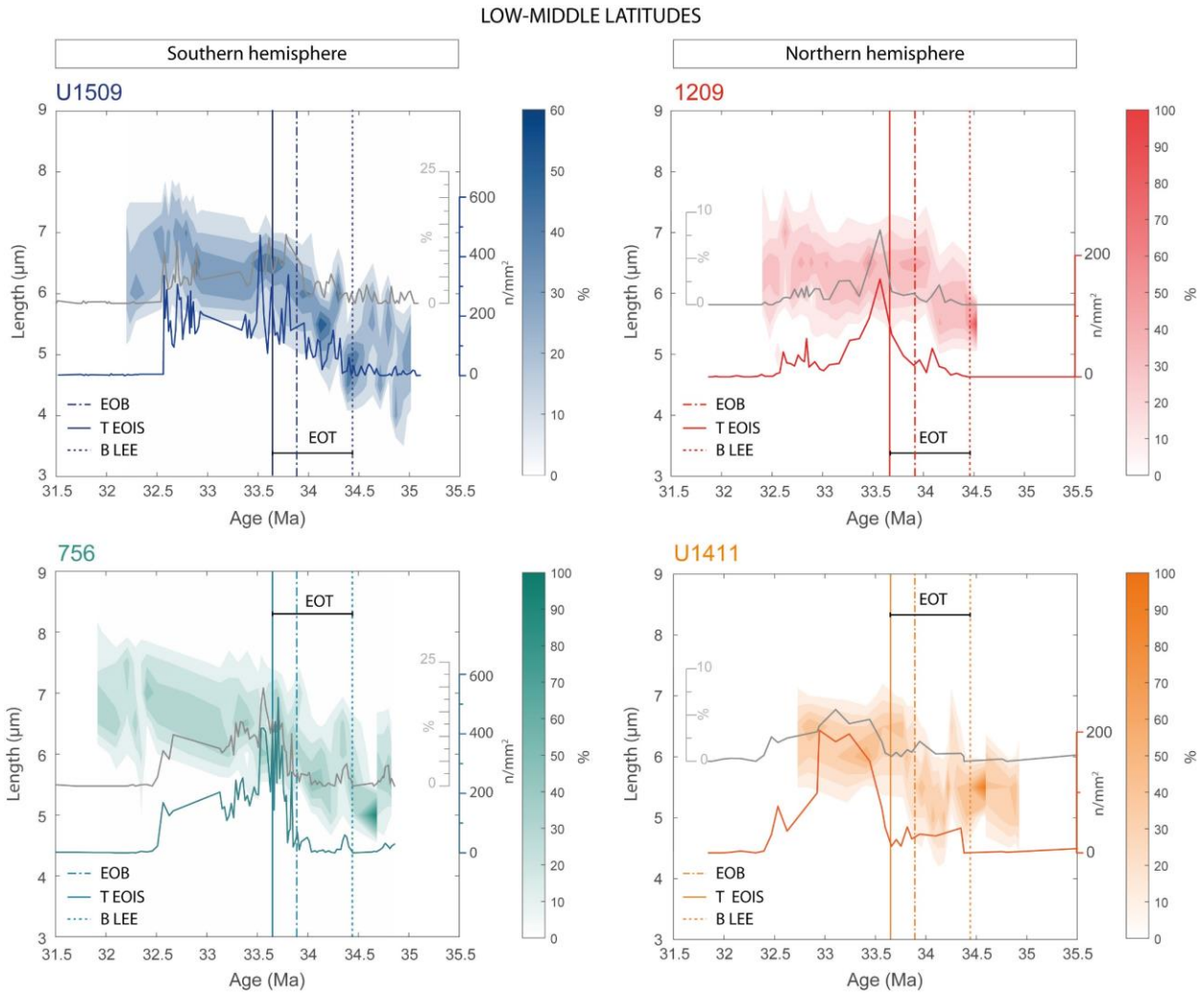

Figure 6.4 *Clausicoccus subdisthicus* gr. density plots for size distribution (%, in bins of 0.5µm) vs quantitative and semiquantitative abundances (%, n/mm2) for the studied sites. Vertical dashed line delimits the base of the Late Eocene Event (LEE); the solid line denotes the top of EOIS and the pointed-dashed line highlights the age of Eocene-Oligocene boundary (EOB; GTS2012).

Abundance distributions. The sharp and synchronous shifts in abundance (acme) of *Clausicoccus subdistichus* gr. documented during the Eocene-Oligocene transition are interpreted as a response of this group to global increases in surface nutrient availability. A significant eutrophication at middle-low and high-latitude in sea surface waters across the EOT was supported by several studies on calcareous nannofossil assemblages (Dunkley Jones et al., 2008; Villa et al., 2014; 2021; Bordiga et al., 2015; Fioroni et al., 2015; Jones et al., 2019). Enhanced paleoproductivity conditions during this time were also recorded by a variety of paleontological and geochemical proxies from the southern high (Diester-Haass, 1995; Diester-Haass and Zahn, 1996; Salamy and Zachos, 1999; Schumacher and Lazarus, 2004; Plancq et al., 2014) and from low-middle (Hartl et al., 1995; Diester-Haass and Zahn, 2001; Diester-Haass and Zachos, 2003; Ravizza and Paquay, 2008; Coxall and Wilson, 2011) latitudes. Moreover, changes in the chemistry of intermediate waters and nutrient distribution have been related to different upwelling systems (Nilsen et al., 2003; Fontorbe et al., 2017).

Previous paleoecological assignments suggest a preference of *Clausicoccus subdistichus* gr. for middle to high latitudes (Wei and Wise, 1990). More recently, a temperate-eutrophic affinity has been proposed for this taxon (See Chapter 2 and 4). An increase in abundance of this group would thus indicate a shift toward more eutrophic/cooler environmental conditions, a scenario that perfectly fits the one inferred for the late Eocene – early Oligocene interval based on independent proxies. The eutrophic affinity of *Clausicoccus subdistichus* gr. is further corroborated by the strong and direct correlation of our quantitative records with the opal (Salamy and Zachos 1999) and benthic foraminifera accumulation rates as reported from the Southern Ocean (Diester-Haass and Zahn 1996) and from the Equatorial Pacific (Coxall and Wilson 2011) (Figure 6.2). The increased export production of diatoms and benthic foraminifera are considered strong indicators of high water productivity (primarily silica, phosphorous, nitrogen) and primary export production (Barron and Baldauf 1989, Diester-Haass and Zahn 1996, 2001, Salamy and Zachos 1999, Coxall and Wilson 2011). Changes observed at high latitudes reinforce the connection with low-middle latitudes and provide a further evidence for a widespread increase in paleoproductivity occurred during the EOT and culminated with the EOGM.

However, small differences in the abundance pattern of *Clausicoccus subdistichus* gr. were observed between the Northern and Southern hemisphere and may possibly suggest some geographically-related variations in the intensity of paleoproductivity. In fact, productivity is also a function of local or regional hydrology and it is it realistic that the global signal is amplified or attenuated worldwide depending on the geographic location and depositinal setting.

Size distributions. Despite some differences in lithology among study sites, we do not find any correlation between sediment % $CaCO_3$ (Figure S6.1) and mean length. Instead, our morphometric analysis reveals a major size increase of *Clausicoccus subdistichus* gr. closely coupled with the positive $\delta^{13}C$ anomaly (Figure 6.3 and Figure 6.4). A possible explanation for the size increase of *Clausicoccus subdistichus* gr. is related to a change in sea-water carbonate geochemistry, as suggested by the strong connection with the positive $\delta^{13}C$ anomaly.

This anomaly is likely caused by a shelf to basin shift in marine carbonate deposition (Opdyke and Wilkinson 1989, Coxall et al. 2005, Lear and Rosenthal 2006, Merico et al. 2008), with the potential contribution of other

mechanisms (e.g., shelf carbonate weathering, increase organic carbon burial into capacitors, and possibly increased ocean ventilation; Armstrong Mckay et al., 2016). The consequent erosion of widespread "fresh" limestone increases CO_3^{2-} fluxes to the oceans, producing an oversaturation of carbonate in the sea water (increasing alkalinity) with the dramatic deepening of CCD (Merico et al., 2008).

Another driver that could have contributed to the deepening of the CCD and the positive $\delta^{13}C$ excursion is a shift from calcareous to siliceous plankton producers (e.g. Harrison, 2000; Coxall et al., 2005). Unfortunately, *Clausicoccus subdistichus* gr. became extinct in the lower part of Burdigalian, thus the precise phisiological behaviour of this taxon is not directly known. Despite this, based on the previous considerations, our assumption is that the increase in the calcite saturation state (Ω) of the oceans likely enhanced the calcification of *Clausicoccus subdistichus* gr. during the EOT.

Our morphometric dataset is particularly intriguing, especially considering that the increase in size and abundances of *Clausicoccus subdistichus* gr. seems not to follow the expected general trends usually observed in calcareous phytoplankton evolution (Finkel et al., 2007). Specifically, the abundance of specimens is inversely related to organism size with regard to the "abundance vs cell-size rule" (i.e.), revealing a possible different strategy of this group to cope with climate and related paleoceanographic changes. Smaller marine phytoplankton cells are generally more competitive than the larger ones and result in a higher nutrient-uptwake and metabolic rates (growth, photosyntesis, etc.) (Raven, 1998; Henderiks, 2008; Finkel et al., 2010; Moore et al., 2013). Thus, these forms have an advantage in acquiring and processing energy and resources from the environment, resulting in increased absolute abundances. This seems not to be the case for *Clausicoccus subdistichus* gr. Not only coccoliths get larger and as the cell does (Henderiks, 2008; Aloisi, 2015) but the individuals become more abundant. However, several studies have documented that the response of calcareous phytoplankton is species specific in many cases and numerous taxa have a clear preference for particular environmental conditions, exhibiting different physiological traits (e.g. Rickaby et al., 2010; Gibbs et al., 2013).

Based on previous reasoning, we hypothesize that a combination of increased trophic resources (e.g. nitrogen, phosphorus, iron and silica), derived from an invigorated Southern Ocean circulation (Sauermilch et al., 2021, Villa et al., 2021), and increased sea-water [CO_3^{2-}] have favored the size increase of *Clausicoccus subdistichus* gr. and, at the same time, allowed this taxon to achieve considerably high abundances, without the pressure of a limiting-nutrient environment.

Species or morphotypes? The two species (*C. subdistichus* and *C. fenestratus*) appear to represent an intra-specific variation rather than an inter-specific variation. Our morphometric results suggest that these forms sole and exclusively differ from the number of holes in their central areas, which are only clearly visible in exceptionally preserved material in trasmitted light microscope and/or during scanning electron microscopy (SEM) analysis. This is because slight overgrowth can easily obscure these holes and prevent the identification at the species level (Wei and Wise, 1990). Consequently, these two morphotypes were combined into a single taxonomic entity with the same biostratigraphic and paleoecological meaning, the *C. subdistichus* gr.

6.5 Conclusions

In conclusion, the observed morphometric and abundance variations of *C. subdistichus* gr. reflect the biomineralization response of this group to global changes in sea-water carbon geochemistry and nutrient availability. Morphometric changes were likely promoted by the increase of carbonate ions concentrations closely tied to the positive $\delta^{13}C$ anomaly and to the dramatic deepening of the CCD.

The enhance alkalinity was triggered by 1) the global $CaCO_3$ burial fractionation from shelf to deep ocean basins, with the consequent augment in the ocean carbonate saturation - buffered by the deepening of CCD (Opdyke and Wilkinson, 1989; Coxall et al., 2005; Merico et al. 2008) and by 2) the switch from calcareous to siliceous plankton producers (Diester-Haass, 1995; Salamy and Zachos, 1999; Harrison, 2000; Coxall et al., 2005) coincident with an explosive diversification and proliferation of diatoms in the Southern Ocean (Egan et al., 2013). We also document that *C. subdistichus* gr. had a unique and worldwide response to environmental changes, showing a great sensitivity to trophic variations during the E-O transition. The simultaneous increase in size and abundance of this group was likely triggered by an oversaturation of [CO_3^{2-}] in the sea water and by the northward transport of higher concentrations of nutrients from the Southern Ocean to the low-middle latitudes (Villa et al., 2021), where mixing and regional-scale upwelling eventually support primary production (Sarmiento et al., 2004; Moore et al., 2013).

Acknoledgments

This research used samples provided by the Integrated Ocean Drilling Program (IODP) and Ocean Drilling Program (ODP). Funding for this work was provided by the University of Padova. Isabella Raffi and Davide Persico are deeply thanked for their constructive comments in the capacity of reviewers of A.V.' s PhD thesis during the evaluation process required by Italian law.

Supplementary information (including Figures S6.1–S6.3; Plate S6.1) associated with this chapter can be found in the **Appendix VII**.

References

Agnini, C., Fornaciari, E., Raffi, I., Catanzariti, R., Pälike, H., Backman, J., Rio, D., 2014. Biozonation and biochronology of Paleogene calcareous nannofossils from low and middle latitudes. Newsletters on Stratigraphy 47, 131–181.

Aloisi, G., 2015. Covariation of metabolic rates and cell size in coccolithophores. Biogeosciences 12, 4665–4692.

Armstrong Mckay, D.I., Tyrrell, T., Wilson, P.A., 2016. Global carbon cycle perturbation across the Eocene-Oligocene climate transition. Paleoceanography 31, 311–329.

Aubry, M.-P., 1992. Late Paleogene Calcareous Nannoplankton Evolution: A Tale of Climatic Deterioration. In: Eocene-Oligocene Climatic and Biotic Evolution. p. 272–279.

Backman, J., 1987. Quantitative Calcareous Nannofossil Biochronology of Middle Eocene through Early Oligocene Sediment from DSDP Sites 522 and 523. Abhandlungen der Geologischen Bundesanstalt 39, 21–31.

Barron, J.A., Baldauf, J.G., 1989. Tertiary cooling steps and paleoproductivity as reflected by diatoms and biosiliceous sediments. In: Berger, W.H., Smetacek, V.S., Wefer, G. (Eds.), Productivity of the Ocean: Present and Past. J Wiley and Sons, Ltd., Chichester, UK, p. 341–354.

Bohaty, S.M., Zachos, J.C., Delaney, M.L., 2012. Foraminiferal Mg/Ca evidence for Southern Ocean cooling across the Eocene-Oligocene transition. Earth and Planetary Science Letters 317–318, 251–261.

Bordiga, M., Henderiks, J., Tori, F., Monechi, S., Fenero, R., Legarda-Lisarri, A., Thomas, E., 2015. Microfossil evidence for trophic changes during the Eocene-Oligocene transition in the South Atlantic (ODP Site 1263, Walvis Ridge). Climate of the Past 11, 1249–1270.

Bown, Paul R., Young, J.R., 1998. Techniques. In: Bown, P.R. (Ed.), Calcareous Nannofossil Biostratigraphy. Kluwer Academic Publishers, London, p. 16–28.

Bralower, T.J., Premoli Silva, I., Malone, M.J., Shipboard Scientific Party, 2002. Site 1209. In: Proceedings of the Ocean Drilling Program, Initial Reports Volume 198, College Station, TX (Ocean Drilling Program). p. 1–102.

Coxall, H.K., Wilson, P.A., 2011. Early Oligocene glaciation and productivity in the eastern equatorial Pacific: Insights into global carbon cycling. Paleoceanography 26, 1–18.

Coxall, H.K., Wilson, P.A., Pälike, H., Lear, C.H., Backman, J., 2005. Rapid stepwise onset of Antarctic glaciation and deeper calcite compensation in the Pacific Ocean. Nature 433, 53–7.

Diester-Haass, L., 1995. Middle Eocene to early Oligocene paleoceanography of the Antarctic Ocean (Maud Rise, ODP Leg 113, Site 689): change from a low to a high productivity ocean. Palaeogeography, Palaeoclimatology, Palaeoecology 113, 311–334.

Diester-Haass, L., Zachos, J.C., 2003. The Eocene-Oligocene transition in the Equatorial Atlantic (ODP Site 925); Paleoproductivity increase and positive $\delta^{13}C$ excursion. In: Prothero, D.R., Ivany, C.L., Nesbitt, E.A. (Eds.), From Greenhouse to Icehouse; The Marine Eocene-Oligocene Transition. Columbia Univ. Press, New York, NY, USA, p. 397–416.

Diester-Haass, L., Zahn, R., 1996. Eocene-Oligocene transition in the Southern Ocean: History of water mass

circulation and biological productivity. Geology 24, 163–166.

Diester-Haass, L., Zahn, R., 2001. Paleoproductivity increase at the Eocene - Oligocene climatic transition: ODP/DSDP sites 763 and 592. Palaeogeography, Palaeoclimatology, Palaeoecology 172, 153–170.

Dunkley Jones, T., 2008. The response of low-latitude calcareous phytoplankton to global change through the Eocene-Oligocene transition.

Dunkley Jones, T., Bown, P.R., Pearson, P.N., Wade, B.S., Coxall, H.K., Lear, C.H., 2008. Major shifts in calcareous phytoplankton assemblages through the Eocene-Oligocene transition of Tanzania and their implications for low-latitude primary production. Paleoceanography 23, 1–14.

Egan, K.E., Rickaby, R.E.M., Hendry, K.R., Halliday, A.N., 2013. Opening the gateways for diatoms primes Earth for Antarctic glaciation. Earth and Planetary Science Letters 375, 34–43.

Finkel, Z. V., Beardall, J., Flynn, K.J., Quigg, A., Rees, T.A. V., Raven, J.A., 2010. Phytoplankton in a changing world: Cell size and elemental stoichiometry. Journal of Plankton Research 32, 119–137.

Finkel, Z. V., Sebbo, J., Feist-Burkhardt, S., Irwin, A.J., Katz, M.E., Schofield, O.M.., Young, J.R., Falkowski, P.G., 2007. A universal driver of macroevolutionary change in the size of marine phytoplankton over the Cenozoic. Proc. Natl. Acad. Sci. 104, 20416–20420.

Fioroni, C., Villa, G., Persico, D., Jovane, L., 2015. Middle Eocene-Lower Oligocene calcareous nannofossil biostratigraphy and paleoceanographic implications from Site 711 (equatorial Indian Ocean). Marine Micropaleontology 118, 50–62.

Fontorbe, G., Frings, P.J., De La Rocha, C.L., Hendry, K.R., Carstensen, J., Conley, D.J., 2017. Enrichment of dissolved silica in the deep equatorial Pacific during the Eocene-Oligocene. Paleoceanography 32, 848–863.

Fornaciari, E., Agnini, C., Catanzariti, R., Rio, D., Bolla, E.M.E.M., Valvasoni, E., 2010. Mid-latitude calcareous nannofossil biostratigraphy and biochronology across the middle to late eocene transition. Stratigraphy 7, 229–264.

Gibbs, S.J., Poulton, A.J., Bown, P.R., Daniels, C.J., Hopkins, J., Young, J.R., Jones, H.L., Thiemann, G.J., Dea, S.A.O., Newsam, C., 2013. Species-specific growth response of coccolithophores to Palaeocene – Eocene environmental change. Nature Geoscience 6, 1–5.

Gradstein, F.M., Ogg, J.G., Schmitz, M.D., Ogg, G.M., 2012. The Geologic Time Scale 2012. Elsevier, Amsterdam, Netherlands.

Hammer, Ø., Harper, D.T., Ryan, D.D., 2001. Past: Paleontological Statistics Software Package for Education and Data Analysis. Palaeontologia Electronica 4, 5–7.

Harrison, K.G., 2000. Role of increased marine silica input on paleo-pCO2 levels. Paleoceanography 15, 292–298.

Hartl, P., Tauxe, L., Herbert, T., 1995. Earliest Oligocene increase in South Atlantic productivity as interpreted from “rock magnetics” at Deep Sea Drilling Project Site 522. Paleoceanography 10, 311–325.

Henderiks, J., 2008. Coccolithophore size rules - Reconstructing ancient cell geometry and cellular calcite quota from fossil coccoliths. Marine Micropaleontology 67, 143–154.

Hutchinson, D.K., Coxall, H.K., Lunt, D.J., Steinthorsdottir, M., de Boer, A.M., Baatsen, M., von der Heydt,

A., Huber, M., Kennedy-Asser, A.T., Kunzmann, L., Ladant, J.B., Lear, C.H., Moraweck, K., Pearson, P.N., Piga, E., Pound, M.J., Salzmann, U., Scher, H.D., Sijp, W.P., Śliwińska, K.K., Wilson, P.A., Zhang, Z., 2021. The Eocene–Oligocene transition: a review of marine and terrestrial proxy data, models and model–data comparisons. Climate of the Past 17, 269–315.

Jones, A.P., Dunkley Jones, T., Coxall, H.K., Pearson, P.N., Nala, D., Hoggett, M., 2019. Low-Latitude Calcareous Nannofossil Response in the Indo-Pacific Warm Pool Across the Eocene-Oligocene Transition of Java, Indonesia. Paleoceanography and Paleoclimatology 34, 1833–1847.

Katz, M.E., Miller, K.G., Wright, J.D., Wade, B.S., Browning, J. V., Cramer, B.S., Rosenthal, Y., 2008. Stepwise transition from the Eocene greenhouse to the Oligocene icehouse. Nature Geoscience 1, 329–333.

Ladant, J.B., Donnadieu, Y., Bopp, L., Lear, C.H., Wilson, P.A., 2018. Meridional Contrasts in Productivity Changes Driven by the Opening of Drake Passage. Paleoceanography and Paleoclimatology 33, 302–317.

Lear, C.H., Bailey, T.R., Pearson, P.N., Coxall, H.K., Rosenthal, Y., 2008. Cooling and ice growth across the Eocene-Oligocene transition. Geology 36, 251–254.

Lear, C.H., Rosenthal, Y., 2006. Benthic foraminiferal Li/Ca: Insights into Cenozoic seawater carbonate saturation state. Geology 34, 985–988.

Merico, A., Tyrrell, T., Wilson, P.A., 2008. Eocene/Oligocene ocean de-acidification linked to Antarctic glaciation by sea-level fall. Nature 452, 979–982.

Miller, K.G., Wright, J.D., Fairbanks, R.G., 1991. Unlocking the Ice House: Oligocene-Miocene oxygen isotopes, eustasy, and margin erosion. Journal of Geophysical Research: Solid Earth 96, 6829–6848.

Monechi, S., 1986a. Biostratigraphy of Fuente Caldera Section by Means of Calcareous Nannofossils. Developments in Palaeontology and Stratigraphy 9, 65/69.

Monechi, S., 1986b. Calcareous nannofossil events around the Eocene-Oligocene boundary in the Umbrian Appenines (Italy). Palaeogeography, Palaeoclimatology, Palaeoecology 57, 61–69.

Moore, C.M., Mills, M.M., Arrigo, K.R., Berman-Frank, I., Bopp, L., Boyd, P.W., Galbraith, E.D., Geider, R.J., Guieu, C., Jaccard, S.L., Jickells, T.D., La Roche, J., Lenton, T.M., Mahowald, N.M., Marañón, E., Marinov, I., Moore, J.K., Nakatsuka, T., Oschlies, A., Saito, M.A., Thingstad, T.F., Tsuda, A., Ulloa, O., 2013. Processes and patterns of oceanic nutrient limitation. Nature Geoscience 6, 701–710.

Nilsen, E.B., Anderson, L.D., Delaney, M.L., 2003. Paleoproductivity, nutrient burial, climate change and the carbon cycle in the western equatorial Atlantic across the Eocene/Oligocene boundary. Paleoceanography 18.

Nocchi, M., Parisi, G., Monaco, P., Monechi, S., Madile, M., 1988. Eocene and early Oligocene micropaleontology and paleoenvironments in SE Umbria, Italy. Palaeogeography, Palaeoclimatology, Palaeoecology 67, 181–244.

Nocchi, M., Parisi, G., Monaco, P., Monechi, S., Madile, M., Napoleone, G., Ripepe, M., Orlando, M., Premoli Silva, I., Bice, D.M., 1986. The Eocene-Oligocene Boundary in the Umbrian Pelagic Sequences, Italy. In: Developments in Palaeontology and Stratigraphy. Elsevier, Amsterdam, p. 25–40.

Norris, R.D., Wilson, P.A., Blum, P., Fehr, A., Agnini, C., Bornemann, A., Boulila, S., Bown, P.R., Cournede, C., Friedrich, O., Ghosh, A.K., Hollis, C.J., Hull, P.M., Jo, K., Junium, C.K., Kaneko, M., Liebrand, D., Lippert, P.C., Liu, Z., Matsui, H., Moriya, K., Nishi, H., Opdyke, B.N., Penman, D.E., Romans, B.W., Scher, H.D., Sexton, P., Takagi, H., Turner, S.K., Whiteside, J.H., Yamaguchi, T., Yamamoto, Y., 2014. Site U1411. Proceedings of the Integrated Ocean Drilling Program 342.

Opdyke, B.N., Wilkinson, B.H., 1989. Surface area control of shallow cratonic to deep marine carbonate accumulation. Paleoceanography 3, 685–703.

Pälike, H., Lyle, M.W., Nishi, H., Raffi, I., Ridgwell, A., Gamage, K., Klaus, A., Acton, G., Anderson, L., Backman, J., Baldauf, J., Beltran, C., Bohaty, S.M., Bown, P.R., Busch, W., Channell, J.E.T., Chun, C.O.J., Delaney, M.L., Dewangan, P., Dunkley Jones, T., Edgar, K.M., Evans, H., Fitch, P., Foster, G.L., Gussone, N., Hasegawa, H., Hathorne, E.C., Hayashi, H., Herrle, J.O., Holbourn, A.E., Hovan, S., Hyeong, K., Iijima, K., Ito, T., Kamikuri, S.I., Kimoto, K., Kuroda, J., Leon-Rodriguez, L., Malinverno, A., Moore, T.C., Murphy, B.H., Murphy, D.P., Nakamura, H., Ogane, K., Ohneiser, C., Richter, C., Robinson, R., Rohling, E.J., Romero, O., Sawada, K., Scher, H.D., Schneider, L., Sluijs, A., Takata, H., Tian, J., Tsujimoto, A., Wade, B.S., Westerhold, T., Wilkens, R., Williams, T., Wilson, P.A., Yamamoto, Y., Yamamoto, S., Yamazaki, T., Zeebe, R.E., 2012. A Cenozoic record of the equatorial Pacific carbonate compensation depth. Nature 488, 609–614.

Peirce, J., Weissel, J., et al., 1989. Site 756. Proceeding ODP, Initial Reports, 121: College Station, TX (Ocean Drilling Program).

Perch-Nielsen, K., 1986. Calcareous nannofossil events at Eocene/Oligocene boundary. In: Pomerol, C., Premoli Silva, I. (Eds.), Terminal Eocene Events. Elsevier, Amsterdam, p. 275–282.

Plancq, J., Mattioli, E., Pittet, B., Simon, L., Grossi, V., 2014. Productivity and sea-surface temperature changes recorded during the late Eocene-early Oligocene at DSDP Site 511 (South Atlantic). Palaeogeography, Palaeoclimatology, Palaeoecology 407, 34–44.

Raven, J.A., 1998. The twelfth Tansley Lecture. Small is beautiful: The picophytoplankton. Functional Ecology 12, 503–513.

Ravizza, G., Paquay, F., 2008. Os isotope chemostratigraphy applied to organic-rich marine sediments from the Eocene-Oligocene transition on the West African margin (ODP Site 959). Paleoceanography 23, 1–11.

Rickaby, R.E.M., Henderiks, J., Young, J.N., 2010. Perturbing phytoplankton: response and isotopic fractionation with changing carbonate chemistry in two coccolithophore species. Climate of the Past 6, 771–785.

Salamy, K.A., Zachos, J.C., 1999. Latest Eocene-Early Oligocene climate change and Southern Ocean fertility: Inferences from sediment accumulation and stable isotope data. Palaeogeography, Palaeoclimatology, Palaeoecology 145, 61–77.

Sarmiento, J.L., Gruber, N., Brzezinski, M.A., Dunne, J.P., 2004. High-latitude controls of thermocline nutrients and low latitude biological productivity. Nature 427, 56–60.

Sauermilch, I., Whittaker, J.M., Klocker, A., Munday, D.R., Hochmuth, K., Bijl, P.K., LaCasce, J.H., 2021.

Gateway-driven weakening of ocean gyres leads to Southern Ocean cooling. Nature Communications 12, 1–8.

Schumacher, S., Lazarus, D., 2004. Regional differences in pelagic productivity in the late Eocene to early Oligocene—a comparison of southern high latitudes and lower latitudes. Palaeogeography, Palaeoclimatology, Palaeoecology 214, 243–263.

Sutherland, R., Dickens, G.R., Blum, P., Agnini, C., Alegret, L., Bhattacharya, J., Bordenave, A., Chang, Li., Collot, J., Cramwinckel, M.J., Dallanave, E., Drake, M.K., Etienne, S.J.G., Giorgioni, M., Gurnis, M., Harper, D.T., Huang, H., Keller, A.L., Lam, A.R., Li, H., Matsui, H., Morgans, H.E.G., Newsam, C., Park, Y.H., Pascher, K.M., Pekar, S.F., Penman, D.E., Saito, S., Stratford, W.R., Westerhold, T., Zhou, X., 2019. Site U1509. Tasman Frontier Subduction Initiation and Paleogene Climate. Proceedings of the International Ocean Discovery Program, 371: College Station, TX (International Oce 371.

Villa, G., Fioroni, C., Persico, D., Roberts, A.P., Florindo, F., 2014. Middle Eocene to Late Oligocene Antarctic glaciation/deglaciation and Southern Ocean productivity. Paleoceanography 29, 223–237.

Villa, G., Florindo, F., Persico, D., Lurcock, P., de Martini, A.P., Jovane, L., Fioroni, C., 2021. Integrated calcareous nannofossil and magnetostratigraphic record of ODP Site 709: Middle Eocene to late Oligocene paleoclimate and paleoceanography of the Equatorial Indian Ocean. Marine Micropaleontology 169, 102051.

Wade, B.S., O'Neill, J.F., Phujareanchaiwon, C., Ali, I., Lyle, M., Witkowski, J., 2020. Evolution of deep-sea sediments across the Paleocene-Eocene and Eocene-Oligocene boundaries. Earth-Science Reviews 211, 103403.

Wei, W., Wise, S.W., 1990. Biogeographic gradients of middle Eocene-Oligocene calcareous nannoplankton in the South Atlantic Ocean. Palaeogeography, Palaeoclimatology, Palaeoecology 79, 29–61.

Zachos, J.C., Dickens, G.R., Zeebe, R.E., 2008. An early Cenozoic perspective on greenhouse warming and carbon-cycle dynamics. Nature 451, 279–283.

Zachos, J.C., Quinn, T.M., Salamy, K.A., 1996. High-resolution (10^4 years) deep-sea foraminiferal stable isotope records of the Eocene-Oligocene climate transition. Paleoceanography 11, 251–266.

Chapter 7

Conclusions

The Eocene-Oligocene transition (EOT) is a major evolutionary break of the Cenozoic that lead to the onset of the Antarctic glaciation; not a single "terminal event", but rather a series of events centered around the E-O boundary (EOB) (Pomerol and Premoli-Silva, 1986). In the following, we report the main conclusions achieved by this PhD project with particular regard to biostratigraphy, paleoclimate and preservation. The main motivation of this PhD project was to investigate the timing and magnitude of calcareous nannofossil response to the onset of Antarctica ice-sheet. The ~5 Myr interval across the EOT investigated in this PhD thesis allows to document the ecological dynamics of calcareous nannofossil communities, as well as their preservation state, across the Eocene-Oligocene transition. Finally, the correlation between different sites located worldwide and characterized by different depositional settings offers a unique opportunity to improve the current biostratigraphic framework and provide a reliable paleoclimatic reconstruction for this crucial time.

7.1 The Eocene-Oligocene CN biostratigraphic framework

The biostratigraphy of the Indian (Hole 756C), Pacific (Site 1209 and Site U1509) and Atlantic oceans (Hole U1411B) has been refined based on semi-quantitative calcareous nannofossil data.

In our first case study we propose additional biohorizons, which possibly implement the overall biostratigraphic framework for this interval: the Bases and Tops of acme of *Clausicoccus subdistichus* gr. and *Lanternithus minutus*, the Bases and Tops of *Sphenolithus akropodus* and the Top common (Tc) of *Isthmolithus recurvus*, at least at regional scale (**Chapter 2**).

In **Chapter 3**, calcareous nannofossil biohorizons are tied to magnetic reversals and this permits the assessment of the reliability of the aforementioned events. The comparison of low-middle and high latitudes age estimates of CN biohorizons points to support the Tc of *C. subdistichus* and the Tc of *I. recurvus*, as valuable stratigraphic tools to correlate Chron C12r.

Among the investigated taxa, *C. subdistichus* gr. has proven to be a good biostratigraphic and paleoenvironmental tool for this crucial time. The striking acme interval of *C. subdistichus* gr. is synchronous and easily recognizable at all the studied sites, even in the poorly preserved sediments of ODP Site 1209. This event has also been recognized in several Italian sections (e.g. Monechi, 1986; Nocchi et al., 1986) and in many other E-O DSDP/ODP /IODP sites (Wise, 1983; Backman, 1987; Toffanin et al., 2013). The base common (Bc) of *C. subdistichus* gr., although sometimes difficult to place, represents the best nannofossil bioevent to approximate the E-O boundary (EOB), while the highest abundance of this taxon exactly correlates with the early Oligocene Glacial Maximum – EOGM (Liu et al., 2004).

Finally, we have followed the Top common and continuous (Tc) of *C. subdistichus* gr., and establish a relative ranking with the extinction of *E. formosa* (32.92 Ma). The age estimate for the Tc of *C. subdistichus* gr. is 32.33 Ma at Site U1509 (Tasman Sea, Chapter 3) and 32.74 at Hole U1411B (North Atlantic, Chapter 5).

7.2 The Eocene-Oligocene boundary and the definition of the EOT

At Hole 756C, we documented important changes and a major turnover among calcareous nannofossil in the late Eocene -early Oligocene time. A remarkable increase in abundance (acme) of *C. subdistichus* gr. was documented very close to the extinction of the planktonic foraminiferal genus *Hantkenina* (124.37 ± 0.13 mbsf). Here, the disappearance of calcareous nannofossil *D. saipanensis* (127.18 mbsf), occurred well before the extinction of the hantkeninids and was used as a baseline to define the start of the oxygen stable isotopic shift (EOT; Hutchinson et al., 2021). During the EOT, our benthic foraminifera and bulk stable isotope $\delta^{18}O$ records gradually become more positive and culminated in a second sharp and globally distinctive positive excursion, the "early Oligocene oxygen isotope step" (EOIS), as named by Hutchinson et al. (2021). Biostratigraphically speaking, the EOIS shift occurs after the extinction level of the hantkeninids (~0.7 m above), which means 240 kyrs later than the foraminiferal event. This is the first pelagic Indian Ocean record in which this pattern, that is the "expected pattern" has been observed (**Chapter 2**). At Site U1509, our data provide a further support for the definition of the onset of the EOT positive shift based on the extinction of *D. saipanensis* (34.43 ± 0.01 Ma). These two events are approximately coincident with the base of the Late Eocene Event - LEE ($\Delta^{18}O_{bulk}$= +0.38‰). The LEE, as defined by Katz et al. (2008) (Hutchinson et al., 2021), is visible at Pacific Site U1509. The global extension of the LEE is corroborated by the recognition both in the South Pacific Ocean (Site U1509) and at Site 1209 (North Pacific), where this positive shift is recorded with a similar magnitude (**Chapter 5**).

7.3 Preservation and diagenetic issues

A detailed SEM analysis on the preservation state of nannofossils across the main phases of the E/O transition was carried out at Site U1411 and Site 1209. The clay enriched sediments at Site U1411 allow for an exceptional preservation of calcareous nannofossils that helped to document even delicate and fragile forms and micromorphologic structures. In contrast, at Site 1209, diagenesis severely affects calcareous nannofossil assemblages, preventing from any paleoecological interpretation. Despite this, for most of the section, diagenesis seems to have not alter the primary bulk isotopic signal which still retains the pristine geochemical signature. As far as biostratigraphic results are concerned, it is worth noting that many of the index species are in fact solution-resistant forms, and, thus these data are still highly reliable. Consistent age models, based on the GTS12 (Gradstein et al., 2012), were generated at each site, in order to guarantee a robust site-to-site correlation.

7.4 A global picture of paleoenvironmental changes across the EOT

Our first case study, Site 756, is a sedimentary succession recovered at Ninetyeast Ridge, in the Indian Ocean (~43°S paleolatitude) (**Chapter 2**). At this Site, shallow water depths (~400 m) permit moderate to good preservation of calcareous nannofossils as well as planktonic foraminifera. Thus, sediments from this site represent a good archive to document the ecological preferences for a number of different genera that constitute the nannofossil assemblages. Our paleoecological interpretation based on principal components analysis (PCA) and

previous literature data, allows the creation of three different eco-groups (warm-oligotrophic, temperate-eutrophic and cold-mesotrophic). Changes in the relative abundance of calcareous nannofossil taxa are consistent with changes observed in the oxygen stable isotope curve across the E-O transition. Some of the genera present in the assemblages (i.e., *Zygrhablithus*, *Dictyococcites*, *Sphenolithus* and *Isthmolithus*) have not been included in these three clusters because they display a complex behavior, and thus more studies are needed to comprehensively understand their intricate ecologies. Among them, *Isthmolithus* (i.e., *I. recurvus*), which exhibits several fluctuations in abundance, is probably the most enigmatic. Our study seems to confirm previous observations (Bukry, 1978; Wei and Wise, 1990) that suggest a latitudinal dependency for *I. recurvus.*

During the late Eocene/early Oligocene transition, calcareous nannofossil assemblages underwent an abrupt turnover with a permanent decline of the warm-oligotrophic taxa (e.g., *Discoaster* and *Ericsonia*), a decrease in species diversity and a remarkable increase in eutrophic taxa (e.g., *Clausicoccus* and *Chiasmolithus*). We interpret this profound reorganization in nannoplankton assemblages as the result of two major paleoenvironmental changes: a decrease in SST coupled with an increase in nutrient availability. A comparison with other sites from the Indo-Pacific area suggests a strong similarity in the timing and magnitude of calcareous nannofossil response, supporting the idea of global modifications in the surface water structure.

At Site U1509, based on trends and shifts recorded in the assemblages, the ~5 Myr study interval was subdivided in four distinct phases, which were also identified based on changes observed in 1) diversity indices (i.e., species richness, dominance, H-index and evenness), 2) the warm-oligotrophic taxa abundance (*Discoaster saipanensis, D. barbadiensis* and *Ericsonia formosa*), 3) the principal component (PC1 and PC2) scores, and 4) bulk stable isotopes and the carbonate content. Changes in these parameters/proxies reflect the overall decline of warm-oligotrophic communities and the increase of genera better adapted to cooler and more eutrophic conditions. The most prominent shift in the assemblages occurred in an interval of ~500 kyr, named as “the precursor phase”, with a relative increase in bulk $\delta^{18}O$ and % $CaCO_3$ values, that predated the phase of maximum glacial expansion (Early Oligocene Glacial Maximum – EOGM; Liu et al., 2004) and document the permanent loss of the late Eocene k-selected community, characterized by warm and oligotrophic taxa.

The biometric investigation performed on *C. subdistichus* gr. in the Indian, Pacific and Atlantic oceans provides key information on *C. subdistichus* gr. sensitivity to paleoenvironmental changes across different basins and geographic location and enabled us to investigate in detail the two species ascribed to this genus (i.e., *C. subdistichus* and *C. fenestratus*), which appear to represent intra-specific variations rather than inter-specific variations. The synchronous increase in abundance and size of *C. subdistichus* gr. was likely favored by high nutrient concentrations and an oversaturation of CO_3^{2-} in the sea surface waters. This latter work provides further evidence for global increases in paleoproductivity during the EOT.

7.5 Take-home messages and future perspectives

One of the main aims of this PhD thesis was to assess the impact of climate change (Antarctica glaciation) on calcareous nannofossils, including major assemblage shifts and morphometrical changes within specific groups.The main conclusion is that calcareous nannofossil assemblages from the Indian and Pacific oceans have recorded a consistent and synchronous response across the EOT, when compared with the main shifts in bulk C and O stable isotopes (**Chapter 2** and **Chapter 4**). At both studied sites (i.e., Site 756 and Site U1509), the turnover between the warm-oligotrophic community and the temperate-eutrophic community took place within the transitional conditions characterizing the EOT, but the main reorganization of the assemblage only occurred during the maximum glacial expansion in the earliest Oligocene (EOGM). These profound perturbations among calcareous nannofossils have likely been triggered by a combination of decreased temperatures and enhanced nutrient availability, likely driven by an invigorated Southern Ocean circulation. Our results further support the growing number of studies that document a global increase in surface ocean productivity in coincidence with the Antarctic glaciation (e.g. Dunkley Jones et al., 2008; Fioroni et al., 2015; Jones et al., 2019; Villa et al., 2021).

Although, the prevailing working hypothesis is that the tectonic opening of the Southern Ocean gateways was not the primary driver for the Antarctic glaciation (DeConto and Pollard, 2003; Huber et al., 2004; Liu et al., 2009), it is clear that evolving oceanographic conditions and invigorated oceanic circulation around Antarctica (Houben et al., 2019; Sauermilch et al., 2021), including deep ocean and surface water cooling (Sijp et al., 2011; Bohaty et al., 2012; Cramwinckel et al., 2018; Sauermilch et al., 2021), undoubtedly have influenced and shaped nannoplankton assemblages during this time (e.g. Villa et al., 2021), as well as entailed significant changes on ocean biochemistry and carbon uptake (Sijp et al., 2011). As the debate on the relative importance played by atmospheric CO_2 over of the opening of Southern Ocean gateways continues, it is becoming more evident that both have had a fundamental impact on Earth climate (Lear et al. 2008, Galeotti et al. 2022) and, in turn, on marine biota. In this context, this project provides key insights into the timing and relationships between global cooling/ice-growth and biotic changes in calcareous phytoplankton assemblages. Our results are also consistent with existing sea surface paleotemperature reconstructions from proxy records (Lear et al., 2008; Bohaty et al., 2012; Hutchinson et al., 2021), nannoplankton biogeographic gradients (Wei and Wise, 1990) and to the most recent high-resolution model results provided by Sauermilch et al. (2021). Data from this work also suggest that *C. subdistichus* gr. had a unique response to the environmental changes occurred at the E-O transition, showing either a great sensitivity to trophic variations or the importance of passing climate thresholds. The morphometric size increase of this group, recorded both in the Southern and Northern hemispheres, was closely coupled to the major perturbation in the global carbon cycle (positive $\delta^{13}C$ anomaly) - and the CCD deepening. Nevertheless, there are questions that are still unanswered. As for instance: which is the real signal of *C. subdistichus* gr. at low (i.e., in the equatorial belt) and high latitudes? Do on-land, open-ocean and shallow water (shelf) sections document global changes or they rather record local/regional signals? Are the enhanced productivity conditions homogeneously recorded at different latitudes? Is there any polar amplification effect?

References

Backman, J., 1987. Quantitative Calcareous Nannofossil Biochronology of Middle Eocene through Early Oligocene Sediment from DSDP Sites 522 and 523. Abhandlungen der Geologischen Bundesanstalt 39, 21–31.

Bohaty, S.M., Zachos, J.C., Delaney, M.L., 2012. Foraminiferal Mg/Ca evidence for Southern Ocean cooling across the Eocene-Oligocene transition. Earth and Planetary Science Letters 317–318, 251–261.

Bukry, D., 1978. Cenozoic silicoflagellate and coccolith stratigraphy, South Atlantic Ocean, Deep Sea Drilling Project 36.

Cramwinckel, M.J., Huber, M., Kocken, I.J., Agnini, C., Bijl, P.K., Bohaty, S.M., Frieling, J., Goldner, A., Hilgen, F.J., Kip, E.L., Peterse, F., Van Der Ploeg, R., Röhl, U., Schouten, S., Sluijs, A., 2018. Synchronous tropical and polar temperature evolution in the Eocene letter. Nature 559, 382–386.

DeConto, R.M., Pollard, D., 2003. Rapid Cenozoic glaciation of Antarctica induced by declining atmospheric CO_2. Nature 1317, 1313–1317.

Dunkley Jones, T., Bown, P.R., Pearson, P.N., Wade, B.S., Coxall, H.K., Lear, C.H., 2008. Major shifts in calcareous phytoplankton assemblages through the Eocene-Oligocene transition of Tanzania and their implications for low-latitude primary production. Paleoceanography 23, 1–14.

Fioroni, C., Villa, G., Persico, D., Jovane, L., 2015. Middle Eocene-Lower Oligocene calcareous nannofossil biostratigraphy and paleoceanographic implications from Site 711 (equatorial Indian Ocean). Marine Micropaleontology 118, 50–62.

Galeotti, S., Bijl, P., Brinkuis, H., M. DeConto, R., Escutia, C., Florindo, F., G.W. Gasson, E., Francis, J., Hutchinson, D., Kennedy-Asser, A., Lanci, L., Sauermilch, I., Sluijs, A., Stocchi, P., 2022. The Eocene-Oligocene boundary climate transition: an Antarctic perspective. In: Antarctic Climate Evolution. BV, p. 297–361.

Gradstein, F.M., Ogg, J.G., Schmitz, M.D., Ogg, G.M., 2012. The Geologic Time Scale 2012. Elsevier, Amsterdam, Netherlands.

Houben, A.J.P., Bijl, P.K., Sluijs, A., Schouten, S., Brinkhuis, H., 2019. Late Eocene Southern Ocean Cooling and Invigoration of Circulation Preconditioned Antarctica for Full-Scale Glaciation. Geochemistry, Geophysics, Geosystems 20, 2214–2234.

Huber, M., Brinkhuis, H., Stickley, C.E., Döös, K., Sluijs, A., Warnaar, J., Schellenberg, S.A., Williams, G.L., 2004. Eocene circulation of the Southern Ocean: Was Antarctica kept warm by subtropical waters? Paleoceanography 19, 1–12.

Hutchinson, D.K., Coxall, H.K., Lunt, D.J., Steinthorsdottir, M., de Boer, A.M., Baatsen, M., von der Heydt, A., Huber, M., Kennedy-Asser, A.T., Kunzmann, L., Ladant, J.B., Lear, C.H., Moraweck, K., Pearson, P.N., Piga, E., Pound, M.J., Salzmann, U., Scher, H.D., Sijp, W.P., Śliwińska, K.K., Wilson, P.A., Zhang, Z., 2021. The Eocene–Oligocene transition: a review of marine and terrestrial proxy data, models and model–data

comparisons. Climate of the Past 17, 269–315.

Jones, A.P., Dunkley Jones, T., Coxall, H.K., Pearson, P.N., Nala, D., Hoggett, M., 2019. Low-Latitude Calcareous Nannofossil Response in the Indo-Pacific Warm Pool Across the Eocene-Oligocene Transition of Java, Indonesia. Paleoceanography and Paleoclimatology 34, 1833–1847.

Katz, M.E., Miller, K.G., Wright, J.D., Wade, B.S., Browning, J. V., Cramer, B.S., Rosenthal, Y., 2008. Stepwise transition from the Eocene greenhouse to the Oligocene icehouse. Nature Geoscience 1, 329–333.

Lear, C.H., Bailey, T.R., Pearson, P.N., Coxall, H.K., Rosenthal, Y., 2008. Cooling and ice growth across the Eocene-Oligocene transition. Geology 36, 251–254.

Liu, Z., Pagani, M., Zinniker, D., Deconto, R.M.R.., Huber, M., Brinkhuis, H., Shah, S.. S.R., Leckie, R.M.M., Pearson, A., 2009. Global cooling during the Eocene-Oligocene climate transition. Science 323, 1187–1190.

Liu, Z., Tuo, S., Zhao, Q., Cheng, X., Huang, W., 2004. Deep-water earliest Oligocene glacial maximum (EOGM) in South Atlantic. Chinese Science Bulletin 49, 2190–2197.

Monechi, S., 1986. Biostratigraphy of Fuente Caldera Section by Means of Calcareous Nannofossils. Developments in Palaeontology and Stratigraphy 9, 65/69.

Nocchi, M., Parisi, G., Monaco, P., Monechi, S., Madile, M., Napoleone, G., Ripepe, M., Orlando, M., Premoli Silva, I., Bice, D.M., 1986. The Eocene-Oligocene Boundary in the Umbrian Pelagic Sequences, Italy. In: Developments in Palaeontology and Stratigraphy. Elsevier, Amsterdam, p. 25–40.

Pomerol, C., Premoli-Silva, I., 1986. Terminal Eocene Events. Elsevier.

Sauermilch, I., Whittaker, J.M., Klocker, A., Munday, D.R., Hochmuth, K., Bijl, P.K., LaCasce, J.H., 2021. Gateway-driven weakening of ocean gyres leads to Southern Ocean cooling. Nature Communications 12, 1–8.

Sijp, W.P., England, M.H., Huber, M., 2011. Effect of the deepening of the Tasman Gateway on the global ocean. Paleoceanography 26, 1–18.

Toffanin, F., Agnini, C., Rio, D., Acton, G., Westerhold, T., 2013. Middle eocene to early oligocene calcareous nannofossil biostratigraphy at IODP site U1333 (equatorial pacific). Micropaleontology 59, 69–82.

Villa, G., Florindo, F., Persico, D., Lurcock, P., de Martini, A.P., Jovane, L., Fioroni, C., 2021. Integrated calcareous nannofossil and magnetostratigraphic record of ODP Site 709: Middle Eocene to late Oligocene paleoclimate and paleoceanography of the Equatorial Indian Ocean. Marine Micropaleontology 169, 102051.

Wei, W., Wise, S.W., 1990. Biogeographic gradients of middle Eocene-Oligocene calcareous nannoplankton in the South Atlantic Ocean. Palaeogeography, Palaeoclimatology, Palaeoecology 79, 29–61.

Wise, S.W., 1983. Mesozoic and Cenozoic calcareous nannofossils recovered by Deep Sea Drilling Project Leg 71 in the Falkland Plateau region, southwest Atlantic Ocean. Init. Repts. DSDP, 71 481–550.

Appendices

Appendix I Description of relevant EOT cores

Appendix II Taxonomic list (Hole 756C)

Appendix III Dataset S1 to S6 (Hole 756C)

Appendix IV Site U1509 Calcareous nannofossil semi-quantitative data (n/mm^2)

Appendix V Site U1509 Calcareous nannofossil data (%) and geochemical data.

Appendix VI Hole 1411B and Site 1209 Calcareous nannofossil semi-quantitative data (n/mm^2), Site 1209 geochemical dataset

Appendix VII Morphometric data and additional information on *C. subdistichus* gr.

Appendix I Description of relevant EOT cores

Relevant Eocene-Oligocene cores						
North Atlantic	**Sites**	**Location**	**Latitude**	**Longitude**	**Datum type**	**References**
	ODP 913	Greenland-Norwegian Sea, North Atlantic Ocean	75.49	6.95	$\delta^{13}C_{37:2}$; $U^{K'}_{37}$; TEX86; IRD; mass susceptibility; minor elements (Zr, Ti)	Pagani et al.2011; Eldrett et al. 2007
	ODP 643	Greenland-Norwegian Sea, North Atlantic Ocean	67.72	1.03	IRD; Mass susceptibility; minor elements (Zr, Ti)	Eldrett et al. 2007
	DSDP 338	Greenland-Norwegian Sea, North Atlantic Ocean	67.78	5.39	IRD; Mass susceptibility; minor elements (Zr, Ti)	Eldrett et al. 2007
	DSDP 336	Iceland-Faroe Ridge, North Atlantic Ocean	63.35	-7.79	$\delta^{13}C_{37:2}$; $U^{K'}_{37}$; TEX86	Pagani et al. 2011
	IODP U1411	Newfoundland Ridge, NW Atlantic Ocean	41.62	-49.00	CN	Bown and Newsam 2017; This study
	ASP 5	North Carolina Slope, NW Atlantic Ocean			$\delta^{13}C_{BF}$; $\delta^{18}O_{BF}$; Mg/Ca_{BF}	Katz et al. 2011
	ODP 1053	Blake Nose, NW Atlantic Ocean	29.99	-76.52	$\delta^{13}C_{BF}$; $\delta^{18}O_{BF}$; Mg/Ca_{BF}	Katz et al. 2011
	ODP 628	Little Bahama Bank, Central Atlantic Ocean	27.53	-78.32	$\delta^{13}C_{37:2}$; $U^{K'}_{37}$; TEX86	Pagani et al. 2011
Equatorial Atlantic	ODP 929	Ceara Rise, Western Equatorial Atlantic Ocean	5.98	-43.74	$\delta^{13}C_{37:2}$; $U^{K'}_{37}$; TEX86	Pagani et al. 2011
	DSDP 366	Sierra Leone Rise, Equatorial Atlantic Ocean	5.68	-19.85	CN	Wei and Wise 1990
	ODP 925	Ceara Rise, Western Equatorial Atlantic Ocean	4.20	-43.49	$\delta^{13}C_{37:2}$; $U^{K'}_{37}$; TEX86; bio-Ba, Opal, $CaCO_3$; preactive MAR, MnEF UEF	Pagani et al. 2011; Nilsen et al. 2003
	ODP 959	West African margin, Western Equatorial Atlantic Ocean	3.63	-2.74	Os	Ravizza and Paquay 2008
	DSDP 522	Walvis Ridge, SE Atlantic Ocean	−26.1	-5.13	$\delta^{13}C_{BF}$; $\delta^{18}O_{BF}$; CN	Zachos et al. 1996; Backman 1987; Wei and Wise 1990

South Atlantic	DSDP 523	Walvis Ridge, SE Atlantic Ocean	-28.55	-2.25	CN	Backman 1987; Wei and Wise 1990
	ODP 1265	Walvis Ridge, Southern Atlantic Ocean			$\delta^{13}C_{BF}$; $\delta^{18}O_{BF}$; Mg/Ca_{BF}	Pusz et al. 2011
	DSDP 516	Rio Grande Rise, SW Atlantic Ocean	-30.28	-35.29	CN	Wei and Wise 1990
	DSDP 360	Cape Basin Continental Rise, SE Atlantic Ocean	-35.85	18.10	CN	Wei and Wise 1990
	ODP 1090	Agulhas Ridge, SE Atlantic Ocean	-42.91	8.90	$\delta^{13}C_{BF}$; $\delta^{18}O_{BF}$; $Mg/Ca_{BF;}$ $\delta^{13}C_{37:2}$; $U^{K'}_{37}$; TEX86; εNd (fossil fish teeth); CN; $\delta^{30}Si$ (sponge spicule); $BaSO_4$, $CaCO_3$,Opal, $C_{org,}$ terrigenous MAR; preactive MAR MnEF UEF; major and minor elements (Cu, Ni, Zn); Clay; Al, Ba, Ca, Fe, Mg, Mn, P, Ti, Sr, Zn; PF	Pusz et al. 2011; Pagani et al. 2011; Scher and Martin 2006, 2008; Marino and Flores 2002; Egan et al. 2013; Anderson and Delaney 2005; Diekmann et al. 2004; Latimer and Filippelli 2002; Galeotti et al. 2002.
	DSDP 513	Falkland Plateau, Atlantic Sector of Southern Ocean	-47.58	-24.64	CN	Wei and Wise 1990
	DSDP 511	Falkland Plateau, Atlantic Sector of Southern Ocean	-51.00	-46.97	CN	Wei and Wise 1990
	ODP 696	Weddell Sea, Atlantic Sector of Southern Ocean	-61.84	-42.93	Dinocyst assemblages	Houben et al. 2013
	ODP 689	Maud Rise, Atlantic Sector of Southern Ocean	-64.54	3.10	CN; BF, PF; diatoms, radiolarians MARs; CN; BFAR, $\delta^{13}C_{BF\ and\ PF}$; $\delta^{18}O_{BF\ and\ PF}$; $\delta^{30}Si$ (diatoms); εNd (fossil fish teeth); $CaCO_3$, opal, terrigenous wt%; clay; BFAR.	Persico and Villa 2004; Diester-Haass and Zahn 1993; Diester-Haass and Zahn 1996; Villa et al. 2013; Bohaty et al.2012; Sher and Martin 2004, 2006; Stott and Kennet 1990; Stott et al. 1990; Wei and Wise 1990; Egan et al. 2013; Ehrmann and Mackensen 1992; Robert et al. 2002
	ODP 690	Maud Rise, Atlantic Sector of Southern Ocean	-65.16	1.20	BF; PF; diatoms; radiolarians; CN; $CaCO_3$, opal, terrigenous wt%; clay assemblages	Diester-Haass and Zahn 1996; Villa et al. 2013; Stott and Kennet 1990; Ehrmann and Mackensen 1992
Indian Ocean	ODP 711	Madingley Rise, western Equatorial Indian Ocean	-2.74	61.16	CN	Wei et al. 1992; Fioroni et al. 2015
	ODP 709	Western equatorial Indian Ocean	-3.92	60.55	CN	Villa et al. 2021

	TDP 11, 12, 17	Kilwa Group, coastal Tanzania	-9.12	39.548	CN; PF; $\delta^{13}C_{BF}$;$Mg/Ca_{PF;}$ $\delta^{11}B$;	Dunkley Jones et al. 2008; Pearson et al. 2008; Lear et al. 2008; Pearson et al. 2009;
	NKK1	Nanggulan Section, Java	-7.79	110.21	CN; PF; BF	Jones et al. 2019; Coxall et al. 2021
	ODP 763	Exmouth Plateau, Central Indian Ocean	-20.59	112.21	$\delta^{13}C_{BF}$; $\delta^{18}O_{BF}$; $CaCO_{3;}$ Opal and terrigenous MAR; BFAR	Diester-Haass and Zahn 2001
	ODP 756	Ninetyeast Ridge, Central Indian Ocean	-27.35	87.60	CN; $\delta^{13}C_{bulk\ and\ BF}$; $\delta^{18}O_{bulk\ and\ BF}$	This study
	ODP 748	Kerguelen Plateau, Indian Sector of Southern Ocean	-58.44	78.98	CN; $\delta^{13}C_{BF}$; $\delta^{18}O_{BF}$; $Mg/Ca_{BF\ and\ PF}$; IRD	Villa et al. 2008; Bohaty et al. 2012; Diester-Haass and Zahn 2001
	ODP 744	Kerguelen Plateau, Indian Sector of Southern Ocean	-61.58	80.60	CN; BF; PF; diatoms, rdiolarians; CN; $\delta^{13}C_{BF}$; $\delta^{18}O_{BF}$;Opal, $CaCO_3$, terrigenous MAR; $Mg/Ca_{BF\ and\ PF;}$ $CaCO_{3,}$ opal, terrigenous wt% and clay; BFAR	Persico and Villa 2004; Diester-Haass and Zahn 1996; Villa et al. 2013; Zachos et al. 1996
	ODP 739	Prydz Bay, Indian Sector of Southern Ocean	-67.59	75.08	Dinocyst assemblages	Houben et al. 2013
	ODP 738	Kerguelen Plateau, Indian Sector of Southern Ocean	-62.71	82.79	CN; $\delta^{18}O_{BF}$; εNd (fossil fish teeth); IRD; MAR; $\delta^{18}O_{BF\ and\ PF}$; $Mg/Ca_{BF\ and\ PF}$; CaCO3, Opal, terrigenous wt%; clay	Villa et al. 2013; Sher et al. 2011; Bohaty et al. 2012; Ehrmann and Mackensen 1992
	ODP 1172	Tasmanian Seaway, Indian Sector of Southern Ocean	-43.96	149.93	Dinocyst; $CaCO_3$ and C_{org} wt %; diatoms	Stickley et al. 2004
	ODP 1170	Tasmanian Seaway, Indian Sector of Southern Ocean	-47.15	146.05	Dinocyst	Sluijs et al. 2003
	ODP 1171	Tasmanian Seaway, Indian Sector of Southern Ocean	-48.50	149.11	Dinocyst	Sluijs et al. 2003
	IODP 1356	Tasmanian Seaway, Indian Sector of Southern Ocean	-63.31	136.00	Dinocyst	Houben et al. 2013
	IODP 1360	Tasmanian Seaway, Indian Sector of Southern Ocean	-66.37	142.75	Dinocyst	Houben et al. 2013

North Pacific	**ODP 1209**	Shatsky Rise, Western Equatorial Pacific Ocean	32.65	158.51	CN; $\delta^{13}C_{bulk}$; $\delta^{18}O_{bulk}$ (this study); εNd (fossil fish teeth); $BaSO_4$, $CaCO_3$ MARs and wt%	This study; Thomas et al. 2003; Averyt et al. 2004; Griffith et al. 2010
	ODP 1210	Shatsky Rise, Western Equatorial Pacific Ocean	32.22	158.26	εNd (fossil fish teeth); $BaSO_4$, $CaCO_3$ MARs and wt %	Thomas et al. 2003; Averyt et al. 2004; Griffith et al. 2010
	ODP 1211	Shatsky Rise, Western Equatorial Pacific Ocean	32.00	157.85	εNd (fossil fish teeth); $BaSO_4$, $CaCO_3$ MARs and wt%	Thomas et al. 2003; Averyt et al. 2004; Griffith et al. 2010
Equatorial Pacific	ODP 803	Ontong-Java Plateau, Central Pacific Ocean	2.43	160.54	$\delta^{13}C_{37:2}$; $U^{K'}_{37}$; TEX86	Pagani et al. 2011
	IODP U1333	Eastern Equatorial Pacific Ocean	10.52	-138.42	CN; $BaSO_4$ MAR	Toffanin et al. 2013; Erhardt et al. 2013
	ODP 1218	Eastern Equatorial Pacific Ocean	8.89	-135.37	CN; δ^{13}CBF; δ^{18}OBF; BFAR and $CaCO_3$ MAR; $BaSO_4$ and $CaCO_3$ MARs; $\delta^{13}C_{37:2}$; $U^{K'}_{37}$; TEX86	Blaj et al. 2009; Coxall et al. 2005; Pälike et al. 2006; Coxall and Wilson 2011; Griffith et al. 2010; Pagani et al. 2011
	DSDP 574	Eastern Equatorial Pacific Ocean	4.21	-133.33	$BaSO_4$ MAR $CaCO_3$ MAR	Griffith et al. 2010
South Pacific	**IODP U1509**	New Caledonia Trough, Tasman Sea; Southern Pacific Ocean	-34.65	165.83	CN; $\delta^{13}C_{bulk}$; $\delta^{18}O_{bulk}$	This study
	DSDP 592	Lord Howe Rise, Tasman Sea; Southern Pacific Ocean	-36.47	165.44	$\delta^{13}C_{BF}$ $\delta^{18}O_{BF;}$ $CaCO_3$ opal and terrigenous MARs; BFAR	Diester-Haass and Zahn 2001
	DSDP 277	Pacific Sector of Southern Ocean	-55.22	166.19	$\delta^{13}C_{37:2}$; $U^{K'}_{37}$; TEX86;	Pagani et al. 2011

Appendix II Taxonomic list (Hole 756C)

Genus/species	Author year	Original name (author year)
Brameletteius	Gartner 1969	
Bramletteius serraculoides	Gartner 1969	
Chiasmolithus	Hay et al. 1966	
Chiasmolithus altus	Bukry and Percival 1971	
Chiasmolithus eoaltus	Persico and Villa 2008	
Chiasmolithus oamaruensis	Hay et al. 1966	*Tremalithus oamaruensis* (Deflandre 1954)
Clausicoccus	Prins 1979	
Clausicoccus fenestratus	Prins 1979	*Discolithus fenestratus* (Deflandre and Fert 1954)
Clausicoccus subdistichus	Prins 1979	*Ellipsolithus subdistichus* (Roth and Hay *in* Hay et al. 1967)
Coccolithus	Schwarz 1894	
Coccolithus cachaoi	Bown 2005	
Coccolithus eopelagicus (16-20µm)	Bramlette and Sullivan 1961	*Tremalithus eopelagicus* (Bramlette and Riedel 1954)
Coccolithus miopelagicus (13-16µm)	Bukry 1971	
Coccolithus pelagicus (6-13µm)	Schiller 1930	*Coccolithophora pelagica* (Wallich 1877)
Coronocyclus	Hay Mohler and Wade 1966	
Coronocyclus nitescens	Bramlette and Wilcoxon 1967	*Umbilicosphaera nitescens* (Kamptner 1963)
Cyclicargolithus	Bukry 1971	
Cyclicargolithus floridanus	Bukry 1971	*Coccolithus floridanus* (Roth and Hay in Hay et al. 1967)
Dictyococcites	Black 1967	
Dictyococcites (4-10µm; 10-14µm)	Black 1967	
Dictyococcites cf. bisectus <10µm		
Dictyococcites bisectus >10µm	Bukry and Percival 1972	*Syracosphaera bisecta* (Hay et al. 1966)
Dictyococcites filewiczii	Wise and Wiegand *in* Wise 1983	
Dictyococcites hesslandii	Haq 1971	
Discoaster	Tan Sin Hok 1927	
Discoaster barbadiensis	Tan 1927	
Discoaster deflandrei	Bramlette and Riedel 1954	
Discoaster distinctus	Martini 1958	
Discoaster robustus	Haq 1969	
Discoaster saipanensis	Bramlette and Riedel 1954	
Discoaster tani nodifer	Bramlette and Riedel 1954	
Discoaster tanii	Bramlette and Riedel 1954	
Ericsonia	Black 1964	
Ericsonia formosa	Haq 1971	*Cyclococcolithus formosus* (Kamptner 1963)
Helicosphaera	Kamptner 1954	
Helicosphaera compacta	Bramlette and Wilcoxon 1967	
Helicosphaera euphratis	Haq 1966	
Isthmolithus	Deflandre in Deflandre and Fert 1954	
Isthmolithus recurvus	Deflandre in Deflandre and Fert 1954	
Lanternithus	Stradner 1962	
Lanternithus minutus	Stradner 1962	
Pontosphaera	Lohmann 1902	
Reticulofenestra	Hay et al. 1966	
Reticulofenestra (<4µm; 4-10µm; 10-14µm)	Hay et al. 1966	
Reticulofenestra daviesii	Haq 1971	*Stradnerius daviesi* (Haq 1968)
Reticulofenestra umbilicus ≥ 14µm	Martini and Ritzkowski 1968	*Coccolithus umbilicus* (Levin 1965)
Sphenolithus	Deflandre *in* Grassè 1952	
Sphenolithus akropodus	de Kaenel and Villa 1996	
Sphenolithus cf. spiniger		
Sphenolithus distentus	Bramlette and Wilcoxon 1967	*Furcatolithus distentus* (Martini 1965)
Sphenolithus intercalaris	Martini 1976	
Sphenolithus moriformis	Bramlette and Wilcoxon 1967	*Nannoturbella moriformis* (Brönnimann and Stradner 1960)
Sphenolithus predistentus	Bramlette and Wilcoxon 1967	
Sphenolithus predistentus/distentus		
Sphenolithus radians	Deflandre *in* Grassè 1952	
Sphenolithus tribulosus	Roth 1970	
Thoracosphaera	Kamptner 1927	
Umbilicosphaera	Lohmann 1902	
Zygrhablithus	Deflandre 1959	
Zygrhablithus bijugatus	Deflandre 1959	*Zygolithus bijugatus* (Deflandre *in* Deflandre and Fert 1954)

Appendix III. Dataset S1

Leg	Sample source	Depth (mbsf)	*Braarudosphaera spp.* %	*Bramletteius serraculoides* %	*Chiasmolithus altus* %	*Chiasmolithus oamaruensis* %	*Chiasmolithus* cf. *oamaruensis* %	*Chiasmolithus spp.* %	*Clausicoccus fenestratus* %	*Clausicoccus subdistichus* %	*Clausicoccus spp.* %	*Coccolithus cachaoi* %	*Coccolithus eopelagicus* (16-20µm) %	*Coccolithus miopelagicus* (13-16µm) %
121	UO756C-5X-5W, 0.0-2.0 cm	113.46	0.00	0.00	0.00	0.00	0.00	0.00	0.00	0.30	0.00	0.00	0.30	0.00
121	UO756C-5X-5W, 20.0-22.0 cm	113.66	0.00	0.00	0.00	0.00	0.00	0.00	0.00	0.00	0.00	0.00	0.00	0.00
121	UO756C-5X-5W, 40.0-42.0 cm	113.86	0.00	0.00	0.00	0.00	0.00	0.00	0.00	0.00	0.00	0.00	0.00	0.00
121	UO756C-5X-5W, 60.0-63.0 cm	114.06	0.00	0.32	0.00	0.00	0.00	0.00	0.00	0.00	0.00	0.00	0.00	0.00
121	UO756C-5X-5W, 79.0-81.0 cm	114.25	0.00	0.00	0.00	0.00	0.00	0.00	0.00	0.00	0.00	0.00	0.00	0.00
121	UO756C-5X-6W, 0.0-2.0 cm	114.28	0.00	0.00	0.00	0.00	0.00	0.00	0.00	0.00	0.00	0.00	0.00	0.00
121	UO756C-5X-6W, 20.0-22.0 cm	114.48	0.00	0.00	0.00	0.00	0.00	0.00	0.00	0.00	0.29	0.00	0.00	0.00
121	UO756C-5X-6W, 40.0-42.0 cm	114.68	0.00	0.00	0.00	0.00	0.00	0.62	0.00	0.00	0.00	0.00	0.00	0.00
121	UO756C-5X-6W, 60.0-62.0 cm	114.88	0.00	0.32	0.00	0.00	0.00	0.32	0.00	0.00	0.00	0.00	0.00	0.32
121	UO756C-5X-6W, 78.5-80.5 cm	115.07	0.00	0.00	0.00	0.00	0.00	0.00	0.00	0.00	0.00	0.00	0.00	0.00
121	UO756C-5X-6W, 100.0-102.0 cm	115.28	0.00	0.00	0.00	0.00	0.00	0.00	0.00	0.00	0.00	0.00	0.00	0.00
121	UO756C-5X-6W, 120.0-122.0 cm	115.48	0.00	0.00	0.00	0.00	0.00	0.00	0.00	0.00	0.00	0.00	0.00	0.00
121	UO756C-5X-7W, 0.0-2.0 cm	115.61	0.00	0.00	0.00	0.00	0.00	0.00	0.00	0.27	0.00	0.00	0.00	0.00
121	UO756C-5X-7W, 20.0-22.0 cm	115.81	0.00	0.00	0.00	0.00	0.00	0.00	0.00	0.00	0.00	0.00	0.00	0.00
121	UO756C-5X-7W, 40.0-42.0 cm	116.01	0.00	0.00	0.00	0.00	0.00	0.00	0.00	0.00	0.00	0.00	0.00	0.00
121	UO756C-5X-7W, 60.0-62.0 cm	116.21	0.00	0.00	0.00	0.00	0.00	0.00	0.00	0.00	0.00	0.00	0.26	0.00
121	UO756C-5X-7W, 79.0-81.0 cm	116.40	0.00	0.00	0.00	0.00	0.00	0.00	0.00	0.00	0.00	0.00	0.00	0.00
121	UO756C-5X-7W, 100.0-102.0 cm	116.61	0.00	0.00	0.00	0.00	0.00	0.00	0.00	0.00	0.00	0.00	0.00	0.00
121	UO756C-5X-7W, 120.0-122.0 cm	116.81	0.00	0.00	0.30	0.00	0.00	0.60	0.00	0.00	0.00	0.00	0.00	0.00
121	UO756C-5X-7W, 140.0-142.0 cm	117.01	0.00	0.00	0.00	0.00	0.00	0.31	0.00	0.31	0.00	0.00	0.00	0.00
121	UO756C-5X-8W, 0.0-2.0 cm	117.11	0.00	0.00	0.00	0.00	0.00	0.30	0.00	0.00	0.00	0.00	0.00	0.00
121	UO756C-5X-8W, 20.0-22.0 cm	117.31	0.00	0.00	0.28	0.00	0.00	0.00	0.00	0.28	0.00	0.00	0.00	0.00
121	UO756C-5X-8W, 40.0-42.0 cm	117.51	0.00	0.00	0.00	0.00	0.00	0.98	0.00	0.33	0.00	0.00	0.00	0.00
121	UO756C-5X-8W, 60.0-62.0 cm	117.71	0.00	0.00	0.67	0.00	0.00	0.67	0.00	0.00	0.00	0.00	0.00	0.00
121	UO756C-5X-8W, 79.0-81.0 cm	117.90	0.00	0.00	0.63	0.00	0.00	0.63	0.00	1.90	0.00	0.00	0.00	0.00
121	UO756C-5X-8W, 100.0-102.0 cm	118.10	0.00	0.00	0.30	0.00	0.00	0.00	0.00	7.51	0.00	0.00	0.00	0.00
121	UO756C-5X-8W, 121.0-123.0 cm	118.32	0.00	0.27	0.54	0.00	0.00	0.00	0.27	5.41	0.00	0.00	0.00	0.00
121	UO756C-5X-CCW, 10.5-12.5 cm	118.47	0.00	0.00	0.78	0.00	0.00	0.26	0.00	10.88	0.00	0.00	0.00	0.00
121	UO756C-6X-1W, 10.0-12.0 cm	120.30	0.00	0.00	0.26	0.00	0.00	0.26	0.00	7.95	0.00	0.00	0.00	0.00
121	UO756C-6X-1W, 20.0-22.0 cm	120.40	0.00	0.00	0.59	0.00	0.00	0.00	0.00	7.04	0.00	0.00	0.00	0.29
121	UO756C-6X-1W, 30.0-32.0 cm	120.50	0.00	0.60	0.00	0.00	0.00	0.30	0.00	7.55	0.00	0.30	0.00	0.00
121	UO756C-6X-1W, 40.0-42.0 cm	120.60	0.00	0.92	0.61	0.31	0.00	0.31	0.00	8.26	0.00	0.00	0.00	0.31
121	UO756C-6X-1W, 50.0-52.0 cm	120.70	0.00	1.26	0.31	0.00	0.00	0.63	0.31	8.18	0.00	0.00	0.31	0.31
121	UO756C-6X-1W, 60.0-62.0 cm	120.80	0.00	1.19	0.30	0.00	0.00	0.00	0.00	10.68	0.00	0.00	0.00	0.00
121	UO756C-6X-1W, 70.0-72.0 cm	120.90	0.00	0.00	0.55	0.00	0.00	0.55	0.00	6.59	0.00	0.00	0.00	0.27
121	UO756C-6X-1W, 80.0-82.0 cm	121.00	0.00	2.85	0.28	0.00	0.00	0.00	0.00	13.39	0.00	0.00	0.00	0.00
121	UO756C-6X-1W, 90.0-92.0 cm	121.10	0.00	2.32	0.00	0.00	0.00	0.29	0.29	10.14	0.00	0.00	0.00	0.00
121	UO756C-6X-1W, 100.0-102.0 cm	121.20	0.00	0.30	0.89	0.30	0.30	0.30	0.59	13.02	0.00	0.00	0.00	0.30
121	UO756C-6X-1W, 110.0-112.0 cm	121.30	0.00	1.20	0.00	0.00	0.00	0.60	0.00	13.47	0.00	0.00	0.00	0.30
121	UO756C-6X-1W, 120.0-122.0 cm	121.40	0.00	0.81	1.35	0.00	0.00	1.08	0.00	11.32	0.00	0.00	0.27	0.81
121	UO756C-6X-1W, 130.0-132.0 cm	121.50	0.00	0.00	0.60	0.00	0.00	0.30	0.00	12.28	0.00	0.00	0.00	0.00
121	UO756C-6X-1W, 140.0-142.0 cm	121.60	0.00	0.00	0.00	0.00	0.00	0.00	0.00	9.97	0.00	0.00	0.00	0.00
121	UO756C-6X-2W, 10.0-12.0 cm	121.80	0.00	0.66	1.32	0.00	0.00	0.33	0.00	10.86	0.00	0.33	0.00	0.33
121	UO756C-6X-2W,19.5-21.5 cm	121.90	0.00	0.00	0.00	0.00	0.00	2.59	0.00	10.36	0.00	0.00	0.00	0.32
121	UO756C-6X-2W, 28.5-30.5 cm	121.99	0.00	0.00	0.00	0.00	0.00	1.31	0.00	8.20	0.00	0.00	0.00	0.00
121	UO756C-6X-2W, 40.0-42.0 cm	122.10	0.00	1.34	0.00	0.00	0.00	0.80	0.00	17.11	0.00	0.00	0.00	0.00
121	UO756C-6X-2W, 50.0-52.0 cm	122.20	0.00	0.29	0.00	0.00	0.00	0.29	0.00	20.76	0.00	0.00	0.00	0.29
121	UO756C-6X-2W, 60.0-62.0 cm	122.30	0.00	0.00	0.30	0.30	0.00	1.22	0.00	16.77	0.00	0.00	0.00	0.00
121	UO756C-6X-2W, 71.5-73.5 cm	122.42	0.00	0.00	0.28	0.00	0.00	2.56	0.00	14.20	0.00	0.28	0.00	0.00
121	UO756C-6X-2W, 81.0-83.0 cm	122.51	0.00	0.00	0.00	0.00	0.00	0.59	0.29	10.85	0.00	0.00	0.00	0.00
121	UO756C-6X-2W, 90.0-92.0 cm	122.60	0.00	0.28	0.00	0.00	0.00	1.10	0.00	14.09	0.00	0.00	0.83	0.00
121	UO756C-6X-2W, 101.0-103.0 cm	122.71	0.33	0.33	0.33	0.00	0.00	1.31	0.00	11.48	0.00	0.00	0.00	0.00

121	UO756C-6X-2W, 110.0-112.0 cm	122.80	0.00	0.00	0.00	0.00	0.00	0.58	0.00	13.41	0.00	0.00	0.00	0.00
121	UO756C-6X-2W, 121.0-123.0 cm	122.91	0.00	0.00	0.00	0.00	0.00	1.31	0.00	11.48	0.00	0.00	0.00	0.66
121	UO756C-6X-2W, 131.5-133.5 cm	123.02	0.00	0.00	0.00	0.00	0.00	0.31	0.00	17.39	0.00	0.00	0.00	0.00
121	UO756C-6X-2W, 142.0-144.0 cm	123.12	0.00	0.00	0.80	0.00	0.27	0.80	0.53	11.47	0.00	0.27	0.00	0.53
121	UO756C-6X-3W, 10.0-12.0 cm	123.30	0.00	0.00	0.00	0.00	0.00	0.54	0.00	13.35	0.00	0.00	0.00	0.00
121	UO756C-6X-3W, 20.0-22.0 cm	123.40	0.00	0.61	0.00	0.00	0.00	1.22	0.00	9.42	0.00	0.00	0.00	0.30
121	UO756C-6X-3W, 30.0-32.0 cm	123.50	0.00	0.00	0.00	0.00	0.00	0.00	0.00	7.55	0.00	0.00	0.00	0.00
121	UO756C-6X-3W, 40.0-42.0 cm	123.60	0.00	0.00	0.00	0.00	0.00	0.99	0.00	7.24	0.00	0.00	0.00	0.00
121	UO756C-6X-3W, 50.0-52.0 cm	123.70	0.00	0.62	0.00	0.00	0.00	0.00	0.00	2.17	0.00	0.00	0.62	0.62
121	UO756C-6X-3W, 60.0-62.0 cm	123.80	0.00	0.00	0.00	0.00	0.00	0.00	0.27	2.14	0.00	0.00	0.27	1.07
121	UO756C-6X-3W, 69.0-71.0 cm	123.89	0.00	0.63	0.00	0.00	0.00	0.00	0.00	3.45	0.00	0.00	0.63	0.63
121	UO756C-6X-3W, 79.0-81.0 cm	123.99	0.00	0.28	0.28	0.00	0.00	0.28	0.28	10.80	0.00	0.00	0.00	0.28
121	UO756C-6X-3W, 90.0-94.0 cm	124.10	0.00	1.13	0.00	0.00	0.00	0.00	0.00	2.27	0.57	0.85	0.00	0.00
121	UO756C-6X-3W, 102.5-104.5 cm	124.23	0.00	0.00	0.00	0.00	0.00	0.00	0.00	2.13	0.00	0.27	0.00	0.00
121	UO756C-6X-3W, 111.5-113.5 cm	124.32	0.00	0.00	0.00	0.00	0.00	0.00	0.00	2.10	0.00	0.00	0.30	0.00
121	UO756C-6X-3W, 120.0-122.0 cm	124.40	0.00	0.32	0.00	0.00	0.00	0.00	0.00	2.91	0.00	0.65	0.00	0.00
121	UO756C-6X-3W, 129.5-131.5 cm	124.50	0.00	0.00	0.00	0.00	0.00	0.30	0.00	0.90	0.00	0.00	0.00	0.00
121	UO756C-6X-3W, 139.5- 141.5 cm	124.60	0.00	0.58	0.00	0.00	0.00	0.00	0.00	2.33	0.29	0.87	0.00	0.00
121	UO756C-6X-4W, 20.0-22.0 cm	124.90	0.00	0.00	0.00	0.00	0.00	0.00	0.28	1.94	0.00	0.00	0.00	0.28
121	UO756C-6X-4W, 30.0-32.0 cm	125.00	0.00	0.00	0.00	0.00	0.00	0.00	0.00	2.86	0.00	0.00	0.00	0.00
121	UO756C-6X-4W, 41.5-43.5 cm	125.12	0.00	0.27	0.00	0.27	0.00	0.00	0.00	0.27	0.00	0.00	0.27	0.27
121	UO756C-6X-4W, 60.0-64.0 cm	125.30	0.00	0.00	0.00	0.00	0.00	0.87	0.00	1.17	0.00	0.00	0.29	0.29
121	UO756C-6X-4W, 70.0-72.0 cm	125.40	0.00	0.00	0.00	0.00	0.00	0.00	0.00	0.30	0.00	0.00	0.00	0.00
121	UO756C-6X-4W, 80.0-82.0 cm	125.50	0.00	0.62	0.31	0.31	0.00	1.86	0.00	0.62	0.31	0.00	0.62	0.00
121	UO756C-6X-4W, 90.0-92.0 cm	125.60	0.00	0.00	0.00	0.00	0.00	3.18	0.00	0.64	0.00	0.00	0.00	0.00
121	UO756C-6X-4W, 100.0-102.0 cm	125.70	0.00	0.33	0.00	0.00	0.00	0.33	0.00	0.00	0.00	1.31	0.00	0.33
121	UO756C-6X-4W, 111.0-113.0 cm	125.81	0.00	0.00	0.00	0.27	0.00	0.81	0.00	0.00	0.00	0.00	0.27	0.81
121	UO756C-6X-4W, 129.0-131-0 cm	125.99	0.00	0.65	0.00	0.00	0.00	1.30	0.00	0.65	0.00	1.30	0.00	0.32
121	UO756C-6X-4W, 140.0-142.0 cm	126.10	0.00	0.30	0.00	0.00	0.00	0.61	0.00	0.30	0.00	0.00	0.00	0.61
121	UO756C-6X-5W, 10.0-12.0 cm	126.30	0.00	0.00	0.00	0.00	0.00	0.00	0.00	0.00	0.00	0.00	0.00	0.28
121	UO756C-6X-5W, 20.0-22.0 cm	126.40	0.00	0.32	0.00	0.00	0.00	0.96	0.00	2.57	0.00	0.00	0.32	0.00
121	UO756C-6X-5W, 40.0-42.0 cm	126.60	0.00	1.86	0.00	0.00	0.00	0.31	0.00	0.62	0.00	0.00	0.00	0.00
121	UO756C-6X-5W, 50.0-52.0 cm	126.70	0.00	0.00	0.00	0.00	0.00	0.00	0.31	3.13	0.00	0.00	0.31	0.63
121	UO756C-6X-5W, 60.0-62.0 cm	126.80	0.00	0.90	0.00	0.00	0.00	0.30	0.00	4.22	0.00	0.30	0.00	0.00
121	UO756C-6X-5W, 70.0-72.0 cm	126.90	0.00	0.63	0.00	0.00	0.00	0.94	0.31	3.77	0.63	0.00	0.00	0.00
121	UO756C-6X-5W, 80.0-82.0 cm	127.00	0.00	1.12	0.00	0.00	0.00	0.56	0.00	1.68	0.00	0.28	0.28	0.56
121	UO756C-6X-5W, 90.0-92.0 cm	127.10	0.00	1.21	0.00	0.00	0.00	0.00	0.00	0.91	0.60	0.00	0.00	0.00
121	UO756C-6X-CCW, 10.0-12.0 cm	127.25	0.00	1.39	0.00	0.00	0.00	0.00	0.00	0.00	0.00	0.00	0.00	1.11
121	UO756C-7X-1W, 0.0-2.0 cm	129.80	0.00	0.30	0.00	0.00	0.00	0.00	0.00	0.61	0.00	0.00	0.00	0.30
121	UO756C-7X-1W, 20.0-22.0	130.00	0.00	0.28	0.00	0.00	0.00	0.00	0.00	0.00	0.00	0.00	0.28	0.00
121	UO756C-7X-1W, 60.0-62.0 cm	130.40	0.00	0.00	0.00	0.00	0.00	0.28	0.00	0.56	0.00	0.00	0.28	0.56
121	UO756C-7X-1W, 80.0-82.0 cm	130.60	0.00	0.00	0.28	0.00	0.00	0.57	0.00	1.13	0.00	0.00	1.13	0.00
121	UO756C-7X-1W, 99.0-101.0 cm	130.79	0.00	0.30	0.00	0.00	0.00	0.59	0.00	0.89	0.00	0.00	0.30	0.30
121	UO756C-7X-1W, 141.5-143.5 cm	131.22	0.00	0.30	0.00	0.00	0.00	0.30	0.00	2.13	0.00	0.00	0.00	0.00
121	UO756C-7X-2W, 0.0-2.0 cm	131.30	0.00	0.88	0.00	0.00	0.00	0.29	0.00	1.75	0.00	0.00	0.58	0.29
121	UO756C-7X-2W, 19.0-21.0 cm	131.49	0.00	0.58	0.58	0.00	0.00	0.00	0.00	4.03	0.00	0.29	1.44	0.00
121	UO756C-7X-2W, 60-0-62.0 cm	131.90	0.00	0.95	0.00	0.00	0.00	0.00	0.00	4.42	0.00	0.63	0.00	0.00
121	UO756C-7X-2W, 80-0-82.0 cm	132.10	0.00	3.15	0.00	0.00	0.00	0.86	0.29	0.29	0.00	0.57	0.86	0.00
121	UO756C-7X-2W, 99.0-101.0 cm	132.29	0.00	1.62	0.00	0.00	0.00	0.00	0.00	1.62	0.00	0.00	0.00	0.00
121	UO756C-7X-2W, 140.0-142.0 cm	132.70	0.00	0.91	0.00	0.00	0.00	0.00	0.00	0.00	0.00	0.00	0.00	0.00

Coccolithus pelagicus (6-13µm) %	*Coronocyclus nitescens* %	*Cyclicargolithus floridanus* %	*Dictyococcites spp.* <4µm %	*Dictyococcites spp.* 4-10µm %	*Dictyococcites spp.* 10-14µm %	*Dictyococcites bisectus* >10µm %	*Dictyococcites aff. bisectus* <10µm %	*Dictyococcites filewiczii* %	*Dictyococcites hesslandii* %	*Discoaster barbadiensis* %	*Discoaster deflandrei* %	*Discoaster distinctus* %	*Discoaster robustus* %	*Discoaster saipanensis* %	*Discoaster saipanensis* (<6µm) %	*Discoaster tanii* %	*Discoaster tanii gr.* %	*Discoaster tani nodifer* %
8.96	0.00	6.27	0.00	0.00	0.00	3.28	2.99	0.00	1.19	0.00	0.30	0.00	0.00	0.00	0.00	0.60	0.00	0.30
10.23	0.00	4.95	0.00	0.00	0.00	0.99	1.65	0.33	0.33	0.00	0.00	0.00	0.00	0.00	0.00	0.00	0.00	0.00
19.68	0.00	12.90	0.00	0.00	0.00	4.19	1.29	0.32	0.65	0.00	0.00	0.00	0.00	0.00	0.00	0.00	0.00	0.00
13.18	0.00	9.65	0.00	0.00	0.00	0.32	0.32	0.00	0.00	0.00	0.00	0.00	0.00	0.00	0.00	0.32	0.00	0.00
21.47	0.00	22.76	0.00	0.00	0.00	2.24	1.28	0.00	0.96	0.00	0.00	0.00	0.00	0.00	0.00	0.00	0.00	0.00
12.42	0.00	9.15	0.00	0.98	0.33	0.65	0.98	0.33	0.33	0.00	0.00	0.00	0.00	0.00	0.00	0.00	0.00	0.00
14.24	0.00	14.24	0.00	0.00	0.00	2.62	1.16	0.00	1.16	0.00	0.00	0.00	0.00	0.00	0.00	0.29	0.00	0.00
21.30	0.00	4.63	0.00	0.00	0.00	2.16	1.54	0.00	2.47	0.00	0.00	0.00	0.00	0.00	0.00	0.00	0.00	0.00
25.95	0.00	8.23	0.00	0.00	0.00	6.96	3.16	0.00	0.63	0.00	0.00	0.00	0.00	0.00	0.00	0.00	0.00	0.00
18.44	0.52	7.27	0.00	0.00	0.00	2.34	2.86	0.26	1.30	0.00	0.52	0.00	0.00	0.00	0.00	0.00	0.00	0.00
19.34	0.00	2.95	0.00	0.00	0.00	3.61	1.31	0.00	0.66	0.00	0.00	0.00	0.00	0.00	0.00	0.33	0.00	0.00
10.91	0.00	6.67	0.00	0.00	0.00	0.61	0.30	0.00	0.30	0.00	0.00	0.00	0.00	0.00	0.00	0.00	0.00	0.00
14.32	0.00	13.79	0.00	0.00	0.00	2.92	1.06	0.00	1.33	0.00	0.00	0.00	0.00	0.00	0.00	0.53	0.00	0.00
11.68	0.00	10.87	0.00	0.00	0.00	0.54	2.72	0.00	0.54	0.00	0.00	0.00	0.00	0.00	0.00	0.27	0.00	0.00
12.54	0.00	17.09	0.00	0.00	0.00	3.99	3.13	0.00	0.85	0.00	0.00	0.00	0.00	0.00	0.00	0.00	0.00	0.00
16.14	0.00	10.58	0.00	0.00	0.00	2.91	2.91	0.26	0.79	0.00	0.00	0.26	0.00	0.00	0.00	0.26	0.00	0.00
18.18	0.00	10.30	0.00	0.00	0.00	4.24	3.03	0.00	0.61	0.00	0.00	0.00	0.00	0.00	0.00	0.00	0.00	0.00
28.42	0.00	4.65	0.00	0.52	0.00	3.36	1.03	0.52	2.07	0.00	0.00	0.00	0.00	0.00	0.00	0.00	0.00	0.00
22.16	0.00	5.69	0.00	0.00	0.00	2.69	1.50	0.60	0.60	0.00	0.00	0.00	0.00	0.00	0.00	0.00	0.00	0.00
19.88	0.00	8.56	0.00	0.61	0.00	3.67	1.53	0.00	1.22	0.00	0.00	0.00	0.00	0.00	0.00	0.31	0.00	0.00
26.51	0.00	4.22	0.00	0.00	0.00	2.41	3.92	0.30	0.00	0.00	0.00	0.00	0.00	0.00	0.00	0.60	0.00	0.00
24.72	0.00	9.27	0.00	0.00	0.00	3.93	2.81	0.00	0.56	0.00	0.00	0.00	0.00	0.00	0.00	0.56	0.00	0.00
14.66	0.00	2.61	0.00	0.00	0.00	1.63	1.30	0.33	0.98	0.00	0.00	0.00	0.00	0.00	0.00	0.00	0.00	0.00
15.33	0.00	7.67	0.00	0.00	0.00	0.67	1.67	0.33	1.00	0.00	0.00	0.00	0.00	0.00	0.00	0.33	0.00	0.00
8.25	0.00	4.44	0.00	0.00	0.00	4.13	1.90	0.32	1.27	0.00	0.00	0.00	0.00	0.00	0.00	0.00	0.00	0.00
14.11	0.00	7.21	0.00	0.00	0.00	0.00	1.80	0.60	2.70	0.00	0.00	0.00	0.00	0.00	0.00	0.00	0.00	0.00
17.30	0.27	10.54	0.00	0.00	0.00	2.43	2.16	0.00	1.89	0.00	0.00	0.27	0.00	0.00	0.00	0.27	0.00	0.00
19.95	0.00	6.99	0.00	0.00	0.00	1.55	1.55	0.26	3.37	0.00	0.00	0.00	0.00	0.00	0.00	0.00	0.00	0.00
16.41	0.00	3.59	0.00	0.00	0.00	0.51	1.28	0.26	1.28	0.00	0.00	0.00	0.00	0.00	0.00	0.00	0.00	0.00
14.66	0.00	2.35	0.00	0.29	0.00	3.52	3.23	0.59	2.93	0.00	0.00	0.00	0.00	0.00	0.00	0.00	0.00	0.00
21.45	0.00	3.02	0.00	0.00	0.00	1.81	0.60	0.30	3.63	0.00	0.00	0.00	0.00	0.00	0.00	0.00	0.00	0.00
13.76	0.00	2.75	0.00	0.00	0.00	1.53	3.36	0.31	3.98	0.00	0.00	0.00	0.00	0.00	0.00	0.00	0.00	0.00
16.04	0.00	2.52	0.00	0.00	0.00	1.89	4.09	0.31	3.14	0.00	0.00	0.00	0.00	0.00	0.00	0.00	0.00	0.00
15.73	0.00	4.15	0.00	0.30	0.00	0.89	2.08	0.00	2.37	0.00	0.00	0.00	0.00	0.00	0.00	0.30	0.00	0.00
14.01	0.00	2.20	0.00	0.00	0.00	4.67	4.12	0.27	2.47	0.00	0.00	0.27	0.00	0.00	0.00	0.27	0.00	0.00
21.37	0.00	3.42	0.00	0.00	0.00	1.99	1.14	0.28	3.42	0.00	0.00	0.00	0.00	0.00	0.00	0.28	0.00	0.00
11.30	0.00	4.64	0.00	0.00	0.00	0.87	1.74	0.00	3.19	0.00	0.00	0.00	0.00	0.00	0.00	0.00	0.00	0.00
20.71	0.00	4.14	0.00	0.00	0.00	1.18	2.66	0.30	0.89	0.00	0.30	0.00	0.00	0.00	0.00	0.00	0.00	0.00
18.56	0.00	5.39	0.00	0.00	0.00	1.20	5.09	0.00	1.50	0.00	0.30	0.00	0.00	0.00	0.00	0.00	0.00	0.00
24.53	0.00	3.50	0.00	0.00	0.00	1.89	3.23	0.00	1.62	0.00	0.27	0.00	0.00	0.00	0.00	0.54	0.00	0.00
17.37	0.00	8.08	0.00	0.00	0.00	2.69	2.99	0.30	0.90	0.00	0.60	0.00	0.00	0.00	0.00	0.30	0.00	0.00
22.51	0.00	2.25	0.00	0.00	0.32	0.96	1.93	0.00	2.89	0.00	0.64	0.00	0.00	0.00	0.00	0.32	0.00	0.00
20.72	0.00	2.96	0.00	0.00	0.00	3.29	1.97	0.00	1.64	0.00	0.33	0.00	0.00	0.00	0.00	0.00	0.00	0.00
19.74	0.00	2.59	0.00	0.00	0.00	1.29	2.27	0.65	4.21	0.00	0.32	0.00	0.00	0.00	0.00	0.32	0.00	0.00
17.38	0.00	0.98	0.00	0.00	0.00	3.93	2.95	0.00	2.30	0.00	0.00	0.00	0.00	0.00	0.00	0.00	0.00	0.00
13.90	0.53	3.74	0.00	0.00	0.00	1.07	2.14	0.27	2.94	0.00	0.00	0.00	0.00	0.00	0.00	0.00	0.00	0.00
15.20	0.00	4.97	0.00	0.00	0.00	1.75	2.34	0.00	1.46	0.00	0.00	0.00	0.00	0.00	0.00	0.00	0.00	0.00
14.33	0.30	3.35	0.00	0.00	0.00	1.22	0.61	0.00	3.05	0.00	0.00	0.00	0.00	0.00	0.00	0.30	0.00	0.30
15.06	0.00	3.69	0.00	0.00	0.00	1.99	1.99	0.00	1.42	0.00	0.00	0.00	0.00	0.00	0.00	0.00	0.00	0.00
16.13	0.00	2.64	0.00	0.00	0.00	1.47	2.05	0.00	3.23	0.00	0.00	0.00	0.00	0.00	0.00	0.00	0.00	0.00
14.64	0.28	4.42	0.00	0.00	0.00	1.66	2.76	0.28	1.38	0.00	0.00	0.00	0.00	0.00	0.00	0.00	0.00	0.00
19.67	0.00	4.92	0.00	0.00	0.00	2.95	2.30	0.00	3.28	0.00	0.00	0.00	0.00	0.00	0.00	0.98	0.00	0.00

16.03	0.00	3.50	0.00	0.00	0.00	2.62	1.75	0.00	2.62	0.00	0.00	0.00	0.00	0.00	0.00	0.00	0.00	0.00
17.05	0.00	2.95	0.00	0.00	0.00	0.98	2.95	0.00	4.26	0.00	0.33	0.00	0.00	0.00	0.00	0.00	0.00	0.00
22.36	0.00	3.11	0.00	0.00	0.00	1.24	0.00	0.00	1.86	0.00	0.00	0.00	0.00	0.00	0.00	0.00	0.00	0.00
15.20	0.00	2.93	0.00	0.00	0.00	0.80	0.53	0.53	1.33	0.00	0.00	0.00	0.00	0.00	0.00	0.53	0.00	0.00
20.98	0.00	0.82	0.00	0.00	0.00	0.82	2.72	0.00	1.36	0.00	0.00	0.00	0.00	0.00	0.00	0.00	0.00	0.00
26.44	0.30	1.52	0.00	0.00	0.00	0.61	1.52	0.00	2.74	0.00	0.00	0.00	0.00	0.00	0.00	0.30	0.00	0.00
34.77	0.00	1.89	0.00	0.00	0.00	1.62	1.35	0.00	1.08	0.00	0.00	0.00	0.00	0.00	0.00	0.27	0.00	0.00
25.99	0.33	2.63	0.00	0.00	0.00	0.66	1.32	0.66	2.30	0.00	0.00	0.00	0.00	0.00	0.00	0.66	0.00	0.00
29.41	0.00	2.48	0.00	0.00	0.00	4.95	3.41	0.62	4.95	0.00	0.00	0.00	0.00	0.00	0.00	0.00	0.31	0.00
22.99	0.00	5.08	0.00	0.00	0.00	2.14	1.34	0.53	2.41	0.00	0.00	0.00	0.00	0.00	0.00	0.00	0.27	0.00
25.08	0.00	3.13	0.00	0.00	0.00	5.02	4.39	0.94	2.19	0.00	0.00	0.00	0.00	0.00	0.00	0.00	0.00	0.00
19.67	0.00	3.32	0.00	0.00	0.00	1.94	2.49	0.28	2.49	0.00	0.00	0.28	0.00	0.00	0.00	0.28	0.00	0.00
28.05	0.00	2.55	0.00	0.00	0.00	2.27	4.25	0.00	2.27	0.00	0.00	0.00	0.00	0.00	0.00	0.28	0.00	0.00
22.34	0.00	1.60	0.00	0.00	0.00	3.99	6.65	0.00	2.66	0.00	0.00	0.00	0.00	0.00	0.00	0.53	0.00	0.00
28.83	0.00	2.10	0.00	0.00	0.00	3.00	2.70	0.00	3.30	0.00	0.00	0.00	0.00	0.00	0.00	2.10	0.00	0.00
19.74	0.32	2.59	0.00	0.00	0.00	2.27	1.62	0.32	1.62	0.00	0.00	0.00	0.00	0.00	0.00	0.32	0.00	0.00
25.97	0.00	0.60	0.00	0.00	0.00	3.58	3.28	0.30	1.79	0.00	0.00	0.00	0.00	0.00	0.00	1.49	0.00	0.30
21.28	0.00	0.87	0.00	0.00	0.00	3.21	2.92	0.00	2.62	0.00	0.00	0.00	0.00	0.00	0.00	0.00	0.00	0.00
21.94	0.00	0.56	0.00	0.00	0.00	0.83	2.22	0.56	1.39	0.00	0.00	0.00	0.00	0.00	0.00	0.56	0.00	0.28
20.57	0.00	2.86	0.00	0.00	0.00	2.00	1.43	0.29	0.86	0.00	0.00	0.00	0.00	0.00	0.00	0.00	0.00	0.00
18.83	0.00	0.27	0.00	0.00	0.00	1.06	1.06	0.53	1.33	0.00	0.00	0.00	0.00	0.00	0.00	0.53	0.00	0.00
13.99	0.00	1.75	0.00	0.00	0.00	2.04	3.50	0.58	5.54	0.00	0.00	0.00	0.29	0.00	0.00	0.87	0.00	0.00
28.19	0.00	0.30	0.00	0.00	0.00	0.89	0.30	0.00	2.97	0.00	0.00	0.00	0.00	0.00	0.00	1.19	0.00	0.00
18.32	0.00	1.86	0.00	0.00	0.00	2.17	5.90	0.00	1.24	0.00	0.00	0.00	0.00	0.00	0.00	2.48	0.00	0.00
27.71	0.00	0.96	0.00	0.00	0.00	0.64	0.96	0.00	1.27	0.00	0.00	0.00	0.00	0.00	0.00	1.91	0.00	0.00
23.93	0.00	1.97	0.00	0.33	0.00	1.97	3.28	0.98	0.00	0.00	0.00	0.00	0.00	0.00	0.00	0.66	0.00	0.00
27.03	0.00	0.00	0.00	0.00	0.00	3.51	2.70	0.27	3.24	0.00	0.00	0.00	0.00	0.00	0.00	2.16	0.00	0.00
27.60	0.00	0.32	0.00	0.00	0.00	3.90	3.90	0.32	1.30	0.00	0.32	0.00	0.00	0.00	0.00	1.30	0.00	0.00
32.73	0.00	0.30	0.00	0.00	0.00	2.12	1.52	0.00	1.82	0.00	0.00	0.00	0.00	0.00	0.00	2.12	0.00	0.00
25.77	0.00	0.56	0.00	0.28	0.00	0.84	1.96	0.28	2.52	0.00	0.56	0.00	0.00	0.00	0.00	0.28	0.00	0.00
28.30	0.00	0.96	0.00	0.00	0.00	1.29	0.64	0.00	0.32	0.00	0.00	0.00	0.00	0.00	0.00	1.61	0.00	0.00
31.06	0.00	0.00	0.00	0.00	0.00	0.00	1.55	0.31	1.55	0.00	0.00	0.00	0.00	0.00	0.00	1.24	0.00	0.00
39.50	0.31	0.31	0.00	0.00	0.00	2.19	0.63	0.00	1.25	0.00	0.00	0.00	0.00	0.00	0.00	1.25	0.00	0.00
27.11	0.00	1.81	0.00	0.00	0.00	1.81	0.90	0.00	0.60	0.00	0.00	0.00	0.00	0.00	0.00	0.90	0.00	0.00
22.96	0.00	2.20	0.00	0.00	0.00	0.63	2.52	0.31	1.26	0.00	0.00	0.00	0.00	0.00	0.00	1.89	0.00	0.31
21.51	0.00	1.96	0.00	0.00	0.00	1.40	1.12	0.28	0.28	0.00	0.00	0.00	0.00	0.00	0.00	0.56	0.00	0.00
18.73	0.00	3.02	0.00	0.00	0.00	0.30	0.30	0.30	0.30	0.00	0.00	0.00	0.00	0.00	0.00	0.00	0.00	0.00
30.08	0.00	0.28	0.00	0.00	0.00	0.00	5.01	0.00	1.67	0.00	0.00	0.00	0.00	0.28	0.00	1.11	0.00	0.28
26.06	0.00	0.30	0.00	0.00	0.00	3.64	0.30	0.00	0.91	0.00	0.00	0.00	0.00	0.00	0.00	1.82	0.00	0.00
26.91	0.00	2.55	0.00	0.00	0.00	2.83	0.28	0.00	2.55	0.00	0.00	0.00	0.00	0.28	0.00	0.57	1.13	0.00
29.81	0.00	0.84	0.00	0.00	0.00	4.46	1.67	0.00	1.67	0.00	0.00	0.00	0.00	0.00	0.00	0.56	0.00	0.56
22.10	0.00	4.82	0.00	0.00	0.28	2.55	0.57	0.28	3.40	0.00	0.00	0.00	0.00	0.00	0.00	0.57	0.28	0.57
32.94	0.00	0.30	0.00	0.00	0.00	1.78	2.37	0.00	2.97	0.00	0.00	0.00	0.00	0.00	0.00	1.48	0.00	0.30
30.09	0.00	9.12	0.00	0.00	0.61	1.52	0.30	0.30	2.74	0.00	0.00	0.00	0.00	0.00	0.00	0.30	0.00	0.00
27.49	0.29	1.17	0.00	0.00	0.00	1.75	0.88	0.00	0.58	0.00	0.00	0.00	0.00	0.00	0.00	0.00	0.00	0.29
25.07	0.00	11.24	0.00	0.00	0.00	0.58	1.73	0.00	1.44	0.00	0.00	0.00	0.00	0.00	0.00	0.58	0.29	0.29
35.96	0.00	1.89	0.00	0.00	0.00	0.95	0.63	0.32	0.63	0.00	0.00	0.00	0.00	0.00	0.00	0.95	0.00	0.00
28.08	0.00	0.57	0.00	0.00	0.00	1.15	1.15	0.29	1.15	0.00	0.00	0.00	0.00	0.29	0.86	0.86	0.57	0.00
32.47	0.00	0.97	0.00	0.32	0.32	0.65	0.32	0.00	0.32	0.00	0.00	0.00	0.00	0.00	0.00	0.00	0.97	0.00
28.57	0.00	10.03	0.00	0.00	0.00	0.61	1.22	0.00	1.22	0.00	0.00	0.00	0.00	1.22	0.00	0.00	0.30	0.00

Discoaster spp. %	*Ericsonia formosa* %	*Helicosphaera compacta* %	*Helicosphaera euphratis* %	*Helicosphaera spp.* %	*Isthmolithus recurvus* %	*Lanternithus minutus* %	*Markalius spp.* %	*Pontosphaera spp.* %	*Reticulofenestra spp.* <4µm %	*Reticulofenestra spp.* 4-10µm %	*Reticulofenestra spp.* 10-14µm %	*Reticulofenestra daviesii* %	*Reticulofenestra umbilicus* >14µm %	*Sphenolithus akropodus* morphotype A %	*Sphenolithus akropodus* morphotype B %	*Sphenolithus distentus* %	*Sphenolithus intercalaris* %	*Sphenolithus moriformis* %
0.00	0.00	0.00	0.00	0.00	0.00	0.00	0.00	0.00	0.00	66.57	2.39	0.00	0.00	0.00	0.00	0.00	0.00	4.78
0.00	0.00	0.00	0.00	0.00	0.00	0.00	0.00	0.00	0.00	76.24	0.99	0.00	0.00	0.00	0.00	0.00	0.00	3.30
0.00	0.00	0.00	0.00	0.00	0.00	0.00	0.00	0.00	0.00	56.45	0.97	0.32	0.00	0.00	0.00	0.00	0.00	0.97
0.00	0.00	0.00	0.00	0.00	0.00	0.00	0.00	0.00	0.00	73.63	0.00	0.00	0.00	0.00	0.00	0.00	0.00	2.25
0.00	0.00	0.00	0.00	0.00	0.00	0.00	0.00	0.00	0.00	47.76	0.64	0.32	0.00	0.00	0.00	0.00	0.00	1.60
0.00	0.00	0.00	0.00	0.00	0.00	0.00	0.00	0.00	0.00	70.26	0.65	1.63	0.00	0.65	0.00	0.00	0.00	1.31
0.00	0.00	0.00	0.00	0.00	0.00	0.00	0.00	0.00	0.00	59.59	1.74	0.00	0.00	0.00	0.00	0.00	0.00	2.03
0.00	0.00	0.00	0.00	0.00	0.00	0.00	0.00	0.00	0.00	62.96	0.00	0.62	0.00	0.31	0.00	0.00	0.00	2.78
0.00	0.00	0.00	0.00	0.00	0.00	0.00	0.00	0.00	0.00	52.22	0.00	0.00	0.00	0.00	0.00	0.00	0.00	0.63
0.26	0.00	0.00	0.00	0.00	0.00	0.00	0.00	0.00	0.00	58.96	0.00	0.52	0.00	0.00	0.78	0.00	0.00	2.08
0.00	0.00	0.00	0.00	0.00	0.33	0.00	0.00	0.00	0.00	68.20	0.00	0.00	0.00	0.00	0.00	0.00	0.00	0.33
0.00	0.00	0.00	0.00	0.00	0.00	0.00	0.00	0.00	0.00	77.88	0.30	0.00	0.00	0.30	0.30	0.00	0.00	1.82
0.27	0.00	0.00	0.00	0.00	0.00	0.00	0.00	0.00	0.00	61.01	0.00	0.27	0.00	0.00	0.00	0.00	0.00	1.59
0.00	0.00	0.00	0.00	0.00	0.00	0.00	0.00	0.27	0.00	67.66	0.27	0.00	0.00	0.27	0.00	0.00	0.00	2.99
0.28	0.00	0.00	0.00	0.00	0.00	0.00	0.00	0.00	0.00	57.83	0.28	0.00	0.00	0.00	0.00	0.00	0.00	0.57
0.53	0.00	0.00	0.00	0.00	0.00	0.00	0.00	0.00	0.00	59.79	0.00	0.79	0.00	0.26	0.00	0.00	0.00	2.65
0.00	0.00	0.00	0.00	0.00	0.00	0.30	0.00	0.00	0.00	54.24	0.30	0.00	0.00	0.00	0.00	0.00	0.00	3.03
0.26	0.00	0.00	0.00	0.00	0.26	0.00	0.00	0.00	0.00	50.90	0.26	0.26	0.00	0.00	0.00	0.00	0.00	5.17
0.00	0.00	0.00	0.00	0.00	0.00	0.30	0.00	0.00	0.00	55.09	0.60	0.90	0.60	0.00	0.00	0.30	0.00	2.40
0.00	0.00	0.31	0.00	0.00	0.00	0.31	0.00	0.00	0.00	53.52	0.00	0.61	0.61	0.31	0.00	0.00	0.00	3.36
0.00	0.00	0.00	0.00	0.00	0.00	0.30	0.00	0.00	0.00	50.60	0.00	0.00	0.00	0.00	0.00	0.00	0.00	5.42
0.00	0.00	0.28	0.00	0.00	0.28	0.28	0.00	0.00	0.00	46.91	0.28	0.56	0.28	0.28	0.28	0.00	0.00	1.69
0.00	0.00	0.00	0.00	0.00	0.00	0.00	0.00	0.00	0.00	66.78	0.00	0.00	0.65	0.33	0.00	0.00	0.00	2.61
0.00	0.00	0.33	0.00	0.00	0.00	0.00	0.00	0.33	0.00	63.67	0.33	1.00	0.00	0.00	0.33	0.00	0.00	2.67
0.32	0.00	0.00	0.00	0.00	0.32	0.00	0.00	0.00	0.00	66.03	0.00	0.00	1.90	0.00	0.00	0.00	0.00	0.95
0.00	0.00	0.00	0.00	0.00	0.00	1.20	0.00	0.60	0.00	55.86	0.00	2.10	0.00	0.60	0.60	0.00	0.00	2.10
0.00	0.00	0.27	0.00	0.00	0.00	1.89	0.00	0.00	0.00	43.24	0.00	6.22	0.00	0.00	0.00	0.00	0.00	2.97
0.00	0.00	0.00	0.00	0.00	0.00	3.63	0.00	0.26	0.00	36.01	0.52	6.99	0.52	0.00	0.00	0.00	0.00	2.33
0.00	0.00	0.00	0.00	0.00	0.00	3.08	0.00	0.00	0.26	39.74	0.00	8.97	0.00	0.00	0.00	0.00	0.00	6.15
0.29	0.29	0.00	0.00	0.00	0.00	4.11	0.00	0.00	0.00	40.18	0.59	3.52	0.00	0.29	0.29	0.00	0.00	4.99
0.00	0.30	0.00	0.00	0.00	0.30	1.81	0.00	0.00	0.00	41.99	0.00	3.02	0.00	0.00	0.00	0.00	0.00	5.44
0.00	0.61	0.00	0.00	0.00	0.00	3.36	0.00	0.31	0.00	40.06	0.31	2.45	0.31	0.00	0.00	0.00	0.00	7.34
0.00	0.63	0.00	0.00	0.00	0.63	4.72	0.00	0.00	0.00	44.97	0.31	1.26	0.00	0.00	0.00	0.00	0.00	2.52
0.30	0.00	0.00	0.00	0.00	0.30	2.97	0.00	0.00	0.00	45.40	0.59	0.30	0.30	0.30	0.00	0.00	0.00	4.15
0.00	0.00	0.00	0.00	0.27	0.00	3.85	0.00	0.00	0.00	49.45	0.00	0.82	1.37	0.00	0.00	0.00	0.00	3.57
0.00	0.28	0.00	0.00	0.00	0.00	4.27	0.00	0.00	0.00	35.90	0.28	1.42	0.57	0.00	0.00	0.00	0.00	3.99
0.29	0.00	0.00	0.29	0.00	0.00	3.48	0.00	0.00	0.00	50.14	0.00	1.45	0.00	0.00	0.00	0.00	0.00	4.93
0.00	1.48	0.00	0.00	0.00	0.00	3.85	0.00	0.00	0.00	37.57	0.59	1.48	0.30	0.00	0.00	0.00	0.00	3.55
0.00	0.60	0.00	0.00	0.00	0.00	2.99	0.00	0.00	0.00	35.03	0.60	2.10	0.60	0.00	0.00	0.00	0.00	6.29
0.54	1.35	0.00	0.00	0.00	0.00	4.85	0.00	0.00	0.00	25.07	4.31	2.70	1.08	0.00	0.00	0.00	0.00	5.12
0.00	1.50	0.00	0.00	0.30	0.00	2.40	0.00	0.30	0.00	33.53	0.30	3.59	1.80	0.00	0.00	0.00	0.00	5.99
0.00	0.96	0.00	0.00	0.00	0.00	2.57	0.00	0.00	0.00	32.15	0.64	5.47	0.96	0.00	0.00	0.00	0.00	7.07
0.00	1.64	0.00	0.00	0.00	0.33	0.66	0.00	0.00	0.00	30.26	0.66	5.59	2.30	0.00	0.00	0.00	0.00	4.61
0.00	2.59	0.00	0.00	0.00	0.00	2.59	0.00	0.00	0.00	26.21	0.97	2.91	4.53	0.00	0.00	0.00	0.00	3.56
0.00	1.64	0.00	0.00	0.33	0.00	1.64	0.00	0.00	0.00	34.10	2.95	5.25	1.64	0.00	0.00	0.00	0.00	1.97
0.00	0.80	0.00	0.00	0.00	0.53	3.74	0.00	0.00	0.00	31.28	0.27	6.95	0.53	0.00	0.00	0.00	0.00	3.74
0.00	0.88	0.00	0.00	0.00	0.29	0.88	0.00	0.00	0.00	35.09	0.00	4.97	1.17	0.00	0.00	0.00	0.00	2.34
0.30	1.83	0.00	0.00	0.00	0.30	3.05	0.00	0.00	0.00	37.80	1.22	3.35	0.91	0.30	0.00	0.00	0.00	4.27
0.00	0.85	0.00	0.00	0.00	0.57	2.56	0.00	0.00	0.00	36.65	3.13	2.84	0.28	0.00	0.00	0.00	0.00	5.40
0.88	2.05	0.00	0.00	0.00	0.88	3.52	0.00	0.00	0.00	39.30	0.88	5.28	0.29	0.00	0.00	0.00	0.00	5.28
0.00	2.76	0.00	0.00	0.00	0.28	3.87	0.00	0.00	0.00	37.29	1.10	0.83	0.28	0.00	0.00	0.00	0.00	7.46
0.00	2.30	0.00	0.00	0.00	0.98	3.28	0.00	0.00	0.00	27.87	2.62	2.30	3.28	0.00	0.00	0.00	0.00	2.30

0.00	0.58	0.00	0.00	0.00	2.62	0.87	0.00	0.00	0.00	45.19	0.29	1.75	0.87	0.00	0.00	0.00	0.00	2.33
0.00	0.98	0.00	0.00	0.00	0.98	0.66	0.00	0.00	0.00	40.33	0.98	1.64	0.98	0.00	0.00	0.00	0.00	4.26
0.00	1.55	0.00	0.00	0.00	0.00	0.31	0.00	0.00	0.00	39.44	1.24	1.24	2.17	0.00	0.00	0.00	0.00	3.73
0.00	2.13	0.00	0.00	0.00	1.33	0.27	0.00	0.00	0.00	42.40	1.07	1.87	1.87	0.00	0.00	0.00	0.00	5.60
0.00	1.09	0.00	0.00	0.00	0.82	0.00	0.00	0.00	0.00	45.23	1.09	3.54	0.82	0.00	0.00	0.00	0.00	4.36
0.30	2.13	0.00	0.00	0.00	1.22	0.00	0.00	0.00	0.00	33.74	2.43	3.34	4.86	0.00	0.00	0.00	0.00	3.34
0.00	2.70	0.00	0.00	0.00	0.81	0.00	0.00	0.00	0.00	38.27	1.08	1.89	1.89	0.00	0.00	0.00	0.00	2.16
0.00	2.30	0.00	0.00	0.00	0.99	0.00	0.00	0.00	0.00	40.79	3.62	2.30	2.30	0.00	0.00	0.00	0.00	2.63
0.00	4.02	0.00	0.00	0.00	0.93	0.31	0.00	0.00	0.00	29.10	3.10	2.17	3.41	0.00	0.00	0.00	0.00	2.48
0.00	4.28	0.00	0.00	0.00	0.80	0.27	0.00	0.00	0.00	40.37	1.60	4.01	1.07	0.00	0.00	0.00	0.00	2.94
0.00	2.51	0.00	0.00	0.00	0.31	0.00	0.00	0.00	0.00	34.80	1.25	4.39	3.13	0.00	0.00	0.00	0.00	1.88
0.00	3.05	0.00	0.00	0.00	1.66	0.00	0.00	0.00	0.00	35.73	0.55	4.16	2.77	0.00	0.00	0.00	0.00	4.43
0.00	5.95	0.00	0.00	0.00	0.85	0.00	0.00	0.00	0.00	26.06	1.13	5.38	1.70	0.00	0.00	0.00	0.28	5.95
0.00	5.05	0.00	0.00	0.00	2.13	0.53	0.00	0.00	0.00	34.57	0.80	5.85	0.00	0.00	0.00	0.00	0.00	5.05
0.00	4.20	0.00	0.00	0.00	0.60	0.30	0.00	0.00	0.00	29.13	3.30	8.41	3.30	0.00	0.00	0.00	0.00	2.70
0.00	4.85	0.00	0.00	0.00	0.32	0.00	0.00	0.00	0.00	40.78	4.53	8.74	0.32	0.00	0.00	0.00	0.00	3.56
0.00	6.27	0.00	0.00	0.00	0.90	0.00	0.00	0.00	0.00	30.45	5.97	9.85	2.39	0.00	0.00	0.00	0.00	1.49
0.00	2.62	0.00	0.00	0.00	1.46	0.29	0.00	0.29	0.00	34.11	1.17	7.87	1.46	0.00	0.00	0.00	0.29	5.25
0.00	0.83	0.00	0.00	0.00	1.94	1.11	0.00	0.00	0.00	45.56	0.83	9.17	0.56	0.00	0.00	0.00	0.00	2.50
0.00	0.57	0.00	0.00	0.00	1.14	0.86	0.00	0.00	0.00	46.29	0.86	8.57	0.29	0.00	0.00	0.00	0.00	3.71
0.00	2.12	0.00	0.00	0.00	1.06	0.27	0.00	0.00	0.00	46.95	2.65	8.22	1.86	0.00	0.00	0.00	0.00	3.18
0.00	2.04	0.00	0.00	0.00	0.58	2.62	0.00	0.00	0.00	43.73	3.79	4.96	2.04	0.00	0.00	0.00	0.00	3.21
0.00	3.26	0.00	0.00	0.00	1.78	2.08	0.00	0.00	0.00	37.09	2.08	8.31	0.89	0.00	0.00	0.00	0.00	3.26
0.31	2.48	0.00	0.00	0.00	1.24	4.04	0.00	0.00	0.00	29.50	2.80	7.14	1.86	0.00	0.00	0.00	0.00	6.52
0.00	3.50	0.00	0.00	0.00	1.59	2.23	0.00	0.00	0.00	32.17	4.14	5.73	2.55	0.00	0.00	0.00	0.00	5.73
0.00	3.61	0.00	0.00	0.00	0.98	0.33	0.00	0.00	0.00	31.80	1.31	8.52	1.97	0.00	0.00	0.00	0.00	3.28
0.00	2.16	0.00	0.00	0.00	0.27	0.27	0.00	0.00	0.00	30.81	5.68	7.30	2.43	0.00	0.00	0.00	0.00	2.97
0.00	5.84	0.00	0.00	0.00	0.32	0.97	0.00	0.00	0.00	25.97	4.55	5.52	2.27	0.00	0.00	0.00	0.00	2.27
0.00	7.27	0.00	0.00	0.00	1.21	0.61	0.00	0.00	0.00	23.64	3.64	8.79	0.61	0.00	0.00	0.00	0.00	2.42
0.28	3.36	0.00	0.00	0.00	1.96	0.00	0.00	0.00	0.00	36.97	5.32	5.60	0.28	0.00	0.00	0.00	0.00	1.40
0.00	3.86	0.00	0.00	0.00	1.29	1.29	0.00	0.00	0.00	37.62	3.22	3.22	1.93	0.00	0.00	0.00	0.00	4.50
0.31	6.52	0.00	0.00	0.00	0.00	0.00	0.00	0.00	0.00	35.40	5.59	2.48	1.24	0.00	0.00	0.00	0.00	1.55
0.00	5.33	0.00	0.00	0.00	0.00	0.00	0.00	0.00	0.00	29.15	2.82	1.57	3.45	0.00	0.00	0.00	0.00	0.94
0.00	4.52	0.00	0.00	0.00	0.30	0.90	0.00	0.00	0.00	34.34	1.20	4.52	1.20	0.00	0.00	0.00	0.30	4.82
0.00	4.09	0.00	0.00	0.00	0.94	0.00	0.00	0.00	0.00	37.42	2.52	4.40	1.26	0.00	0.00	0.00	0.00	3.14
0.00	4.47	0.00	0.00	0.00	1.96	0.28	0.00	0.00	0.00	45.81	1.40	2.79	1.96	0.00	0.00	0.00	0.00	2.51
0.60	1.51	0.00	0.00	0.00	0.60	0.30	0.00	0.00	0.00	48.94	1.81	4.23	0.60	0.00	0.00	0.00	0.00	6.04
0.56	6.13	0.00	0.00	0.00	0.84	0.00	0.00	0.00	0.00	26.18	5.85	1.67	1.39	0.00	0.00	0.00	0.00	2.23
0.30	2.12	0.00	0.00	0.00	0.91	0.00	0.00	0.00	0.00	44.55	3.03	5.15	3.03	0.00	0.00	0.00	0.00	1.21
0.00	2.83	0.00	0.00	0.00	1.42	0.00	0.00	0.00	0.00	37.96	3.40	3.12	5.38	0.00	0.00	0.00	0.00	1.70
0.28	3.90	0.00	0.00	0.28	1.11	0.00	0.00	0.28	0.00	40.95	2.51	1.11	2.23	0.00	0.00	0.00	0.00	2.79
0.28	6.80	0.00	0.00	0.00	1.70	0.00	0.00	0.00	0.00	36.83	4.25	1.42	3.68	0.00	0.00	0.00	0.00	4.25
0.30	3.26	0.00	0.00	0.00	0.30	0.30	0.00	0.30	0.00	37.39	5.04	0.89	2.67	0.00	0.00	0.00	0.00	2.08
0.00	3.34	0.00	0.00	0.00	0.91	0.00	0.00	0.61	0.61	30.40	0.91	5.47	0.00	0.00	0.00	0.00	0.00	2.43
0.00	2.05	0.00	0.00	0.00	1.75	0.29	0.00	0.29	0.00	41.23	1.46	3.80	1.75	0.00	0.00	0.00	0.00	4.68
0.00	6.63	0.00	0.00	0.00	1.73	0.00	0.00	0.00	0.00	24.78	3.17	6.34	2.31	0.00	0.00	0.00	0.00	2.02
0.00	4.42	0.00	0.00	0.00	0.63	0.00	0.00	0.32	0.00	35.33	1.58	2.84	1.89	0.00	0.00	0.00	0.00	3.79
0.00	8.31	0.00	0.00	0.00	0.86	0.00	0.00	0.00	0.00	30.09	5.73	4.58	3.44	0.00	0.00	0.00	0.00	3.44
0.32	3.57	0.32	0.00	0.00	0.97	0.00	0.00	1.30	0.00	31.82	4.22	5.19	0.97	0.32	0.00	0.00	0.00	6.82
0.00	3.95	0.00	0.00	0.00	1.82	0.00	0.00	0.00	0.91	25.23	1.82	5.78	0.91	0.00	0.00	0.00	0.00	6.38

Sphenolithus predistentus %	*Sphenolithus predistentus/distentus* %	*Sphenolithus radians* %	*Sphenolithus* cf. *spiniger* %	*Sphenolithus tribulosus* %	*Sphenolithus spp.* %	*Thoracosphaera spp.* %	*Umbilicosphaera spp.* %	*Zygrhablithus bijugatus* %	Reworked %	Indetermined %
0.90	0.30	0.00	0.00	0.00	0.00	0.00	0.00	0.60	0.00	0.00
0.66	0.33	0.00	0.00	0.00	0.00	0.00	0.00	0.00	0.00	0.00
0.65	0.32	0.00	0.00	0.00	0.00	0.65	0.00	0.65	0.00	0.00
0.00	0.00	0.00	0.00	0.00	0.00	0.00	0.00	0.00	0.00	0.00
0.32	0.00	0.00	0.00	0.00	0.00	0.64	0.00	0.00	0.00	0.00
0.00	0.00	0.00	0.00	0.00	0.00	0.00	0.00	0.33	0.00	0.00
1.45	0.58	0.00	0.00	0.00	0.00	0.29	0.00	0.29	0.00	0.00
0.00	0.00	0.00	0.00	0.00	0.00	0.00	0.00	0.31	0.00	0.31
0.00	0.32	0.00	0.00	0.00	0.00	0.32	0.00	0.63	0.00	0.00
1.30	0.52	0.00	0.00	0.00	0.00	0.26	0.00	1.30	0.00	0.52
0.66	0.66	0.00	0.00	0.00	0.00	0.00	0.00	1.64	0.00	0.00
0.30	0.00	0.00	0.00	0.00	0.00	0.00	0.30	0.00	0.00	0.00
1.06	0.00	0.00	0.00	0.00	0.00	0.53	0.00	1.06	0.00	0.00
0.27	0.00	0.00	0.00	0.00	0.00	0.00	0.00	1.36	0.00	0.27
1.14	0.00	0.00	0.00	0.00	0.00	0.57	0.00	1.71	0.00	0.00
0.26	0.00	0.00	0.00	0.00	0.00	0.26	0.00	1.06	0.00	0.00
0.91	0.00	0.00	0.00	0.00	0.00	1.21	0.00	3.64	0.00	0.00
0.00	0.00	0.00	0.00	0.00	0.00	0.52	0.00	1.81	0.00	0.00
1.20	0.00	0.00	0.00	0.00	0.00	0.30	0.00	4.19	0.00	0.00
0.00	0.31	0.00	0.00	0.00	0.00	0.92	0.00	3.06	0.00	0.31
0.90	0.00	0.00	0.00	0.00	0.00	0.00	0.00	4.52	0.00	0.00
1.12	0.00	0.00	0.00	0.00	0.00	0.28	0.00	5.06	0.00	0.00
0.65	0.00	0.00	0.00	0.00	0.00	0.33	0.00	5.86	0.00	0.00
0.67	0.00	0.00	0.00	0.00	0.00	0.33	0.00	2.00	0.00	0.00
1.27	0.00	0.00	0.00	0.00	0.00	0.00	0.00	5.71	0.00	0.00
0.00	0.00	0.00	0.00	0.00	0.00	0.00	0.30	2.40	0.00	0.00
0.54	0.00	0.27	0.00	0.00	0.00	0.00	0.00	2.97	0.00	0.00
0.00	0.00	0.00	0.00	0.00	0.00	0.00	0.00	4.15	0.00	0.00
2.05	0.51	0.00	0.00	0.00	0.00	0.00	0.26	7.18	0.00	0.00
0.29	0.00	0.00	0.00	0.00	0.29	0.00	0.59	8.50	0.00	0.29
0.00	0.30	0.00	0.00	0.00	0.00	0.00	0.00	6.95	0.00	0.30
0.00	0.00	0.00	0.00	0.00	0.00	0.00	0.00	8.87	0.00	0.00
0.94	0.00	0.00	0.00	0.00	0.00	0.31	0.00	4.09	0.00	0.31
0.30	0.00	0.00	0.00	0.00	0.00	0.30	0.00	6.82	0.00	0.00
0.00	0.00	0.00	0.00	0.00	0.00	0.27	0.00	4.12	0.00	0.00
0.28	0.00	0.00	0.00	0.00	0.00	0.28	0.00	4.27	0.00	0.00
0.87	0.00	0.00	0.00	0.00	0.00	0.00	0.00	3.77	0.00	0.00
0.59	0.30	0.00	0.00	0.00	0.00	0.89	0.00	3.25	0.00	0.00
0.00	0.00	0.00	0.00	0.00	0.00	0.00	0.00	4.19	0.00	0.00
0.00	0.00	0.00	0.00	0.00	0.00	0.27	0.00	2.43	0.00	1.08
0.00	0.00	0.00	0.00	0.00	0.00	0.00	0.00	3.89	0.00	0.00
0.00	0.00	0.00	0.00	0.00	0.00	0.96	0.00	7.07	0.00	0.32
0.33	0.00	0.00	0.00	0.00	0.00	0.00	0.00	8.88	0.00	0.00
0.00	0.00	0.00	0.00	0.00	0.00	0.00	0.00	11.33	0.00	0.65
0.00	0.00	0.00	0.00	0.00	0.00	0.33	0.00	13.11	0.00	0.00
0.00	0.00	0.00	0.00	0.00	0.00	0.27	0.00	8.02	0.00	0.00
0.00	0.00	0.00	0.00	0.00	0.00	0.00	0.00	6.73	0.00	0.29
0.00	0.00	0.00	0.00	0.00	0.00	0.00	0.30	4.27	0.00	0.00
0.00	0.00	0.00	0.00	0.00	0.00	0.00	0.00	6.25	0.00	0.00
0.00	0.00	0.00	0.00	0.00	0.00	0.29	0.00	4.11	0.00	0.00
0.00	0.00	0.00	0.00	0.00	0.00	0.00	0.00	4.42	0.00	0.00
0.00	0.00	0.00	0.00	0.00	0.00	0.66	0.33	6.23	0.00	0.00

0.00	0.00	0.00	0.00	0.00	0.00	0.29	0.00	4.66	0.00	0.00
0.00	0.00	0.00	0.00	0.00	0.00	0.33	0.00	6.56	0.00	0.33
0.31	0.00	0.00	0.00	0.00	0.00	0.00	0.00	3.73	0.00	0.00
0.00	0.00	0.00	0.00	0.00	0.53	0.00	0.00	6.13	0.00	0.27
0.00	0.00	0.00	0.00	0.00	0.00	0.00	0.00	2.45	0.00	0.00
0.00	0.00	0.00	0.00	0.00	0.00	0.00	0.00	3.34	0.00	0.30
0.00	0.00	0.00	0.00	0.00	0.00	0.00	0.00	2.70	0.00	0.00
0.00	0.00	0.00	0.00	0.00	0.00	0.00	0.00	2.30	0.00	0.00
0.00	0.00	0.00	0.00	0.00	0.00	1.24	0.00	3.10	0.00	0.00
0.00	0.00	0.00	0.27	0.00	0.00	0.27	0.00	5.08	0.00	0.53
0.00	0.00	0.00	0.00	0.00	0.00	0.00	0.00	5.64	0.00	0.00
0.00	0.00	0.00	0.00	0.00	0.00	0.28	0.00	3.05	0.00	1.39
0.00	0.00	0.00	0.00	0.00	0.00	0.00	0.00	8.22	0.00	0.00
0.00	0.00	0.00	0.00	0.00	0.00	0.27	0.00	5.05	0.00	0.53
0.00	0.00	0.00	0.00	0.00	0.00	0.00	0.00	3.60	0.00	0.00
0.00	0.00	0.00	0.00	0.00	0.00	0.32	0.00	2.91	0.32	0.65
0.00	0.00	0.00	0.00	0.00	0.00	0.00	0.00	4.18	0.00	0.00
0.00	0.00	0.00	0.00	0.00	0.00	0.00	0.00	9.33	0.00	0.87
0.00	0.00	0.00	0.00	0.00	0.00	0.00	0.00	6.67	0.00	0.00
0.00	0.00	0.00	0.00	0.00	0.00	0.00	0.00	6.86	0.00	0.00
0.00	0.00	0.00	0.27	0.00	0.00	0.00	0.00	8.49	0.00	0.00
0.00	0.00	0.00	0.00	0.00	0.00	0.00	0.00	5.25	0.00	0.58
0.00	0.00	0.00	0.00	0.00	0.00	0.00	0.00	7.12	0.00	0.00
0.00	0.00	0.00	0.00	0.00	0.00	0.31	0.00	6.52	0.00	0.62
0.00	0.00	0.00	0.00	0.00	0.00	0.00	0.00	5.10	0.00	0.00
0.00	0.00	0.00	0.00	0.00	0.00	0.00	0.00	12.13	0.00	0.66
0.00	0.00	0.00	0.00	0.00	0.00	0.00	0.00	7.03	0.00	0.00
0.00	0.00	0.00	0.00	0.00	0.00	0.00	0.00	9.09	0.00	0.00
0.00	0.00	0.00	0.00	0.00	0.00	0.00	0.00	9.39	0.00	0.00
0.00	0.00	0.00	0.00	0.00	0.00	0.56	0.00	10.92	0.00	0.00
0.00	0.00	0.00	0.00	0.00	0.00	0.32	0.00	5.47	0.00	0.00
0.00	0.00	0.00	0.00	0.00	0.00	0.00	0.00	8.39	0.00	0.00
0.00	0.00	0.00	0.00	0.00	0.00	0.00	0.00	6.90	0.00	0.00
0.00	0.00	0.00	0.00	0.00	0.00	0.00	0.00	9.04	0.00	0.00
0.00	0.00	0.00	0.00	0.00	0.00	0.00	0.00	7.86	0.00	0.00
0.00	0.00	0.00	0.00	0.00	0.00	0.00	0.00	7.26	0.00	0.00
0.00	0.00	0.00	0.00	0.00	0.00	0.00	0.60	9.06	0.00	0.00
0.00	0.00	0.00	0.00	0.00	0.00	0.00	0.00	13.93	0.00	0.00
0.00	0.00	0.00	0.00	0.00	0.00	0.00	0.00	5.45	0.00	0.00
0.00	0.00	0.00	0.00	0.00	0.00	0.00	0.00	6.52	0.00	0.00
0.00	0.00	0.00	0.00	0.00	0.00	0.00	0.00	3.34	0.00	0.00
0.00	0.00	0.00	0.00	0.00	0.00	0.00	0.00	2.27	0.00	0.00
0.00	0.00	0.00	0.00	0.00	0.00	0.59	0.00	2.37	0.00	0.00
0.00	0.00	0.00	0.00	0.00	0.00	0.30	0.61	6.69	0.00	0.00
0.00	0.00	0.00	0.00	0.00	0.00	0.58	0.00	5.85	0.00	0.00
0.00	0.00	0.00	0.00	0.00	0.00	0.00	0.29	4.61	0.00	0.00
0.00	0.00	0.00	0.00	0.00	0.00	0.32	0.00	1.58	0.00	0.00
0.00	0.00	0.00	0.00	0.00	0.00	0.00	0.00	2.58	0.00	0.00
0.00	0.00	0.00	0.00	0.00	0.00	0.32	0.00	4.22	0.00	0.00
0.00	0.00	0.00	0.00	0.00	0.00	1.22	0.00	4.26	0.00	3.65

Appendix III. Dataset S2 (n/mm^2)

Leg	Sample source	Depth (mbsf)	*Chiasmolithus altus*	*Chiasmolithus oamaruensis*	*Clausicoccus fenestratus*	*Clausicoccus subdistichus*	*Dictyococcites bisectus*	*Dictyococcites* cf. *bisectus*	*Dictyococcites hesslandii*	*Discoaster barbadiensis*
121	UO756C-5X-5W, 0.0-2.0 cm	113.46	1	0	0	0	46	26	23	0
121	UO756C-5X-5W, 20.0-22.0 cm	113.66	5	0	0	1	25	25	10	0
121	UO756C-5X-5W, 40.0-42.0 cm	113.86	0	0	0	0	45	15	26	0
121	UO756C-5X-5W, 60.0-63.0 cm	114.06	1	0	0	0	27	16	6	0
121	UO756C-5X-5W, 79.0-81.0 cm	114.25	0	0	0	1	26	16	13	0
121	UO756C-5X-6W, 0.0-2.0 cm	114.28	2	0	0	0	29	23	5	0
121	UO756C-5X-6W, 20.0-22.0 cm	114.48	1	0	0	0	42	15	13	0
121	UO756C-5X-6W, 40.0-42.0 cm	114.68	0	0	0	0	28	27	20	0
121	UO756C-5X-6W, 60.0-62.0 cm	114.88	0	0	0	0	62	31	17	0
121	UO756C-5X-6W, 78.5-80.5 cm	115.07	0	0	0	0	50	52	23	0
121	UO756C-5X-6W, 100.0-102.0 cm	115.28	0	0	0	0	46	18	8	0
121	UO756C-5X-6W, 120.0-122.0 cm	115.48	0	0	0	1	22	15	7	0
121	UO756C-5X-7W, 0.0-2.0 cm	115.61	0	0	0	2	90	35	13	0
121	UO756C-5X-7W, 20.0-22.0 cm	115.81	0	0	0	2	25	41	15	0
121	UO756C-5X-7W, 40.0-42.0 cm	116.01	1	0	0	1	87	44	15	0
121	UO756C-5X-7W, 60.0-62.0 cm	116.21	0	0	0	1	49	44	20	0
121	UO756C-5X-7W, 79.0-81.0 cm	116.40	2	0	0	0	89	34	22	0
121	UO756C-5X-7W, 100.0-102.0 cm	116.61	5	0	0	0	41	23	24	0
121	UO756C-5X-7W, 120.0-122.0 cm	116.81	5	0	0	0	77	32	18	0
121	UO756C-5X-7W, 140.0-142.0 cm	117.01	8	0	0	1	37	13	18	0
121	UO756C-5X-8W, 0.0-2.0 cm	117.11	0	0	0	0	63	42	8	0
121	UO756C-5X-8W, 20.0-22.0 cm	117.31	4	0	1	4	52	49	20	0
121	UO756C-5X-8W, 40.0-42.0 cm	117.51	3	0	0	3	55	35	27	0
121	UO756C-5X-8W, 60.0-62.0 cm	117.71	11	2	0	6	30	44	20	0
121	UO756C-5X-8W, 79.0-81.0 cm	117.90	4	0	0	23	77	32	14	0
121	UO756C-5X-8W, 100.0-102.0 cm	118.10	7	2	3	166	35	85	42	0
121	UO756C-5X-8W, 121.0-123.0 cm	118.32	13	2	0	125	59	46	24	0
121	UO756C-5X-CCW, 10.5-12.5 cm	118.47	14	1	0	141	26	37	40	0
121	UO756C-6X-1W, 10.0-12.0 cm	120.30	3	0	0	204	36	33	45	0
121	UO756C-6X-1W, 20.0-22.0 cm	120.40	14	0	0	148	63	60	59	0
121	UO756C-6X-1W, 30.0-32.0 cm	120.50	6	0	0	155	27	27	29	0
121	UO756C-6X-1W, 40.0-42.0 cm	120.60	13	4	0	109	35	57	43	0
121	UO756C-6X-2W, 50.0-52.0 cm	120.70	4	0	0	124	34	28	31	0
121	UO756C-6X-1W, 60.0-62.0 cm	120.80	6	0	2	164	21	37	35	0
121	UO756C-6X-1W, 70.0-72.0 cm	120.90	11	0	0	118	73	58	36	0
121	UO756C-6X-1W, 80.0-82.0 cm	121.00	8	2	0	244	36	32	64	0

121	UO756C-6X-1W, 90.0-92.0 cm	121.10	0	0	0	179	31	38	41	0
121	UO756C-6X-1W, 100.0-102.0 cm	121.20	20	4	0	233	38	58	30	0
121	UO756C-6X-1W, 110.0-112.0 cm	121.30	1	0	0	252	49	77	43	0
121	UO756C-6X-1W, 120.0-122.0 cm	121.40	23	0	0	176	39	46	56	0
121	UO756C-6X-1W, 130.0-132.0 cm	121.50	13	0	0	193	45	43	17	0
121	UO756C-6X-1W, 140.0-142.0 cm	121.60	15	0	1	157	28	28	66	0
121	UO756C-6X-2W, 10.0-12.0 cm	121.80	11	2	0	221	55	40	35	0
121	UO756C-6X-2W,19.5-21.5 cm	121.90	5	0	0	197	36	61	75	0
121	UO756C-6X-2W, 28.5-30.5 cm	121.99	4	0	0	195	73	71	39	0
121	UO756C-6X-2W, 40.0-42.0 cm	122.10	5	0	0	418	30	30	66	0
121	UO756C-6X-2W, 50.0-52.0 cm	122.20	4	0	0	419	37	41	38	0
121	UO756C-6X-2W, 60.0-62.0 cm	122.30	10	4	0	406	31	39	57	0
121	UO756C-6X-2W, 71.5-73.5 cm	122.42	11	3	0	301	50	64	37	0
121	UO756C-6X-2W, 81.0-83.0 cm	122.51	0	1	1	204	20	37	53	0
121	UO756C-6X-2W, 90.0-92.0 cm	122.60	5	5	0	415	63	101	45	0
121	UO756C-6X-2W, 101.0-103.0 cm	122.71	2	0	0	144	27	26	44	0
121	UO756C-6X-2W, 110.0-112.0 cm	122.80	1	0	0	441	38	42	35	0
121	UO756C-6X-2W, 121.0-123.0 cm	122.91	1	1	0	235	18	29	61	0
121	UO756C-6X-2W, 131.5-133.5 cm	123.02	4	1	0	522	36	50	42	0
121	UO756C-6X-2W, 142.0-144.0 cm	123.12	7	0	2	248	16	12	50	0
121	UO756C-6X-3W, 10.0-12.0 cm	123.30	0	0	0	360	13	24	31	0
121	UO756C-6X-3W, 20.0-22.0 cm	123.40	0	2	0	210	26	17	45	0
121	UO756C-6X-3W, 30.0-32.0 cm	123.50	0	0	0	174	43	39	36	0
121	UO756C-6X-3W, 40.0-42.0 cm	123.60	0	0	0	193	23	29	63	0
121	UO756C-6X-3W, 50.0-52.0 cm	123.70	0	0	0	34	38	33	52	0
121	UO756C-6X-3W, 60.0-62.0 cm	123.80	0	0	1	72	70	37	57	0
121	UO756C-6X-3W, 69.0-71.0 cm	123.89	0	0	0	79	49	42	62	0
121	UO756C-6X-3W, 79.0-81.0 cm	123.99	1	0	4	267	43	29	53	0
121	UO756C-6X-3W, 90.0-94.0 cm	124.10	0	0	0	20	17	50	45	0
121	UO756C-6X-3W, 102.5-104.5 cm	124.23	0	0	0	34	51	82	49	0
121	UO756C-6X-4W, 111.5-113.5 cm	124.32	0	0	0	48	49	48	36	0
121	UO756C-6X-3W, 120.0-122.0 cm	124.40	0	0	1	69	91	97	63	0
121	UO756C-6X-3W, 129.5-131.5 cm	124.50	0	0	0	10	54	50	17	0
121	UO756C-6X-3W, 139.5- 141.5 cm	124.60	0	0	0	37	41	62	56	0
121	UO756C-6X-4W, 20.0-22.0 cm	124.90	0	2	0	52	29	39	24	0
121	UO756C-6X-4W, 30.0-32.0 cm	125.00	0	0	1	38	35	40	22	0
121	UO756C-6X-4W, 41.5-43.5 cm	125.12	0	2	0	3	28	39	33	0
121	UO756C-6X-4W, 60.0-64.0 cm	125.30	4	0	0	7	80	99	77	0
121	UO756C-6X-4W, 70.0-72.0 cm	125.40	0	0	0	2	20	25	40	0
121	UO756C-6X-4W, 80.0-82.0 cm	125.50	4	6	0	7	73	96	64	0
121	UO756C-6X-4W, 90.0-92.0 cm	125.60	0	5	0	7	20	23	44	0
121	UO756C-6X-4W, 100.0-102.0 cm	125.70	0	0	0	10	51	66	10	0
121	UO756C-6X-4W, 111.0-113.0 cm	125.81	1	2	0	2	43	57	64	0
121	UO756C-6X-4W, 129.0-131-0 cm	125.99	0	0	0	7	41	49	12	0
121	UO756C-6X-4W, 140.0-142.0 cm	126.10	0	1	0	2	25	16	31	0
121	UO756C-6X-5W, 10.0-12.0 cm	126.30	0	0	0	0	16	28	41	0
121	UO756C-6X-5W, 20.0-22.0 cm	126.40	1	0	0	12	16	11	21	0
121	UO756C-6X-5W, 40.0-42.0 cm	126.60	0	0	0	11	7	34	13	0
121	UO756C-6X-5W, 50.0-52.0 cm	126.70	0	0	0	42	16	12	18	0
121	UO756C-6X-5W, 60.0-62.0 cm	126.80	0	1	0	60	29	27	8	0

121	UO756C-6X-5W, 70.0-72.0 cm	126.90	2	0	1	52	24	19	17	0
121	UO756C-6X-5W, 80.0-82.0 cm	127.00	1	0	0	21	21	24	7	0
121	UO756C-6X-5W, 90.0-92.0 cm	127.10	1	0	0	12	19	22	9	0
121	UO756C-6X-CCW, 10.0-12.0 cm	127.25	1	0	0	0	7	43	23	0
121	UO756C-7X-1W, 0.0-2.0 cm	129.80	0	0	0	3	18	8	7	0
121	UO756C-7X-1W, 20.0-22.0	130.00	0	1	2	3	43	15	46	0
121	UO756C-7X-1W, 60.0-62.0 cm	130.40	0	2	0	4	34	11	23	0
121	UO756C-7X-1W, 80.0-82.0 cm	130.60	4	4	0	8	50	27	67	0
121	UO756C-7X-1W, 99.0-101.0 cm	130.79	2	0	0	10	31	66	65	0
121	UO756C-7X-1W, 141.5-143.5 cm	131.22	0	0	0	19	10	4	37	0
121	UO756C-7X-2W, 0.0-2.0 cm	131.30	0	0	0	25	9	5	7	0
121	UO756C-7X-2W, 19.0-21.0 cm	131.49	3	1	1	31	10	13	21	5
121	UO756C-7X-2W, 60-0-62.0 cm	131.90	0	0	0	21	6	5	4	0
121	UO756C-7X-2W, 80-0-82.0 cm	132.10	0	1	1	13	10	12	27	1
121	UO756C-7X-2W, 99.0-101.0 cm	132.29	0	0	0	22	5	3	1	0
121	UO756C-7X-2W, 140.0-142.0 cm	132.70	2	1	0	29	10	16	23	2

Discoaster saipanensis	*Ericsonia formosa*	*Isthmolithus recurvus*	*Reticulofenestra umbilicus* >14µm	*Sphenolithus akropodus* morphotype A	*Sphenolithus akropodus* morphotype B	*S. akropodus*	*Sphenolithus distentus*	*Sphenolithus predistentus/distentus*	*Sphenolithus predistentus*
0	0	0	0	0	0	0	0	6	13
0	0	0	0	0	0	0	4	3	10
0	0	0	0	0	0	0	0	2	7
0	0	0	0	0	0	0	3	7	9
0	0	0	0	0	0	0	0	2	6
0	0	0	0	4	1	5	0	0	1
0	0	0	0	0	0	0	0	7	11
0	0	0	0	1	0	1	0	0	1
0	0	0	0	0	0	0	0	2	1
0	0	0	0	9	7	16	0	0	8
0	0	1	0	0	0	0	0	2	5
0	0	0	0	2	5	7	0	0	7
0	0	0	0	0	0	0	0	0	24
0	0	0	0	4	2	6	0	0	5
0	0	0	0	0	0	0	0	1	23
0	0	0	2	1	0	1	0	0	1
0	0	0	4	0	0	0	0	1	15
0	0	1	1	0	0	0	0	0	2
0	0	3	6	1	1	2	1	1	22
0	0	0	16	1	0	1	0	1	5
0	0	2	0	0	0	0	0	0	7
0	0	2	12	4	1	5	0	0	10
0	1	0	11	1	0	1	0	1	13
0	0	0	9	3	2	5	0	0	6
0	0	1	15	0	0	0	0	0	15
0	0	0	5	6	3	9	0	0	4
0	0	1	21	2	0	2	0	0	5
0	0	1	5	0	0	0	0	0	3
0	1	0	1	2	0	2	0	8	31
0	4	1	5	0	4	4	0	0	4
0	6	6	6	1	0	1	0	1	17
0	11	1	7	0	0	0	0	0	1
0	6	3	2	0	1	1	0	2	17
0	3	2	5	2	1	3	0	0	2
0	4	0	25	0	0	0	0	1	1
0	9	1	15	1	1	2	0	0	0

0	3	2	3	0	0	0	0	0	9
0	39	1	14	0	0	0	0	1	6
0	39	1	10	0	0	0	0	0	1
0	32	1	14	0	0	0	0	0	0
0	18	1	22	0	0	0	0	0	1
0	38	1	36	0	0	0	0	0	0
0	36	1	38	0	0	0	0	0	1
0	51	0	41	0	0	0	0	0	0
0	36	0	37	0	0	0	0	0	0
0	30	5	27	0	0	0	0	0	0
0	32	7	21	0	0	0	0	0	0
0	42	13	16	1	1	2	0	0	0
0	43	13	34	0	0	0	0	0	0
0	39	13	6	0	0	0	0	0	0
0	61	24	35	0	0	0	0	0	0
0	23	10	25	0	0	0	0	0	0
0	17	28	16	0	0	0	0	0	0
0	18	20	24	0	0	0	0	0	0
0	48	18	40	0	0	0	0	0	0
0	21	16	43	0	0	0	0	0	0
0	19	23	11	0	0	0	0	0	0
0	41	14	71	0	0	0	0	0	0
0	68	24	40	0	0	0	0	0	0
0	64	23	37	0	0	0	0	0	0
0	59	12	35	0	0	0	0	0	0
0	94	29	41	0	0	0	0	0	0
0	75	8	57	0	0	0	0	0	0
0	56	24	67	0	0	0	0	0	0
0	67	8	17	0	0	0	0	0	0
0	88	22	11	0	0	0	0	0	0
0	77	12	51	0	0	0	0	0	0
0	151	12	113	0	0	0	0	0	0
0	62	11	39	0	0	0	0	0	0
0	70	16	21	0	0	0	0	0	0
0	32	30	41	0	0	0	0	0	0
0	26	20	8	0	0	0	0	0	0
0	45	16	42	0	0	0	0	0	0
0	70	16	50	0	0	0	0	0	0
0	41	20	16	0	0	0	0	0	0
0	78	28	47	0	0	0	0	0	0
0	76	18	38	0	0	0	0	0	0
0	51	31	26	0	0	0	0	0	0
0	42	11	27	0	0	0	0	0	0
0	59	15	29	0	0	0	0	0	0
0	112	22	17	0	0	0	0	0	0
0	57	26	11	0	0	0	0	0	0
0	47	8	34	0	0	0	0	0	0
0	55	10	22	0	0	0	0	0	0
0	66	3	35	0	0	0	0	0	0
0	74	17	34	0	0	0	0	0	0

0	74	13	29	0	0	0	0	0	0
0	69	20	40	0	0	0	0	0	0
0	75	19	35	0	0	0	0	0	0
1	116	12	20	0	0	0	0	0	0
0	23	8	20	0	0	0	0	0	0
1	46	46	157	0	0	0	0	0	0
0	46	8	30	0	0	0	0	0	0
0	107	26	102	0	0	0	0	0	0
0	78	6	40	0	0	0	0	0	0
0	43	7	12	0	0	0	0	0	0
0	42	10	23	0	0	0	0	0	0
1	64	7	37	0	0	0	0	0	0
0	26	6	13	0	0	0	0	0	0
8	95	3	31	0	0	0	0	0	0
0	27	13	7	1	0	1	0	0	0
21	77	32	15	0	0	0	0	0	0

Appendix III. Dataset S3

Leg	Sample source	Depth (mbsf)	PC 1 score	PC 2 score
121	UO756C-5X-5W, 0.0-2.0 cm	113.46	-2.870	-0.728
121	UO756C-5X-5W, 20.0-22.0 cm	113.66	-3.781	-1.279
121	UO756C-5X-5W, 40.0-42.0 cm	113.86	-2.922	-1.546
121	UO756C-5X-5W, 60.0-63.0 cm	114.06	-3.756	-2.007
121	UO756C-5X-5W, 79.0-81.0 cm	114.25	-3.451	-1.740
121	UO756C-5X-6W, 0.0-2.0 cm	114.28	-3.818	-1.779
121	UO756C-5X-6W, 20.0-22.0 cm	114.48	-3.464	-1.185
121	UO756C-5X-6W, 40.0-42.0 cm	114.68	-2.309	-1.081
121	UO756C-5X-6W, 60.0-62.0 cm	114.88	-1.754	-1.371
121	UO756C-5X-6W, 78.5-80.5 cm	115.07	-1.960	-0.918
121	UO756C-5X-6W, 100.0-102.0 cm	115.28	-2.222	-1.840
121	UO756C-5X-6W, 120.0-122.0 cm	115.48	-3.941	-1.783
121	UO756C-5X-7W, 0.0-2.0 cm	115.61	-3.064	-1.513
121	UO756C-5X-7W, 20.0-22.0 cm	115.81	-3.458	-1.322
121	UO756C-5X-7W, 40.0-42.0 cm	116.01	-3.434	-1.357
121	UO756C-5X-7W, 60.0-62.0 cm	116.21	-2.482	-1.434
121	UO756C-5X-7W, 79.0-81.0 cm	116.40	-2.163	-0.547
121	UO756C-5X-7W, 100.0-102.0 cm	116.61	-0.988	-0.884
121	UO756C-5X-7W, 120.0-122.0 cm	116.81	-1.636	-0.405
121	UO756C-5X-7W, 140.0-142.0 cm	117.01	-1.747	-0.496
121	UO756C-5X-8W, 0.0-2.0 cm	117.11	-0.779	-0.278
121	UO756C-5X-8W, 20.0-22.0 cm	117.31	-0.921	-0.760
121	UO756C-5X-8W, 40.0-42.0 cm	117.51	-2.041	-0.389
121	UO756C-5X-8W, 60.0-62.0 cm	117.71	-2.475	-0.534
121	UO756C-5X-8W, 79.0-81.0 cm	117.90	-2.252	-0.185
121	UO756C-5X-8W, 100.0-102.0 cm	118.10	-2.413	0.350
121	UO756C-5X-8W, 121.0-123.0 cm	118.32	-1.818	0.644
121	UO756C-5X-CCW, 10.5-12.5 cm	118.47	-1.205	1.908
121	UO756C-6X-1W, 10.0-12.0 cm	120.30	-1.115	2.578
121	UO756C-6X-1W, 20.0-22.0 cm	120.40	-0.248	3.015
121	UO756C-6X-1W, 30.0-32.0 cm	120.50	-0.322	1.398
121	UO756C-6X-1W, 40.0-42.0 cm	120.60	-0.214	3.486
121	UO756C-6X-1W, 50.0-52.0 cm	120.70	-0.317	2.584
121	UO756C-6X-1W, 60.0-62.0 cm	120.80	-0.508	1.952
121	UO756C-6X-1W, 70.0-72.0 cm	120.90	-1.006	2.207
121	UO756C-6X-1W, 80.0-82.0 cm	121.00	0.094	2.802
121	UO756C-6X-1W, 90.0-92.0 cm	121.10	-1.386	2.475
121	UO756C-6X-1W, 100.0-102.0 cm	121.20	-0.059	2.934
121	UO756C-6X-1W, 110.0-112.0 cm	121.30	-0.463	2.787
121	UO756C-6X-1W, 120.0-122.0 cm	121.40	1.210	3.510
121	UO756C-6X-1W, 130.0-132.0 cm	121.50	-0.486	2.177
121	UO756C-6X-1W, 140.0-142.0 cm	121.60	0.570	1.954
121	UO756C-6X-2W, 10.0-12.0 cm	121.80	0.714	1.880
121	UO756C-6X-2W,19.5-21.5 cm	121.90	1.525	3.006
121	UO756C-6X-2W, 28.5-30.5 cm	121.99	0.610	1.743
121	UO756C-6X-2W, 40.0-42.0 cm	122.10	0.093	3.281
121	UO756C-6X-2W, 50.0-52.0 cm	122.20	-0.665	1.680
121	UO756C-6X-2W, 60.0-62.0 cm	122.30	-0.034	2.894

121	UO756C-6X-2W, 71.5-73.5 cm	122.42	-0.187	3.476
121	UO756C-6X-2W, 81.0-83.0 cm	122.51	0.151	1.908
121	UO756C-6X-2W, 90.0-92.0 cm	122.60	-0.169	3.456
121	UO756C-6X-2W, 101.0-103.0 cm	122.71	1.323	2.090
121	UO756C-6X-2W, 110.0-112.0 cm	122.80	0.045	0.547
121	UO756C-6X-2W, 121.0-123.0 cm	122.91	0.239	1.540
121	UO756C-6X-2W, 131.5-133.5 cm	123.02	-0.716	0.881
121	UO756C-6X-2W, 142.0-144.0 cm	123.12	0.348	1.553
121	UO756C-6X-3W, 10.0-12.0 cm	123.30	-0.651	0.472
121	UO756C-6X-3W, 20.0-22.0 cm	123.40	0.949	0.025
121	UO756C-6X-3W, 30.0-32.0 cm	123.50	0.703	-1.365
121	UO756C-6X-3W, 40.0-42.0 cm	123.60	0.300	-0.672
121	UO756C-6X-3W, 50.0-52.0 cm	123.70	1.551	-0.763
121	UO756C-6X-3W, 60.0-62.0 cm	123.80	0.433	-1.086
121	UO756C-6X-3W, 69.0-71.0 cm	123.89	0.260	-0.643
121	UO756C-6X-3W, 79.0-81.0 cm	123.99	0.935	0.343
121	UO756C-6X-3W, 90.0-94.0 cm	124.10	2.240	-0.164
121	UO756C-6X-3W, 102.5-104.5 cm	124.23	1.952	-0.361
121	UO756C-6X-3W, 111.5-113.5 cm	124.32	1.590	-1.667
121	UO756C-6X-3W, 120.0-122.0 cm	124.40	-0.032	-1.033
121	UO756C-6X-3W, 129.5-131.5 cm	124.50	1.892	-2.087
121	UO756C-6X-3W, 139.5- 141.5 cm	124.60	1.310	0.153
121	UO756C-6X-4W, 20.0-22.0 cm	124.90	0.393	-1.118
121	UO756C-6X-4W, 30.0-32.0 cm	125.00	-0.688	-0.504
121	UO756C-6X-4W, 41.5-43.5 cm	125.12	0.110	-1.032
121	UO756C-6X-4W, 60.0-64.0 cm	125.30	0.029	0.646
121	UO756C-6X-4W, 70.0-72.0 cm	125.40	1.783	-1.115
121	UO756C-6X-4W, 80.0-82.0 cm	125.50	2.532	2.262
121	UO756C-6X-4W, 90.0-92.0 cm	125.60	2.440	0.859
121	UO756C-6X-4W, 100.0-102.0 cm	125.70	1.896	-0.719
121	UO756C-6X-4W, 111.0-113.0 cm	125.81	1.680	-0.775
121	UO756C-6X-4W, 129.0-131-0 cm	125.99	2.873	-0.393
121	UO756C-6X-4W, 140.0-142.0 cm	126.10	3.914	-1.683
121	UO756C-6X-5W, 10.0-12.0 cm	126.30	2.205	-1.895
121	UO756C-6X-5W, 20.0-22.0 cm	126.40	1.977	-0.586
121	UO756C-6X-5W, 40.0-42.0 cm	126.60	2.574	-1.868
121	UO756C-6X-5W, 50.0-52.0 cm	126.70	2.526	-2.099
121	UO756C-6X-5W, 60.0-62.0 cm	126.80	1.675	-0.104
121	UO756C-6X-5W, 70.0-72.0 cm	126.90	1.964	-0.856
121	UO756C-6X-5W, 80.0-82.0 cm	127.00	1.478	-1.352
121	UO756C-6X-5W, 90.0-92.0 cm	127.10	-0.082	-0.313
121	UO756C-6X-CCW, 10.0-12.0 cm	127.25	4.053	-1.594
121	UO756C-7X-1W, 0.0-2.0 cm	129.80	0.962	-2.347
121	UO756C-7X-1W, 20.0-22.0	130.00	1.518	-2.265
121	UO756C-7X-1W, 60.0-62.0 cm	130.40	1.614	-1.744
121	UO756C-7X-1W, 80.0-82.0 cm	130.60	1.754	-1.554
121	UO756C-7X-1W, 99.0-101.0 cm	130.79	1.730	-1.661
121	UO756C-7X-1W, 141.5-143.5 cm	131.22	1.007	-1.090
121	UO756C-7X-2W, 0.0-2.0 cm	131.30	1.248	-0.780
121	UO756C-7X-2W, 19.0-21.0 cm	131.49	1.788	-1.731

121	UO756C-7X-2W, 60-0-62.0 cm	131.90	1.544	-1.569
121	UO756C-7X-2W, 80-0-82.0 cm	132.10	3.482	-1.842
121	UO756C-7X-2W, 99.0-101.0 cm	132.29	2.215	-0.781
121	UO756C-7X-2W, 140.0-142.0 cm	132.70	2.472	-0.879

Appendix III. Dataset S4 Bulk stable isotopes and carbonate content (Hole 756C)

Leg	Identifier sample	Depth (mbsf)	$\delta^{13}C$ (PDB,‰)	$\delta^{18}O$ (PDB,‰)	$CaCO_3$ (wt, %)
121	756C-5X-7W-140	115.81	1.13	0.88	88.95
121	756C-5X-8W-020	117.31	1.21	0.90	86.27
121	756C-5X-8W-060	117.71	1.55	1.00	78.04
121	756C-5X-8W-100	118.11	1.41	1.07	80.47
121	756C-5X-CC-010	118.47	1.33	1.18	97.53
121	756C-6X-1W-020	120.30	1.34	1.12	95.23
121	756C-6X-1W-040	120.60	1.49	1.19	77.07
121	756C-6X-1W-060	120.80	1.33	0.98	100.00
121	756C-6X-1W-080	121.00	1.51	1.17	83.47
121	756C-6X-1W-100	121.20	1.57	1.09	94.55
121	756C-6X-1W-120	121.40	1.51	1.04	84.01
121	756C-6X-1W-140	121.60	1.57	1.05	90.28
121	756C-6X-2W-019	121.90	1.75	1.13	96.34
121	756C-6X-2W-040	122.10	1.83	1.01	87.29
121	756C-6X-2W-060	122.30	1.95	1.05	84.60
121	756C-6X-2W-081	122.51	1.91	1.08	84.49
121	756C-6X-2W-101	122.71	1.91	0.97	75.29
121	756C-6X-2W-121	122.91	1.86	0.96	79.73
121	756C-6X-2W-142	123.12	1.90	0.76	83.18
121	756C-6X-3W-020	123.40	1.89	0.54	84.48
121	756C-6X-3W-040	123.60	1.80	0.44	83.86
121	756C-6X-3W-050	123.70	1.88	0.66	73.32
121	756C-6X-3W-060	123.80	1.72	0.64	87.41
121	756C-6X-3W-069	123.89	1.71	0.66	83.24
121	756C-6X-3W-079	123.99	1.72	0.64	81.74
121	756C-6X-3W-090	124.10	1.51	0.10	70.18
121	756C-6X-3W-102	124.23	1.73	0.67	79.86
121	756C-6X-3W-120	124.40	1.52	0.33	69.68
121	756C-6X-3W-139	124.60	1.76	0.67	64.76
121	756C-6X-4W-030	125.00	1.54	0.62	91.22
121	756C-6X-4W-060	125.30	1.58	0.72	88.22
121	756C-6X-4W-080	125.50	1.58	0.67	83.37
121	756C-6X-4W-100	125.70	1.30	0.49	74.38
121	756C-6X-4W-129	125.99	1.26	0.62	71.79
121	756C-6X-5W-010	126.30	1.24	0.53	70.98
121	756C-6X-5W-040	126.60	1.28	0.54	92.69
121	756C-6X-5W-060	126.80	1.41	0.46	80.18
121	756C-6X-5W-070	126.90	1.42	0.56	76.94
121	756C-6X-5W-080	127.00	1.32	0.43	81.95
121	756C-6X-5W-090	127.10	1.48	0.53	67.29
121	756C-6X-CC-010	127.25	1.31	0.48	66.01
121	756C-7X-1W-020	130.00	1.48	0.24	72.86
121	756C-7X-1W-080	130.60	1.56	0.47	70.91
121	756C-7X-1W-141	131.22	1.51	0.54	70.60
121	756C-7X-2W-019	131.49	1.51	0.39	73.90
121	756C-7X-2W-080	132.10	1.46	0.35	77.99
121	756C-7X-2W-140	132.70	1.34	0.10	59.14

Appendix III. Dataset S5

Benthic foraminifera C and O stable isotopes (Hole 756C)

Leg	Sample source	Depth (mbsf)	Species	Preservation	No.	Weight (mg)
121	756C-5X-5 W, 0.0-2.0 cm	113.46	*C. havanensis*	Good - moderate	2	0.15
121	756C-5X-5 W, 20.0-22.0 cm	113.66	*C. havanensis*	Good - moderate	2	0.14
121	756C-5X-5 W, 40.0-42.0 cm	113.86	*C. havanensis*	Good - moderate	2	0.18
121	756C-5X-5 W, 60.0-63.0 cm	114.06	*C. havanensis*	Good - moderate	2	0.16
121	756C-5X-5 W, 79.0-81.0 cm	114.25	*C. havanensis*	Good - moderate	2	0.16
121	756C-5X-6 W, 0.0-2.0 cm	114.28	*C. havanensis*	Good - moderate	2	0.17
121	756C-5X-6 W, 20.0-22.0 cm	114.48	*C. havanensis*	Good - moderate	2	0.14
121	756C-5X-6 W, 40.0-42.0 cm	114.68	*C. havanensis*	Good - moderate	2	0.17
121	756C-5X-6 W, 60.0-62.0 cm	114.88	*C. havanensis*	Good - moderate	2	0.15
121	756C-5X-6 W, 78.5-80.5 cm	115.07	*C. havanensis*	Good - moderate	2	0.13
121	756C-5X-6 W, 100.0-102.0 cm	115.28	*C. havanensis*	Good - moderate	2	0.20
121	756C-5X-6 W, 120.0-122.0 cm	115.48	*C. havanensis*	Good - moderate	2	0.15
121	756C-5X-7 W, 0.0-2.0 cm	115.61	*C. havanensis*	Good - moderate	2	0.20
121	756C-5X-7 W, 20.0-22.0 cm	115.81	*C. havanensis*	Good - moderate	2	0.19
121	756C-5X-7 W, 40.0-42.0 cm	116.01	*C. havanensis*	Good - moderate	2	0.16
121	756C-5X-7 W, 60.0-62.0 cm	116.21	*C. havanensis*	Good - moderate	2	0.19
121	756C-5X-7 W, 79.0-81.0 cm	116.40	*C. havanensis*	Good - moderate	2	0.19
121	756C-5X-7 W, 100.0-102.0 cm	116.61	*C. havanensis*	Good - moderate	2	0.15
121	756C-5X-7 W, 120.0-122.0 cm	116.81	*C. havanensis*	Good - moderate	2	0.13
121	756C-5X-7 W, 140.0-142.0 cm	117.01	*C. havanensis*	Good - moderate	2	0.15
121	756C-5X-8 W, 0.0-2.0 cm	117.11	*C. havanensis*	Good - moderate	2	0.17
121	756C-5X-8 W, 20.0-22.0 cm	117.31	*C. havanensis*	Good - moderate	2	0.14
121	756C-5X-8 W, 40.0-42.0 cm	117.51	*C. havanensis*	Good - moderate	2	0.15
121	756C-5X-8 W, 60.0-62.0 cm	117.71	*C. havanensis*	Good - moderate	2	0.16
121	756C-5X-8 W, 79.0-81.0 cm	117.90	*C. havanensis*	Good - moderate	2	0.19
121	756C-5X-8 W, 100.0-102.0 cm	118.11	*C. havanensis*	Good - moderate	2	0.17
121	756C-5X-8 W, 121.0-123.0 cm	118.32	*C. havanensis*	Good - moderate	2	0.16
121	756C-5X-CC W, 10.5-12.5 cm	118.47	*C. havanensis*	Good - moderate	2	0.16
121	756C-6X-1 W, 10.0-12.0 cm	120.30	*C. havanensis*	Good - moderate	2	0.18
121	756C-6X-1 W, 20.0-22.0 cm	120.40	*C. havanensis*	Good - moderate	2	0.20
121	756C-6X-1 W, 30.0-32.0 cm	120.50	*C. havanensis*	Good - moderate	2	0.13
121	756C-6X-1 W, 40.0-42.0 cm	120.60	*C. havanensis*	Good - moderate	2	0.18
121	756C-6X-1 W, 50.0-52.0 cm	120.70	*C. havanensis*	Good - moderate	2	0.17
121	756C-6X-1 W, 60.0-62.0 cm	120.80	*C. havanensis*	Good - moderate	2	0.15
121	756C-6X-1 W, 70.0-72.0 cm	120.90	*C. havanensis*	Good - moderate	2	0.18
121	756C-6X-1 W, 80.0-82.0 cm	121.00	*C. havanensis*	Good - moderate	2	0.17
121	756C-6X-1 W, 90.0-92.0 cm	121.10	*C. havanensis*	Good - moderate	2	0.18
121	756C-6X-1 W, 100.0-102.0 cm	121.20	*C. havanensis*	Good - moderate	2	0.20
121	756C-6X-1 W, 110.0-112.0 cm	121.30	*C. havanensis*	Good - moderate	2	0.17
121	756C-6X-1 W, 120.0-122.0 cm	121.40	*C. havanensis*	Good - moderate	2	0.20
121	756C-6X-1 W, 130.0-132.0 cm	121.50	*C. havanensis*	Good - moderate	2	0.20
121	756C-6X-1 W, 140.0-142.0 cm	121.60	*C. havanensis*	Good - moderate	2	0.15
121	756C-6X-2 W, 10.0-12.0 cm	121.80	*C. havanensis*	Good - moderate	2	0.15
121	756C-6X-2 W, 19.5-21.5 cm	121.90	*C. havanensis*	Good - moderate	2	0.18
121	756C-6X-2 W, 28.5-30.5 cm	121.99	*C. havanensis*	Good - moderate	2	0.16
121	756C-6X-2 W, 40.0-42.0 cm	122.10	*C. havanensis*	Good - moderate	2	0.19

121	756C-6X-2 W, 50.0-52.0 cm	122.20	*C. havanensis*	Good - moderate	2	0.18
121	756C-6X-2 W, 60.0-62.0 cm	122.30	*C. havanensis*	Good - moderate	2	0.17
121	756C-6X-2 W, 71.5-73.5 cm	122.42	*C. havanensis*	Good - moderate	2	0.13
121	756C-6X-2 W, 81.0-83.0 cm	122.51	*C. havanensis*	Good - moderate	2	0.15
121	756C-6X-2 W, 90.0-92.0 cm	122.60	*C. havanensis*	Good - moderate	2	0.18
121	756C-6X-2 W, 101.0-103.0 cm	122.71	*C. havanensis*	Good - moderate	2	0.20
121	756C-6X-2 W, 110.0-112.0 cm	122.80	*C. havanensis*	Good - moderate	2	0.19
121	756C-6X-2 W, 121.0-123.0 cm	122.91	*C. havanensis*	Good - moderate	2	0.19
121	756C-6X-2 W, 131.5-133.5 cm	123.02	*C. havanensis*	Good - moderate	2	0.18
121	756C-6X-2 W, 142.0-144.0 cm	123.12	*C. havanensis*	Good - moderate	2	0.17
121	756C-6X-3 W, 10.0-12.0 cm	123.30	*C. havanensis*	Good - moderate	2	0.15
121	756C-6X-3 W, 20.0-22.0 cm	123.40	*C. havanensis*	Good - moderate	2	0.13
121	756C-6X-3 W, 30.0-32.0 cm	123.50	*C. havanensis*	Good - moderate	2	0.19
121	756C-6X-3 W, 40.0-42.0 cm	123.60	*C. havanensis*	Good - moderate	2	0.13
121	756C-6X-3 W, 50.0-52.0 cm	123.70	*C. havanensis*	Good - moderate	2	0.13
121	756C-6X-3 W, 60.0-62.0 cm	123.80	*C. havanensis*	Good - moderate	2	0.19
121	756C-6X-3 W, 69.0-71.0 cm	123.89	*C. havanensis*	Good - moderate	2	0.20
121	756C-6X-3 W, 79.0-81.0 cm	123.99	*C. havanensis*	Good - moderate	2	0.19
121	756C-6X-3 W, 90.0-94.0 cm	124.10	*C. havanensis*	Good - moderate	2	0.19
121	756C-6X-3 W, 102.5-104.5 cm	124.23	*C. havanensis*	Good - moderate	2	0.18
121	756C-6X-3 W, 111.5-113.5 cm	124.32	*C. havanensis*	Good - moderate	2	0.19
121	756C-6X-3 W, 120.0-122.0 cm	124.40	*C. havanensis*	Good - moderate	2	0.16
121	756C-6X-3 W, 129.5-131.5 cm	124.50	*C. havanensis*	Good - moderate	2	0.17
121	756C-6X-3 W, 139.5-141.5 cm	124.60	*C. havanensis*	Good - moderate	2	0.19
121	756C-6X-4, 10 cm	124.80	*C.mundulus*		3	0.23
121	756C-6X-4 W, 20.0-22.0 cm	124.90	*C. havanensis*	Good - moderate	2	0.18
121	756C-6X-4 W, 30.0-32.0 cm	125.00	*C. havanensis*	Good - moderate	2	0.18
121	756C-6X-4 W, 41.5-43.5 cm	125.12	*C. havanensis*	Good - moderate	2	0.19
121	756C-6X-4 W, 60.0-64.0 cm	125.30	*C. havanensis*	Good - moderate	2	0.17
121	756C-6X-4, 53 cm	125.30	*C.mundulus*		3	0.27
121	756C-6X-4 W, 70.0-72.0 cm	125.40	*C. havanensis*	Good - moderate	2	0.15
121	756C-6X-4 W, 80.0-82.0 cm	125.50	*C. havanensis*	Good - moderate	2	0.14
121	756C-6X-4 W, 90.0-92.0 cm	125.60	*C. havanensis*	Good - moderate	2	0.13
121	756C-6X-4 W, 100.0-102.0 cm	125.70	*C. havanensis*	Good - moderate	2	0.17
121	756C-6X-4 W, 111.0-113.0 cm	125.81	*C. havanensis*	Good - moderate	2	0.15
121	756C-6X-4, 122 cm	125.92	*C.mundulus*		3	0.23
121	756C-6X-4 W, 129.0-131.0 cm	125.99	*C. havanensis*	Good - moderate	2	0.20
121	756C-6X-4 W, 140.0-142.0 cm	126.10	*C. havanensis*	Good - moderate	2	0.18
121	756C-6X-5 W, 10.0-12.0 cm	126.30	*C. havanensis*	Good - moderate	2	0.17
121	756C-6X-5 W, 20.0-22.0 cm	126.40	*C. havanensis*	Good - moderate	2	0.19
121	756C-6X-5, 35.5 cm	126.56	*C.mundulus*		3	0.27
121	756C-6X-5 W, 40.0-42.0 cm	126.60	*C. havanensis*	Good - moderate	2	0.16
121	756C-6X-5 W, 50.0-52.0 cm	126.70	*C. havanensis*	Good - moderate	2	0.13
121	756C-6X-5 W, 60.0-62.0 cm	126.80	*C. havanensis*	Good - moderate	2	0.16
121	756C-6X-5 W, 70.0-72.0 cm	126.90	*C. havanensis*	Good - moderate	2	0.15
121	756C-6X-5 W, 80.0-82.0 cm	127.00	*C. havanensis*	Good - moderate	2	0.15
121	756C-6X-5 W, 90.0-92.0 cm	127.10	*C. havanensis*	Good - moderate	2	0.15
121	756C-6X-CC W, 10.0-12.0 cm	127.25	*C. havanensis*	Good - moderate	2	0.16
121	756C-7X-1 W, 0.0-2.0 cm	129.80	*C. havanensis*	Good - moderate	2	0.16
121	756C-7X-1 W, 20.0-22.0 cm	130.00	*C. havanensis*	Good - moderate	2	0.14

121	756C-7X-1, 41 cm	130.21	*C.mundulus*		3	0.25
121	756C-7X-1 W, 60.0-62.0 cm	130.40	*C. havanensis*	Good - moderate	2	0.18
121	756C-7X-1 W, 80.0-82.0 cm	130.60	*C. havanensis*	Good - moderate	2	0.20
121	756C-7X-1 W, 99.0-101.0 cm	130.79	*C. havanensis*	Good - moderate	2	0.19
121	756C-7X-1, 115 cm	130.95	*C.mundulus*		3	0.22
121	756C-7X-1 W, 141.5-143.5 cm	131.22	*C. havanensis*	Good - moderate	2	0.19
121	756C-7X-2 W, 0.0-2.0 cm	131.30	*C. havanensis*	Good - moderate	2	0.15
121	756C-7X-2 W, 19.0-21.0 cm	131.49	*C. havanensis*	Good - moderate	2	0.15
121	756C-7X-2, 48 cm	131.78	*C.mundulus*		3	0.28
121	756C-7X-2 W, 60.0-62.0 cm	131.90	*C. havanensis*	Good - moderate	2	0.16
121	756C-7X-2 W, 80.0-82.0 cm	132.10	*C. havanensis*	Good - moderate	2	0.16
121	756C-7X-2 W, 99.0-101.0 cm	132.29	*C. havanensis*	Good - moderate	2	0.14
121	756C-7X-2, 115 cm	132.45	*C.mundulus*		3	0.24
121	756C-7X-2 W, 140.0-142.0 cm	132.70	*C. havanensis*	Good - moderate	2	0.15
121	756C-7X-3, 40 cm	133.20	*C.mundulus*		3	0.24
121	756C-7X-3, 115 cm	133.95	*C.mundulus*		3	0.20
121	756C-7X-4, 35 cm	134.65	*C.mundulus*		3	0.27
121	756C-7X-4, 110 cm	135.40	*C.mundulus*		3	0.30
121	756C-7X-5, 50 cm	136.30	*C.mundulus*		3	0.28
121	756C-7X-5, 110 cm	136.90	*C.mundulus*		3	0.27
121	756C-7X-6, 50 cm	137.80	*C.mundulus*		3	0.25
121	756C-8X-1, 10 cm	139.50	*C.mundulus*		3	0.24
121	756C-8X-1, 115 cm	140.55	*C.mundulus*		3	0.16
121	756C-8X-2, 17 cm	141.07	*C.mundulus*		3	0.26
121	756C-8X-2, 100 cm	141.90	*C.mundulus*		3	0.29
121	756C-8X-3, 25 cm	142.65	*C.mundulus*		3	0.61

Analyzer	Date	$\delta^{13}C$ (PDB,‰)	$\delta^{18}O$ (PDB, ‰)
Elias Chadli	2015	1.01	1.29
Elias Chadli	2015	0.93	1.20
Elias Chadli	2015	1.08	1.20
Elias Chadli	2015	1.01	1.31
Elias Chadli	2015	0.93	1.18
Elias Chadli	2015	0.86	1.11
Elias Chadli	2015	1.04	0.93
Elias Chadli	2015	0.74	1.31
Elias Chadli	2015	0.96	1.15
Elias Chadli	2015	1.06	0.91
Elias Chadli	2015	0.98	1.25
Elias Chadli	2015	1.16	1.10
Elias Chadli	2015	1.14	1.25
Elias Chadli	2015	0.98	1.17
Elias Chadli	2015	0.85	0.99
Elias Chadli	2015	0.92	1.11
Elias Chadli	2015	0.79	0.94
Elias Chadli	2015	0.92	1.06
Elias Chadli	2015	0.99	0.96
Elias Chadli	2015	1.07	1.08
Elias Chadli	2015	1.09	1.15
Elias Chadli	2015	0.98	0.97
Elias Chadli	2015	0.99	1.07
Elias Chadli	2015	1.02	1.08
Elias Chadli	2015	0.89	1.16
Elias Chadli	2015	1.07	1.08
Elias Chadli	2015	1.14	1.08
Elias Chadli	2015	1.42	1.16
Elias Chadli	2015	1.17	1.22
Elias Chadli	2015	1.39	1.39
Elias Chadli	2015	1.37	1.08
Elias Chadli	2015	1.26	1.20
Elias Chadli	2015	1.28	1.27
Elias Chadli	2015	1.39	1.20
Elias Chadli	2015	1.32	1.23
Elias Chadli	2015	1.41	1.06
Elias Chadli	2015	1.44	1.20
Elias Chadli	2015	1.65	1.47
Elias Chadli	2015	1.52	1.17
Elias Chadli	2015	1.70	1.36
Elias Chadli	2015	1.57	1.41
Elias Chadli	2015	1.57	1.28
Elias Chadli	2015	1.73	1.10
Elias Chadli	2015	1.63	1.13
Elias Chadli	2015	1.70	1.19
Elias Chadli	2015	1.73	1.06

Elias Chadli	2015	1.66	1.26
Elias Chadli	2015	1.87	1.45
Elias Chadli	2015	1.93	1.25
Elias Chadli	2015	1.81	1.37
Elias Chadli	2015	1.83	1.41
Elias Chadli	2015	1.81	1.46
Elias Chadli	2015	1.65	1.24
Elias Chadli	2015	1.77	1.30
Elias Chadli	2015	1.45	1.06
Elias Chadli	2015	1.49	0.93
Elias Chadli	2015	1.46	0.92
Elias Chadli	2015	1.61	0.87
Elias Chadli	2015	1.35	0.80
Elias Chadli	2015	1.33	0.54
Elias Chadli	2015	1.40	0.49
Elias Chadli	2015	1.32	1.01
Elias Chadli	2015	1.33	1.05
Elias Chadli	2015	1.42	0.81
Elias Chadli	2015	1.33	0.81
Elias Chadli	2015	1.30	0.96
Elias Chadli	2015	1.32	0.99
Elias Chadli	2015	1.31	0.83
Elias Chadli	2015	1.38	0.63
Elias Chadli	2015	1.31	0.99
Elias Chadli	2014	1.40	0.94
Elias Chadli	2015	1.27	0.74
Elias Chadli	2015	1.07	0.72
Elias Chadli	2015	1.19	0.82
Elias Chadli	2015	1.35	0.84
Max Holmstrom	2014	1.29	0.96
Elias Chadli	2015	1.36	0.67
Elias Chadli	2015	1.39	0.56
Elias Chadli	2015	1.06	0.43
Elias Chadli	2015	1.15	0.77
Elias Chadli	2015	0.91	0.55
Max Holmstrom	2014	1.18	0.90
Elias Chadli	2015	0.89	0.84
Elias Chadli	2015	0.85	0.86
Elias Chadli	2015	0.85	0.66
Elias Chadli	2015	0.72	0.55
Max Holmstrom	2014	1.00	0.70
Elias Chadli	2015	0.97	0.46
Elias Chadli	2015	0.98	0.33
Elias Chadli	2015	1.17	0.50
Elias Chadli	2015	0.94	0.49
Elias Chadli	2015	1.01	0.48
Elias Chadli	2015	1.00	0.26
Elias Chadli	2015	1.19	0.29
Elias Chadli	2015	1.06	0.49
Elias Chadli	2015	1.29	0.27

Max Holmstrom	2014	1.27	0.62
Elias Chadli	2015	1.14	0.64
Elias Chadli	2015	1.11	0.62
Elias Chadli	2015	1.30	0.62
Max Holmstrom	2014	1.16	0.64
Elias Chadli	2015	0.98	0.50
Elias Chadli	2015	1.17	0.56
Elias Chadli	2015	0.98	0.29
Max Holmstrom	2014	1.35	0.93
Elias Chadli	2015	1.30	0.52
Elias Chadli	2015	0.87	0.31
Elias Chadli	2015	1.15	0.48
Max Holmstrom	2014	1.29	0.73
Elias Chadli	2015	1.22	0.23
Max Holmstrom	2014	1.34	0.76
Max Holmstrom	2014	1.28	0.71
Max Holmstrom	2014	1.31	0.89
Max Holmstrom	2014	1.37	0.69
Max Holmstrom	2014	1.40	0.62
Max Holmstrom	2014	1.26	0.47
Max Holmstrom	2014	1.45	0.78
Max Holmstrom	2014	1.29	0.80
Max Holmstrom	2014	1.11	0.72
Max Holmstrom	2014	1.04	0.97
Max Holmstrom	2014	1.19	0.90
Max Holmstrom	2014	1.13	1.01

Appendix III. Dataset S6 Planktonic foraminifera

>180 µm fraction

Sample source	Depth (mbsf)	Perservation (1-5: poor to very good)	No. Count	*Globigerinatheka index*	*Globigerinatheka tropicalis*	*Globigerinatheka luterbacheri*	*Hantkenina alabamensis*	*Hantkenina primitiva*	*Pseudohastigerina micra*	*Pseudohastigerina naguewichiensis*
756C-5X-7, 40.0-42.0 cm	116.01	4	300							
756C-5X-7, 140.0-142.0 cm	117.01	4	302							
756C-5X-8, 40.0-42.0 cm	117.51	5	307							
756C-5X-8, 100.0-102.0 cm	118.11	4	310							
756C-5X-CC, 10.5-12.5 cm	118.47	4	301							
756C-6X-1, 10.0-12.0 cm	120.30	4	300							
756C-6X-1, 40.0-42.0 cm	120.60	4	308							
756C-6X-1, 80.0-82.0 cm	121.00	4	317							
756C-6X-1, 110.0-112.0 cm	121.30	4	301							
756C-6X-1, 140.0-142.0 cm	121.60	4	310							
756C-6X-2, 19.5-21.5 cm	121.90	5	301							
756C-6X-2, 50.0-52.0 cm	122.20	5	307							
756C-6X-2, 71.5-73.5 cm	122.42	5	302							
756C-6X-2, 90.0-92.0 cm	122.60	5	300							
756C-6X-2, 110.0-112.0 cm	122.80	5	306							
756C-6X-2, 131.5-133.5 cm	123.02	5	312							
756C-6X-3, 10.0-12.0 cm	123.30	5	312							
756C-6X-3, 30.0-32.0 cm	123.50	5	318							
756C-6X-3, 50.0-52.0 cm	123.70	5	303							
756C-6X-3, 69.0-71.0 cm	123.89	5	304							
756C-6X-3, 102.5-104.5 cm	124.23	5	300							
756C-6X-3, 129.5-131.5 cm	124.50	5	314				X*			
756C-6X-4, 10 cm	124.80	3	305	6						
756C-6X-4, 30.0-32.0 cm	125.00	4	303				1			
756C-6X-4, 53 cm	125.3	4	313							
756C-6X-4, 80.0-82.0 cm	125.50	4	300							
756C-6X-4, 100.0-102.0 cm	125.70	5	302							
756C-6X-4, 111.0-113.0 cm	125.81	5	307					1		
756C-6X-4, 140.0-142.0 cm	126.10	4	304							
756C-6X-5, 20.0-22.0 cm	126.40	4	313				1			
756C-6X-5, 40.0-42.0 cm	126.60	4	304							
756C-6X-5, 60.0-62.0 cm	126.80	4	307	2						
756C-6X-5, 80.0-82.0 cm	127.00	4	303							1
756C-6X-CC, 10.0-12.0 cm	127.25	4	303	1		1				1
756C-7X-1, 0.0-2.0 cm	129.80	4	300	4					3	
756C-7X-1, 20.0-22.0 cm	130.00	4	303	11	4		1			
756C-7X-1, 41 cm	130.21	2	302	62	2	1				
756C-7X-1, 60.0-62.0 cm	130.40	4	307	77	6	3				
756C-7X-1, 80.0-82.0 cm	130.60	5	310	78	19	3				1
756C-7X-1, 115 cm	130.95	2	312	133	2	1	1			
756C-7X-2, 0.0-2.0 cm	131.30	4	300	87	21	2			1	
756C-7X-2, 19.0-21.0 cm	131.49	5	303	95	15	8			2	
756C-7X-2, 60.0-62.0 cm	131.90	4	305	77	6		2			
756C-7X-2, 80.0-82.0 cm	132.10	4	306	94	10	3				
756C-7X-2, 115 cm	132.45	4	301	64	3				1	
756C-7X-2, 140.0-142.0 cm	132.70	4	300	50	6	2				
756C-7X-3, 40 cm	133.20	2	300	61	7	7				
756C-7X-3, 115 cm	133.95	1	300	49	6	3				
756C-7X-4, 35 cm	134.65	4	301	47	3	1				
756C-7X-4, 110 cm	135.40	4	301	73	6	1				

756C-7X-5, 50 cm	136.30	2	300	53	2	1		4
756C-7X-5, 110 cm	136.90	3	300	42	2		1	
756C-7X-6, 50 cm	137.80	1	300	48	1			

X* species found to be present after a wider scouring of the whole >180 micron fraction

>63 µm fraction

Sample source	Depth (mbsf)	Splits	Perservation (1-5: poor to very good)	In-situ Fragments	Reworked Fragments	Reworked forams	No. Count	*Globigerinatheka index*	*Hantkenina primitiva*	*Pseudohastigerina micra*	*Pseudohastigerina naguewichiensis*
756C-5X-7, 40.0-42.0 cm	116.01										
756C-5X-7, 140.0-142.0 cm	117.01										
756C-5X-8, 40.0-42.0 cm	117.51	7	4	O	O	R	310			7	1
756C-5X-8, 100.0-102.0 cm	118.11										
756C-5X-CC, 10.5-12.5 cm	118.47										
756C-6X-1, 10.0-12.0 cm	120.30	9	4	F	O	O	303			7	
756C-6X-1, 40.0-42.0 cm	120.60										
756C-6X-1, 80.0-82.0 cm	121.00	8	4	O	O	O	305			3	1
756C-6X-1, 110.0-112.0 cm	121.30										
756C-6X-1, 140.0-142.0 cm	121.60										
756C-6X-2, 19.5-21.5 cm	121.90	8	4	F	F	F	305			2	
756C-6X-2, 50.0-52.0 cm	122.20										
756C-6X-2, 71.5-73.5 cm	122.42	7	5	O	O	R	301			8	1
756C-6X-2, 90.0-92.0 cm	122.60										
756C-6X-2, 110.0-112.0 cm	122.80										
756C-6X-2, 131.5-133.5 cm	123.02	7	4	C	F	F	307			11	1
756C-6X-3, 10.0-12.0 cm	123.30										
756C-6X-3, 30.0-32.0 cm	123.50	6	4	O	O	O	309			10	1
756C-6X-3, 50.0-52.0 cm	123.70										
756C-6X-3, 69.0-71.0 cm	123.89										
756C-6X-3, 102.5-104.5 cm	124.23	6	4	A	C	F	305			3	
756C-6X-3, 129.5-131.5 cm	124.50										
756C-6X-4, 10 cm	124.80	6	4	F	O	O	305	2		3	
756C-6X-4, 30.0-32.0 cm	125.00										
756C-6X-4, 53 cm	125.3	5	4	C	F	C	314			1	
756C-6X-4, 80.0-82.0 cm	125.50										
756C-6X-4, 100.0-102.0 cm	125.70										
756C-6X-4, 111.0-113.0 cm	125.81	6	4	F	O	O	301				2
756C-6X-4, 140.0-142.0 cm	126.10										
756C-6X-5, 20.0-22.0 cm	126.40										
756C-6X-5, 40.0-42.0 cm	126.60	6	5	F	O	O	303				
756C-6X-5, 60.0-62.0 cm	126.80										
756C-6X-5, 80.0-82.0 cm	127.00										
756C-6X-CC, 10.0-12.0 cm	127.25	6	4	O	O	O	317			3	
756C-7X-1, 0.0-2.0 cm	129.80										
756C-7X-1, 20.0-22.0 cm	130.00	6	5	C	F	F	340			5	1
756C-7X-1, 41 cm	130.21										
756C-7X-1, 60.0-62.0 cm	130.40										
756C-7X-1, 80.0-82.0 cm	130.60	6	4	O	O	O	334	7		2	
756C-7X-1, 115 cm	130.95										
756C-7X-2, 0.0-2.0 cm	131.30	6	4	C	F	F	307				
756C-7X-2, 19.0-21.0 cm	131.49										
756C-7X-2, 60.0-62.0 cm	131.90										
756C-7X-2, 80.0-82.0 cm	132.10	6	4	O	O	O	316	1		3	1
756C-7X-2, 115 cm	132.45										
756C-7X-2, 140.0-142.0 cm	132.70	6	4	C	F	F	312	1		2	1
756C-7X-3, 40 cm	133.20										
756C-7X-3, 115 cm	133.95										
756C-7X-4, 35 cm	134.65	5	4	F	O	O	302	2		2	
756C-7X-4, 110 cm	135.40										

756C-7X-5, 50 cm	136.30										
756C-7X-5, 110 cm	136.90										
756C-7X-6, 50 cm	137.80	5	2	A	C	C	304	12	1	52	4

Magn. strat. age (Ma) GTS12																									
			IODP U1509									ODP 1218			IODP U1333			ODP 711			DSDP 522, 523		DSDP 516		IODP U1411	
Oceanographic domain			Pacific Ocean															Indian Ocean			Atlantic Ocean					
			Tasman Sea									Equatorial Pacific						Eq. Indian Ocean			South Atlantic				North Atlantic	
			This study									Blaj et al. 2009			Toffanin et al. 2013			Fioroni et al. (2015)			Backman (1987)		Wei & Wise (1989)		Newsam (2016)	
Event/Chron boundary	CN ZONE	Chron	Sample Top	Sample Base	Mid point (CSF-a, m)	Error (± m)	Age (Ma)	Error (± Myr)	Position from Top Chron	Sed. Rate (m/Myr)		Age (Ma)	Error (± Myr)	|Δt| (Myr)	Age (Ma)	Error (± Myr)	|Δt| (Myr)	Age (Ma)	Error (± Myr)	|Δt| (Myr)	Age (Ma)	|Δt| (Myr)	Age (Ma)	|Δt| (Myr)	Age (Ma)	|Δt| (Myr)
T *Reticulofenestra umbilicus*	CNO2	no data	U1509A-23R-1W, 100-101	U1509A-23R-2W, 8-9	203.395	0.29	31.382	0.015	0.16	19.09		32.042	0.004	0.660				31.156	0.074	0.227	31.833	0.451	32.544	1.162		
T *Sphenolithus akropodus*			U1509A-24R-2W, 132-133	U1509A-24R-3W, 42-43	209.705	0.30	31.712	0.016	0.32	19.09																
Tc *Chiasmolithus altus*			U1509A-24R-3W, 42-43	U1509A-24R-3W, 102-103	210.305	0.30	31.744	0.016	0.33	19.09																
Tc *Clausicoccus subdistichus*		C12r	U1509A-26R-1W, 11-12	U1509A-26R-2W, 2-3	221.560	0.14	**32.333**	0.008	0.61	19.09											32.322	0.011	32.988 ?	0.655	32.646	0.313
Tc *Lanternithus minutus*			U1509A-26R-3W, 122-123	U1509A-26R-4W, 32-33	224.705	0.30	32.497	0.016	0.69	19.09																
Tc(2) *Isthmolithus recurvus*			U1509A-26R-8W, 15-16	U1509A-26R-8W, 45-46	230.555	0.15	32.803	0.008	0.83	19.09											32.837 (T)	0.034	32.722 (T)	0.081		
T *Ericsonia formosa*	CNO1		U1509A-27R-3W, 9-10	U1509A-27R-3W, 70-71	234.300	0.31	32.999	0.016	0.93	19.09		32.974	0.004	0.025	32.984	0.251	0.015	32.342	0.006	0.657	32.784	0.215	32.988	0.011	33.129	0.130
C13n-C12r			U1509A-27R-2W, 110-112	U1509A-28R-1W, 50-52	237.260	3.75	33.157																			
B *Sphenolithus akropodus*		C13n	U1509A-27R-3W, 70-71	U1509A-28R-1W, 40-41	237.755	3.15	33.183	0.165	0.05	19.09								34.538 (B)	0.230	1.538						
Tc *Sphenolithus intercalaris*			U1509A-28R-1W, 40-41	U1509A-28R-1W, 100-101	241.205	0.30	33.364	0.016	0.38	19.09								32.675	0.055	0.688						
Tc(1) *Isthmolithus recurvus*			U1509A-28R-2W, 130-131	U1509A-28R-3W, 40-41	243.605	0.30	33.489	0.016	0.61	19.09																
Bc *Lanternithus minutus*			U1509A-28R-3W, 40-41	U1509A-28R-3W, 100-101	244.205	0.30	33.521	0.016	0.66	19.09																
C13r-C13n			U1509A-28R-5W, 56-58	U1509A-28R-6W, 56-58	247.720	0.75	33.705																			
EOB					250.085		33.890			12.78																
Bc *Clausicoccus subdistichus*	CNE21		U1509A-29R-1W, 9-10	U1509A-29R-1W, 40-41	250.350	0.16	**33.911**	0.012	0.16	12.78					33.897	0.175	0.013	33.654	0.051	0.257	33.894	0.017			33.807	0.104
T *Discoaster saipanensis*	CNE20	C13r	U1509A-29R-5W, 67-68	U1509A-29R-5W, 96-97	256.960	0.15	34.428	0.011	0.56	12.78		34.691	0.012	0.264	34.247	0.175	0.181	34.143	0.164	0.285	34.508	0.080	34.206	0.222	34.610	0.182
Bc *Sphenolithus intercalaris*			U1509A-30R-1W, 130-131	U1509A-30R-2W, 9-10	261.150	0.15	34.756	0.011	0.81	12.78																
T *Discoaster barbadiensis*			U1509A-30R-2W, 70-71	U1509A-30R-2W, 100-101	262.058	0.15	34.827	0.012	0.87	12.78		34.943	0.010	0.116				34.874	0.106	0.047	34.735	0.092	34.489	0.338	34.775	0.052
C15n-C13r			U1509A-30R-3W, 105-107	U1509A-30R-4W, 105-107	264.260	0.75	34.999																			
Tc *Cribrocentrum reticulatum*	CNE19	C15n	U1509A-30R-4W, 65-66	U1509A-30R-4W, 95-96	264.755	0.15	35.038	0.012	0.13	12.71								35.057	0.070	0.019	35.294 (T)	0.256	35.240 (T)	0.202	35.115 (Tc)	0.077
C15r-C15n			U1509A-30R-6W-0-2	U1509A-31R-1W-20-22	268.010	1.50	35.294																			

Appendix IV. Calcareous nannofossils bioevents investigated at IODP U1509) are tied to magnetostratigraphy and calibrated using the Geological Time Scale (GTS12, Gradstein et al. 2012).
Our age estimates are herein compared with those from different sites. Chron boundaries (grey bars) are used as tie points and sedimentation rates are assumed to remain constant between ties-points. Below the first and above the last tie point, we assume a sed. rate equal to that calculate for the last complete chron in the section. CN biozone is from Agnini et al. 2014.
|Δt|= absolute time difference (Myr) between ``This study'' Age (Ma) column and the corresponding age estimate for each site.
B = Base, Bc= Base continuous and common, T = Top, Tc= Top continuous and common;

Appendix V. Site U1509 calcareous nannofossil data (%)

Core	Type	Sect	A/W	Interval		Top depth CSF-A (m)	Bottom depth CSF-A (m)	CSF-A (m)	*Blackites spp.*	*Bramletteius serraculoides*	*Calcidiscus? edgariae*	*Chiasmolithus altus*	*Chiasmolithus cf. altus*	*Chiasmolithus oamaruensis*	*Chiasmolithus spp.*
21	R	1	W	30	31	183.3	183.3	183.305	0.00	0.00	0.00	0.00	0.00	0.00	0.00
21	R	1	W	90	91	183.9	183.9	183.905	0.00	0.27	0.00	0.00	0.00	0.00	0.00
21	R	2	W	0	1	184.5	184.5	184.505	0.28	0.00	0.00	0.00	0.00	0.00	0.00
21	R	2	W	60	61	185.1	185.1	185.105	0.00	0.00	0.00	0.64	0.00	0.00	0.00
21	R	3	W	35	36	185.7	185.7	185.705	0.00	0.27	0.00	0.00	0.00	0.00	0.55
21	R	CC	W	11	12	186.3	186.3	186.305	0.00	0.24	0.00	0.71	0.00	0.00	0.24
22	R	1	W	30	31	192.9	192.9	192.905	0.73	0.00	0.00	0.24	0.00	0.00	0.00
22	R	1	W	90	91	193.5	193.5	193.505	1.10	0.00	0.00	0.55	0.00	0.00	0.55
22	R	2	W	29	30	194.4	194.4	194.405	0.50	0.00	0.00	0.25	0.00	0.00	0.00
22	R	2	W	89	90	195	195	195.005	1.80	0.00	0.00	0.23	0.00	0.00	0.00
22	R	3	W	29	30	195.9	195.9	195.905	1.55	0.00	0.00	0.00	0.26	0.00	0.00
22	R	CC	W	9	10	196.4	196.4	196.405	1.36	0.00	0.00	0.00	0.00	0.00	0.00
23	R	1	W	40	41	202.5	202.5	202.505	0.93	0.00	0.00	0.00	0.00	0.00	0.00
23	R	1	W	100	101	203.1	203.1	203.105	0.88	0.29	0.00	0.00	0.00	0.00	0.00
23	R	2	W	8	9	203.7	203.7	203.685	0.91	0.00	0.00	0.00	0.00	0.30	0.00
23	R	2	W	70	71	204.3	204.3	204.305	0.77	0.00	0.00	0.00	0.00	0.00	0.00
23	R	2	W	130	131	204.9	204.9	204.905	2.39	0.00	0.00	0.00	0.00	0.00	0.00
24	R	1	W	30	31	207	207	207.005	0.79	0.00	0.00	0.00	0.00	0.00	0.00
24	R	1	W	90	91	207.6	207.6	207.605	0.97	0.00	0.00	0.00	0.00	0.00	0.00
24	R	2	W	14	15	208.2	208.2	208.225	0.80	0.00	0.27	0.00	0.00	0.00	0.00
24	R	2	W	72	73	208.8	208.8	208.805	1.29	0.00	0.00	0.00	0.00	0.00	0.00
24	R	2	W	132	133	209.4	209.4	209.405	1.08	0.00	0.00	0.00	0.00	0.00	0.00
24	R	3	W	42	43	210	210	210.005	1.40	0.00	0.00	0.00	0.00	0.00	0.00
24	R	3	W	102	103	210.6	210.6	210.605	1.66	0.00	0.00	0.55	0.00	0.00	0.00
25	R	1	W	40	41	212.1	212.1	212.105	1.30	0.32	0.00	0.00	0.00	0.00	0.00
25	R	1	W	100	101	212.7	212.7	212.705	1.25	0.00	0.00	0.00	0.00	0.00	0.00
25	R	2	W	15	16	213.3	213.3	213.305	2.01	0.00	0.00	0.00	0.00	0.00	0.25
26	R	1	W	11	12	221.4	221.4	221.415	1.52	0.00	0.00	1.52	0.00	0.00	0.61
26	R	2	W	32	33	222	222	222.005	0.93	0.00	0.00	0.46	0.00	0.00	0.00
26	R	2	W	92	93	222.6	222.6	222.605	1.39	0.00	0.00	0.28	0.00	0.00	0.00
26	R	3	W	2	3	223.2	223.2	223.205	0.71	0.00	0.00	0.94	0.00	0.00	0.24
26	R	3	W	64	65	223.8	223.8	223.825	1.18	0.00	0.00	0.30	0.00	0.00	0.30
26	R	3	W	122	123	224.4	224.4	224.405	0.56	0.00	0.00	0.56	0.00	0.00	0.00
26	R	4	W	32	33	225	225	225.005	2.02	0.00	0.00	0.76	0.00	0.00	0.00
26	R	4	W	92	93	225.6	225.6	225.605	2.01	0.00	0.00	0.29	0.00	0.00	0.00
26	R	5	W	2	3	226.2	226.2	226.205	1.57	0.00	0.22	0.45	0.00	0.00	0.00
26	R	5	W	66	67	226.8	226.9	226.845	1.55	0.31	0.00	0.62	0.00	0.00	0.00
26	R	5	W	122	123	227.4	227.4	227.405	0.69	0.00	0.00	0.23	0.00	0.00	0.00

26	R	6	W	32	33	228	228	228.005	2.10	0.00	0.00	0.60	0.00	0.00	0.60
26	R	6	W	92	93	228.6	228.6	228.605	1.15	0.00	0.00	0.46	0.00	0.00	0.00
26	R	7	W	2	3	229.2	229.2	229.205	1.86	0.00	0.00	0.00	0.00	0.00	0.23
26	R	7	W	64	65	229.8	229.8	229.825	0.25	0.00	0.00	0.00	0.00	0.00	0.25
26	R	8	W	15	16	230.4	230.4	230.405	0.27	0.00	0.00	0.00	0.00	0.00	0.00
27	R	1	W	9	10	231	231	230.995	1.16	0.00	0.00	0.00	0.00	0.00	0.29
27	R	1	W	70	71	231.6	231.6	231.605	1.67	0.00	0.00	0.24	0.00	0.00	0.00
27	R	1	W	130	131	232.2	232.2	232.205	1.98	0.00	0.00	0.25	0.00	0.00	0.00
27	R	2	W	40	41	232.8	232.8	232.805	0.27	0.00	0.00	0.80	0.00	0.00	0.27
27	R	2	W	100	101	233.4	233.4	233.405	2.87	0.00	0.00	0.26	0.00	0.00	0.00
27	R	3	W	9	10	234	234	233.995	2.29	0.57	0.00	0.38	0.00	0.00	0.00
27	R	3	W	70	71	234.6	234.6	234.605	1.65	0.00	0.24	0.47	0.00	0.00	0.00
28	R	1	W	40	41	240.9	240.9	240.905	1.63	0.27	0.00	0.00	0.00	0.00	0.00
28	R	1	W	100	101	241.5	241.5	241.505	2.33	0.19	0.00	0.00	0.00	0.00	0.00
28	R	2	W	9	10	242.1	242.1	242.095	2.99	0.00	0.60	1.49	0.00	0.00	0.00
28	R	2	W	70	71	242.7	242.7	242.705	1.37	0.00	0.00	0.39	0.00	0.00	0.20
28	R	2	W	130	131	243.3	243.3	243.305	3.21	0.00	0.00	0.23	0.00	0.00	0.00
28	R	3	W	40	41	243.9	243.9	243.905	1.82	0.20	0.00	0.00	0.00	0.20	0.00
28	R	3	W	100	101	244.5	244.5	244.505	1.90	0.00	0.24	0.00	0.00	0.00	0.48
28	R	4	W	20	21	245.1	245.1	245.105	2.53	0.00	0.00	0.63	0.00	0.00	0.63
28	R	4	W	80	81	245.7	245.7	245.705	4.00	0.00	0.00	0.00	0.00	0.00	0.00
28	R	4	W	140	141	246.3	246.3	246.305	2.09	0.60	0.00	0.30	0.00	0.00	0.30
28	R	5	W	20	21	246.6	246.6	246.605	1.09	0.00	0.00	0.55	0.00	0.00	0.27
28	R	5	W	50	51	246.9	246.9	246.905	3.45	0.63	0.00	0.00	0.00	0.00	0.00
28	R	5	W	80	81	247.2	247.2	247.205	1.72	0.29	0.00	0.00	0.00	0.00	0.00
28	R	5	W	109	110	247.5	247.5	247.495	1.23	0.00	0.00	0.93	0.00	0.00	0.00
28	R	5	W	140	141	247.8	247.8	247.805	1.92	0.32	0.00	0.96	0.00	0.00	0.00
28	R	6	W	20	21	248.1	248.1	248.105	2.09	0.26	0.00	1.31	0.00	0.00	0.00
28	R	6	W	50	51	248.4	248.4	248.405	3.07	0.84	0.00	0.56	0.00	0.00	0.00
29	R	1	W	9	10	250.2	250.2	250.195	3.42	0.00	0.31	0.93	0.00	0.00	0.31
29	R	1	W	40	41	250.5	250.5	250.505	2.17	0.00	0.00	0.62	0.00	0.00	0.00
29	R	1	W	70	71	250.8	250.8	250.805	2.38	0.00	0.00	0.30	0.00	0.00	0.89
29	R	1	W	100	101	251.1	251.1	251.105	1.50	0.21	0.00	0.64	0.00	0.00	0.43
29	R	1	W	130	131	251.4	251.4	251.405	3.23	0.00	0.00	0.27	0.00	0.00	0.00
29	R	2	W	6	7	251.7	251.7	251.705	1.30	0.00	0.00	0.26	0.00	0.00	0.00
29	R	2	W	36	37	252	252	252.005	1.22	0.00	0.00	0.61	0.00	0.00	0.91
29	R	2	W	66	67	252.3	252.3	252.305	1.54	0.00	0.00	0.22	0.00	0.00	0.22
29	R	2	W	96	97	252.6	252.6	252.605	2.28	0.00	0.00	0.98	0.00	0.00	0.33
29	R	2	W	126	127	252.9	252.9	252.905	1.47	0.00	0.00	0.24	0.00	0.00	0.49
29	R	3	W	6	7	253.2	253.2	253.205	1.11	0.00	0.00	0.22	0.00	0.00	0.22
29	R	3	W	36	37	253.5	253.5	253.505	1.20	0.24	0.00	0.00	0.00	0.00	0.24
29	R	3	W	66	67	253.8	253.8	253.805	1.65	0.47	0.00	0.24	0.00	0.00	0.00
29	R	3	W	96	97	254.1	254.1	254.105	1.92	0.00	0.00	0.00	0.00	0.00	0.00
29	R	3	W	126	127	254.4	254.4	254.405	1.35	0.00	0.00	0.00	0.00	0.00	0.00
29	R	4	W	6	7	254.7	254.7	254.705	1.52	0.00	0.00	0.43	0.00	0.00	0.22
29	R	4	W	36	37	255	255	255.005	2.48	0.00	0.23	0.45	0.00	0.00	0.68
29	R	4	W	66	67	255.3	255.3	255.305	0.76	0.00	0.25	0.00	0.00	0.00	0.00
29	R	4	W	96	97	255.6	255.6	255.605	1.08	0.00	0.00	0.27	0.00	0.00	0.00
29	R	4	W	126	127	255.9	255.9	255.905	5.97	0.31	0.00	0.00	0.00	0.00	0.00
29	R	5	W	6	7	256.2	256.2	256.205	1.48	0.00	0.00	0.25	0.00	0.25	0.00

29	R	5	W	36	37	256.5	256.5	256.505	2.80	0.00	0.00	0.22	0.00	0.00	0.65
29	R	5	W	67	68	256.8	256.8	256.815	1.68	0.00	0.24	0.48	0.00	0.00	0.48
29	R	5	W	96	97	257.1	257.1	257.105	1.93	0.00	0.00	0.00	0.00	0.00	0.48
29	R	5	W	126	127	257.4	257.4	257.405	1.74	0.00	0.00	0.29	0.00	0.00	0.29
29	R	6	W	6	7	257.7	257.7	257.705	1.27	0.00	0.00	0.32	0.00	0.00	0.00
29	R	6	W	36	37	258	258	258.005	1.75	0.00	0.00	0.25	0.00	0.00	0.00
29	R	6	W	66	67	258.3	258.3	258.305	0.81	0.00	0.00	0.27	0.00	0.00	0.00
29	R	6	W	96	97	258.6	258.6	258.605	1.90	0.00	0.00	0.00	0.00	0.00	0.32
29	R	6	W	126	127	258.9	258.9	258.905	1.02	0.26	0.00	0.00	0.00	0.00	0.00
29	R	7	W	6	7	259.2	259.2	259.205	1.59	0.00	0.00	0.32	0.00	0.00	0.96
29	R	7	W	36	37	259.5	259.5	259.505	0.32	0.00	0.00	0.00	0.00	0.00	0.00
30	R	1	W	40	41	260.1	260.1	260.105	1.36	0.00	0.00	0.54	0.00	0.00	0.00
30	R	1	W	70	71	260.4	260.4	260.405	0.86	0.00	0.00	0.22	0.00	0.00	0.00
30	R	1	W	100	101	260.7	260.7	260.705	1.95	0.28	0.28	0.00	0.00	0.00	0.00
30	R	1	W	130	131	261	261	261.005	2.36	0.00	0.29	0.29	0.00	0.00	0.00
30	R	2	W	9	10	261.3	261.3	261.295	2.56	0.28	1.42	0.00	0.00	0.00	0.00
30	R	2	W	40	41	261.6	261.6	261.605	3.77	0.31	0.00	0.00	0.00	0.00	0.00
30	R	2	W	70	71	261.9	261.9	261.905	4.67	0.33	0.67	0.00	0.00	0.00	0.00
30	R	2	W	100	101	262.2	262.2	262.205	1.70	0.00	0.00	0.00	0.00	0.00	0.00
30	R	3	W	5	6	262.5	262.5	262.505	1.54	0.31	0.00	0.00	0.00	0.00	0.00
30	R	3	W	35	36	262.8	262.8	262.805	2.92	0.00	0.00	0.00	0.00	0.00	0.00
30	R	3	W	65	66	263.1	263.1	263.105	0.64	0.32	0.00	0.00	0.00	0.00	0.00
30	R	3	W	96	97	263.4	263.4	263.415	3.16	0.00	0.00	0.00	0.00	0.24	0.00
30	R	3	W	125	126	263.7	263.7	263.705	1.12	0.00	0.00	0.00	0.00	0.00	0.00
30	R	4	W	5	6	264	264	264.005	2.25	0.28	0.00	0.00	0.00	0.00	0.00
30	R	4	W	35	36	264.3	264.3	264.305	0.87	0.29	0.00	0.00	0.00	0.00	0.29
30	R	4	W	65	66	264.6	264.6	264.605	1.50	0.00	0.00	0.00	0.00	0.00	0.00
30	R	4	W	95	96	264.9	264.9	264.905	2.31	0.00	0.00	0.00	0.00	0.00	0.00
30	R	4	W	125	126	265.2	265.2	265.205	0.30	0.00	0.00	0.00	0.00	0.00	0.00
30	R	5	W	3	4	265.5	265.5	265.485	2.28	0.00	0.00	0.00	0.00	0.00	0.00
30	R	5	W	35	36	265.8	265.8	265.805	1.82	0.30	0.00	0.00	0.00	0.00	0.00
30	R	5	W	65	66	266.1	266.1	266.105	4.01	0.00	0.00	0.00	0.00	0.00	0.00
30	R	5	W	95	96	266.4	266.4	266.405	2.43	0.00	0.00	0.00	0.00	0.00	0.00
30	R	6	W	20	21	266.7	266.7	266.705	1.22	0.00	0.00	0.00	0.00	0.00	0.00
30	R	6	W	49	50	267	267	266.995	0.76	0.00	0.00	0.00	0.00	0.00	0.00
30	R	CC	W	19	20	267.3	267.3	267.305	1.09	0.00	0.00	0.00	0.00	0.00	0.00

Clausicoccus fenestratus	*Clausicoccus subdistichus*	*Clausicoccus spp.*	*Coccolithus cachaoi*	*Coccolithus eopelagicus* (16-20µm)	*Coccolithus miopelagicus* (13-16µm)	*Coccolithus pelagicus* (6-13µm)	*Coronocyclus nitescens*	*Dictyoccocites spp. distal shield (ellip*	*Cyclicargolithus floridanus*	*Dictyococcites spp. <4µm*	*Dictyococcites spp. 4-10µm*
0.00	0.00	0.00	0.00	0.00	0.00	3.04	0.00	0.00	14.29	0.00	2.13
0.00	0.00	0.27	0.00	0.00	0.00	8.09	0.00	0.00	9.16	0.00	2.43
0.00	0.00	0.00	0.00	0.00	0.00	6.44	0.00	0.00	20.73	0.00	1.12
0.00	0.64	0.00	0.00	0.00	0.00	9.62	0.00	0.00	8.65	0.00	2.88
0.00	0.00	0.00	0.00	0.00	0.00	10.38	0.00	0.00	13.11	0.00	0.55
0.00	0.47	0.00	0.00	0.00	0.00	8.75	0.00	0.00	16.55	0.00	1.89
0.00	0.00	0.00	0.00	0.00	0.00	10.73	0.49	0.00	8.29	0.00	1.46
0.00	0.00	0.00	0.00	0.00	0.00	6.91	0.28	0.00	9.67	0.00	1.38
0.00	0.00	0.00	0.00	0.00	0.00	10.20	0.00	0.00	4.23	0.00	1.99
0.00	0.45	0.00	0.00	0.00	0.00	9.46	0.00	0.00	9.23	0.00	2.25
0.00	0.00	0.00	0.00	0.26	0.00	9.04	0.00	0.00	7.75	0.00	3.10
0.00	0.00	0.27	0.00	0.00	0.00	10.84	0.00	0.00	10.30	0.00	0.81
0.00	0.31	0.00	0.00	0.00	0.00	20.74	0.00	0.00	5.57	0.00	1.24
0.00	0.00	0.00	0.00	0.00	0.00	18.53	0.00	0.00	4.71	0.29	2.06
0.00	0.30	0.00	0.00	0.00	0.00	19.03	0.00	0.00	3.63	0.00	3.02
0.00	0.00	0.00	0.00	0.00	0.00	13.52	0.00	0.26	3.83	0.00	1.79
0.00	0.00	0.00	0.00	0.00	0.00	10.02	0.00	0.00	9.07	0.00	1.91
0.00	0.00	0.00	0.00	0.20	0.00	10.83	0.00	0.00	6.10	0.00	1.57
0.00	0.00	0.00	0.00	0.00	0.24	11.35	0.00	0.00	8.21	0.00	1.69
0.00	0.00	0.00	0.00	0.00	0.27	9.12	0.00	0.00	9.92	0.00	1.61
0.00	0.00	0.00	0.00	0.00	0.00	10.36	0.00	0.00	7.77	0.00	2.27
0.00	0.00	0.00	0.00	0.00	0.00	10.63	0.00	0.00	10.20	0.00	2.17
0.00	0.00	0.00	0.00	0.00	0.00	7.26	0.00	0.00	9.78	0.00	1.40
0.00	0.00	0.00	0.00	0.00	0.00	14.96	0.00	0.00	6.09	0.00	1.66
0.32	0.00	0.00	0.00	0.00	0.00	9.09	0.00	0.00	3.25	0.00	0.65
0.00	0.00	0.00	0.00	0.00	0.00	12.97	0.00	0.00	2.00	0.00	1.00
0.00	0.00	0.00	0.00	0.00	0.50	10.78	0.00	0.00	4.51	0.00	0.75
0.00	0.30	0.00	0.00	0.00	0.00	10.67	0.00	0.00	1.83	0.00	2.74
0.00	6.02	0.00	0.00	0.00	0.00	6.02	0.00	0.00	3.24	1.39	1.85
0.00	9.75	0.00	0.00	0.00	0.00	5.29	0.00	0.00	2.23	0.00	0.56
0.24	4.72	0.00	0.00	0.00	0.24	5.19	0.00	0.00	1.89	0.00	0.94
0.00	2.66	0.00	0.00	0.00	0.00	4.44	0.00	0.00	2.96	0.00	1.18
0.00	2.80	0.00	0.00	0.00	0.00	7.28	0.00	0.00	5.88	0.00	1.12
0.25	3.02	0.00	0.00	0.00	0.00	6.80	0.00	0.00	2.52	0.00	0.00
0.00	5.46	0.00	0.00	0.00	0.00	8.05	0.00	0.00	1.44	0.00	1.15
0.67	3.36	0.00	0.00	0.00	0.00	6.26	0.00	0.00	0.45	0.00	1.12
0.93	10.84	0.00	0.00	0.00	0.00	8.98	0.00	0.00	2.48	0.00	2.48
0.23	5.05	0.00	0.00	0.00	0.00	4.13	0.00	0.00	2.29	0.00	0.69

0.30	2.99	0.00	0.00	0.00	0.00	6.59	0.00	0.00	2.10	0.00	2.40
0.23	3.69	0.00	0.00	0.00	0.23	6.68	0.00	0.00	6.45	0.00	0.92
0.46	4.64	0.00	0.00	0.00	0.00	6.73	0.00	0.00	3.02	0.00	0.93
0.50	4.28	0.00	0.00	0.00	0.00	6.30	0.00	0.00	4.79	0.00	2.02
0.27	4.51	0.00	0.00	0.00	0.00	8.49	0.00	0.00	0.53	0.00	5.04
0.29	3.19	0.00	0.00	0.00	0.29	7.54	0.00	0.00	4.06	0.00	0.87
0.00	3.57	0.00	0.00	0.00	0.00	3.10	0.00	0.00	3.10	0.00	0.24
0.00	7.43	0.00	0.00	0.00	0.00	6.68	0.00	0.00	0.99	0.00	3.22
0.53	4.27	0.00	0.00	0.00	0.00	3.73	0.00	0.00	1.87	0.27	2.40
0.26	9.92	0.00	0.00	0.00	0.00	5.48	0.00	0.00	1.57	0.00	2.35
0.00	5.73	0.00	0.00	0.00	0.00	7.25	0.00	0.00	2.10	0.00	0.95
0.47	4.02	0.00	0.00	0.00	0.24	4.26	0.00	0.00	7.09	0.00	3.07
0.54	5.43	0.00	0.00	0.00	0.00	12.50	0.00	0.00	2.45	0.00	2.72
0.00	4.86	0.00	0.00	0.00	0.00	6.42	0.00	0.00	1.95	0.00	0.00
0.00	3.28	0.00	0.00	0.00	0.00	9.25	0.00	0.00	5.67	0.00	0.00
0.00	3.92	0.00	0.00	0.00	0.00	7.84	0.00	0.00	2.16	0.00	0.00
0.23	8.94	0.00	0.00	0.00	0.00	18.81	0.00	0.00	3.21	0.00	0.46
0.20	9.90	0.00	0.00	0.00	0.00	11.92	0.00	0.00	3.03	0.00	0.00
0.00	8.55	0.00	0.00	0.00	0.00	10.21	0.00	0.00	3.56	0.00	0.00
1.27	4.11	0.00	0.00	0.00	0.00	13.92	0.00	0.00	4.43	0.00	1.27
1.00	11.33	0.00	0.00	0.00	0.00	14.67	0.00	0.00	3.33	0.00	0.67
0.30	5.37	0.00	0.00	0.00	0.00	12.24	0.00	0.00	3.28	0.00	0.30
1.91	4.92	0.00	0.00	0.00	0.00	11.48	0.00	0.00	3.28	0.00	0.27
1.57	7.21	0.00	0.00	0.00	0.00	14.73	0.00	0.00	3.45	0.00	0.63
3.44	5.16	0.00	0.00	0.00	0.00	15.76	0.00	0.00	3.72	0.00	0.29
0.62	6.48	0.00	0.00	0.00	0.00	12.35	0.00	0.00	0.31	0.00	0.00
1.28	6.41	0.00	0.00	0.00	0.00	13.46	0.00	0.00	1.28	0.00	0.00
0.26	12.79	0.00	0.00	0.00	0.00	13.05	0.00	0.00	0.52	0.00	0.52
0.56	10.89	0.00	0.00	0.00	0.00	17.60	0.00	0.00	0.56	0.00	0.84
0.00	6.21	0.93	0.00	0.00	0.31	13.35	0.00	0.00	5.28	0.00	0.00
0.00	2.79	0.00	0.00	0.00	0.62	16.41	0.00	0.00	6.50	0.00	0.00
0.00	1.79	0.00	0.00	0.00	0.00	17.56	0.00	0.00	5.36	0.00	0.00
0.21	1.07	0.00	0.00	0.21	0.21	17.34	0.00	0.00	1.07	0.00	0.00
0.00	1.34	0.00	0.00	0.00	0.27	12.37	0.00	0.00	0.54	0.00	0.00
0.00	1.81	0.00	0.00	0.00	0.00	13.21	0.00	0.00	0.78	0.00	0.26
0.00	3.35	0.30	0.00	0.00	0.00	12.80	0.00	0.00	0.00	0.00	0.30
0.00	4.18	0.00	0.00	0.22	0.22	12.97	0.00	0.00	1.54	0.00	0.00
0.00	3.26	0.65	0.00	0.00	0.33	14.98	0.00	0.00	0.33	0.00	0.65
0.00	1.96	0.00	0.00	0.00	0.49	12.96	0.00	0.00	0.24	0.00	0.00
0.00	1.11	0.00	0.00	0.00	0.00	11.78	0.00	0.00	0.00	0.00	0.00
0.00	3.61	0.48	0.00	0.00	0.00	12.50	0.00	0.24	0.48	0.00	0.00
0.00	3.55	0.24	0.00	0.00	0.00	11.82	0.00	0.24	0.24	0.00	0.00
0.00	4.27	1.28	0.00	0.00	0.00	5.98	0.00	0.00	0.64	0.00	0.00
0.00	3.24	1.08	0.00	0.00	0.00	10.54	0.00	0.00	1.08	0.00	0.00
0.00	3.03	0.00	0.00	0.00	0.22	13.85	0.00	0.22	0.22	0.00	0.22
0.23	2.25	0.45	0.00	0.00	0.68	16.22	0.00	0.00	1.35	0.00	0.23
0.00	0.76	0.00	0.00	0.00	0.00	8.59	0.00	0.00	2.02	0.00	0.25
0.00	1.08	0.27	0.00	0.00	0.00	10.78	0.00	0.00	1.62	0.00	0.00
0.00	1.26	0.63	0.00	0.00	0.00	12.26	0.00	0.00	1.26	0.00	0.00
0.00	1.48	0.49	0.00	0.00	0.00	7.88	0.00	0.00	1.97	0.00	0.00

0.00	0.00	0.22	0.00	0.00	0.43	12.28	0.00	0.00	1.94	0.00	0.65
0.00	1.20	0.72	0.00	0.00	0.00	7.93	0.00	0.24	0.00	0.00	0.00
0.00	0.00	0.48	0.00	0.00	0.24	15.66	0.00	0.00	2.89	0.00	0.00
0.00	0.00	0.00	0.00	0.00	0.29	14.49	0.00	0.00	0.58	0.00	0.00
0.00	1.27	0.32	0.00	0.00	0.00	12.34	0.00	0.00	0.00	0.00	0.32
0.00	2.01	0.75	0.00	0.00	0.00	16.04	0.00	0.00	0.75	0.00	0.00
0.00	2.15	0.00	0.00	0.00	0.00	15.32	0.00	0.27	0.81	0.00	0.27
0.00	0.32	0.00	0.32	0.00	0.00	16.46	0.00	0.00	2.22	0.00	0.32
0.26	1.28	0.00	0.00	0.00	0.00	15.82	0.00	0.00	1.02	0.00	1.28
0.00	3.50	0.00	0.00	0.00	0.32	14.65	0.00	0.00	1.91	0.00	0.00
0.00	1.91	0.00	0.00	0.00	0.00	13.06	0.00	0.00	0.00	0.00	0.00
0.00	0.27	0.00	0.00	0.00	0.27	15.76	0.00	0.00	0.27	0.00	0.27
0.00	1.51	0.65	0.00	0.00	0.00	14.66	0.00	0.00	1.51	0.00	0.00
0.00	1.11	0.00	0.00	0.00	0.84	15.60	0.00	0.00	1.67	0.00	0.84
0.00	0.00	0.00	0.00	0.00	0.00	12.09	0.00	0.00	3.54	0.00	0.00
0.00	0.00	0.00	0.00	0.00	0.00	8.55	0.00	0.00	3.42	0.00	1.42
0.00	0.00	0.00	0.63	0.00	0.00	11.64	0.00	0.00	2.83	0.00	0.00
0.00	0.33	0.00	0.00	0.00	0.00	13.33	0.00	0.00	3.00	0.00	0.67
0.00	0.57	0.00	0.00	0.00	0.00	16.43	0.00	0.00	3.68	0.00	0.57
0.00	0.00	0.00	0.00	0.00	0.00	14.46	0.00	0.00	1.23	0.00	1.54
0.00	0.00	0.00	0.00	0.58	0.00	16.33	0.00	0.00	2.04	0.00	0.58
0.00	3.19	0.00	0.00	0.00	0.00	15.02	0.00	0.00	0.96	0.00	0.64
0.00	0.73	0.00	0.00	0.00	0.00	11.19	0.00	0.00	0.49	0.00	0.00
0.00	0.00	0.00	0.00	0.00	0.00	15.64	0.00	0.00	0.00	0.00	0.28
0.00	0.56	0.00	0.00	0.00	0.28	15.17	0.00	0.00	0.28	0.00	0.28
0.00	0.00	0.00	0.00	0.00	0.29	17.92	0.00	0.00	1.73	0.00	0.58
0.00	2.10	0.00	0.00	0.00	0.00	11.41	0.00	0.00	2.70	0.00	0.00
0.00	0.99	0.33	0.00	0.00	0.33	12.87	0.00	0.00	0.66	0.00	1.65
0.00	0.60	0.00	0.00	0.00	0.60	16.12	0.00	0.00	1.19	0.00	0.00
0.00	1.30	0.00	0.00	0.00	0.00	10.10	0.00	0.00	3.58	0.00	0.00
0.00	2.12	0.00	0.00	0.00	0.00	12.73	0.00	0.00	1.21	0.00	0.00
0.00	2.29	0.00	0.00	0.00	0.00	10.89	0.00	0.00	0.00	0.00	0.00
0.00	0.81	0.27	0.00	0.00	0.00	8.92	0.00	0.00	3.24	0.00	0.00
0.00	0.00	0.00	0.00	0.00	0.00	9.17	0.00	0.00	0.61	0.00	0.92
0.00	0.00	0.00	0.00	0.00	0.00	7.59	0.00	0.00	1.01	0.00	0.00
0.00	0.00	0.00	0.00	0.00	0.00	11.14	0.00	0.00	0.82	0.00	0.00

Dictyococcites spp. 10-14µm	*Dictyococcites bisectus >10µm*	*Dictyococcites aff. bisectus <10µm*	*Dictyococcites cf. filewiczii*	*Dictyococcites filewiczii*	*Dictyococcites hesslandii*	*Discoaster barbadiensis*	*Discoaster deflandrei*	*Discoaster distinctus*	*Discoaster cf. distinctus*	*Discoaster robustus*	*Discoaster saipanensis*
0.00	0.30	0.30	0.00	0.00	0.00	0.00	0.00	0.00	0.00	0.00	0.00
0.27	0.81	2.43	0.00	0.00	0.00	0.00	0.00	0.00	0.00	0.00	0.00
0.28	1.12	0.84	0.00	0.28	0.00	0.00	0.00	0.00	0.00	0.00	0.00
0.00	0.96	1.60	0.00	0.00	0.32	0.00	0.00	0.00	0.00	0.00	0.00
0.27	0.82	0.55	0.00	0.00	0.00	0.00	0.00	0.00	0.00	0.00	0.00
0.24	0.47	1.89	0.00	0.00	0.00	0.00	0.24	0.00	0.00	0.00	0.00
0.24	1.22	3.66	0.00	0.00	0.24	0.00	0.00	0.00	0.00	0.00	0.00
0.28	1.66	1.10	0.00	0.00	0.00	0.00	0.00	0.00	0.00	0.00	0.00
0.00	0.50	7.46	0.00	0.00	0.00	0.00	0.00	0.00	0.00	0.00	0.00
0.00	2.03	3.60	0.00	0.00	0.00	0.00	0.00	0.00	0.00	0.00	0.00
0.52	1.29	3.36	0.00	0.00	0.26	0.00	0.00	0.00	0.00	0.00	0.00
0.00	2.98	2.71	0.00	0.00	0.00	0.00	0.00	0.00	0.00	0.00	0.00
0.00	2.79	1.86	0.00	0.00	0.00	0.00	0.31	0.00	0.00	0.00	0.00
0.29	0.88	1.47	0.00	0.00	0.00	0.00	0.00	0.00	0.00	0.00	0.00
0.30	1.81	3.63	0.00	0.00	0.00	0.00	0.00	0.00	0.00	0.00	0.00
0.00	1.28	3.32	0.00	0.00	0.00	0.00	0.26	0.00	0.00	0.00	0.00
0.24	0.72	2.15	0.00	0.24	0.00	0.00	0.00	0.00	0.00	0.00	0.00
0.00	3.15	4.33	0.00	0.00	0.39	0.00	0.00	0.20	0.00	0.20	0.00
0.00	3.38	6.04	0.00	0.97	0.00	0.00	0.00	0.00	0.00	0.00	0.00
0.54	1.88	3.22	0.00	0.00	0.00	0.00	0.00	0.00	0.00	0.00	0.00
0.00	1.29	0.97	0.00	0.00	0.00	0.00	0.00	0.00	0.00	0.00	0.00
0.00	0.22	1.95	0.00	0.43	0.00	0.00	0.00	0.00	0.00	0.00	0.00
0.00	1.40	5.03	0.00	0.00	0.00	0.00	0.00	0.00	0.00	0.00	0.00
0.00	1.39	3.32	0.00	0.00	0.00	0.00	0.00	0.00	0.00	0.00	0.00
0.00	0.97	4.22	0.00	0.00	0.00	0.00	0.00	0.00	0.00	0.00	0.00
0.00	1.25	1.75	0.00	0.00	0.00	0.00	0.00	0.00	0.00	0.00	0.25
0.00	5.01	8.02	0.00	0.00	0.00	0.00	0.25	0.00	0.00	0.00	0.00
0.00	3.96	5.79	0.00	0.00	0.30	0.00	0.00	0.00	0.00	0.00	0.00
0.00	2.08	4.63	0.00	0.00	0.00	0.00	0.00	0.23	0.23	0.00	0.00
0.00	1.39	7.52	0.00	0.00	0.00	0.00	0.00	0.00	0.28	0.00	0.00
0.00	0.47	3.77	0.00	0.00	0.00	0.00	0.00	0.00	0.00	0.00	0.00
0.00	1.78	3.85	0.00	0.00	0.00	0.00	0.00	0.89	0.00	0.00	0.00
0.00	0.56	3.36	0.00	0.00	0.00	0.00	0.00	0.00	0.00	0.00	0.00
0.00	0.50	2.77	0.00	0.00	0.25	0.00	0.50	0.00	0.00	0.00	0.00
0.00	0.86	4.89	0.00	0.00	0.00	0.00	0.00	0.00	0.00	0.00	0.00
0.00	1.34	2.68	0.00	0.00	0.00	0.00	0.00	0.00	0.00	0.00	0.00
0.00	1.24	3.41	0.00	0.00	0.62	0.00	0.31	0.00	0.00	0.00	0.00
0.00	1.38	3.90	0.00	0.00	0.00	0.00	0.00	0.00	0.00	0.00	0.00

0.00	1.50	4.49	0.00	0.00	0.00	0.00	0.00	0.00	0.00	0.00	0.00
0.00	0.69	3.00	0.00	0.00	0.00	0.00	0.00	0.00	0.00	0.00	0.00
0.00	2.09	2.55	0.00	0.00	0.00	0.00	0.00	0.00	0.00	0.00	0.00
0.00	1.26	3.53	0.00	0.00	0.00	0.00	0.00	0.00	0.00	0.00	0.00
0.00	1.59	5.04	0.00	0.00	0.00	0.00	0.00	0.27	0.00	0.00	0.00
0.00	1.45	2.61	0.00	0.00	0.00	0.00	0.00	0.00	0.00	0.00	0.00
0.00	0.71	1.67	0.00	0.24	0.00	0.00	0.00	0.00	0.00	0.00	0.00
0.00	2.48	6.19	0.25	0.74	0.00	0.00	0.00	0.00	0.00	0.00	0.00
0.00	1.07	4.53	0.00	0.00	0.00	0.00	0.00	0.00	0.00	0.00	0.00
0.00	3.13	5.74	0.00	0.52	0.00	0.00	0.00	0.00	0.00	0.00	0.00
0.19	1.53	6.11	0.19	0.00	0.38	0.00	0.00	0.00	0.00	0.00	0.00
0.24	3.07	5.44	0.00	0.24	0.24	0.00	0.00	0.00	0.00	0.00	0.00
0.00	1.09	4.08	0.00	0.27	0.00	0.00	0.00	0.00	0.00	0.00	0.00
0.39	1.75	2.14	0.00	0.00	0.00	0.00	0.00	0.00	0.00	0.00	0.00
0.60	1.19	3.28	0.00	0.00	0.00	0.00	0.00	0.00	0.00	0.00	0.00
1.18	0.98	2.35	0.00	0.20	0.00	0.00	0.00	0.00	0.00	0.00	0.00
0.23	0.92	3.67	0.00	0.00	0.00	0.00	0.00	0.00	0.00	0.00	0.00
0.00	0.81	3.64	0.20	0.00	0.20	0.00	0.00	0.00	0.00	0.00	0.00
0.00	2.61	4.51	0.24	0.24	0.48	0.00	0.00	0.00	0.00	0.00	0.00
0.63	2.22	6.65	0.00	0.32	0.00	0.00	0.00	0.00	0.00	0.00	0.00
0.00	0.67	2.00	0.00	0.00	0.33	0.00	0.00	0.00	0.00	0.00	0.00
0.00	3.28	2.69	0.00	0.00	0.60	0.00	0.00	0.00	0.00	0.00	0.00
0.00	1.91	1.37	0.00	0.00	0.00	0.00	0.00	0.27	0.00	0.00	0.00
0.00	2.51	3.76	0.31	0.00	0.00	0.00	0.00	0.00	0.00	0.00	0.00
0.00	0.57	0.86	0.00	0.00	0.29	0.00	0.00	0.29	0.00	0.00	0.00
0.00	2.16	8.33	0.00	0.31	0.00	0.00	0.00	0.31	0.00	0.00	0.00
0.00	2.88	10.26	0.32	0.00	0.00	0.00	0.00	0.00	0.00	0.00	0.00
0.00	1.31	6.53	0.00	0.26	0.26	0.00	0.00	0.00	0.00	0.00	0.00
0.00	1.40	8.38	0.00	0.28	0.56	0.00	0.00	0.00	0.00	0.00	0.00
0.00	0.62	3.11	0.00	0.31	0.00	0.00	0.00	0.00	0.00	0.00	0.00
0.00	0.93	5.88	0.00	0.31	0.00	0.00	0.00	0.00	0.00	0.00	0.00
0.00	1.49	5.65	0.00	0.89	0.00	0.00	0.00	0.00	0.00	0.00	0.00
0.00	1.71	5.35	0.00	0.21	0.00	0.00	0.00	0.00	0.00	0.00	0.00
0.00	4.30	5.91	0.00	0.00	0.54	0.00	0.00	0.00	0.00	0.00	0.00
0.00	1.81	5.70	0.26	0.00	0.52	0.00	0.00	0.00	0.00	0.00	0.00
0.00	1.22	7.01	0.00	0.61	0.00	0.00	0.00	0.00	0.00	0.00	0.00
0.00	3.08	4.62	0.00	0.00	0.44	0.00	0.00	0.00	0.00	0.00	0.00
0.00	1.63	3.26	0.00	0.00	1.30	0.00	0.00	0.00	0.00	0.00	0.00
0.00	3.42	7.58	0.49	0.24	0.49	0.00	0.00	0.00	0.00	0.00	0.00
0.00	1.56	4.67	0.00	0.22	0.89	0.00	0.00	0.00	0.00	0.00	0.00
0.00	1.20	4.33	0.00	0.48	0.00	0.00	0.00	0.00	0.00	0.00	0.00
0.00	2.36	5.20	0.00	0.00	0.00	0.00	0.00	0.00	0.00	0.00	0.00
0.00	0.64	3.85	0.00	0.21	0.85	0.00	0.00	0.00	0.00	0.00	0.00
0.00	1.62	5.41	0.00	0.00	0.54	0.00	0.00	0.00	0.00	0.00	0.00
0.22	2.60	3.03	0.00	0.22	0.22	0.00	0.00	0.00	0.00	0.00	0.00
0.00	3.15	4.73	0.23	0.00	0.45	0.00	0.00	0.00	0.00	0.00	0.00
0.00	4.04	5.56	0.00	0.00	0.51	0.00	0.00	0.00	0.00	0.00	0.00
0.00	3.77	8.36	0.00	0.00	1.08	0.00	0.00	0.00	0.00	0.00	0.00
0.00	1.89	7.86	0.00	0.31	0.63	0.00	0.00	0.00	0.00	0.00	0.00
0.25	2.71	5.17	0.00	0.00	0.49	0.00	0.00	0.00	0.00	0.00	0.00

0.00	1.08	7.54	0.00	0.22	0.43	0.00	0.22	0.00	0.00	0.00	0.00
0.00	2.40	4.81	0.00	0.00	0.72	0.00	0.00	0.00	0.00	0.00	0.00
0.00	3.61	5.06	0.00	0.00	0.48	0.00	0.00	0.00	0.00	0.00	0.48
0.00	4.35	7.83	0.00	0.58	0.58	0.29	0.00	0.00	0.00	0.00	2.32
0.00	1.90	6.96	0.00	0.32	0.32	0.00	0.00	0.00	0.00	0.00	0.63
0.00	2.26	5.26	0.00	0.25	0.50	0.00	0.00	0.00	0.00	0.00	4.01
0.00	3.76	5.65	0.00	0.54	0.81	0.00	0.00	0.00	0.00	0.00	1.61
0.00	4.11	8.54	0.95	0.95	1.90	0.00	0.00	0.00	0.00	0.00	0.00
0.00	2.81	6.63	0.00	2.04	1.53	0.00	0.00	0.00	0.00	0.00	1.02
0.00	4.14	4.46	0.00	1.59	0.96	0.00	0.00	0.00	0.00	0.00	0.96
0.00	1.27	4.46	0.00	1.27	0.64	0.00	0.00	0.00	0.00	0.00	0.64
0.00	1.90	4.08	0.54	0.27	1.63	0.00	0.00	0.00	0.00	0.00	1.09
0.00	2.16	3.66	0.00	1.72	2.59	0.00	0.00	0.00	0.00	0.00	1.08
0.00	1.39	4.18	0.00	0.84	0.28	0.00	0.00	0.00	0.00	0.00	0.28
0.00	1.77	5.01	0.00	1.47	1.77	0.00	0.00	0.00	0.00	0.00	0.88
0.00	1.99	3.70	0.28	0.85	1.71	0.00	0.00	0.00	0.00	0.00	0.28
0.31	0.63	3.14	0.00	0.94	1.26	0.00	0.00	0.00	0.00	0.00	0.63
0.00	1.00	3.33	0.00	0.00	1.33	0.00	0.00	0.00	0.00	0.00	0.33
0.00	1.13	3.12	0.28	0.28	2.55	0.00	0.00	0.00	0.00	0.00	2.27
0.00	2.77	4.62	0.00	1.23	1.85	0.00	0.00	0.00	0.00	0.00	1.54
0.00	1.46	1.75	0.00	0.29	2.33	0.29	0.00	0.00	0.00	0.00	1.17
0.00	0.32	2.24	0.32	0.64	1.28	0.00	0.00	0.00	0.00	0.00	0.00
0.00	1.22	2.92	0.00	0.73	1.95	0.97	0.00	0.00	0.00	0.00	0.97
0.00	2.23	3.07	0.00	0.28	3.91	0.00	0.00	0.00	0.00	0.00	0.84
0.00	1.97	0.84	0.28	0.00	3.65	0.28	0.00	0.00	0.00	0.00	0.56
0.00	1.73	2.02	0.00	1.16	3.47	0.29	0.00	0.00	0.00	0.00	0.58
0.00	2.70	5.11	0.00	0.90	1.80	0.00	0.00	0.00	0.00	0.00	0.60
0.00	1.32	2.31	0.00	0.33	2.97	0.00	0.00	0.00	0.00	0.00	1.98
0.00	2.09	4.18	0.00	0.30	1.19	0.00	0.00	0.00	0.00	0.00	0.30
0.00	0.65	6.19	0.00	0.00	2.93	0.00	0.00	0.00	0.00	0.00	0.33
0.00	2.73	7.27	0.00	0.30	6.97	0.00	0.00	0.00	0.00	0.00	0.91
0.00	2.29	1.72	0.00	0.57	2.87	0.00	0.00	0.00	0.00	0.00	0.86
0.00	1.08	2.70	0.00	0.00	2.70	0.00	0.00	0.00	0.00	0.00	0.27
0.00	2.14	5.20	0.61	0.61	2.45	0.00	0.00	0.00	0.00	0.00	0.31
0.00	1.01	0.76	0.00	0.00	2.53	0.00	0.00	0.00	0.00	0.00	0.00
0.00	2.17	2.99	0.00	0.00	1.63	0.00	0.00	0.00	0.00	0.00	0.82

Discoaster saipanensis <7µm	*Discoaster tanii*	*Discoaster tanii gr.*	*Discoaster tani nodifer*	*Discoaster spp.*	*Ericsonia formosa*	*Helicosphaera bipuncta*	*Helicosphaera compacta*	*Helicosphaera euphratis*	*Helicosphaera cf. huangii*	*Helicosphaera recta*	*Helicosphaera cf. recta*
0.00	0.00	0.00	0.00	0.00	0.00	0.00	0.00	0.00	0.00	0.30	0.00
0.00	0.00	0.00	0.00	0.00	0.27	0.00	0.00	0.00	0.00	0.00	0.00
0.00	0.28	0.00	0.00	0.00	0.00	0.00	0.00	0.00	0.00	0.00	0.00
0.00	0.00	0.00	0.00	0.00	0.00	0.00	0.32	0.00	0.00	0.00	0.00
0.00	0.00	0.00	0.00	0.00	0.00	0.00	0.00	0.00	0.27	0.00	0.00
0.00	0.00	0.00	0.00	0.00	0.00	0.00	0.00	0.00	0.00	0.00	0.00
0.00	0.00	0.00	0.00	0.00	0.00	0.00	0.00	0.00	0.00	0.00	0.00
0.00	0.00	0.00	0.00	0.00	0.00	0.00	0.00	0.00	0.00	0.00	0.00
0.00	0.00	0.00	0.00	0.00	0.00	0.00	0.00	0.00	0.00	0.00	0.00
0.00	0.00	0.00	0.00	0.23	0.00	0.00	0.00	0.00	0.00	0.00	0.00
0.00	0.00	0.00	0.00	0.00	0.00	0.00	0.00	0.00	0.00	0.00	0.00
0.00	0.00	0.00	0.00	0.27	0.27	0.00	0.00	0.00	0.00	0.00	0.00
0.00	0.00	0.00	0.00	0.31	0.00	0.00	0.00	0.00	0.00	0.00	0.00
0.00	0.00	0.00	0.00	0.00	0.00	0.00	0.00	0.00	0.00	0.00	0.00
0.00	0.30	0.00	0.00	0.00	0.30	0.00	0.00	0.00	0.00	0.00	0.00
0.00	0.51	0.00	0.00	0.00	0.00	0.00	0.00	0.00	0.00	0.00	0.00
0.00	0.00	0.00	0.00	0.24	0.00	0.00	0.00	0.00	0.00	0.72	0.00
0.00	0.00	0.00	0.00	0.00	0.20	0.00	0.00	0.00	0.00	0.00	0.00
0.00	0.00	0.00	0.00	0.00	0.00	0.00	0.00	0.00	0.00	0.00	0.00
0.00	0.00	0.00	0.27	0.00	0.00	0.00	0.00	0.00	0.00	0.00	0.00
0.00	0.00	0.00	0.00	0.00	0.00	0.00	0.00	0.00	0.00	0.00	0.32
0.00	0.00	0.00	0.00	0.00	0.00	0.00	0.00	0.00	0.00	0.00	0.00
0.00	0.00	0.00	0.00	0.00	0.00	0.00	0.00	0.00	0.00	0.00	0.00
0.00	0.00	0.00	0.00	0.00	0.28	0.00	0.00	0.00	0.00	0.00	0.00
0.00	0.00	0.00	0.00	0.00	0.00	0.00	0.00	0.32	0.00	0.00	0.00
0.00	0.25	0.00	0.00	0.00	0.00	0.00	0.00	0.00	0.00	0.00	0.00
0.00	0.00	0.00	0.00	0.00	0.00	0.00	0.00	0.00	0.00	0.00	0.00
0.00	0.00	0.00	0.00	0.00	0.00	0.00	0.00	0.00	0.00	0.00	0.00
0.00	0.00	0.00	0.00	0.00	0.00	0.00	0.00	0.00	0.00	0.00	0.00
0.00	0.00	0.00	0.00	0.00	0.00	0.00	0.00	0.00	0.00	0.00	0.00
0.00	0.00	0.00	0.00	0.00	0.00	0.00	0.00	0.00	0.00	0.00	0.00
0.00	0.30	0.00	0.00	0.00	0.00	0.00	0.00	0.00	0.00	0.00	0.00
0.00	0.56	0.00	0.00	0.00	0.00	0.00	0.00	0.00	0.00	0.00	0.00
0.00	0.50	0.00	0.00	0.00	0.00	0.00	0.00	0.00	0.00	0.00	0.00
0.00	0.57	0.00	0.00	0.29	0.00	0.00	0.00	0.00	0.00	0.00	0.00
0.00	0.67	0.00	0.00	0.22	0.00	0.00	0.00	0.00	0.00	0.00	0.00
0.00	0.31	0.00	0.00	0.00	0.00	0.00	0.00	0.00	0.00	0.00	0.00
0.00	0.00	0.00	0.00	0.00	0.00	0.00	0.00	0.00	0.00	0.00	0.00

0.00	0.00	0.00	0.00	0.00	0.00	0.00	0.00	0.00	0.00	0.00	0.00
0.00	0.00	0.00	0.00	0.00	0.00	0.00	0.00	0.00	0.00	0.00	0.00
0.00	0.00	0.00	0.00	0.00	0.00	0.00	0.00	0.00	0.00	0.00	0.00
0.00	0.00	0.00	0.00	0.00	0.00	0.00	0.00	0.00	0.00	0.00	0.00
0.00	0.00	0.00	0.00	0.00	0.00	0.00	0.00	0.00	0.00	0.00	0.00
0.00	0.00	0.00	0.00	0.00	0.00	0.00	0.00	0.00	0.00	0.00	0.00
0.00	0.00	0.00	0.00	0.00	0.00	0.00	0.24	0.00	0.00	0.00	0.00
0.00	0.00	0.00	0.00	0.00	0.00	0.00	0.00	0.00	0.00	0.00	0.00
0.00	0.00	0.00	0.00	0.00	0.00	0.00	0.00	0.00	0.00	0.00	0.00
0.00	0.52	0.00	0.00	0.00	0.00	0.00	0.00	0.00	0.00	0.00	0.00
0.00	0.00	0.00	0.00	0.00	0.00	0.00	0.00	0.00	0.00	0.00	0.00
0.00	0.24	0.00	0.00	0.00	0.00	0.00	0.47	0.00	0.00	0.00	0.00
0.00	0.00	0.00	0.00	0.00	0.00	0.00	0.00	0.00	0.00	0.00	0.00
0.00	0.00	0.00	0.00	0.00	0.00	0.00	0.00	0.00	0.00	0.00	0.00
0.00	0.00	0.00	0.00	0.00	0.30	0.00	0.00	0.00	0.00	0.00	0.00
0.00	0.00	0.00	0.00	0.00	0.00	0.00	0.00	0.00	0.00	0.00	0.00
0.00	0.00	0.00	0.00	0.23	0.46	0.00	0.00	0.00	0.00	0.00	0.00
0.00	0.00	0.00	0.00	0.00	0.00	0.00	0.20	0.00	0.00	0.00	0.00
0.00	0.24	0.00	0.00	0.00	0.00	0.00	0.00	0.00	0.00	0.00	0.00
0.00	0.00	0.00	0.00	0.00	0.00	0.00	0.00	0.00	0.00	0.00	0.00
0.00	0.00	0.00	0.00	0.00	0.00	0.00	0.00	0.00	0.00	0.00	0.00
0.00	0.00	0.00	0.00	0.30	0.00	0.00	0.30	0.00	0.00	0.00	0.00
0.00	0.00	0.00	0.00	0.00	0.82	0.00	0.00	0.00	0.00	0.00	0.00
0.00	0.00	0.00	0.00	0.00	0.00	0.00	0.00	0.00	0.00	0.00	0.00
0.00	0.00	0.00	0.00	0.00	0.00	0.00	0.29	0.00	0.00	0.00	0.00
0.00	0.00	0.00	0.00	0.00	0.31	0.00	0.31	0.00	0.00	0.00	0.00
0.00	0.00	0.00	0.00	0.00	0.64	0.00	0.00	0.00	0.00	0.00	0.00
0.00	0.00	0.00	0.00	0.00	0.26	0.00	0.00	0.00	0.00	0.00	0.00
0.00	0.00	0.00	0.00	0.00	0.28	0.00	0.00	0.00	0.00	0.00	0.00
0.00	0.00	0.00	0.00	0.00	1.24	0.00	0.00	0.00	0.00	0.00	0.00
0.00	0.00	0.00	0.31	0.00	2.17	0.00	0.00	0.00	0.00	0.00	0.00
0.00	0.00	0.00	0.00	0.00	1.49	0.00	0.00	0.00	0.00	0.00	0.00
0.00	0.00	0.00	0.00	0.00	1.07	0.00	0.43	0.00	0.00	0.00	0.00
0.00	0.00	0.00	0.00	0.00	2.42	0.00	0.00	0.00	0.00	0.00	0.00
0.00	0.00	0.00	0.00	0.00	1.04	0.00	0.00	0.00	0.00	0.00	0.00
0.00	0.61	0.00	0.00	0.00	0.30	0.00	0.00	0.00	0.00	0.00	0.00
0.00	0.00	0.00	0.00	0.00	0.88	0.00	0.00	0.00	0.00	0.00	0.00
0.00	0.33	0.00	0.00	0.00	0.33	0.00	0.00	0.00	0.00	0.00	0.00
0.00	0.00	0.00	0.00	0.00	1.22	0.00	0.00	0.00	0.00	0.00	0.00
0.00	0.22	0.00	0.00	0.00	1.56	0.00	0.00	0.00	0.00	0.00	0.00
0.00	0.48	0.00	0.00	0.00	1.68	0.00	0.00	0.00	0.00	0.00	0.00
0.00	0.24	0.00	0.00	0.00	1.89	0.00	0.00	0.00	0.00	0.00	0.00
0.00	0.00	0.00	0.00	0.00	0.21	0.00	0.00	0.00	0.00	0.00	0.00
0.00	0.00	0.00	0.00	0.00	0.54	0.00	0.00	0.00	0.00	0.00	0.00
0.00	0.00	0.00	0.00	0.00	2.16	0.00	0.00	0.00	0.00	0.00	0.00
0.00	0.23	0.00	0.00	0.00	0.90	0.00	0.00	0.00	0.00	0.00	0.00
0.00	0.51	0.00	0.00	0.25	2.02	0.00	0.00	0.00	0.00	0.00	0.00
0.00	0.00	0.00	0.00	0.00	1.08	0.00	0.27	0.00	0.00	0.00	0.00
0.00	0.00	0.00	0.00	0.00	1.26	0.00	0.00	0.00	0.00	0.00	0.00
0.00	0.00	0.00	0.00	0.25	1.23	0.00	0.25	0.00	0.00	0.00	0.00

0.00	0.22	0.00	0.00	0.00	1.29	0.00	0.00	0.00	0.00	0.00	0.00
0.00	0.00	0.00	0.00	0.00	0.00	0.00	0.00	0.00	0.00	0.00	0.00
0.24	0.24	0.48	0.24	0.00	1.93	0.00	0.00	0.00	0.00	0.00	0.00
0.29	0.87	0.58	0.00	1.16	2.32	0.00	0.00	0.00	0.00	0.00	0.00
0.32	0.32	0.00	0.32	0.00	1.58	0.00	0.00	0.00	0.00	0.00	0.00
0.00	0.50	0.00	0.00	0.00	0.50	0.00	0.00	0.00	0.00	0.00	0.00
0.27	0.00	0.00	0.00	0.00	3.76	0.00	0.00	0.00	0.00	0.00	0.00
0.00	0.00	0.00	0.00	0.00	2.85	0.00	0.00	0.00	0.00	0.00	0.00
0.26	0.51	0.00	0.00	0.00	2.04	0.00	0.00	0.00	0.00	0.00	0.00
0.00	0.00	0.00	0.00	0.32	1.59	0.00	0.32	0.00	0.00	0.00	0.00
0.00	0.00	0.32	0.00	0.00	2.23	0.00	0.00	0.00	0.00	0.00	0.00
0.00	0.00	0.00	0.00	0.00	0.54	0.00	0.54	0.00	0.00	0.00	0.00
0.00	0.00	0.00	0.00	0.00	1.08	0.00	0.00	0.00	0.00	0.00	0.00
0.28	0.00	0.00	0.00	0.00	0.84	0.00	0.00	0.00	0.00	0.00	0.00
0.29	0.00	0.00	0.00	0.29	2.06	0.00	0.29	0.00	0.00	0.00	0.00
1.14	0.28	0.00	0.00	0.00	1.42	0.00	0.00	0.00	0.00	0.00	0.00
0.31	0.94	0.00	0.00	0.31	0.00	0.00	0.31	0.00	0.00	0.00	0.00
0.00	0.00	0.00	0.00	0.00	2.33	0.00	0.33	0.00	0.00	0.00	0.00
0.00	0.00	0.00	0.00	0.00	1.98	0.00	1.13	0.00	0.00	0.00	0.00
0.00	0.00	0.00	0.00	0.00	1.54	0.00	0.31	0.00	0.00	0.00	0.00
0.00	0.29	0.00	0.00	0.00	0.87	0.00	0.00	0.00	0.00	0.00	0.00
0.00	0.00	0.00	0.00	0.00	0.32	0.00	0.00	0.00	0.00	0.00	0.00
0.00	0.00	0.00	0.00	0.00	1.46	0.00	0.00	0.00	0.00	0.00	0.00
0.00	0.00	0.00	0.00	0.00	1.12	0.00	0.00	0.00	0.00	0.00	0.00
0.00	0.00	0.00	0.00	0.00	4.78	0.00	0.00	0.00	0.00	0.00	0.00
0.00	0.00	0.00	0.00	0.00	1.45	0.00	0.00	0.00	0.00	0.00	0.00
0.00	0.00	0.00	0.00	0.00	3.00	0.00	0.00	0.00	0.00	0.00	0.00
0.00	0.00	0.00	0.00	0.00	1.32	0.00	0.00	0.00	0.00	0.00	0.00
0.00	0.60	0.00	0.60	0.00	2.69	0.00	0.00	0.00	0.00	0.00	0.00
0.00	0.00	0.00	0.00	0.00	0.00	0.00	0.00	0.00	0.00	0.00	0.00
0.00	0.30	0.00	0.00	0.30	0.91	0.00	0.00	0.00	0.00	0.00	0.00
0.00	0.29	0.00	0.00	0.29	0.29	0.00	0.00	0.00	0.00	0.00	0.00
0.00	0.27	0.00	0.00	0.00	1.89	0.00	0.00	0.00	0.00	0.00	0.00
0.00	0.31	0.00	0.00	0.00	0.61	0.00	0.00	0.00	0.00	0.00	0.00
0.00	0.00	0.00	0.00	0.00	0.76	0.00	0.00	0.00	0.00	0.00	0.00
0.00	0.27	0.00	0.00	0.00	1.09	0.00	0.00	0.00	0.00	0.00	0.00

Helicosphaera cf. wilcoxonii	*Helicosphaera wilcoxonii*	*Helicosphaera cf. leesiae*	*Helicosphaera lophota*	*Helicosphaera spp.*	*Isthmolithus recurvus*	*Lanternithus cf. minutus*	*Lanternithus minutus*	*Lanternithus spp.*	*Markalius apertus*	*Markalius inversus*	*Pontosphaera cf. pulchripora*
0.00	0.00	0.00	0.00	0.00	0.00	0.00	0.00	0.00	0.00	0.00	0.00
0.00	0.00	0.00	0.00	0.00	0.00	0.00	0.00	0.00	0.00	0.00	0.00
0.00	0.00	0.00	0.00	0.00	0.00	0.00	0.00	0.00	0.00	0.00	0.00
0.00	0.00	0.00	0.00	0.00	0.00	0.00	0.00	0.00	0.00	0.00	0.00
0.00	0.00	0.00	0.00	0.00	0.00	0.00	0.00	0.00	0.00	0.00	0.00
0.00	0.00	0.00	0.00	0.00	0.00	0.00	0.00	0.00	0.00	0.00	0.00
0.00	0.00	0.00	0.00	0.00	0.00	0.00	0.00	0.00	0.00	0.00	0.00
0.28	0.00	0.00	0.00	0.00	0.00	0.00	0.55	0.00	0.00	0.00	0.00
0.00	0.00	0.00	0.00	0.00	0.00	0.00	0.25	0.00	0.00	0.00	0.00
0.00	0.00	0.00	0.00	0.00	0.00	0.00	0.00	0.00	0.00	0.00	0.00
0.00	0.00	0.00	0.00	0.00	0.00	0.00	0.00	0.00	0.00	0.00	0.00
0.00	0.00	0.00	0.00	0.00	0.00	0.00	0.00	0.00	0.00	0.00	0.00
0.00	0.00	0.00	0.00	0.00	0.00	0.00	0.00	0.00	0.00	0.00	0.00
0.00	0.00	0.00	0.00	0.00	0.00	0.00	0.00	0.00	0.00	0.29	0.00
0.00	0.00	0.00	0.00	0.00	0.00	0.00	0.00	0.00	0.00	0.30	0.00
0.00	0.00	0.00	0.00	0.00	0.00	0.00	0.00	0.00	0.00	0.00	0.00
0.48	0.00	0.00	0.00	0.00	0.00	0.00	0.00	0.00	0.00	0.00	0.00
0.00	0.00	0.00	0.00	0.00	0.20	0.00	0.00	0.00	0.00	0.00	0.00
0.00	0.00	0.00	0.24	0.00	0.00	0.00	0.00	0.00	0.00	0.00	0.00
0.00	0.00	0.00	0.00	0.00	0.00	0.00	0.00	0.00	0.00	0.00	0.00
0.00	0.00	0.32	0.00	0.00	0.00	0.00	0.00	0.00	0.00	0.00	0.00
0.00	0.00	0.00	0.00	0.00	0.00	0.00	0.00	0.00	0.00	0.00	0.00
0.00	0.00	0.00	0.00	0.00	0.00	0.00	0.00	0.00	0.00	0.00	0.00
0.00	0.00	0.00	0.00	0.00	0.28	0.00	0.00	0.00	0.00	0.00	0.00
0.00	0.00	0.00	0.00	0.32	0.00	0.00	0.32	0.00	0.00	0.00	0.00
0.00	0.00	0.00	0.00	0.00	0.00	0.00	0.00	0.00	0.00	0.00	0.00
0.00	0.00	0.00	0.00	0.00	0.00	0.00	0.00	0.00	0.00	0.00	0.00
0.00	0.00	0.00	0.00	0.00	0.00	0.00	0.00	0.00	0.00	0.00	0.00
0.00	0.00	0.00	0.00	0.00	0.00	0.00	0.00	0.00	0.00	0.00	0.00
0.00	0.00	0.00	0.00	0.00	0.00	0.00	0.00	0.00	0.00	0.00	0.00
0.00	0.00	0.00	0.00	0.00	0.00	0.00	0.24	0.00	0.00	0.00	0.00
0.00	0.00	0.00	0.00	0.00	0.00	0.00	0.00	0.00	0.00	0.00	0.00
0.00	0.00	0.00	0.00	0.00	0.00	0.00	0.00	0.00	0.00	0.00	0.00
0.00	0.00	0.00	0.00	0.00	0.00	0.00	0.00	0.00	0.00	0.00	0.00
0.29	0.00	0.00	0.00	0.00	0.00	1.15	0.00	0.00	0.00	0.00	0.00
0.22	0.22	0.00	0.00	0.00	0.22	0.00	0.89	0.00	0.00	0.00	0.00
0.62	0.00	0.00	0.00	0.00	0.31	0.00	0.00	0.00	0.00	0.00	0.00
0.23	0.00	0.00	0.00	0.00	0.00	0.00	0.69	0.23	0.00	0.23	0.00

0.30	0.00	0.00	0.00	0.00	0.00	0.00	0.60	0.00	0.00	0.00	0.00
0.00	0.00	0.00	0.00	0.00	0.23	0.00	0.23	0.00	0.00	0.00	0.00
0.00	0.00	0.00	0.00	0.00	0.00	0.00	0.46	0.00	0.00	0.00	0.00
0.00	0.00	0.00	0.00	0.00	0.00	0.00	2.02	0.00	0.00	0.00	0.00
0.00	0.00	0.00	0.00	0.00	0.00	0.00	0.27	0.00	0.00	0.00	0.00
0.00	0.00	0.00	0.00	0.00	0.29	0.00	0.87	0.00	0.00	0.00	0.00
0.00	0.00	0.00	0.00	0.00	0.24	0.00	1.43	0.00	0.00	0.00	0.00
0.00	0.00	0.00	0.00	0.00	0.25	0.00	0.74	0.00	0.00	0.00	0.00
0.00	0.00	0.00	0.00	0.00	0.27	0.00	0.53	0.00	0.00	0.00	0.00
0.00	0.00	0.00	0.00	0.00	0.52	0.00	0.26	0.00	0.00	0.00	0.00
0.00	0.00	0.00	0.00	0.00	0.38	0.00	0.57	0.00	0.00	0.00	0.00
0.00	0.00	0.00	0.00	0.00	0.24	0.00	0.95	0.00	0.00	0.00	0.00
0.00	0.00	0.00	0.00	0.00	0.00	0.00	1.90	0.00	0.00	0.00	0.00
0.00	0.00	0.00	0.00	0.00	0.00	0.00	2.92	0.39	0.00	0.00	0.00
0.00	0.00	0.00	0.00	0.00	0.00	0.00	1.79	1.19	0.00	0.00	0.00
0.00	0.00	0.00	0.00	0.00	0.00	0.00	4.31	0.98	0.00	0.00	0.00
0.00	0.00	0.00	0.00	0.00	0.92	0.00	0.00	0.00	0.00	0.00	0.00
0.00	0.00	0.00	0.00	0.00	0.81	0.00	2.63	0.00	0.00	0.00	0.20
0.00	0.00	0.00	0.00	0.00	0.71	0.00	0.00	0.48	0.00	0.24	0.00
0.00	0.00	0.00	0.00	0.00	0.63	0.00	0.32	0.00	0.00	0.00	0.00
0.00	0.00	0.00	0.00	0.00	0.33	0.00	0.00	0.00	0.00	0.00	0.00
0.00	0.00	0.00	0.00	0.00	2.09	0.00	0.00	0.00	0.00	0.00	0.00
0.00	0.00	0.00	0.00	0.00	1.91	0.00	0.00	0.27	0.00	0.00	0.27
0.00	0.00	0.00	0.00	0.00	1.88	0.00	0.00	0.00	0.00	0.00	0.31
0.00	0.00	0.00	0.00	0.00	1.72	0.29	0.00	0.00	0.00	0.00	0.00
0.00	0.00	0.00	0.00	0.00	0.31	0.00	0.00	0.00	0.00	0.00	0.31
0.00	0.00	0.00	0.00	0.00	0.00	0.00	0.00	0.00	0.00	0.00	0.32
0.00	0.00	0.00	0.00	0.00	1.57	0.00	0.00	0.00	0.00	0.00	0.00
0.00	0.00	0.00	0.00	0.00	1.40	0.00	0.00	0.00	0.00	0.00	0.00
0.00	0.00	0.00	0.00	0.00	0.93	0.00	0.00	0.00	0.00	0.00	0.00
0.00	0.00	0.00	0.00	0.00	0.93	0.00	0.00	0.00	0.00	0.00	0.00
0.00	0.00	0.00	0.00	0.00	1.19	0.00	0.00	0.00	0.30	0.00	0.00
0.00	0.00	0.00	0.00	0.00	0.21	0.00	0.00	0.00	0.00	0.00	0.43
0.00	0.00	0.00	0.00	0.00	0.00	0.00	0.00	0.00	0.00	0.00	0.27
0.00	0.00	0.00	0.00	0.00	0.78	0.00	0.00	0.00	0.00	0.00	0.00
0.00	0.00	0.00	0.00	0.00	0.61	0.00	0.00	0.00	0.00	0.00	0.00
0.00	0.00	0.00	0.00	0.00	1.32	0.00	0.00	0.00	0.00	0.22	0.44
0.00	0.00	0.00	0.00	0.00	0.00	0.00	0.00	0.00	0.00	0.00	0.00
0.24	0.00	0.00	0.00	0.00	0.73	0.00	0.00	0.00	0.00	0.00	0.00
0.00	0.00	0.00	0.00	0.00	0.44	0.00	0.00	0.00	0.00	0.00	0.22
0.00	0.00	0.00	0.00	0.00	0.96	0.00	0.00	0.00	0.00	0.00	0.00
0.00	0.00	0.00	0.00	0.00	0.95	0.00	0.00	0.00	0.00	0.00	0.00
0.21	0.00	0.00	0.00	0.00	0.43	0.00	0.00	0.00	0.00	0.00	0.00
0.00	0.00	0.00	0.00	0.00	1.35	0.00	0.00	0.00	0.27	0.00	0.00
0.00	0.00	0.00	0.00	0.00	0.43	0.00	0.00	0.00	0.22	0.00	0.00
0.23	0.00	0.00	0.00	0.00	0.90	0.00	0.00	0.00	0.00	0.23	0.00
0.00	0.00	0.00	0.00	0.00	0.51	0.00	0.00	0.00	0.00	0.00	0.00
0.00	0.00	0.00	0.00	0.00	0.54	0.00	0.00	0.27	0.00	0.00	0.00
0.00	0.00	0.00	0.00	0.00	0.63	0.00	0.00	0.00	0.00	0.00	0.00
0.49	0.00	0.00	0.00	0.00	1.48	0.00	0.00	0.00	0.00	0.00	0.00

0.00	0.00	0.00	0.00	0.00	0.43	0.00	0.43	0.00	0.00	0.00	0.00
0.24	0.00	0.00	0.00	0.00	0.48	0.00	0.00	0.00	0.24	0.00	0.00
0.72	0.00	0.00	0.00	0.00	1.69	0.00	0.00	0.00	0.00	0.00	0.00
0.00	0.00	0.00	0.00	0.00	1.45	0.00	0.00	0.00	0.00	0.00	0.00
0.00	0.00	0.00	0.00	0.00	0.32	0.00	0.00	0.00	0.00	0.00	0.00
0.00	0.00	0.00	0.00	0.00	0.25	0.00	0.00	0.25	0.00	0.00	0.00
0.00	0.00	0.00	0.00	0.00	0.81	0.00	0.00	0.27	0.00	0.27	0.00
0.00	0.00	0.00	0.00	0.00	0.63	0.00	0.00	0.00	0.00	0.00	0.00
0.00	0.00	0.00	0.00	0.00	1.53	0.00	0.00	0.00	0.26	0.00	0.00
0.00	0.00	0.00	0.00	0.00	0.64	0.00	0.00	0.32	0.00	0.00	0.00
0.00	0.00	0.00	0.00	0.00	0.32	0.00	0.00	0.00	0.00	0.00	0.00
0.00	0.00	0.00	0.00	0.00	0.82	0.00	0.00	0.00	0.00	0.00	0.00
0.22	0.00	0.00	0.00	0.00	0.86	0.00	0.00	0.00	0.00	0.22	0.00
0.00	0.00	0.00	0.00	0.00	0.28	0.00	0.00	0.00	0.00	0.28	0.00
0.00	0.00	0.00	0.00	0.00	0.59	0.00	0.00	0.00	0.00	0.00	0.00
0.00	0.00	0.00	0.00	0.00	0.85	0.00	0.00	0.00	0.00	0.00	0.00
0.00	0.00	0.00	0.00	0.00	0.94	0.00	0.00	0.00	0.00	0.00	0.00
0.00	0.00	0.00	0.00	0.33	0.67	0.00	0.00	0.00	0.00	0.00	0.00
0.00	0.00	0.00	0.00	0.00	0.57	0.00	0.00	0.28	0.00	0.00	0.00
0.00	0.00	0.00	0.00	0.00	0.62	0.00	0.00	0.00	0.62	0.00	0.00
0.00	0.00	0.00	0.00	0.00	0.58	0.00	0.00	0.29	0.00	0.29	0.00
0.00	0.00	0.00	0.00	0.00	0.64	0.00	0.00	0.00	0.00	0.00	0.00
0.00	0.00	0.00	0.00	0.00	1.70	0.00	0.00	0.00	0.00	0.24	0.00
0.00	0.00	0.00	0.00	0.00	0.56	0.00	0.00	0.00	0.00	0.00	0.00
0.00	0.00	0.00	0.00	0.00	0.00	0.00	0.00	0.00	0.00	0.00	0.00
0.00	0.00	0.00	0.00	0.00	0.29	0.00	0.00	0.00	0.00	0.29	0.00
0.00	0.00	0.00	0.00	0.00	0.30	0.00	0.00	0.00	0.00	0.60	0.00
0.00	0.00	0.00	0.00	0.00	0.00	0.00	0.00	0.00	0.00	0.00	0.00
0.00	0.00	0.00	0.00	0.00	0.60	0.00	0.00	0.00	0.00	0.30	0.00
0.00	0.00	0.00	0.00	0.00	0.00	0.00	0.00	0.00	0.00	0.00	0.00
0.00	0.00	0.00	0.00	0.00	0.61	0.00	0.30	0.00	0.00	0.00	0.00
0.00	0.00	0.00	0.00	0.00	0.57	0.00	0.00	0.00	0.00	0.00	0.00
0.00	0.00	0.00	0.00	0.00	0.27	0.00	0.00	0.00	0.00	0.00	0.00
0.00	0.00	0.00	0.00	0.00	0.92	0.00	0.00	0.00	0.00	0.00	0.00
0.00	0.00	0.00	0.00	0.00	0.25	0.00	0.00	0.00	0.00	0.00	0.00
0.00	0.00	0.00	0.00	0.00	0.82	0.00	0.27	0.00	0.00	0.00	0.00

Pontosphaera spp.	*Reticulofenestra spp. <4µm*	*Reticulofenestra spp. 4-10µm*	*Reticulofenestra spp. 10-14µm*	*Reticulofenestra daviesii*	*Reticulofenestra umbilicus >14µm*	*Sphenolithus akropodus A*	*Sphenolithus akropodus B*	*Sphenolithus cf. intercalaris*	*Sphenolithus intercalaris*	*Sphenolithus sp. 1*	*Sphenolithus sp. 2*
0.00	16.72	60.18	0.00	1.22	0.00	0.00	0.00	0.00	0.00	0.00	0.00
0.00	13.21	55.80	0.27	2.96	0.00	0.00	0.00	0.00	0.00	0.00	0.00
0.00	18.77	43.70	0.28	2.52	0.00	0.00	0.00	0.28	0.00	0.00	0.00
0.00	11.86	57.05	0.00	2.24	0.00	0.00	0.00	0.00	0.00	0.00	0.00
0.00	13.66	51.37	0.00	1.91	0.00	0.00	0.00	0.00	0.27	0.00	0.00
0.00	13.71	48.94	0.00	1.89	0.00	0.00	0.00	0.00	0.47	0.00	0.00
0.00	39.27	28.05	0.00	1.95	0.00	0.00	0.24	0.00	0.24	0.00	0.00
0.00	40.88	30.11	0.28	0.55	0.00	0.00	0.00	0.00	0.00	0.00	0.00
0.00	45.27	25.87	0.00	0.00	0.00	0.00	0.00	0.00	0.00	0.00	0.00
0.00	37.39	28.83	0.23	0.68	0.00	0.00	0.00	0.00	0.00	0.00	0.00
0.00	48.06	21.45	0.00	1.03	0.00	0.00	0.00	0.00	0.00	0.00	0.00
0.00	47.43	20.33	0.54	0.54	0.00	0.00	0.00	0.00	0.00	0.00	0.00
0.00	37.77	21.98	0.00	2.48	0.00	0.00	0.00	0.00	0.00	0.00	0.00
0.00	45.88	22.94	0.00	0.88	0.00	0.00	0.00	0.00	0.00	0.00	0.00
0.00	45.02	19.34	0.00	0.00	0.00	0.00	0.00	0.00	0.00	0.00	0.00
0.00	51.02	20.15	0.00	1.53	0.51	0.00	0.00	0.00	0.00	0.00	0.00
0.00	44.87	21.72	0.00	1.19	0.24	0.00	0.00	0.00	0.00	0.00	0.00
0.00	36.42	27.56	0.39	1.18	0.59	0.00	0.00	0.00	0.00	0.00	0.00
0.00	39.13	20.77	0.24	2.66	0.48	0.00	0.00	0.00	0.00	0.00	0.00
0.00	41.02	27.08	0.00	1.34	0.54	0.00	0.00	0.00	0.00	0.00	0.00
0.00	43.37	29.13	0.32	0.00	0.32	0.00	0.00	0.00	0.00	0.00	0.00
0.00	31.02	39.48	0.65	0.65	0.43	0.00	0.00	0.00	0.00	0.00	0.00
0.00	21.51	46.65	0.28	0.84	0.56	0.00	0.28	0.00	0.00	0.00	0.00
0.00	32.13	32.13	0.55	1.11	0.55	0.00	0.00	0.00	0.00	0.00	0.00
0.00	34.74	39.94	0.32	0.00	1.30	0.00	0.00	0.00	0.00	0.00	0.00
0.00	46.63	28.18	0.25	1.00	0.50	0.50	0.00	0.00	0.00	0.00	0.00
0.00	29.32	33.58	0.50	1.25	0.75	0.25	0.00	0.00	0.25	0.00	0.00
0.00	25.00	42.07	0.00	0.00	0.30	0.30	0.61	0.00	0.00	0.00	0.00
0.00	32.18	36.11	0.00	0.93	0.23	0.00	0.69	0.00	0.00	0.00	0.00
0.00	30.64	33.98	0.56	3.34	0.28	0.00	0.00	0.00	0.00	0.00	0.00
0.00	49.76	25.94	0.24	0.94	0.71	0.00	0.00	0.00	0.00	0.00	0.00
0.00	43.79	30.18	0.00	3.55	0.00	0.00	0.00	0.00	0.00	0.00	0.00
0.00	36.97	32.21	0.28	4.76	0.56	0.28	0.00	0.00	0.00	0.00	0.00
0.00	43.07	30.98	0.50	2.77	0.50	0.00	0.25	0.00	0.00	0.00	0.00
0.00	39.37	28.45	0.57	2.87	0.00	0.00	0.00	0.00	0.00	0.00	0.00
0.00	44.74	30.43	0.00	2.68	0.22	0.00	0.00	0.00	0.00	0.00	0.00
0.00	39.01	18.89	0.62	4.02	0.62	0.00	0.00	0.00	0.00	0.00	0.00
0.00	48.62	27.52	0.46	1.61	0.69	0.00	0.00	0.00	0.00	0.00	0.00

0.00	42.51	26.35	0.00	3.29	0.00	0.00	0.00	0.00	0.00	0.00	0.00
0.00	40.78	29.95	0.23	3.00	0.00	0.00	0.00	0.00	0.00	0.00	0.00
0.00	45.01	26.45	0.00	1.86	0.23	0.00	0.00	0.00	0.00	0.00	0.00
0.00	38.04	31.23	0.25	1.26	0.00	0.25	0.00	0.00	0.00	0.00	0.00
0.00	35.01	29.97	0.53	5.31	0.27	0.00	0.00	0.00	0.00	0.00	0.00
0.00	47.54	25.51	0.00	0.87	0.29	0.00	0.00	0.00	0.00	0.00	0.00
0.00	35.71	41.90	0.24	1.90	0.00	0.00	0.24	0.00	0.00	0.00	0.00
0.00	21.53	40.84	0.00	1.49	0.00	0.00	0.00	0.00	0.00	0.00	0.00
0.00	28.80	40.80	0.53	3.20	0.00	0.00	0.00	0.00	0.00	0.00	0.00
0.00	36.03	22.98	1.31	3.66	0.52	0.00	0.00	0.00	0.00	0.00	0.00
0.00	36.45	28.05	0.95	2.86	0.19	0.00	0.00	0.00	0.00	0.00	0.00
0.00	38.30	25.06	1.18	0.95	0.00	0.00	0.00	0.00	0.00	0.00	0.00
0.27	20.38	30.16	0.54	12.50	0.00	0.00	0.00	0.00	0.27	0.00	0.00
0.00	33.66	28.02	0.19	10.31	0.00	0.00	0.00	0.00	0.00	0.00	0.00
0.00	27.46	22.99	0.30	11.04	0.00	0.00	0.00	0.00	0.00	0.00	0.00
0.20	46.67	13.14	0.78	8.43	1.18	0.00	0.00	0.00	0.00	0.00	0.00
0.00	23.85	19.95	0.69	12.84	0.23	0.00	0.00	0.00	0.00	0.00	0.00
0.20	29.49	16.97	0.61	11.31	0.20	0.00	0.00	0.00	0.40	0.00	0.00
0.24	24.47	30.40	0.71	7.60	0.48	0.00	0.00	0.00	0.00	0.00	0.00
0.00	13.61	26.58	1.58	14.87	0.63	0.00	0.00	0.00	0.32	0.00	0.00
0.00	13.00	36.00	0.67	7.67	0.33	0.00	0.00	0.00	1.00	0.00	0.00
0.00	14.33	32.84	0.30	12.84	0.60	0.00	0.00	0.00	0.00	0.00	0.00
0.27	16.67	37.70	0.55	9.84	1.09	0.00	0.00	0.00	0.00	0.00	0.00
0.00	21.32	27.27	0.00	7.84	0.63	0.00	0.00	0.00	0.63	0.00	0.00
0.57	23.21	30.37	1.43	5.73	1.15	0.00	0.00	0.00	0.86	0.00	0.00
0.00	15.74	37.96	0.31	9.57	0.62	0.00	0.00	0.00	0.00	0.00	0.00
0.00	21.79	28.85	0.32	7.37	0.64	0.00	0.00	0.00	0.00	0.00	0.00
0.00	21.41	25.85	1.57	7.57	0.78	0.00	0.00	0.00	0.52	0.00	0.26
0.28	13.41	27.65	1.40	7.54	0.00	0.00	0.00	0.00	0.00	0.00	0.00
0.00	21.43	26.40	4.04	7.45	1.24	0.00	0.00	0.00	0.00	0.00	0.00
0.00	9.60	31.58	2.48	10.53	1.55	0.00	0.00	0.00	0.00	0.31	0.00
0.00	12.80	38.39	2.08	4.76	0.60	0.00	0.00	0.00	0.00	0.00	0.00
0.00	14.56	43.90	1.07	6.21	0.00	0.00	0.00	0.21	0.21	0.21	0.00
0.00	11.56	47.85	0.27	5.91	0.00	0.00	0.00	0.00	0.00	0.27	0.00
0.00	15.03	46.89	0.78	6.22	1.55	0.00	0.00	0.00	0.00	0.00	0.00
0.00	7.01	54.27	0.61	5.79	0.91	0.00	0.00	0.00	0.00	0.00	0.00
0.44	11.65	44.62	0.66	7.03	0.00	0.00	0.00	0.00	0.00	0.00	0.00
0.00	11.73	43.97	0.98	9.77	0.33	0.00	0.00	0.00	0.33	0.00	0.00
0.00	11.49	40.10	3.67	9.29	0.98	0.00	0.00	0.00	0.00	0.00	0.00
0.00	11.78	48.22	2.89	9.78	0.67	0.00	0.00	0.00	0.22	0.00	0.00
0.00	16.59	43.99	1.44	7.93	0.48	0.00	0.00	0.00	0.00	0.00	0.00
0.00	11.58	44.68	2.13	8.75	0.47	0.00	0.00	0.00	0.00	0.00	0.00
0.00	10.90	55.34	0.85	8.55	0.21	0.00	0.00	0.00	0.21	0.00	0.00
0.00	11.35	43.24	1.35	13.78	1.35	0.00	0.00	0.00	0.00	0.00	0.00
0.22	10.17	42.64	0.87	13.20	2.16	0.00	0.00	0.00	0.00	0.00	0.00
0.00	12.16	34.46	0.45	15.09	0.45	0.00	0.00	0.00	0.00	0.00	0.00
0.00	9.09	46.46	0.00	16.16	0.25	0.00	0.00	0.00	0.00	0.00	0.00
0.00	4.31	47.98	0.27	14.56	1.35	0.00	0.00	0.00	0.00	0.00	0.00
0.00	5.97	44.03	0.31	12.58	0.63	0.00	0.00	0.00	0.00	0.00	0.00
0.00	8.87	46.55	1.48	11.33	0.74	0.00	0.00	0.00	0.00	0.00	0.00

0.00	6.47	42.03	0.86	12.07	1.72	0.00	0.00	0.00	0.22	0.00	0.00
0.00	19.95	42.07	0.00	11.30	0.48	0.00	0.00	0.00	0.00	0.24	0.24
0.00	8.67	50.36	0.24	2.65	0.00	0.00	0.00	0.00	0.00	0.24	0.00
0.00	11.88	43.19	0.87	1.45	0.29	0.00	0.00	0.00	0.00	0.00	0.00
0.00	15.19	46.52	0.00	5.70	0.63	0.00	0.00	0.00	0.00	0.00	0.00
0.00	16.79	40.35	0.75	5.01	0.75	0.00	0.00	0.00	0.00	0.00	0.00
0.00	12.37	40.59	1.08	3.49	1.08	0.00	0.00	0.00	0.00	0.00	0.00
0.00	7.59	38.92	0.32	7.59	0.63	0.00	0.00	0.00	0.00	0.00	0.00
0.00	22.19	26.79	1.02	6.89	1.02	0.00	0.00	0.00	0.26	0.00	0.00
0.00	11.78	38.22	0.96	6.05	0.64	0.00	0.00	0.00	0.32	0.00	0.00
0.00	20.70	38.85	0.96	7.01	0.64	0.00	0.00	0.00	0.00	0.00	0.00
0.00	23.91	32.88	1.09	8.97	0.82	0.00	0.00	0.00	0.00	0.27	0.00
0.00	14.01	36.64	1.72	7.97	0.43	0.00	0.00	0.00	0.22	0.22	0.22
0.00	27.86	30.36	0.56	5.57	1.11	0.00	0.00	0.00	0.28	0.56	0.28
0.29	18.29	35.10	0.88	7.67	0.29	0.00	0.00	0.00	1.47	0.29	0.00
0.00	18.23	37.89	0.28	8.83	0.00	0.00	0.00	0.00	1.71	0.00	0.28
0.00	17.92	41.82	0.31	6.60	0.31	0.00	0.00	0.00	0.94	0.94	0.00
0.00	15.33	40.67	0.00	8.00	0.33	0.00	0.00	0.00	0.33	0.33	0.00
0.00	10.76	41.93	1.13	6.80	0.85	0.00	0.00	0.00	0.00	0.00	0.00
0.00	12.31	42.15	0.92	5.54	0.92	0.00	0.00	0.00	0.00	0.00	0.00
0.00	28.57	28.57	1.17	6.71	0.00	0.00	0.00	0.00	0.00	0.00	0.00
0.00	17.57	48.24	0.00	3.51	0.00	0.00	0.00	0.00	0.32	0.00	0.00
0.00	32.60	30.41	0.49	2.43	0.97	0.00	0.00	0.00	0.00	0.00	0.00
0.00	28.49	36.87	0.56	3.07	0.00	0.00	0.00	0.00	0.00	0.00	0.00
0.00	19.66	41.57	1.40	4.21	0.28	0.00	0.00	0.00	0.00	0.00	0.00
0.00	23.99	31.21	1.73	4.91	1.45	0.00	0.00	0.00	0.00	0.00	0.00
0.00	9.91	50.45	0.00	5.41	0.00	0.00	0.00	0.00	0.00	0.00	0.00
0.00	22.77	41.58	0.99	3.63	0.33	0.00	0.00	0.00	0.00	0.00	0.00
0.30	18.51	37.61	1.79	5.67	1.49	0.00	0.00	0.00	0.00	0.00	0.00
0.00	26.06	36.81	0.00	5.86	0.00	0.00	0.00	0.00	0.00	0.00	0.00
0.00	30.91	22.12	0.00	5.45	0.00	0.00	0.00	0.00	0.00	0.00	0.00
0.00	35.82	28.08	0.29	5.16	0.57	0.00	0.00	0.00	0.00	0.00	0.00
0.00	33.78	34.59	0.27	3.51	0.00	0.00	0.00	0.00	0.00	0.00	0.00
0.00	36.09	32.42	0.92	2.45	0.92	0.00	0.00	0.00	0.00	0.00	0.00
0.00	70.63	10.13	0.25	1.52	0.25	0.00	0.00	0.00	0.00	0.00	0.00
0.00	45.92	23.10	2.17	1.36	0.82	0.00	0.00	0.00	0.00	0.00	0.00

Sphenolithus moriformis gr.	*Sphenolithus cf. predistentus*	*Sphenolithus predistentus*	*Sphenolithus predistentus-distentus*	*Sphenolithus distentus*	*Sphenolithus cf. spiniger*	*Sphenolithus tribulosus*	*Sphenolithus cf. tribulosus*	*Sphenolithus spp.*	*Thoracosphaera* spp.	*Umbilicosphaera spp.*	*Zygrhablithus bijugatus*
0.61	0.00	0.61	0.00	0.00	0.00	0.00	0.00	0.00	0.00	0.00	0.00
2.16	0.00	0.81	0.54	0.00	0.00	0.00	0.00	0.00	0.27	0.00	0.00
1.40	0.00	0.56	0.28	0.00	0.00	0.00	0.00	0.00	0.00	0.00	0.56
1.28	0.00	0.64	0.00	0.00	0.00	0.00	0.00	0.00	0.00	0.00	0.32
2.73	0.00	1.64	0.27	0.00	0.00	0.00	0.00	0.00	0.00	0.00	0.55
1.65	0.00	0.71	0.00	0.00	0.00	0.00	0.00	0.00	0.24	0.00	0.47
0.73	0.00	0.73	0.24	0.00	0.24	0.00	0.00	0.00	0.00	0.24	0.24
0.55	0.00	1.38	0.00	0.00	0.00	0.00	0.00	0.00	0.00	0.00	1.38
1.24	0.00	1.99	0.00	0.00	0.00	0.00	0.00	0.00	0.00	0.00	0.00
1.35	0.00	1.13	0.00	0.00	0.00	0.00	0.00	0.00	0.23	0.00	0.68
1.03	0.00	0.00	0.00	0.00	0.00	0.00	0.00	0.00	0.00	0.00	0.78
0.81	0.00	0.00	0.00	0.00	0.00	0.00	0.00	0.00	0.27	0.00	0.27
0.62	0.00	0.62	0.00	0.00	0.00	0.31	0.00	0.00	0.00	0.00	2.17
0.59	0.00	0.00	0.00	0.00	0.00	0.00	0.00	0.00	0.00	0.00	0.00
0.91	0.00	0.60	0.00	0.00	0.00	0.00	0.00	0.00	0.00	0.00	0.30
0.77	0.00	0.51	0.00	0.00	0.00	0.00	0.00	0.00	0.00	0.00	0.00
2.15	0.00	1.43	0.00	0.00	0.00	0.00	0.00	0.00	0.00	0.00	0.24
2.95	0.00	0.00	0.00	0.00	0.00	0.00	0.00	0.00	0.20	0.00	2.36
0.97	0.00	0.48	0.00	0.00	0.00	0.00	0.00	0.00	0.00	0.00	1.93
1.88	0.00	0.00	0.00	0.00	0.00	0.00	0.00	0.00	0.00	0.00	0.00
0.65	0.00	0.65	0.00	0.00	0.00	0.00	0.00	0.00	0.00	0.00	0.32
0.87	0.00	0.22	0.00	0.00	0.00	0.00	0.00	0.00	0.00	0.00	0.00
0.84	0.00	0.84	0.00	0.00	0.00	0.00	0.00	0.00	0.00	0.00	1.68
1.94	0.00	0.28	0.00	0.00	0.00	0.00	0.00	0.00	0.00	0.00	1.11
0.97	0.00	0.32	0.00	0.00	0.00	0.00	0.00	0.00	0.00	0.00	1.30
1.25	0.00	0.50	0.00	0.00	0.00	0.00	0.00	0.00	0.25	0.00	0.25
1.00	0.00	0.00	0.00	0.00	0.00	0.00	0.00	0.00	0.00	0.00	1.00
0.61	0.00	0.91	0.00	0.00	0.00	0.00	0.00	0.00	0.30	0.00	0.30
0.69	0.00	0.69	0.00	0.00	0.00	0.00	0.00	0.00	0.00	0.00	1.39
1.39	0.00	0.00	0.00	0.00	0.00	0.00	0.00	0.00	0.00	0.00	0.56
1.42	0.00	0.47	0.00	0.00	0.00	0.00	0.00	0.00	0.00	0.00	0.00
1.18	0.59	0.00	0.00	0.00	0.00	0.00	0.00	0.00	0.00	0.00	0.89
1.96	0.00	0.28	0.00	0.00	0.00	0.00	0.00	0.00	0.00	0.00	0.00
1.01	0.00	0.00	0.00	0.00	0.00	0.00	0.00	0.00	0.00	0.00	1.01
1.15	0.00	0.00	0.00	0.00	0.00	0.00	0.00	0.00	0.00	0.00	0.57
0.45	0.00	0.22	0.00	0.00	0.00	0.00	0.00	0.00	0.00	0.00	0.67
1.55	0.00	0.31	0.00	0.00	0.00	0.00	0.00	0.00	0.00	0.00	0.00
0.46	0.00	0.00	0.00	0.00	0.00	0.00	0.00	0.00	0.00	0.00	0.69

0.90	0.00	0.60	0.00	0.00	0.00	0.00	0.00	0.00	0.30	0.00	1.50
1.38	0.00	0.46	0.00	0.00	0.00	0.00	0.00	0.00	0.00	0.00	0.00
0.46	0.00	0.46	0.00	0.00	0.00	0.00	0.23	0.00	0.00	0.00	1.86
1.01	0.00	0.25	0.00	0.00	0.25	0.00	0.00	0.25	0.00	0.00	2.02
0.53	0.00	0.53	0.00	0.00	0.00	0.00	0.00	0.00	0.00	0.00	1.33
0.58	0.00	0.00	0.00	0.00	0.00	0.00	0.00	0.00	0.00	0.00	2.32
0.48	0.00	0.24	0.00	0.00	0.00	0.00	0.00	0.00	0.00	0.00	2.86
1.24	0.00	0.00	0.00	0.00	0.00	0.00	0.00	0.00	0.00	0.00	3.22
2.40	0.00	0.00	0.00	0.00	0.00	0.00	0.00	0.00	0.00	0.27	2.93
1.04	0.00	0.26	0.00	0.00	0.00	0.00	0.00	0.00	0.00	0.00	0.52
1.15	0.00	0.00	0.00	0.00	0.00	0.00	0.00	0.00	0.38	0.00	1.15
1.18	0.00	0.24	0.00	0.00	0.00	0.00	0.00	0.00	0.00	0.00	0.00
0.82	0.00	0.00	0.00	0.00	0.00	0.00	0.00	0.00	0.00	0.00	2.17
0.97	0.00	0.00	0.00	0.00	0.00	0.00	0.00	0.00	0.00	0.00	3.50
1.79	0.00	0.30	0.00	0.00	0.00	0.00	0.00	0.00	0.00	0.00	4.48
0.98	0.00	0.00	0.00	0.00	0.00	0.00	0.00	0.00	0.00	0.00	2.75
0.00	0.00	0.46	0.00	0.00	0.00	0.00	0.00	0.00	0.23	0.00	0.00
0.61	0.00	0.20	0.00	0.00	0.00	0.00	0.00	0.00	0.00	0.00	3.84
0.95	0.00	0.00	0.00	0.00	0.00	0.00	0.00	0.00	0.00	0.00	0.48
0.95	0.00	0.00	0.00	0.00	0.00	0.00	0.00	0.00	0.00	0.00	1.90
1.33	0.00	1.33	0.00	0.00	0.00	0.00	0.00	0.00	0.00	0.00	0.33
2.09	0.00	0.30	0.00	0.00	0.00	0.00	0.00	0.00	0.00	0.00	2.69
0.27	0.00	0.00	0.00	0.00	0.00	0.00	0.00	0.00	0.00	0.00	3.01
0.94	0.00	0.00	0.00	0.00	0.00	0.00	0.00	0.00	0.00	0.00	0.94
1.15	0.00	0.29	0.00	0.00	0.00	0.00	0.00	0.00	0.29	0.00	0.29
0.31	0.00	0.31	0.00	0.00	0.00	0.00	0.00	0.00	0.00	0.00	0.93
0.64	0.00	0.00	0.00	0.00	0.00	0.00	0.00	0.00	0.00	0.00	0.00
0.26	0.00	0.52	0.00	0.00	0.00	0.00	0.00	0.00	0.00	0.00	0.26
0.28	0.00	0.56	0.00	0.00	0.00	0.00	0.00	0.00	0.84	0.00	0.84
0.62	0.00	0.00	0.00	0.00	0.00	0.00	0.00	0.00	0.00	0.00	1.55
1.55	0.00	0.00	0.00	0.00	0.00	0.00	0.00	0.00	0.00	0.00	2.79
0.60	0.00	0.00	0.00	0.00	0.00	0.00	0.00	0.00	0.00	0.00	1.49
0.64	0.00	0.64	0.00	0.00	0.00	0.00	0.00	0.00	0.00	0.00	0.00
0.81	0.00	0.81	0.00	0.00	0.27	0.00	0.00	0.00	0.00	0.00	0.54
1.04	0.00	0.26	0.00	0.00	0.00	0.00	0.00	0.00	0.00	0.00	0.26
0.61	0.00	0.00	0.00	0.00	0.00	0.00	0.00	0.00	0.00	0.00	0.91
1.54	0.00	0.22	0.00	0.00	0.00	0.00	0.00	0.00	0.00	0.00	1.76
1.63	0.00	0.33	0.00	0.00	0.00	0.00	0.00	0.00	0.00	0.00	0.33
1.47	0.00	0.00	0.00	0.00	0.00	0.00	0.00	0.00	0.00	0.00	0.73
1.11	0.00	0.22	0.00	0.00	0.00	0.00	0.00	0.00	0.00	0.00	0.89
0.72	0.00	0.48	0.00	0.00	0.00	0.00	0.00	0.00	0.00	0.00	0.24
2.13	0.00	0.95	0.00	0.00	0.00	0.00	0.00	0.00	0.00	0.00	0.24
1.71	0.00	0.21	0.00	0.00	0.00	0.00	0.00	0.00	0.00	0.00	1.50
1.08	0.00	0.54	0.00	0.00	0.00	0.00	0.00	0.00	0.00	0.00	0.27
0.65	0.00	0.22	0.00	0.00	0.00	0.00	0.00	0.00	0.00	0.00	0.43
0.45	0.00	0.23	0.00	0.00	0.00	0.00	0.00	0.00	0.23	0.00	0.23
1.26	0.00	0.25	0.00	0.00	0.25	0.00	0.00	0.00	0.00	0.00	0.25
0.54	0.00	0.27	0.00	0.00	0.00	0.00	0.00	0.00	0.00	0.00	0.27
0.31	0.00	0.63	0.00	0.00	0.00	0.00	0.00	0.00	0.31	0.00	0.94
1.48	0.00	0.00	0.00	0.00	0.00	0.00	0.00	0.00	0.00	0.00	3.20

1.08	0.22	0.00	0.00	0.00	0.00	0.00	0.00	0.00	0.00	0.00	3.66
1.68	0.00	0.00	0.00	0.00	0.00	0.00	0.00	0.00	0.00	0.00	2.16
0.48	0.00	0.00	0.00	0.00	0.00	0.00	0.00	0.00	0.48	0.00	0.00
0.58	0.00	0.29	0.00	0.00	0.29	0.00	0.00	0.00	0.58	0.00	0.29
1.27	0.00	0.00	0.00	0.00	0.00	0.00	0.00	0.00	0.00	0.32	1.58
0.25	0.00	0.00	0.00	0.00	0.00	0.00	0.00	0.00	0.00	0.00	0.50
2.15	0.00	0.00	0.00	0.00	0.00	0.00	0.00	0.00	0.27	0.00	1.34
0.63	0.00	0.63	0.00	0.00	0.00	0.00	0.00	0.00	0.95	0.32	0.63
0.77	0.00	0.26	0.00	0.00	0.00	0.00	0.00	0.00	0.51	0.00	0.77
0.96	0.00	0.00	0.00	0.00	0.32	0.00	0.00	0.00	0.64	0.32	0.96
1.91	0.00	0.00	0.00	0.00	0.00	0.00	0.00	0.00	1.27	0.00	2.23
0.00	0.00	0.00	0.00	0.00	0.00	0.00	0.00	0.00	0.54	0.00	1.09
1.51	0.00	0.65	0.00	0.00	0.22	0.00	0.00	0.22	0.43	0.22	2.37
0.56	0.00	0.28	0.00	0.00	0.00	0.00	0.00	0.00	0.56	0.28	0.56
0.88	0.00	0.29	0.00	0.00	0.00	0.00	0.00	0.00	0.59	0.00	0.88
0.57	0.00	0.57	0.00	0.00	0.00	0.00	0.00	0.00	0.28	0.00	0.85
1.26	0.00	0.00	0.00	0.00	0.00	0.00	0.00	0.00	0.31	0.00	0.63
0.67	0.00	0.00	0.00	0.00	0.00	0.00	0.00	0.00	0.33	0.33	1.00
0.28	0.00	0.00	0.00	0.00	0.00	0.00	0.00	0.00	0.85	0.00	0.85
1.23	0.00	0.00	0.00	0.00	0.00	0.00	0.00	0.00	0.62	0.31	1.85
0.87	0.29	0.00	0.00	0.00	0.00	0.00	0.00	0.00	0.00	0.00	1.75
0.96	0.00	0.00	0.00	0.00	0.00	0.00	0.00	0.00	0.32	0.00	2.56
1.46	0.00	0.24	0.00	0.00	0.24	0.00	0.00	0.00	1.22	0.49	1.46
0.84	0.00	0.00	0.00	0.00	0.00	0.00	0.00	0.00	0.00	0.00	0.84
0.00	0.00	0.28	0.00	0.00	0.00	0.00	0.00	0.00	0.56	0.00	0.28
0.87	0.00	0.00	0.00	0.00	0.00	0.00	0.00	0.00	0.87	0.00	0.87
0.30	0.00	0.00	0.00	0.00	0.00	0.00	0.00	0.00	0.60	0.30	0.00
0.66	0.00	0.00	0.00	0.00	0.00	0.00	0.00	0.00	0.00	0.33	0.00
0.60	0.00	0.00	0.00	0.00	0.00	0.00	0.00	0.00	0.60	0.00	0.60
0.65	0.33	0.00	0.00	0.00	0.00	0.00	0.00	0.00	0.00	0.00	0.65
0.00	0.00	0.00	0.00	0.00	0.00	0.00	0.00	0.00	0.61	0.00	2.12
0.29	0.00	0.29	0.00	0.00	0.00	0.00	0.00	0.00	0.86	0.57	1.15
0.54	0.00	0.00	0.00	0.00	0.00	0.00	0.00	0.00	0.27	1.62	0.54
0.31	0.00	0.00	0.00	0.00	0.31	0.00	0.00	0.00	0.61	0.00	0.92
0.76	0.00	0.00	0.00	0.00	0.00	0.00	0.00	0.00	0.51	0.25	1.01
1.36	0.00	0.00	0.00	0.00	0.00	0.00	0.00	0.00	0.00	0.27	1.90

Indetermined placolith	*Cribrocentrum cf. erbae*	*Cribrocentrum cf. reticulatum*	*Cribrocentrum reticulatum*	*Reworking*
0.00	0.00	0.00	0.00	0.30
0.00	0.00	0.00	0.00	0.00
0.28	0.00	0.00	0.00	0.00
0.00	0.00	0.00	0.00	0.96
0.00	0.00	0.00	0.00	0.82
0.24	0.00	0.00	0.00	0.00
0.24	0.00	0.00	0.00	0.24
0.28	0.00	0.00	0.00	0.28
0.25	0.00	0.00	0.00	0.00
0.23	0.00	0.00	0.00	0.00
0.00	0.00	0.00	0.00	0.26
0.00	0.00	0.00	0.00	0.00
0.00	0.00	0.00	0.00	0.00
0.00	0.00	0.00	0.00	0.00
0.00	0.00	0.00	0.00	0.00
0.00	0.00	0.00	0.00	0.00
0.00	0.00	0.00	0.00	0.00
0.20	0.00	0.00	0.00	0.00
0.00	0.00	0.00	0.00	0.24
0.00	0.00	0.00	0.27	0.00
0.00	0.00	0.00	0.00	0.65
0.00	0.00	0.00	0.00	0.00
0.00	0.00	0.00	0.00	0.28
0.00	0.00	0.00	0.00	0.00
0.00	0.00	0.00	0.00	0.00
0.00	0.00	0.00	0.00	0.00
0.00	0.00	0.00	0.00	0.00
0.00	0.00	0.00	0.00	0.30
0.00	0.00	0.00	0.00	0.00
0.00	0.00	0.28	0.00	0.28
0.00	0.00	0.00	0.00	0.94
0.00	0.00	0.00	0.00	0.00
0.00	0.00	0.00	0.00	0.00
0.00	0.00	0.00	0.00	0.00
0.00	0.00	0.00	0.00	0.57
0.00	0.00	0.00	0.00	0.00
0.00	0.00	0.00	0.00	0.00
0.00	0.00	0.00	0.00	0.00

0.00	0.00	0.00	0.00	0.00
0.00	0.00	0.00	0.00	0.23
0.46	0.00	0.00	0.00	0.00
0.00	0.00	0.00	0.00	0.00
0.27	0.00	0.00	0.00	0.00
0.00	0.00	0.00	0.00	0.00
0.00	0.00	0.00	0.00	0.00
0.25	0.00	0.00	0.00	0.25
0.27	0.00	0.00	0.00	0.00
0.26	0.00	0.00	0.00	0.00
0.00	0.00	0.00	0.00	0.19
0.24	0.00	0.00	0.00	0.24
0.00	0.00	0.00	0.00	0.00
0.00	0.00	0.00	0.00	0.00
0.00	0.00	0.00	0.00	0.00
0.00	0.00	0.00	0.00	0.00
0.23	0.00	0.00	0.00	0.00
0.00	0.00	0.00	0.00	0.20
0.00	0.00	0.00	0.00	0.00
0.00	0.00	0.00	0.00	0.00
0.00	0.00	0.00	0.00	0.00
0.00	0.00	0.00	0.00	0.00
0.00	0.00	0.00	0.00	0.00
0.00	0.00	0.00	0.00	0.00
0.00	0.00	0.00	0.00	0.00
0.00	0.00	0.00	0.32	0.00
0.00	0.00	0.00	0.00	0.00
0.00	0.00	0.00	0.00	0.00
0.00	0.00	0.00	0.00	0.00
0.00	0.00	0.00	0.00	0.00
0.00	0.00	0.00	0.00	0.00
0.00	0.00	0.00	0.27	0.00
0.26	0.00	0.00	0.00	0.00
0.00	0.00	0.00	0.00	0.00
0.00	0.00	0.00	0.00	0.00
0.00	0.00	0.00	0.00	0.00
0.00	0.00	0.00	0.00	0.00
0.00	0.00	0.00	0.00	0.00
0.00	0.00	0.00	0.00	0.00
0.00	0.00	0.00	0.00	0.00
0.00	0.00	0.00	0.00	0.00
0.00	0.00	0.00	0.00	0.00
0.22	0.00	0.22	0.00	0.00
0.00	0.00	0.00	0.00	0.00
0.00	0.00	0.00	0.00	0.00
0.00	0.00	0.00	0.00	0.00
0.00	0.00	0.00	0.00	0.00
0.25	0.00	0.00	0.00	0.00

0.22	0.00	0.00	0.22	0.22
0.00	0.00	0.00	0.00	0.00
0.00	0.00	0.00	0.00	0.00
0.00	0.00	0.00	0.00	0.00
0.00	0.00	0.00	0.00	0.00
0.00	0.00	0.00	0.25	0.00
0.00	0.00	0.00	0.00	0.00
0.00	0.00	0.00	0.00	0.00
0.00	0.00	0.00	0.00	0.00
0.00	0.32	0.00	0.00	0.00
0.00	0.00	0.00	0.00	0.00
0.00	0.00	0.00	0.27	0.00
0.00	0.00	0.00	0.00	0.00
0.00	0.00	0.00	0.00	0.00
0.00	0.00	0.00	0.00	0.00
0.00	0.00	0.00	0.28	0.00
0.00	0.00	0.00	0.00	0.00
0.00	0.00	0.00	0.00	0.00
0.00	0.00	0.00	0.00	0.00
0.00	0.00	0.00	0.00	0.00
0.00	0.00	0.00	0.00	0.00
0.00	0.00	0.00	0.00	0.00
0.00	0.28	0.00	0.00	0.00
0.00	0.00	0.00	0.28	0.00
0.00	0.00	0.00	0.87	0.00
0.00	0.00	0.00	0.00	0.30
0.00	0.00	0.00	0.33	0.00
0.00	0.00	0.00	1.19	0.00
0.00	0.00	0.00	2.28	0.00
0.00	0.00	0.00	0.00	0.00
0.00	0.00	0.00	0.00	0.00
0.00	0.00	0.00	0.00	0.00
0.00	0.00	0.00	0.00	0.00
0.00	0.00	0.00	0.00	0.00
0.00	0.00	0.00	0.00	0.00

Appendix V. Site U1509 Bulk geochemical data

Identifier 1	Depth (CSF-A, m)	$\delta^{13}C$	$\delta^{18}O$	$CaCO_3$ (wt, %)
U1509A-21R-1W-0-1	183.00	2.46	0.67	85.98
U1509A-21R-1W-30-31	183.30	2.42	0.69	83.79
U1509A-21R-1W-60-61	183.60	2.14	0.51	89.47
U1509A-21R-1W-90-91	183.90	1.89	0.47	75.57
U1509A-21R-1W-120-121	184.20	1.75	0.48	83.22
U1509A-21R-2W-0-1	184.50	1.71	0.56	87.46
U1509A-21R-2W-30-31	184.80	1.81	0.46	73.31
U1509A-21R-2W-60-61	185.10	1.45	0.56	86.97
U1509A-21R-3W-5-6	185.40	1.83	0.47	79.07
U1509A-21R-3W-35-36	185.70	1.91	0.57	49.29
U1509A-21R-3W-65-66	186.00	1.50	0.48	78.68
U1509A-21R-CCW-11-12	186.30	1.53	0.38	81.73
U1509A-22R-1W-30-31	192.90	1.82	0.45	73.82
U1509A-22R-1W-59-60	193.19	1.86	0.50	68.38
U1509A-22R-1W-90-91	193.50	1.75	0.39	78.33
U1509A-22R-1W-120-121	193.80	1.85	0.59	75.22
U1509A-22R-2W-29-30	194.40	1.86	0.52	72.56
U1509A-22R-2W-59-60	194.70	1.80	0.50	71.65
U1509A-22R-2W-89-90	195.00	1.78	0.49	71.51
U1509A-22R-2W-119-120	195.30	1.68	0.45	64.10
U1509A-22R-3W-29-30	195.90	1.73	0.60	79.33
U1509A-22R-3W-59-60	196.20	1.82	0.25	74.40
U1509A-22R-CCW-9-10	196.40	1.84	0.36	72.77
U1509A-23R-1W-9-10	202.19	1.70	0.31	65.78
U1509A-23R-1W-40-41	202.50	1.86	0.52	68.26
U1509A-23R-1W-70-71	202.80	1.70	0.26	73.80
U1509A-23R-1W-100-101	203.10	1.86	0.35	69.62
U1509A-23R-1W-130-131	203.40	1.72	0.17	71.40
U1509A-23R-2W-8-9	203.68	1.77	0.44	53.43
U1509A-23R-2W-40-41	204.00	1.82	0.44	71.65
U1509A-23R-2W-70-71	204.30	1.85	0.48	69.09
U1509A-23R-2W-100-101	204.60	1.81	0.45	75.23
U1509A-23R-2W-130-131	204.90	1.95	0.32	58.78
U1509A-24R-1W-0-1	206.70	1.51	0.40	73.76
U1509A-24R-1W-30-31	207.00	1.71	0.55	74.04
U1509A-24R-1W-59-60	207.29	1.78	0.37	69.54
U1509A-24R-1W-90-91	207.60	1.69	0.38	65.31
U1509A-24R-1W-120-121	207.90	1.66	0.48	69.03
U1509A-24R-2W-14-15	208.22	1.96	0.56	69.78
U1509A-24R-2W-42-43	208.50	2.04	0.38	75.10
U1509A-24R-2W-72-73	208.80	1.83	0.32	76.48
U1509A-24R-2W-102-103	209.10	1.77	0.45	80.18
U1509A-24R-2W-132-133	209.40	1.68	0.40	71.52
U1509A-24R-3W-13-14	209.71	2.03	0.43	79.85
U1509A-24R-3W-42-43	210.00	1.77	0.39	82.42
U1509A-24R-3W-72-73	210.30	1.78	0.45	86.90

U1509A-24R-3W-102-103	210.60	1.80	0.43	82.88
U1509A-25R-1W-10-11	211.80	1.98	0.47	74.04
U1509A-25R-1W-40-41	212.10	1.99	0.50	79.52
U1509A-25R-1W-70-71	212.40	1.92	0.50	80.06
U1509A-25R-1W-100-101	212.70	1.76	0.36	82.92
U1509A-25R-1W-130-131	213.00	1.84	0.50	81.01
U1509A-25R-2W-15-16	213.30	1.65	0.38	80.13
U1509A-25R-2W-45-46	213.60	1.97	0.56	82.63
U1509A-26R-1W-11-12	221.41	1.91	0.47	77.28
U1509A-26R-2W-2-3	221.70	1.85	0.50	71.48
U1509A-26R-2W-32-33	222.00	1.76	0.55	78.62
U1509A-26R-2W-64-65	222.32	1.69	0.38	80.93
U1509A-26R-2W-92-93	222.60	1.84	0.41	77.02
U1509A-26R-2W-122-123	222.90	1.94	0.51	79.13
U1509A-26R-3W-2-3	223.20	1.82	0.38	75.83
U1509A-26R-3W-32-33	223.50	1.94	0.56	81.94
U1509A-26R-3W-64-65	223.82	1.86	0.54	78.83
U1509A-26R-3W-92-93	224.10	1.98	0.56	81.89
U1509A-26R-3W-122-123	224.40	1.83	0.53	86.95
U1509A-26R-4W-2-3	224.70	2.01	0.75	81.04
U1509A-26R-4W-32-33	225.00	1.84	0.44	74.84
U1509A-26R-4W-64-65	225.32	2.07	0.56	82.62
U1509A-26R-4W-92-93	225.60	1.89	0.54	80.93
U1509A-26R-4W-122-123	225.90	2.00	0.60	84.58
U1509A-26R-5W-2-3	226.20	1.95	0.59	83.88
U1509A-26R-5W-32-33	226.50	1.84	0.68	85.18
U1509A-26R-5W-66-67	226.84	1.83	0.51	76.75
U1509A-26R-5W-92-93	227.10	1.92	0.58	81.27
U1509A-26R-5W-122-123	227.40	1.78	0.63	82.75
U1509A-26R-6W-2-3	227.70	1.85	0.64	84.03
U1509A-26R-6W-32-33	228.00	1.90	0.58	77.26
U1509A-26R-6W-64-65	228.32	1.95	0.78	83.56
U1509A-26R-6W-92-93	228.60	1.89	0.59	88.19
U1509A-26R-6W-122-123	228.90	2.00	0.61	83.26
U1509A-26R-7W-2-3	229.20	2.04	0.77	87.25
U1509A-26R-7W-32-33	229.50	1.91	0.66	82.71
U1509A-26R-7W-64-65	229.82	2.00	0.61	73.87
U1509A-26R-7W-92-93	230.10	1.91	0.70	80.98
U1509A-26R-8W-15-16	230.40	1.88	0.70	83.32
U1509A-26R-8W-45-46	230.70	1.94	0.64	81.18
U1509A-27R-1W-9-10	230.99	2.01	0.62	76.99
U1509A-27R-1W-40-41	231.30	1.88	0.56	76.25
U1509A-27R-1W-70-71	231.60	2.08	0.61	87.28
U1509A-27R-1W-100-101	231.90	2.00	0.46	69.86
U1509A-27R-1W-130-131	232.20	2.07	0.61	82.08
U1509A-27R-2W-9-10	232.49	2.05	0.51	83.67
U1509A-27R-2W-40-41	232.80	2.20	0.55	87.41
U1509A-27R-2W-69-70	233.09	1.93	0.48	82.14
U1509A-27R-2W-100-101	233.40	1.85	0.59	78.24
U1509A-27R-2W-130-131	233.70	1.87	0.42	77.85

U1509A-27R-3W-9-10	233.99	2.07	0.58	75.44
U1509A-27R-3W-40-41	234.30	2.04	0.56	76.52
U1509A-27R-3W-70-71	234.60	2.18	0.46	83.16
U1509A-28R-1W-9-10	240.59	2.26	0.63	85.33
U1509A-28R-1W-40-41	240.90	2.21	0.63	85.40
U1509A-28R-1W-70-71	241.20	2.28	0.61	69.04
U1509A-28R-1W-100-101	241.50	2.20	0.68	85.80
U1509A-28R-1W-130-131	241.80	2.18	0.68	80.77
U1509A-28R-2W-9-10	242.09	2.26	0.68	80.68
U1509A-28R-2W-40-41	242.40	2.28	0.64	77.49
U1509A-28R-2W-70-71	242.70	2.40	0.77	81.41
U1509A-28R-2W-100-101	243.00	2.30	0.61	79.43
U1509A-28R-2W-130-131	243.30	2.40	0.78	76.82
U1509A-28R-3W-10-11	243.60	2.34	0.62	79.52
U1509A-28R-3W-40-41	243.90	2.42	0.78	82.12
U1509A-28R-3W-69-70	244.19	2.44	0.65	81.72
U1509A-28R-3W-100-101	244.50	2.37	0.51	72.97
U1509A-28R-3W-130-131	244.80	2.52	0.72	78.93
U1509A-28R-4W-20-21	245.10	2.38	0.56	80.42
U1509A-28R-4W-50-51	245.40	2.46	0.66	76.06
U1509A-28R-4W-80-81	245.70	2.44	0.68	75.33
U1509A-28R-4W-109-110	245.99	2.64	0.65	82.24
U1509A-28R-4W-140-141	246.30	2.47	0.72	95.28
U1509A-28R-5W-20-21	246.60	2.50	0.71	73.59
U1509A-28R-5W-50-51	246.90	2.36	0.60	79.82
U1509A-28R-5W-80-81	247.20	2.27	0.50	85.70
U1509A-28R-5W-109-110	247.49	2.33	0.44	79.97
U1509A-28R-5W-140-141	247.80	2.24	0.28	84.25
U1509A-28R-6W-20-21	248.10	2.25	0.29	76.60
U1509A-28R-6W-50-51	248.40	2.27	0.28	85.73
U1509A-29R-1W-9-10	250.19	2.24	0.20	90.59
U1509A-29R-1W-40-41	250.50	2.11	0.15	81.08
U1509A-29R-1W-70-71	250.80	2.10	0.39	87.74
U1509A-29R-1W-100-101	251.10	2.23	0.25	83.08
U1509A-29R-1W-130-131	251.40	2.09	0.15	82.24
U1509A-29R-2W-6-7	251.70	2.25	0.20	83.98
U1509A-29R-2W-36-37	252.00	2.20	0.22	88.02
U1509A-29R-2W-66-67	252.30	2.29	0.24	99.36
U1509A-29R-2W-96-97	252.60	2.08	0.23	83.62
U1509A-29R-2W-126-127	252.90	2.20	0.33	90.67
U1509A-29R-3W-6-7	253.20	2.31	0.41	91.83
U1509A29R-3W-36-37	253.50	2.22	0.27	88.02
U1509A-29R-3W-66-67	253.80	2.23	0.30	92.21
U1509A-29R-3W-96-97	254.10	2.18	0.33	81.44
U1509A-29R-3W-126-127	254.40	2.10	0.18	90.84
U1509A-29R-4W-6-7	254.71	2.23	0.36	83.48
U1509A-29R-4W-36-37	255.01	2.20	0.22	85.21
U1509A-29R-4W-66-67	255.31	2.25	0.35	96.00
U1509A-29R-4W-96-97	255.61	2.06	0.22	77.55
U1509A-29R-4W-126.127	255.91	2.08	0.22	86.03

U1509A-29R-5W-6-7	256.20	1.99	0.27	96.17
U1509A-29R-5W-36-37	256.50	2.03	0.42	94.40
U1509A-29R-5W-67-68	256.81	1.85	0.21	100.00
U1509A-29R-5W-96-97	257.10	2.32	0.18	70.19
U1509A-29R-5W-126-127	257.40	2.18	0.04	71.81
U1509A-29R-6W-6-7	257.70	2.08	0.13	72.21
U1509A-29R-6W-36-37	258.00	1.94	0.04	72.44
U1509A-29R-6W-66-67	258.30	1.89	0.17	73.36
U1509A-29R-6W-96-97	258.60	1.96	0.19	78.31
U1509A-29R-6W-126-127	258.90	2.00	0.03	69.88
U1509A-29R-7W--6-7	259.20	1.99	0.02	68.92
U1509A-29R-7W-36-37	259.50	2.20	0.17	75.92
U1509A-30R-1W-40-41	260.10	2.27	0.05	76.65
U1509A-30R-1W-70-71	260.40	2.22	-0.01	83.66
U1509A-30R-1W-100-101	260.70	2.16	0.04	52.84
U1509A-30R-1W-130.131	261.00	2.34	0.12	70.59
U1509A-30R-2W-9-10	261.29	2.36	0.23	74.84
U1509A-30R-2W-40-41	261.60	2.38	0.19	74.53
U1509A-30R-2W-70-71	261.90	2.32	0.00	83.44
U1509A-30R-2W-100-101	262.20	2.36	0.14	78.10
U1509A-30R-3W-5-6	262.50	2.35	0.01	67.86
U1509A-30R-3W-35-36	262.80	2.21	-0.11	73.69
U1509A-30R-3W-65-66	263.10	2.15	0.23	71.43
U1509A-30R-3W-96-97	263.41	2.06	-0.06	69.19
U1509A-30R-3W-125-126	263.70	2.19	0.28	79.92
U1509A-30R-4W-5-6	264.00	2.09	0.10	70.04
U1509A-30R-4W-35-36	264.30	2.20	0.04	67.42
U1509A-30R-4W-65-66	264.60	2.45	0.04	70.58
U1509A-30R-4W-95-96	264.90	2.31	0.07	58.42
U1509A-30R-4W-125-126	265.20	2.21	-0.11	64.70
U1509A-30R-5W-3-4	265.48	2.22	0.14	73.08
U1509A-30R-5W-35-36	265.80	2.07	0.25	72.06
U1509A-30R-5W-65-66	266.10	2.08	0.06	69.58
U1509A-30R-5W-95-96	266.40	2.16	0.17	67.66
U1509A-30R-6W-20-21	266.70	2.34	0.09	69.04
U1509A-30R-6W-49-50	266.99	2.41	0.22	67.87
U1509A-30R-CCW-19-20	267.30	2.50	0.15	61.26

Appendix V

Reworked calcareous nannofossils

At Site U1509, the presence of reworked calcareous nannofossils (Figure S4.1), mainly of middle-late Eocene age, is well recorded and considerably increases in the upper part of the section, as previously observed (Sutherland et al. 2019). Reworking, despite being considered a disturbing factor, can provide additional clues on the erosion/transport processes occurred in the area surrounding the investigatedsedimentary basin. The presence of older nannofossils is related to the redeposition during the early Oligocene of middle-late Eocene sediments present in the nearby areas. Images of a representative selection of reworked nannofossils are provided in **Plates S4.1 and 4.2**.

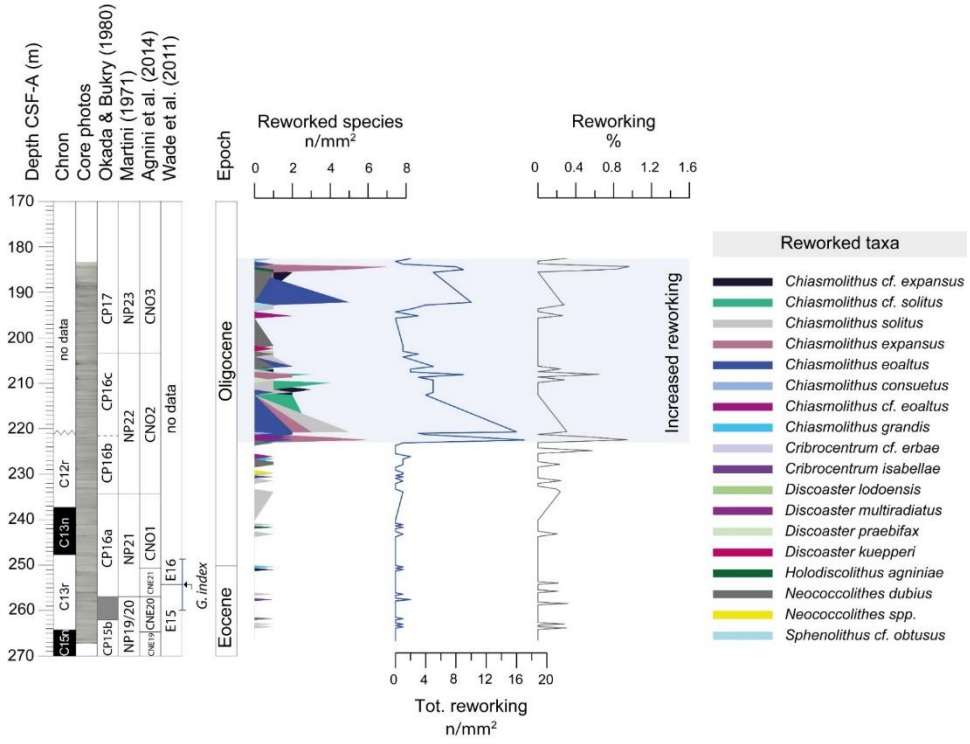

Figure S4.1 Reworked calcareous nannofossil plots (n/mm^2 and %) with the corresponding reworked species reported on the right side.

PLATE S4.1

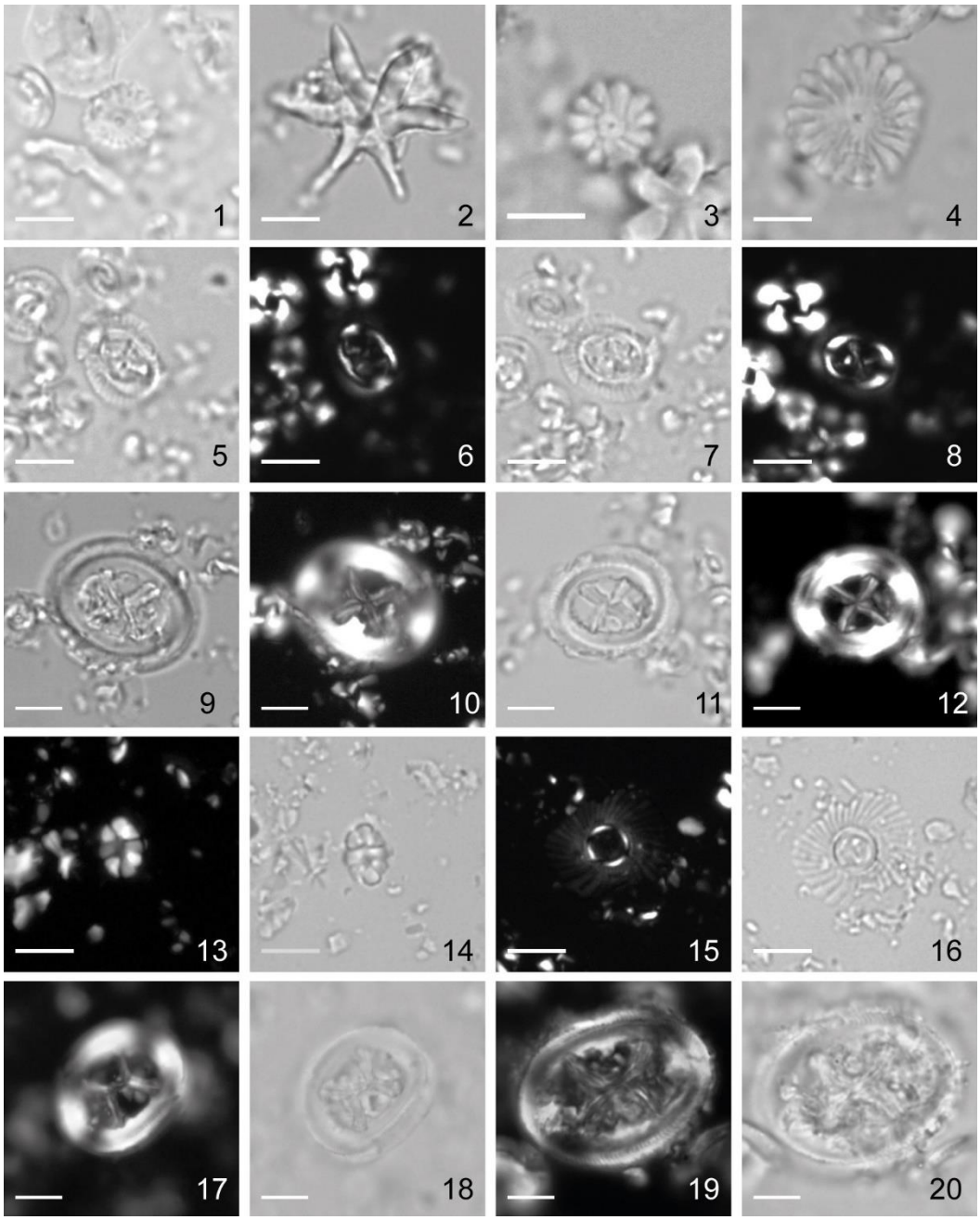

Plate S4.1 LM (magnification 1250x) microphotographs of reworked calcareous nannofossils and other occasional taxa from IODP Site U1509. Scale bar = 5 µm. Photos 1-5, 7, 9, 11, 14, 16, 18,20 are in crossed nicols; photos 6,8,10,12,13,15,17,19 are in parallel light. **1.** *Discoaster praebifax*. Sample U1509A-24R-3W, 42-43 cm. **2.** *Discoaster lodoensis*. Sample U1509A-24R-2W, 14-15 cm. **3.** *Discoaster kuepperi*. Sample U1509A-23R-1W, 100-101 cm. **4.** *Discoaster multiradiatus*. Sample U1509A-26R-5W, 66-67 cm. **5-8.** *Chiasmolithus consuetus*. Sample U1509A-21R-1W, 30-31 cm. **9-12.** *Chiasmolithus* cf. *expansus.* Samples U1509A-21R-1W, 30-31 cm; U1509A-21R-22W, 60-61 cm. **13, 14.** *Holodiscolithus agniniae*. Sample U1509A-21R-CCW, 11-12 cm. **5, 16.** *Pedinocyclus larvalis*. Sample U1509A-29R-2W, 96-97 cm. **17, 18.** *Chiasmolithus expansus*. Sample U1509A-26R-5W, 66-67 cm. **19, 20.** *Chiasmolithus grandis.* Sample U1509A-26R-5W, 122-123 cm.

PLATE S4.2

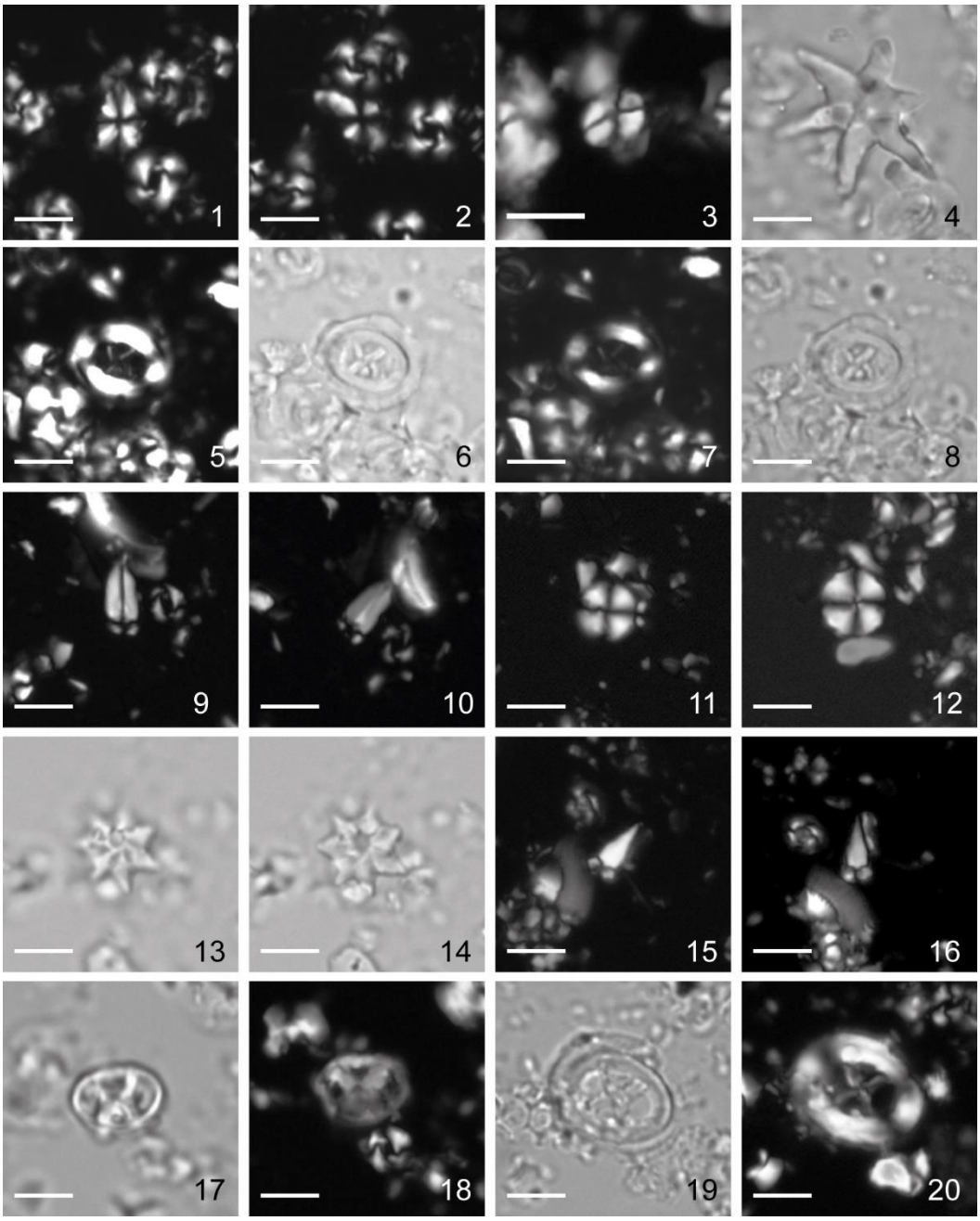

Plate S4.2 LM (magnification 1250x) microphotographs of reworked calcareous nannofossils from IODP Site U1509. Scale bar = 5 µm. Photos 1-3, 5, 7, 9-12, 15,16,18,20 are in crossed nicols; photos 4,6,8,13,14,17,19 are in parallel light. **1, 2.** *Sphenolithus radians* (0°, 45°). Sample U1509A-21R-1W, 30-31 cm. **3.** *Octolithus* spp. Sample U1509A-28R-1W, 100-101 cm. **4.** *Discoaster lodoensis*. Sample U1509-24R-3W, 42-43 cm. **5-8.** *Chiasmolithus solitus*. Sample U1509A-27R-1W, 130-131cm. **9,10.** *Sphenolithus obtusus* (0°, 45°). Sample U1509A-30R-2W, 9-10 cm. **11,12.** *Cyclicargolithus luminis*. Samples U1509A-29R-6W, 96-97 cm; U1509A-30R-3W, 5-6 cm. **13, 14.** *Discoaster saipanensis*. Sample U1509A-22R-1W, 90-91 cm. **15, 16.** *Sphenolithus* cf. *obtusus*. Sample U1509A-22R-1W, 90-91 cm. **17, 18.** *Neococcolithes dubius*. Sample U1509A-26R-8W, 15-16 cm. **19, 20.** *Chiasmolithus* cf. *expansus*. Sample U1509A-22R-1W, 90-91 cm.

Appendix VI. Hole U1411B semi-quantitative data (n/mm^2)

Exp	Site	Hole	Core	Type	Sect	A/W	Top offset (cm)	Bottom offset (cm)	Mean (mbsf)	Preservation	Abundance	*C. subdistichus*	*C. fenestratus*	*C. subdistichus gr.*	*% C. subdistichus gr.*	*D. barbadiensis*	*D. saipanensis*	*E. formosa*	*I. recurvus*	*R. umbilicus* >14um	*S. akropodus* A	*S. akropodus* B
342	U1411	B	11	H	CC		46	54	96.25	P	R	0	0	0	0	0	0	0	0	0	0	0
342	U1411	B	12	H	2	W	30	30	97.70	M	F	0	0	0	0	0	0	0	0	0	0	0
342	U1411	B	12	H	5	W	30	30	102.20	M/G	C	3	0	0	0	0	0	0	0	1	0	0
342	U1411	B	12	H	CC		33	41	105.36	P/M	F/C	1	0	1	0	0	0	0	4	0	0	0
342	U1411	B	13	H	3	W	75	77	109.16	M	C	3	0	3	0	0	0	0	4	1	0	0
342	U1411	B	13	H	CC				115.38	P	F/C	0	0	0	0	0	0	0	2	3	0	0
342	U1411	B	14	H	3	W	75	77	118.66	P	F	3	0	3	1	0	0	0	10	1	0	0
342	U1411	B	14	H	5	W	75	77	121.66	M	F/C	27	3	30	3	0	0	0	4	1	0	1
342	U1411	B	14	H	7	W	30		124.28	M/G	C	73	4	77	2	0	0	0	7	6	0	1
342	U1411	B	15	H	3	W	70		128.01	M	F/C	34	2	36	3	0	0	0	6	12	0	0
342	U1411	B	15	H	CC		66	71	133.58	G	C/A	95	4	99	3	0	0	2	33	10	0	2
342	U1411	B	16	H	1	W	50		134.11	M/G	C	187	16	203	4	0	0	21	40	31	0	0
342	U1411	B	16	H	3	W	150	150	138.10	G	C/A	170	14	184	6	0	0	43	2	45	0	0
342	U1411	B	16	H	6	W	27	27	141.38	M/G	C/A	173	24	197	4	0	0	27	13	35	0	0
342	U1411	B	17	H	3	W	150	150	147.60	G	C/A	148	4	152	5	1	0	34	5	31	0	0
342	U1411	B	17	H	7	A	25	25	152.25	G	C/A	74	0	74	2	0	0	42	28	29	0	0
342	U1411	B	18	H	1	W	90	91	153.51	G	A	42	0	42	1	0	0	17	23	33	0	0
342	U1411	B	18	H	3	W	30	31	155.91	G	C	10	1	11	1	0	0	47	26	31	0	0
342	U1411	B	18	H	4	W	60	61	157.71	G	C/A	21	1	22	1	0	0	27	16	18	0	0
342	U1411	B	18	H	5	W	90	91	159.51	M/G	C/A	10	1	11	1	1	0	29	21	4	0	0
342	U1411	B	18	H	7	W	30	31	161.91	G	C	43	0	43	1	0	0	9	31	17	0	0
342	U1411	B	19	H	1	W	150	150	163.60	M/G	C/A	22	1	23	1	0	0	39	72	23	0	0
342	U1411	B	19	H	3		150	150	166.60	G	C/A	31	0	31	2	0	0	54	31	28	0	0
342	U1411	B	19	H	5	W	103	105	169.14	M/G	C/A	28	0	28	1	0	8	67	31	31	0	0
342	U1411	B	20	H	1	W	40	41	172.01	G	C/A	40	1	41	1	25	12	79	60	30	0	0
342	U1411	B	19	H	CC		67	74	172.38	G	C	5	0	5	1	5	3	83	24	31	0	0
342	U1411	B	19	H	CC	W	74	74	172.41	M/G	C	0	0	0	0	8	4	58	30	24	0	0
342	U1411	B	20	H	4	W	133	133	177.43	M/G	C	2	0	2	0	7	11	27	13	21	0	0
342	U1411	B	21	X	CC		25	33	178.05	G	C	1	0	1	0	24	17	55	11	14	0	0
342	U1411	B	22	X	CC		10	19	187.35	M/G	C	7	0	7	1	13	14	20	21	23	0	0

P= poor
M= moderate
G= good

R= rare
F= few
C= common
A= abundant

S. akropodus	*S. predistentus*	*S. tribulosus*	*C. reticulatum*	*C. isabellae* (>12um)
0	0	0	0	0
0	5	0	0	0
0	13	0	0	0
0	0	1	0	0
0	7	1	0	0
0	0	0	0	0
0	3	0	0	0
1	9	0	0	0
1	8	0	0	0
0	2	0	0	0
2	5	0	0	0
0	2	1	0	0
0	19	1	0	0
0	9	1	0	0
0	3	11	0	0
0	10	6	0	0
0	6	1	0	0
0	1	2	0	0
0	9	0	0	0
0	0	0	0	0
0	5	0	0	0
0	7	3	0	0
0	4	1	0	0
0	0	0	0	0
0	2	3	0	0
0	1	0	0	0
0	0	0	0	0
0	0	0	0	2
0	0	0	15	0
0	0	0	24	4

Appendix VI. Site 1209 semi-quantitative data (n/mm^2)

Site	Hole	Core	Type	Section	Interval	adj-rmcd	*Clausicoccus subdistichus* gr.	% *Clausicoccus subdistichus* gr.	*Discoaster barbadiensis*	*Discoaster saipanensis*	*Ericsonia formosa*	*Ericsonia formosa* (dissolved)	*Isthmolithus recurvus*	*Reticulofenestra umbilicus* >14µm	*S. akropodus*	*Sphenolithus predistentus*	*Sphenolithus predistentus/distentu*	*Sphenolithus intercalaris*	*Sphenolithus* cf. *S. intercalaris*	Reworking
1209	A	13	H	2	87	125.80	0	0	2	1	0	0	0	0	31	102	17	1	0	1
1209	A	13	H	2	112	126.05	0	0	2	1	1	1	0	0	4	120	3	3	2	1
1209	A	13	H	2	137	126.30	1	0	4	1	0	0	0	0	1	43	0	0	1	1
1209	A	13	H	3	12	126.55	0	0	0	0	1	1	0	0	7	284	0	8	1	3
1209	A	13	H	3	37	126.80	0	0	1	0	1	0	0	1	7	204	3	3	0	1
1209	A	13	H	3	87	127.30	0	0	0	0	1	0	0	1	9	137	0	1	0	0
1209	A	13	H	3	137	127.80	2	0	0	0	1	0	0	1	10	126	1	0	0	0
1209	A	13	H	4	37	128.30	0	0	0	0	2	0	2	1	8	132	0	7	0	0
1209	A	13	H	4	87	128.80	0	0	0	0	1	0	1	1	25	203	3	2	0	0
1209	A	13	H	4	137	129.30	1	0	1	0	1	0	0	1	40	145	0	4	0	0
1209	A	13	H	5	12	129.55	4	0	0	1	0	0	0	3	35	243	0	5	1	0
1209	C	3	H	1	115	129.80	1	0	0	0	1	0	0	3	32	141	1	1	0	0
1209	C	3	H	1	140	130.05	1	0	0	0	0	0	0	0	36	266	0	0	3	0
1209	C	3	H	2	20	130.35	1	0	0	0	1	0	0	2	25	138	0	4	0	0
1209	C	3	H	2	45	130.60	5	0	0	0	0	0	0	1	13	150	0	7	5	0
1209	C	3	H	2	70	130.85	7	0	0	0	0	0	0	0	14	90	0	1	0	0
1209	C	3	H	2	95	131.10	41	1	0	0	0	0	0	0	12	216	0	6	5	0
1209	C	3	H	2	120	131.35	23	1	0	0	0	0	1	1	9	171	0	0	0	0
1209	C	3	H	2	145	131.60	22	1	0	0	2	0	0	2	3	251	0	16	3	0
1209	C	3	H	3	25	131.90	18	2	0	0	0	0	0	1	11	115	0	1	0	0
1209	C	3	H	3	50	132.15	36	1	0	0	0	0	0	3	15	190	0	14	2	1
1209	C	3	H	3	75	132.40	28	2	0	0	0	0	0	1	32	162	0	0	0	0
1209	C	3	H	3	95	132.60	25	1	0	0	0	0	0	2	1	121	0	0	0	0
1209	C	3	H	3	110	132.75	63	2	0	0	0	0	0	2	19	245		5	2	0
1209	C	3	H	3	125	132.90	16	1	0	0	2	0	0	2	3	102	0	0	1	0
1209	C	3	H	4	5	133.20	25	2	0	0	33	0	0	1	22	172	0	7	0	0
1209	C	3	H	4	30	133.45	13	2	0	0	15	0	3	0	4	134	0	0	1	0
1209	C	3	H	4	50	133.65	10	1	1	0	20	0	2	0	10	112	0	1	0	0
1209	C	3	H	4	80	133.95	20	1	0	0	33	0	2	1	1	27	0	3	2	0
1209	C	3	H	4	130	134.45	22	3	0	0	34	0	2	3	0	43	0	1	0	0
1209	C	3	H	5	35	135.00	60	3	0	0	109	0	0	7	0	25	0	0	0	1
1209	C	3	H	5	85	135.50	63	1	0	0	140	0	0	4	0	52	0	0	0	0
1209	C	3	H	5	135	136.00	96	4	0	0	103	0	2	2	0	52	0	1	0	1
1209	C	3	H	6	40	136.55	161	8	0	0	65	0	0	7	0	76	0	1	0	0
1209	C	3	H	6	90	137.05	70	1	2	0	67	0	1	32	0	67	0	0	0	0
1209	A	14	H	3	35	137.55	35	1	0	0	66	0	4	11	0	90	0	0	0	0
1209	A	14	H	3	80	138.00	19	1	0	0	72	0	2	17	0	51	0	2	0	0
1209	A	14	H	3	105	138.25	28	1	0	0	86	0	1	13	0	117	0	3	0	0
1209	A	14	H	3	135	138.55	7	0	1	0	46	0	2	3	0	47	0	2	0	0
1209	A	14	H	4	10	138.80	47	1	1	0	32	0	8	21	0	106	0	6	0	1
1209	A	14	H	4	40	139.10	17	2	2	0	62	0	3	7	0	45	0	2	0	0
1209	A	14	H	4	65	139.35	14	0	0	0	57	0	7	7	0	36	0	7	0	0
1209	A	14	H	4	90	139.60	3	1	0	0	32	0	4	8	0	9	0	1	0	0
1209	A	14	H	4	115	139.85	6	0	1	1	71	0	14	4	0	14	0	2	1	0
1209	C	4	H	2	13	140.10	2	0	2	2	75	0	3	5	0	12	0	3	0	0
1209	C	4	H	2	38	140.35	0	0	2	1	57	2	18	50	0	4	0	6	0	0
1209	C	4	H	2	63	140.60	0	0	7	3	62	1	12	72	0	2	0	12	0	2
1209	C	4	H	2	78	140.75	0	0	5	6	38	0	22	24	0	0	0	12	0	0
1209	C	4	H	2	113	141.10	0	0	9	4	35	3	8	14	0	0	0	20	0	1
1209	C	4	H	2	138	141.35	0	0	12	10	20	0	3	35	0	0	0	25	0	0
1209	C	4	H	3	13	141.60	0	0	42	29	8	4	17	136	0	0	0	40	0	8
1209	C	4	H	3	43	141.90	0	0	99	62	19	9	0	77	0	0	0	20	1	0
1209	C	4	H	3	93	142.40	0	0	372	367	6	10	11	6	0	0	0	4	0	2
1209	B	15	H	2	40	142.90	0	0	106	159	10	0	0	5	0	0	0	28	0	0
1209	B	15	H	2	90	143.40	0	0	199	192	7	0	1	2	0	0	0	20	0	1
1209	B	15	H	2	140	143.90	0	0	183	243	1	5	0	1	0	0	0	10	2	0
1209	B	15	H	3	45	144.45	0	0	95	267	0	0	0	0	0	0	0	1	3	0
1209	B	15	H	3	95	144.95	0	0	159	240	0	0	0	0	0	0	0	0	1	0

Appendix VI. Site 1209 bulk C and O stable isotopes and carbonate content (wt, %)

Identifier 1	Depth (adj-rmcd)	$\delta^{13}C$	$\delta^{18}O$	$CaCO_3$ (wt, %)
1209C-3H-2-70	130.85	1.79	0.67	76.6
1209C-3H-2-80	130.95	1.64	0.61	81.1
1209C-3H-2-90	131.05	1.55	0.63	80.4
1209C-3H-2-100	131.15	1.54	0.70	77.7
1209C-3H-2-110	131.25	1.67	0.65	84.4
1209C-3H-2-120	131.35	1.77	0.77	82.7
1209C-3H-2-130	131.45	1.71	0.77	74.9
1209C-3H-2-140	131.55	1.68	0.72	76.7
1209C-3H-3-5	131.70	1.70	0.76	79.6
1209C-3H-3-15	131.80	1.82	0.84	78.6
1209C-3H-3-25	131.90	1.92	0.89	80.2
1209C-3H-3-35	132.00	2.00	0.96	94.4
1209C-3H-3-45	132.10	1.92	0.99	83.8
1209C-3H-3-55	132.20	1.98	0.94	85.5
1209C-3H-3-65	132.30	1.95	1.04	78.6
1209C-3H-3-70	132.35	1.92	0.96	86.0
1209C-3H-3-75	132.40	2.00	1.12	84.2
1209C-3H-3-80	132.45	1.86	0.97	78.4
1209C-3H-3-85	132.50	1.88	0.98	88.6
1209C-3H-3-90	132.55	1.85	0.97	83.4
1209C-3H-3-95	132.60	1.79	0.81	83.4
1209C-3H-3-100	132.65	1.84	0.93	85.0
1209C-3H-3-105	132.70	1.88	0.91	75.3
1209C-3H-3-110	132.75	1.96	0.96	84.0
1209C-3H-3-115	132.80	1.93	0.83	70.1
1209C-3H-3-120	132.85	1.90	0.88	90.1
1209C-3H-3-125	132.90	1.76	0.85	82.4
1209C-3H-3-130	132.95	1.82	0.86	82.6
1209C-3H-3-135	133.00	1.85	0.90	94.2
1209C-3H-3-140	133.05	1.82	0.62	85.1
1209C-3H-3-145	133.10	1.84	0.77	88.6
1209C-3H-4-5	133.20	1.94	0.76	85.0
1209C-3H-4-10	133.25	1.91	0.70	90.3
1209C-3H-4-15	133.30	1.95	0.72	84.7
1209C-3H-4-20	133.35	1.79	0.49	86.9
1209C-3H-4-25	133.40	1.95	0.80	65.6
1209C-3H-4-30	133.45	1.91	0.97	100.0
1209C-3H-4-35	133.50	1.96	0.86	78.2
1209C-3H-4-40	133.55	1.93	0.77	76.3
1209C-3H-4-45	133.60	1.91	0.71	84.4
1209C-3H-4-50	133.65	1.86	0.74	82.6
1209C-3H-4-55	133.70	1.89	0.88	93.3
1209C-3H-4-60	133.75	1.99	0.90	91.2
1209C-3H-4-65	133.80	2.00	0.70	86.4
1209C-3H-4-70	133.85	1.99	0.65	77.4

1209C-3H-4-75	133.90	1.86	0.71	75.5
1209C-3H-4-80	133.95	1.95	0.70	82.3
1209C-3H-4-85	134.00	1.97	0.71	84.3
1209C-3H-4-90	134.05	1.92	0.79	76.0
1209C-3H-4-95	134.10	1.95	0.72	76.2
1209C-3H-4-100	134.15	1.98	0.79	82.5
1209C-3H-4-105	134.20	1.92		61.7
1209C-3H-4-110	134.25	2.00	0.81	78.2
1209C-3H-4-115	134.30	2.08	0.93	68.8
1209C-3H-4-120	134.35	2.08	0.91	65.4
1209C-3H-4-125	134.40	2.15	0.84	81.9
1209C-3H-4-130	134.45	2.15	0.77	83.5
1209C-3H-4-135	134.50	2.20	0.80	77.1
1209C-3H-4-140	134.55	2.17	0.83	80.3
1209C-3H-4-145	134.60	2.18	0.81	68.3
1209C-3H-5-5	134.70	2.12	0.76	81.1
1209C-3H-5-10	134.75	2.19	0.75	78.8
1209C-3H-5-15	134.80	2.11	0.79	85.8
1209C-3H-5-20	134.85	2.14	0.82	82.4
1209C-3H-5-25	134.90	2.04	0.83	85.0
1209C-3H-5-30	134.95	2.12	1.01	74.3
1209C-3H-5-35	135.00	2.14	1.05	81.7
1209C-3H-5-40	135.05	2.07	1.04	79.4
1209C-3H-5-45	135.10	2.03	1.11	81.8
1209C-3H-5-50	135.15	2.10	0.93	84.6
1209C-3H-5-55	135.20	2.12	1.22	83.1
1209C-3H-5-60	135.25	2.13	1.17	83.4
1209C-3H-5-65	135.30	2.12	1.05	83.0
1209C-3H-5-70	135.35	2.11	1.02	76.8
1209C-3H-5-75	135.40	2.08	1.13	81.3
1209C-3H-5-80	135.45	2.11	1.02	75.1
1209C-3H-5-85	135.50	2.17	1.10	72.8
1209C-3H-5-90	135.55	2.20	1.13	90.9
1209C-3H-5-95	135.60	2.26	1.14	80.4
1209C-3H-5-100	135.65	2.20	0.84	65.2
1209C-3H-5-105	135.70	2.12	1.00	81.8
1209C-3H-5-110	135.75	2.08	0.88	80.2
1209C-3H-5-115	135.80	2.11	0.92	81.0
1209C-3H-5-120	135.85	2.19	0.89	80.7
1209C-3H-5-125	135.90	2.27	0.85	84.2
1209C-3H-5-130	135.95	2.28	0.98	81.9
1209C-3H-5-135	136.00	2.19	0.82	95.0
1209C-3H-5-140	136.05	2.26	0.84	91.9
1209C-3H-5-145	136.10	2.23	0.96	80.9
1209C-3H-6-10	136.20	2.13	0.84	85.8
1209C-3H-6-15	136.25	2.13	0.85	78.1
1209C-3H-6-20	136.30	2.14	0.79	87.5
1209C-3H-6-25	136.35	2.22	0.79	93.3
1209C-3H-6-30	136.40	2.31	0.81	75.8
1209C-3H-6-35	136.45	2.38	0.91	64.8

1209C-3H-6-40	136.50	2.34	0.84	61.7
1209C-3H-6-45	136.55	2.30	0.84	81.0
1209C-3H-6-5	136.60	2.13	0.83	83.3
1209C-3H-6-50	136.65	2.26	0.79	62.5
1209C-3H-6-55	136.70	2.13	0.75	78.4
1209C-3H-6-60	136.75	2.09	0.77	80.6
1209C-3H-6-65	136.80	2.08	0.69	80.1
1209C-3H-6-70	136.85	1.90		77.6
1209C-3H-6-75	136.90	2.07	0.54	75.9
1209C-3H-6-80	136.95	2.01	0.50	79.1
1209C-3H-6-85	137.00	2.01	0.52	83.7
1209C-3H-6-90	137.05	1.99	0.46	82.9
1209C-3H-6-95	137.10	1.97	0.55	72.6
1209C-3H-6-100	137.15	1.96	0.40	84.4
1209C-3H-6-105	137.20	1.97	0.47	77.2
1209A-14H-3-5	137.25	1.95	0.47	77.7
1209A-14H-3-10	137.30	1.94	0.44	75.3
1209A-14H-3-15	137.35	1.88	0.33	78.6
1209A-14H-3-20	137.40	1.84	0.20	65.7
1209A-14H-3-25	137.45	1.87	0.43	75.0
1209A-14H-3-30	137.50	1.88	0.41	79.0
1209A-14H-3-35	137.55	1.84	0.37	81.2
1209A-14H-3-40	137.60	1.82	0.26	71.1
1209A-14H-3-45	137.65	1.84	0.36	85.0
1209A-14H-3-50	137.70	1.92	0.24	79.4
1209A-14H-3-55	137.75	1.91	0.25	78.4
1209A-14H-3-60	137.80	1.98	0.31	77.5
1209A-14H-3-65	137.85	1.90	0.09	65.2
1209A-14H-3-70	137.90	1.89	0.24	78.9
1209A-14H-3-75	137.95	1.90	0.29	78.5
1209A-14H-3-80	138.00	1.89	0.25	78.4
1209A-14H-3-90	138.10	1.91	0.42	78.9
1209A-14H-3-95	138.15	1.82	0.32	77.2
1209A-14H-3-100	138.20	1.86	0.32	78.0
1209A-14H-3-105	138.25	1.88	0.42	76.9
1209A-14H-3-110	138.30	1.80	0.38	78.6
1209A-14H-3-115	138.35	1.82	0.45	76.2
1209A-14H-3-120	138.40	1.79	0.47	78.5
1209A-14H-3-125	138.45	1.76	0.66	83.9
1209A-14H-3-130	138.50	1.67	0.42	69.4
1209A-14H-3-135	138.55	1.68	0.52	77.0
1209A-14H-3-140	138.60	1.64	0.57	87.5
1209A-14H-3-145	138.65	1.69	0.57	77.2
1209A-14H-4-5	138.75	1.74	0.38	78.1
1209A-14H-4-10	138.80	1.90	0.46	76.1
1209A-14H-4-15	138.85	1.77	0.51	79.2
1209A-14H-4-20	138.90	1.79	0.44	72.4
1209A-14H-4-25	138.95	1.73	0.43	76.5
1209A-14H-4-30	139.00	1.75	0.38	66.7
1209A-14H-4-35	139.05	1.74	0.40	72.3

1209A-14H-4-40	139.10	1.72	0.42	75.5
1209A-14H-4-45	139.15	1.71	0.39	74.7
1209A-14H-4-50	139.20	1.78	0.53	73.6
1209A-14H-4-55	139.25	1.78	0.62	72.2
1209A-14H-4-60	139.30	1.79	0.55	74.6
1209A-14H-4-65	139.35	1.76	0.60	69.2
1209A-14H-4-70	139.40	1.73	0.48	73.8
1209A-14H-4-75	139.45	1.77	0.59	72.1
1209A-14H-4-80	139.50	1.79	0.66	74.2
1209A-14H-4-85	139.55	1.75	0.57	75.6
1209A-14H-4-90	139.60	1.76	0.58	77.6
1209A-14H-4-95	139.65	1.82	0.67	76.5
1209A-14H-4-100	139.70	1.73	0.56	78.0
1209A-14H-4-105	139.75	1.75	0.44	54.0
1209A-14H-4-110	139.80	1.71	0.32	80.6
1209A-14H-4-115	139.85	1.66	0.36	51.0
1209A-14H-4-120	139.90	1.74	0.42	79.6
1209A-14H-4-125	139.95	1.73	0.40	57.5
1209A-14H-4-130	140.00	1.69	0.31	86.5
1209A-14H-4-135	140.05	1.66	0.41	85.6
1209C-4H-2-13	140.10	1.55	0.14	53.3
1209C-4H-2-18	140.15	1.48	0.13	88.1
1209C-4H-2-23	140.20	1.46	0.16	86.6
1209C-4H-2-33	140.30	1.44	0.14	78.8
1209C-4H-2-38	140.35	1.42	-0.04	59.2
1209C-4H-2-48	140.45	1.41	0.23	77.0
1209C-4H-2-53	140.50	1.37	-0.02	64.5
1209C-4H-2-58	140.55	1.34	0.07	87.6
1209C-4H-2-63	140.60	1.23	-0.11	64.4
1209C-4H-2-73	140.70	1.10	-0.11	82.0
1209C-4H-2-78	140.75	0.98	-0.11	69.8
1209C-4H-2-83	140.80	1.00	-0.02	72.0
1209C-4H-2-93	140.90	0.99	-0.02	77.9
1209C-4H-2-98	140.95	1.03	-0.05	77.5
1209C-4H-2-103	141.00	1.03	-0.16	84.2
1209C-4H-2-113	141.10	1.05	-0.14	74.1
1209C-4H-2-118	141.15	1.18	-0.18	78.3
1209C-4H-2-123	141.20	1.20	-0.05	82.6
1209C-4H-2-128	141.25	1.27	-0.13	40.9
1209C-4H-2-133	141.30	1.28	-0.28	73.3
1209C-4H-2-138	141.35	1.32	-0.23	73.8
1209C-4H-2-143	141.40	1.39	-0.28	60.9
1209C-4H-3-3	141.50	1.52	-0.20	69.9
1209C-4H-3-8	141.55	1.62	-0.27	45.5
1209C-4H-3-13	141.60	1.64	-0.30	69.0
1209C-4H-3-18	141.65	1.66	-0.30	68.8
1209C-4H-3-23	141.70	1.68	-0.54	43.3
1209C-4H-3-28	141.75	1.66	-0.48	69.8
1209C-4H-3-33	141.80	1.72	-0.20	74.3
1209C-4H-3-38	141.85	1.69	-0.32	72.6

1209C-4H-3-43	141.90	1.71	-0.43	74.0
1209C-4H-3-48	141.95	2.11	0.18	72.6
1209C-4H-3-53	142.00	2.08	0.30	79.5
1209C-4H-3-58	142.05	2.28	0.35	70.7
1209C-4H-3-63	142.10	2.35	0.40	77.7
1209C-4H-3-68	142.15	2.50	0.39	73.2
1209C-4H-3-73	142.20	2.55	0.77	73.5
1209C-4H-3-78	142.25	2.50	0.82	61.1
1209C-4H-3-83	142.30	2.42	0.60	75.6
1209C-4H-3-88	142.35	2.39	0.63	62.1
1209C-4H-3-93	142.40	2.31	0.73	80.1

Appendix VII. Site 1209 Morphometric data (*C. subdistichus* gr.)

Sample	Depth (adj-rmcd)	Mean Length (L)	Mean Width (W)	± Error (L)	± Error (W)	St. dev. Length (σ)	N	Min Length (µm)	Max Length (µm)
1209C-4H-2, 13	140.10	5.54	4.39	0.04	0.04	0.18	6	5.28	5.71
1209A-14H-4, 90	139.60	5.80	4.66	0.05	0.03	0.46	20	4.69	6.64
1209A-14H-4, 40	139.10	5.93	4.68	0.04	0.04	0.48	50	5.01	6.96
1209A-14H-3, 135	138.55	5.76	4.52	0.04	0.04	0.41	41	5.02	6.77
1209A-14H-3, 80	138.00	6.54	5.25	0.03	0.03	0.50	50	5.13	7.63
1209A-14H-3, 35	137.55	6.34	5.12	0.04	0.04	0.48	50	5.14	7.31
1209C-3H-6, 90	137.05	6.41	5.20	0.03	0.03	0.46	50	5.35	7.75
1209C-3H-6, 40	136.55	6.38	5.25	0.03	0.03	0.50	50	5.43	7.28
1209C-3H-5, 135	136.00	6.29	5.13	0.03	0.03	0.46	50	5.15	7.51
1209C-3H-5, 85	135.50	6.46	5.21	0.03	0.03	0.37	50	5.67	7.64
1209C-3H-5, 35	135.00	6.26	5.11	0.04	0.03	0.46	50	5.52	7.31
1209C-3H-4, 130	134.45	6.34	5.16	0.03	0.03	0.57	50	4.52	7.62
1209C-3H-4, 80	133.95	6.21	5.04	0.03	0.03	0.56	50	5.20	7.66
1209C-3H-4, 50	133.65	6.18	5.01	0.03	0.03	0.45	50	5.18	7.17
1209C-3H-4, 30	133.45	6.29	5.11	0.03	0.03	0.44	50	5.38	7.28
1209C-3H-3, 125	132.90	6.37	5.15	0.03	0.03	0.56	50	5.27	7.68
1209C-3H-3, 95	132.60	6.62	5.41	0.03	0.03	0.59	50	5.37	7.65
1209C-3H-3, 75	132.40	6.50	5.28	0.03	0.03	0.48	50	5.28	7.71
1209C-3H-3, 25	131.90	6.45	5.28	0.03	0.03	0.51	50	4.92	7.68
1209C-3H-2, 120	131.35	6.40	5.18	0.03	0.03	0.49	50	5.57	7.37
1209C-3H-2, 70	130.85	6.77	5.53	0.03	0.03	0.52	50	5.73	7.90
1209C-3H-2, 20	130.35	6.10	5.02	0.03	0.04	0.59	6	5.08	6.78
1209C-3H-1, 115	129.80	6.28	5.06	0.04	0.02	0.46	19	5.57	7.16
1209A-13H-4, 137	129.30	6.46	5.16	0.03	0.03	0.71	10	5.07	7.50

N = number of specimens measured per sample

Appendix VII. Hole U1411B Morphometric data (*C. subdistichus* gr.)

Sample	Depth (mbsf)	Mean Length (L)	Mean Width (W)	± Error (L)	± Error (W)	St. dev. Length (σ)	N	Min Length (µm)	Max Length (µm)
1411B-19H-CC, 67-74	172.41	5.31	4.38	0.03	0.03	0.50	30	4.26	6.27
1411B-20H-1W, 40-41	172.01	5.30	4.24	0.03	0.03	0.35	30	4.52	6.15
1411B-19H-7W, 24	171.35	5.28	4.33	0.03	0.02	0.43	30	4.24	6.34
1411B-19H-5W, 103-105	169.14	5.50	4.44	0.02	0.02	0.44	30	4.29	6.20
1411B-19H-3W,150-150	166.60	5.29	4.38	0.03	0.03	0.35	30	4.58	6.00
1411B-19H-1W, 150-150	163.60	5.73	4.73	0.03	0.03	0.48	30	4.86	6.70
1411B-18H-7W, 30-31	161.91	6.14	5.04	0.03	0.03	0.54	30	4.89	6.85
1411B-18H-6W, 60-61	160.71	5.46	4.56	0.03	0.03	0.35	30	4.58	6.13
1411B-18H-5W, 90-91	159.51	5.23	4.15	0.03	0.03	0.68	21	4.35	7.09
1411B-18H-4W, 60-61	157.71	5.14	4.17	0.03	0.03	0.51	30	4.23	6.35
1411B-18H-3W, 30-31	155.91	5.24	4.25	0.03	0.03	0.45	30	4.30	6.13
1411B-18H-1W, 90-91	153.51	5.60	4.56	0.03	0.03	0.40	30	4.77	6.28
1411B-17H-7A, 25-25	152.25	5.45	4.42	0.03	0.04	0.54	30	4.29	6.75
1411B-17H-5W, 25	149.36	5.77	4.75	0.03	0.03	0.68	30	4.32	6.93
1411B-17H-3W, 150-150	147.60	5.97	4.94	0.03	0.03	0.45	30	5.11	6.95
1411B-17H-3W, 25	146.36	6.18	5.10	0.03	0.03	0.41	30	5.18	6.83
1411B-16H-6W, 27-27	141.38	6.26	5.19	0.03	0.03	0.43	30	5.65	7.16
1411B-16H-3W, 150-150	138.10	6.07	5.00	0.03	0.04	0.35	30	5.20	6.66
1411B-16H-1W, 50	134.11	6.06	4.98	0.03	0.04	0.41	30	5.36	6.93
1411B-15H-3W, 70	128.01	6.28	5.27	0.04	0.04	0.39	30	5.52	7.09
1411B-14H-7W, 30	124.28	6.26	5.25	0.03	0.03	0.46	30	5.15	7.20

N = number of specimens measured per sample

Appendix VII. Site 1509 Morphometric data (*C. subdistichus* gr.)

Sample	Depth (CSF-a, m)	Mean Length (L)	Mean width (W)	± Error (L)	± Error (W)	St. dev. (L)	N	Min length (µm)	Max length (µm)
1509A-30R-5W, 65-66	266.11	4.96	3.85	0.06	0.06	0.43	30	4.06	5.63
1509A-30R-4W, 95-96	264.96	4.71	3.63	0.06	0.08	0.56	30	3.60	5.95
1509A-30R-3W, 125-126	263.71	4.64	3.55	0.04	0.04	0.52	20	3.86	5.53
1509A-30R-3W, 5-6	262.51	5.44	4.28	0.07	0.04	0.43	30	4.69	5.99
1509A-30R-2W, 9-10	261.30	5.05	3.97	0.07	0.08	0.70	30	4.19	6.83
1509A-30R-1W, 40-41	260.11	5.45	4.37	0.06	0.07	0.64	30	3.91	6.38
1509A-29R-6W, 96-97	258.61	5.13	4.07	0.05	0.07	0.56	30	3.97	6.11
1509A-29R-5W, 126-127	257.41	4.97	3.97	0.06	0.08	0.52	20	3.89	5.95
1509A-29R-5W, 6-7	256.21	4.84	3.88	0.05	0.06	0.41	30	3.86	5.83
1509A-29R-4W, 36-37	255.01	5.91	4.80	0.06	0.06	0.45	30	4.81	6.63
1509A-29R-3W, 66-67	253.81	5.35	4.28	0.05	0.07	0.42	30	4.63	6.26
1509A-29R-2W, 96-97	252.61	5.47	4.40	0.04	0.05	0.37	30	4.76	6.18
1509A-29R-1W, 130-131	251.41	6.04	4.82	0.04	0.05	0.55	30	5.06	7.25
1509A-29R-1W, 9-10	250.20	5.90	4.79	0.05	0.05	0.48	30	4.99	6.76
1509A-28R-5W, 109-110	247.50	6.16	5.11	0.04	0.05	0.46	30	5.20	6.86
1509A-28R-4W, 140-141	246.31	6.40	5.26	0.04	0.04	0.41	30	5.66	7.31
1509A-28R-4W, 20-21	245.11	6.48	5.37	0.03	0.04	0.51	30	5.45	7.57
1509A-28R-3W, 40-41	243.91	6.23	5.14	0.04	0.05	0.47	30	5.16	7.16
1509A-28R-2W, 70-71	242.71	6.19	4.98	0.05	0.03	0.46	30	5.09	6.94
1509A-28R-1W, 100-101	241.51	6.27	5.01	0.04	0.07	0.56	30	5.13	7.27
1509A-27R-3W, 70-71	234.61	6.41	5.24	0.04	0.04	0.53	30	5.32	7.57
1509A-27R-2W, 100-101	233.41	6.50	5.28	0.04	0.05	0.39	30	5.82	7.53
1509A-27R-1W, 130-131	232.21	6.59	5.37	0.04	0.04	0.54	30	5.47	7.49
1509A-27R-1W, 9-10	231.00	6.55	5.33	0.04	0.04	0.47	30	5.34	7.35
1509A-26R-7W, 64-65	229.83	6.75	5.51	0.04	0.04	0.53	30	5.78	7.57
1509A-26R-6W, 92-93	228.61	6.67	5.48	0.03	0.04	0.52	30	5.57	7.83
1509A-26R-5W, 122-123	227.41	6.81	5.69	0.04	0.04	0.61	30	5.59	7.93
1509A-26R-5W, 2-3	226.21	6.78	5.57	0.04	0.03	0.51	30	5.62	7.74
1509A-26R-4W, 32-33	225.01	6.91	5.73	0.03	0.03	0.56	30	5.74	7.75
1509A-26R-3W, 64-65	223.83	6.55	5.44	0.03	0.03	0.61	30	5.20	7.71
1509A-26R-2W, 92-93	222.61	6.86	5.74	0.04	0.04	0.56	30	5.69	7.94
1509A-26R-1W, 11-12	221.42	6.57	5.42	0.03	0.05	0.52	30	5.09	7.36
1509A-25R-1W, 100-101	212.71	6.38	5.25	0.04	0.04	0.61	30	4.95	7.60
1509A-24R-3W, 102-103	210.61	6.25	5.06	0.03	0.04	0.67	30	4.62	7.46
1509A-24R-2W, 132-133	209.41	6.32	5.19	0.04	0.03	0.64	30	5.21	7.59

N = number of specimens measured per sample

Appendix VII. Hole 756C Morphometric data (*C. subdistichus* gr.)

Sample	Depth (mbsf)	Mean Length (L)	Mean Width (w)	± Error (L)	± Error (W)	St. dev. Length (σ)	N	Min Length (µm)	Max Length (µm)
756C-7X-2W, 99-101	132.29	5.67	4.50	0.04	0.05	0.52	30	4.46	6.73
756C-7X-2W, 60-62	131.90	5.75	4.70	0.03	0.04	0.49	30	5.01	6.54
756C-7X-2W, 0-2	131.30	5.66	4.50	0.04	0.05	0.54	30	4.70	6.46
756C-7X-1W, 60-62	130.40	5.72	4.66	0.04	0.06	0.49	30	4.77	6.80
756C-6X-5W, 90-92	127.10	5.67	4.54	0.05	0.05	0.46	30	4.97	6.72
756C-6X-5W, 50-52	126.70	5.99	4.82	0.05	0.06	0.52	30	4.71	6.79
756C-6X- 4W, 140-142	126.10	5.58	4.42	0.04	0.04	0.63	20	4.03	6.74
756C-6X-4W, 90-92	125.60	5.68	4.54	0.06	0.06	0.38	30	5.11	6.61
756C-6X- 4W, 41.5-43.5	125.12	5.68	4.43	0.05	0.05	0.49	30	4.41	6.48
756C-6X-3W, 129.5-131.5	124.50	6.36	5.12	0.05	0.06	0.60	30	4.99	7.41
756C-6X-3W, 90-94	124.10	6.10	4.87	0.05	0.07	0.52	30	5.28	7.06
756C-6X-3W, 50-52	123.70	6.16	4.94	0.04	0.06	0.47	30	5.30	7.26
756C-6X-3W, 10-12	123.30	6.38	5.25	0.07	0.05	0.52	30	5.54	7.56
756C-6X-2W, 110-112	122.80	6.48	5.35	0.07	0.06	0.50	30	5.28	7.20
756C-6X-2W, 71.5-73.5	122.42	6.50	5.23	0.06	0.06	0.64	30	5.52	8.04
756C-6X-2W, 40-42	122.10	6.38	5.31	0.06	0.08	0.56	30	5.45	7.58
756C-6X-2W, 28.5-30.5	121.99	6.32	5.16	0.07	0.08	0.55	30	5.48	7.48
756C-6X-1W, 130-132	121.50	6.56	5.35	0.06	0.07	0.60	30	5.48	7.64
756C-6X-1W, 90-92	121.10	6.62	5.47	0.05	0.06	0.47	30	5.49	7.52
756C-6X-1W, 50-52	120.70	6.57	5.36	0.05	0.06	0.56	30	5.66	7.67
756C-6X-1W, 10-12	120.30	6.50	5.25	0.05	0.06	0.48	30	5.48	7.50
756C-5X-8W, 79-81	117.90	6.83	5.70	0.04	0.05	0.50	30	5.47	7.74
756C-5X-8W, 40-42	117.51	7.15	5.83	0.04	0.09	0.47	30	6.01	8.36
756C-5X-8W, 20-22	117.31	6.48	5.20	0.07	0.07	0.85	30	5.11	7.84
756C-5X-8W, 0-2	117.11	6.85	5.73	0.05	0.08	0.65	20	5.79	8.39
756C-5X-7W, 120-122	116.81	6.97	5.77	0.04	0.04	0.61	20	5.63	6.61
756C-5X-7W, 79-81	116.40	6.64	5.45	0.04	0.04	0.58	20	5.63	7.56
756C-5X-7W, 40-42	116.01	7.08	5.86	0.03	0.04	0.60	30	5.75	8.43

N = number of specimens measured per sample

Enhanced primary productivity and carbonate oversaturation across the Eocene Oligocene Transition: a global perspective

Taxonomy notes

Order COCCOLITHALES Haeckel, 1894 emend. Young and Bown, 1997

Family COCCOLITHACEAE Poche, 1913 emend. Young and Bown, 1997

Genus *Clausicoccus* Prins 1979

Clausicoccus subdistichus (Roth & Hay in Hay et al 1967) Prins 1979.

Remarks: small to medium elliptical species with a narrow central area spanned by a disjoint plate with perforations that are only clearly visible in SEM.

Basionym: *Ellipsolithus subdistichus* Roth & Hay *in* Hay et al., 1967

Junior synonym: *Clausicoccus obrutus*

Other synonims:

Clausicoccus bireticulata (Roth, 1970) Prins 1979 (= *Ericsonia bireticulata*) - distinguished by Roth on basis of having fine grills within the pores but this is a typical feature of well-preserved *Clausicoccus*

Ericsonia obruta, Perch-Nielsen 1971

Ericsonia subdisticha Roth, in Baumann & Roth 1969

Clausicoccus fenestratus (Deflandre & Fert 1954) Prins 1979

Remarks: medium sized elliptical species with a wider central area spanned by perforations visible in LM.

In this work we use *Clausicoccus subdistichus* gr., an informal taxonomic group that includes*C. subdistichus* and *C. fenestratus*.

Paleoproductivity proxies

There are several lines of evidence for enhanced productivity and export production based on a variety of proxies. These include the diversification of diatoms (Falkowski et al. 2004, Finkel 2007), the increase in the biogenic opal accumulation rates (Salamy and Zachos 1999), the increase in the benthic foraminiferal accumulation rates (BFAR) (Coxall and Wilson 2011), the increase in marine micro- and macro- fossil accumulation rates (Diester-Haass 1995, Diester-Haass and Zahn 1996, 2001, Diester-Haass and Zachos 2003), the Ba excess (Anderson and Delaney 2005), the barium-based proxies i.e. high Ba/Ti ratios (Latimer and Filippelli 2002), the Os isotopes (Ravizza and Paquay 2008). Other studies, instead, find no evidence for increased productivity in equatorial regions (Nilsen et al. 2003, Schumacher and Lazarus 2004) and in some case document a decrease (Griffith et al. 2010, Erhardt et al. 2013) suggesting variation in regional circulation and site-specific productivity responses.

Abundances and biometry

A minimum of 300 specimens per slide were counted to obtain the relative abundance (%) of *C. subdistichus* gr.. Semiquantitative countings on *C. subdistichus* gr.were performed in to obtain the number of specimes a prefixed area of 1 mm^2 (Backman and Shackleton 1983). Biometric analyses were performed on a total of 3453 entire placoliths at ODP Site 756 (28 samples, 800 specimens), IODP Site U1509 (35 samples, 1030 specimens), ODP Site 1209 (24 samples, 1002 specimens), IODP Site U1411 (21 samples, 621 specimens), respectively. Statistical mean, median, maximum and minimum values, standard deviation, the error of measurements (approximately ± 0.05 µm) and 95% confidence interval have been calculated for each sample.

Carbonate content and bulk stable isotopes

Bulk oxygen and carbon isotopes from the Pacific and Indian oceans show similar trends (Figure 6.2E, F), and are consistent with the global signatures of the reference sections for this interval, with remarkably similar $\delta^{18}O$ and $\delta^{13}C$ mean values (Site U1509 $\delta^{18}O$= 0.41±0.21‰(SD), $\delta^{13}C$= 2.04±0.24‰; Site 1209 $\delta^{18}O$ = 0.56±0.38 ‰, $\delta^{13}C$= 1.87±0.30‰; Site 756 $\delta^{18}O$= 0.73±0.29‰, $\delta^{13}C$= 1.55±0.22‰). Instead, the carbonate content (weight, %) varies significantly among the study sites, as reported in Figure S6.1.

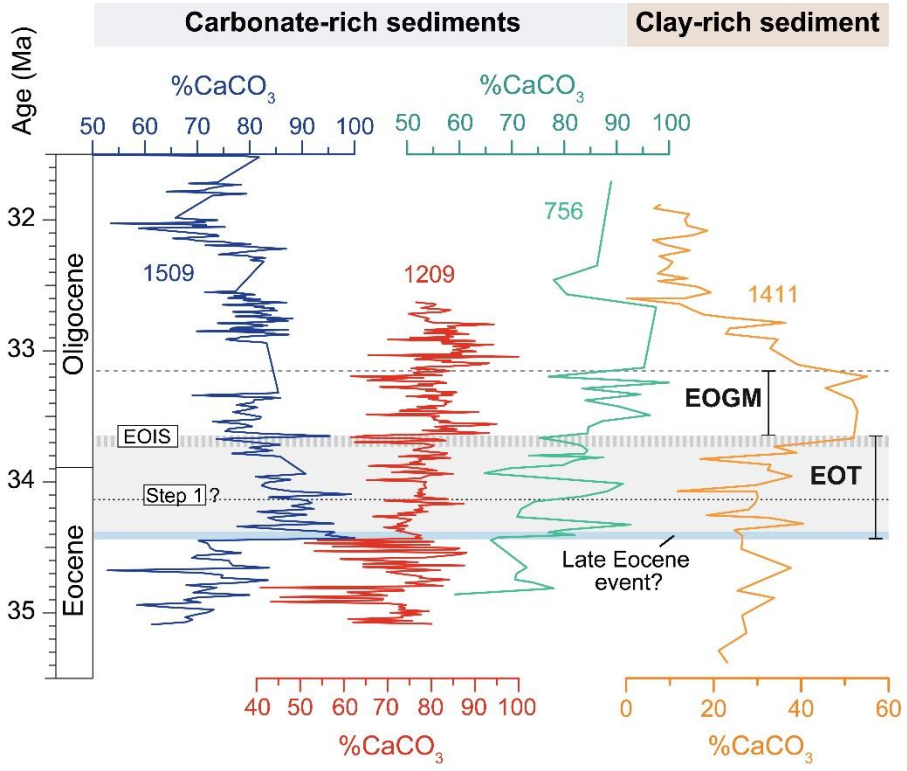

Figure S6.1 Carbonate content (CaCO3, %) from bulk sediments at Site U1509, Site 756, Site 1209 (see Chapters 2 and 4) and at Site U1411 (from Norris et al. 2014). Age models for the study sites are provided in previously published records (Chapters 2, 3, and 5).

Size increase

The morphometric analysis carried out at the four study sites is synthesized as a scatter plot (Figure S6.2) of length vs width, which reveals a progressive increase in size trough the main phases of the E-O transition (PRE-EOT, EOT, EOGM and Oligocene) associated with a gradual increase in the circularity of the placoliths, documented at all the studied sites (Site U1509, Site U1411, Site 756 and Site1209). This dataset is consistent with the coccolith size-rules documented by Henderiks (2008).

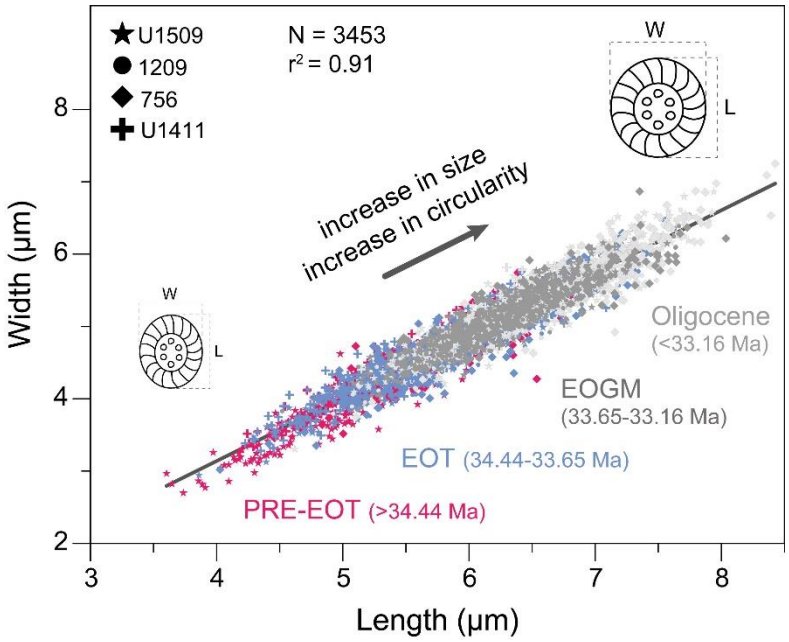

Figure S6.2 Scatter plot of length versus width of placoliths ascribed to *C. subdistichus* gr.. A remarkable increase in size is documented starting from the PRE-EOT (pink), during the EOT (light blue) and up to the EOGM (grey) and Oligocene (light grey). The solid black line is the regression line (coefficient r^2= 0.91). The size changes include also an increased circularity trough time at all the studied sites.

Age models

Age models presented in this work are calibrated to GTS12 (GTS2012) (Gradstein et al. 2012). For ODP Site 756 we use an integrated age model based on plankton biostratigraphic (including calcareous nannofossils and the extinction of planktonic foraminifer *Hantkenina*) and oxygen stable isotope events. IODP Site U1509 and ODP 1209 chronologies are based on nannofossils and oxygen stable isotopes.

IODP Site U1411, is based on nannofossil biostratigraphic events with additional control tie-points provided by magnetostratigraphy (Norris et al. 2014).

Frequency histograms

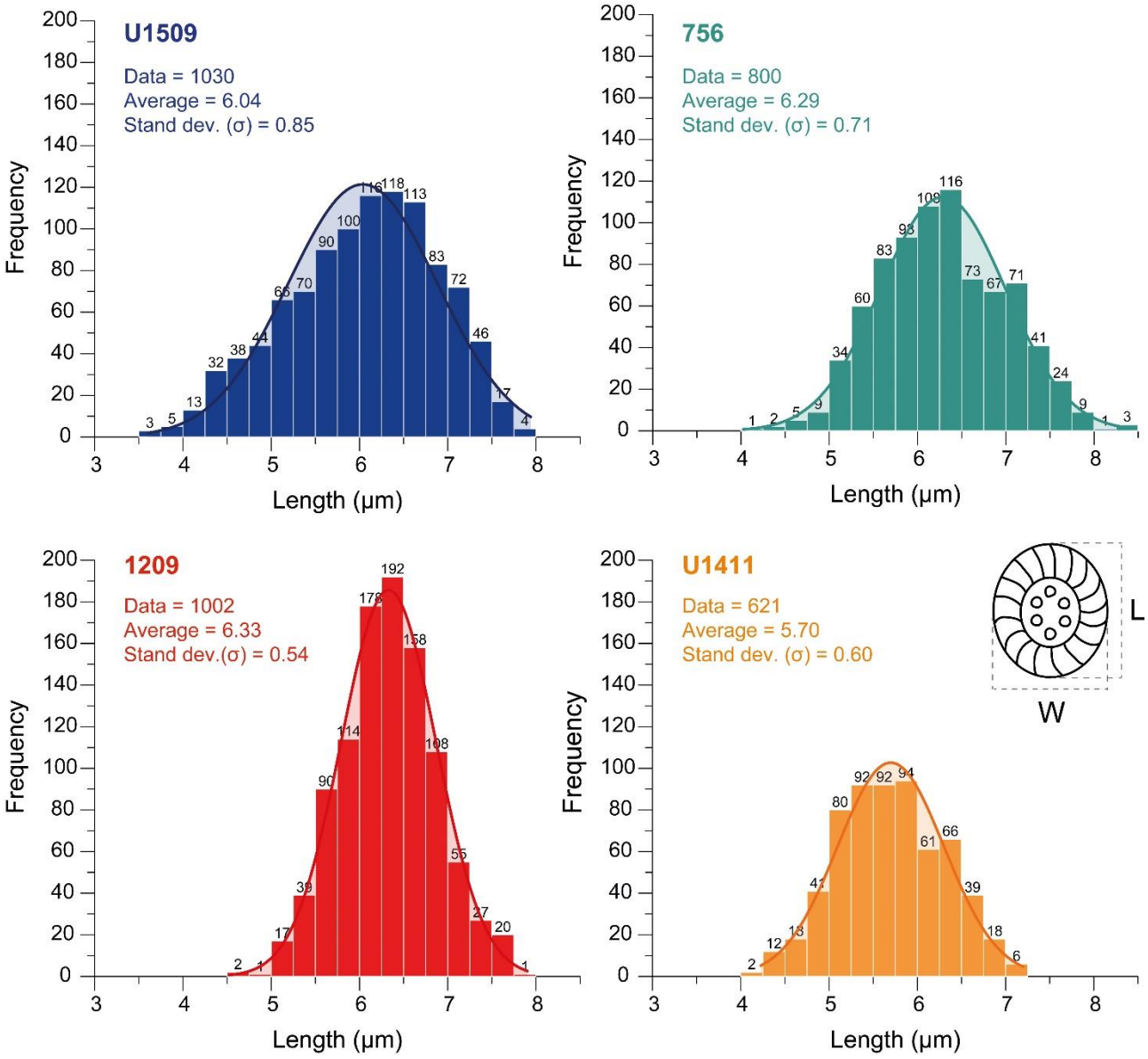

Figure S6.3 Frequency histograms of placolith length documented at Site U1509, Site 756, Site 1209, and Site U1411.

Plate S6.1. LM images of *Clausicoccus subdistichus* taken at Sites 756, 1209, U1411 and U1509. Photos are in crossed nicols and parallel light. Scale bar 2 µm. **1-4.** Sample 756C-7X-2W, 60-62. **5-12.** Sample 756C-5X-8W, 79-81. **13-18.** Sample 1209C-3H-4, 80. **19-20.** Sample 1209C-3H-4, 130. **21-22.** Sample 1209C-3H-5, 35. **23-24.** Sample 1209C-3H-5, 85. **25-26.** Sample 1411B-16H-1W, 50. **27-28.** Sample 1411B-16H-3W, 150. **29-32.** Sample 1411B-18H-1W, 90. **33-36.** Sample 1411B-18H-3W, 30. **37-38.** Sample 1509A-28R-4W, 20. **39-42.** Sample 1509A-28R-4W, 140. **43-48.** Sample 1509A-28R-4W, 140

PLATE S6.1

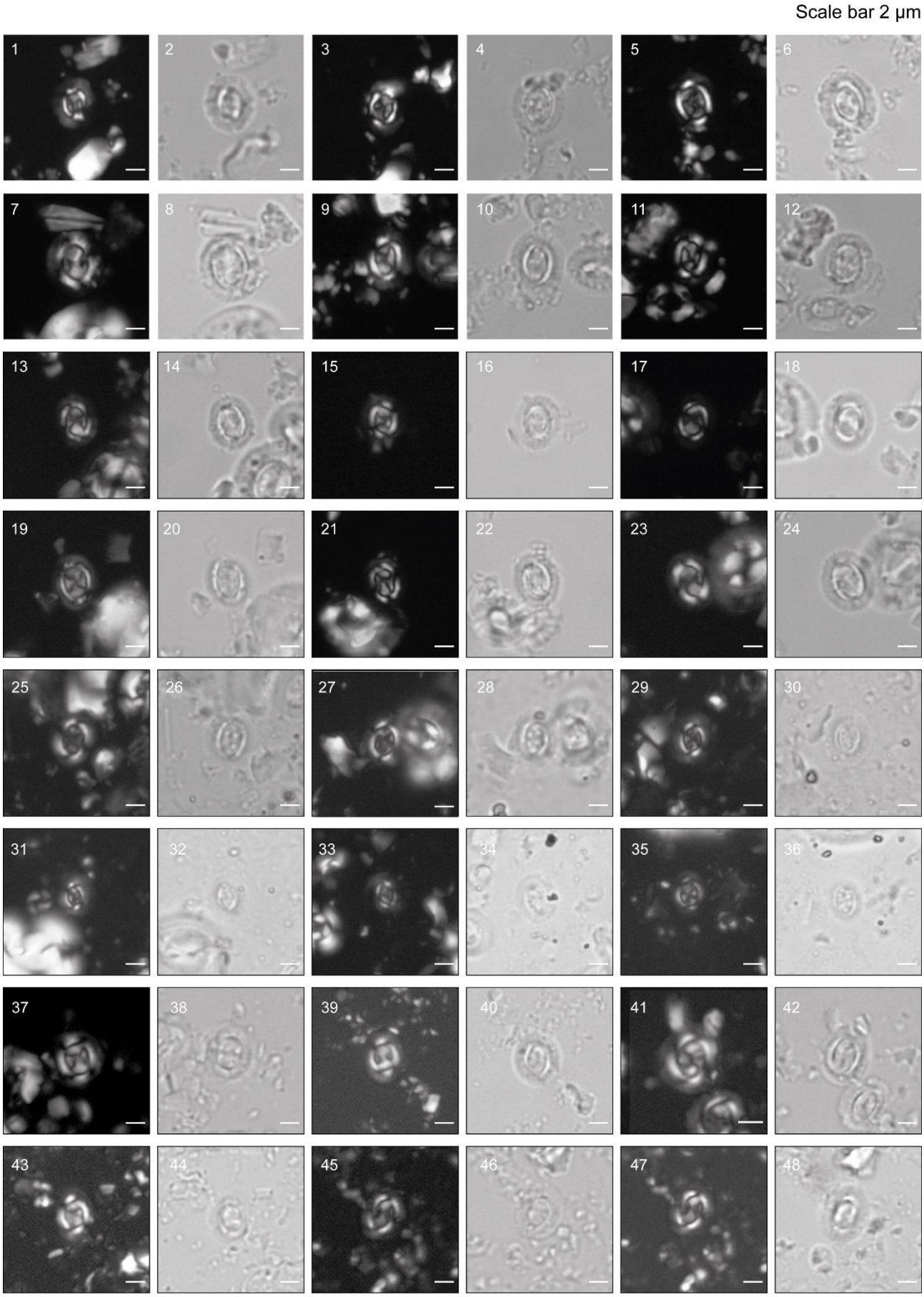
Scale bar 2 µm
1
2
3
4
5
6
7
8
9
10
11
12
13
14
15
16
17
18
19
20
21
22
23
24
25
26
27
28
29
30
31
32
33
34
35
36
37
38
39
40
41
42
43
44
45
46
47
48

References

Anderson, L.D., Delaney, M.L., 2005. Middle Eocene to early Oligocene paleoceanography from Agulhas Ridge, Southern Ocean (Ocean Drilling Program Leg 177, Site 1090). Paleoceanography 20, 1–13.

Backman, J., Shackleton, N.J., 1983. Quantitative biochronology of Pliocene and early Pleistocene calcareous nannofossils from the Atlantic, Indian and Pacific oceans. Marine Micropaleontology 8, 141–170.

Coxall, H.K., Wilson, P.A., 2011. Early Oligocene glaciation and productivity in the eastern equatorial Pacific: Insights into global carbon cycling. Paleoceanography 26, 1–18.

Diester-Haass, L., 1995. Middle Eocene to early Oligocene paleoceanography of the Antarctic Ocean (Maud Rise, ODP Leg 113, Site 689): change from a low to a high productivity ocean. Palaeogeography, Palaeoclimatology, Palaeoecology 113, 311–334.

Diester-Haass, L., Zachos, J.C., 2003. The Eocene-Oligocene transition in the Equatorial Atlantic (ODP Site 925); Paleoproductivity increase and positive $\delta^{13}C$ excursion. In: Prothero, D.R., Ivany, C.L., Nesbitt, E.A. (Eds.), From Greenhouse to Icehouse; The Marine Eocene-Oligocene Transition. Columbia Univ. Press, New York, NY, USA, p. 397–416.

Diester-Haass, L., Zahn, R., 1996. Eocene-Oligocene transition in the Southern Ocean: History of water mass circulation and biological productivity. Geology 24, 163–166.

Diester-Haass, L., Zahn, R., 2001. Paleoproductivity increase at the Eocene - Oligocene climatic transition: ODP/DSDP sites 763 and 592. Palaeogeography, Palaeoclimatology, Palaeoecology 172, 153–170.

Erhardt, A.M., Pälike, H., Paytan, A., 2013. High-resolution record of export production in the eastern equatorial Pacific across the Eocene-Oligocene transition and relationships to global climatic records. Paleoceanography 28, 130–142.

Falkowski, P.G., Katz, M.E., Knoll, A.H., Quigg, A., Raven, J.A., Schofield, O., Taylor, F.J.R., 2004. The evolution of modern eukaryotic phytoplankton. Science 305, 354–360.

Finkel, Z. V., 2007. Does Phytoplankton Cell Size Matter? The Evolution of Modern Marine Food Webs. In: Falkowski, P.G., Knoll, A.H. (Eds.), Evolution of Primary Producers in the Sea. Elsevier Academic Press, p. 333–350.

Gradstein, F.M., Ogg, J.G., Schmitz, M.D., Ogg, G.M., 2012. The Geologic Time Scale 2012. Elsevier, Amsterdam, Netherlands.

Griffith, E., Calhoun, M., Thomas, E., Averyt, K.B., Erhardt, A.M., Bralower, T.J., Lyle, M.W., Olivarez-Lyle, A., Paytan, A., 2010. Export productivity and carbonate accumulation in the Pacific Basin at the transition from a greenhouse to icehouse climate (late Eocene to early Oligocene). Paleoceanography 25, 1–15.

Henderiks, J., 2008. Coccolithophore size rules - Reconstructing ancient cell geometry and cellular calcite quota from fossil coccoliths. Marine Micropaleontology 67, 143–154.

Latimer, J.C., Filippelli, G.M., 2002. Eocene to Miocene terrigenous inputs and export production: Geochemical evidence from ODP Leg 177, Site 1090. Palaeogeography, Palaeoclimatology, Palaeoecology 182, 151–164.

Nilsen, E.B., Anderson, L.D., Delaney, M.L., 2003. Paleoproductivity, nutrient burial, climate change and the carbon cycle in the western equatorial Atlantic across the Eocene/Oligocene boundary. Paleoceanography 18.

Norris, R.D., Wilson, P.A., Blum, P., Fehr, A., Agnini, C., Bornemann, A., Boulila, S., Bown, P.R., Cournede, C., Friedrich, O., Ghosh, A.K., Hollis, C.J., Hull, P.M., Jo, K., Junium, C.K., Kaneko, M., Liebrand, D., Lippert, P.C., Liu, Z., Matsui, H., Moriya, K., Nishi, H., Opdyke, B.N., Penman, D.E., Romans, B.W., Scher, H.D., Sexton, P., Takagi, H., Turner, S.K., Whiteside, J.H., Yamaguchi, T., Yamamoto, Y., 2014. Site U1411. Proceedings of the Integrated Ocean Drilling Program 342.

Ravizza, G., Paquay, F., 2008. Os isotope chemostratigraphy applied to organic-rich marine sediments from the Eocene-Oligocene transition on the West African margin (ODP Site 959). Paleoceanography 23, 1–11.

Salamy, K.A., Zachos, J.C., 1999. Latest Eocene-Early Oligocene climate change and Southern Ocean fertility: Inferences from sediment accumulation and stable isotope data. Palaeogeography, Palaeoclimatology, Palaeoecology 145, 61–77.

Schumacher, S., Lazarus, D., 2004. Regional differences in pelagic productivity in the late Eocene to early Oligocene—a comparison of southern high latitudes and lower latitudes. Palaeogeography, Palaeoclimatology, Palaeoecology 214, 243–263.

Young, J.R., Bown, P.R., 1997. Cenozoic calcareous nannoplankton classification. Journal of Nannoplankton Research 19, 36–47.

Acknowledgements

I am extremely grateful to my supervisor Claudia Agnini for giving me the chance to work on this project and for her constant support and guidance. I would like to thank her for sharing with me her knowledge and love for micropaleontology. My PhD would not have been possible without her help, patience, and precious moment of discussions. My sincere gratitude also to Edoardo Dallanave, for allowing the use of his magnetostratigraphic data within my thesis. Many thanks also to Maria Chiara Dalconi, for giving me the opportunity to perform my studies at the SEM ad for her help in teaching me how to use it.

Many thanks as well to Carlotta for always being beside me and ready to help and to Livio for the counseling and the early-morning coffee supply. A huge thank also to Elena, for sharing this journey with me and for always being there from day one to the end. There are far too many people to name from the Department of Geosciences who have contributed to these great years; all of the PhD students, Marta and Alice, and other friends from the coffee room and the laboratories, including Ornella.

I would like also to thank Prof. Massimiliano Ghinassi and Prof. Andrea D'Alpaos for always making me laugh, especially during the long hours spent under the microscope.

Finally, I am extremely grateful to all my family who have provided incessant encouragement over the past years. And, above all, I thank Ivana, for be my best friend since the first year of kindergarten and Mario for his love and endless confidence in me.